Impact des mécanismes moléculaires impliquant la muqueuse orale et les protéines salivaires sur la perception de la flaveur : exemples de l'astringence et de la perception aromatique

Francis Canon

Université de Bourgogne – Franche-Comté

Habilitation à Diriger les Recherches

Ecole doctorale E2S Environnement - Santé

Présentée et soutenue publiquement par

Francis Canon

le 03 Décembre 2019

Impact des mécanismes moléculaires impliquant la muqueuse orale et les protéines salivaires sur la perception de la flaveur : exemples de l'astringence et de la perception aromatique

JURY

Dr Gabelica Valérie	INSERM, Bordeaux	rapporteur
Dr Marchal Axel	Université de Bordeaux	rapporteur
Dr Mercier-Bonin Muriel	INRA, Toulouse	rapporteur
Dr Briand Loïc	INRA, Dijon	examinateur
Dr Lesniewska Eric	Université de Dijon	examinateur
Dr Giuliani Alexandre	INRA, Saint-Aubin	examinateur

Table des matières

Curriculum vitae

Etat civil

Francis CANON
Né le 18/01/1981 à le Creusot, France

Identifiants

Orcid: http://orcid.org/0000-0002-6140-5007
Research ID: http://www.researcherid.com/rid/E-7692-2013
Scopus Author ID: http://www.scopus.com/authid/detail.url?authorId=36861075000

Etudes et Diplômes

2007-2010	Doctorat en biochimie, chimie des aliments "Mention très honorable". *Centre international d'études supérieures en sciences agronomique*, Montpellier, France. Sous la direction de Dr Véronique Cheynier
2006	Master recherche en Chimie et Biochimie alimentaire (Major) *Ecole nationale supérieure de biologie appliquée à la nutrition et à l'alimentation*, Dijon, France.

Expérience professionnelle

2012 – aujourd'hui :	Chargé de recherche à l'INRA - CSGA "Centre des sciences du goût et de l'alimentation", Dijon, France
2010 – 2011	Chercheur Post-Doctorant au Synchrotron SOLEIL, Gif-sur-Yvette, France. Sous la direction d'Alexandre Giuliani
2007 – 2010	Doctorant à l'INRA - SPO (Science pour l'Oenologie), Montpellier, France. Sous la direction de Véronique Cheynier et Pascale Sarni-Manchado

Contrats

2013 – 2014	ANS attribuée par le département CEPIA-INRA (Budget annuel renouvelé 1 fois), 15 000€
2012 – 2013	Faber bourse attribuée par le conseil régional de Bourgogne (Budget annuel renouvelé 1 fois), 30,000€

Encadrement d'étudiants et de chercheurs post-doctorants

2012 – 2019	3 Postdoctorants : Le Joubioux F.; Aybeke E.; Muñoz-Gonzáles C.) 4 Doctorants : Pagès-Hélary S. (2012-2015); Ployon S. (2013-2016); Wang M. (2018-2022); Clément Nivet (2019-2022) 5 étudiants en Master : Courtin J.; Toutain P.M.; Julio R.; Thierry A. & Laheurte M.

Activité d'enseignement

2018 – Aujourd'hui	Intervention en tant qu'expert en perception de la flaveur et chimie analytique dans le cadre du Master P2FOOD, Université de Bourgogne – Franche-Comté

Organisation de conférences scientifiques

2014	Membre du Comité d'organisation pour le 24th ECRO Congress (European Chemoreception Research Organization) (10-13 septembre 2014, Dijon, France)
2009	Membre du Comité d'organisation pour le 25th International Conference on Polyphenols (24 – 27 Août 2010, Montpellier, France)

Responsabilités institutionnelles

2017 – Aujourd'hui	Membre élu du conseil d'unité du CSGA
2017 – Aujourd'hui	Membre élu du conseil scientifique du département CEPIA INRA
2016 – Aujourd'hui	Membre nominé du conseil scientifique de la plateforme ChemoSens

Participation à des comités de lecture et jury

2012 – Aujourd'hui	Évaluateur pour les journaux : Tetrahedron, Food Chemistry, Journal of Agriculture and Food Chemistry, Chinese Journal of Chemistry, Journal of Texture Studies & Food Research International
2018	Membre du jury de la thèse de Mélanie MILLET.
2015	Membre du jury de la thèse de Guilherme TAVARES.

Membre de sociétés scientifiques

2008 – Aujourd'hui	Membre de la société française de spectrométrie masse

Collaborations majeures

Académique

- Lesniewska E. & Bourillot E. from the ("Institut Carnot de Bourgogne", Université Bourgogne – Franche Comté, Dijon, France) sur le développement de méthodologies utilisant AFM pour la caractérisation des surfaces biologiques. Ils sont équipés avec les techniques AFM de dernière génération telles que high-speed AFM, nano-IR ou SMM.
- Zahouani H. & Vargiolu R. ("Laboratoire de Tribologie et Dynamique des Systèmes", Ecole Centrale Lyon) sur le développement de méthodologie pour la caractérisation en bouche des forces de friction.
- Del Pozo Bayón M. (Dept. de Microbiología y Biotecnología-Biotechnology and Microbiology Dept., Instituto de Investigación en Ciencias de la Alimentación, Madrid, Spain) sur les effets de la salive sur la libération des molécules d'arôme *in vivo* lors de la consommation de vin.
- Piombino P. département des sciences de l'Agriculture, Université de Naples Federico II, Naples, Italie sur le couplage de la méthode de caractérisation des

dominances sensorielles temporelles et de la spectrométrie de masse de type PTR-MS pour la caractérisation de l'effet de protection de la fraction volatile des vins par les tannins lors de l'oxydation des vins.
- Guyot S. (Unité Biopolymères, Interaction & Assemblage, INRA, Rennes, France) sur la caractérisation de l'astringence des tannins de pommes.

Industrielle

- Nestlé Research via Benjamin Le Révérend & Christoph Hartmann, Head of Perception Physiology Group sur les aspects d'astringence et de libération des molécules d'arôme.
- Oenobrands avec Rémy Schneider sur l'effet des protéines de la matrice vin et de la salive sur la libération des molécules d'arôme.
- Lallemand sur les effets des molécules de la paroi de levure sur la libération des molécules d'arôme et la perception.

Prix et distinctions

2014	ANR-JCJC, intitulée "MUcosal salivary Film & Flaveur INteractions" (ANR-14-CE20-0001), 398'662€ (incluant les salaires pour un post-doctorant et un assitant ingénieur)
2013-2014	Bourse ANS attribuée par le département CEPIA-INRA (budget d'un an renouvellé une fois), 15'000€
2012-2013	Bourse Faber du conseil générale de la région Bourgogne (budget d'un an renouvellé une fois), 30'000€
2010	Prix de la meilleure conférence orale à la "journée de l'école doctorale science des procédés – sciences des aliments "
2009	Prix du meilleur poster à la "journée de l'école doctorale science des procédés – sciences des aliments"
2008	Prix du meilleur poster à la "journées françaises de la spectrométrie de masse"

I. Synthèse de mes travaux de recherche

L'activité de recherche que j'ai mise en place a pour but de mieux comprendre le rôle des protéines salivaires dans la perception de la flaveur.

La flaveur est l'un des principaux moteurs de la prise alimentaire et de l'acceptabilité des aliments. Il s'agit d'une perception multimodale correspondant à l'intégration fonctionnelle des informations en provenance des sens chimiques de l'olfaction, la gustation et de la perception trigéminale(Thomas-Danguin 2009). Une partie des mécanismes moléculaires impliqués dans ces différents sens ne sont toujours pas connus. Ainsi malgré l'importance de la sensation d'astringence, les bases moléculaires de cette sensation n'ont toujours pas été élucidés. De même les mécanismes moléculaires péri-récepteurs sont encore peu connus, alors qu'ils sont susceptibles de moduler la répartition, la disponibilité et la nature des molécules de la flaveur activant les récepteurs sensoriels. Il a ainsi été récemment rapporté que la salive pouvait moduler la libération des molécules d'arôme en fonction de sa composition et de son activité enzymatique. Les protéines salivaires ancrées à la surface de la muqueuse orale et formant la pellicule mucosale pourraient également être impliquées dans la rémanence aromatique. Malgré leur importance, il existe encore peu d'information sur ces mécanismes.

Dans ce contexte mon projet de recherche a pour objectif de répondre à trois questions scientifiques :

- Quel(s) est (sont) le(s) mécanisme(s) moléculaire(s) à l'origine de la sensation d'astringence ?
- Quels sont les mécanismes moléculaires en bouche modifiant la perception aromatique et à l'origine de la persistance aromatique ?
- Comment ces mécanismes s'impactent ils les uns et les autres ?

Il me semble important d'adresser ces trois questions en même temps pour les raisons suivantes :

Premièrement, des mécanismes moléculaires distincts mais impliquant chacun des protéines salivaires identiques et la muqueuse orale interviennent dans la perception aromatique(Buffo et al. 2005; Doyennette et al. 2014; Linforth and Taylor 2000; Wright et al. 2003) et de l'astringence(Nayak and Carpenter 2008; Ployon et al. 2018) en bouche. Deuxièmement, les tanins, qui sont des composés astringents, modifieraient la persistance aromatique. Ainsi, certaines compagnies œnologiques proposent des fractions de tannins pour leurs effets sur la persistance aromatique. Cependant, à l'heure actuelle il n'existe aucune étude ayant permis de montrer par quel mécanisme moléculaire croisé les tanins modifieraient la persistance aromatique. Troisièmement, les interactions à un niveau perceptuel entre l'astringence et la perception aromatique contribuent aux propriétés sensorielles global de l'aliment.

Mon projet de recherche vise donc à avoir une compréhension claire de ces mécanismes et de leurs interactions à un niveau moléculaire et perceptuel, afin de proposer des solutions pour une meilleurs acceptation des aliments astringents. En effet, les tanins ont des propriétés antioxydantes bénéfiques pour la santé et pourraient contribuer à réduire le risque de certaines maladies comme les maladies cardiovasculaires. Cependant, les aliments riches en tanins sont généralement rejetés par le consommateur à cause de l'impact négatif de l'astringence sur l'image sensorielle de la flaveur des aliments. L'astringence est également

un problème pour l'utilisation de certaines fractions de protéines végétales alors qu'elles constituent des sources de protéines pertinentes et durables.

II. Stratégie de recherche

Afin d'étudier ces différents mécanismes, mes travaux de recherche s'appuient sur des approches *in-vivo*, *ex-vivo* et *in-vitro*, multidisciplinaires mêlant biophysique, biochimie, biologie moléculaire, chimie analytique et analyse sensorielle.

Les approches *in-vitro* reposent sur le développement d'objets modèles tels que la production et la purification de protéines cibles ou le développement d'un modèle de muqueuse orale. Les interactions de ces objets avec les molécules de la flaveur sont ensuite étudiées en milieu modèle afin d'être correctement caractérisées.

Les approches *ex-vivo* permettent de mieux rendre compte de la réalité biologique des systèmes étudiés et portent par exemple sur l'effet des tannins sur les forces de friction à la surface de langue de porc.

Enfin les approches *in vivo* chez l'homme sont généralement plus difficiles à mettre en œuvre et requièrent le développement d'instruments ou de méthodologies spécifiques. De plus, elles nécessitent de prendre en compte plusieurs variables en même temps qui ne peuvent pas être toutes contrôlées ou même mesurées ainsi que la forte variabilité interindividuelle.

Les allers-et-retours entre ces trois approches sont nécessaires afin d'affiner notre compréhension du rôle des mécanismes moléculaires étudiés dans la perception.

III. Développement et caractérisation d'un modèle de muqueuse orale

La muqueuse orale et la salive sont des barrières de défense qui assurent la protection des tissus oraux profonds contre l'abrasion mécanique lors de la mastication, qui contrôlent la pénétration de micro-organismes et de molécules potentiellement toxiques pour l'organisme. Pour cela, la muqueuse orale est constituée d'un épithélium stratifié qui est recouvert d'une fine couche de protéines, appelée pellicule mucosale. Cette couche détermine les propriétés de surface de la muqueuse orale. Ainsi, ces propriétés de lubrification lui permettent de limiter les forces de friction à la surface de la muqueuse orale, pendant que sa composition détermine sa capacité à interagir avec les composés de la matrice alimentaire ou les micro-organismes. Malgré le fait que plusieurs études aient suggéré son implication dans la perception de la flaveur, il existe encore peu de données sur les mécanismes moléculaires d'interaction entre la pellicule mucosale et les molécules de la flaveur. En effet, peu d'études se sont intéressées à ces mécanismes. La plupart d'entre elles ont été réalisées *in vivo*(Wright et al. 2003) sans être capables d'identifier la contribution spécifique de la pellicule mucosale. Les études réalisées *in vitro* ont utilisé une pellicule mucosale reconstituée sur une surface synthétique(Bongaerts et al. 2007) qui différaient de la pellicule mucosale *in vivo* en terme de composition, ultrastructure et propriétés(Dresselhuis et al. 2008; Joiner et al. 2004). La capacité des protéines à interagir avec les composés de la flaveur ou de lubrifier la surface de la pellicule mucosale dépend de leur structure(Canon et al. 2011; Canon et al. 2018; Pagès-Hélary et al. 2014). Ceci suggère que la composition de la pellicule mucosale intervient sur son action dans la perception de la flaveur.

A. Formation de la pellicule mucosale et rôle de MUC1

La pellicule mucosale résulte d'un ancrage spécifique des protéines salivaires à la surface des cellules épithéliales composant la muqueuse orale. MUC5B, l'α-amylase salivaire, les cystatines, les protéines riches en prolines acides(Bradway et al. 1992) ainsi que l'immunoglobuline A(Gibbins and Carpenter 2013) figurent parmi les protéines qui ont été identifiées au niveau de la pellicule mucosale. Cependant, le mécanisme exact d'absorption de ces protéines à la surface des cellules épithéliales et de formation de la pellicule mucosale est mal connu(Ployon et al. 2016). A côté des protéines salivaires, une mucine transmembranaire, MUC1, a été identifiée parmi les protéines composant la pellicule mucosale(Gibbins et al. 2013). Son expression par les cellules orales épithéliales a été confirmée(Ukkonen et al. 2017). La pellicule mucosale assure un rôle de lubrification de la surface de la muqueuse orale. Ainsi sa présence modifie les propriétés de surface de la muqueuse orale. Cependant, les modèles de muqueuses orales qui existaient jusqu'à présent ne la prenaient pas en compte. Récemment, Teubl *et al.* (2013) ont développé un modèle d'épithélium oral basé sur la lignée TR146, sur lequel est déposé un film constitué de mucines gastriques de porc. Cependant, de par la composition de leur film réduite à la seule présence de mucines et la nature de celles-ci, ce modèle ne constitue pas un modèle réaliste. J'ai donc développé un nouveau modèle de muqueuse orale prenant en compte la pellicule mucosale. Ce développement a été réalisé dans le cadre de la thèse de Sarah Ployon que j'ai co-dirigé

et financé par une projet ANR Jeune Chercheuse – Jeune Chercheur (ANR JC-JC) intitulé « MUcosal salivary Film and Flavor Interaction » (MUFFIN), que j'ai dirigé. Le développement d'un modèle réaliste de muqueuse orale prenant en compte la pellicule salivaire représente une innovation majeure pour la communauté scientifique travaillant sur les processus oraux intervenant dans la perception de la flaveur.

Publication n°1: Ployon, S.; Belloir, C.; Bonnotte, A.; Lherminier, J.; Canon, F.; Morzel, M., The membrane-associated MUC1 improves adhesion of salivary MUC5B on buccal cells. Application to development of an in vitro cellular model of oral epithelium. *Arch. Oral Biol.* **2016,** *61*, 149-55.

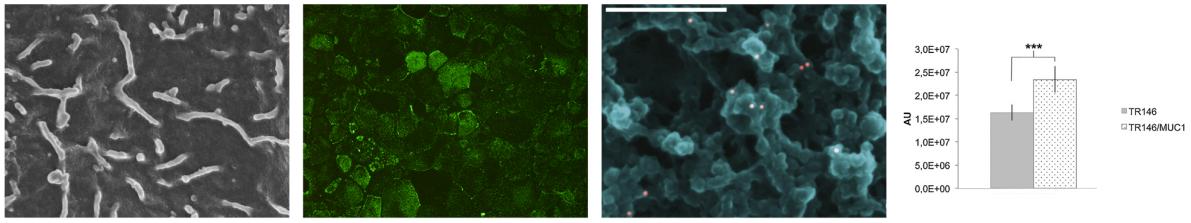

a. TR146 cells observed by SEM | b. MUC5B immunostaining of TR146/MUC1/Y-LSD | c. Immuno-SEM detection of salivary MUC5B on the MP (scale bars 500 nm) | d. Semi-quantification of MUC5B retained on cells by immunocyto-chemistry

Figure 1. Développement d'un modèle de muqueuse orale.

Le modèle mis au point utilise la lignée cellulaire immortalisée TR146, issue d'un carcinome de muqueuse orale. Ces cellules présentent à leur surface des structures topographiques typiques des cellules buccales humaines, appelées microplicae(Rupniak et al. 1985) (Figure 1a). Ces structures pourraient faciliter la formation de la pellicule mucosale sans que cela n'ait été démontré. Des expériences d'immunocytochimie ont montré que MUC1 n'était pas exprimé à la surface des cellules TR146. Ainsi, la lignée TR146 a été transfectée de manière stable par un gène codant pour la protéine MUC1/Y-LSP, donnant naissance à la lignée cellulaire TR146-MUC1/Y-LSP. Un protocole pour reformer la pellicule mucosale à la surface des cellules a été mis au point. Il a été validé par des expériences d'immunomarquage confirmant l'ancrage de MUC5B, protéine composant majoritairement la pellicule mucosale, à la surface des cellules après rinçage de ces dernières (figure 1b et 1c). Des expériences d'immunocytochimie ont montré que la présence de MUC1 augmentait de manière significative l'ancrage de MUC5B (figure 1d). Ainsi, MUC1 semble jouer un rôle clé dans la formation de la pellicule mucosale(Gibbins et al. 2013), en fournissant un point d'ancrage aux protéines salivaires mucosales. MUC1 est une protéine polymorphique avec une importante variabilité interindividuelle(Hanisch and Müller 2000). Ainsi, comme les interactions protéine-protéine dépendent de la structure des deux partenaires, la variabilité structurale de MUC1 pourrait impacter la composition et donc les propriétés de la pellicule mucosale et son impact sur la flaveur.

B. Impact de la pellicule mucosale sur les propriétés de surface de la muqueuse orale.

Je présente ci-dessous un article se rapportant au travail de post-doctorat de Ece Aybeke, financé dans le cadre du projet ANR MUFFIN que j'ai dirigé. Ce travail porte sur la caractérisation des changements de propriétés de la surface cellulaire suite à la formation de

la pellicule mucosale, en utilisant une approche basée sur la microscopie à force atomique (AFM).

Publication n°2: Aybeke, E. N.; Ployon, S.; Brulé, M.; De Fonseca, B.; Bourillot, E.; Morzel, M.; Lesniewska, E.; Canon, F., Nano-imaging of the physical surface properties of human buccal cells and changes induced by saliva. *Langmuir* 2019.

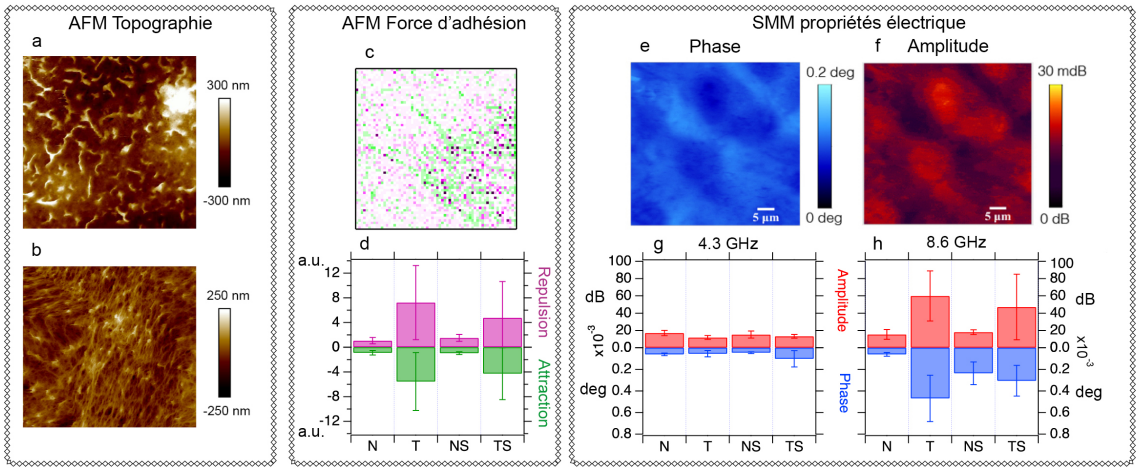

Figure 2. Caractérisation du modèle de muqueuse orale cellulaire par AFM: topographie des cellules transfectées avec (b) et sans (a) pellicule mucosale; cartographie des forces de rétention et répulsion avec une pointe fonctionnalisée avec une molécule hydrophobe d'une cellules transfectées (c) et comparaison des valeurs moyennes pour les 4 conditions ; cartographie de la phase (e) et de l'amplitude (f) des ondes réfléchies à 8,6 GHz d'une cellule transfectée et comparaison des valeurs moyennes de la phase et de l'amplitude pour les différentes conditions testées à 4,3 (g) et 8,6 (h) GHz. Conditions testées : cellules natives TR146 sans (N) et avec pellicule mucosale (NS); cellules transfectées TR146-MU1/Y-LSD sans (T) et avec pellicule mucosale (TS).

Dans cette étude, la topographie, l'hydrophobicité et les propriétés électriques de la surface cellulaire, des cellules natives et transfectées avec et sans pellicule mucosale, ont été caractérisées avec différentes techniques basées sur l'AFM. L'AFM classique a permis de caractériser la topographie de la surface des cellules (figures 2a et 2b). La fonctionnalisation de la pointe AFM (Chemical force microscopy (CFM)) avec un alcanthiol a permis de sonder le caractère hydrophobe de la surface de la muqueuse (figures 2c et 2d). Enfin, l'utilisation de la microscopie à sonde locale micro-onde (SMM ; scanning microwave microscopy) a rendu possible la mesure des propriétés diélectriques à la surface du modèle de muqueuse (figures 2e, 2f, 2g et 2h).

Ces mesures ont montré que la transfection de la lignée cellulaire TR146 ne modifiait pas la topographie de la surface des cellules. Elles ont également révélé l'existence de zones plus hydrophobes et plus hydrophiles à la surface des cellules transfectées par MUC1/Y-LSP (figure 2c et 2d). Ceci suggère la présence à la fois de domaines hydrophiles et hydrophobes au niveau de la partie extracellulaire de MUC1. MUC1/Y-LSP présente une version raccourcie de sa partie extra-cellulaire par rapport aux autres isoformes de MUC1, avec en particulier l'absence de la région VNTR fortement glycosylée. De plus, le SEA domaine présente une délétion de 15 acides aminés, conduisant à une altération de sa structure tridimensionnelle. Cette déstructuration du SEA domaine pourrait être à l'origine de l'émergence en surface de régions hydrophobes normalement enfouies dans le cœur hydrophobe de ce domaine.

En parallèle la présence de ce domaine extracellulaire, induit d'importants changements de la constante diélectrique à la surface du modèle cellulaire, se traduisant par des modifications de la phase et de l'amplitude des micro-ondes réfléchies au longueurs d'ondes les plus élevées (8.6 GHz) (figure 2h). Des changements sont également observables à une longueur d'onde plus courte (4.3 GHz) traduisant des changements plus en profondeur, qui pourraient résulter de changements au niveau intracellulaire dus à la présence de la queue cytosolique de MUC1/Y-LSP (figure 2g).

La formation de la pellicule mucosale, correspondant à l'ancrage spécifique de protéines salivaires à la surface cellulaire, ne modifie pas de manière significative les propriétés d'hydrophobicité à la surface des cellules natives bien que modifiant les propriétés électriques (changement significatif de la phase à 8.6 GHz). En revanche, elle tend à diminuer la présence des zones les plus hydrophobes et les plus hydrophiles en présence de MUC1/Y-LSP. Ces zones sont probablement masquées suite à l'ancrage des protéines salivaires, et seraient donc impliquées dans les interactions entre MUC1/Y-LSP et les protéines salivaires. Ceci suggère que des interactions non-covalentes de différentes natures, impliquant à la fois des effets hydrophobes et des liaisons électrostatiques, participent à l'ancrage des protéines salivaires à MUC1.

Ainsi, la présence des protéines formant la pellicule induit de forts changements des propriétés de surface de la muqueuse orale pouvant moduler ses interactions avec les molécules de la flaveur.

IV. Etude des mécanismes moléculaires à l'origine de la sensation d'astringence

A. Rôle de la muqueuse orale dans la sensation d'astringence

La sensation d'astringence est une sensation de sécheresse, de rugosité et de constriction des muqueuses. Cette sensation présente la particularité d'être rémanente et de mettre plusieurs dizaines de secondes (20-40s) à se développer (Lyman and Green 1990) après que l'aliment ait été mise en bouche. Cette sensation est généralement ressentie lors de la consommation d'aliments d'origine végétale riches en tanins. Ces derniers participent aux mécanismes de défense des végétaux et présentent des effets antinutritionnels dus à leur capacité à inhiber les enzymes digestives. Les tanins ne sont pas les seules molécules astringentes et d'autres molécules telles que certaines protéines ou des ions sont décrits comme étant astringents. Malgré l'importance de l'astringence dans la perception de la flaveur de l'aliment, les mécanismes moléculaires impliqués restent encore mal compris.

Il a été récemment confirmé que l'astringence est médiée via le nerf trijumaux sans que la nature des récepteurs sensoriels impliqués n'ait été clairement identifiée(Schöbel et al. 2014). Les auteurs suggèrent l'implication de chemorécepteurs de type « transient receptor potential » (TRP), qui seraient activés par certains tanins(Kurogi et al. 2012) ou leurs métabolites(Kurogi et al. 2015). Ces récepteurs sont exprimés au niveau de terminaisons nerveuses libres trigéminales enfouies dans la muqueuse orale(Kichko et al. 2018). Ainsi, cette hypothèse suppose que les tanins diffusent à travers la pellicule mucosale et la muqueuse orale jusqu'à ces récepteurs. Cette hypothèse souffre également du fait que l'astringence est généralement décrite comme une sensation tactile(Breslin et al. 1993; Green 1993). Ainsi, l'astringence aurait pour origine l'activation de mécanorécepteurs(Guinard and Mazzucchelli 1996) situés au niveau de la muqueuse orale. Cette activation résulterait d'une augmentation des forces de friction à la surface de la muqueuse orale suite à la perte du pouvoir de lubrification des protéines salivaires et/ou de la pellicule mucosale. L'hypothèse la plus couramment admise postule que l'agrégation et la précipitation des protéines salivaires par les molécules astringentes, à l'origine de la perte de leur pouvoir de lubrification(Bate-Smith 1973) et/ou de changements au niveau de la pellicule mucosale(Horne et al. 2002), serait à l'origine des changements de force de friction en bouche. Cependant, il a été montré que la présence de salive n'est pas nécessaire à la perception de l'astringence et qu'à l'inverse elle diminue sa perception (Nayak and Carpenter 2008). Dans cette autre hypothèse, les protéines salivaires joueraient un rôle de protection de la pellicule mucosale qui serait plus directement impliquée dans la perception de l'astringence. En faveur de cette hypothèse, il a été montré chez l'animal qu'un régime riche en tanin induit une augmentation de la sécrétion de protéines riches en proline (PRP) salivaires (Ann and Carlson 1985; Clauss et al. 2005; Mehansho et al. 1983; Mehansho et al. 1985; Mehansho et al. 1987; Shimada 2006) et que ces protéines ont une affinité particulière pour les tanins(Hagerman and Butler 1981). Afin d'étudier la validité de cette hypothèse, j'ai mis en place une étude présentée dans la publication suivante.

Publication n°3 : Ployon, S.; Morzel, M.; Belloir, C.; Bonnotte, A.; Bourillot, E.; Briand, L.; Lesniewska, E.; Lherminier, J.; Aybeke, E.; Canon, F., Mechanisms of astringency:

Structural alteration of the oral mucosal pellicle by dietary tannins and protective effect of bPRPs. *Food Chem.* **2018,** *253*, 79-87.

Dans ce travail, le modèle de muqueuse précédemment développé a été mis en présence de deux tanins (l'épigallocachine gallate (EgCG) et l'épigallocatéchine (EgC)) à différentes concentrations. Ces deux tanins diffèrent par la présence d'un groupe galloyle au niveau de la structure de l'EgCG (figure 3). Des expériences d'immunofluorescences et de microscopie électronique à balayage, présentées sur la figure 3, ont montré la formation de larges agrégats au niveau de la pellicule mucosale en présence des deux tanins étudiés, lorsqu'ils sont à des concentrations supérieures à leur seuil de perception de la sensation d'astringence.

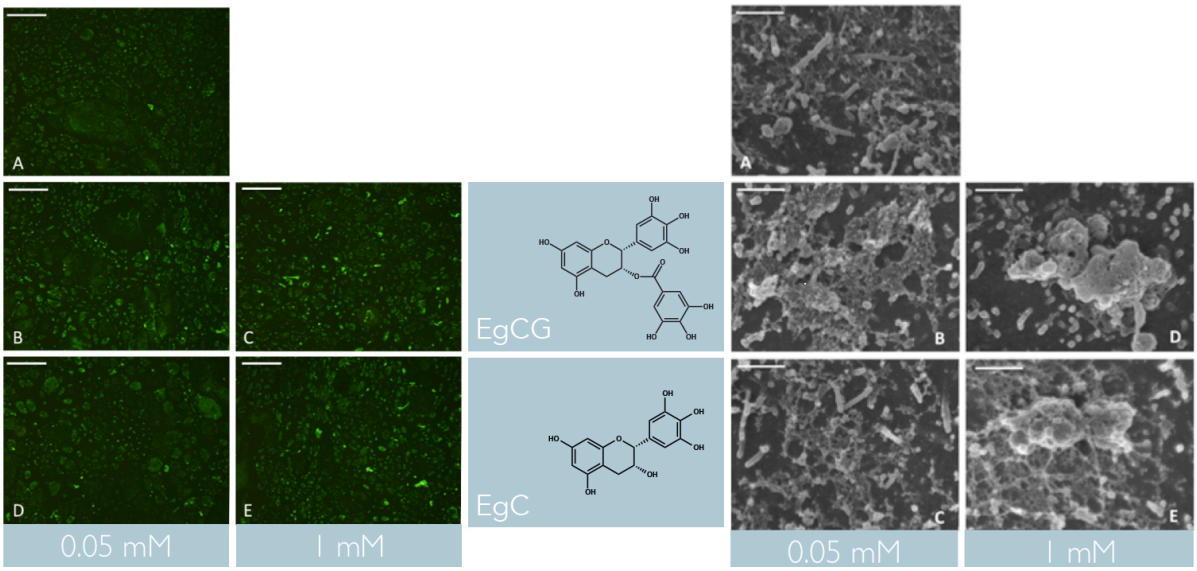

Figure 3. Sur la gauche, immunofluorescence des mucines MUC5 à la surface des cellules TR146/MUC1/Y-LSP en fonction de la présence d'EgCG ou EgC aux concentrations de 0.05 mM et 1mM. Sur la droite, images de microscopie électronique à balayage de la surface des cellules TR146/MUC1/Y-LSP en fonction de la présence d'EgCG ou EgC aux concentrations de 0.05 mM et 1 mM.

La figure 4 présente le pourcentage de l'aire des agrégats en fonction de leur taille. L'analyse de la taille des particules à 75% de l'aire totale montre une augmentation significative de la taille des agrégats avec la concentration en tanins. La présence du groupe galloyle supplémentaire sur l'EgCG tend à augmenter la taille des agrégats formés, bien que cette différence ne soit pas significative. L'ajout au milieu de culture cellulaire de la PRP IB5 à une concentration physiologique avant l'addition de tanins, a réduit de manière significative l'agrégation de la pellicule mucosale. En parallèle, des expériences de microscopie à force atomique (AFM) ont mise en évidence une augmentation des forces de friction au niveau de la pellicule mucosale avec la formation d'agrégats.
Ainsi, cette étude a montré que les tanins agrègent la pellicule mucosale, induisant une augmentation des forces de friction à la surface de la muqueuse orale, et que la présence de PRP diminue cette agrégation.

Ces observations penchent donc en faveur d'un rôle de protection de la pellicule mucosale des PRP salivaires alors que l'agrégation de la pellicule mucosale par les tanins induit une augmentation des forces de friction.

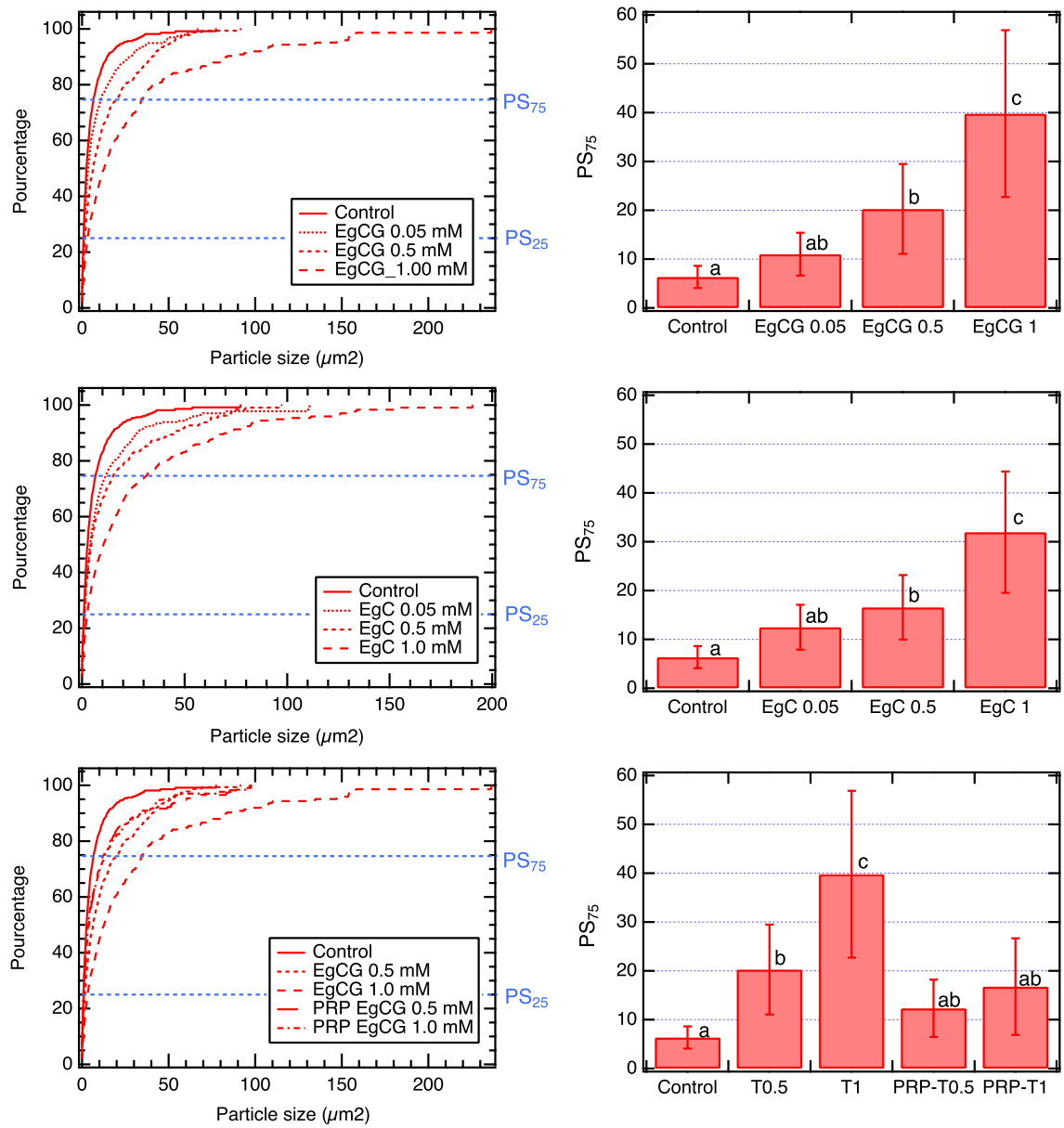

Figure 4. Répartition de l'aire total des agrégats en fonction de la taille des agrégats et taille des particules à 75% de l'aire totale en fonction des conditions étudiées.

B. Caractérisation des interactions tanins – protéines riches en prolines

La synthèse de PRP salivaires constitue un mécanisme d'adaptation à la consommation d'aliments riches en tanins (Ann and Carlson 1985; Clauss et al. 2005; Mehansho et al. 1983; Mehansho et al. 1985; Mehansho et al. 1987; Shimada 2006). Chez l'homme, l'ensemble des PRP synthétisées est codé par seulement 6 gènes (PRB1, PRB2, PRB3, PRB4, PRH1 et PRH2), tous situés sur le chromosome 12 (Maeda 1985; Maeda et al. 1985). Parmi ces gènes qui semblent avoir un ancêtre commun (Azen et al. 1996; Stubbs et al. 1998), deux codent pour des PRP acides (PRH1 et PRH2) et quatre pour des PRP basiques et glycosylées (PRB1, PRB2, PRB3 et PRB4) (Kim and Maeda 1986). Ils codent pour des pro-protéines qui subissent divers processus de maturation au cours de leur excrétion. Ces modifications post-traductionnelles

(glycosylation, phosphorylation et clivage) conduisent à la sécrétion d'une vingtaine de PRP dans la salive (Bennick 2002; Lyons et al. 1988).

Comme leur nom l'indique, les PRP montrent une richesse "anormale" en proline. Alors que cet acide aminé ne représente que 5% des acides aminés totaux chez les protéines structurées, un minimum de 20% est rencontré chez les PRP. Ce taux peut atteindre 40% pour les PRPs de certaines espèces comme l'homme, le rat et la souris (Kauffman and Keller 1979; Mehansho and Carlson 1983; Mehansho et al. 1985; Mole et al. 1990). La présence accrue de glycine, acide glutamique et glutamine est aussi une caractéristique de ces protéines. Le taux de ces quatre acides aminés avoisine les 70 à 90% (Mole et al. 1990). Ces protéines ont ainsi un index de complexité très faible. Ces quatre acides aminés qui empêchent la formation de structures secondaires chez ces protéines (Dunker et al. 2001) sont qualifiés de casseurs d'hélice. De plus, chez les PRP, ces acides aminés sont organisés sous la forme de nombreuses séquences répétées au sein de la chaîne peptidique. Ainsi, les PRP appartiennent à la famille des protéines intrinsèquement désordonnées (IDP). Sur la base de la valeur de leur point isoélectrique (pI) et de leur éventuelle glycosylation, les PRP salivaires sont divisées en trois classes, les PRP acides (*a*PRP), les PRP basiques (*b*PRP) et les PRP glycosylées (*g*PRP).

Parmi la vingtaine de PRP salivaires humaines, je me suis plus particulièrement intéressé à IB5. Cette protéine a été choisie comme modèle pour étudier la structure des PRP et leurs interactions avec les tanins. Les protéines salivaires humaines IB5, PRP basique, et II-1, PRP glycosylée, résultant du clivage de la pro-protéines PRB4S, ont été produites par voie hétérologue. L'étude de leur structure a utilisé la diffusion des rayons-X aux petits angles.

Publication n°4 : Boze, H.; Marlin, T.; Durand, D.; Pérez, J.; Vernhet, A.; Canon, F.; Sarni-Manchado, P.; Cheynier, V.; Cabane, B., Proline-rich salivary proteins have extended conformations. *Biophys. J.* **2010,** *99*, 656-665.

Cette étude a permis de caractériser la structure globale adoptée par IB5 en solution ainsi que son rayon de giration. Les résultats ont montré que les PRP basique sont présents en solution sous la forme d'une chaine allongée avec une conformation inhabituellement étendue par rapport aux autres IDP.

Afin de caractériser les complexes établis en solution entre les PRP et les tanins, une approche basée sur la spectrométrie de masse (MS) a été développée. Une première étude a étudié les complexes IB5•*n*EgCG formés en solution.

Publication n°5 : Canon, F.; Paté, F.; Meudec, E.; Marlin, T.; Cheynier, V.; Giuliani, A.; Sarni-Manchado, P., Characterization, stoichiometry and stability of salivary protein-tannin complexes by ESI-MS and ESI-MS/MS. *Anal. Bioanal. Chem.* **2009,** *395* (8), 2535-2545.

L'étude des interactions par ESI-MS a confirmé la présence en solution de complexes non-covalents IB5•tanin(s) et permis de préciser leurs stœchiométries. Ces expériences ont permis de montrer que les PRP présentaient plusieurs sites d'interactions leur permettant de fixer plusieurs tanins en même temps. Ainsi, la structure allongée des PRP pourrait leur permettre de maximiser le rapport nombre de site de fixation / nombre d'acides aminés. En effet, l'unique fonction décrite pour les PRP basiques est de lier et piéger les tanins.
Une autre étude a permis de caractériser l'impact de la structure des tanins sur ces interactions.

Publication n°6 : Canon, F.; Giuliani, A.; Paté, F.; Sarni-Manchado, P., Ability of a salivary intrinsically unstructured protein to bind different tannin targets revealed by mass spectrometry. *Anal. Bioanal. Chem.* **2010,** *398*, 815-822.

Des expériences de compétition entre différents tanins et de dissociation des complexes IB5•tanin ont mis en évidence l'influence des principales caractéristiques structurales des tanins sur cette interaction. En outre, ces expériences ont permis de montrer l'implication de liaisons hydrogènes dans les interactions PRP•tanins.

Une étude précédente comparant l'affinité d'une PRP entière avec celle d'une PRP tronquée avait montré une plus forte affinité des PRP entières pour les tanins. Afin d'expliquer cette observation, les auteurs ont proposé l'hypothèse qu'un changement de conformation des PRP au cours de l'interaction permet au PRP de s'enrouler autour des tanins et de maximiser les zones d'interaction (Charlton et al. 1996). Cette hypothèse a été étudiée dans la publication suivante :

Publication n°7 : Canon, F.; Ballivian, R.; Chirot, F.; Antoine, R.; Sarni-Manchado, P.; Lemoine, J. r. m.; Dugourd, P., Folding of a Salivary Intrinsically Disordered Protein upon Binding to Tannins. *J. Am. Chem. Soc.* **2011,** *133* (20), 7847-7852.

L'étude structurale des édifices IB5•tanin par spectrométrie de mobilité ionique couplée à la MS, a mis en évidence pour la première fois des changements conformationnels de la protéine IB5 induit par la fixation des tanins en fonction de la stœchiométrie d'interaction. Ces réarrangements structuraux ont été confirmés par des expériences couplant la MS à la spectroscopie infra-rouge (unplublished data).

Afin d'identifier les sites d'interaction des tanins sur IB5, une nouvelle méthodologie basée sur le couplage de la spectrométrie de masse (MS) et de la spectroscopie ultraviolette sous vide en utilisant le rayonnement synchrotron (SR) a été développée. Cette nouvelle méthodologie permet de fragmenter la chaîne peptidique tout en conservant les liaisons faibles. Elle fait l'objet de la publication suivante :

Publication n°8 : Canon, F.; Milosavljević, A. R.; van der Rest, G.; Réfrégiers, M.; Nahon, L.; Sarni-Manchado, P.; Cheynier, V.; Giuliani, A., Photodissociation and dissociative photoionization mass spectrometry of proteins and noncovalent protein-ligand complexes. *Angew. Chem. Int. Ed.* **2013,** *52* (32), 8377-8381.

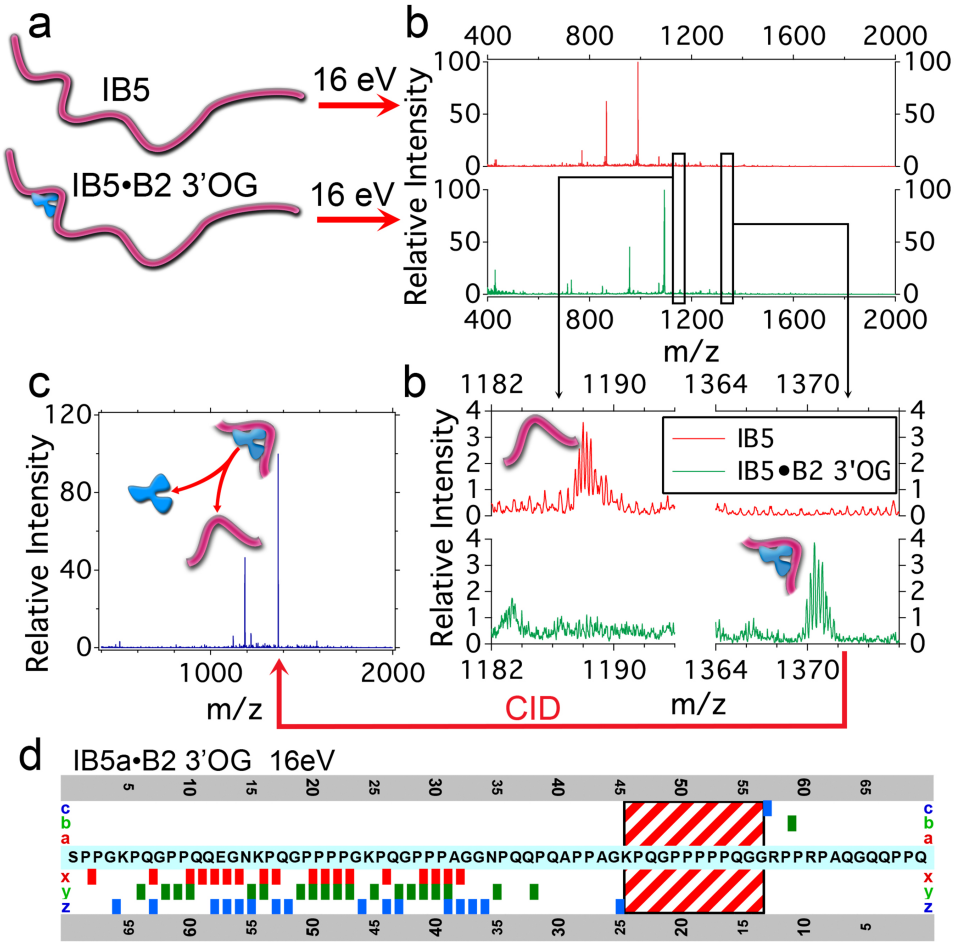

Figure 5. Les ions correspondants à la protéine IB5 et au complexe IB5•B2 3'OG ont été sélectionnés et irradiés par une longueur d'onde de 16 eV (a). Les spectres MS/MS générés (b) ont montré la présence de fragments de la chaîne peptidique liés au tanin lorsque le complexe IB5•B2 3'OG était sélectionné. Les spectres MS^3 VUV/CID de ces fragments liés à B2 3'OG montrent le détachement de B2 3'OG. L'analyse des fragments porteur de B2 3'OG a permis de mettre en évidence le site d'interaction de ce tanin sur IB5.

Cette étude a permis de déterminer le site d'interaction préférentiel d'un tanin (B2 3'OG) sur IB5(Canon et al. 2013). Cette méthodologie a ensuite été appliquée à d'autres tanins afin de comparer les sites d'interactions en fonction de leur structure chimique.

Publication n°9 : Canon, F.; Ployon, S.; Mazauric, J.-P.; Sarni-Manchado, P.; Réfrégiers, M.; Giuliani, A.; Cheynier, V., Binding site of different tannins on a human salivary proline-rich protein evidenced by dissociative photoionization tandem mass spectrometry. *Tetrahedron* **2015,** *71* (20), 3039-3044.

Les sites d'interaction de trois tanins (EgCG, B2 et B2 3'OG) sur IB5 ont été comparés. Les résultats obtenus ont montré que les trois tanins se lient préférentiellement sur le même site d'interaction constitué de la séquence : **« KPQGPPPPPQGG »**(Canon et al. 2015). Cette séquence comprend un cluster de 5 prolines qui adopte probablement une conformation de type hélice poly-proline II. Ce segment rigide constitue vraisemblablement un point d'ancrage initial à la fixation des tanins. Il est entouré de régions flexibles permettant des réarrangements de conformation favorable à l'établissement de liaisons hydrogène additionnelles.

Concernant le mécanisme d'agrégation, une approche multi-technique utilisant les informations apportées par la spectrométrie de masse, la diffusion dynamique de la lumière (DLS) et la diffusion des rayons X aux petits angles (SAXS, Small Angle X-ray Scattering) a permis de caractériser le processus d'agrégation d'IB5 avec l'épigallocatéchine gallate (EgCG, un tanin modèle).

Publication n°10 : Canon, F.; Paté, F.; Cheynier, V.; Sarni-Manchado, P.; Giuliani, A.; Pérez, J.; Durand, D.; Li, J.; Cabane, B., Aggregation of the salivary proline-rich protein IB5 in the presence of the tannin EgCG. *Langmuir* **2013,** *29* (6), 1926-1937.

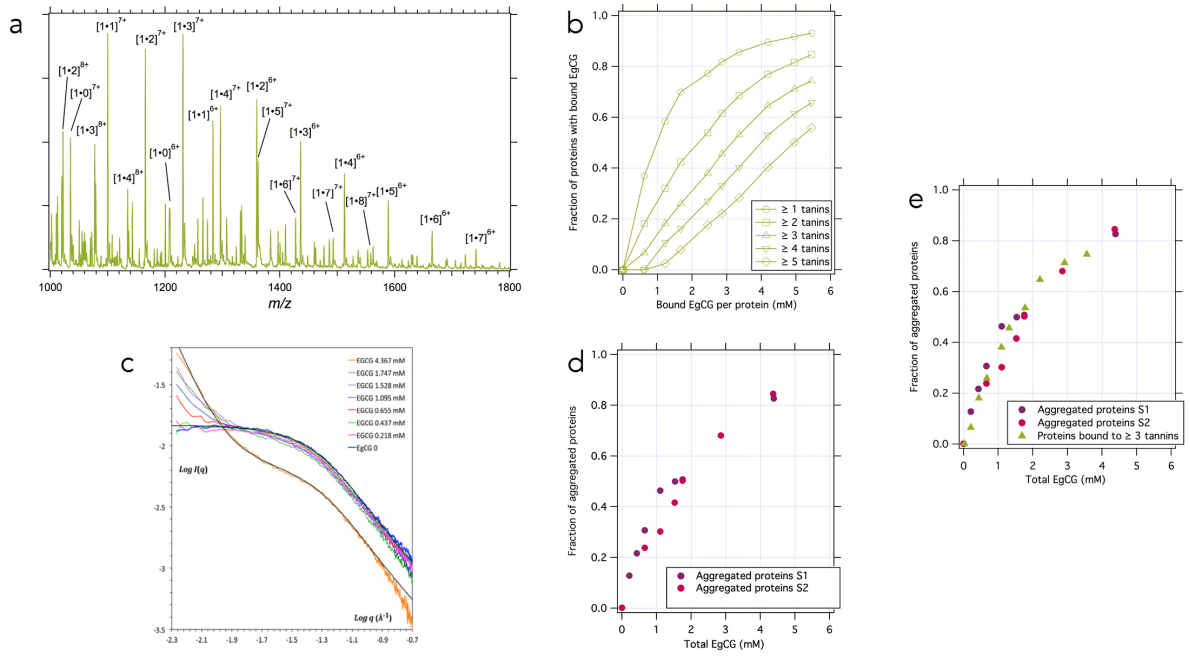

Figure 6. a. Spectre ESI-MS d'une solution IB5 – EgCG; b. fractions d'IB5 ayant liées au moins n EgCG; c. spectres SAXS de solutions IB5 - EgCG; d. fractions d'IB5 agrégées en fonction de la concentration en EgCG; e. Fractions d'IB5 agrégées et ayant liée au moins 3 EgCG en fonction de la concentration en EgCG.

Les informations obtenues ont permis de déterminer l'affinité de l'interaction, ainsi que la stœchiométrie des complexes IB5•*n*EgCG lorsque ces derniers commencent à s'agréger. Cette dernière information a permis de montrer qu'il fallait au moins 3 tanins par protéine pour former des agrégats. Enfin, il a été montré au cours de ces expériences que la concentration en EgCG au seuil d'agrégation IB5-EgCG était proche du seuil de sensibilité à l'astringence de ce tanin. Ceci suggère qu'une fois les PRP précipitées, ces dernières ne peuvent plus protéger la pellicule mucosale des tanins qui commencent alors à l'agréger.

Conclusion

L'ensemble de ces travaux ont permis de confirmer certaines hypothèses présentes dans la littérature sur les mécanismes moléculaires impliqués dans la sensation d'astringence. Il a été montré pour la première fois que les tanins agrégent la pellicule mucosale avec pour conséquence l'augmentation des forces de friction à la surface des cellules épithéliales. La présence de PRP protège l'agrégation de la pellicule mucosale. Ces travaux ont montré que ces protéines intrinsèquement désordonnées présentaient une conformation très allongée en

solution, leur permettant de fixer plusieurs tanins. Ces derniers se fixent de préférence au niveau de clusters polyproline rigides, alors que les acides aminés environnant forment des zones de jonction flexibles permettant des réarrangements structuraux lors de l'interaction avec les tanins et la maximisation du nombre de liaison hydrogènes.

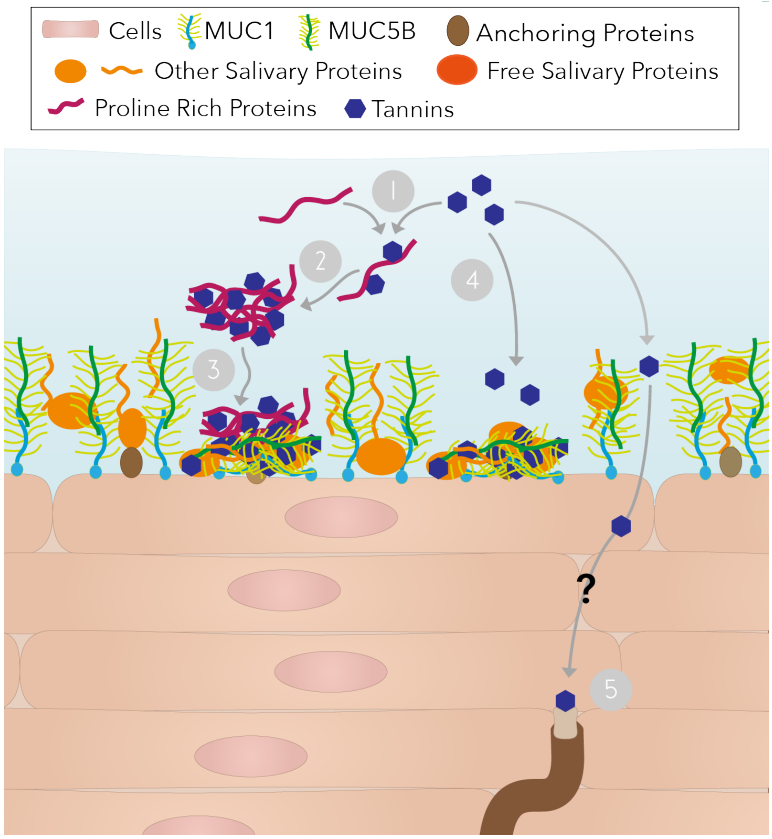

Figure 7. Schéma récapitulant les différentes hypothèses expliquant l'astringence. Les PRP interagissent avec les tanins (1) et forment des complexes supramoléculaires solubles (2), formant ensuite des agrégats qui finissent par précipiter (3). Les tanins agrègent également la pellicule mucosale (4) et pourraient activer les récepteurs de type TRP présents au niveau des extrémités trigéminales libres.

V. Etude des mécanismes moléculaires en bouche impliquée dans la libération des molécules d'arôme

Différentes études ont montré des différences de perception pour une même molécule, suivant que cette dernière atteigne les récepteurs olfactifs via la voie ortho- ou retro-nasale (Burdach et al. 1984; Kuo et al. 1993; Linforth et al. 2002 ; Voirol and Daget 1986). Ces observations suggèrent que les processus oraux impactent la quantité et/ou la qualité des molécules volatiles atteignant et activant les récepteurs olfactifs. Parmi les différents facteurs oraux, il a été montré un impact de la salive sur la libération des molécules d'arômes. Les premières études, qui se sont intéressées à l'effet de la salive, ont été réalisées *in vitro* en utilisant de la salive artificielle (Friel and Taylor 2001; van Ruth and Roozen 2000; van Ruth et al. 2001). D'autres études *in vitro* ont également montré un impact de la salive humaine sur la libération des molécules d'arôme. Il a ainsi été proposé que des différences de composition salivaire, et plus particulièrement des protéines salivaires, puissent être à l'origine de la variabilité interindividuelle observée lors la perception de la flaveur(Cabras et al. 2012; Dsamou et al. 2012; Mounayar et al. 2013). La salive contient plus de 1200 protéines salivaires dont les concentrations varient énormément entre individus(Quintana et al. 2009) sous l'effet de différents facteurs tels que l'âge(Dodds et al. 2005; Morzel et al. 2011; Morzel et al. 2012; Sevenhuysen et al. 1984), les pathologies et la prise médicamenteuse(Dodds et al. 2005), la diète (Morzel et al. 2011; Morzel et al. 2012; Perry et al. 2007) etc… La muqueuse orale est un des autres facteurs oraux suspectés d'intervenir dans la libération en bouche des molécules d'arôme. Il a ainsi été proposé que cette dernière soit à l'origine de la persistance aromatique en bouche (Buettner et al. 2002; Buffo et al. 2005; Doyennette et al. 2014; Esteban-Fernãndez et al. 2016; Wright et al. 2003). Cependant, peu d'études se sont intéressées à vérifier cette hypothèse, probablement à cause des difficultés d'une telle étude. En effet, une approche *in vivo* permettant d'isoler spécifiquement l'effet de la muqueuse orale tout en mesurant la libération des molécules d'arôme est difficile à mettre en place, alors qu'une approche *in vitro* requière le développement de modèle réaliste de muqueuse orale. Cette dernière est composée d'un épithélium oral recouvert par une fragile et fine couche de protéines salivaires ancrées à sa surface, appelée la pellicule mucosale. Ainsi, la composition de la pellicule mucosale est susceptible d'évoluer en fonction de la composition salivaire ; et des différences de composition pourraient être à l'origine de différence de perception entre individus.

Une partie de mes travaux de recherche a pour but de mieux comprendre le rôle des protéines salivaires et de la muqueuse orale dans la perception aromatique à travers l'étude des mécanismes moléculaires impliqués. Ce chapitre sera divisé en deux parties portant sur l'effet des protéines salivaires et sur celui de la muqueuse orale dans la libération des molécules d'arôme.

A. Etude des interactions entre les protéines salivaires libres (PSL) et les molécules de la flaveur

Afin de vérifier que les effets des protéines salivaires ont un impact sur la libération des molécules d'arôme au niveau de la cavité nasale, j'ai mis en place une approche *in vivo*. Cette étude a mesuré par Atmospheric Pressure Chemical Ionization – Mass Spectrometry

(APCI-MS) la libération de molécules d'arôme au niveau de la cavité nasale lors de la consommation d'eaux aromatisées dans trois conditions physiologiques différentes (sécrétion salivaire au repos ou stimulée et bouche rincée). Les résultats obtenus montrent un effet de la variabilité interindividuelle, des conditions physiologiques et de l'hydrophobicité des molécules sur les paramètres de libération. L'étude des corrélations entre les paramètres physiologiques des sujets et les paramètres de libération des molécules d'arôme a montré de fortes corrélations entre les temps de libération « longs » et les concentrations en certaines protéines salivaires (alpha-amylase, lipocaline) avec des « p-values » significatives selon l'hydrophobicité de la molécule. Ces observations indiquent que la présence de protéines au niveau de la salive favorise la rémanence en bouche des molécules d'arôme via des interactions non-covalentes impliquant des effets hydrophobes.

Afin de vérifier l'effet de protéines salivaires telles que l'alpha-amylase, une étude *in vitro* a été mise en place dans le cadre de la thèse de Sandy Pagès-Hélary. Cette étude s'est plus particulièrement intéressée à l'impact de l'alpha-amylase et des mucines qui sont les familles de protéines salivaires majoritaires. Cet effet a été mis en regard avec celui d'un pool de salive humaine.

Publication n°11 : Pagès-Hélary, S.; Andriot, I.; Guichard, E.; Canon, F., Retention effect of human saliva on aroma release and respective contribution of salivary mucin and **α**-amylase. *Food Res. Int.* **2014,** *64*, 424-431.

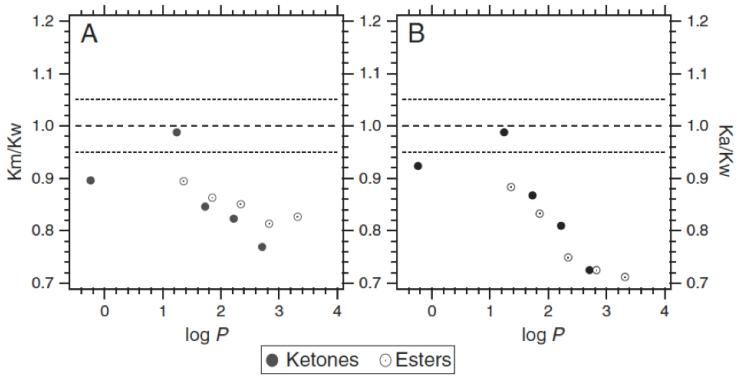

Figure 8. Rapport des coefficients de partage air/liquide en présence de mucine et d'eau (Km/Kw) (A) et en présence d'alpha-amylase et d'eau (Ka/Km) (B) en fonction du log P des esters et cétones étudiés.

Cette étude a montré un effet de rétention des molécules d'arôme par l'alpha-amylase et une mucine. Une corrélation linéaire entre **l'hydrophobicité** des molécules d'arôme (pour deux familles chimiques : cétone et ester) et leur **rétention par l'alpha-amylase et les mucines** est observée. Cette étude a également montré que lorsque les **l'alpha-amylase et les mucines** étaient toutes les deux en solution, l'effet de rétention observé ne correspondait pas à la somme de leur effet individuel, mais était inférieur. Cette observation suggère que des **interactions inter-protéiques** peuvent s'établir entre ces deux familles de protéines comme précédemment reporté conduisant à des effets de compétition et/ou d'encombrement stérique au niveau des sites d'interactions avec les molécules d'arôme. La comparaison avec un pool de salive humaine a montré une **activité hydrolytique de la salive humaine sur les esters**, comme précédemment observé.

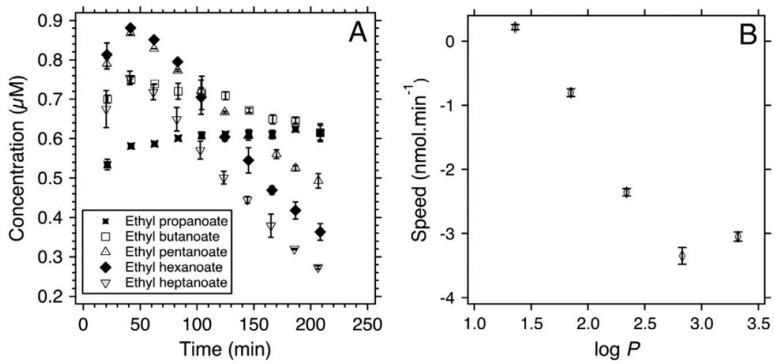

Figure 9. Concentration dans l'espace de tête des différentes cétones en fonction du temps (A) et vitesse de dégradation enzymatique en fonction du log P des molécules.

Les résultats de cette étude m'ont conduit à m'interroger sur l'effet de la variabilité interindividuelle de l'activité enzymatique salivaire sur la libération des molécules d'arôme. Je présente ci-dessous un article se rapportant au travail de Carolina Muñoz-González (post-doctorat financé par l'obtention d'un financement dans le cadre du programme « Agreenskills plus »).

Publication n°12 : Muñoz-González, C.; Feron, G.; Brulé, M.; Canon, F., Understanding the release and metabolism of aroma compounds using micro-volume saliva samples by ex vivo approaches. *Food Chem.* **2018,** *240*, 275-285.

Au cours de cette étude, nous avons comparé l'effet de la salive de trois individus sur 3 familles de molécules d'arôme (cétones, aldéhydes et alcools). Le tableau 1 présente l'effet des salives individuelles sur la libération des molécules d'arôme avec à gauche la salive non-traitée et à droite la salive après centrifugation. Nous observons des effets très contrastés en fonction de la famille chimique des molécules d'arôme. Alors que certaines molécules sont très peu (alcools) affectées par la salive, d'autres (aldéhydes et cétones) le sont très fortement telles que l'hexanal et l'octanal. Concernant, l'effet de la variabilité interindividuelle, nous observons des différences significatives entre les différentes salives non-traitées alors que la centrifugation des salives tend à gommer ces différences. Ainsi, il apparaît que la salive affecte la libération des molécules d'arômes en fonction de leur structure et de sa composition. Le niveau d'activité salivaire a été corrélé à la capacité anti-oxydante totale de la salive, comme précédemment reporté(Piombino et al. 2014).
Les résultats obtenus ont montré que cet effet était attribuable à une réduction des aldéhydes en alcool et était dépendant de la concentration en NADH. Les molécules affectées et les métabolites identifiés sont présentés dans le tableau 2.

Tableau 1. Concentration relative en molécules d'arôme dans l'espace de tête par rapport à l'eau par « Headspace Sampling – Gas chromatography » (HS-GC). Des lettres différentes entre les différentes salives indiquent des différences significatives.

Compounds	whole saliva					clarified saliva				
	w	S1	S2	S3	mean whole saliva	w	S1	S2	S3	mean clarified saliva
Ketones										
2-butanone	100 b	106 a	104 a	105 a	105	100 a	103 a	101 a	99 a	101
2,3-butanedione	100 a	93 b	90 b	52 c	78	100 a	95 bc	98 ab	94 c	96
2-pentanone	100 a	101 a	99 a	99 a	100	100 b*	105 a*	103 ab*	100 a*	103
2,3-pentanedione	100 a	94 b	92 b	72 c	86	100 a	92 b	91 b	92 b	92
2-octanone	100 a	105 a	101 a	102 a	103	100 a	99 a	97 a	100 a	99
1-octen-3-one	100 a	86 b	85 b	40 c	70	100 a	85 b	85 b	49 c	73
Alcohols										
1-pentanol	100 b*	103 ab*	105 ab*	110 a*	106	100 b	106 a	106 a	103 ab	105
1-hexanol	100 a	103 a	101 a	101 a	102	100 a	103 a	103 a	103 a	103
(Z)-3-hexen-1-ol	100 a	103 a	101 a	101 a	102	100 a	105 a	105 a	105 a	105
1-octanol	100 c	104 b	109 a	107 ab	107	100 b*	103 ab*	105 a*	105 a*	104
1-octen3-ol	100 a*	100 a*	100 a*	96 b*	99	100 a	99 a	102 a	98 a	100
linalool	100 a	102 a	99 a	102 a	101	100 a	103 a	105 a	106 a	105
menthol	100 b*	104 ab*	105 a*	99 b*	103	100 a	102 a	99 a	100 a	100
Aldehydes										
Hexanal	100 a	96 a	88 b	39 c	74	100 a	100 a	98 a	90 b	96
Octanal	100 a	89 b	77 c	23 d	63	100 a	100 a	102 a	94 b	99
Octenal	100 a	105 a	100 a	71 b	92	100 a	101 a	99 a	89 b	96
Benzaldehyde	100 ab	96 b	103 a	73 c	91	100 a	99 a	100 a	103 a	101

Ces réactions résultent probablement de l'activité d'enzymes appartenant à la super-famille des oxydo-reductases, qui sont des enzymes NAD(P)H+ dépendantes. Parmi celles-ci, les Aldo-Keto Reductases (AKR) sont de bonnes candidates(Barski et al. 2008). Ces enzymes interviennent dans la détoxification et l'élimination des groupements carbonyles chimiquement réactifs. La réduction des groupes carbonyle est rapide en une seule étape, modifie la polarité et prépare les molécules xénobiotiques à être conjuguée (Bachur 1976). Ces réactions affectent les aldéhydes et cétones générés de manières endogènes ou rencontrés dans l'environnement et l'alimentation. Ainsi, la capacité de la salive humaine à catalyser ces réactions pourrait représenter un mode d'inactivation et de détoxification de composés potentiellement toxiques à l'entrée de l'organisme. Bien qu'il s'agisse d'une étude ex-vivo, ces réactions ont été récemment reportées au niveau de l'épithélium olfactif dans des expériences ex-vivo et in-vitro (Robert-Hazotte et al. 2019; Schoumacker et al. 2016). Ainsi, elles apparaissent comme un mécanisme général de détoxification de ces molécules. D'autre part, un article tend à montrer que ces réactions métaboliques modulent la perception aromatique (Ijichi et al. 2019) et pourraient donc être à l'origine de différence interindividuelle de perception de la flaveur.

Tableau 2. Molécules et métabolites correspondants identifiés par HS-SPME-GC/MS en présence de salive.

Compounds significantly reduced by the presence of saliva	Metabolites identified in the HS above saliva samples	
2,3-butanedione (diacetyl)  «Buttery» OT: 2,3-6,5 ppb	3-hydroxy-2-butanone (acetoin)  «Sour milk» OT: 800 ppb	
2,3-pentanedione  «Butter, cream» OT: 78 ppb	3-hydroxypentan-2-one  «Herbaceous, truffle» OT: ?	2-hydroxypentan-2-one
1-octen-3-one 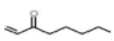 «Mushroom-like» OT: 0,005 ppb	3-octanone 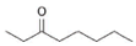 «Fruity, floral» OT: 28 ppb	1-octen-3-ol 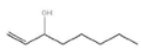 «Mushroom» OT : 1 ppb
Hexanal 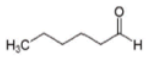 «Green, grassy» OT: 4,5 ppb	1-hexanol  «Fatty, floral, green» OT: 2500 ppb	
Octanal 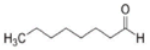 «Green grassy» OT: 0,7 ppb	1-octanol  «Green» OT: 110 ppb	
Octenal  «Green» OT: 3 ppb	(E)-2-octen-1-ol  «?» OT: ?	1-octanol, (Z)-3-octen-1-ol, and others
Benzaldehyde  «Almond, burnt sugar» OT: 350 ppb	Benzyl alcohol  «Sweet, flower» OT: 10000 ppb	

Ainsi après avoir montré que la variabilité interindividuelle affectait la libération des molécules d'arôme, nous avons proposé l'hypothèse que des troubles de la salivation puissent modifier la libération des molécules d'arôme en bouche et conduire à des troubles de la perception. Les personnes âgées sont souvent atteintes de trouble de la salivation et de la perception aromatique. Ces troubles de la perception peuvent avoir des conséquences importantes comme elles peuvent influer sur la prise alimentaire. L'article ci-dessous présente une étude systématique de la littérature étudiant les relations entre prise alimentaire et trouble de la salivation, qui a été réalisé dans le cadre du post-doctorat de Carolina Muñoz-González.

Publication n°13 : Muñoz-González, C.; Vandenberghe-Descamps, M.; Feron, G.; Canon, F.; Labouré, H.; Sulmont-Rossé, C., Association between salivary hypofunction and food consumption in the elderlies. A systematic literature review. *The journal of nutrition, health & aging* **2018,** *22* (3), 407-419.

Cette étude a montré que l'hyposalivation était corrélée avec une perte de l'appétit, une diète déséquilibrée mais pas avec la prise alimentaire totale. Une relation entre les déficiences salivaires et la malnutrition a également été mis en évidence. Cependant, l'observation de ces corrélations ne donnent pas d'information sur l'impact de ces troubles salivaires sur la libération des molécules d'arôme. Ainsi, nous avons posé l'hypothèse que l'hyposalivation liée à l'âge impactait la libération des molécules d'arôme. L'article ci-dessous présente l'étude de cette hypothèse et a été réalisé dans le cadre du travail de post-doctorat de Carolina Muñoz-González.

Publication n°14 : Muñoz-González, C.; Brulé, M.; Feron, G.; Canon, F., Does interindividual variability of saliva affect the release and metabolization of aroma compounds ex vivo? The particular case of elderly suffering or not from hyposalivation. *Journal of Texture Studies* **2019,** *50*, 36–44.

A partir d'un panel de 110 personnes âgées, 15 personnes souffrant d'hyposalivation et 15 personnes avec une salivation normale ont été recrutées. Ces deux groupes étaient appariés en sexe et en âge. Les deux groupes différaient de manière significative au niveau de leurs flux salivaires stimulés et non-stimulés ainsi que de leur indice de masse corporelle. Les personnes souffrant d'hyposalivation présentent un indice de masse corporelle significativement plus élevé que les individus normaux. Les salives des 30 sujets ont été incubées avec trois molécules d'arôme : Ethyl hexanoate, octanal, 2-nonanone.

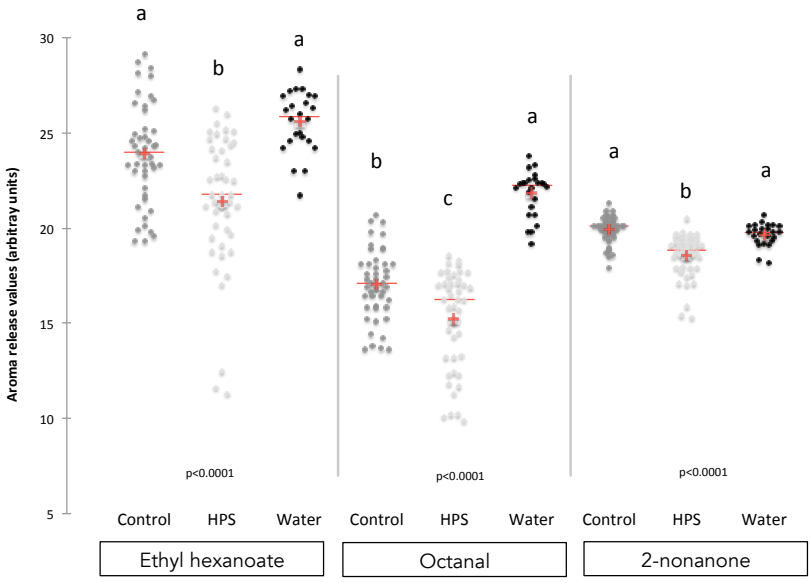

Figure 10. Libération de l'éthyl hexanoate, de l'octanal et de la 2-nonanone en présence d'eau, des salives des individus du groupe contrôle (control) et de celles des individus hyposalivateurs (HPS).

La figure 10 présente les résultats obtenus et montre que la salive des hyposalivateurs affecte de manière significative la libération des molécules d'arôme par rapport à la salive du groupe contrôle et à de l'eau pour les trois molécules étudiées. Ainsi, les trois molécules sont

sensiblement moins libérées en présence de la salive des hyposalivateurs. Il a pu être confirmé seulement pour l'octanal que cette différence provenait de l'activité métabolique de la salive. Nous avons également observé que la capacité antioxydante totale de la salive était significativement plus élevée chez les hyposalivateurs. Ainsi la capacité antioxydante apparaît comme un facteur important de la modulation de la métabolisation des molécules d'arôme en bouche et pourrait être à l'origine de différence de perception aromatique.

B. Etude des interactions entre les protéines de la pellicule de la muqueuse orale et les molécules de la flaveur

Différents auteurs ont suggéré que la muqueuse orale était impliquée dans la persistance aromatique en bouche. Cependant les mécanismes moléculaires impliqués dans ce phénomène sensoriel n'ont pas été caractérisés jusqu'à présent. Dans la partie précédente, j'ai montré que les protéines salivaires libres, pouvaient affecter la libération des molécules d'arôme via l'établissement de liaisons non-covalentes ou la métabolisation de ces dernières. Les protéines salivaires libres sont avalées à chaque déglutition, alors que les protéines de la pellicule mucosale sont ancrées à la surface des cellules épithéliales. Ainsi, une des hypothèses expliquant l'origine de la persistance aromatique en bouche propose que ce phénomène résulte de l'absorption et de la désorption des molécules d'arômes à la surface de la muqueuse via des liaisons faibles (non-covalentes) entre protéines salivaires liées à la pellicule mucosale et molécules d'arôme.

A l'aide du modèle de muqueuse développé, j'ai mis en place une étude *in vitro* afin de tester l'hypothèse proposée ci-dessus. L'effet du modèle de muqueuse a été étudié à la fois en condition statique par GC-FID et dynamique par PTR-MS. En conditions statiques, 300 µL de tampon contenant la molécule testée à une concentration de 10^{-4} mol/l (10^{-3} mol/ pour le guaicol et les pyrazines et 7 x 10^{-5} pour la 2-decanone) ont été ajoutés dans un flacon contenant les cellules épithéliales avec ou sans pellicule. La figure 11 présente les ratios des coefficients de partage en présence des cellules avec ou sans pellicule et en condition contrôle. Ainsi, un ratio inférieur à 1 indique un effet de « rétention » des cellules avec ou sans pellicule. Les significativités sont indiquées par rapport au contrôle. Ainsi, cette figure montre que les molécules suivantes sont significativement moins libérées en présence des cellules épithliales : pentan 2,3 dione, le trans-2-hexenal, ethyl-hexanoate, nonan-2-one et decan-2-one. Le graphique 10 présente les ratios de K de la série des méthyl kétones en fonction de leur hydrophobicité ici apparentée à leur log P (coefficient de partage eau/octanol). Une corrélation linéaire est observée à la fois pour les coefficients de partage en présence de cellules sans pellicule et de cellules avec pellicule. Cette observation indique que l'effet des cellules sur la libération des cétones linéaires augmente avec l'hydrophobicité de ces molécules. Une telle observation a été précédemment observée en présence de mucine et d'alpha-amylase, dont l'origine avait été attribué à l'établissement d'interactions non-covalentes. L'analyse des solutions d'arôme mises en présence des cellules a montré l'apparition d'un nouveau composé pour les molécules significativement impactée par la présence des cellules. La nature de ce nouveau composé varie en fonction de la molécule mise présence des cellules, suggérant une métabolisation de cette dernière en un nouveau composé par les cellules épithéliales avec ou sans pellicule.

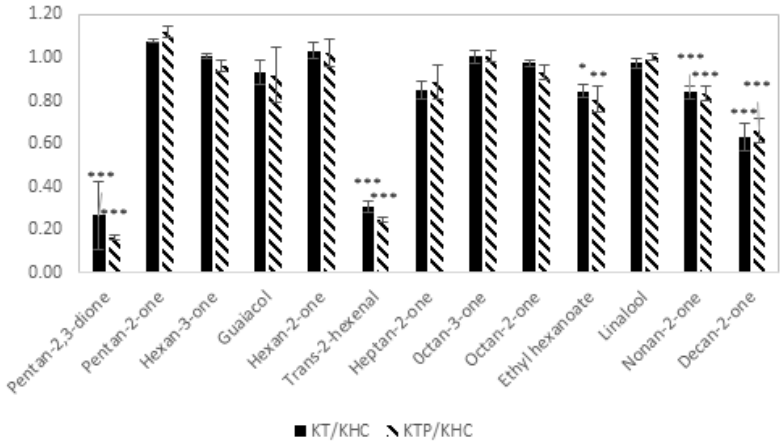

Figure 11. Ratios des coefficients de partage (air/liquide) des molécules d'arôme en présence en présence des cellules épithéliales TR146/MUC1-Y-LSP avec (K_{TP}/K_{HC}) ou sans (K_T/K_{HC}) pellicule mucosale et d'une condition contrôle. Les significativités sont indiquées par rapport à la condition contrôle.

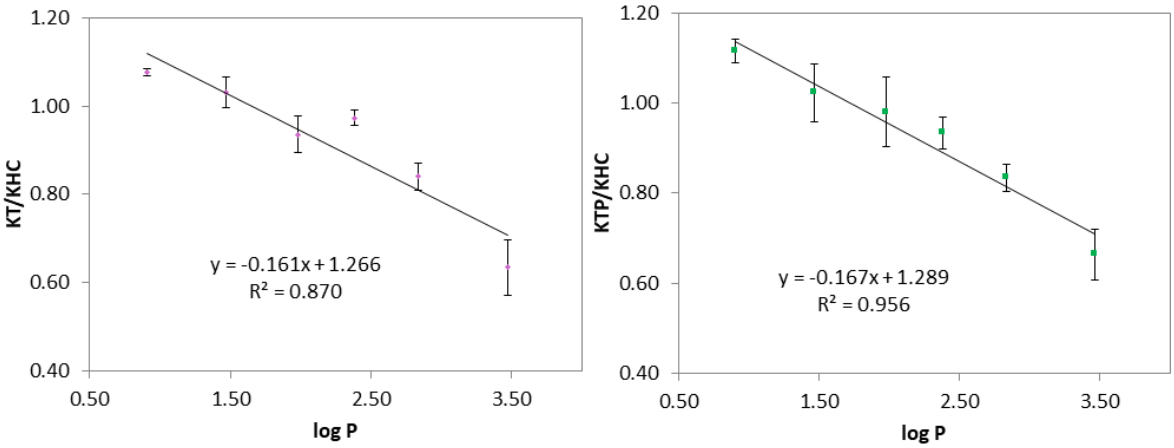

Figure 12. Présentation des coefficients de partage K_{TP}/K_{HC} et K_T/K_{HC} en fonction du log P des molécules appartenant à la série linéaire des cétones méthylées étudiées.

Tableau 3. Composés nouveaux identifiés en fonction de la molécule initiale mise au contact des cellules épithéliales.

Molécule initiale	Molécule nouvelle identifiée
Non-2-anone	Nonan-2-ol
Decan-2-one	Decan-2-ol
Pentan-2,3-dione	2-hydroxy-pentan-3-one + 3-hydroxy-pentan-2-one
Trans-2-hexenal	Acide hexanoïque
Hexanoate d'éthyle	Acide hexanoïque

Concernant la métabolisation des molécules d'arôme, il est observé comme dans les études précédentes une réduction des groupement carbonyle avec la réduction des cétones en alcool mais également une oxydation du groupe carbonyle du trans-2-hexenal en groupe carboxyle. Il est également observé l'hydrolyse d'un ester, l'hexanoate d'éthyle, en un acide carboxylique, l'acide hexanoïque.

En parallèle une étude en condition dynamique a été réalisée en mesurant la composition de l'espace de tête par PTR-MS de solutions de pentan-2-one et d'octan-2-one en présence des cellules TR146/MUC1/Y-LSP avec et sans pellicule mucosale. De même qu'en condition statique, les spectres de masse n'ont pas révélé la formation de métabolite pour ces deux molécules.

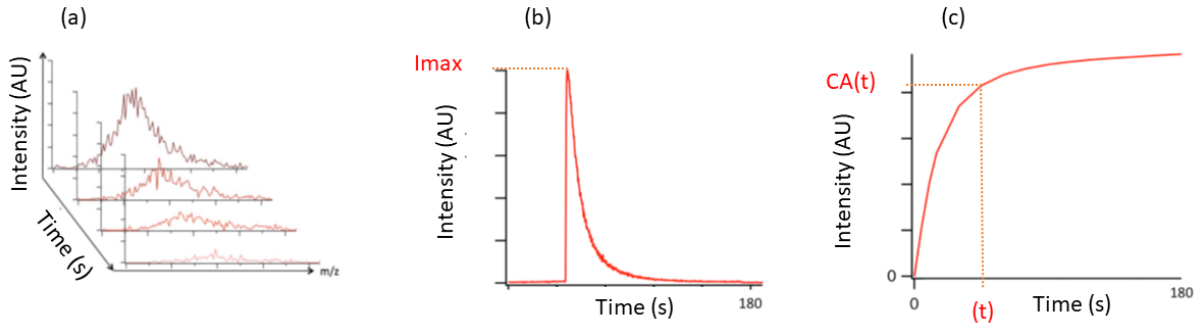

Figure 13. Spectres PTR-MS au cours du temps (a), intégration des aires des ions au cours du temps (b), et aire cumulée au cours du temps.

Table 1. Effet des cellules TR146/MUC1/Y-LSD avec (TP) ou sans (T) pellicule mucosale sur les aires cumulées de libération au cours du temps de la pentan-2-one.

Pentan-2-one								
Condition	Imax	CA(5)	CA(15)	CA(30)	CA(60)	CA(90)	CA(120)	CA(150)
T	1,11 ^{b,1}	1,06 ^{a,1}	1,04 ^{a,1}	1,01 ^{a,1}	0,98 ^{a,1}	0,96 ^{a,1}	0,94 ^{b,1}	0,93 ^{b,1}
TP	1,12 ^{b,2}	1,04 ^{a,1}	1,00 ^{a,1}	0,97 ^{a,1}	0,93 ^{b,2}	0,91 ^{b,2}	0,89 ^{b,2}	0,88 ^{b,2}

Table 2. Effet des cellules TR146/MUC1/Y-LSD avec (TP) ou sans (T) pellicule mucosale sur les aires cumulées de libération au cours du temps de la pentan-2-one.

Octan-2-one								
Condition	Imax	CA(5)	CA(15)	CA(30)	CA(60)	CA(90)	CA(120)	CA(150)
T	1,06 ^{a,1}	1,05 ^{a,1}	1,02 ^{a,1}	0,97 ^{a,1}	0,91 ^{a,1}	0,88 ^{b,2}	0,85 ^{b,1}	0,83 ^{b,1}
TP	1,01 ^{a,1}	1,08 ^{a,1}	1,06 ^{a,1}	1,01 ^{a,1}	0,95 ^{a,1}	0,92 ^{a,1}	0,91 ^{b,1}	0,90 ^{b,1}

Pour ces deux molécules, il est observé un effet significatif sur les aires cumulées au cours du temps en présence des cellules avec une diminution de la quantité de molécule libérée, à partir de 60s. Un effet de la présence de la pellicule mucosale est également observé pour les deux molécules avec dans le cas de la penta-2-one un effet d'augmentation de la rétention et dans le cas de l'octan-2-one une diminution de la rétention pour les temps les plus longs. Cet effet de rétention pourrait avoir pour origine l'établissement de liaisons non-covalentes entre les molécules d'arôme et la surface des cellules. La caractérisation des propriétés physico-chimiques de la surface des cellules a montré la présence à la fois de zones très hydrophobes et de zones très hydrophyles lors de l'expression de MUC1/Y-LSP et une diminution des zones les plus hydrophobes et hydrophyles après formation de la pellicule mucosale. Ainsi, la diminution de rétention de l'octan-2one en présence de la pellicule mucosale pourrait être due à la disparition de ces zones très hydrophobes, qui à l'inverse favoriseraient les interactions avec la pentan-2-one, qui présente une hydrophobicité moindre.

Conclusion

La thématique de recherche que j'ai développée autour des mécanismes moléculaires en bouche affectant la libération des molécules d'arôme s'est appuyée sur les travaux pionniers d'Andy Taylor, Andreas Buettner ou encore de Saskia van Ruth, qui ont révélé les mécanismes moléculaires impliqués. Ainsi, l'originalité de mes travaux réside dans la mise en évidence de nouvelles réactions métaboliques, de la forte variabilité interindividuelle de cette réactivité au niveau salivaire, et de l'existence de ces mécanismes au niveau de la muqueuse orale. L'ensemble de ces mécanismes moléculaires peut à la fois impacter la quantité et la qualité des molécules d'arôme atteignant les récepteurs olfactifs. Ceci apparaît d'autant plus important qu'un article récemment publié a montré que ces mécanismes pouvaient modifier la perception(Ijichi et al. 2019), venant renforcer l'intérêt de continuer d'explorer cette thématique de recherche.

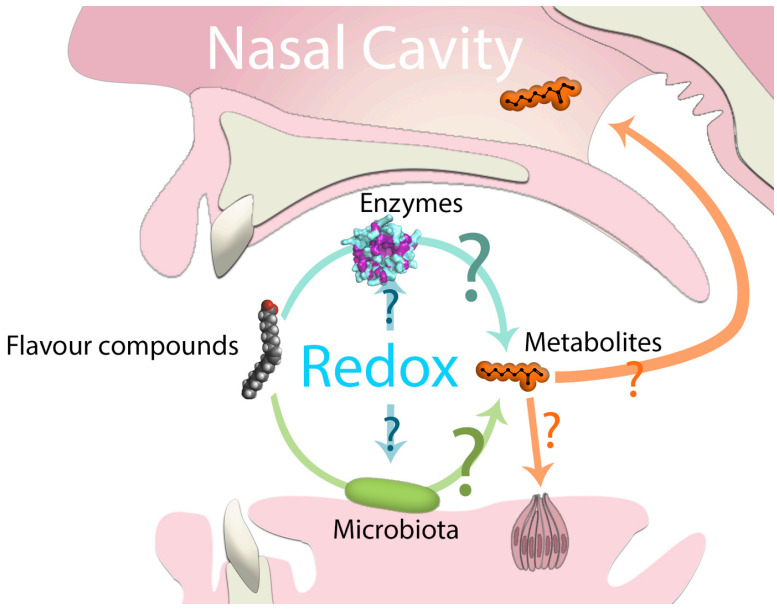

Figure 14. Schéma résumant les réactions de métabolisation des molécules d'arôme en bouche.

VI. Perspectives de mon activité de recherche

A. Développement d'un nouveau modèle de muqueuse orale

La figure 15 présente la structure de MUC1 et de ces différentes isoformes. Le modèle de muqueuse précédemment développé repose sur la transfection de la lignée TR146 par un gène codant pour l'isoforme MUC1/Y-LSP. Cette isoforme a été caractérisée dans le cas de cellules cancéreuses alors que les isoformes 1 et 2 sont les isoformes sauvages. Ainsi, MUC1/Y-LSP diffère des isoformes sauvages par l'absence de la région « variable number tandem repeat » (VNTR) et par la délétion de 15 acides aminés au niveau du SEA domaine. La région VNTR est composée de la répétition (20 à 120 répétitions) pratiquement à l'identique de la séquence de 20 acides aminés (PDTRPAPGSTAPPAHGVTSA). Ce domaine forme une structure rigide fortement glycosylée, commune aux mucines et conférant aux surfaces qu'elles recouvrent des propriétés hydrophiles et répulsives à la fois électrostatiquement et stériquement. Cette délétion entraine l'absence d'auto-clivage de MUC1 en sous-unités α et β (Zhang et al. 2013). A l'inverse, les isoformes sauvages sont composées de deux sous-unités, reliées entre elles par des liaisons non-covalentes au niveau du domaine SEA bien structuré (Macao et al. 2005; Parry et al. 2001). Ce clivage pourrait avoir une fonction de protection de la muqueuse en permettant le largage de la sous-unité α en cas d'agrégation de cette dernière par des molécules exogènes (Macao et al. 2005).

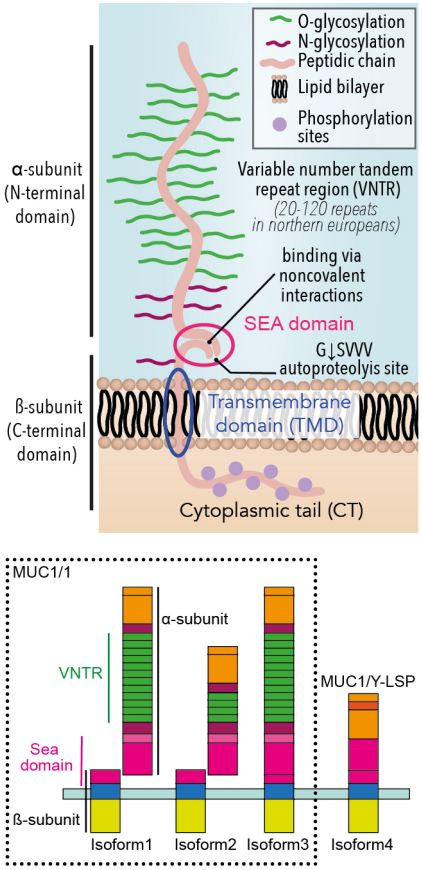

Figure 15. Structure et isoformes de MUC1.

La partie cytoplasmique de MUC1 comporte 7 sites potentiels de phosphorylation, suggérant un rôle de signalisation de MUC1. Ainsi un changement de conformation ou la rupture des 2 sous-unités pourrait activer un mécanisme de signalisation intra-cellulaire.

B. Application du nouveau modèle de muqueuse à la sensation d'astringence

L'agrégation de la pellicule mucosale par les tanins pourrait conduire à des changements de conformation de MUC1 ou à une rupture de ses deux unités, activant le mécanisme de signalisation cellulaire. D'autre part, les cellules épithéliales ont la capacité de libérer de l'acétylcholine, qui est un neurotransmetteur (Kummer et al. 2008), alors que les terminaisons nerveuses libres trigéminales possèdent des récepteurs à cette molécule (Alimohammadi and Silver 2000; Hans et al. 2012). Ainsi, je propose ici l'hypothèse qu'un tel mécanisme puisse être impliqué dans la sensation d'astringence. En faveur de cette hypothèse, il a été montré une relation entre la sensibilité trigéminale de personnes souffrant du burning-mouth syndrome et l'expression de MUC1.

Une seconde hypothèse est que la rupture des deux sous-unités de MUC1 suite à l'agrégation de la pellicule mucosale entraîne un détachement de cette dernière. Ainsi, la pellicule mucosale ne pourrait plus remplir sa fonction de lubrification à la surface de la muqueuse orale, entrainant une augmentation des forces de frictions et par voie de conséquence l'activation des mécanorécepteurs enfouis dans la muqueuse. Ces hypothèses seront testées dans le cadre de la thèse de Clément Niveau (2019-2022), qui a obtenu un financement de l'école doctorale E2S Environnement – Santé.

C. Application du nouveau modèle de muqueuse à la perception aromatique

La caractérisation du modèle de muqueuse orale par AFM a montré que l'expression de MUC1/Y-LSP à la surface des cellules épithéliales modifiait fortement les propriétés de surface de ces dernières. Sachant que MUC1/Y-LSP ne possède pas le domaine VNTR richement glycosylé à l'origine des propriétés de lubrification de MUC1, il est probable que les propriétés de surface de cellules épithéliales exprimant les isoformes 1 ou 2 de MUC1 soient différentes de celles de la lignée TR146/MUC1/Y-LSP. Ces différences pourraient impacter les interactions entre la muqueuse et les molécules d'arôme.

D. Identification et caractérisation des enzymes salivaires impliquées dans la métabolisation des molécules d'arôme en bouche

Après avoir mis en évidence l'existence de réactions enzymatiques au niveau de la salive, l'étape suivante est d'identifier les enzymes impliquées et de caractériser leur structure et leur réactivité. Un nouveau chargé de recherche, Mathieu Schwartz, a été recruté cette année pour mener à bien cette thématique. Nous nous attèlerons également à mettre en évidence l'impact de ces réactions sur la perception.

E. Caractérisation *in vivo* de la sensation d'astringence

Afin de mettre en regard les informations obtenues par les approches *in vitro* et la perception de l'astringence, il est également important de mieux caractériser la perception des stimuli astringents. En effet, l'évaluation sensorielle des seuils de sensibilité aux molécules astringentes est difficile à réaliser à cause de la rémanence de cette sensation et de l'effet cumulatif des expositions. De plus, les molécules astringentes sont souvent amères. Cette dimension multimodale du stimuli perturbe l'évaluation de la seule composante sensorielle astringente. En effet, les différentes composantes sensorielles de la flaveur interagissent entre elles lors de l'intégration cérébrale, avec des effets de potentialisation positive ou négative. Ainsi, il semble important de développer de nouvelles méthodologies d'évaluation des propriétés astringente d'un stimuli.

Un autre axe de travail porte sur le développement de méthodes d'évaluation objectives des changements de lubrification en bouche se produisant lors de la

consommation de produits astringents. Ces méthodes permettront de mieux quantifier l'effet des tanins en conditions *in vivo*. Une collaboration a été développée avec Roberto Vargiolu et Hassan Zahouani de l'Ecole Centrale de Lyon dans ce cadre. Ces chercheurs sont des spécialistes des mesures tribologiques. Une collaboration a été initiée avec eux afin de développer des instruments permettant de mieux caractériser les changements de forces de friction en bouche. Ils ont élaboré un premier prototype, qui est en phase de test. Cet instrument permettra de réaliser des mesures non-subjectives du niveau de rugosité en bouche en présence ou non de stimuli astringents.

F. Couplage des méthodes d'analyses sensorielles temporelles et de la mesure de l'espace gazeux en bouche.

La mise en regard des données sensorielles et analytiques concerne également la perception aromatique. Les méthodes d'analyse sensorielle telles que la méthode de « temporal dominance sensation » (TDS) ou celle de « Temporal Check-All-That-Apply » (T-CATA) permettent de caractériser la cinétique des sensations perçues lors de la dégustation d'un aliment au cours du temps, qu'il s'agisse pour le sujet de noter seulement la sensation dominante (TDS) ou toutes les sensations perçues à un instant T (T-CATA). La spectrométrie de masse de type PTR-MS permet de suivre la libération des molécules d'arôme au niveau de la cavité nasale d'un sujet au cours du temps. Ainsi, nous travaillons actuellement sur le couplage des données TDS / T-CATA et PTR-MS. Ce couplage permettra d'associer les données de composition de l'espace gazeux au niveau de la cavité nasale (nosespace) aux sensations aromatiques perçues.

Ce couplage n'est pas aussi évident qu'il n'y paraît car les temps de réponse entre les individus et entre les individus et le PTR-MS ne sont pas identiques. De plus, les méthodes sensorielles citées caractérisent la cinétique des sensations au niveau d'un panel d'individus alors que le PTR-MS caractérise la libération des molécules d'arôme au niveau de la cavité nasale d'un seul individu. Enfin, l'intensité mesurée par PTR-MS d'un ion dépend de son rendement d'ionisation, ici en lien avec son affinité protonique.

G. Etude des relations entre tanins et perception aromatique

Les fournisseurs de tanins œnologiques vantent l'impact positif de leurs produits sur les arômes des vins et en particulier sur leur longueur en bouche. Cependant, à ma connaissance, cet effet n'a pas été clairement établi. Il suggère que les interactions des tanins avec la muqueuse orale influencent de manière positive la capacité de cette dernière à interagir avec les molécules d'arôme. D'autre part, il a été montré que la perception de l'astringence pouvait être influencée par la perception d'autre sensation telle que le goût sucré. En effet, la perception du sucré diminue l'intensité de l'astringence perçue (Lyman and Green 1990). Il est ainsi possible que la perception de certaines notes odorantes, comme des notes sucrées, puissent diminuer l'astringence perçue d'un produit. Ainsi, astringence et perception aromatique pourrait interagir à la fois à un niveau moléculaire et perceptuel. Une meilleure compréhension de ces interactions permettrait de proposer de nouvelles stratégies

de reformulation des produits alimentaires, afin par exemple d'augmenter leur richesse en polyphénols tout en gardant une bonne acceptabilité.

VII. Bibliographie

Alimohammadi H, Silver WLJCs. 2000. Evidence for nicotinic acetylcholine receptors on nasal trigeminal nerve endings of the rat. 25:61-66.

Ann DK, Carlson DM. 1985. The structure and organization of a proline-rich protein gene of a mouse multigene family. Journal of Biological Chemistry 260:15863-15872.

Azen EA, Amberger E, Fisher S, Prakobphol A, Niece RL. 1996. Prb1, prb2, and prb4 coded polymorphisms among human salivary concanavalin-a binding, ii-1, and po proline-rich proteins. American Journal of Human Genetics 58:143-153.

Bachur NR. 1976. Cytoplasmic aldo-keto reductases: A class of drug metabolizing enzymes. Science 193:595-597.

Barski OA, Tipparaju SM, Bhatnagar A. 2008. The aldo-keto reductase superfamily and its role in drug metabolism and detoxification. Drug Metab Rev 40:553-624.

Bate-Smith EC. 1973. Haemanalysis of tannins : The concept of relative astringency. Phytochemistry 12:907-912.

Bennick A. 2002. Interaction of plant polyphenol with salivary proteins. Critical Reviews in Oral Biology & Medicine 13:184-196.

Bongaerts JHH, Rossetti D, Stokes JR. 2007. The lubricating properties of human whole saliva. Tribology Letters 27:277-287.

Bradway SD, Bergey EJ, Scannapieco FA, Ramasubbu N, Zawacki S, Levine MJ. 1992. Formation of salivary-mucosal pellicle: The role of transglutaminase. Biochem J 284:557-564.

Breslin PA, Gilmore M, Beauchamp GK, Green BG. 1993. Psychophysical evidence that oral astringency is a tactile sensation. Chem Senses 18:405-417.

Buettner A, Beer A, Hannig C, Settles M, Schieberle P. 2002. Quantitation of the in-mouth release of heteroatomic odorants. In: Heteroatomic aroma compounds, Vol. 826:American Chemical Society, 296-311.

Buffo RA, Rapp JA, Krick T, Reineccius GA. 2005. Persistence of aroma compounds in human breath after consuming an aqueous model aroma mixture. Food Chem 89:103-108.

Burdach KJ, Kroeze JHA, Koster EP. 1984. Nasal, retronasal, and gustatory perception - an experimental comparison. Perception & Psychophysics 36:205-208.

Cabras T, Melis M, Castagnola M, Padiglia A, Tepper BJ, Messana I, et al. 2012. Responsiveness to 6-n-propylthiouracil (prop) is associated with salivary levels of two specific basic proline-rich proteins in humans. PLoS ONE 7:e30962.

Canon F, Ballivian R, Chirot F, Antoine R, Sarni-Manchado P, Lemoine Jrm, et al. 2011. Folding of a salivary intrinsically disordered protein upon binding to tannins. J Am Chem Soc 133:7847-7852.

Canon F, Milosavljević AR, van der Rest G, Réfrégiers M, Nahon L, Sarni-Manchado P, et al. 2013. Photodissociation and dissociative photoionization mass spectrometry of proteins and noncovalent protein-ligand complexes. Angew Chem Int Ed 52:8377-8381.

Canon F, Ployon S, Mazauric J-P, Sarni-Manchado P, Réfrégiers M, Giuliani A, et al. 2015. Binding site of different tannins on a human salivary proline-rich protein evidenced by dissociative photoionization tandem mass spectrometry. Tetrahedron 71:3039-3044.

Canon F, Neiers F, Guichard E. 2018. Saliva and flavor perception: Perspectives. J Agric Food Chem 66:7873-7879.

Charlton AJ, Baxter NJ, Lilley TH, Haslam E, McDonald CJ, Williamson MP. 1996. Tannin interactions with a full-length human salivary proline -rich protein display a stronger affinity than with single proline-rich repeats. FEBS Lett 382:289-292.

Clauss M, Gehrke J, Hatt JM, Dierenfeld ES, Flach EJ, Hermes R, et al. 2005. Tannin-binding salivary proteins in three captive rhinoceros species. Comparative Biochemistry and Physiology Part A: Molecular & Integrative Physiology 140:67-72.

Dodds MWJ, Johnson DA, Yeh C-K. 2005. Health benefits of saliva: A review. J Dent 33:223-233.

Doyennette M, Deleris I, Feron G, Guichard E, Souchon I, Trelea IC. 2014. Main individual and product characteristics influencing in-mouth flavour release during eating masticated food products with different textures: Mechanistic modelling and experimental validation. J Theor Biol 340:209-221.

Dresselhuis D, Dehoog E, Cohenstuart M, Vanaken G. 2008. Application of oral tissue in tribological measurements in an emulsion perception context. Food Hydrocoll 22:323-335.

Dsamou M, Palicki O, Septier C, Chabanet C, Lucchi G, Ducoroy P, et al. 2012. Salivary protein profiles and sensitivity to the bitter taste of caffeine. Chem Senses 37:87-95.

Dunker AK, Lawson JD, Brown CJ, Williams RM, Romero P, Oh JS, et al. 2001. Intrinsically disordered protein. Journal of Molecular Graphics and Modelling 19:26-59.

Esteban-Fernãndez A, Rocha-Alcubilla N, Munoz-Gonzalez C, Moreno-Arribas MV, Pozo-Bayon MA. 2016. Intra-oral adsorption and release of aroma compounds following in-mouth wine exposure. Food Chem 205:280-288.

Friel EN, Taylor AJ. 2001. Effect of salivary components on volatile partitioning from solutions. J Agric Food Chem 49:3898-3905.

Gibbins H, Proctor G, Yakubov G, Wilson S, Carpenter G. 2013. Concentration of salivary protective proteins within the bound oral mucosal pellicle. Oral Dis.

Gibbins HL, Carpenter GH. 2013. Alternative mechanisms of astringency - what is the role of saliva? Journal of Texture Studies 44:364-375.

Green BG. 1993. Oral astringency: A tactile component of flavor. Acta Psychol 84:119-125.

Guinard JX, Mazzucchelli R. 1996. The sensory perception of texture and mouthfeel. Trends Food Sci Technol 7:213-219.

Hagerman AE, Butler LG. 1981. The specificity of proanthocyanidin-protein interactions. J Biol Chem 256:4494-4497.

Hanisch F-G, Müller S. 2000. Muc1: The polymorphic appearance of a human mucin. Glycobiology 10:439-449.

Hans M, Wilhelm M, Swandulla D. 2012. Menthol suppresses nicotinic acetylcholine receptor functioning in sensory neurons via allosteric modulation. Chem Senses 37:463-469.

Horne J, Hayes J, Lawless HT. 2002. Turbidity as a measure of salivary protein reactions with astringent substances. Chem Senses 27:653-659.

Ijichi C, Wakabayashi H, Sugiyama S, Ihara Y, Nogi Y, Nagashima A, et al. 2019. Metabolism of odorant molecules in human nasal/oral cavity affects the odorant perception. Chem Senses 44:465-481.

Joiner A, Muller D, Elofsson UM, Arnebrant T. 2004. Ellipsometry analysis of the in vitro adsorption of tea polyphenols onto salivary pellicles. Eur J Oral Sci 112:510-515.

Kauffman DL, Keller PJ. 1979. The basic proline-rich proteins in human parotid saliva from a single subject. Arch Oral Biol 24:249-256.

Kichko TI, Neuhuber W, Kobal G, Reeh PW. 2018. The roles of trpv1, trpa1 and trpm8 channels in chemical and thermal sensitivity of the mouse oral mucosa. European Journal of Neuroscience 47:201-210.

Kim HS, Maeda N. 1986. Structures of two haeii-types genes in the human salivary proline-rich protein multigene family. J Biol Chem 261:6712-6718.

Kummer W, Lips KS, Pfeil U. 2008. The epithelial cholinergic system of the airways. Histochem Cell Biol 130:219-234.

Kuo Y-L, Pangborn RM, Noble AC. 1993. Temporal patterns of nasal, oral, and retronasal perception of citral and vanillin and interaction of these odourants with selected tastants. International Journal of Food Science & Technology 28:127-137.

Kurogi M, Miyashita M, Emoto Y, Kubo Y, Saitoh O. 2012. Green tea polyphenol epigallocatechin gallate activates trpa1 in an intestinal enteroendocrine cell line, stc-1. Chem Senses 37:167-177.

Kurogi M, Kawai Y, Nagatomo K, Tateyama M, Kubo Y, Saitoh O. 2015. Auto-oxidation products of epigallocatechin gallate activate trpa1 and trpv1 in sensory neurons. Chem Senses 40:27-46.

Linforth R, Taylor AJ. 2000. Persistence of volatile compounds in the breath after their consumption in aqueous solutions. J Agric Food Chem 48:5419-5423.

Linforth R, Martin F, Carey M, Davidson J, Taylor AJ. 2002. Retronasal transport of aroma compounds. J Agric Food Chem 50:1111-1117.

Lyman BJ, Green BG. 1990. Oral astringency: Effects of repeated exposure and interactions with sweeteners. Chem Senses 15:151-164.

Lyons KM, Azen EA, Goodman PA, Smithies O. 1988. Many protein products from a few loci: Assignement of human salivary proline-rich proteins to specific loci. Genetics 120:255-265.

Macao B, Johansson DGA, Hansson GC, Härd T. 2005. Autoproteolysis coupled to protein folding in the sea domain of the membrane-bound muc1 mucin. Nature Structural &Amp; Molecular Biology 13:71.

Maeda N. 1985. Inheritance of the human salivary proline-rich proteins : A reinterpretation in terms of six loci forming two subfamilies. Biochem Genet 23:455-464.

Maeda N, Kim HS, Azen EA, Smithies O. 1985. Differential rna splicing and post-translational cleavages in the human salivary prolice-rich protein gene system. J Biol Chem 260:1123-1130.

Mehansho H, Carlson DM. 1983. Induction of protein and glycoprotein synthesis in rat submandibular glands by isoproterenol. J Biol Chem 258:6616-6620.

Mehansho H, Hagerman A, Clements S, Butler LG, Rogler JC, Carlson DM. 1983. Modulation of prolin-rich protein biosynthesis in rat parotid glands by sorghums with high tannin levels. Proc Natl Acad Sci USA 80:3948-3952.

Mehansho H, Clements S, Sheares BT, Smith S, Carlson DM. 1985. Induction of proline-rich glycoprotein synthesis in mouse salivary glands by isoproterenol and by tannins. J Biol Chem 260:4418-4423.

Mehansho H, Butler LG, Carlson DM. 1987. Dietary tannins and salivary proline-rich proteins : Interactions, induction, and defense mechanisms. Annu Rev Nutr 7:423-440.

Mole S, Butler LG, Iason G. 1990. Defense against dietary tannins in herbivores: A survey for proline-rich salivary proteins in mammals. Biochemical Systematics and Ecology 18:287-293.

Morzel M, Palicki O, Chabanet C, Lucchi G, Ducoroy P, Chambon C, et al. 2011. Saliva electrophoretic protein profiles in infants: Changes with age and impact of teeth eruption and diet transition. Arch Oral Biol 56:634-642.

Morzel M, Jeannin A, Lucchi G, Truntzer C, Pecqueur D, Nicklaus S, et al. 2012. Human infant saliva peptidome is modified with age and diet transition. Journal of Proteomics 75:3665-3673.

Mounayar R, Septier C, Chabanet C, Feron G, Neyraud E. 2013. Oral fat sensitivity in humans: Links to saliva composition before and after stimulation by oleic acid. Chemosensory Perception 6:118-126.

Nayak A, Carpenter GH. 2008. A physiological model of tea-induced astringency. Physiology & Behavior 95:290-294.

Pagès-Hélary S, Andriot I, Guichard E, Canon F. 2014. Retention effect of human saliva on aroma release and respective contribution of salivary mucin and **α**-amylase. Food Res Int 64:424-431.

Parry S, Silverman HS, McDermott K, Willis A, Hollingsworth MA, Harris A. 2001. Identification of muc1 proteolytic cleavage sites in vivo. Biochem Biophys Res Commun 283:715-720.

Perry GH, Dominy NJ, Claw KG, Lee AS, Fiegler H, Redon R, et al. 2007. Diet and the evolution of human amylase gene copy number variation. Nat Genet 39:1256-1260.

Piombino P, Genovese A, Esposito S, Moio L, Cutolo PP, Chambery A, et al. 2014. Saliva from obese individuals suppresses the release of aroma compounds from wine. PLoS One 9:e85611.

Ployon S, Belloir C, Bonnotte A, Lherminier J, Canon F, Morzel M. 2016. The membrane-associated muc1 improves adhesion of salivary muc5b on buccal cells. Application to development of an in vitro cellular model of oral epithelium. Arch Oral Biol 61:149-155.

Ployon S, Morzel M, Belloir C, Bonnotte A, Bourillot E, Briand L, et al. 2018. Mechanisms of astringency: Structural alteration of the oral mucosal pellicle by dietary tannins and protective effect of bprps. Food Chem 253:79-87.

Quintana M, Palicki O, Lucchi G, Ducoroy P, Chambon C, Salles C, et al. 2009. Inter-individual variability of protein patterns in saliva of healthy adults. Journal of Proteomics 72:822-830.

Robert-Hazotte A, Faure P, Neiers F, Potin C, Artur Y, Coureaud G, et al. 2019. Nasal mucus glutathione transferase activity and impact on olfactory perception and neonatal behavior. Scientific reports 9:3104.

Rupniak HT, Rowlatt C, Lane EB, Steele JG, Trejdosiewicz LK, Laskiewicz B, et al. 1985. Characteristics of four new human cell lines derived from squamous cell carcinomas of the head and neck. J Natl Cancer Inst 75:621-635.

Schöbel N, Radtke D, Kyereme J, Wollmann N, Cichy A, Obst K, et al. 2014. Astringency is a trigeminal sensation that involves the activation of g protein-coupled signaling by phenolic compounds. Chem Senses.

Schoumacker R, Robert-Hazotte A, Heydel JM, Faure P, Le Quere JL. 2016. Real-time monitoring of the metabolic capacity of ex vivo rat olfactory mucosa by proton transfer reaction mass spectrometry (ptr-ms). Anal Bioanal Chem 408:1539-1543.

Sevenhuysen GP, Holodinsky C, Dawes C. 1984. Development of salivary alpha-amylase in infants from birth to 5 months. Am J Clin Nutr 39:584-588.

Shimada T. 2006. Salivary proteins as a defense against dietary tannins. J Chem Ecol 32:1149-1163.

Stubbs M, Chan J, Kwan A, So J, Barchynsky U, Rassouli-Rahsti M, et al. 1998. Encoding of human basic and glycosylated proline-rich proteins by the prb gene complex and proteolytic processing of their precursor proteins. Arch Oral Biol 43:753-770.

Thomas-Danguin T. 2009. Flavor. In: Encyclopedia of neuroscience:Springer, 1580-1582.

Ukkonen H, Pirhonen P, Herrala M, Mikkonen JJW, Singh SP, Sormunen R, et al. 2017. Oral mucosal epithelial cells express the membrane anchored mucin muc1. Arch Oral Biol 73:269-273.

van Ruth SM, Roozen JP. 2000. Influence of mastication and saliva on aroma release in a model mouth system. Food Chem 71:339-345.

van Ruth SM, Grossmann I, Geary M, Delahunty CM. 2001. Interactions between artificial saliva and 20 aroma compounds in water and oil model systems. J Agric Food Chem 49:2409-2413.

Voirol E, Daget N. 1986. Comparative study of nasal and retronasal olfactory perception. Food Science and Technology - Lebensmittel - Wissenschaft & Technologie 19:316-319.

Wright KM, Hills BP, Hollowood TA, Linforth RST, Taylor AJ. 2003. Persistence effects in flavour release from liquids in the mouth. Int J Food Sci Technol 38:343-350.

Zhang L, Vlad A, Milcarek C, Finn OJ. 2013. Human mucin muc1 rna undergoes different types of alternative splicing resulting in multiple isoforms. Cancer Immunology, Immunotherapy 62:423-435.

VIII. Animation de recherche et autres activités (représentation, expertise,…)

A. Projets significatifs

J'ai choisi de présenter brièvement trois projets, deux auxquels j'ai participés et un que j'ai développé mais qui n'a pour l'instant pas été retenu pour financement.

Projet ANR Protannin : Protannin est le premier projet ANR auquel j'ai participé. Ce projet avait pour objectif de caractériser la relation structure – fonction des PRP dans le cadre des interactions PRP - tanins. Cette première participation à un projet ANR a été très enrichissante pour moi car elle m'avait montré à l'époque le mode de fonctionnement de la recherche sur projet. J'ai eu en charge la caractérisation des interactions PRP-tanins par spectrométrie de masse.

Projet ANR MUFFIN : Le projet d'ANR MUcosal salivary Film and Flavor Interaction est le premier projet de recherche d'envergure que j'ai mis en place et dirigé. Il a débuté en 2015 et s'est terminé en septembre 2019. L'objectif de ce projet était de développer un nouveau modèle de muqueuse orale prenant en compte pour la première fois la pellicule mucosale afin de caractériser les interactions entre la muqueuse orale et les molécules de la flaveur.
Ce projet fut une expérience enrichissante sur le plan du management car j'ai eu à encadrer une petite équipe de recherche composée d'une étudiante en thèse, de deux post-doctorantes, d'une assistante ingénieure et d'une étudiante en master.

Projet MACARON : MACARON est un projet d'ERC consolidator que j'ai déposé en février 2019. Ce projet a été classé B et n'a donc pas été retenu. Je le cite néanmoins car il m'a permis de formuler mes nouvelles hypothèses de travail et de structurer mon futur projet de recherche. Ce projet va être adapté au format ANR et une évolution sera proposée à l'appel ERC Consolidator Grant 2021. Ce projet a pour objectif d'explorer les nouvelles hypothèses que j'ai proposées sur le rôle de MUC1 dans la sensation d'astringence.

B. Encadrement d'étudiant et postdoctorants

Encadrement de thèses (soutenues)

Co-encadrement de la thèse de Sandy Pagès-Hélary (2012-2015)

- Encadrement : Elisabeth Guichard – Francis Canon
- J'ai co-encadré le travail de thèse de Sandy Pagès-Hélary qui portait la « Libération en bouche des molécules de la flaveur : influence des composés salivaires au niveau macroscopique et moléculaire ». Cette thèse était composées de trois parties : une approche sur la libération des molécules d'arôme *in vivo*, une approche sur la libération des molécules d'arôme *in vitro* en présence de salive artificielle, enfin une troisième partie a abordé les liens entre libération et paramètres physiologiques et

biochimique. Cette première expérience de co-encadrement m'a permis de mettre en place m'a thématique de recherche en explorant des premières pistes d'investigation. Cette expérience fut très enrichissante pour moi, au travers des difficultés rencontrées sur le plan des résultats scientifiques et des difficultés rencontrées lors de l'étude des molécules volatiles et de l'encadrement. Ce travail a conduit à la rédaction d'une publication qui a aujourd'hui un assez bon taux de citation (27 citations en 5 ans). Cependant, une partie des résultats de cette thèse est encore à valoriser.

Co-encadrement de la thèse de Sarah Ployon (2013-2016)

- Encadrement : Martine Morzel – Francis Canon
- J'ai co-encadré le travail de Sarah Ployon sur les « Interactions entre muqueuse orale, salive et molécules de la flaveur ». Cette thèse a comporté trois volets : le développement du modèle de muqueuse orale, les interactions tanins – muqueuse orale et les interactions molécules d'arôme – muqueuse orale. Ce travail a fait l'objet de trois publications et d'une quatrième en correction. Ce travail a été réalisé dans le cadre de l'ANR MUFFIN bien qu'il s'agisse d'un financement de type bourse MENRT. Il s'agissait d'une thèse ambitieuse qui a débouché sur des résultats significatifs avec le développement du premier modèle de muqueuse orale et les premiers résultats sur ses interactions avec les tanins et les molécules d'arôme.

Encadrement de thèses (en cours)

Co-encadrement de la thèse de Mei Wang (2018-2022)

- Encadrement : Gilles Féron – Francis Canon
- Je co-encadre le travail de Mei Wang sur l'« Impact du vieillissement sur la perception de la sensation d'astringence : comparaison de la population française et chinoise ». Mei est une étudiante chinoise dont la bourse est financée par le gouvernement chinois. L'encadrement de cette thèse est particulièrement enrichissant sur le plan des différences culturelles. Un premier article devrait être soumis l'année prochaine.

Co-encadrement de la thèse de Clément Nivet (2019-2022)

- Encadrement : Martine Morzel – Francis Canon
- Je vais co-encadrer le travail de Clément Nivet sur « le rôle de MUC1 dans la sensation d'astringence ». Cette thèse va explorer les hypothèses que j'ai proposées sur le rôle de MUC1 dans la sensation d'astringence.

Encadrement de chercheuses post-doctorantes

Encadrement du post-doctorat de Carolina Muñoz-González (2015-2018)

- Encadrement : Francis Canon
- J'ai encadré le projet de Carolina Muñoz-González sur le développement d'une alimentation adaptée aux personnes âgées. Ces travaux ont conduit à la publication de 5 articles et 2 autres sont en cours de rédaction.

Encadrement du post-doctorat d'Ece Aybeke (2015-2018)

- Encadrement : Francis Canon

- J'ai encadré Ece dans le cadre de l'ANR MUFFIN. Ce post-doctorat avait pour objectif la caractérisation des propriétés de surface du modèle de muqueuse orale par AFM. Il a débouché sur deux publications (dont une en commun avec Sarah Ployon), une partie des résultats est encore en cours d'analyse.

Encadrement d'étudiants

J'ai également encadré ou co-encadré différents étudiants en stage allant du BTS au Master II recherche.

Nom Prénom	Année	Niveau	Sujet
Courtin Justine	2014	Mater 2	Etude du rôle de la Lipocaline salivaire humaine dans la perception du goût du gras
Laheurte Maxime	2014-2015	BTS	Etude du rôle de la Lipocaline salivaire humaine dans la perception du goût du gras
Pradels Claire	2015	Master I	Etude *in vitro* du rôle de la pellicule mucosale sur la libération des arômes
Toutain Paul-Marie	2016	Ecole d'ingénieur	Production et purification d'une protéine recombinante, la lipocaline salivaire (LCN1), et analyse de ses interactions avec les molécules de la flaveur
Julio Raphaël	2018	Master I	Étude de l'effet des mannoprotéines sur la rétention et la libération des arômes du vin
Thierry Alban	2018	Ecole d'ingénieur	Développement d'un système de vannes automatisées

C. Jury de thèse

J'ai été membre du jury des thèses suivantes :

- Examinateur de la thèse de Mélanie MILLET (2018, Rennes) « Etude des interactions entre (macro-) molécules dans des boissons pouvant conduire à des déstabilisations colloïdales ».
- Examinateur de la thèse de Guilherme TAVARES (2015, Rennes) « Coacervats de ß-lactoglobuline et de lactoferrine : caractérisation et application potentielle pour l'encapsulation de bioactifs ».

D. Autres activités

Membre nommé du comité scientifique de la plateforme Chemosens

Je siège en tant qu'expert en chimie analytique au comité scientifique de la plateforme Chemosens depuis 2016. Cette fonction consiste à fournir des conseils d'orientation ou de choix scientifiques lors des réunions du comité.

Membre élu du comité scientifique du département CEPIA

J'ai été élu en tant que suppléant au comité scientifique du département CEPIA en 2017. Cette fonction m'amène à participer aux réunions du conseil scientifiques quand mon binôme ne peut le faire, à participer à l'évaluation des postes de chargés de recherche et d'ingénieur de recherche remontés au département annuellement ou à représenter le CS lors des évaluations HCERES d'UMR CEPIA, afin d'aider le CS dans la formulation de ses recommandations.

Membre élu du conseil d'unité du CSGA

J'ai été élu en tant que suppléant au conseil d'unité en 2017, ainsi je siège à ce conseil lors ce que mon binôme ne peut le faire afin d'apporter un avis sur les décisions concernant l'unité.

IX. Liste des travaux.

Liste des publications scientifiques

2019

1. Aybeke, E. N.; Ployon, S.; Brulé, M.; De Fonseca, B.; Bourillot, E.; Morzel, M.; Lesniewska, E.; Canon, F., Nanoscale Mapping of the Physical Surface Properties of Human Buccal Cells and Changes Induced by Saliva. *Langmuir* **2019**.
2. Heydel, J.-M.; Menetrier, F.; Belloir, C.; Canon, F.; Faure, P.; Lirussi, F.; Chavanne, E.; Saliou, J.-M.; Artur, Y.; Canivenc-Lavier, M.-C.; Briand, L.; Neiers, F., Characterization of rat glutathione transferases in olfactory epithelium and mucus. *PLOS ONE* **2019,** *14* (7), e0220259.
3. Muñoz-González, C.; Canon, F.; Feron, G.; Guichard, E.; Pozo-Bayón, M. A., Assessment Wine Aroma Persistence by Using an in Vivo PTR-ToF-MS Approach and Its Relationship with Salivary Parameters. *Molecules* **2019,** *24* (7), 1277.
4. Tournier, C.; Demonteil, L.; Canon, F.; Marduel, A.; Feron, G.; Nicklaus, S., A new masticatory performance assessment method for infants: a feasibility study. *Journal of texture studies* **2019**.

2018

5. Canon, F.; Neiers, F.; Guichard, E., Saliva and Flavor Perception: Perspectives. ***J. Agric. Food Chem.*** 2018, 66 (30), 7873-7879. (I.F.; Notoriety: ; Time Cited : 0)
6. Deuscher Z., Bonny J.-M., Boué F., Cheynier V., Clerjon S., Devaux M.-F., Meneghel J., Guillon F., Jamme F., Le Feunteun S., Passot S., Réfrégiers M., Rogniaux H., Ropartz D., Thévenot J., Vallverdu-Queralt A., & **Canon F.** (2017). Selected case studies presenting advanced methodologies to study food and chemical industry materials: From the structural characterization of raw materials to the multisensory integration of food. ***Innovative Food Science & Emerging Technologies***. (I.F.; Notoriety: ; Time Cited : 0)
7. Ployon S., Morzel M., Belloir C., Bonnotte A., Bourillot E., Briand L., Lesniewska E., Lherminier J., Aybeke E., & **Canon F.** (2018). Mechanisms of astringency: Structural alteration of the oral mucosal pellicle by dietary tannins and protective effect of bPRPs. ***Food Chemistry***, *253*, 79-87. (I.F.; Notoriety: Acceptable ; Time Cited : 3)
8. Muñoz-González, C. ; Brulé, M. ; Feron, G.; **Canon, F. (2018)**. Does interindividual variability of saliva affect the release and metabolization of aroma compounds ex vivo? The particular case of elderly suffering or not from hyposalivation. ***Journal of Texture Studies***. (I.F. 1.591 ; Notoriety: Acceptable ; Time Cited : 0).
9. Muñoz-González C., Feron G., **Canon F. (2018)**, Main effects of human saliva on flavour perception and the potential contribution to food consumption. ***Proceedings of the Nutrition Society***.
10. Muñoz-González C. Feron G., Brule M. & **Canon F**. (2018). Understanding the release and metabolism of aroma compounds using micro-volume saliva samples by ex vivo approaches. ***Food Chemistry***, *240*, 275-285. (I.F.; Notoriety: ; Time Cited : 4)
11. Muñoz-González C., Vandenberghe-Descamps M., Feron G., **Canon F.**, Labouré H., & Sulmont-Rossé C. (2018). Association between salivary hypofunction and food consumption in the elderlies. A systematic literature review. ***The journal of nutrition, health & aging***, 22(3), 407-419. (Facteur d'impact à 2 ans:; Notoriété à 2 ans:; Nombre de citation dans le WoS: 1)

2017

12. Ployon S., Morzel M., & **Canon F**. (2017). The role of saliva in aroma release and perception. ***Food Chemistry***, *226*, 212-220. (I.F.; Notoriety: ; Time Cited : 9)

2016

13. Ployon S., Belloir C., Bonnotte A., Lherminier J., **Canon F.** and Morzel M. (2016) The membrane-associated MUC1 improves adhesion of salivary MUC5B on buccal cells. Application to development of an in vitro cellular model of oral epithelium. ***Archives of Oral Biology**, 61*, pp. 149-55. (I.F. 1,733; Notoriety: ; Time Cited : 5)

2015

14. **Canon F.**, Milosavljevic A.R., Nahon L. and Giuliani A. Action spectroscopy of a protonated peptide in the far ultraviolet range. ***Physical Chemistry Chemical Physics**, 17*(39), pp. 25725-25733. (Facteur d'impact à 2 ans: 4,449; Notoriété à 2 ans: Excellent; Nombre de citation dans le WoS: 11)

15. **Canon F.**, Ployon S., Mazauric J.-P., Sarni-Manchado P., Réfrégiers M., Giuliani A., & Cheynier V. Binding site of different tannins on a human salivary proline-rich protein evidenced by dissociative photoionization tandem mass spectrometry. ***Tetrahedron**, 71*(20), pp. 3039-3044. (Facteur d'impact à 2 ans: 2,645; Notoriété à 2 ans: Excellent; Nombre de citation dans le WoS: 17)

16. Milosavljevic A. R., Nicolas C., Rankovic M. L. J., **Canon F.**, Miron C. and Giuliani A. 2015. K-Shell Excitation and Ionization of a Gas-Phase Protein: Interplay between Electronic Structure and Protein Folding. ***Journal of Physical Chemistry Letters**, 6*(16), pp. 3132-3138. (Facteur d'impact à 2 ans: 6,585; Notoriété à 2 ans: Exceptionnelle; Nombre de citation dans le WoS: 9)

17. Rankovic M. L., **Canon F.**, Nahon L., Giuliani A. and Milosavljević A. R. (2015) VUV action spectroscopy of protonated leucine-enkephalin peptide in the 6-14 eV range. ***Journal of Chemical Physics**, 143*(24). (Facteur d'impact à 2 ans: 2,894; Notoriété à 2 ans: Exceptionnelle; Nombre de citation dans le WoS: 4)

18. Rankovic M. L., **Canon F.**, Nahon L., Giuliani A. and Milosavljević A. R. (2015) Photoinduced fragmentation of gas-phase protonated leucine-enkephalin peptide in the VUV range. in Diaz, C., Rabadan, I., Garcia, G., Mendez, L. and Martin, F., (eds.) ***Xxix International Conference on Photonic, Electronic, and Atomic Collisions***. (I.F.; Notoriety: ; Time Cited : 0)

19. Tournier C., Rodrigues J., Canon F., Salles, C., & Feron G. A method to evaluate chewing efficiency in infants through food bolus characterization: a preliminary study. ***Journal of Texture Studies**, 46,* 113-119. (Facteur d'impact à 2 ans: 1,261; Notoriété à 2 ans: Acceptable; Nombre de citation dans le WoS: 1)

2014

20. Giuliani A., Milosavljević A. R., **Canon F.**, Nahon L. (2014) Contribution of synchrotron radiation to photoactivation studies of biomolecular ions in the gas phase. ***Mass Spectrometry Review***, 33(5), 424-441. (Facteur d'impact à 2 ans: 7,735; Notoriété à 2 ans: Exceptionnelle; Nombre de citation dans le WoS: 16)

21. Milosavljević A. R., Cerovski V. Z., **Canon F.**, Ranković, M. L., Škoro N., Nahon L., & Giuliani A. (2014). Energy-Dependent UV Photodissociation of Gas-Phase Adenosine Monophosphate Nucleotide Ions: The Role of a Single Solvent Molecule. ***The Journal of Physical Chemistry Letters**, 5*(11), 1994-1999. (Facteur d'impact à 2 ans: 6,585; Notoriété à 2 ans: Exceptionnelle; Nombre de citation dans le WoS: 7)

22. Milosavljević A. R., Cerovski V. Z., Rankovic M. L., **Canon F.**, Nahon L., & Giuliani A. (2014). VUV photofragmentation of protonated leucine-enkephalin peptide dimer below ionization energy. ***European Physical Journal D**, 68*(3). (Facteur d'impact à 2 ans: 1,513; Notoriété à 2 ans: Correct ; Nombre de citation dans le WoS: 2)

23. Pagès-Hélary, S., Andriot, I., Guichard, E., & Canon, F. (2014). Retention effect of human saliva on aroma release and respective contribution of salivary mucin and α-amylase. ***Food Research International****, 64*, 424-431. (Facteur d'impact à 2 ans: 3,005; Notoriété à 2 ans: Excellente ; Nombre de citation dans le WoS: 20)

2013

24. Brunet C., Antoine R., Dugourd P., Duflot D., **Canon F.**, Giuliani A., Nahon L. (2013) Valence shell direct double photodetachment in polyanions. ***New Journal of Physics*** 15**:** 063024. (Facteur d'impact à 2 ans: 4,063; Notoriété à 2 ans: Exceptionnelle ; Nombre de citation dans le WoS: 4).

25. Brunet C., Antoine R., Dugourd P, Canon F., Giuliani A., Nahon L. (2013) Photo-induced electron detachment of protein polyanions in the VUV range. ***The Journal of Chemical Physics*** 138, 064301. (Facteur d'impact à 2 ans: 3,164; Notoriété à 2 ans: Excellente ; Nombre de citation dans le WoS: 10)

26. **Canon F.**, Paté F., Cheynier V., Sarni-Manchado P., Giuliani A., Pérez J., Durand D., Li J. & Cabane B. (2013) Aggregation of the Salivary Proline-Rich Protein IB5 in the Presence of the Tannin EgCG. ***LANGMUIR 29***, 1926-1937. (Facteur d'impact à 2 ans: 4,187; Notoriété à 2 ans: Excellente ; Nombre de citation dans le WoS: 44)

27. **Canon F.**, Milosavljević A. R., van der Rest G., Réfrégiers M., Nahon L., Sarni-Manchado P., Cheynier V., & Giuliani A. (2013). Photodissociation and dissociative photoionization mass spectrometry of proteins and noncovalent protein-ligand complexes. ***Angewandte Chemie International Edition****, 52*(32), 8377-8381. (Facteur d'impact à 2 ans: 13,734; Notoriété à 2 ans: Exceptionnelle; Nombre de citation dans le WoS: 27)

28. Milosavljević A.R., Cerovski V.Z., Canon F., Nahon L. & Giuliani A. (2013) Nanosolvation-Induced Stabilization of a Protonated Peptide Dimer Isolated in the Gas Phase. ***Angewandte Chemie International Edition***, 52, 7286-7290. (Facteur d'impact à 2 ans: 13,734; Notoriété à 2 ans: Exceptionnelle; Nombre de citation dans le WoS: 11)

2012

29. Brunet C., Antoine R., Dugourd P., **Canon F.**, Giuliani A., Nahon L. (2011) Formation and Fragmentation of Radical Peptide Anions: Insights from Vacuum Ultra Violet Spectroscopy. ***Journal of the American Society for Mass Spectrometry***, 23(2): 274-281. (Facteur d'impact à 2 ans: 4,002; Notoriété à 2 ans: Excellente; Nombre de citation dans le WoS: 34)

30. Giuliani A., Milosavljević A. R., Hinsen K., **Canon F.**, Nicolas C., Réfrégiers M., Nahon L., (2012) Structure and Charge-State Dependence of the Gas-Phase Ionization Energy of Proteins ***Angewandte Chemie International Edition***, 51, 9552-9556. (Facteur d'impact à 2 ans: 13,734; Notoriété à 2 ans: Exceptionnelle; Nombre de citation dans le WoS: 20)

31. Milosavljević A.R., **Canon F.,** Nicolas C., Miron C., Nahon L., Giuliani A. (2012) Gas-Phase Protein Inner-Shell Spectroscopy by Coupling an Ion Trap with a Soft X-ray Beamline. *The* ***Journal of Physical Chemistry Letters*** 3**,** 1191-1196. (Facteur d'impact à 2 ans: 6,585; Notoriété à 2 ans : Exceptionnelle; Nombre de citation dans le WoS: 33)

32. Milosavljević A. R., Nicolas C., Gil J.-F., **Canon F.**, Réfrégiers M., Nahon L., and Giuliani A. (2012) Fast *in-vacuo* photon shutter for synchrotron radiation quadrupole ion trap tandem mass spectrometry. ***Nuclear Instruments and Methods in Physics Research Section B: Beam Interactions with Materials and Atoms*** 2012, 279, 34-36. (Facteur d'impact à 2 ans : 1,266; Notoriété à 2 ans : Correcte ; Nombre de citation dans le WoS: 11)

33. Milosavljević A.R., Nicolas C., Gil J.-F., **Canon F.,** Réfrégiers M., Nahon L. and Giuliani A. (2012) VUV synchrotron radiation: a new activation technique for tandem mass spectrometry.

Journal of Synchrotron Radiation 19, 174-178. (Facteur d'impact à 2 ans : 2,186; Notoriété à 2 ans : excellente ; ; Nombre de citation dans le WoS: 26)

2011

34. Bagag, A., Giuliani, A., **Canon, F.**, Réfrégiers, M., Naour, F. (2011) Separation of peptides from detergents using ion mobility spectrometry. ***Rapid Commun. Mass Spectrom.***, *25*, 3436-3440. (Facteur d'impact à 2 ans : 2,79 ; Notoriété à 2 ans : excellente; Nombre de citation dans le WoS: 5)
35. Brunet C., Antoine R., Allouche A.-R., Dugourd P., **Canon F.**, Giuliani A., Nahon L. (2011) Gas phase Photo-Formation and Vacuum UV Photofragmentation Spectroscopy of Tryptophan and Tyrosine Radical-Containing Peptides. ***The Journal of Physical Chemistry A,*** *115*, 8933-8939. (Facteur d'impact à 2 ans: 2,946; Notoriété à 2 ans: Excellente ; ; Nombre de citation dans le WoS: 23)
36. **Canon F.,** Ballivian R., Chirot F., Antoine R., Sarni-Manchado P., Lemoine J. and Dugourd P. (2011) Folding of a salivary intrinsically unstructured protein upon binding to tannins. ***Journal of American Chemical Society,*** 2011, 133, 7847. (Facteur d'impact à 2 ans: 9,907; Notoriété à 2 ans: Exceptionnelle; ; Nombre de citation dans le WoS: 53)

2010

37. Boze H., Marlin T., Durand D., Pérez J., Vernhet A., **Canon F.**, Sarni-Manchado P., Cheynier V. and Cabane, B. (2010) Proline-rich salivary proteins have extended conformations. ***Biophysical Journal,*** 99, 656-665. (Facteur d'impact à 2 ans: 4,218; Notoriété à 2 ans: Excellente; Nombre de citation dans le WoS: 53)
38. **Canon F.,** Giuliani A., Paté F. and Sarni-Manchado P. (2010) Ability of a salivary intrinsically unstructured protein to bind different tannin targets revealed by mass spectrometry. ***Analytical and Bioanalytical Chemistry***, 398, (2), 815-822. (Facteur d'impact à 2 ans: 3,841; Notoriété à 2 ans: Excellente ; Nombre de citation dans le WoS: 30)
39. Tarascou I., Souquet J.M., Mazauric J.P., Carrillo S., Coq S., **Canon F.**, Fulcrand H. and Cheynier V. (2010) The hidden face of food phenolic composition. ***Archives of Biochemistry and Biophysics,*** 501, (1), 16-22. (Facteur d'impact à 2 ans: 3,022; Notoriété à 2 ans: Excellente; Nombre de citation dans le WoS: 48)

2009

40. **Canon F.,** Paté F., Meudec E., Marlin T., Cheynier V., Giuliani A. and Sarni-Manchado P. (2009) Characterization, stoichiometry and stability of salivary protein-tannin complexes by ESI-MS and ESI-MS/MS. ***Analytical and Bioanalytical Chemistry***, 395, 2535-2545. (Facteur d'impact à 2 ans: 3,48; Notoriété à 2 ans: Excellente; Nombre de citation dans le WoS: 33)

2008

41. Sautour M., **Canon F.,** Miyamoto T., Dongmo A. and Lacaille-Dubois M.A. (2008) A new ecdysteroid and other constituents from two Dioscorea species. ***Biochemical Systematics and Ecology***, 36, 559-563. (Facteur d'impact à 2 ans: 1,136; Notoriété à 2 ans: Correcte; Nombre de citation dans le WoS: 4)

Liste des proceedings

2013

1. Giuliani A., Milosavljevic A., **Canon F.**, Nahon L. & Réfrégiers M.(2013). Application of VUV synchrotron radiation to proteomic and analytical mass spectrometry. *11th International Conference on Synchrotron Radiation Instrumentation (Sri 2012), 425.*

2007

2. Sautour M., **Canon F.,** Miyamoto T., Dongmo A. and Lacaille-Dubois M.A. (2007) Ecdysteroids from Dioscorea dumetorum, Planta Medica, 73, 418. (Facteur d'impact à 2 ans: 1,848; Notoriété à 2 ans : Correcte)

Liste des présentations orales dans des congrès nationaux & internationaux

2019

1. Muñoz-gonzález C., Brulé M., Féron G., **Canon F.**, (2019). Interindividual variability of oral metabolization and release of aroma compounds in elderly. In 12th Wartburg Symposium on Flavor Chemistry and Biology, Eisenach, Germany, May 21 – 24, 2019.

2018

2. Canon F., Interactions between saliva, mucosae and flavor compounds (2018). In International Conference on Mediterranean Diet and Gastronomy, Evora, Portugal. *(Invited Keynote Speaker)*
3. Ployon S., Morzel M., Belloir C., Bonotte A. Bourillot E., Briand L., Lesniewska E., Lhermiinier J., Aybeke E., Muñoz-González C., **Canon F.** (2018) New insight into the role of the oral mucosa in flavour perception. In The 5th International Conference on Agricultural and Biological Sciences, Hangzhou, China. *(Invited Keynote Speaker)*
4. Muñoz-gonzález C., Brulé M., Féron G., **Canon F.**, (2018). Application of an in vivo ptr-tof-ms approach to determine differences in wine aroma release among wines spiked with different types of oenological tannins. In the 5th International Conference on Food Oral Processing, Leeds, United Kingdom.
5. Muñoz-gonzález C., Brulé M., Féron G., **Canon F.**, (2018). Effets de la variabilité interindividuelle de la salive humaine (flux et composition) sur la libération d'arômes et la perception de la flaveur chez le sujet âgé afin de mettre en place des stratégies d'élaboration des produits alimentaires pour un vieillissement en bonne santé « Food4Elderly ». In Les Journées Francophones de Nutrition, Nice, France.

2017

6. Muñoz-gonzález C., **Canon F.**, Semon E., Feron G., Guichard E., Pozo-bayón M.Á. (2017). Application of an in vivo ptr-tof-ms approach to determine differences in wine aroma release among wines spiked with different types of oenological tannins. In the 4th Wine Active Compounds internation conference, Beaune, France.
7. Muñoz-González C., Brulé M., Féron G. & **Canon F.** (2017). Does human saliva drive flavour perception? London, United-Kingdom.
8. Ployon S., Brulé M., Pradels C., Morzel M., **Canon F.** (2017). New insight on the role of the oral mucosa in aroma release. In 15th Weurman Flavour Research Symposium, Graz, Austria.

2016

9. *Aybeke E.N., Ployon S., Belloir C., Bourillot E., Lesniewska E., Morzel M., **Canon F.** (2016).* Impact of mucosal pellicle on the physical properties of oral epithelial cells. In 19th International Scanning Probe Microscopy Conference. Kyoto, Japan.
10. Ployon S., Pradels C., Belloir C., Morzel M., **Canon F.** (2016). Interactions between aroma compounds and the oral mucosa could be responsible for aroma persistence. In 4th International Conference on Food Oral Processing. Lausanne, Switzerland.

2015

11. Canon F. 2015. Mass spectrometry for the study of protein-ligand interactions and supramolecular complexes: Application to an intrinsically disordered protein. In Paper Presented to the 8th SMAP, Ajaccio, France. (Invited Keynote Speaker)
12. Canon F., Giuliani A., Réfrégiers M., Nahon L., Pérez J., Durand D., Cabane B., Sarni-Manchado P., Cheynier V. (2015). Astringency and the interactions between a human salivary proline-rich protein and tannins. Saint-Aubin, France *(Invited Keynote Speaker)*
13. Canon F. (2015). Contribution des interactions tanins - protéines salivaires dans la sensation d'astringence. In *14ème Forum Oenologique de Davayé*. Davayé, France. *(Invited Keynote Speaker)*

2014

14. Canon F., Ployon S., Milosavljevic A. R., Sarni-Manchado P., Cheynier V., Réfrégiers M., Nahon L., & Giuliani, A. (2014). Localization of the binding site of different model tannins on the salivary PRP IB5. In *3rd International Conference on Food Oral Processing*, (pp. 85). Wageningen, The Netherlands.
15. Pagès-Hélary S., Guichard E., & **Canon F.** (2014). Does salivary composition impact the release of aroma? In *14th Weurman Flavour Research Symposium*). Cambridge, United Kingdom.

2013

16. Giuliani A., Milosavljević A. R., Hinsen K., Canon F., Nicolas C., Réfrégiers M., & Nahon, L. (2012). Ionization energy of gas phase protein cations and its dependence on charge state_and structure. In *Synchrotron SOLEIL Users Meeting*. Orsay.
17. Milosavljević A. R., **Canon F.**, Cerovski V. Z., Nicolas C., Réfrégiers M., Nahon, L., & Giuliani A. (2013). Interaction of energetic photons with bare and nanosolvated biopolymers isolated in the gas phase. In *2nd Nanoscale Insights into Ion Beam Cancer Therapy*. Sopot, Poland.

2012

18. Canon F, Milosavljević AR, Sarni-Manchado P, Cheynier V, van der Rest G, Réfrégiers M, Nahon L & Giuliani A (2012) Localization of non-covalent protein-ligand binding sites by top-down mass spectrometry based on vacuum ultra-violet (VUV) activation. In *29ème Journées Françaises de la Spectrométrie de Masse*, (pp 59). Orléan, France.
19. Canon F., Sarni-Manchado P., Paté F., Marlin T., Giuliani A., Durand D., Cheynier V. & Cabane B. (2012) Astringency, a new insight into salivary PRP – tannin interaction. In *Food Oral Processing*, Beaune, France.

2011

20. Canon F., Cabane B., Durand D. Perez J., Paté F., Giuliani A., Marlin T., Cheynier V. & Sarni-Manchado P. (2011) Study of interactions occurring between proline rich proteins and tannins. In *Synchrotron SOLEIL Users Meeting*, Orsy.

2010

21. Canon F., Giuliani A., Ballivian R., Chirot F., Albrieux F., Paté F., Cheynier V., Lemoine J., Antoine R., & Dugourd P. & Sarni-Manchado P.(2010) Tannin interactions with a human basic salivary proline rich protein studied by mass spectrometry. In *XXVth International Conference on Polyphenols*, Montpellier.
22. Canon F., Paté F., Giuliani A., Cheynier V. & Sarni-Manchado P. (2010) Understanding functions of a human intrinsically unstructured protein involved in astringency. In *Journée de l'école doctorale Sciences des Aliments - Sciences des Procédés*, Montpellier, France.

2009

23. Canon F., Giuliani A., Ballivian R., Chirot F., Albrieux F., Paté F., Cheynier V., Lemoine J., Antoine R., Dugourd P. & Sarni-Manchado P. (2009) Mass spectrometry contribution to understand function of an human intrinsically unstructured protein involved in astringency. In *18th International Mass Spectrometry Conference*, Bremen, Germany.

2008

24. Canon F., Giuliani A., Marlin T., Boze H., Paté F., Bouchut C., Meudec E., Cheynier V. & Sarni-Manchado P. (2008) Tannins interactions with a human basic salivary proline rich protein studied by mass spectrometry. In *XXIVth International Conference on Polyphenols*, pp. 67-68, Salamanca, Spain.
25. Canon F., Meudec E., Marlin T., Sarni- Manchado P. & Cheynier V. (2008) Basic salivary proline rich proteins involved in astringency studied by mass spectrometry. In *8th European Symposium on saliva*, pp. 33, Egmund aan Zee, The Netherlands.

Liste des Posters

2018

1. Jay L., **Canon F.**, Tournier C., Vargiolu R., Zahouani H. (2018). Impact of saliva and astringent compounds on tongue mechanical properties : an ex vivo investigation. In the 5th International Conference on Food Oral Processing, Leeds, United Kingdom.
2. Féron G., Brignot H., Schöps F., Neirs F., **Canon F.**, Walliczek-dworschak U., Muñoz-González C. & Hummel T. (2018). Salivary redox status: a key parameter involved in the release and perception of sensory stimuli in human. In the 5th International Conference on Food Oral Processing, Leeds, United Kingdom.

2017

3. Muñoz-González C., Brulé M., Féron G. & **Canon F.** (2016). Unravelling the effects of interindividual variability of human saliva (flow and composition) on aroma compounds. In15th Weurman Flavour Research Symposium, Graz, Austria, 18th – 22nd September 2017.

2016

4. Aybeke EN, Ployon S, Brulé, Bourillot E, Morzel M, Lesniewska E & **Canon F.** (2016). Impact of a mucosal pellicle on the physical properties of oral epithelial cells. International Scanning Probe Microscopy Conference, Grindelwald, Switzerland,12th-15th June 2016.
5. Ployon S, Pradels C, Belloir C, Morzel M & **Canon F.** (2016). Role of oral mucosa and mucosal pellicle in aroma persistence. 94th IADR (International Association for Dental Research) General Session, Seoul, Korea, 22nd-25th June 2016
6. Ployon S, Pradels C, Belloir C, Morzel M & **Canon F.** (2016). Interactions between aroma compounds and the oral mucosa could be responsible for aroma persistence. 4th International Conference on Food Oral Processing (FOP), Lausanne, Switzerland, 3rd-6th July 2016.

2015

7. Canon, F., Pages-Helary, S. and Guichard, E. (2015). In nose concentration of aroma compounds is modified by salivary protein composition and saliva stimulation. Chemical Senses, 40(3), pp. 237.
8. Ployon S, Sémon E, Le Quéré J-L, Belloir C, Tromelin A, Guichard E, Morzel M & Canon F. (2015). Développement d'une méthode d'analyse de la désorption de composés d'arôme par

PTR-MS sur un modèle in vitro de muqueuse orale. Congrès français de Spectrométrie de Masse et d'Analyse Protéomique, Ajaccio, 15-18 Septembre 2015.

2014

9. **Canon F.**, Milosavljevic A. R., Sarni-Manchado P., Cheynier V., Réfrégiers M., Nahon L., & Giuliani A. (2014). Localization of the binding site of different model tannins on the salivary PRP IB5. In *10th European Symposium on Saliva*, (pp. 51). Egmond aan Zee, The Netherlands.
10. Giuliani A., Milosavljevic A. R., **Canon F.**, Nahon, L., & Réfrégiers M. (2014). Electronic spectroscopy of polypeptides in the gas phase. In *2nd International Conference on Physics and Biological Systems*. Gif-sur-Yvette, France.
11. Milosavljevic A. R., Nicolas C., Ranković M. L., **Canon F**., Miron C., & Giuliani A. (2014). N K-shell X-ray tandem mass spectrometry of gas-phase ubiquitin protein In *27th Summer School and International Symposium on the Physics of Ionized Gases*. Belgrade, Serbia.
12. Pagès-Hélary S., Guichard E., & **Canon F.** (2014). Impact of the main salivary proteins on aroma release. In *10th European Symposium on Saliva*, (pp. 52). Egmond aan Zee, The Netherlands.
13. Ployon S., Belloir C., Bonnot A., **Canon F.**, & Morzel M. (2014). Design of an in-vitro model of oral mucosa: microscopic characterization. In *10th European Symposium on Saliva*, (pp. 76). Egmond aan Zee, The Netherlands.
14. Tournier C., Rodrigues J., Mielle P., Feron G., **Canon F.**, & Salles C. (2014). Development of methods to study food oral processing in infants. In *3rd International Conference on Food Oral Processing*, (pp. 99). Wageningen, The Netherlands.

2013

15. Giuliani A., Milosavljevic A., Canon F., Nahon L., & Refregiers M. (2013). Application of VUV synchrotron radiation to proteomic and analytical mass spectrometry. *11th International Conference on Synchrotron Radiation Instrumentation (Sri 2012), 425*.
16. Milosavljevic A. R., **Canon F.**, Ranković M. L., Cerovski V. Z., Nahon L., & Giuliani A. (2013). VUV photofragmentation of protonated leucine-enkephalin peptide: partial ion yield dependence on type of sequence fragments. In *28th International Conference on Photonic, Electronic and Atomic Collisions*). Lanzhou, China.
17. Милосављевић А. Р., Ранковић М. Љ., Церовски В. З., **Канон Ф.**, Наон Л., & Ђулијани и. А. (2013). УТИЦАЈ НАНОСОЛВАТАЦИЈЕ НА СТАБИЛНОСТ ПЕПТИДА ИЗОЛОВАНОГ У ГАСНОЈ ФАЗИ. In *XII Congress of Serbian Physicists*. Vrnjačka Banja, Serbia.
18. Milosavljević A. R., **Canon F.**, Cerovski V. Z., Ranković M. L., Nahon L., & Giuliani A. (2013). VUV photodissociation of bare and nanosolvated protonated nucleotide isolated in the gas phase. In *2nd Nanoscale Insights into Ion Beam Cancer Therapy*. Sopot, Poland.

2012

19. Pagès S., **Canon F.,** Andriot I., Tromelin A., Ayed C., Deprêtre N., Feron G., Salles C., & Guichard E. (2012). Does saliva modify the volatility of aroma compounds? In *2nd International Conference on Food Oral Processing*, (pp. 156). Beaune, France.

2011

20. Brunet C., Antoine R., Dugourd P., **Canon F.**, Giuliani A., & Nahon L. (2011). Photofragmentation and action spectroscopy of gas phase peptide ans protein polyanions. From near-UV to vacuum UV. In *SMAP*, (pp. 133). Avignon, France.

21. Canon F., Milosavljević A.R., Sarni-Manchado P., Cheynier V., van der Rest G., Réfrégiers M., Nahon L. & Giuliani A. (2011). VUV-photodissociation of peptides in the gas phase probed by synchrotron radiation. In *ASMS Conference*. Denver.
22. Canon F., Milosavljević A. R., Sarni-Manchado P., Cheynier, V., Van der Rest, G., Réfrégiers, M., Nahon, L., & Giuliani, A. (2011). VUV-photodissociation of peptides in the gas phase probed by synchrotron radiation. In *SMAP*). Avignon, France.
23. Giuliani A., Canon F., Réfrégiers M., & Nahon L. (2011). Coupling of a linear ion trap with a VUV beamline. In *SMAP*, (pp. 293). Avignon, France.

2008

24. Canon F., Giuliani A., Marlin T, Boze H., Mazauric J.-P., Bouchut C., Paté F., Meudec E., Cheynier V., & Sarni-Manchado P. (2008). Contribution de la spectrométrie de masse à l'étude d'une protéine non structurée riche en proline impliquée dans le phénomène d'astringence. In *25èmes Journées Françaises de Spectrométrie de Masse*). Grenoble, France.

Liste des communiqués de presse

2018

1. Canon F. (2018). La sensation d'astringence, une histoire de protéines. In). inra.fr: INRA.

2013

2. Canon F., Milosavljević A. R., van der Rest G., Réfrégiers M., Nahon L., Sarni-Manchado P., Cheynier V., & Giuliani, A. (2013). La sensation d'astringence sous les rayons UV / [The secrets of astringency revealed through UV radiation]. In *INRA Presse*, (pp. 2 p.). Paris (France): Service Presse INRA.

Liste des articles de communication et de vulgarisation

2018

1. Canon F. (2018). La Chimie de l'astringence mieux décrite. In Cahier du « Monde », Actualité, Science & Médecine, Mercredi 7 Février 2018, N°22728, (pp. 3).
2. Canon F. (2018). La sensation d'astringence, une histoire de protéines. In Sciences et Vie, Avril 2018.

2016

3. Canon F., Cabane B., Durand D, Sarni-Manchado P., Réfrégier M., Nahon L., Pérez J. Giuliani A. & Cheynier V. (2016). Astringency and the interaction between a human salivary proline rich-protein and tannins. In INRA-SOLEIL 10 years, (pp. 68-69).

2015

4. Canon, F. (2015). Contribution des interactions tanins - protéines salivaires dans la sensation d'astringence. In *Revue Française d'œnologie*, Mars/Avril 2015 n°269, (pp. 10-11).

2014

5. Canon, F., Milosavljevic, A. R., Van der Rest, G., Réfrégier, M., Nahon, L., Sarni-Manchado, P., Cheynier, V., & Giuliani, A. (2014). Synchrotron radiation -tandem mass spectrometry for proteomic and structural biology. In *SOLEIL highlights 2013*, (pp. 60-61).

6. **Canon F.,** Giuliani A., & Cheynier V. (2014). Comprendre la perception de l'astringence. In *Faits marquants CEPIA 2013*, (pp. 4). Nantes (France): INRA.
7. Milosavljević A. R., Cerovski V. Z., **Canon F.**, Nahon L., & Giuliani A. (2014). Nanosolvation-induced stabilization of a protonated peptide dimer isolated in the gas phase. In *SOLEIL highlights 2013*, (pp. 86-87).
8. **Canon F.** (2014). Comprendre les mécanismes de perception de l'astringence. In *1er CRU Journal d'information du Centre INRA de Dijon*, (pp. 2 p.). Dijon (France): INRA.

2013

9. **Canon F.**, Milosavljević, A. R., Van der Rest, G., Réfrégier, M., Nahon, L., Sarni-Manchado, P., Cheynier, V., & Giuliani, A. (2013). Interaction ligand – proteine : la sensation d'astringence sous les rayons VUV de DESIRS. In *La Recherche à Soleil, le magazine du Synchrotron SOLEIL*, (pp. 04-06).
10. **Canon F.** (2013). Ne dites plus goût, mais flaveur. In *Portail actus*, vol. 2013. Paris (France): INRA.
11. **Canon F.,** & Cheynier, V. (2013). Tanins du vin : des interactions avec les protéines de la salive à la sensastion d'astringence. In *Vitisphere.com*, (pp. 8 p.). Montpellier (France): Société Vitisphere SA.
12. Milosavljevic A. R., **Canon F.**, Nicolas C., Miron C., Nahon, L., & Giuliani, A. (2013). Inner-sell spectroscopy of gas-phase protein ions. In *SOLEIL highlights 2012*, (pp. 90-91).

2012

13. Sarni-Manchado P., Cheynier V., Giuliani A., Réfrégiers M., Nahon L., & **Canon F.** (2012). Etude structurale de la protéine salivaire humaine IB5 seule et en interaction avec un tanin In *INRA en lumière - 5 ans de partenariat avec SOLEIL* (pp. 14): INRA.

PUBLICATIONS ILLUSTRATIVES

Publication n°1: The membrane-associated MUC1 improves adhesion of salivary MUC5B on buccal cells. Application to development of an in vitro cellular model of oral epithelium.

Ployon, S.; Belloir, C.; Bonnotte, A.; Lherminier, J.; Canon, F.; Morzel, M.,

Archives of Oral Biology **2016,** *61*, 149-55.

Archives of Oral Biology 61 (2016) 149–155

Contents lists available at ScienceDirect

Archives of Oral Biology

journal homepage: www.elsevier.com/locate/aob

The membrane-associated MUC1 improves adhesion of salivary MUC5B on buccal cells. Application to development of an in vitro cellular model of oral epithelium

Sarah Ployon[a,b,c], Christine Belloir[a,b,c], Aline Bonnotte[d], Jeannine Lherminier[e], Francis Canon[a,b,c], Martine Morzel[a,b,c,*]

[a] CNRS, UMR 6265 Centre des Sciences du GoÛt et de l'Alimentation, F-21000 Dijon, France
[b] INRA, UMR1324 Centre des Sciences du GoÛt et de l'Alimentation, F-21000 Dijon, France
[c] Université de Bourgogne, UMR Centre des Sciences du GoÛt et de l'Alimentation, F-21000 Dijon, France
[d] Université de Bourgogne, UMR 1347 Agroécologie, Plateforme DImaCell, Centre de Microscopie INRA/Université de Bourgogne, F-21000 Dijon, France
[e] INRA, UMR1347 Agroécologie, ERL CNRS 6300, Plateforme DImaCell, Centre de Microscopie INRA/Université de Bourgogne, F-21000 Dijon, France

ARTICLE INFO

Article history:
Received 20 August 2015
Received in revised form 2 November 2015
Accepted 3 November 2015

Keywords:
Oral mucosa
Mucosal pellicle
TR146 cells
Mucins
Immunocytochemistry
Scanning electron microscopy

ABSTRACT

Objectives: The mucosal pellicle is a thin layer of salivary proteins, mostly MUC5B mucins, anchored to epithelial oral cells. This pellicle is involved in protection of oral mucosae against abrasion, pathogenic microorganisms or chemical xenobiotics. The present study aimed at studying the involvement of MUC1 in mucosal pellicle formation and more specifically in salivary MUC5B binding using a cell-based model of oral epithelium.
Design: MUC1 mRNAs were not detected in TR146 cells, and therefore a stable cell line named TR146/MUC1 expressing this protein was developed by transfection. TR146 and TR146/MUC1 were incubated with human saliva in order to evaluate retention of MUC5B by epithelial cells.
Results: The cell surface of both TR146 and TR146/MUC1 was typical of a squamous non-keratinized epithelium, with the presence of numerous microplicae. After incubation for 2 h with saliva diluted in culture medium (1:1) and two washes with PBS, saliva deposits on cells appeared as a loose filamentous thin network. MUC5B fluorescent immunostaining evidenced a heterogeneous lining of confluent cell cultures by this salivary mucin but with higher fluorescence on TR146/MUC1 cells. Semi-quantification of MUC5B bound to cells confirmed a better retention by TR146/MUC1, evaluated by Dot Blot (+34.1%, $p < 0.05$) or by immunocytochemistry (+44%, $p < 0.001$).
Conclusion: The membrane-bound mucin MUC1 is a factor enhancing the formation of the mucosal pellicle by increasing the binding of salivary MUC5B to oral epithelial cells. An in vitro model suitable to study specifically the function and properties of the mucosal pellicle is proposed.

1. Introduction

The oral cavity is lined by a thin layer of salivary proteins anchored onto mucosae (Bradway, Bergey, Jones, & Levine, 1989) and teeth (Hay, 1967), termed the mucosal and dental pellicles respectively. The mucosal pellicle is the inner structure of the protective mucus layer on mucosae, the upper structure being a mobile layer of saliva (Pramanik, Osailan, Challacombe, Urquhart, & Proctor, 2010). Salivary pellicles are known to have an essential role in oral health (Tabak, Levine, Mandel, & Ellison, 1982). For example, the dental pellicle ensures lubrication and buffering of dental surface (Hannig & Joiner, 2006). Regarding more specifically the mucosal pellicle, by similarity with the dental pellicle, it could contribute to moisture retention, lubrication or protection against microbial colonization (Bradway et al., 1989). It could also play a role in sensory perception of astringency (Nayak & Carpenter, 2008). Finally, similarly to intestinal mucus which is a gel barrier to drug delivery (Boegh & Nielsen, 2015), it is likely that the salivary mucus modulates diffusion properties of drugs and other chemical compounds through the oral mucosa (Teubl et al., 2013). Based on these functions of the mucosal pellicle, it appears necessary to include this biological structure to in vitro models of oral mucosa.

* Corresponding author at: INRA-CSGA, 17 rue Sully, 21000 Dijon, France. Fax: +33 380 69 32 27.
E-mail address: martine.morzel@dijon.inra.fr (M. Morzel).

http://dx.doi.org/10.1016/j.archoralbio.2015.11.002
0003-9969/

The mucosal pellicle contains salivary proteins such as amylase, IgA, cystatins (Bradway et al., 1989), carbonic anhydrase IV, secretory component or mucins (Gibbins, Yakubov, Proctor, Wilson, & Carpenter, 2014). Among these salivary proteins, MUC5B has been identified as a major component of *in vivo*(Gibbins, Proctor, Yakubov, Wilson, & Carpenter, 2014) and *in vitro*(Cardenas, Elofsson, & Lindh, 2007) mucosal pellicles. Detecting MUC5B on cells sampled from human buccal surfaces confirmed its attachment to epithelial cells (Morzel, Tai, Brignot, & Lherminier, 2014).

The mechanisms of pellicle formation are not fully understood. Hydrophobic effects between the cell surface and salivary proteins have been suggested to be a prominent factor in pellicle formation (Gibbins, Yakubov et al., 2014). Surface wettability has also been reported to be involved in the structural organization of pellicle components (Aroonsang, Sotres, El-Schich, Arnebrant, & Lindh, 2014). From a biochemical point of view, cross-linking between salivary components by transglutaminase was demonstrated (Bradway et al., 1992; Gibbins, Yakubov et al., 2014). The involvement of the membrane-bound mucins MUC1 in MUC5B adhesion to cells through direct binding between the two mucins has also been suggested (Gibbins, Yakubov et al., 2014; Offner & Troxler, 2000). A recent study further supported the hypothesis of a role of membrane-bound mucins, by demonstrating that MUC5B could bind to HT29 intestinal cells only when they were induced to secrete the membrane-bound mucins MUC5AC(Gibbins, Proctor, Yakubov, Wilson, & Carpenter, 2015).

MUC1 is a polymorphic membrane-associated glycoprotein (Hanisch & Muller, 2000), expressed in most healthy epithelial tissues. In relation to tissues of the human oral cavity, MUC1 mRNAs were found in salivary glands (Sengupta et al., 2001) but also in epithelial oral cells (Chang, Chang, Kim, Lee, & Kho, 2011). Recently, the protein MUC1 was detected in the superficial part of oral epithelium (Kullaa, Asikainen, Herrala, Ukkonen, & Mikkonen, 2014). Decrease of MUC1 levels in epithelial cells of elderly has been associated to lower mucosal defences in the oral cavity (Chang et al., 2011), supporting its implication in the formation of the mucosal pellicle.

The aim of the present study was to investigate the role of MUC1 in the binding of MUC5B to oral mucosae. We opted for a cell-based model using TR146 cells, which have been shown to be suitable for establishing a model of oral epithelium (Jacobsen, Van Deurs, Pedersen, & Rassing, 1995). TR146 cells were stably transfected in order to over-express MUC1, and adhesion of human salivary MUC5B on either transfected or native cell lines was compared. The resulting models, constituted of epithelial cells lined by a salivary pellicle, were characterized by microscopic approaches

2. Materials and methods

2.1. Saliva collection

The study was performed following the guidelines of the declaration of Helsinki. Written informed consent was obtained from the participants. Saliva was obtained from fifteen volunteers who declared to be in good oral health. Subjects were instructed to refrain from smoking, eating or drinking for at least two hours before saliva collection. Subjects donated saliva for approximately 1 h by spitting out saliva accumulating spontaneously in their mouth into plastic vessels. All samples were pooled and centrifuged at 14 000 g for 20 min at 4 °C. The resulting pool of clarified saliva was aliquoted and immediately frozen at − 80 °C.

2.2. Cell culture

TR146 epithelial cells, derived from a human buccal squamous cell carcinoma (Rupniak et al., 1985), were obtained from the European Collection of Cell Cultures (ECACC, Salisbury, Wiltshire, UK). TR146 cells were routinely grown in DMEM/F12—GlutaMAX medium from Gibco® (1:1, v:v), supplemented with 10% fetal bovine serum (FBS) and 100 units/ml penicillin, 100 μg/ml streptomycin in T75 flasks (all obtained from Life Technologies). Cells were subcultured at 7 days intervals and medium was changed every 2 days. Cells were incubated at 37 °C in a humidified atmosphere containing 7.5% CO_2. Cells were seeded at a density of 4×10^4 cells/cm^2 in 96-well plates for viability assay, in 12-well culture plates for semi-quantification of MUC5B by dot blot, in 8-well culture slides coated with Cell-Tak™ (Corning) for MUC5B and MUC1 immunostaining or on 10 mm diameter glass slips coated with Cell-Tak™ for Scanning Electron Microscopy (SEM) and confocal microscopy. In these conditions, confluence was reached in 48 h and cells formed a multi-layer culture after five days. Cells were grown for five days before depositing clarified saliva at the culture surface.

2.3. Exposure of cells to human saliva: viability assay and formation of a salivary pellicle

At confluence, cells were incubated for 24 h with clarified saliva diluted in growth medium (1:1, v:v). DMSO 50% was used as a positive control of cytotoxic effect. Cytotoxic effect of saliva was assessed using the Neutral Red assay using a fluorimetric method (Rat, Korwinzmijowska, Warnet, & Adolphe, 1994). Briefly, cells were incubated for 3 h at 37 °C with 200 μl of medium containing neutral red at 50 μg/ml, washed twice with PBS that was removed, and then incubated at room temperature for 1 h in neutral red eluent (ethanol:H_2O:acetic acid, 50:49:1) with gentle agitation. Reading of fluorescence was performed with Victor^{3}V microplate reader (PerkinElmer) with excitation and emission wavelengths fixed at 544 nm and 595 nm, respectively. 80% of viability was considered as an indicator of non-cytotoxicity. Assays were performed in triplicates.

A salivary pellicle was deposited onto cells by incubating cell subcultures for 2 h with clarified saliva diluted into growth medium (1:1). After incubation, samples were washed twice with PBS in order to eliminate the non-adsorbed saliva.

2.4. Measurement of the cell multi-layer thickness

Five-day subcultures were stained using LIVE/DEAD® BacLight™ (LifeTechnologies), which stains live cells with Syto 9 and dead cells with propidium iodide. Confocal microscopy was used in order to observe throughout the culture. Pictures were taken from the glass surface to the upper cells' surface with 160 nm steps imaging and were merged in order to obtain an overlay projection, which allowed evaluating the cell model thickness.

2.5. Cell transfection

The vector (pCMV6) carrying the gene of MUC1 variant 2 from OriGene (OriGene Technologies, ref. SC302125) was used. The protein encoded by the gene matches with the isoform Y of the human MUC1 (Uniprot identifier P15941-7). The plasmid was amplified by subcloning in DH5α *Escherichia coli* (Life Technologies) and purified using PureYield™ Plasmid Miniprep System (Promega). Cells were transfected when 80% confluence was reached. FuGENE®-HD (Promega) was used as transfection reagent at a FuGENE®-HD:DNA ratio of 3.0:1 following the manufacturer's instructions. After 48 h, cells were subjected to drug selection in 0.2 mg/ml geneticin (G418 sulfate, LifeTechnologies) for 2–3 weeks. Surviving cell colonies were then picked up and subcloned using cloning rings. Twenty-four clones were expanded stepwise in 96, 24, 6-well plates and screened for gene expression of MUC1

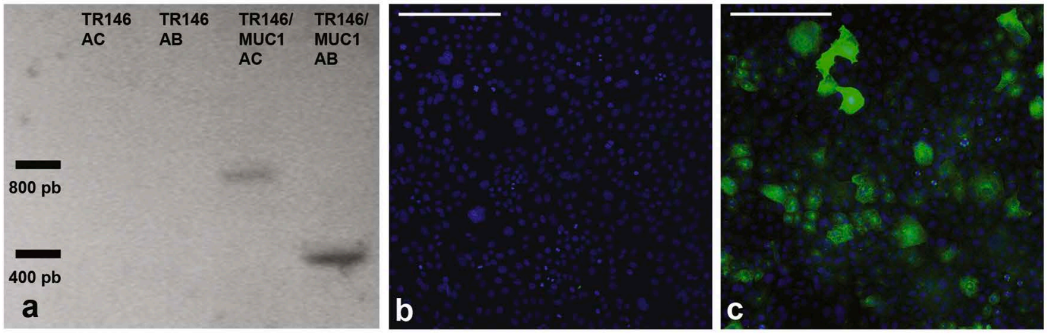

Fig. 1. Over-expression of MUC1 in TR146/MUC1 cells evidenced by (a) RT-PCR in native TR146 cells and transfected TR146/MUC1 cells, (b) and (c) immunostaining of MUC1 on TR146 and TR146/MUC1 transfected cells, respectively. Cell nuclei are stained in blue by DAPI. Scale bars 100 μm. (For interpretation of the references to color in this figure legend, the reader is referred to the web version of this article.)

by RT-PCR. The best stable cell line named TR146/MUC1 was obtained after 55 days of selection and growth.

2.6. Expression of MUC1 by RT-PCR

For preparation of cDNA from the cells, total RNA was extracted from TR146 and TR146/MUC1 confluent cells using RNAeasy Plus Mini Kit (QIAGEN) and quantified using a NanoDrop ND-1000 spectrophotometer (Thermo Scientific). Reverse transcription was performed using Biorad iScript™ cDNA Synthesis Kit on 450 ng of total RNA in a final volume of 10 μl. PCR was performed using Taq PCR Master Mix Kit (QIAGEN) with 2.5 μl of template DNA and 0.2 μM primers in a total reaction volume of 25 μl. The following cycling parameters were applied: 94 °C for 3 min and 30 cycles of amplification (94 °C for 50 s; 60 °C for 50 s and 72 °C for 2 min). Gene specific primers were designed according to standard recommendations with primer design software (Primer-Blast and Vector NTI® software). Two primers pairs were ordered at Eurogentec. A first pair (AB, 5′TGCTTACAGCTACCACAGCC3′ and 5′CCAGACTGGGCAGAGAAAGG3′) was designed in order to hybrid with all MUC1 mRNA forms (cDNA sequence of 436 pb). A second pair (AC, 5′TGCTTACAGCTACCACAGCC3′ and 5′ATTAGGACAAGGCTGGTGGG3′) was designed in order to target specifically insertion sequence MUC1 of 795 bp length specific for *pCMV6-MUC1* construction. Amplified products were resolved by agarose gel electrophoresis (0.8%) at 100 V for 20 min. Gel was stained with ethidium bromide and viewed under UV transilluminator Geldoc 2000 imaging system (Bio-Rad).

2.7. Fluorescence immunostaining of MUC1 and MUC5B

Immunostaining of MUC1 was performed on TR146 and TR146/MUC1 cells without a salivary pellicle. Immunostaining of MUC5B was performed on native or transfected cells with or without a salivary pellicle.

Samples on glass slides were fixed by immersion in cold methanol for 10 min. Non-specific binding was prevented using 0.3% fat-free milk and 5% non-immune goat serum in PBS for

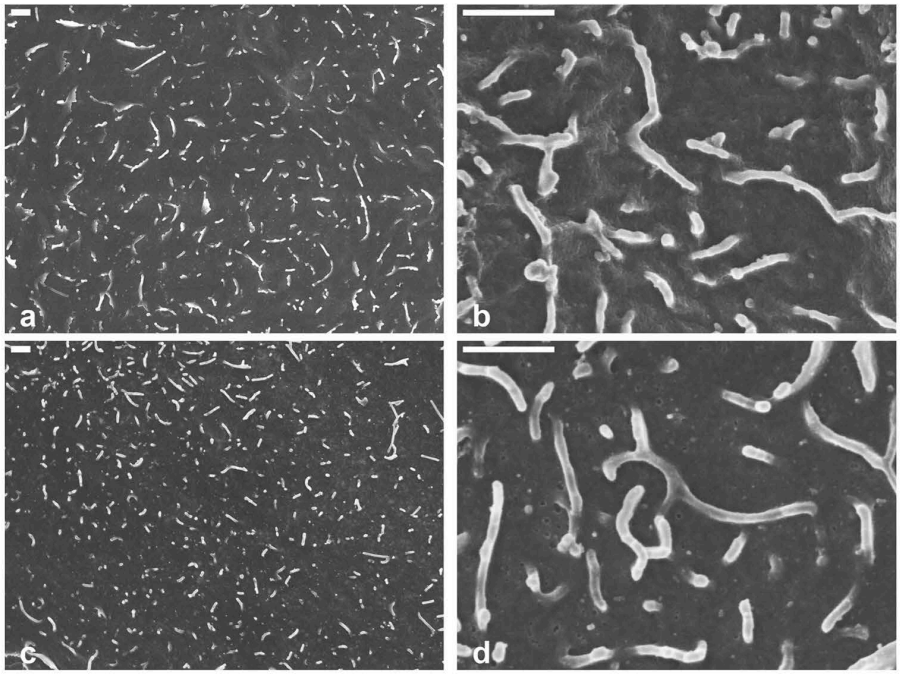

Fig. 2. TR146 (a and b) and TR146/MUC1 (c and d) cells observed by SEM. Scale bars 1 μm.

15 min. For MUC1 immunostaining, a mouse monoclonal anti-MUC1 antibody clone 4A5 (OriGene Technologies) was used (1:200 in PBS, 1 h). For MUC5B immunostaining, a mouse monoclonal anti-MUC5B antibody F2 (kind gift from Prof. Veerman, Free University of Amsterdam) was used (1:25 in PBS, 1.5 h). Negative controls were obtained by omitting primary antibodies in the incubation medium. Alexa 488 Goat anti-mouse IgG (Invitrogen) was used as the secondary antibody (1:400 in PBS, 1 h). The samples were mounted into Prolong Gold antifade reagent with DAPI (Invitrogen). Fluorescence was observed with a Nikon Eclipse E600 microscope (Nikon Instruments) equipped with UV-2A (excitation 330–380 nm, emission 400 nm) and B-2A (excitation 450–490 nm, emission 505 nm) filters. Images were acquired using a Nikon Dxm1200C camera. The Nikon NIS-Br software was used for data acquisition. MUC5B were semi-quantified using ImageJ software on 5 images of either TR146 or TR146/MUC1 samples, extracting the raw integrated density values of the green channel. Results were expressed in arbitrary units (AU). The difference between TR146 and TR146/MUC1 cells was tested by ANOVA.

2.8. Semi-quantification of MUC5B in cellular extracts by Dot-Blot

Dot Blot was performed on lysates of TR146 and TR146/MUC1 cells with a salivary pellicle. Three biological replicates were produced and analysed. Cells were lysed in 150 μl of RIPA buffer (Sigma–Aldrich) and proteins were quantified using the DC protein assay (Bio-Rad). The volume of lysate containing 5 μg of proteins was deposited per well on nitrocellulose membranes, in triplicate for each biological replicate. For detection of MUC5B, the primary antibody F2 (1:400 in PBS, 1 h) and the secondary antibody goat-anti mouse IgG coupled to HRP (LifeTechnologies, 1:2000, 1 h) were used. Non-specific binding was prevented using 0.3% fat-free milk. HRP activation was performed using the Clarity Western ECL Substrate Kit (Bio-Rad). Blot images were acquired using the Chemidoc imaging system (Bio-Rad). Semi-quantification of chemiluminescence detected within boundaries of each dot was performed using the ImageLab software. Results were expressed in arbitrary units (AU). The median values of technical replicates were calculated for each biological replicate, and the difference between TR146 and TR146/MUC1 cells was tested by ANOVA.

2.9. Scanning electron microscopy

Fixation of TR146 cells and TR146/MUC1 cells was carried out with 2.5% glutaraldehyde in PBS for 30 min, followed by 0.4% osmium tetroxide in PBS for 30 min. Dehydration was done through graded baths of ethanol (from 30 to 100%). Drying was performed by the critical point drying (CPD) method using Leica CPD 030. Samples were then coated with a thin carbon layer using a CRESSINGTON 308R and observed with a scanning electron microscope JEOL JSM 7600F (JEOL, Ltd.). SEM was operated at 2 kV and samples were observed at a working distance of 5 mm.

2.10. Immuno-scanning electron microscopy

Fixation of cells was achieved with 4% (v/v) paraformaldehyde for 20 min at 4 °C. Blocking and incubation with the antibody anti-MUC5B were performed as described for fluorescence immunostaining. The primary antibody was detected with 15 nm gold-labeled Goat Anti Mouse (GAM) IgG (Aurion, 1:15 in PBS, 1 h). After immunological reactions, samples were fixed with 2.5% glutaraldehyde in PBS. Finally, samples were dehydrated with ethanol, dried with CPD and carbon coated as described above. Samples were observed with a Hitachi SU5000 Schottky Field Emission—scanning electron microscope and gold particles were detected with a Backscattered Electron (BSE) detector. SEM was operated at 5 kV and samples were observed at a working distance of 8 mm.

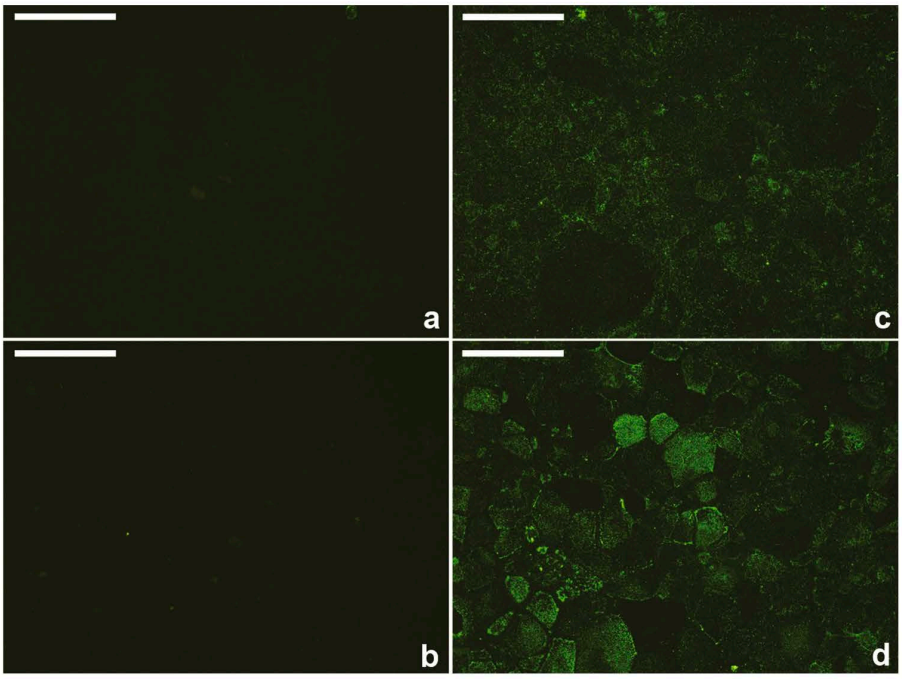

Fig. 3. MUC5B immunostaining of (a) TR146 cells, (b) TR146/MUC1cells, (c) TR146 cells incubated for 2 h with human saliva, (d) TR146/MUC1 cells incubated for 2 h with human saliva. Scale bars 100 μm.

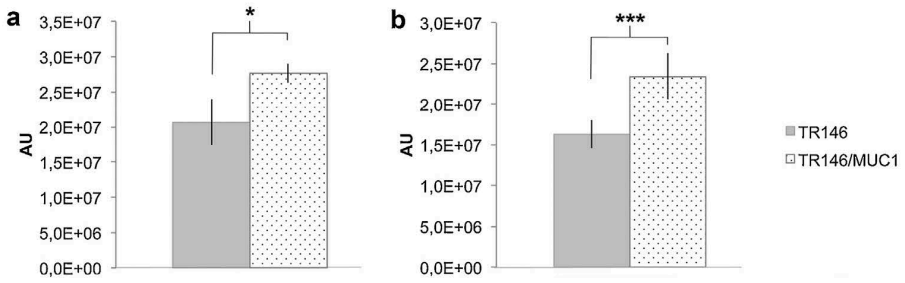

Fig. 4. Semi-quantification (mean ± STD) of MUC5B retained on TR146 and TR146/MUC1 cells after incubation for 2 h with human saliva by Dot-Blot chemiluminescence assay (a) and immunocytochemistry followed by image analysis (b).

3. Results

3.1. Expression of MUC1 in transfected cells

In order to confirm the efficiency of MUC1 transfection, RT-PCR and fluorescence immunostaining of MUC1 were carried on native TR146 cells and transfected TR146/MUC1 cells (Fig. 1). After amplification, the sequences AB and AC measuring 436 and 795 pb respectively were detected only in transfected cells (Fig. 1a), indicating that MUC1 was not detectable at the mRNA level in native cells and that transcription of the recombinant MUC1 gene was efficiently performed in the transfected cells. Compared to TR146 native cells (Fig. 1b), transfected TR146/MUC1 cells showed Alexa fluorescent green staining (Fig. 1c) that confirmed expression of MUC1 membrane-associated mucin at the protein level. Only some cells were stained, probably because superficial cells are not necessarily at the same stage of growth, inducing differences in MUC1 expression or MUC1 integration into the membrane.

3.2. Morphology of TR146 and TR146/MUC1 cells

After five days of growth, *i.e.*, three days after confluence was reached, cells formed a multi-layer culture whose thickness was approximated to 12.7 μm. No dead cells were observed (data not shown).

The cells surface was investigated by SEM and observations are presented in Fig. 2. The cells surface exhibited numerous membrane folds (microplicae) (Fig. 2a and c). These microplicae were clearly visualized at higher magnification (see arrows in Fig. 2b and d). The density and size of microplicae showed some cell-to-cell variability within one culture. However, overall, there was no substantial morphological difference between the two cell types.

3.3. Binding of saliva and MUC5B to TR146 and TR146/MUC1 cells

First, cell viability assays revealed that diluted clarified saliva was not toxic to cells for up to 24 h of exposure. Then, the ability of salivary mucins MUC5B to adsorb onto cells was evaluated by Dot-Blot which was performed on cells lysates, and by fluorescent immunostaining of cells. Fig. 3 shows immunostaining of MUC5B on cells and revealed that, expectedly, no fluorescence was detected in the absence of saliva (Fig. 3a and b). In contrast, MUC5B was detectable after incubation of cells with saliva for 2 h (Fig. 3c and d) on both cell types but not after incubation for 10 min (data not shown). TR146/MUC1 presented a higher fluorescent intensity than TR146, translating a higher amount of salivary MUC5B retained on the cells surface (Fig. 3c and d). Similarly to what was observed for MUC1 staining, clear between-cells variability was observed in the TR146/MUC1 culture while the lining appeared more homogenous in TR146 cells. From a semi-quantitative point of view (Fig. 4), TR146/MUC1 cells showed a significantly higher retention of salivary MUC5B than native TR146 cells indicated both by the Dot-Blot method (+34.1%, $p < 0.05$) and by immunocytochemistry (+44%, $p < 0.001$).

SEM allowed to observe the structure of the salivary deposit (Fig. 5a and b) and revealed that it was made of a loose filamentous network. No major differences were observed between transfected and native cells. Membrane folds were still visible under this network indicating that the saliva deposit was overall thin. However, some thicker and larger aggregates were also observed translating an uneven structure. SEM coupled to immunostaining of MUC5B was carried out (Fig. 5c) and it confirmed that the deposits contained MUC5B. The mesh size was approximated to a maximum of 0.5 μm.

4. Discussion

The objective of the present study was to evaluate the role of MUC1 in the anchoring of MUC5B onto oral epithelial cells, and more generally to obtain a deeper understanding of its involvement in the formation of the mucosal pellicle. Overall, we found that MUC5B binding was quantitatively enhanced when oral epithelial cells expressed MUC1. An in vitro model constituted of

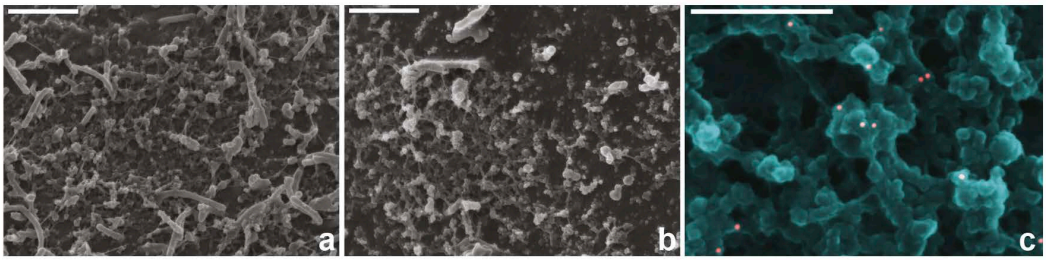

Fig. 5. SEM observations of TR146 (a) and TR146/MUC1 (b) cells, both incubated for 2 h with human saliva (scale bars 1 μm), and immuno-SEM detection of salivary MUC5B on salivary aggregates (scale bars 500 nm). Gold particles are coloured in pink. (For interpretation of the references to color in this figure legend, the reader is referred to the web version of this article.)

epithelial cells lined with a mucosal pellicle is proposed, based on the use of transfected TR146/MUC1 cells.

The experimental choice of using the TR146 cell line was guided by considerations on the structure of membrane-bound mucins and on the morphology of oral cells. Some epithelial cell lines are able to secrete membrane-bound mucins. For example, Gibbins et al. (2015) recently used HT29-MTX intestinal cells, which produce the membrane-bound mucins MUC5AC, to study mucosal pellicle formation. However, MUC5AC mucins can form a layer gel whose thickness varies from approximately 100–300 μm along the gastro-intestinal tract (Pelaseyed et al., 2014), which differs from the situation in the oral cavity where the pellicle thickness has been evaluated to a maximum of 100 nm (Morzel et al., 2014). Moreover, MUC5AC mucins do not possess the MUC1 amino-acid sequence which is thought to interact with MUC5B (Wang et al., 2004). Other human epithelial cell lines naturally express MUC1. MUC1 mRNAs were for example detected in several intestinal cell lines such as Caco-2 (Van Klinken et al., 1996). However, the morphology of intestinal cells differs quite substantially from that of oral cells, for example regarding their shape (columnar *vs* squamous) and the presence of microvilli at the apical surface of intestinal cells. In order to model closely the in vivo surface of oral mucosae, in particular that of soft tissues which represent the largest area in the oral cavity, we therefore opted for a well-characterized non-keratinized cell line, the TR146 cell line. TR146 also exhibits high similarity in terms of permeability with human oral cells (Jacobsen et al., 1995; Teubl et al., 2013). However, experiments performed in the present study indicated that MUC1 were not detectable in TR146 cells at the mRNA or protein level. Therefore, in order to study the involvement of MUC1 in oral mucosal pellicle formation, we stably transfected the TR146 cell line.

In the oral cavity, the thickness of the mucosa can vary from 500 and 800 μm (Wertz & Squier, 1991) with epithelial thickness varying from approximately 100 μm on the floor of the mouth to 300 μm on buccal surfaces (Prestin, Rothschild, Betz, & Kraft, 2012). The present model is thinner than oral epithelium and we suggest that it could represent the upper layer of mucosa, which directly interacts with compounds diluted in saliva. From a morphological point of view, non-keratinized surfaces of cheeks, lips or soft palate are made of cells characterised by membrane folds termed microplicae (Asikainen, Mikkonen, Ruotsalainen, Koistinen, & Kullaa, 2014, Kullaa-Mikkonen, 1986). Such folds were clearly present either on TR146 or on TR146/MUC1 cell membranes. This is particularly interesting knowing that these structures have been described as the basis for mucosal pellicle formation *in vivo*(Asikainen et al., 2012). Overall, SEM observations demonstrate that the morphologies of both types of cells are suitable for a model including a mucosal pellicle layer.

The ability of mucins MUC5B to bind to cells surface was demonstrated in both types of cells, and we showed that adsorption of salivary components to the mucosa is not immediate as indicated by undetectable MUC5B on cells incubated with saliva for 10 min. Furthermore, we noticed that with a longer incubation (24 h of incubation, data not shown), mucins formed dense and patchy aggregates, possibly due to local acidification by the cells. On synthetic surfaces also, time appears to be a determinant factor for mucin retention: MUC5B was detected on silica after 1 h incubation with saliva (Aroonsang et al., 2014) but was not after 20 min (Gibbins, Yakubov et al., 2014). The time used in the present study (2 h) was chosen to be compatible with the in vivo situation since the time of turnover of the superficial layer of oral epithelium was calculated to be 2.7 h (Dawes, 2003).

The specific mechanism of adsorption of MUC5B to oral surfaces is not fully elucidated to date. Some studies have demonstrated that MUC5B are retained better on hydrophobic than hydrophilic surfaces (Aroonsang et al., 2014; Cardenas et al., 2007) suggesting a role of hydrophobic effects. Moreover, the involvement of the membrane bound mucins MUC1 has also been proposed (Gibbins, Yakubov et al., 2014; Offner & Troxler, 2000). For example, Gibbins, Yakubov et al., 2014 and Gibbins, Proctor et al., 2014 pointed out that retention of MUC5B was limited on hydrophobic surfaces, and suggested that MUC1 is essential to pellicle formation. With regards to the possible biochemical interaction between the two mucins, an in vitro assay showed that multiple MUC5B domains could bind to the N-terminal domain of MUC1, especially with the last 107 amino acids (Wang et al., 2004). Here, our results provide an argument in favour of MUC1 implication, since TR146/MUC1 cells retained better MUC5B. Furthermore, the observation of between-cell variability in binding of salivary MUC5B to TR146/MUC1 cells may be correlated to the expression of MUC1 that was also observed to be uneven among the cells. However, bioadhesion of salivary mucins to epithelial cells, even if reduced, also occurred in TR146 cells. Thus the binding of MUC5B to epithelial cells is probably a multimodal process enhanced by the presence of membrane-associated mucins MUC1.

From a structural point of view, the salivary deposits observed by SEM both on TR146 and TR146/MUC1 cells were somehow comparable to the observations of human dried saliva (Teubl et al., 2013) where mucins form a filamentous network. However, the spatial organisation of mucins was different. In particular, the apparent mesh size is smaller in our model (up to 0.5 μm) than in dried saliva (up to 0.9 μm), which may be due to specific interactions of MUC5B with the underlying cell surface. The distribution of MUC5B over the surface of individual cells was comparable to the in vivo situation, where MUC5B appeared clustered on sections of buccal cells sampled on healthy subjects (Morzel et al., 2014). This clustering was all the more visible on TR146/MUC1 cells. In addition, although we did not observe by SEM structural differences of mucins network between TR146 and TR146/MUC1, the higher amount of MUC5B on TR146/MUC1 may have an impact on the pellicle functionality such as its lubricating properties. For example, Pramanik et al. (2010) related the reduction of oral lubrication in dry mouth patients with a lower expression of MUC1. Altogether, the model developed using TR146/MUC1 appeared to mimic more faithfully a healthy physiological situation compared to a TR146-based model.

As any in vitro model, the model presented in this study shows some limitations. First, no dead cells were observed and the nuclei integrity was preserved, which differs from the cell status in the superficial layer of a squamous non-keratinized epithelium previously described (Squier, 1991). Second, the MUC1/Y isoform of MUC1 expressed by TR146/MUC1 is a shorter form of the full-length human membrane-bound mucin that lacks the variable number tandem repeat (VNTR) region (Hanisch & Muller, 2000). Although the function of this region is not clearly described in epithelial oral cells, a correlation between its length and lubrication has been reported in eye epithelium (Imbert et al., 2006). The expression of MUC1 as a single isoform may therefore be a limitation to this model. Nevertheless, the model also presents several advantages. First, compared to synthetic surfaces, a cell-based model ensures that surface properties (*e.g.*, hydrophobicity, wettability, topography) are close to those found on oral mucosa and that salivary proteins can adopt a realistic spatial conformation. Second, it allows studying the biochemical interactions between cell membrane constituents and exogenous molecules, which would not be possible with a synthetic surface. Considering now cell-based models, to our knowledge, only one model based on oral cell cultures had previously taken into account the presence of a mucus layer lining the cells (Teubl et al., 2013). In that model, the mucus layer was dried prior to being deposited onto cells, which may affect its physico-chemical properties. In addition,

the mucus layer measured between 120 and 150 μm, *i.e.*, much thicker than the mucosal pellicle. In contrast, the present model is suitable to focus on the function and properties of the mucosal pellicle, especially since our model takes into consideration the expression of the membrane-bound MUC1, which enhanced the anchoring of MUC5B.

To conclude, the main advantage of the present model is to include a mucosal pellicle, *i.e.*, the layer at the interface between the oral epithelium and saliva. Its physico-chemical properties can control different mechanisms such as adsorption onto or diffusion through the mucosa. Therefore, this model is a promising tool to investigate molecular phenomena occurring at the surface of oral mucosae. As a perspective of this work, this model will be used to study the complex molecular interactions between flavour compounds, epithelial cells and the mucosal pellicle.

Acnowledgements

Prof Veerman (Free university of Amsterdam) is gratefully acknowledged for providing the MUC5B F2 antibody. The authors thank Christine Arnould (INRA, UMR1347 Agroécologie, ERL CNRS 6300, Plateforme DImaCell, Centre de Microscopie INRA/Université de Bourgogne) for confocal microscopy observations and Frédéric Herbst (Institut Carnot de Bourgogne, Université de Bourgogne) for training and assistance in SEM experiments. Hitachi High-Technologies Europe (Roland Schmidt) and Elexience (Thierry Grenut) are acknowledged for obtaining SEM images. Franck Ménétrier and Claire Fenech (Centre des Sciences du GoÛt et de l'Alimentation) are thanked for advice on sample preparation prior to microscopy and on RT-PCR, respectively. This study was funded by the French National Research Agency (Grant ANR-10-ALIA-001 MUFFIN). The French Ministry of Higher Education and Research provided the PhD fellowship for Sarah Ployon.

References

Aroonsang, W., Sotres, J., El-Schich, Z., Arnebrant, T., & Lindh, L. (2014). Influence of substratum hydrophobicity on salivary pellicles: organization or composition? *Biofouling*, *30*(9), 1123–1132.

Asikainen, P., Mikkonen, J. J., Ruotsalainen, T. J., Koistinen, A. P., & Kullaa, A. M. (2014). Microstructure of the superficial epithelial cells of the human oral mucosa. *Ultrastructural Pathology*, *38*(1), 6–12.

Asikainen, P., Ruotsalainen, T. J., Mikkonen, J. J. W., Koistinen, A., ten Bruggenkate, C., & Kullaa, A. M. (2012). The defence architecture of the superficial cells of the oral mucosa. *Medical Hypotheses*, *78*(6), 790–792.

Boegh, M., & Nielsen, H. M. (2015). Mucus as a barrier to drug delivery – understanding and mimicking the barrier properties. *Basic & Clinical Pharmacology & Toxicology*, *116*(3), 179–186.

Bradway, S. D., Bergey, E. J., Jones, P. C., & Levine, M. J. (1989). Oral mucosal pellicle: adsorption and transpeptidation of salivary components to buccal epithelial cells. *Biochemical Journal*, *261*(3), 887–896.

Bradway, S. D., Bergey, E. J., Scannapieco, F. A., Ramasubbu, N., Zawacki, S., & Levine, M. J. (1992). Formation of salivary mucosal pellicle: the role of transglutaminase. *Biochemical Journal*, *284*, 557–564.

Cardenas, M., Elofsson, U., & Lindh, L. (2007). Salivary mucin MUC5B could be an important component of in vitro pellicles of human saliva: an in situ ellipsometry and atomic force microscopy study. *Biomacromolecules*, *8*(4), 1149–1156.

Chang, W.-L., Chang, J.-Y., Kim, Y.-Y., Lee, G., & Kho, H.-S. (2011). MUC1 expression in the oral mucosal epithelial cells of the elderly. *Archives of Oral Biology*, *56*(9), 885–890.

Dawes, C. (2003). Estimates, from salivary analyses, of the turnover time of the oral mucosal epithelium in humans and the number of bacteria in an edentulous mouth. *Archives of Oral Biology*, *48*(5), 329–336.

Gibbins, H. L., Proctor, G. B., Yakubov, G. E., Wilson, S., & Carpenter, G. H. (2014). Concentration of salivary protective proteins within the bound oral mucosal pellicle. *Oral Diseases*, *20*(7), 707–713.

Gibbins, H. L., Proctor, G. B., Yakubov, G. E., Wilson, S., & Carpenter, G. H. (2015). SIgA binding to mucosal surfaces is mediated by mucin–mucin interactions. *PLoS One*, *10*(3), 13. http://dx.doi.org/10.1371/journal.pone.0119677.

Gibbins, H. L., Yakubov, G. E., Proctor, G. B., Wilson, S., & Carpenter, G. H. (2014). What interactions drive the salivary mucosal pellicle formation? *Colloids and Surfaces B-Biointerfaces*, *120*, 184–192.

Hanisch, F. G., & Muller, S. (2000). MUC1: the polymorphic appearance of a human mucin. *Glycobiology*, *10*(5), 439–449.

Hannig, M., & Joiner, A. (2006). The structure, function and properties of the acquired pellicle. *Monographs in Oral Science*, *19*, 29–64.

Hay, D. I. (1967). The adsorption of salivary proteins by hydroxyapatite and enamel. *Archives of Oral Biology*, *12*(8), 937–946.

Imbert, Y., Darling, D. S., Jumblatt, M. M., Foulks, G. N., Couzin, E. G., Steele, P. S., et al. (2006). MUC1 splice variants in human ocular surface tissues: possible differences between dry eye patients and normal controls. *Experimental Eye Research*, *83*(3), 493–501.

Jacobsen, J., Van Deurs, B., Pedersen, M., & Rassing, M. R. (1995). TR146 cells grown on filters as a model for human buccal epithelium: I. Morphology, growth, barrier properties, and permeability. *International Journal of Pharmaceutics*, *125*(2), 165–184.

Kullaa, A. M., Asikainen, P., Herrala, M., Ukkonen, H., & Mikkonen, J. J. W. (2014). Microstructure of Oral Epithelial Cells as an Underlying Basis for Salivary Mucosal Pellicle. *Ultrastructural Pathology*, *38*(6), 382–386.

Kullaa-Mikkonen, A. (1986). Scanning electron microscopic study of surface of human oral mucosa. *European Journal of Oral Sciences*, *94*(1), 50–56.

Morzel, M., Tai, S., Brignot, H., & Lherminier, J. (2014). Immunocytological detection of salivary mucins (MUC5B) on the mucosal pellicle lining human epithelial buccal cells. *Microscopy Research and Technique*, *77*(6), 453–457.

Nayak, A., & Carpenter, G. H. (2008). A physiological model of tea-induced astringency. *Physiology & Behavior*, *95*(3), 290–294.

Offner, G. D., & Troxler, R. F. (2000). Heterogeneity of high-molecular-weight human salivary mucins. *Advances in Dental Research*, *14*, 69–75.

Pelaseyed, T., Bergstrom, J. H., Gustafsson, J. K., Ermund, A., Birchenough, G. M. H., Schutte, A., et al. (2014). The mucus and mucins of the goblet cells and enterocytes provide the first defense line of the gastrointestinal tract and interact with the immune system. *Immunological Reviews*, *260*(1), 8–20.

Pramanik, R., Osailan, S. M., Challacombe, S. J., Urquhart, D., & Proctor, G. B. (2010). Protein and mucin retention on oral mucosal surfaces in dry mouth patients. *European Journal of Oral Sciences*, *118*(3), 245–253.

Prestin, S., Rothschild, S. I., Betz, C. S., & Kraft, M. (2012). Measurement of epithelial thickness within the oral cavity using optical coherence tomography. *Head and Neck-Journal for the Sciences and Specialties of the Head and Neck*, *34*(12), 1777–1781.

Rat, P., Korwinzmijowska, C., Warnet, J. M., & Adolphe, M. (1994). New in-vitro fluorimetric microtitration assays for toxicological screening of drugs. *Cell Biology and Toxicology*, *10*(5–6), 329–337.

Rupniak, H. T., Rowlatt, C., Lane, E. B., Steele, J. G., Trejdosiewicz, L. K., Laskiewicz, B., et al. (1985). Characteristics of 4 new human cell lines derived from squamous cell carcinomas of the head and neck. *Journal of the National Cancer Institute*, *75*(4), 621–635.

Sengupta, A., Valdramidou, D., Huntley, S., Hicks, S. J., Carrington, S. D., & Corfield, A. P. (2001). Distribution of MUC1 in the normal human oral cavity is localized to the ducts of minor salivary glands. *Archives of Oral Biology*, *46*(6), 529–538.

Squier, C. A. (1991). The permeability of oral mucosa. *Critical Reviews in Oral Biology and Medicine*, *2*(1), 13–32.

Tabak, L. A., Levine, M. J., Mandel, I. D., & Ellison, S. A. (1982). Role of salivary mucins in the protection of the oral cavity. *Journal of Oral Pathology & Medicine*, *11*(1), 1–17.

Teubl, B. J., Absenger, M., Froehlich, E., Leitinger, G., Zimmer, A., & Roblegg, E. (2013). The oral cavity as a biological barrier system: design of an advanced buccal in vitro permeability model. *European Journal of Pharmaceutics and Biopharmaceutics*, *84*(2), 386–393.

Van Klinken, B. J. W., Oussoren, E., Weenink, J. J., Strous, G. J., Buller, H. A., Dekker, J., & Einerhand, A. W. C. (1996). The human intestinal cell lines Caco-2 and LS174T as models to study cell-type specific mucin expression. *Glycoconjugate Journal*, *13*(5), 757–768.

Wang, L., Li, X., Bruno, L., Oppenheim, F. G., Troxler, R. F., & Offner, G. D. (2004). MUC1 and MUC5B can form a protective mucin scaffold. *Paper presented at the international association for dental research annual meeting*, Hawai Convention Center, Honolulu.

Wertz, P. W., & Squier, C. A. (1991). Cellular and molecular basis of barrier function in oral epithelium. *Critical Reviews in Therapeutic Drug Carrier Systems*, *8*(3), 237–269.

Publication n°2: Nano-imaging of the physical surface properties of human buccal cells and changes induced by saliva.

Aybeke, E. N.; Ployon, S.; Brulé, M.; De Fonseca, B.; Bourillot, E.; Morzel, M.; Lesniewska, E.; Canon, F.,

Langmuir 2019, *on line*.

LANGMUIR Article
Cite This: Langmuir XXXX, XXX, XXX−XXX
pubs.acs.org/Langmuir

Nanoscale Mapping of the Physical Surface Properties of Human Buccal Cells and Changes Induced by Saliva

Ece Neslihan Aybeke,[†] Sarah Ployon,[†] Marine Brulé,[†] Brice De Fonseca,[‡] Eric Bourillot,[‡] Martine Morzel,[†] Eric Lesniewska,[‡] and Francis Canon*[,†]

[†]Centre des Sciences du Goût et de l'Alimentation, AgroSup Dijon, CNRS, INRA, Université de Bourgogne Franche-Comté, Dijon F-21000, France

[‡]ICB UMR CNRS 6303, Université de Bourgogne Franche-Comté, Dijon F-21078, France

Supporting Information

ABSTRACT: The mucosal pellicle, also called salivary pellicle, is a thin biological layer made of salivary and epithelial constituents, lining oral mucosae. It contributes to their protection against microbiological, chemical, or mechanical insults. Pellicle formation depends on the cells' surface properties, and in turn the pellicle deeply modifies such properties. It has been reported that the expression of the transmembrane mucin MUC1 in oral epithelial cells improves the formation of the mucosal pellicle. Here, we describe an approach combining classical and functionalized tip atomic force microscopy and scanning microwave microscopy to characterize how MUC1 induces changes in buccal cells' morphology, hydrophobicity, and electric properties to elucidate the physicochemical mechanisms involved in the enhancement of the anchoring of salivary proteins. We show that MUC1 expression did not modify drastically the morphology of the epithelial cells' surface. MUC1 expression, however, resulted in the presence of more hydrophobic and more charged areas at the cell surface. The presence of salivary proteins decreased the highest attractive and repulsive forces recorded between the cell surface and a functionalized hydrophobic atomic force microscopy (AFM) tip, suggesting that the most hydrophobic and charged areas participate in the binding of salivary proteins. The cells' dielectric properties were altered by both MUC1 expression and the presence of a mucosal pellicle. We finally show that in the absence of MUC1, the pellicle appeared as a distinct layer poorly interacting with the cells' surface. This integrative AFM/scanning microwave microscopy approach may usefully describe the surface properties of various cell types, with relevance to the bioadhesion or biomimetics fields.

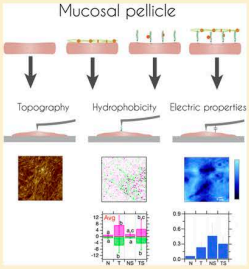

INTRODUCTION

Mucosal surfaces, which line various body cavities (eye, mouth, nose, vagina, etc.) or internal organs (lungs, stomach, gut, etc.), represent the first line of defense against invading pathogens and xenobiotics. They also ensure protection against mechanical wear and dehydration through their lubricating properties. These functions are partly fulfilled by a mucous layer covering the often mucin-secreting epithelial cells. The situation differs slightly for the mucosal surfaces of the oral cavity, where epithelial cells are lined by a thin biological layer, up to 100 nm high, made of both epithelial and salivary constituents. This biological structure termed the mucosal or salivary pellicle is constituted through selective adsorption of salivary proteins (MUC5B, MUC7, sIgA, etc.) onto the cell's surface.[1] Among these, the heavily glycosylated mucins MUC5B are prominently involved in the lubricating and hydrating properties of the pellicle.[2] Adsorption of MUC5B and other salivary proteins to the cells' surface is suggested to occur mainly through noncovalent interactions (in particular hydrophobic effect).[3] We have also shown that the presence of the transmembrane mucin MUC1 enhances anchoring of MUC5B onto the cell's surface,[4] suggesting that protein−protein interactions between MUC1 and salivary proteins are also involved in the mucosal pellicle formation. Cross-linking between salivary proteins mediated by transglutaminase further consolidates the architecture of the pellicle.[1a]

Oral mucosal surfaces play a role in the perception of food sensory attributes, in particular, astringency or aroma persistence. For both sensations, the suggested mechanism by which the oral surface intervenes relies on the ability of the cell surface and mucosal pellicle constituents to interact noncovalently with tannins[5] or aroma compounds.[6] Noncovalent interactions can be of different natures (hydrophobic effect, electrostatic interactions, van der Waals forces, or π-effects) depending on the structure and physicochemical properties of the partners.

Therefore, determining the physicochemical characteristics of epithelial cells and mucosal surfaces may help understand further the nature of noncovalent interactions involved both in the anchoring of salivary proteins forming the mucosal pellicle and in flavor perception. More generally, such information would be of great importance to gain deeper knowledge on the phenomenon of bioadhesion on oral soft surfaces.

To study in vitro biological events involving the mucosal surface, we have recently developed a cellular model of oral

Received: June 28, 2019
Revised: August 14, 2019
Published: August 25, 2019

DOI: 10.1021/acs.langmuir.9b01979
Langmuir XXXX, XXX, XXX−XXX

mucosa surmounted by a mucosal pellicle. The model is based on the use of TR146 cells, which have been stably transfected to express the transmembrane mucin MUC1, incubated with human saliva. We have demonstrated that MUC1 expression increases by 30% the anchoring of salivary MUC5B at its surface.[4] This model proved useful to study the structural alterations of the mucosal pellicle induced by tannins.[5b]

Atomic force microscopy (AFM) is a very high-resolution type of scanning probe microscopy which allows investigating with subnanometer-resolution capacity the morphology and physicochemical properties of biological samples in their physiological environment. The AFM technique consists of scanning the surface of a sample by a sharp tip and recording the interatomic forces between the sample and the tip. AFM can be applied to a variety of biological samples such as protein assemblies,[7] viruses,[8] or live eukaryotic cells.[9] Functionalization of AFM tips with a ligand enables probing specific interactions such as antibody−antigen or DNA−protein interactions.[10] Another AFM technique, termed scanning microwave microscopy (SMM), combines the electromagnetic measurement capabilities of a microwave vector network analyzer (VNA) with the resolution power of AFM. Our laboratory has developed a network analyzer giving access to several frequencies in the range 0.1−16 GHz.[11] The signal characterizes the local conductance and dielectric properties of the sample, enabling to perform three-dimensional tomographic investigations on the electric properties of a sample. While the dielectric properties of a medium determine the strength of interactions between charged species, the dielectric properties of a surface provide indications on its ability to establish electrostatic forces. Moreover, as the dielectric microenvironments are complex and variable, SMM will provide an overview of its spatial variation both horizontally and vertically.

Here, we report an integrative approach combining classical AFM, force spectroscopy, and SMM to identify the physicochemical mechanisms involved in the formation of the mucosal pellicle and characterize the influence of biological supramolecular structures (the transmembrane mucins and/or the mucosal pellicle) present at the cell surface on its physicochemical properties. While classical AFM discriminated the structures present on the cell surface, functionalization of the probe's tip allowed evaluating the hydrophobicity of cell's surface. In parallel, the electric properties of the cell's surface were explored at resonance frequencies of 2, 4.3, and 8.6 GHz by the SMM device. The thorough description of the physicochemical properties of the cell surface and how they are affected by the presence of mucin and salivary proteins will provide new insights into the mechanisms at the origin of bioadhesion on the soft surfaces of the oral cavity. Bioadhesion is crucial to maintain a healthy and comfortable hydrated mouth feeling. Any new knowledge in this field may lead to innovations in, for example, the development of oral hygiene products or saliva substitutes for patients suffering from dry mouth.

■ EXPERIMENTAL SECTION

Saliva Collection. The study was performed in agreement with the guidelines of the Declaration of Helsinki. Informed consent was obtained from the subjects who donated saliva. Unstimulated saliva was collected from 17 volunteers who declared to be in good oral health. The volunteers were instructed to refrain from smoking, eating, and drinking for at least 2 h before the collection sessions. The collection sessions lasted 30 min, during which volunteers spat out the saliva accumulating naturally in their mouth into plastic vessels kept on ice. All samples were pooled and centrifuged at 14 000*g* for 20 min at 4 °C. The clarified saliva was aliquoted and frozen at −80 °C.

Cell Culture. The native (TR146) and transfected (TR146/MUC1) epithelial cells were routinely grown according to the protocol described previously.[4] The cells were seeded at 4×10^4 cells/mL density on Cell-Tak-coated glass cover slips (Agar Scientific). The cells were incubated at 37 °C in a humidified atmosphere containing 7.5% CO_2 for 2 days to reach confluence. The confluent cultures were incubated with clarified saliva for 2 h and then washed twice with phosphate-buffered saline (PBS, pH 7.0−7.3, Gibco) to eliminate unbound saliva. Fixation of cells was carried out with 2.5% glutaraldehyde (Sigma-Aldrich) in PBS (pH 7.8 ± 0.2, Bio-RAD) for 30 min, followed by rinsing with PBS. AFM imaging (topography and tip−sample force measurements) was performed in liquid PBS medium. SMM analysis was performed on samples processed as above and further dehydrated through graded baths of ethanol (from 30 to 100%). Drying was performed by the critical point drying method using a Leica CPD 030.

AFM Imaging. AFM characterizations were performed using a Multimode 8 AFM microscope (Bruker, Santa Barbara, CA). The topographic features of cells without and with a mucosal pellicle were investigated using silicon nitride probes (ScanAsyst Air HR, k = 0.4 N/m and f = 70 kHz, Bruker). The topographic images were acquired at high resolution (512 × 512 pixel^2) using Peak force mode. In the Peak force mode, the AFM tip oscillates at a frequency of 2 kHz with an amplitude of 20 nm. This mode is well adapted for imaging soft and delicate samples such as cells at high resolution.

Tip−Sample Force Measurements. Gold-coated AFM probes were functionalized with hydrophobic self-assembled monolayers (SAMs) using alkanethiols. Forming an SAMs assembly on gold surfaces is a well-controlled process with many practical advantages.[12] The SH groups of alkanethiols have a high affinity on gold substrates[13] via chemical binding, and they can remain stable for days to weeks after their formation.[12] Gold-coated cantilevers, with the nominal spring constant of 0.12 N/m and the nominal resonance frequency of 23 kHz, were purchased from Bruker (NPG-10, Santa Barbara, CA). The self-assembled monolayers were formed on the gold-coated cantilevers according to a previous procedure.[14] Gold-coated cantilevers were immersed in 1 mM solutions of alkanethiols terminated with CH_3 (1-octadecanethiol, Sigma-Aldrich) for 18 h. First, a Teflon substrate (Sigma-Aldrich) was scanned to verify the AFM tip functionalization. Second, the adhesion forces between the functionalized tips and cells were measured using contact imaging mode. AFM enables to probe the forces between the tip and the sample by monitoring the deflection of the cantilever when it approaches, contacts, and retracts from a surface. The contact imaging mode records a force curve for each contact point of tip in function of the approach—retract curves providing information about the elasticity and adhesion. The tip−sample adhesion forces were measured on a 5 × 5 μm^2 area on the cell surface by taking into account 256 × 256 contact points. Images were acquired from four different glass slides per condition (N, NS, T, TS).

Statistical Analysis for Tip−Sample Force Measurements. To determine the characteristic adhesion forces between each sample and the hydrophobic tip, a total of 65 536 force curves were recorded per sample. For each image, cumulated attractive and repulsive forces were plotted against the force intensity. The D25, D50, and D75, which correspond to the force intensities at 25, 50, and 75% of the cumulated force, were extracted. The average attractive and repulsive forces were also extracted. The impact of the sample type on such data was tested using one-way analysis of variance (ANOVA). When a significant difference was observed ($p < 0.05$), the means were compared using a Tukey pairwise comparison test (significance level set at 5%).

SMM Imaging. Scanning microwave microscopy combines the use of atomic force microscopy with a vector network analyzer (VNA). This configuration offers simultaneous measurement of the topography and complex reflection coefficient of a sample with high

DOI: 10.1021/acs.langmuir.9b01979
Langmuir XXXX, XXX, XXX−XXX

sensitivity. The VNA can generate microwaves in the high-frequency range. The incident microwave signal is transmitted through a resonant circuit to a conductive probe. The conductive probe enables to transmit and receive microwaves from the contact point on sample. The applied microwave penetrates into the sample and a part of the signal is reflected back through the cantilever. The VNA detects the reflected signal (alternatively transmitted signal) in the reflection mode and thereby measures the complex reflection coefficient (S_{11}) of the contact point. The measured S_{11} value represents the local impedance resulting from the tip−sample interactions. The amplitude and phase of the S_{11} signal are recorded for each contact point simultaneously with topographic data of the sample.

We have performed SMM analysis using a commercial AFM (Keysight 5600LS, Agilent Technologies) equipped with a vector network analyzer (VNA N5230A, Agilent Technologies). The VNA can generate microwaves ranging from 800 MHz to 13 GHz and detects the reflected signal from the sample. Topography, VNA phase, and VNA amplitude images of the samples were recorded using contact mode in ambient conditions. The surfaces of samples were scanned via a platinum−iridium-coated tip with a nominal radius of 20 nm (SCM-PIT, k = 2.8 N/m and f_0 = 75 kHz, Bruker) at 50 μm scan size with a 1 Hz scan rate. Each sample was analyzed at three frequencies (2, 4.3, and 8.6 GHz). Images were acquired from four different glass slides per condition (N, NS, T, TS).

Statistical Analysis of SMM Images. A total of 174 SMM images were used for statistical analysis: the number of images at each frequency (2, 4.3, and 8.6 GHz) was, respectively, 12, 12, and 10 for native cells (N); 9, 10, and 9 for native cells with a salivary (mucosal) pellicle (NS); 17, 20, and 16 for transfected TR146/MUC1 cells (T); and 19, 19, and 21 for transfected cells with a salivary pellicle (TS). The mean values of each amplitude and phase image were obtained using AFM software.[15] One-way ANOVA was performed to evaluate at each frequency the impact of MUC1 and the mucosal pellicle on the mean amplitude and phase SMM values.

Impedance Images. The complex reflection coefficient was converted into complex impedance data using a Matlab script. The reflection coefficient S_{11} was measured in the reflection mode. In this way, a ratio of the incident/reflected electromagnetic waves was recorded by the VNA. The microwave images (amplitude and phase signals) are induced by interaction variations between the tip and the sample at every contact point, traducing local changes of the constituted equivalent electrical circuit. These local changes give access to nanoscale electrical impedance values of the sample, called device under test (DUT).

Impedance is a complex number with strong frequency dependence. A simple method to measure impedance at microwave frequencies is to connect the DUT (here biological sample) of unknown impedance to the end of a coaxial line (here the AFM tip). The other end of the coaxial line is linked to the VNA, the microwave source. Thus, the SMM measurement allows to calculate the corresponding real and imaginary impedance components by first expressing the real and imaginary parts of the reflection coefficient as follows

$$\Gamma_r = \left|\Gamma_L\right| \cos\left(\phi \frac{\pi}{180}\right) \tag{1}$$

$$\Gamma_i = \left|\Gamma_L\right| \sin\left(\phi \frac{\pi}{180}\right) \tag{2}$$

with ϕ the measured phase and $|\Gamma_L|$ the modulus of the measured amplitude variation of the reflection coefficient expressed as

$$|\Gamma_L| = 10^{(S_{11}/20)} \tag{3}$$

Unknown impedance reflects a part of the microwave signal. Thus, the amount of reflected signal from the DUT, Γ_L, is directly dependent on the degree of mismatch between the microwave source characteristic impedance, Z_0 (a real industry normalized value of 50 Ω), and the DUT impedance. Its expression can be noted as follows

$$\Gamma_L = \frac{V_{refl}}{V_{inc}} = \frac{Z_L - Z_0}{Z_L + Z_0} = \Gamma_r + j\Gamma_i \tag{4}$$

where Z_L is the unknown impedance of the DUT.

By setting Z_0 to 50 Ω, we can then define normalized load impedance by

$$Z = \frac{Z_L}{Z_0} = \frac{R + jX}{Z_0} = r + jx \tag{5}$$

With this simplification, we can rewrite the reflection coefficient formula as

$$\Gamma_L = \Gamma_r + j\Gamma_i = \frac{Z_L - Z_0}{Z_L + Z_0} = \frac{(Z_L - Z_0)/Z_0}{(Z_L + Z_0)/Z_0} = \frac{Z - 1}{Z + 1} = \frac{r + jx - 1}{r + jx + 1} \tag{6}$$

and express the normalized load impedance as

$$Z = r + jx = \frac{1 + \Gamma_L}{1 - \Gamma_L} = \frac{1 + \Gamma_r + j\Gamma_i}{1 - \Gamma_r + j\Gamma_i} \tag{7}$$

By setting the real and the imaginary parts of Z, two independent relationships are obtained

$$r = \frac{1 - \Gamma_r^2 - \Gamma_i^2}{(1 - \Gamma_r)^2 + \Gamma_i^2} \tag{8}$$

$$x = \frac{2\Gamma_i}{(1 - \Gamma_r)^2 + \Gamma_i^2} \tag{9}$$

where r, the real part of the impedance, translates a resistance (Ω) of the DUT and x, the imaginary part, is the reactance of the DUT (Ω).

As the sensitivity of the reflection coefficient Γ_L to impedance r rapidly decreases for very high impedances (r > 10 kΩ for $|\Gamma_L| > 0.99$) and for very low impedances (r < 250 mΩ for $|\Gamma_L| < -0.99$), the imaging frequencies are chosen according to their matching degree with the microwave source to avoid losses in reflection coefficient sensitivity.

In this article, images representing the variation of the real part of the impedance of the DUT are presented as qualitative measurements (one representative image per condition at 8.6 GHz).

Data Availability. The data supporting the findings of this study are available from the corresponding author upon reasonable request.

RESULTS AND DISCUSSION

Morphology of Human Oral Epithelial Cells. Figure 1 presents the retention of the salivary mucins MUC5B on human buccal TR146 native cells (Figure 1b) and on TR146/MUC1 transfected cells (Figure 1c) and the topography of native and transfected cells without or with a mucosal pellicle imaged by AFM (Figure 1a,d−h). As previously reported,[4] the expression of MUC1 in transfected cells enhanced the retention of salivary mucins MUC5B. MUC5B immunostaining showed larger between-cell variability in transfected cells. Cells had a rather flat shape (Figure 1a) with an apex in height in the range of 1−2 μm. There was no substantial difference in the morphological features of native and transfected cells (Figure 1d,e). Membrane folds (microplicae), a few hundreds of nanometers high, were visible on both types of cells. They varied in size and density as previously observed by scanning electron microscopy.[4] Microplicae are typical of squamous epithelial surfaces,[16] where they increase the exchange surface between cells and the external medium, saliva here, with effects on drug absorption, for example. They may also enhance mucus retention, thereby preventing infections.[16]

DOI: 10.1021/acs.langmuir.9b01979
Langmuir XXXX, XXX, XXX−XXX

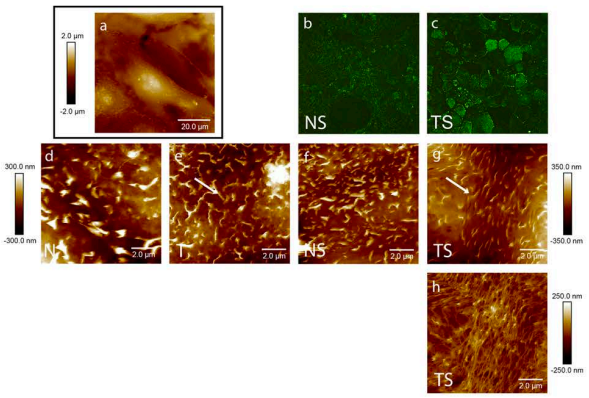

Figure 1. Retention of salivary mucins and topography of human epithelial buccal cells. Immunostaining of MUC5B bound at the cell surface of native TR146 cells (b) and transfected TR146/MUC1 cells (c). Typical topographical image of epithelial cells (here are presented TR146/MUC1 cells) (a). Topography of TR146 native cells (d), TR146/MUC1 transfected cells (e), native cells with a mucosal pellicle (f), and transfected cells with a mucosal pellicle (g, h).

The overall appearance of the cell surface was not drastically modified by the presence of a mucosal pellicle on native cells (Figure 1f). It was not possible to determine precisely its thickness because of the uneven cells' topography. However, microplicae remained distinguishable under the pellicle, as previously found,[5b] indicating that only a very thin layer was deposited on the cell surface. This is also consistent with former measurements of the pellicle's thickness (0−100 nm) on human buccal cells.[17] On transfected cells, the same conclusions applied to most acquired images (Figure 1g), although a fine filamentous network was also occasionally observed (Figure 1h). AFM imaging provided a detailed topographic picture of this fragile structure in liquid medium. This network resembles the filamentous structure observed by cryoscanning electron microscopy in submandibular/sublingual saliva, which was interpreted as a mucin network.[18] It is also comparable to a MUC5B network formed on mica observed by AFM.[5a] This distinctive appearance of some TR146/MUC1 cells can be related to the heterogeneous retention of MUC5B (Figure 1c): it is likely that such a salivary network would form specifically on cells retaining most strongly MUC5B mucins.

Impact of a Mucosal Pellicle on the Hydrophobicity of Epithelial Cells. Chemical force microscopy (CFM) with hydrophobic tip has been previously successfully used to perform direct measurements of hydrophobic forces at the cell surfaces.[19] To investigate the impact of a mucosal pellicle on cells' hydrophobicity, we applied CFM with hydrophobic functionalized gold AFM tips to monitor interactions in liquid medium at the cell surface (Figure 2). Tips were functionalized with alkanethiols terminated with CH_3, as previously reported[14] and checked on hydrophobic Teflon (Supporting Information Figure S1): a greater adhesion force was observed with the functionalized tip. Then, the cell surface was scanned, leading to adhesion force mapping. Figure 2a shows a representative map of adhesion force for the four tested conditions. It reveals that there were both attractive (negative values) and repulsive (positive values) forces between the functionalized tip and the cell surface, with large differences among conditions. Pictures of native TR146 cells without (N) or with a mucosal pellicle (NS) were very similar, with

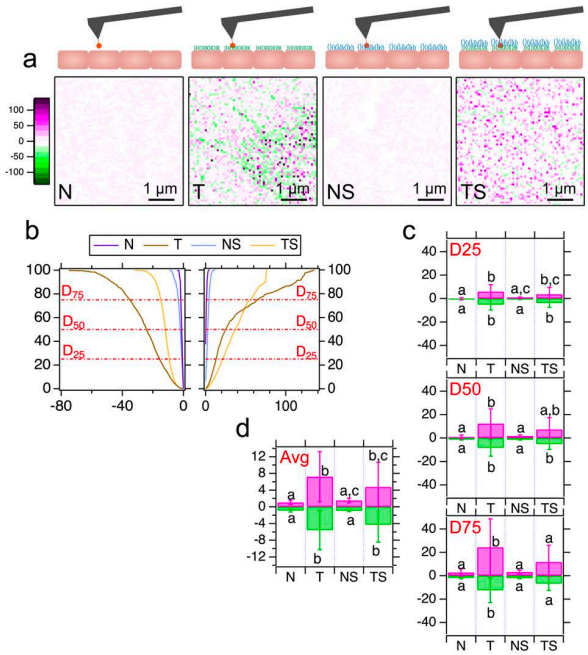

Figure 2. Hydrophobicity of human epithelial buccal cells. (a) Schematic illustration of sample−tip interactions and the corresponding adhesion force maps for TR146 native cells (N), TR146/MUC1 transfected cells (T), native cells with a mucosal pellicle (NS), and transfected cells with a mucosal pellicle (TS). (b) Cumulated attractive (left) and repulsive (right) force curves as a function of force intensity. (c) Means of the D75, D50, and D25 positive and negative values. (d) Means of the average values of repulsive and attractive forces. All forces are expressed in nN.

attractive and repulsive forces at low intensities. Conversely, much higher intensities (both for positive and for negative forces) were recorded on images of TR146/MUC1 transfected cells without (T) or with a mucosal pellicle (TS). In addition, the presence of the mucosal pellicle seemed to decrease overall the number of areas with the highest repulsive and attractive forces.

To compare maps, we plotted for each image the cumulative force as a function of the adhesion forces' intensity, for both attractive (negative values) and repulsive (positive values) forces. Figure 2b provides the resulting curves for the particular images presented in Figure 2a. This confirmed that attractive and repulsive forces recorded at the surface of native cells without or with a mucosal pellicle were weak since their absolute values never exceeded 10 nN. The curves were very close for the two conditions N/NS: the presence of saliva hardly modified attractive and repulsive forces at the cell surface. In contrast, the curves obtained for the transfected cells showed higher attractive (down to −80 nN) and repulsive (up to 130 nN) forces. On these cells, the presence of a mucosal pellicle induced a rather large difference in adhesion forces, particularly with a decrease of the maximum intensity of attractive and repulsive forces.

From these curves were extracted the values D25, D50, and D75, which represent the attractive or repulsive forces at 25, 50, and 75% of the total attractive or repulsive forces, respectively. These were determined for all of the acquired images on different cells (n = 18, 16, 18, and 24 for the conditions N, T, NS, and TS, respectively). Figure 2c represents the repulsive and attractive D25, D50, and D75

DOI: 10.1021/acs.langmuir.9b01979
Langmuir XXXX, XXX, XXX−XXX

values (mean ± STD), while Figure 2d presents the average repulsive and attractive forces at the cell surface (mean ± STD). ANOVA testing evidenced statistical differences between conditions for the D25 (repulsive forces: F = 7.92002, p = 0.00014; attractive forces: F = 10.3863, p = 1.09×10^{-5}), D50 (repulsive forces: F = 7.69584, p = 0.00017; attractive forces: F = 11.0893, p = 5.52×10^{-6}), D75 (repulsive forces: F = 8.99411, p = 4.4724×10^{-5}; attractive forces: F = 11.564, P = 3.49×10^{-6}), and average (repulsive forces: F = 8.29782, p = 9.22×10^{-5}; attractive forces: F = 10.0733, p = 1.50×10^{-5}) values. Tukey pairwise comparison tests were applied. For native cells, the presence of salivary proteins at the surface (N vs NS) did not modify significantly the repulsive and attractive forces. In contrast, the presence of MUC1 alone (N vs T) significantly increased the adhesive and repulsive forces for all extracted values: D25, D50, D75, and average. The anchoring of salivary proteins on TR146/MUC1 transfected cells (T vs TS) slightly reduced adhesion forces, but not significantly, except for the highest attractive and repulsive forces (D75).

Attractive and repulsive forces suggest the occurrence of noncovalent interactions between the AFM tip and the surface of the cells. Attractive forces could be due to the hydrophobic effect, indicating the presence of hydrophobic surfaces, or London dispersion, which are not expected to play an important role due to the weakness of the CH−HC interaction and their too small number, while repulsive forces suggest the presence of hydrophilic surfaces, presenting either formal or partial charges. Therefore, the expression of MUC1 increased the intensity of both hydrophobic and charged areas. The protein encoded by the gene used to transfect TR146 cells (MUC1-Y-LSP) presents a shorter extracellular domain than the full-length MUC1. This 167 amino acid extracellular domain contains 11 basic amino acids (Arg, Lys) and 15 acidic amino acids (Asp, Glu), with a theoretical isoelectric point of 5.08. At the pH of the cell culture medium (6.8−7.2) or PBS (7.0−7.8), it tends to be negatively charged, consistently with the increase in repulsive forces. In addition, although the structure of this extracellular domain is not described, its composition in amino acids suggests that it would comprise both hydrophobic and charged areas, which would explain the present observations. The great variability (indicated by large standard deviations associated with average values) for both attractive and repulsive forces is probably related first to the heterogeneous between-cell and within-cell expression of MUC1, and second to heterogeneity in the surface properties of MUC1-Y-LSP. This isoform of MUC1 could bear five N-glycosylations, but in contrast to other isoforms of MUC1, it does not include the variable number tandem repeat (VNTR) module, which is abundantly glycosylated. Thus, this isoform does not fully represent the properties of other isoforms of MUC1, such as MUC1/1. The numerous glycosylations of the VNTR module are expected to be negatively charged, increasing the hydrophilicity at the cell surface, and should decrease the access to the hydrophobic domain of the peptidic chain through steric hindrance.

The presence of salivary proteins decreased the highest attractive and repulsive forces (Figure 2c,d), suggesting that the most hydrophobic and charged areas participate in the binding of salivary proteins. MUC5B in particular have high affinity for hydrophobic substrates.[20] Therefore, the highly hydrophobic areas observed upon MUC1 expression probably participate in the higher retention of MUC5B on transfected cells compared to native cells (Figure 2a,b). More generally, our results support the previous suggestion that hydrophobic effects and electrostatic interactions intervene in salivary protein binding during pellicle formation.[21]

Mucosal Pellicle Modifies the Dielectric Properties of Epithelial Cells. After documenting cells' hydrophobicity, we investigated the cells' dielectric properties by scanning microwave microscopy (SMM). This technique has been previously applied to cells[22] where the amplitude of the microwave signal yields information about the sample's conductivity determined, for example, by the ionic strength, while the phase of the microwave signal reflects the dielectric losses arising from the fluid density/water content characteristic of the sample. An advantage of microwave near-field investigation over infrared, optical waves or AFM force field is the penetration ability of microwaves, allowing subsurface imaging even in poorly conductive biological materials. Since penetration decreases with increasing frequency, it is possible to estimate whether differences in dielectric properties occur at the sample surface or deeper.

The samples were analyzed using a scanning microwave microscope setup as shown in Figure 3. In the imaging mode,

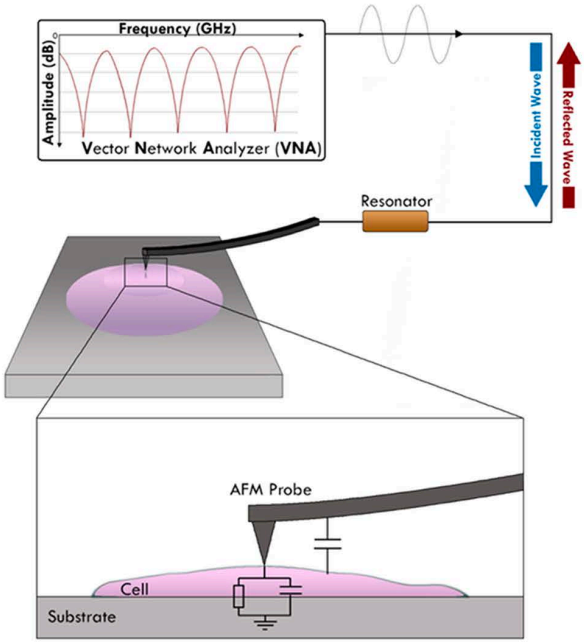

Figure 3. Schematic illustration of cell analysis by scanning microwave microscopy.

where a fixed frequency is chosen, SMM allows to simultaneously obtain the topography of the surface by means of its AFM tip and the reflection coefficient of the microwave signal acquired by the vector network analyzer at each point of measurement. The microwave amplitude and phase images are dependent on the frequency as well as the topography of the cells. In our case, the topography was overall comparable from one sample to another, as shown by AFM images (Figures 1a and 4a). Any significant difference in the amplitude and phase SMM images relates therefore mainly to differences in dielectric properties among samples.

Each sample was examined at resonance frequencies of 2, 4.3, and 8.6 GHz. A typical topography image of each type of

DOI: 10.1021/acs.langmuir.9b01979
Langmuir XXXX, XXX, XXX−XXX

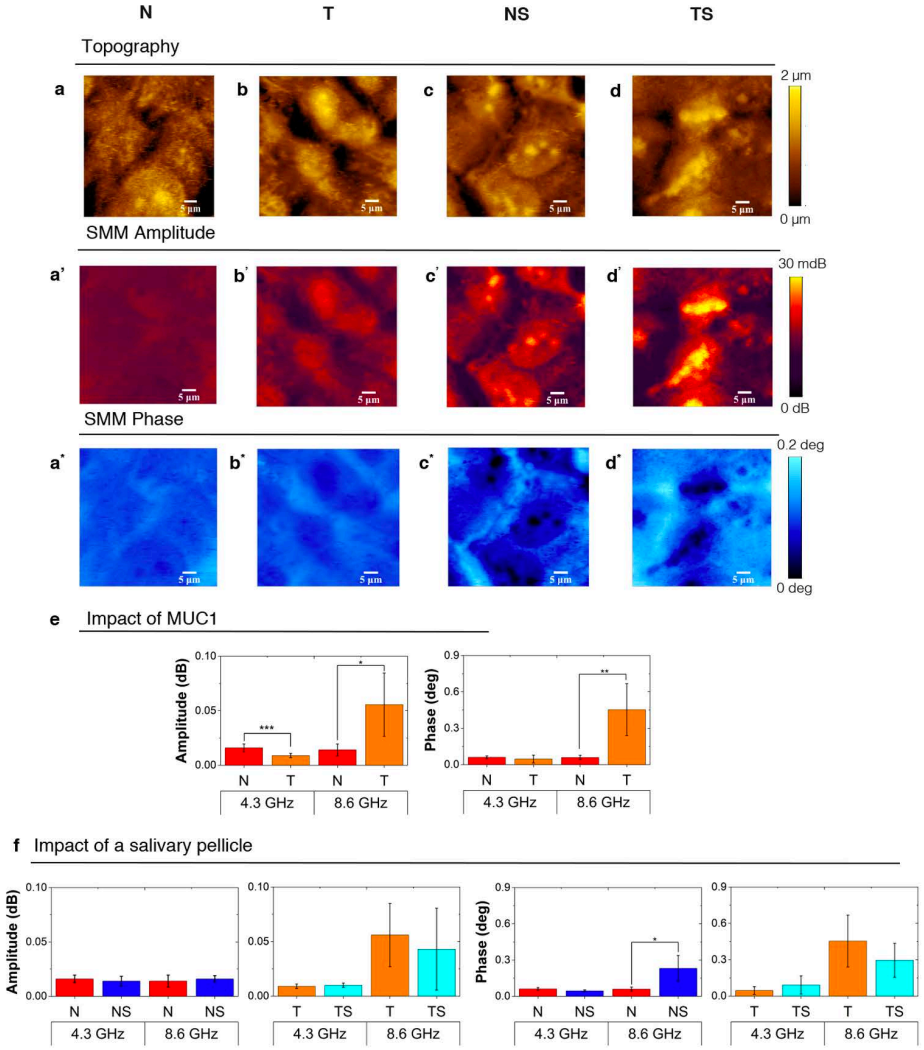

Figure 4. Scanning microwave microscopy analysis of human epithelial buccal cells. Topography (a–d), SMM amplitude (a′–d′), and SMM phase (a*–d*) images for TR146 native cells (N), TR146/MUC1 transfected cells (T), native cells with a mucosal pellicle (NS), and transfected cells with a mucosal pellicle (TS). SMM amplitude and phase images were measured at a resonance frequency of 8.6 GHz. All images are at 50 × 50 μm^2 scanning size. (e, f) SMM amplitude and phase values (mean ± STD) recorded at 4.3 and 8.6 GHz for native (red) and transfected (orange) cells, native cells with a mucosal pellicle (dark blue), and transfected cells with a mucosal pellicle (light blue). ANOVA tests were performed to evaluate the statistical impact of the presence of MUC1 protein (e) or a mucosal pellicle (f) on amplitude and phase values (*p < 0.05, **p < 0.005, and ***p < 0.001).

sample is displayed with the corresponding SMM amplitude and phase images obtained at a resonance frequency of 8.6 GHz (Figure 4). SMM images obtained at 2 and 4.3 GHz are presented in Supporting Information Figure S2. Overall, the contrast of amplitude and phase images between samples increased with resonance frequency (Figure S2). The difference in the dielectric properties between cells was therefore much more visible at high frequency (near the sample's surface) than at low frequency (deeper down). This is expected since cells differ by the presence or absence of a transmembrane mucin and the presence or absence of a mucosal pellicle on their surface.

The impact of MUC1 expression on electric properties was evaluated by comparing native and transfected cells at 4.3 and 8.6 GHz (Figure 4e). At 4.3 GHz, the amplitude microwave signal was significantly higher for native cells (DF = 30, F = 12.70, p = 0.0012). At 8.6 GHz, amplitude and phase signals were significantly higher for transfected cells (amplitude: DF = 25, F = 6.29, p = 0.0190; phase: DF = 24, F = 10.63, p = 0.0033). The large differences in values at 8.6 GHz (e.g., phase of ∼0.060 vs ∼0.50° for N and T, respectively) confirm that the microwave–sample interactions differed mainly near the sample's surface, most likely as a result of the presence of the transmembrane protein. MUC1-Y-LSP contains a short cytoplasmic tail, a membrane-spanning domain, and an extracellular domain overall negatively charged. Charge variations induced by the presence of MUC1 possibly influenced the complex conductivity, thereby the SMM amplitude and phase signals.

The impact of a mucosal pellicle on the electric properties was evaluated by comparing both native and transfected cells without or with a mucosal pellicle at 4.3 and 8.6 GHz (Figure 4f). For both cell types, the presence of the pellicle had no significant impact on the SMM amplitude signal. In contrast,

DOI: 10.1021/acs.langmuir.9b01979
Langmuir XXXX, XXX, XXX–XXX

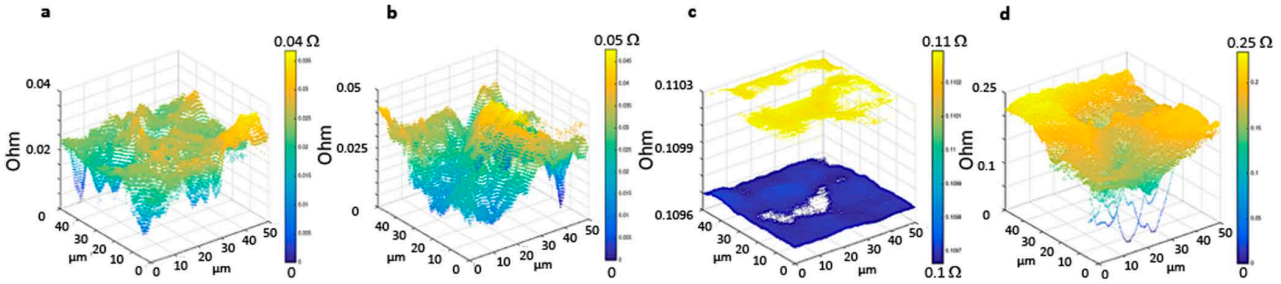

Figure 5. Impedance images of TR146 epithelial buccal cells. Impedance images were constructed for one representative image per condition from amplitude and phase values obtained at 8.6 GHz. (a) TR146 native cells (N); (b) TR146/MUC1 transfected cells (T); (c) native cells with a mucosal pellicle (NS); and (d) transfected cells with a mucosal pellicle (TS).

the SMM phase signal was significantly increased (DF = 17, F = 6.38, p = 0.0217) after pellicle formation for native cells at 8.6 GHz.

The difference in the phase signals of N and NS cells indicated a change in the dielectric environment of the material due to the mucosal pellicle. This change was larger in absolute value at high frequency (8.6 GHz), i.e., near the surface. At microwave frequencies, the dielectric properties of biological tissues are highly influenced by the presence of water. For example, an SMM study on Chinese hamster ovary cells reported that increasing the relative humidity increased their conductance[23] since water adsorbed onto the cells' surface is responsible for the dissipation of microwave energy. With an increase in the humidity content, the dielectric loss values (translated by the phase of the microwave signal) increase. Our results are in line with this: the mucosal pellicle most likely increased residual humidity at the cells' surface.

The results of phase signal for transfected cells were rather unexpected: the presence of MUC1 promotes binding of MUC5B on the cells' surface and enhances mucosal pellicle formation,[4] which was expected to result in higher dielectric losses. Nevertheless, a slight increase in microwave phase signal was observed in TS in comparison to NS (0.30 vs 0.23°), which may relate to a higher wettability of the cell surface. Thus, a direct correlation between mucins concentrations and wettability of saliva was reported: saliva containing more MUC5B presented lower contact angles.[18] Assuming there is an increase in surface wettability in transfected vs native cells would explain the higher microwave phase signal. The only representation of microwave raw signals (phase and amplitude), however, is not sufficient to fully understand the impact of saliva on the dielectric properties of native and transfected cells.

Biological media are defined by their complex conductivity and permittivity, with these properties varying with the frequency of the electric field passing through the medium. In our case, the complex reflection coefficient can be converted into complex impedance to obtain electrical and dielectric properties, i.e., capacitance and conductance properties of the sample.[24] Figure 5 shows the impedance images deduced from phase and amplitude values for one representative image per condition N, T, NS, and TS at 8.6 GHz (Figure 5a–d). After mucosal pellicle formation, the maximum impedance increased. Saliva, containing 99% of water, can be considered as a polar dielectric system. When a dielectric material is excited by an electric field at microwave frequencies, the rotational movement is no longer synchronized with the variations of the electric field and a resonance phenomenon occurs. There is thus a phase difference between the electric field and the rotational movement, thereby producing dielectric losses, translated into the observed increase in impedance. Even more remarkably, the three-dimensional impedance images show that this effect is different between the two cell types. For native cells specifically (Figure 5c), the effect is characterized by the dissociation of the impedance of the native cells (low level) from that induced by the mucosal pellicle formation (high level), which can be interpreted as a low affinity of native cells for saliva, in accordance with the hydrophobic functionalized tip results. In contrast, for transfected cells, the impedance response is not dissociated. In the presence of an electric field, the effects on the impedance are complex: they combine first a dielectric loss effect due to, as previously mentioned, increasing binding between transmembrane MUC1 and salivary MUC5B and thereby formation of the mucosal pellicle and second a conductivity effect induced by the displacement of the charges in dense areas. The present impedance results indicate a strong binding between the transfected cells and the mucosal pellicle.

■ CONCLUSIONS

The present study innovatively combines different techniques and methodologies of atomic force microscopy, to characterize the surface properties of a model of mucosa. The classical AFM technique provided information on the topography of the cells and the structure of the mucosal pellicle. Chemical force microscopy (CFM) investigation, with the CH_3 functionalized tip, allowed to characterize the hydrophobicity at the cell surface and revealed that the expression of MUC1 leads to the presence of more repulsive and attractive forces on the cells' surface, suggesting an increase of both hydrophobic and hydrophilic areas. This indicates that the adhesion of the salivary proteins probably involves the most hydrophobic and charged areas of MUC1. The SMM approach gave complementary information on the electric properties of the cell surface, and the main results obtained indicate that salivary proteins and MUC1 are strongly interacting together. In the absence of MUC1, salivary proteins appeared as a distinct layer poorly interacting with the cells' surface.

These findings open perspectives about the use of AFM to characterize biological structures and their formation. Regarding the oral mucosa and the formation of the mucosal pellicle, these results call for research aiming at gaining a deeper understanding of the mechanisms involved in the formation of the mucosal pellicle and the regions or domains of MUC1 that are involved in the binding of salivary proteins. Future research

DOI: 10.1021/acs.langmuir.9b01979
Langmuir XXXX, XXX, XXX−XXX

is also required to identify the salivary proteins that specifically bind MUC1 and the noncovalent interactions involved.

■ ASSOCIATED CONTENT

Supporting Information

The Supporting Information is available free of charge on the ACS Publications website at DOI: 10.1021/acs.langmuir.9b01979.

Verification of AFM tips functionalization (Figure S1) (PDF)

Scanning microwave microscopy analysis of human epithelial buccal cells (Figure S2) (PDF)

■ AUTHOR INFORMATION

ORCID

Francis Canon: 0000-0002-6140-5007

Author Contributions

E.N.A., E.B., E.L., and F.C. conceived and designed the work. E.N.A. performed all of the AFM experiments. S.P. and M.B. produced the TR146/MUC1 cells, maintained the cell lines, and performed immunohistochemistry. B.D.F. calculated and plotted impedance images. E.N.A., E.B., M.M., E.L., and F.C. analyzed and interpreted the data. E.N.A. drafted the manuscript with input from all authors. E.B., B.D.F., M.M., E.L., and F.C. revised the manuscript. All authors have approved its submitted version.

Notes

The authors declare no competing financial interest.

■ ACKNOWLEDGMENTS

This study was funded by the French National Research Agency (Grant ANR-14-CE20-0001-01 MUFFIN). The French National Research Agency also provided support for establishing and maintaining collaboration between ICB and INRA (Grants ANR-15-IDEX-03 PIA2/iSite-BFC, ANR-15-CE09-0002-02, ANR-17-EURE-0002 EIPHI Graduate School).

■ ABBREVIATIONS

AFM, atomic force microscopy; MUC1, mucin-1; MUC5B, mucin-5B; N, native cells; NS, native cells with a mucosal pellicle; PBS, phosphate-buffered saline; SMM, scanning microwave microscopy; T, TR146/MUC1 transfected cells; TS, transfected cells with a mucosal pellicle; VNA, vector network analyzer

■ REFERENCES

(1) (a) Bradway, S. D.; Bergey, E. J.; Scannapieco, F. A.; Ramasubbu, N.; Zawacki, S.; Levine, M. J. Formation of Salivary-Mucosal Pellicle - the Role of Transglutaminase. *Biochem. J.* **1992**, *284*, 557−564. (b) Gibbins, H. L.; Proctor, G. B.; Yakubov, G. E.; Wilson, S.; Carpenter, G. H. Concentration of salivary protective proteins within the bound oral mucosal pellicle. *Oral Dis.* **2014**, 707−713.

(2) (a) Tabak, L. A. Structure and function of human salivary mucins. *Crit. Rev. Oral Biol. Med.* **1990**, *1*, 229−234. (b) Hannig, C.; Hannig, M.; Morzel, M. *Flavour: From Food to Perception*; Guichard, E.; Salles, C.; Morzel, M.; Bon, A.-M. L., Eds.; John Wiley & Sons; Ltd, 2017; pp 79−108.

(3) Gibbins, H. L.; Yakubov, G. E.; Proctor, G. B.; Wilson, S.; Carpenter, G. H. What interactions drive the salivary mucosal pellicle formation? *Colloids Surf., B* **2014**, *120*, 184−192.

(4) Ployon, S.; Belloir, C.; Bonnotte, A.; Lherminier, J.; Canon, F.; Morzel, M. The membrane-associated MUC1 improves adhesion of salivary MUC5B on buccal cells. Application to development of an in vitro cellular model of oral epithelium. *Arch. Oral Biol.* **2016**, *61*, 149−155.

(5) (a) Davies, H. S.; Pudney, P. D. A.; Georgiades, P.; Waigh, T. A.; Hodson, N. W.; Ridley, C. E.; Blanch, E. W.; Thornton, D. J. Reorganisation of the Salivary Mucin Network by Dietary Components: Insights from Green Tea Polyphenols. *PLoS One* **2014**, *9*, No. e108372. (b) Ployon, S.; Morzel, M.; Belloir, C.; Bonnotte, A.; Bourillot, E.; Briand, L.; Lesniewska, E.; Lherminier, J.; Aybeke, E.; Canon, F. Mechanisms of astringency: Structural alteration of the oral mucosal pellicle by dietary tannins and protective effect of bPRPs. *Food Chem.* **2018**, *253*, 79−87.

(6) Ployon, S.; Morzel, M.; Canon, F. The role of saliva in aroma release and perception. *Food Chem.* **2017**, *226*, 212−220.

(7) Garcia-Alles, L. F.; Lesniewska, E.; Root, K.; Aubry, N.; Pocholle, N.; Mendoza, C. L.; Bourillot, E.; Barylyuk, K.; Pompon, D.; Zenobi, R.; Reguera, D.; Truan, G. Spontaneous non-canonical assembly of CcmK hexameric components from beta-carboxysome shells of cyanobacteria. *PLoS One* **2017**, *12*, No. e0185109.

(8) (a) Alsteens, D.; Newton, R.; Schubert, R.; Martinez-Martin, D.; Delguste, M.; Roska, B.; Muller, D. J. Nanomechanical mapping of first binding steps of a virus to animal cells. *Nat. Nanotechnol.* **2017**, *12*, 177−183. (b) Aybeke, E. N.; Belliot, G.; Lemaire-Ewing, S.; Estienney, M.; Lacroute, Y.; Pothier, P.; Bourillot, E.; Lesniewska, E. HS-AFM and SERS Analysis of Murine Norovirus Infection: Involvement of the Lipid Rafts. *Small* **2017**, *13*, 10.

(9) Cartagena-Rivera, A. X.; Wang, W. H.; Geahlen, R. L.; Raman, A. Fast, multi-frequency, and quantitative nanomechanical mapping of live cells using the atomic force microscope. *Sci. Rep.* **2015**, *5*, No. 11692.

(10) (a) Harada, Y.; Kuroda, M.; Ishida, A. Specific and quantized antigen-antibody interaction measured by atomic force microscopy. *Langmuir* **2000**, *16*, 708−715. (b) Berthier, A.; Elie-Caille, C.; Lesniewska, E.; Delage-Mourroux, R.; Boireau, W. Label-free sensing and atomic force spectroscopy for the characterization of protein-DNA and protein-protein interactions: application to estrogen receptors. *J. Mol. Recognit.* **2011**, *24*, 429−435.

(11) Plassard, C.; Bourillot, E.; Rossignol, J.; Lacroute, Y.; Lepleux, E.; Pacheco, L.; Lesniewska, E. Detection of defects buried in metallic samples by scanning microwave microscopy. *Phys. Rev. B* **2011**, *83*, 4.

(12) Love, J. C.; Estroff, L. A.; Kriebel, J. K.; Nuzzo, R. G.; Whitesides, G. M. Self-assembled monolayers of thiolates on metals as a form of nanotechnology. *Chem. Rev.* **2005**, *105*, 1103−1169.

(13) Nuzzo, R. G.; Allara, D. L. Adsorption of bifunctional organic disulfides on gold surfaces. *J. Am. Chem. Soc.* **1983**, *105*, 4481−4483.

(14) Dorobantu, L. S.; Bhattacharjee, S.; Foght, J. M.; Gray, M. R. Atomic force microscopy measurement of heterogeneity in bacterial surface hydrophobicity. *Langmuir* **2008**, *24*, 4944−4951.

(15) Horcas, I.; Fernandez, R.; Gomez-Rodriguez, J. M.; Colchero, J.; Gomez-Herrero, J.; Baro, A. M. WSXM: A software for scanning probe microscopy and a tool for nanotechnology. *Rev. Sci. Instrum.* **2007**, *78*, No. 013705.

(16) Asikainen, P.; Sirvio, E.; Mikkonen, J. J. W.; Singh, S. P.; Schulten, E. A. J. M.; ten Bruggenkate, C. M.; Koistinen, A. P.; Kullaa, A. M. Microplicae - Specialized Surface Structure of Epithelial Cells of Wet-Surfaced Oral Mucosa. *Ultrastruct. Pathol.* **2015**, *39*, 299−305.

(17) Morzel, M.; Tai, S.; Brignot, H.; Lherminier, J. Immunocytological detection of salivary mucins (MUC5B) on the mucosal pellicle lining human epithelial buccal cells. *Microsc. Res. Technol.* **2014**, *77*, 453−457.

(18) Vijay, A.; Inui, T.; Dodds, M.; Proctor, G.; Carpenter, G. Factors That Influence the Extensional Rheological Property of Saliva. *PLoS One* **2015**, *10*, No. e0135792.

(19) Alsteens, D.; Dague, E.; Rouxhet, P. G.; Baulard, A. R.; Dufrêne, Y. F. Direct Measurement of Hydrophobic Forces on Cell Surfaces Using AFM. *Langmuir* **2007**, *23*, 11977−11979.

(20) Lindh, L.; Glantz, P. O.; Carlstedt, I.; Wickstrom, C.; Arnebrant, T. Adsorption of MUC5B and the role of mucins in early salivary film formation. *Colloids Surf., B* **2002**, *25*, 139−146.
(21) Bradway, S. D.; Bergey, E. J.; Jones, P. C.; Levine, M. J. Oral Mucosal Pellicle - Adsorption and Transpeptidation of Salivary Components to Buccal Epithelial-Cells. *Biochem. J.* **1989**, *261*, 887−896.
(22) Oh, Y. J.; Huber, H. P.; Hochleitner, M.; Duman, M.; Bozna, B.; Kastner, M.; Kienberger, F.; Hinterdorfer, P. High-frequency electromagnetic dynamics properties of THP1 cells using scanning microwave microscopy. *Ultramicroscopy* **2011**, *111*, 1625−1629.
(23) Tuca, S. S.; Badino, G.; Gramse, G.; Brinciotti, E.; Kasper, M.; Oh, Y. J.; Zhu, R.; Rankl, C.; Hinterdorfer, P.; Kienberger, F. Calibrated complex impedance of CHO cells and E. coli bacteria at GHz frequencies using scanning microwave microscopy. *Nanotechnology* **2016**, *27*, No. 135702.
(24) Gramse, G.; Kasper, M.; Fumagalli, L.; Gomila, G.; Hinterdorfer, P.; Kienberger, F. Calibrated complex impedance and permittivity measurements with scanning microwave microscopy. *Nanotechnology* **2014**, *25*, 8.

DOI: 10.1021/acs.langmuir.9b01979
Langmuir XXXX, XXX, XXX−XXX

Publication n°3: Mechanisms of astringency: Structural alteration of the oral mucosal pellicle by dietary tannins and protective effect of bPRPs.

Ployon, S.; Morzel, M.; Belloir, C.; Bonnotte, A.; Bourillot, E.; Briand, L.; Lesniewska, E.; Lherminier, J.; Aybeke, E.; Canon, F.

Food Chem. 2018, *253*, 79-87.

Food Chemistry 253 (2018) 79–87

Contents lists available at ScienceDirect

Food Chemistry

journal homepage: www.elsevier.com/locate/foodchem

Mechanisms of astringency: Structural alteration of the oral mucosal pellicle by dietary tannins and protective effect of *b*PRPs

Sarah Ployon[a], Martine Morzel[a], Christine Belloir[a], Aline Bonnotte[b], Eric Bourillot[c], Loïc Briand[a], Eric Lesniewska[c], Jeannine Lherminier[b], Ece Aybeke[a], Francis Canon[a,*]

[a] Centre des Sciences du Goût et de l'Alimentation, AgroSup Dijon, CNRS, INRA, Université de Bourgogne Franche-Comté, F-21000 Dijon, France
[b] INRA, UMR1347 Agroécologie, ERL CNRS 6300, Plateforme DImaCell, Centre de Microscopie INRA/Université de Bourgogne, F-21000 Dijon, France
[c] ICB UMR CNRS 6303, Université de Bourgogne Franche-Comté, F-21000 Dijon, France

ARTICLE INFO

Keywords:
TR146/MUC1 cells
Salivary mucins MUC5B
EgCG
IB5
Scanning Electron Microscopy
Atomic Force Microscopy
Astringency

ABSTRACT

The interaction of tannins with salivary proteins is involved in astringency. This paper focussed on saliva lining oral mucosae, the mucosal pellicle. Using a cell-based model, the impact of two dietary tannins (EgC and EgCG) on the mucosal pellicle structure and properties was investigated by microscopic techniques. The role of basic Proline-Rich-Proteins (bPRPs) in protecting the mucosal pellicle was also evaluated.

At low (0.05 mM) tannin concentration, below the sensory detection threshold, the distribution of salivary mucins MUC5B on cells remained unaffected. At 0.5 and 1 mM, MUC5B-tannin aggregates were observed and their size increased with tannin concentration and with galloylation. In addition, 3 mM EgCG resulted in higher friction forces measured by AFM. In presence of bPRPs, the size distribution of aggregates was greatly modified and tended to resemble that of the "no tannin" condition, highlighting that bPRPs have a protective effect against the structural alteration induced by dietary tannins.

1. Introduction

Astringency, mostly considered as an unpleasant sensory attribute, is an organoleptic tactile sensation (Green, 1993) mediated by the trigeminal nerve (Schobel et al., 2014). It is defined as the sensation of drying and puckering of oral mucosa. Astringency can be experienced during the consumption of plant food products, such as green tea, red wine or berries. In those products, proanthocyanidins, a group of tannins, have been identified as responsible for this sensation. Tannins are phenolic compounds (*syn.* polyphenols) and have the ability to precipitate proteins. They can be divided into three groups, proanthocyanidins (*syn.* condensed tannins), which are oligomers and polymers of flavan-3-ols, hydrolysable tannins, which are polyesters of sugars and gallic or ellagic acids, and complex tannins in which both types are covalently bound. Tannins are plant secondary metabolites, which play a role in plant defence mechanisms through their deleterious effects for plant predators (i.e. herbivores and omnivores). For instance in mammalian herbivores, tannins can reduce digestibility, damage the gastrointestinal mucosa and epithelium, and lead to kidney or liver failure or endogenous nitrogen loss (Shimada, 2006). In rodents, a tannin-rich diet induces weight loss, which is continuous in hamsters but reversible after three days in rats and mice. In parallel, feeding on tannins induces in rats and mice a dramatic increase in salivary proline-rich proteins (PRPs) within three days, while this is not observed in hamsters (Shimada, 2006).

Indeed in mammals, the presence of PRPs in saliva appears to be linked to the consumption of tannins. PRPs are particularly abundant in human saliva and may constitute up to 70% of parotid saliva proteins (Bennick, 1982). PRPs are classified in three groups depending on their isoelectric point and their degree of glycosylation: acidic, basic and glycosylated PRP (aPRP, bPRP and gPRP, respectively). aPRPs play a role in calcium binding and gPRPs in oral lubrication, while the main function of bPRP is the scavenging of tannins. Thus, investigations on tannin-protein interactions have shown that PRPs have a particular affinity for tannins (Shimada, 2006). Therefore, according to the Red Queen hypothesis, it can be postulated that bPRPs are part of a defence mechanism selected to protect organisms against the detrimental effects of tannins. Astringency is also probably a chemosensory signal for the detection of tannin-rich foods, leading to a shunning behaviour.

Astringency is thought to be due to a loss in the lubrication capacity

* Corresponding author.
E-mail addresses: martine.morzel@inra.fr (M. Morzel), christine.belloir@inra.fr (C. Belloir), aline.bonnotte@u-bourgogne.fr (A. Bonnotte), eric.bourillot@u-bourgogne.fr (E. Bourillot), loic.briand@inra.fr (L. Briand), lesniew@u-bourgogne.fr (E. Lesniewska), jeannine.lherminier@inra.fr (J. Lherminier), ece.aybeke@inra.fr (E. Aybeke), francis.canon@inra.fr (F. Canon).

https://doi.org/10.1016/j.foodchem.2018.01.141
Received 18 July 2017; Received in revised form 22 November 2017; Accepted 22 January 2018
Available online 03 February 2018

of salivary proteins and more particularly of the proteins composing the mucosal pellicle (Nayak & Carpenter, 2008). The mucosal pellicle is a thin biological structure, whose thickness can reach 100 nm (Morzel, Siying, Brignot, & Lherminier, 2014), made of salivary proteins anchored onto oral epithelial thanks to covalent and non-covalent bonds (Bradway et al., 1992; Gibbins, Yakubov, Proctor, Wilson, & Carpenter, 2014). The mucosal pellicle contains MUC5B, MUC7, cystatins and IgA (Gibbins et al., 2014) and also amylases and PRPs (Bradway et al., 1992). Among these salivary proteins, the mucins MUC5B have been identified as major components. Davies et al. have reported that tannins aggregate the salivary mucins MUC5B and MUC7 (Davies et al., 2014). Therefore, interaction of astringent compounds with adsorbed mucins could play an important role in astringency sensation (Biegler, Delius, Käsdorf, Hofmann, & Lieleg, 2016).

In this context, the two hypotheses tested in this study are that 1 – tannins aggregate the mucosal pellicle proteins, with an impact on lubricating properties of this structure and 2 – PRPs play a protective role by scavenging tannins, precluding their access to the mucosa and its consequent structural alteration. As a result, astringency would be perceived only when tannin concentration is high enough to overcome the protective capacity of PRPs. To test these hypotheses, an *in vitro* cell-based model of oral mucosa with a mucosal pellicle previously developed (Ployon et al., 2016) was used. First, to investigate the effect of tannins on the mucosal pellicle structure, the model was exposed to two dietary monomers of proanthocyanidins, Epigallocatechin (EgC) and Epigallocatechin gallate (EgCG), differing in their structure by the presence of a galloylated moiety on EgCG (Fig. 1) and which is detected sensorially at lower concentrations. The mucosal pellicle structure and properties were investigated using three complementary microscopic techniques, fluorescent immunostaining of salivary MUC5B, Scanning Electron Microscopy (SEM) and Atomic Force Microscopy (AFM). Second, in order to evaluate the role of bPRP in the protection of the oral mucosa, the model was covered by a liquid film containing IB5 (a human bPRP) prior to exposure to EgCG. The size of the aggregates with and without PRPs was evaluated by image analysis and compared.

2. Material and methods

2.1. Saliva collection

The study was performed in agreement with the guidelines laid out in the declaration of Helsinki. Written informed consent was obtained from the participants. Unstimulated saliva was obtained by the spitting method from fifteen volunteers who declared to be in good oral health. Subjects were instructed to refrain from smoking, eating or drinking for at least two hours before saliva collection. All samples were pooled and centrifuged at 14,000*g* for 20 min at 4 °C. The resulting pool of clarified saliva was divided into aliquots of 4 ml. Samples were immediately frozen at −80 °C.

2.2. Cell culture and formation of in vitro mucosal pellicle

TR146/MUC1 cells (Ployon et al., 2016) were grown in DMEM/F12–GlutaMAX medium (1:1) supplemented with 10% Foetal Bovine Serum (FBS), 1% penicillin/streptomycin (P/S) and 2.5 mg/ml of neomycin G418 (Gibco® by Life Technologies). Culture conditions were maintained at 37 °C and 7.5% CO_2. Cells were cultured in T75 flasks and the medium was changed every two days. Sub-cultures were prepared at 80% confluence using Trypsin-EDTA. Cells were seeded into eight-chamber glass slides for MUC5B immunostaining, and on 10 mm diameter glass slips for SEM and AFM imaging. All supports were coated with Cell-Tak™ (Corning) prior to seeding at a density of 4×10^6 cells/cm^2. In these conditions, confluence was reached in 48 h. Three days after confluence, a mucosal pellicle was deposited on the cells' surface by incubating cells for 2 h with clarified saliva diluted into growth medium (1:1) (Ployon et al., 2016). After incubation, samples were washed twice with PBS in order to eliminate the non-adsorbed saliva.

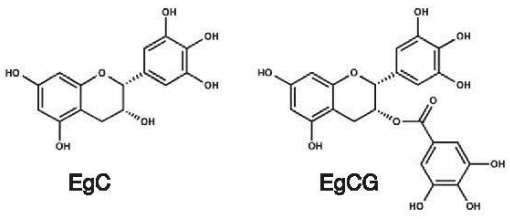

Fig. 1. Structure of Epigallocathechin (EgC) and Epigallocatechin gallate (EgCG).

2.3. Tannins solution

Epigallocatechin (EgC) and Epigallocatechin gallate (EgCG) were purchased from Santa Cruz Biotechnology (Texas, US). EgC and EgCG were diluted in PBS (pH 7.5) immediately before use to avoid compounds oxidation.

2.4. IB5 production

IB5 was produced and purified according to the method described by Boze et al. (2010) and was a kind gift from Dr. Cheynier (INRA Montpellier). The concentration of IB5 was adjusted to 0.66 mM in PBS.

2.5. Viability assay

Cells were cultured into 96-wells plates. When confluence was reached, cells were incubated for 2 h with clarified saliva diluted in growth medium as described above. After two washes with PBS, samples were exposed to tannins solutions (0.05–10 mM) or IB5 solution at 0.33 mM for 1 h. Cytotoxic effects were assessed using the Neutral Red assay, using a fluorimetric method. Briefly, cells were incubated for 3 h at 37 °C with 200 µl of medium containing neutral red at 50 µg/ml, washed twice with PBS and incubated at room temperature for 1 h in neutral red eluent (ethanol:H_2O:acetic acid, 50:49:1) with gentle agitation. Reading of the fluorescence was performed with Victor3V microplate reader (PerkinElmer) with excitation and emission wavelengths fixed at 544 nm and 595 nm, respectively. 80% of viability was considered as an indicator of non-cytotoxicity. Assays were performed in triplicate.

2.6. Exposure of the model to EgC and EgCG

Three concentrations of EgC and EgCG were tested for MUC5B immunostaining and SEM: 0.05, 0.5 and 1 mM. These concentrations were chosen taking into account the sensory detection thresholds of EgC and EgCG which were measured at 0.54 mM and 0.19 mM, respectively (Scharbert, Holzmann, & Hofmann, 2004). For AFM imaging, two concentrations of EgCG (1 and 3 mM) were tested. The cell-based model was covered with a tannin solution in PBS, or PBS alone as a control. After 5 min, the liquid was removed and cells were fixed prior to microscopical observations. Each condition was tested in triplicate.

2.7. Exposure of the model mucosa to EgCG in presence of IB5

The effect of EgCG at 1 mM was evaluated in presence of IB5 at 0.33 mM. The cell-based model was preliminarily covered by 62.5 µl of IB5 solution at 0.66 mM. Then, 62.5 µl of EgCG at 2 mM or 1 mM was added, resulting in final concentrations of 1 mM or 0.5 mM in EgCG and 0.33 mM in IB5. In the control condition, 62.5 µl of PBS were added to the 62.5 µl of IB5 solution.

2.8. Fluorescence immunostaining of MUC5B

Cells were fixed in 4% paraformaldehyde (PFA) for 30 min. Autofluorescence of PFA was blocked with a solution of NH_4Cl at 50 mM. Non-specific binding was prevented using 0.3% free fat milk/5% goat serum in PBS. A primary antibody anti-MUC5B F2 (1:50 in PBS) produced in mouse was used (kind gift from Prof. Veerman, Free University of Amsterdam). Alexa 488 Goat anti-mouse IgG from Invitrogen was used as secondary antibody (1:400 in PBS). The samples were mounted into Prolong Gold antifade reagent with DAPI (Invitrogen). MUC5B immunostaining was observed with a NIKON Eclipse E600 microscope (Nikon Instruments, Melville, New York, USA) after excitation with high-pressure mercury-vapor lamp. Images were acquired using a Nikon Dxm1200C camera. The Nikon NISBR software was used for data acquisition. Three images, taken on different areas of the sample, were acquired for each of the triplicate.

2.9. Scanning Electron Microscopy

Fixation of TR146/MUC1 cells was carried out with 2.5% glutaraldehyde in PBS for 30 min, followed by 0.4% osmium tetroxide in PBS for 30 min. Dehydration was done through graded baths of ethanol (from 30 to 100%). Drying was performed by the critical point drying (CPD) method using Leica CPD 030. Samples were then coated with a thin carbon layer using a CRESSINGTON 308R and observed with a scanning electron microscope JEOL JSM 7600F (JEOL Ltd). SEM was operated at 2 kV and samples were observed at a working distance of 5 mm.

2.10. Atomic Force Microscopy imaging

Fixation of TR146/MUC1 cells was carried out with 2.5% glutaraldehyde in PBS for a minimum of 30 min. Atomic force microscopy experiments were performed using a Multimode 8 AFM microscope (Bruker, Santa Barbara, CA, USA). The topography and friction images were collected in $10 \times 10\ \mu m^2$ of scan size and 1 Hz of scan rate in high resolution (512×512 pixel^2) using contact mode. The surfaces of samples were scanned in trace and retrace directions with V-shaped silicon nitride cantilevers with spring constant of 0.12 N/m (DNP-S, Bruker, Santa Barbara, CA, USA) in PBS medium (pH 7.8 ± 0.2, Bio-Rad). After obtaining a satisfactory topographical image in contact mode, the scan angle switched to 90° from 0° in order to record friction force images. The amount of tracking force was fixed for all samples to be able to compare the friction properties of different samples. In lateral force microscopy, the cantilever scans over the sample surface laterally (perpendicular to their lengths) and is torqued depending on the friction properties of substrate. The lateral forces are recorded by monitoring the horizontal deflection on the 4-segmented photodetector. The measured relative friction forces were in Volts and directly proportional to absolute friction force (in N). The friction force images visualize the high- and low-friction sites on the sample surface and they can provide a comparative analysis of the friction properties of different samples. Topography and friction force images of each sample were acquired in three conditions: 0, 1 and 3 mM EgCG (n = 7 per condition). For each sample, the median friction force was extracted for trace and retrace images and the mean value was calculated. The difference between the 1 and 3 mM conditions and the control (no tannin) was tested by a Student *t*-test.

2.11. Image analysis and statistical analysis

Images of MUC5B immunostained samples were analyzed using IgorPro software (WaveMetrics, Tigard, Oregon). 32-bits coloured images were converted into 8-bits grey level images. Then a thresholding operation, converting grey images into binary images, was performed. Finally, the binary images were submitted to an operation of image particle analysis and particles area in pixels were extracted and converted in mm^2.

The distribution of the total particle area was calculated and the particle sizes, representing 25 and 75% of the total particle area distribution (PS25 and PS75), were determined.

The differences between the different conditions were analyzed using a non-parametric Kruskal-Wallis test, followed by a post hoc Dunn-Holland-Wolfe test for pairwise comparison.

3. Results

3.1. Viability assay

For the exposure time of 1 h, EgC did not affect cell viability at any of the concentrations tested, while EgCG exhibited a cytotoxic effect for a concentration between 6 and 10 mM. The 0.33 mM IB5 solution was not toxic to cells.

3.2. Effect of tannins on the mucosal pellicle structure

The salivary mucin MUC5B, a major constituent of the mucosal pellicle, was immunostained on the *in vitro* model of oral mucosa in the presence, or not, of EgC or EgCG (Fig. 2). In the absence of tannins, salivary MUC5B was detectable as a layer exhibiting some between-cell variability, in accordance with previous observations (Ployon et al., 2016). The appearance of the MUC5B layer was hardly, if at all, affected by EgC and EgCG at 0.05 mM. By contrast, treatment with 1 mM EgC and EgCG (and to a lesser with 0.5 mM EgC and EgCG) was associated with the presence of some larger MUC5B deposits with higher fluorescence intensity (see arrows on Fig. 2), which correspond probably to MUC5B-tannin aggregates. The structure of these objects was investigated by Scanning Electronic Microscopy (SEM) in control conditions (no tannin) and at 0.05 and 1 mM of EgC and EgCG (Fig. 3). In the control condition (Fig. 3A), saliva deposit was made of a thin, loose, filamentous network as previously described by Ployon et al. (2016). When the model was exposed to EgC at 0.05 mM (Fig. 3B), the structural difference was limited, while addition of EgCG at the same concentration resulted in a deposit that appeared slightly thicker (Fig. 3C).

By contrast, when both tannins were added at the higher concentration (1 mM), larger and denser deposits were present on the cells' surface (3D and 3E). The size of these aggregates could reach several µm.

3.3. Effect of tannins on aggregates' population

Fig. 4 presents data obtained by image analysis of MUC5B immunostaining images, translating the size of MUC5B-tannins aggregates: cumulative particle area as a function of particle size (left) and PS75 determined from the cumulative curves (right) for both tannins and each concentration. For both tannins, differences in the cumulative curves can be observed depending on tannin concentration. PS25 was almost identical for the three concentrations while PS75 increased strongly with tannin concentration. In addition, large particles (> 100–$120\ \mu m^2$) were present only at the 1 mM concentration. Therefore, the higher the tannin concentration, the larger were the aggregates. For both tannins, PS75 was not significantly different from the control at 0.05 mM, while the difference became significant from 0.5 mM with p-values below 0.05, 0.001, 0.05 and 0.001 for EgC 0.5 mM, EgC 1 mM, EgCG 0.5 mM and EgCG 1 mM, respectively. Comparing now the two tannins, and although the difference was not significant, PS75 values tended to be higher for EgCG than for EgC at the two higher concentrations. In addition, the highest particle sizes ($> 200\ \mu m^2$) were observed for EgCG at 1 mM. In other words, EgCG generated overall larger particles than EgC, at least at 0.5 and 1 mM. These trends were also observable on mean particle areas, with values of 1.08 (control) 1.33, 1.34 and 2.04 µm^2 for EgC at 0.05, 0.5 and

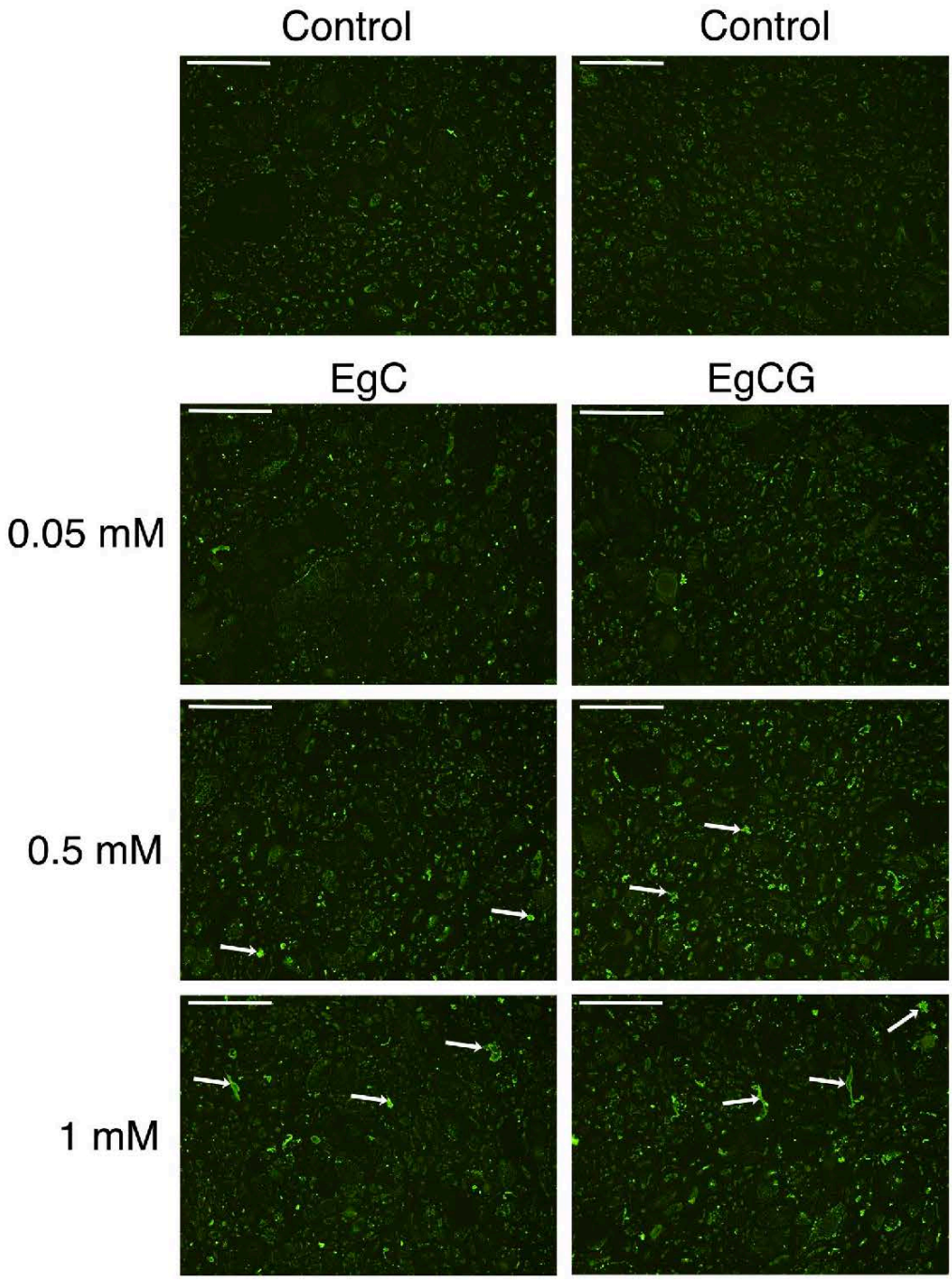

Fig. 2. Immunostaining of MUC5B on the *in vitro* model (TR146/MUC1 cells with a mucosal pellicle) after exposure to tannins (EgC and EgCG) at four concentrations: 0 (Control), 0.05, 0.5 and 1 mM. Scale bar = 100 μm.

1 mM, and 1.17, 1.57 and 2.61 μm^2 for EgCG at 0.05, 0.5 and 1 mM. This corresponds to radii from 600 to 900 nm approximately.

3.4. Effect of EgCG on friction force

Fig. 5 presents atomic force microscopy (AFM) images of topography (left) and friction forces (right) of the oral mucosa model's surface in control condition (no tannin) and in presence of EgCG at 1 and 3 mM. The topography of the *in vitro* model exposed to 1 or 3 mM EgCG was not drastically modified compared to the control condition (Fig. 5, left). In all conditions, the cells' surface was characterized by the presence of microplicae, as also observed on Fig. 3. These structural features are typical of stratified epithelial cells' surface. The microplicae height was in the range of a few hundreds of nm. In contrast to topography, friction force (Fig. 5, right) appeared influenced by EgCG concentration. At 3 mM especially, some areas were characterized by much higher friction force (see arrows) than in the other conditions. Considering the 7 replicates per condition, the average friction force recorded were 0.603 ± 0.186 V (no tannin), 0.560 ± 0.086 V (1 mM EgCG) and 1.313 ± 0.376 V (3 mM EgCG). The 3 mM condition was statistically different from the control ($p = 0.002$).

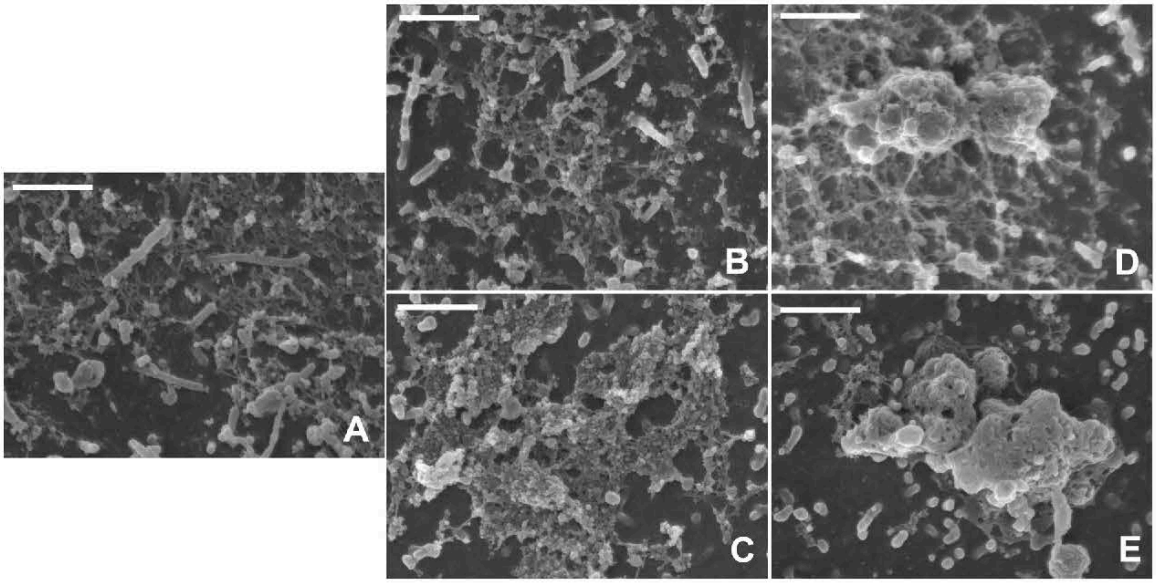

Fig. 3. SEM observation (×25,000) of the *in vitro* mucosal pellicle after exposure to tannins. A. Control (no tannins), B. EgC 0.05 mM, C. EgCG 0.05 mM, D. EgC 1 mM, E. EgCG 1 mM. Scale bar = 1 μm.

3.5. Effect of EgCG on the mucosal pellicle structure in presence of IB5

In order to assess the protective role of PRP toward tannin, the model of mucosa was preliminarily covered by a solution of the bPRP, IB5, prior to MUC5B immunostaining and image analysis. Addition of IB5 alone did not impact on the structure of the pellicle (data not shown).

Following the same format as Fig. 4, Fig. 6 presents data translating the size of MUC5B-tannins aggregates. There were differences in the shape of the cumulative curves. In particular, the presence of PRP modified the curves obtained with EgCG alone in such a way that they tended to resemble the control curve. The difference was especially

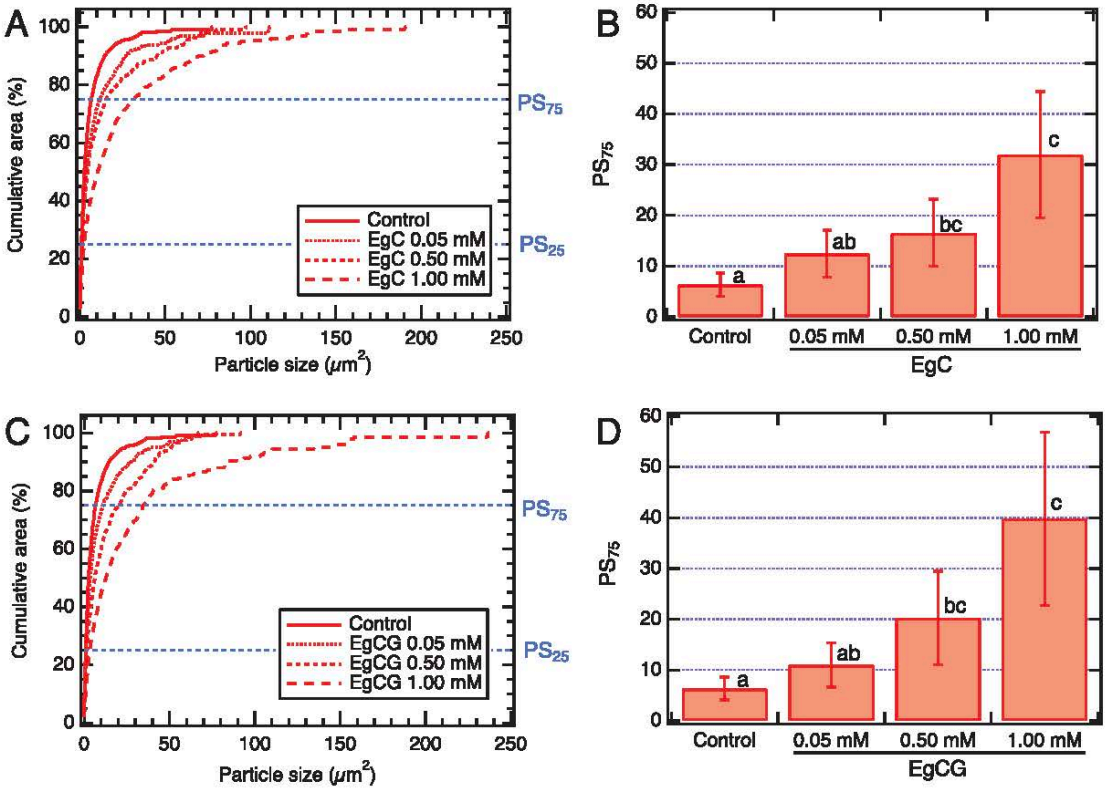

Fig. 4. Impact of the tannin type and concentration on MUC5B-tannins aggregates size. Distribution of particle size and particle size at 75% of the cumulative particle area after exposure of the *in vitro* model to EgC (top) and EgCG (bottom) at 0.05, 0.5 and 1 mM.

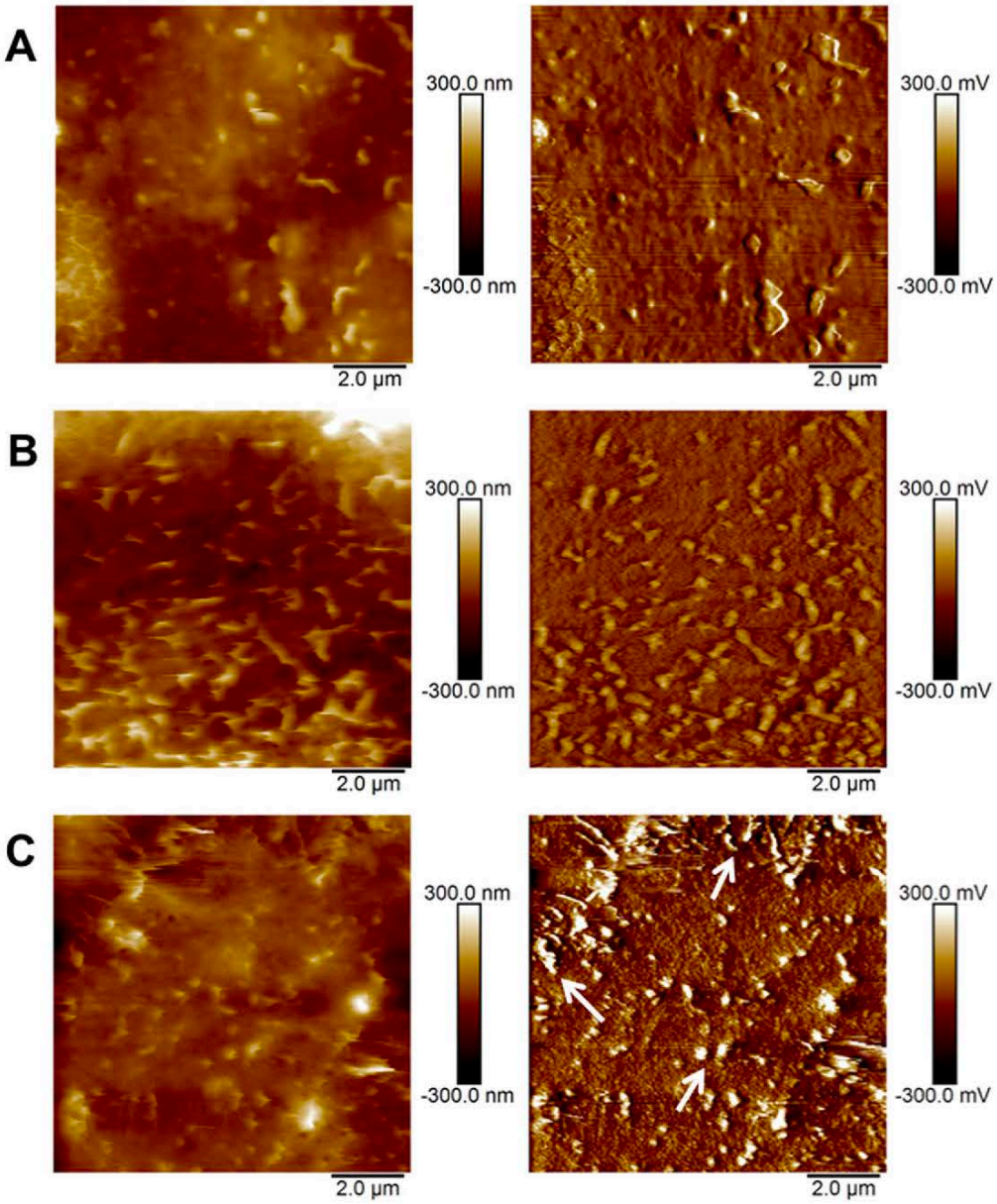

Fig. 5. AFM topography (left) and friction (right) images of the *in vitro* model (TR146/MUC1 cells with a mucosal pellicle). a. Control (no EgCG), b. EgCG 1 M, c EgCG 3 mM.

striking for the 1 mM EgCG: PS75, which was significantly increased by exposure to EgCG alone ($p \leq 0.001$), became non-significantly different from the control when PRP were added.

4. Discussion

The aim of this work was to contribute to the understanding of oral mechanisms involved in the sensation of astringency. Overall, it was found that tannins altered the mucosal pellicle by generating aggregates whose size depended on tannins' structure and concentration. At elevated concentrations, increased friction was measured on oral cells lined with a mucosal pellicle. Finally, we demonstrated that the bPRP IB5 could counteract the effect of tannins in terms of structural alteration.

The choice of focussing on the mucosal pellicle to decipher the mechanisms of astringency was guided by the fact that this sensation is perceived predominantly on mucosal surfaces, which are described as dry and puckered upon exposure to astringents. The mucosal salivary pellicle is a thin protein layer bound onto epithelium cells' surface. It is composed of epithelial and salivary proteins selectively adsorbed onto the cells' surface (Hannig, Hannig, Kensche, & Carpenter, 2017). MUC5B (Gibbins et al., 2014; Morzel et al., 2014; Ployon et al., 2016), amylase, cystatin and acidic proline-rich proteins (aPRPs) (Bradway et al., 1992) but also secretory component and IgA (Gibbins & Carpenter, 2013) have been identified in mucosal pellicles. Structurally, it has been described as organized in two layers (Macakova, Yakubov, Plunkett, & Stokes, 2010): an anchoring layer, constituted of the membrane-bound mucin MUC1 (Ukkonen et al., 2017) and small salivary proteins, and an external layer mainly composed of MUC5B (Macakova et al., 2010). The MUC5B-rich moiety is consistently thought to be chiefly responsible for the lubrication properties of this structure. Therefore, in order to focus on astringency, which is characterized as a loss of lubrication, the impact of tannins of the MUC5B layer was specifically studied.

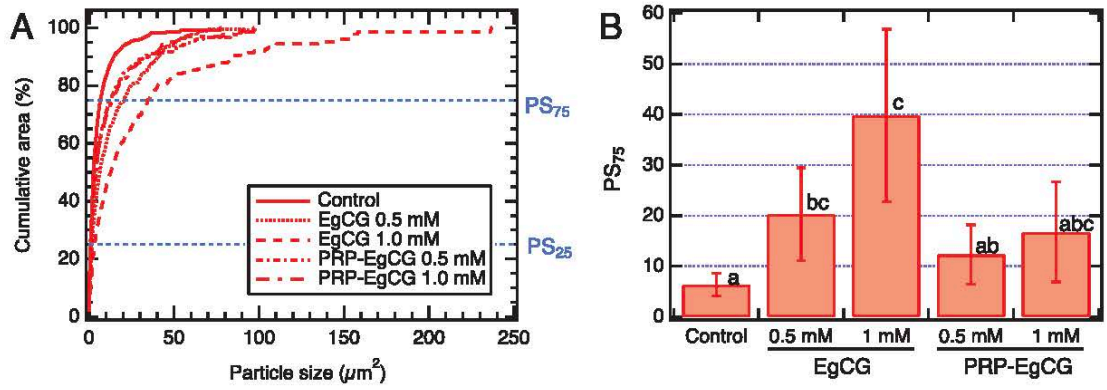

Fig. 6. Impact of PRP on MUC5B-tannins aggregates size. Distribution of particle size and particle size at 75% of the cumulative particle area after exposure of the *in vitro* model to the tannin EgCG at 0.5 mM and 1 mM, in presence or not of the bPRP IB5 (0.33 mM).

The impact of tannins on coating of oral surfaces by mucins has been previously studied. Thus, by quantifying mucins in solutions of tannins swirled in mouth and expectorated, Lee and Vickers (2012) reported that the mucus coating was not substantially altered, and suggested that tannins-mucins complexes may remain on mucosal surfaces. Another study reported that mouth rinsing with tannic acid modified the dental pellicle ultrastructure by making it distinctly more electron dense (Hertel et al., 2017), and the authors proposed that the dental pellicle might be strengthened by the inclusion of PRP-tannic acid complexes. Together, these two studies suggest that mucins are not extensively removed from oral surfaces by tannins. What we observed, namely the formation of aggregates, rather suggests that the spatial distribution of mucins is impacted by tannins. Aggregation of MUC5B by EgCG, and thus modification of the MUC5B network, has been previously reported (Davies et al., 2014). For a concentration of purified MUC5B of 15 $\mu g.ml^{-1}$ (i.e. ~0.027 μM), an increase of aggregate size was observed by AFM for EgCG at 0.075 and 0.375 mM in a dose-dependent manner with an average area reaching ~36,000 nm^2 at the high EgCG level, i.e. an average radius in the range of 100–120 nm (assuming that aggregates are circular-shaped). Using another mucin (porcine gastric mucin) at much higher concentration (~1.8 μM) with also much more concentrated EgCG (up to 22 mM), there was also an increase of aggregates' size with a tannin dose-effect and the average aggregate radius measured either by Dynamic Light Scattering or AFM was not substantially different from the previous study, in the range of 200 nm for the highest EgCG concentration (McColl, Horvath, Yakubov, & Ramsden, 2017). Another study using a much lower EgCG:mucin molar ratio (90 μM EgCG:1.8 μM pig gastric mucin) reported that no large aggregates were present, and estimated the radius of mucin-EgCG blobs (measured by TEM) at ~12–20 nm (Zhao et al., 2012). In our present study, and although the method of measurement (particle detection by image analysis on fluorescent images) may slightly over-estimate the size of aggregates due to the diffusion of fluorescence, the average aggregate size is quite clearly higher (radii range: 600–900 nm) than in the three studies quoted above. The EgCG:mucin molar ratio is not known here, especially since the MUC5B are not in solution but adsorbed to the cells' surface. However, another major difference between our study and the three others is that we worked on whole saliva and not purified mucin. Therefore, the presence of other salivary proteins likely has an effect on the formation of aggregates.

Protein aggregates can be formed in presence of tannins due to the multidentate properties of the latter, allowing to bridge two proteins together (Canon et al., 2013). The aggregation process induced by tannins has been extensively described for bPRPs, where aggregation occurs when at least three tannins are bound per protein and where aggregate size increases with tannin concentration, with radii reaching up to 1000 nm (Canon et al., 2013). In addition, glycosylation of PRPs prevents their aggregation by tannins (Sarni-Manchado, Canals-Bosch, Mazerolles, & Cheynier, 2008), precluding bridging of the peptidic chains due to steric hindrance. This last element is of interest for the process of aggregation of mucins, since these large proteins present a central region that is heavily glycosylated, flanked by the C and N terminal protein domains with relatively little glycosylations. Indeed, Davies et al. (2014) reported the aggregation by EgCG of MUC5B N- and C-terminal protein domains, but not of oligosaccharide-rich regions. Therefore, it is likely that aggregation expands from the unglycosylated regions. We also propose that other salivary proteins may be involved in this process and possibly facilitate the aggregation, especially if their degree of glycosylation is null or limited. The co-precipitation of mucins and other proteins by various astringent compounds has recently been reported and characterized, and it was found that amylase, cystatins and PRPs were particularly abundant in the precipitates formed upon incubation of saliva with EgCG (Delius, Medard, Kuster, & Hofmann, 2017). Cystatins have been described by several authors as constituents of the mucosal pellicle (Bradway et al., 1992; Gibbins & Carpenter, 2013), and MUC5B is known to form heterotypic complexes with salivary proteins, such as amylase and PRPs (Iontcheva, Oppenheim, & Troxler, 1997). This suggests that the MUC5B aggregates which we observed are more precisely aggregates of several types of proteins with tannins, and that the inclusion of other proteins with a propensity to aggregation could explain the larger average size that we observed compared to studies based on purified mucins.

The size of the aggregates was also influenced by the tannin structure, with higher values for EgCG than for EgC. Generally, interaction between the phenolic hydroxyl groups of EgC and EgCG and the amide groups of proteins is responsible for binding of these tannins to saliva proteins (Haslam, Lilley, Magnolato, & Warminski, 1992). However, EgCG differs structurally from EgC by an extra galloyl group and it has been previously shown that galloylation, representing one additional potential site for interaction, enhances aggregation (Poncet-Legrand, Cartalade, Putaux, Cheynier, & Vernhet, 2003). Davies et al. (2014) also observed different behaviours of salivary mucins in the presence of epicatechin (EC) or EgCG, in particular the absence of MUC5B aggregation when exposed to EC as opposed to EgCG. Our results are also in general agreement with those of Schwarz and Hofmann (2008) who measured the protein binding activity of 13 different astringents and found that binding of whole saliva proteins was highest for the compounds containing at least one galloyl group (Schwarz & Hofmann, 2008). Binding being a prerequisite to aggregation, it is consistent with the effect of galloylation on aggregate size that we observed.

Having clearly demonstrated that EgC and EgCG can alter the mucosal pellicle by inducing mucin aggregates, one may wonder what the sensory consequences of such structural modifications are. Overall, saliva is considered responsible for the lubrication between oral

surfaces, by maintaining wetness and reducing abrasion. For example, adsorption for 1 h of human saliva to synthetic surfaces reduces the friction coefficient by a factor of 20 (Berg, Rutland, & Arnebrant, 2003). Among the different proteins thought to participate to the rheological and tribological properties of saliva, the gel-forming MUC5B has received special attention. Mucins are highly hydrated, amphiphilic glycoproteins that facilitate lubrication in each of the three lubrication regimes that can occur in the presence of a fluid (boundary, mixed or hydrodynamic lubrication) (Coles, Chang, & Zauscher, 2010). Boundary lubrication of oral surfaces, which is characterized by a low film thickness (Coles et al., 2010), occurs when the surfaces (e.g. tongue and palate, cheek mucosa and teeth) are in full contact, which we believe occurs inevitably in the context of food oral processing. In addition, salivary pellicles formed on hydrophobic synthetic surfaces result in friction coefficients that remain low, even in the boundary regime (Macakova, Yakubov, Plunkett, & Stokes, 2011). Finally, direct interaction of tannins with proteins of the mucosal pellicle increased the perceived astringency of tea (Nayak & Carpenter, 2008). These two elements (role of mucins in boundary lubrication, importance of salivary pellicles in instrumentally-measured or sensorially-perceived friction) suggest that the MUC5B mucins included in salivary pellicles most likely contribute to the mouthfeel perceived on mucosal surfaces during eating or drinking. Their aggregation induced by tannins, as we measured in this study, would contribute to the loss of lubrication and to the typical dry and rough feeling of astringency. This is consistent with the increase of the friction coefficient of pre-adsorbed salivary pellicle formed onto synthetic surfaces when exposed to EgCG (Rossetti, Bongaerts, Wantling, Stokes, & Williamson, 2009). In the present study, we also measured at the 3 mM EgCC concentration an increased friction force at the surface of the epithelial cells. Besides this loss of lubrication, it is possible that aggregation can also result in a discontinuous and patchy mucosal pellicle, exposing the underneath epithelial cells. Tannins can interact directly with and bind to epithelial cells (Soares et al., 2016), which has been proposed to be another mechanism at the origin of astringency (Green, 1993). The possible involvement of chemoreceptors (Schobel et al., 2014; Sirk, Friedman, & Brown, 2011) or the binding to lipid of cell membranes (Sirk et al., 2011) have, for example, been suggested. Therefore, alteration of the mucosal pellicle by tannins, as documented here, could lead to astringency through these different mechanisms.

It is interesting at this stage to link our observations with the sensory perception of tannins. The intensity of the astringency sensation elicited by tannins depends on both their concentration and structure, for example their degree of polymerization (Vidal et al., 2003) or the stereochemistry of monomers (Thorngate & Noble, 1995). When it comes to sensory thresholds, data are very scarce. This is probably due to the methodological challenge constituted by the relatively slow development of astringency after ingestion and its long persistence and the fact that the perceived intensity of the same astringent solution increases upon repeated exposures (Green, 1993). For these reasons, the classical sensory methods for determination of detection or recognition thresholds are not well adapted. Nevertheless, recognition thresholds of 0.52 and 0.19 mM were reported for EgC and EgCG, respectively (Scharbert et al., 2004). These values are consistent with the fact that the mucin aggregate sizes were overall larger for the more astringent compound EgCG. Therefore, although this would need to be further confirmed, this suggests that the aggregate size distribution (particularly the presence and proportion of larger aggregates) is correlated with the perceived astringency of this class of tannins. One should note that the friction measured by AFM was significantly increased only for a higher concentration (3 mM). This is not entirely surprising since, as we suggested above, the loss of lubrication is probably only one consequence of the mucosal pellicle alteration. Other mechanisms (interactions of tannins with the membrane lipids, activation of specialized receptors) may participate to the astringency sensation, as also suggested in another study focussing on friction coefficients of salivary films (Rossetti et al., 2009). This can explain that human oro-sensory perception is more sensitive than the instrumental measure of only one aspect of the astringency sensation.

Another difference between the various *in vitro* studies and the human physiological situation is the presence of free flowing saliva in the oral cavity when a subject consumes a tannin-containing beverage. Based on this, we tested a second hypothesis, namely that PRPs in solution play a protective role towards tannins, precluding their access to the mucosa and its consequent structural alteration. We indeed observed that in the presence of the human PRP IB5 at physiological concentration, the formation of mucin aggregates induced by EgCG was limited. PRPs belong to the intrinsically disordered proteins, with an unusual extended conformation (Boze et al., 2010). This structure enables bPRPs to bind several tannins but also different types of tannins (Canon, Giuliani, Paté, & Sarni-Manchado, 2010), which could lead to an unfolded to folded structural transition (Canon et al., 2011). bPRP-tannin interaction occurs in three steps: formation of soluble non-covalent complexes, formation of aggregates from these supramolecular edifices and ultimately precipitation (Canon et al., 2013). At 0.33 mM IB5, the use of Small Angle X-ray Scattering enabled to determine that aggregation starts when EgCG concentration exceeds 0.5 mM approximately (Canon et al., 2013). In this study, we also observed visually that the threshold of precipitation of IB5 by EgCG was situated between 0.5 and 1 mM (data not shown). Therefore, in our conditions, it is expected that at 0.5 mM EgCG, aggregates are formed but they do not necessarily precipitate onto the mucosal pellicle. At 1 mM in contrast, aggregates are formed and they also precipitate. In both cases, the interactions between PRP and tannins limit the concentration of tannins which can interact with and alter the mucosal pellicle, as we observed based on mucin aggregates' size. However, the sensory implications are not straightforward, since astringency of tannins results probably from several mechanisms: loss of lubrication properties of free flowing saliva induced for example by salivary proteins aggregation (Lu & Bennick, 1998), direct tactile perception of large aggregates/precipitates of proteins from free saliva (Canon et al., 2013) and/or alteration of the mucosal pellicle (as we demonstrated here) with the several possible consequences discussed above. To sum up, we propose that the different following events occur in the oral cavity, depending on tannin concentration: around the threshold of aggregation of PRP by tannin, soluble aggregates are formed and it is possible that the consequent modification of the lubricating power of saliva is already perceived. Around the threshold of precipitation, in addition to the reduced lubrication properties of free flowing saliva, PRP-EgCG complexes precipitate onto the mucosal surfaces with certainly an impact on the lubricating function of the mucosal pellicle (although it is not at this stage structurally altered to a very large extent). At even higher concentrations, when the tannin concentration exceeds the capacity of interactions between PRPs and tannins, tannins can also alter the mucosal pellicle structure. From a sensory point of view, these different events combine to form the complex astringency sensation.

One should finally keep in mind that these different mechanisms are intimately dependent on the initial concentration of PRPs in saliva, which shows high inter-individual variability (Cabras et al., 2012), but also on the initial mucosal pellicle structure. This topic of inter-individual variability deserves further attention in order to gain a deeper understanding of variability in flavour perception.

Conflict of interest statement

The authors declare no conflict of interest.

Acknowledgments

This work was funded by the French National Research Agency (MUFFIN ANR-14-CE20-0001-01), FEDER and Region Bourgogne Franche-Comte grants.

References

Bennick, A. (1982). Salivary proline-rich proteins. *Molecular and Cellular Biochemistry, 45*, 83–99.

Berg, I. C. H., Rutland, M. W., & Arnebrant, T. (2003). Lubricating properties of the initial salivary pellicle – An AFM Study. *Biofouling, 19*(6), 365–369.

Biegler, M., Delius, J., Käsdorf, B. T., Hofmann, T., & Lieleg, O. (2016). Cationic astringents alter the tribological and rheological properties of human saliva and salivary mucin solutions. *Biotribology, 6*, 12–20.

Boze, H., Marlin, T., Durand, D., Pérez, J., Vernhet, A., Canon, F., ... Cabane, B. (2010). Proline-rich salivary proteins have extended conformations. *Biophysical Journal, 99*, 656–665.

Bradway, S. D., Bergey, E. J., Scannapieco, F. A., Ramasubbu, N., Zawacki, S., & Levine, M. J. (1992). Formation of salivary-mucosal pellicle: The role of transglutaminase. *Biochemical Journal, 284*, 557–564.

Cabras, T., Melis, M., Castagnola, M., Padiglia, A., Tepper, B. J., Messana, I., & Tomassini Barbarossa, I. (2012). Responsiveness to 6-n-propylthiouracil (PROP) is associated with salivary levels of two specific basic proline-rich proteins in humans. *PLoS One, 7*(2), e30962.

Canon, F., Ballivian, R., Chirot, F., Antoine, R., Sarni-Manchado, P., Lemoine, J.r.m., & Dugourd, P. (2011). Folding of a salivary intrinsically disordered protein upon binding to tannins. *Journal of the American Chemical Society, 133*(20), 7847–7852.

Canon, F., Giuliani, A., Paté, F., & Sarni-Manchado, P. (2010). Ability of a salivary intrinsically unstructured protein to bind different tannin targets revealed by mass spectrometry. *Analytical and Bioanalytical Chemistry, 398*, 815–822.

Canon, F., Paté, F., Cheynier, V., Sarni-Manchado, P., Giuliani, A., Pérez, J., ... Cabane, B. (2013). Aggregation of the salivary proline-rich protein IB5 in the presence of the tannin EgCG. *Langmuir, 29*(6), 1926–1937.

Coles, J. M., Chang, D. P., & Zauscher, S. (2010). Molecular mechanisms of aqueous boundary lubrication by mucinous glycoproteins. *Current Opinion in Colloid & Interface Science, 15*(6), 406–416.

Davies, H. S., Pudney, P. D., Georgiades, P., Waigh, T. A., Hodson, N. W., Ridley, C. E., ... Thornton, D. J. (2014). Reorganisation of the salivary mucin network by dietary components: Insights from green tea polyphenols. *PLoS One, 9*(9), e108372.

Delius, J., Medard, G., Kuster, B., & Hofmann, T. (2017). Effect of astringent stimuli on salivary protein interactions elucidated by complementary proteomics approaches. *Journal of Agricultural and Food Chemistry, 65*(10), 2147–2154.

Gibbins, H. L., & Carpenter, G. H. (2013). Alternative mechanisms of astringency – What is the role of saliva? *Journal of Texture Studies, 44*(5), 364–375.

Gibbins, H. L., Yakubov, G. E., Proctor, G. B., Wilson, S., & Carpenter, G. H. (2014). What interactions drive the salivary mucosal pellicle formation? *Colloids and Surfaces B: Biointerfaces, 120*, 184–192.

Green, B. G. (1993). Oral astringency: A tactile component of flavor. *Acta Psychologica, 84*, 119–125.

Hannig, C., Hannig, M., Kensche, A., & Carpenter, G. (2017). The mucosal pellicle – An underestimated factor in oral physiology. *Archives of Oral Biology, 80*, 144–152.

Haslam, E., Lilley, T. H., Magnolato, D., & Warminski, E. E. (1992). The influence of polysaccharides upon polyphenol-protein interactions. JIEP92, 16(2), 266–269.

Hertel, S., Potschke, S., Basche, S., Delius, J., Hoth-Hannig, W., Hannig, M., & Hannig, C. (2017). Effect of tannic acid on the protective properties of the in situ formed pellicle. *Caries Research, 51*(1), 34–45.

Iontcheva, I., Oppenheim, F. G., & Troxler, R. F. (1997). Human salivary mucin MG1 selectively forms heterotypic complexes with amylase, proline-rich proteins, statherin, and histatins supramolecular edificies. *Journal of Dental Research, 76*(3), 734–743.

Lee, C. A., & Vickers, Z. M. (2012). Astringency of foods may not be directly related to salivary lubricity. *Journal of Food Science, 77*(9), S302–306.

Lu, Y., & Bennick, A. (1998). Interaction of tannin with human salivary proline-rich proteins. *Archives of Oral Biology, 43*(9), 717–728.

Macakova, L., Yakubov, G. E., Plunkett, M. A., & Stokes, J. R. (2010). Influence of ionic strength changes on the structure of pre-adsorbed salivary films. A response of a natural multi-component layer. *Colloids and Surfaces B: Biointerfaces, 77*(1), 31–39.

Macakova, L., Yakubov, G. E., Plunkett, M. A., & Stokes, J. R. (2011). Influence of ionic strength on the tribological properties of pre-adsorbed salivary films. *Tribology International, 44*(9), 956–962.

McColl, J., Horvath, R., Yakubov, G. E., & Ramsden, J. J. (2017). Surface rearrangement of adsorbed EGCG–mucin complexes on hydrophilic surfaces. *International Journal of Biological Macromolecules, 95*, 704–712.

Morzel, M., Tai, S., Brignot, H., & Lherminier, J. (2014). Immunocytological detection of salivary mucins (MUC5B) on the mucosal pellicle lining human epithelial buccal cells. *Microscopy Research and Technique, 77*, 453–457.

Nayak, A., & Carpenter, G. H. (2008). A physiological model of tea-induced astringency. *Physiology & Behavior, 95*(3), 290–294.

Ployon, S., Belloir, C., Bonnotte, A., Lherminier, J., Canon, F., & Morzel, M. (2016). The membrane-associated MUC1 improves adhesion of salivary MUC5B on buccal cells. Application to development of an in vitro cellular model of oral epithelium. *Archives of Oral Biology, 61*, 149–155.

Poncet-Legrand, C., Cartalade, D., Putaux, J.-L., Cheynier, V., & Vernhet, A. (2003). Flavan-3-ol aggregation in model ethanolic solutions: Incidence of polyphenol structure, concentration, ethanol content and ionic strength. *Langmuir, 19*(25), 10563–10572.

Rossetti, D., Bongaerts, J. H. H., Wantling, E., Stokes, J. R., & Williamson, A. M. (2009). Astringency of tea catechins: More than an oral lubrication tactile percept. *Food Hydrocolloids, 23*(7), 1984–1992.

Sarni-Manchado, P., Canals-Bosch, J., Mazerolles, G., & Cheynier, V. (2008). Influence of the glycosylation of human salivary proline-rich proteins on their interactions with condensed tannins. *Journal of Agricultural and Food Chemistry, 56*(20), 9563–9569.

Scharbert, S., Holzmann, N., & Hofmann, T. (2004). Identification of the astringent taste compounds in black tea infusions by combining instrumental analysis and human bioresponse. *Journal of Agricultural and Food Chemistry, 52*(11), 3498–3508.

Schobel, N., Radtke, D., Kyereme, J., Wollmann, N., Cichy, A., Obst, K., ... Hatt, H. (2014). Astringency is a trigeminal sensation that involves the activation of g protein-coupled signaling by phenolic compounds. *Chemical Senses*.

Schwarz, B., & Hofmann, T. (2008). Is there a direct relationship between oral astringency and human salivary protein binding? *European Food Research And Technology, 227*(6), 1693–1698.

Shimada, T. (2006). Salivary proteins as a defense against dietary tannins. *Journal of Chemical Ecology, 32*(6), 1149–1163.

Sirk, T. W., Friedman, M., & Brown, E. F. (2011). Molecular binding of black tea theaflavins to biological membranes: Relationship to bioactivities. *Journal of Agricultural and Food Chemistry, 59*(8), 3780–3787.

Soares, S., Ferrer-Galego, R., Brandao, E., Silva, M., Mateus, N., & de Freitas, V. (2016). Contribution of human oral cells to astringency by binding salivary protein/tannin complexes. *Journal of Agricultural and Food Chemistry*.

Thorngate, J. H., & Noble, A. C. (1995). Sensory evaluation of bitterness and astringency of 3R(-)-epicatechin and 3S(+)-catechin. *Journal of the Science of Food and Agriculture, 67*, 531–535.

Ukkonen, H., Pirhonen, P., Herrala, M., Mikkonen, J. J. W., Singh, S. P., Sormunen, R., & Kullaa, A. M. (2017). Oral mucosal epithelial cells express the membrane anchored mucin MUC1. *Archives of Oral Biology, 73*, 269–273.

Vidal, S., Francis, L., Guyot, S., Marnet, N., Kwiatkowski, M., Gawel, R., ... Waters, E. J. (2003). The mouth-feel properties of grape and apple proanthocyanidins in a wine-like medium. *Journal of the Science of Food and Agriculture, 83*(6), 564–573.

Zhao, Y., Chen, L., Yakubov, G., Aminiafshar, T., Han, L., & Lian, G. (2012). Experimental and theoretical studies on the binding of epigallocatechin gallate to purified porcine gastric mucin. *The Journal of Physical Chemistry B, 116*(43), 13010–13016.

Publication n°4: Proline-rich salivary proteins have extended conformations.

Boze, H.; Marlin, T.; Durand, D.; Pérez, J.; Vernhet, A.; Canon, F.; Sarni-Manchado, P.; Cheynier, V.; Cabane, B.

Biophys. J. ***2010,*** *99, 656-665.*

Proline-Rich Salivary Proteins Have Extended Conformations

Hélène Boze,[†] Thérèse Marlin,[†] Dominique Durand,[‡] Javier Pérez,[§] Aude Vernhet,[†] Francis Canon,[†] Pascale Sarni-Manchado,[†] Véronique Cheynier,[†] and Bernard Cabane[¶*]

[†]INRA, Montpellier SupAgro, UMR 1083 Sciences pour l'Œnologie, F-34060 Montpellier, France; [‡]IBBMC, CNRS UMR 8619, Université Paris-Sud, 91405 Orsay, France; [§]Beamline SWING, Synchrotron SOLEIL, BP 48, 91192 Gif-sur-Yvette, France; and [¶]PMMH, CNRS UMR 7636, ESPCI, 75231 Paris cedex 05, France

ABSTRACT Three basic proline-rich salivary proteins have been produced through the recombinant route. IB5 is a small basic proline-rich protein that is involved in the binding of plant tannins in the oral cavity. II-1 is a larger protein with a closely related backbone; it is glycosylated, and it is also able to bind plant tannins. II-1ng has the same polypeptidic backbone as II-1, but it is not glycosylated. Small angle x-ray scattering experiments on dilute solutions of these proteins confirm that they are intrinsically disordered. IB5 and II-1ng can be described through a chain model including a persistence length and cross section. The measured radii of gyration ($R_g = 27.9$ and 41.0 ± 1 Å respectively) and largest distances ($r_{max} = 110$ and 155 ± 10 Å respectively) show that their average conformations are rather extended. The length of the statistical segment (twice the persistence length) is $b = 30$ Å, which is larger than the usual value (18 Å – 20 Å) for unstructured polypeptide chains. These characteristics are presumably related to the presence of polyproline helices within the polypeptidic backbones. For both proteins, the radius of gyration of the chain cross-section is $R_c = 2.7 \pm 0.2$Å. The glycosylated protein II-1 has similar conformations but the presence of large polyoside sidegroups yields the structure of a branched macromolecule with the same hydrophobic backbone and hydrophilic branches. It is proposed that the unusually extended conformations of these proteins in solution facilitate the capture of plant tannins in the oral cavity.

INTRODUCTION

Intrinsically disordered proteins (IDPs), often referred to as naturally unfolded proteins are proteins that lack well-structured 3D folds, and therefore do not have a stable tertiary structure (1–8). These proteins have long remained relatively obscure in our view of the protein universe because they do not crystallize, and therefore do not produce any diffraction spot in x-ray crystallography. More recently, it has been shown that ~30% of all proteins in eukaryotic organisms are intrinsically unstructured (5,9). This discovery challenged the traditional protein structure paradigm, which stated that a specific well-defined structure was required for the correct function of a protein. Biochemical evidence has since shown that intrinsically unfolded proteins are functional and that their lack of folded structures is related to their functions (10).

Intrinsically unstructured proteins have particular sequences. The sequence signature of unfolded proteins (or unfolded regions of proteins) is as follows: 1), a bias toward polar and charged amino acids (Gln, Ser, Pro, Glu, Lys); 2), a bias away from bulky hydrophobic residues Val, Leu, Met, Phe, Trp, Tyr); and 3), in some cases a low sequence complexity with repeated short amino acid sequences.

Salivary proline rich proteins (sPRPs), which constitute about two-thirds of proteins secreted by the human parotid glands, have this type of sequence signature (11,12). They contain repeated sequences with high proportions of Pro, Gly and Gln, or Glu residues (1,3,4). Circular dichroism and NMR studies of some of these proteins give indications of largely disordered structures with short polyproline II helical sections (13–15). sPRPs are divided into glycosylated, acidic, and basic types that, despite their structural similarities, have different functions (16).

The function of basic salivary PRPs (bPRPs) is to bind polyphenolic plant compounds (e.g., tannins) present in food (17,18) and thus protect against their anti-nutritional effects (19). bPRPs are present in the saliva of primates and herbivorous animals but almost absent in that of carnivorous animals. They make it possible for herbivorous animals to consume foods that contain up to 5% tannins by weight. The capacity of bPRPs to bind and precipitate tannins has been ascribed to their proline rich sequences (20,21) that, together with their high glycine content (22), confers them an open structure providing a large binding surface and multiple contact points (3,4,20,23,24). Moreover, the proline residues may provide hydrophobic interactions and hydrogen bond acceptor sites for the binding of tannins.

Glycosylated proline rich proteins (PRPs) ensure oral lubrication, bind oral bacteria, and are also able to bind tannins (20,25,26). Earlier biophysical data suggest that oligosaccharide moieties attached to a protein backbone may be capable of assuming a variety of conformational geometries depending on the oral surface with which it interacts (25,27). Thus, the shape or conformation of these salivary molecules could play an important role in defining their functional role in the oral cavity. These proteins account for ~17% of human parotid salivary proteins (12,28,29).

Submitted January 28, 2010, and accepted for publication April 21, 2010.

*Correspondence: bcabane@pmmh.espci.fr

Editor: Martin Blackledge.

0006-3495/10/07/0656/10 $2.00

doi: 10.1016/j.bpj.2010.04.050

This study is part of a larger project focused on the interactions of plant tannins with salivary proteins. For this purpose, we have developed an heterologous expression system for the production of some human basic PRPs through integration of the gene coding for a human salivary proline-rich pro-protein, PRB4S, into a yeast genome (30). We obtained a nonglycosylated protein (IB5), a glycosylated protein (II-1), and the nonglycosylated form of the latter (II-1ng). Preliminary investigations indicate that these proteins do bind tannins (21,31). Moreover, we have shown the presence in solution of IB5-tannin soluble supramolecular structures with different stoichiometries that show the ability of bPRPs to bind and scavenge tannins (32). Increasing tannin concentration leads to the precipitation of IB5-tannin complexes, whereas only limited aggregation is observed with the glycosylated protein II-1 at the same protein/tannin ratio (33). These different behaviors may be related to the functions of these proteins, involving either complexation of tannin molecules in ingested foods and drinks, which may reduce their toxicity, or formation of precipitates, which may contribute to the perception of astringency in the oral cavity.

We report a small angle x-ray scattering (SAXS) study of these proteins (for general references see Receveur-Bréchot et al. (7) and Bernadó and Blackledge (8)). The aim is to gain a precise view of their conformations and to find out whether these conformations confer functional advantages like the ability to bind several tannin ligands. However, IDPs in solution explore an enormous number of conformations, and SAXS experiments only determine average correlations between the relative positions of atoms in the macromolecules. We addressed this problem in the following way. First, we acquired high quality spectra with a high resolution (10 Å), to maximize the information content of the data. Then we determined a set of geometrical parameters that characterize the average protein structure, such as the radius of gyration, persistence length and cross-section of the polypeptide chain, and we compared these structural parameters to those of other intrinsically disordered proteins. Finally we used mathematical algorithms to produce representative conformations that reproduce the experimental scattering curves.

MATERIALS AND METHODS

Large-scale production and purification of PRPs

The *Pichia pastoris* system for expression of heterologous recombinant proteins has been used. It allows large yields of properly matured proteins and generally yields protein-bound oligosaccharides that are of much shorter chain length than found in *Saccharomyces cerevisiae* (34). As described previously, bPRPs were overexpressed on a large scale in *P. pastoris* using the methanol-inducible alcohol oxidase promoter (35). They were produced during the growth phase and secreted into the culture medium. Five majors bands around the expected molecular weight (apparent molar masses 45–15 KDa) were detected in the supernatant with sodium dodecyl sulfate-polyacrylamide gel electrophoresis (SDS PAGE) analysis (Fig. 1, *lane 1*). The SDS PAGE technique was carried out under reducing conditions using

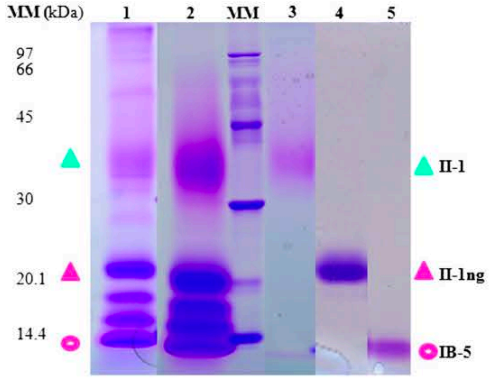

FIGURE 1 SDS-PAGE patterns of proteins obtained at successive stages of purification. (*Lane 1*) Crude supernatant. (*Lane 2*) PRP extract after streamline. (*Lane 3*) Purified fraction of the glycosylated protein II-1 (*blue triangle*). (*Lane 4*) Purified fraction of the nonglycosylated form of II-1 (II1ng) (*pink triangle*). (*Lane 5*) Purified fraction of IB-5 (*pink circle*). MM, molecular mass markers.

12.5% acrylamide running gels, the protein bands were stained by R250 Coomassie brilliant blue (35,36) and the organic solvent was omitted from the acetic acid destaining solution. In these conditions the PRP bands appear pink-violet; IB5 and II-1ng give neat pink bands whereas II-1 gives a very diffuse one.

Ion-exchange chromatography

After centrifugation of the crude medium, the recombinant PRPs were recovered from the supernatant using a single step ion-exchange (cationic) chromatography. Their high isoelectric point (above pH = 11) allows binding to the silica surfaces of the ion exchange column at neutral pH and moderate ionic strength, whereas the other macromolecules (yeast proteins and polysaccharides) of the supernatant do not. We used a FPLC Biocad/Sprint system (Perseptive Biosystems, MA) with a Pharmacia Streamline 50 column (id 2 cm/L 40 cm). The matrix (Streamline SP XL) was equilibrated in buffer (50 mM Tris HCl, pH 8.0). A preparative chromatography technique called expanded bed adsorption was used. The gel was expanded using upside flow at 13 mL/min until the top of the bed was stable. The supernatant obtained after centrifugation of the crude culture (280 mL/run) was applied after dilution (1:2) in the same buffer to the column (upside flow). The flow was subsequently inverted (downside flow) and the plunger was lowered to 1 cm from the top of the bed. The proteins were eluted with 150 mL of the same buffer containing 1 M NaCl at a 5 mL $\times$ min^{-1} flow rate. The protein elution was monitored by measuring absorbance at 230 nm. The purified extract contained five PRPs, and was free of polysaccharides and yeast proteins (Fig. 1, *lane 2*).

Gel filtration chromatography and sample preparation

A partial separation of the five PRPs was carried out through size exclusion chromatography using the FPLC Biocad/Sprint system. Aliquots of the extract purified previously were applied on a Superdex 75 HR 3.2/30 PC or a Hiload 16/60 Superdex 75 column (Pharmacia), using ammonium acetate 50 mM, pH 5.5 buffer at a 0.8 mL $\times$ min^{-1} flow rate. The elution was monitored by absorbance at 230 nm. Collected fractions were checked by SDS-PAGE. Those containing either IB5, II-1, or II-1ng were freeze-dried until use. The purified proteins were checked by MS experiments. The masses obtained from spectra deconvolution were in agreement with

the theoretical ones determined from their primary sequences (32, F. Canon, unpublished). For the SAXS experiments, the protein solutions were prepared by mixing carefully weighted volumes of protein powder and of buffer (ammonium acetate 50 mM pH 5.5 buffer) in such a way that the concentration was known precisely. The samples were then injected in a capillary located on the beam path, at a temperature regulated at 20°C. We checked that solutions made without and with freeze-drying give identical spectra.

SAXS instruments and methods

SAXS experiments were carried out using the Nanostar instrument (Bruker, Karlsruhe, Germany) at IBBMC in Orsay. The x-rays were produced by a rotating anode (Cu Kα, wavelength $\lambda = 1.54$ Å), and the scattered x-rays were collected using a 2D position sensitive detector (Vantec) positioned at 662 mm from the sample. The scattering vector range was $0.011 < q < 0.40$ Å^{-1} where $q = 4\pi\sin\theta/\lambda$ and 2θ is the scattering angle. Further experiments were carried out on the beamline SWING, at the Synchrotron SOLEIL. The incident beam energy was 12 keV, and the sample to detector (Aviex CCD) distance was set to 1927 mm. The scattering vector range was $0.008 < q < 0.49$ Å^{-1}. Several successive frames (typically 25) of 4 s each were recorded for both sample and pure solvent. We checked that x-rays did not cause irradiation damage by comparing the successive frames, before calculating the average intensity and experimental error. For protein IB5, identical spectra were obtained from the Nanostar instrument and from Swing; the data presented in this study are from Swing. For II-1ng and II-1, spectra were obtained with the Nanostar only. Scattering from the pure solvent was measured and subtracted from the corresponding protein spectra. Intensities were scaled using the scattering of water. For each protein, the original solutions (concentrations 5.8–8.7 g $\times$ L^{-1}) were compared to solutions with concentrations two and four times lower. The concentration dependence was very small, indicating that interactions between dissolved proteins were weakly repulsive at such concentrations. Indeed, at this concentration the average distance between the centers of mass of proteins was >14 nm, which is much larger than the Debye screening length in 50 mM salt (1.4 nm). Nevertheless the data at low and high concentrations are spliced to obtain SAXS curves unaffected by interparticle interactions at small angles and to improve the statistics in the outer region. The scattered intensities were measured on an absolute scale; calculations of the molar mass of each protein from the intensity extrapolated to $q \rightarrow 0$ gave values that were within 15% of those determined through ESI-MS, which is a usual accuracy given the uncertainties in the density of the proteins. This agreement confirmed that the dilute solutions contained independent macromolecules only.

RESULTS

Primary structures

The amino acid primary structures were deduced from N-terminal sequencing and mass spectrometry analysis of the proteins referred to the sequence of the cloned PRB4S cDNA. They showed the presence of four main isoforms of IB5 (Fig. 2 *a*), which differ by a few N-terminal amino acids, with molar masses 7481.36 (IB5a, abundance 14.5%), 7238.09 (IB5b, 44.3%), 7079.93 (IB5c, 27.8%), and 6923.74 (IB5d, 13.4%). Note that IB5 cannot be glycosylated because it lacks the N-glycosylation signal on its amino acid sequence.

For II-1 and II-1ng, ESI-MS has shown that two main forms and three minor ones were copurified. The average molar masses of the peptide backbones were 14,479.10 (II-1nga, 38%), 14,093.63 (II-1ngb, 28%), 14,180.72 (II-1ngc, 13%), 14,566.19 (II-1ngd, 8%), and 14,722.38 (II-1nge, 13%), all showing five sites for potential glycosylation (Fig. 2 *b*).

However, mass spectra of EndoH deglycosylated II-1 indicate that the main form of glycosylated II-1 presents one glycosylation (F. Canon, unpublished). The localization of this glycosylation among the five N-X-S sites has not been determined; however, it is known that those closest to the N-terminal are available for glycosylation for a longer time, and therefore are more likely to be glycosylated (38). The total mass of the polyosides bound to the II-1 backbone is estimated to be 26% of the mass of the protein, corresponding to ~20–30 mannose per protein. This is an average from monosaccharide assay after trimethylsilylation of

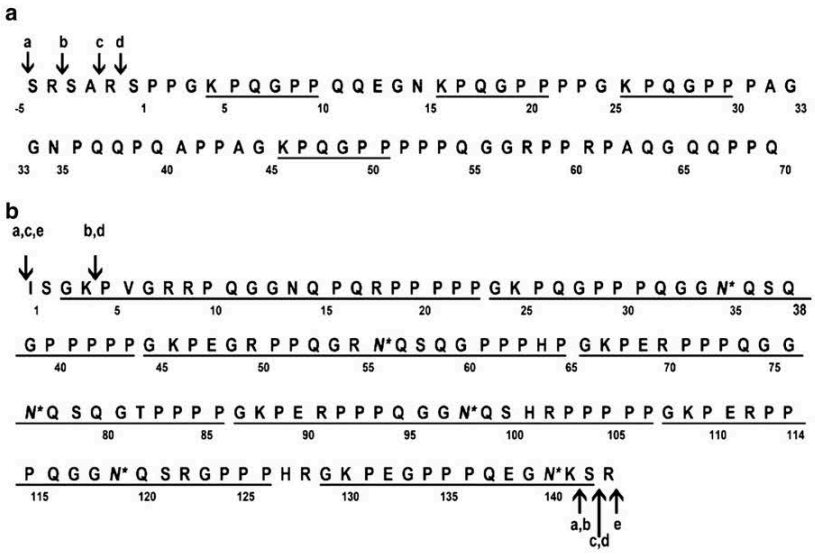

FIGURE 2 Sequences of the recombinant PRP (*a*) IB5 and (*b*) II-1. For IB5, four isoforms, IB5a–d, have been copurified, and five for II-1 (II-1a–e). For the two proteins, the isoforms differ by just a few amino acids. Repeated sequences are underlined and stars indicate potential sites of glycosylation.

polyosides (39) and aldolization methods (40). The broad band observed for protein II-1 in the SDS-PAGE experiments and crowded spectra obtained by ESI-MS indicate glycosylation heterogeneity classically observed during production of recombinant glycoproteins (41). Concerning the structure of these polyosides we can infer that they may be similar to those found in other recombinant glycosylated proteins arising from *P. Pastoris*. Its N-glycosylation synthesis pathway mirrors that of typical mammalian cells up to the point where Man8GlcNAc2 N-glycosylated proteins exit the endoplasmic reticulum. These proteins are a model of human salivary N-glycosylated PRPs (42–44).

Bioinformatic analysis

For proteins that may be partly or fully unstructured, there are some well established programs (www.disprot.org) that predict the extent of folding and structural order of their conformations in solution, on the basis of the amino acid sequence (45). All programs predicted no folding at all and a disorder index near maximum disorder (Fig. SI-1 in the Supporting Material). Such an extreme result is rather uncommon among unstructured proteins. Note, however, that these programs are not able to recognize the presence of short polyproline I (PPI) or polyproline II (PPII) structural elements that occur in proline rich proteins.

Conformations according to SAXS

For unstructured proteins that do not have a permanent secondary or tertiary structure, SAXS experiments determine the average conformation of the protein in solution. This average conformation is described by the pair distance distribution function $P(r)$, i.e., the number of different electron pairs with a mutual distance between r and $r + dr$ within the protein (46,47). For an isolated macromolecule, $P(r)$ is a function that initially grows with the number of chain elements that can be found at a distance r from a given chain element, goes through a maximum value P_{max} at the most populated distance and then decays to reach zero at the maximum distance r_{max} within the macromolecule. For the three proteins, IB5, II-1ng, and II-1, we calculated $P(r)$ from SAXS spectra using the GNOM procedure with the q range 0.015–0.35 $Å^{-1}$ (48) (Fig. 3). For comparison the calculated $P(r)$ of a freely jointed chain are also traced. The $P(r)$ of a dense sphere has a symmetrical shape that reflects the fact that the largest distance within a dense object is rather short; on the other hand, $P(r)$ of a freely jointed chain (i.e., a chain in which the orientations of successive segments are uncorrelated) has a long tail at large distances, because the conformations of such a chain stretch to large distances. The pair distance distributions of the three salivary proteins are similar to that of a freely jointed chain. For IB5 and to a lesser extent for II-1ng, $P(r)$ has a small shoulder around $r = 10$ Å, which may be tentatively ascribed to short and rigid structural elements within the chain (see below).

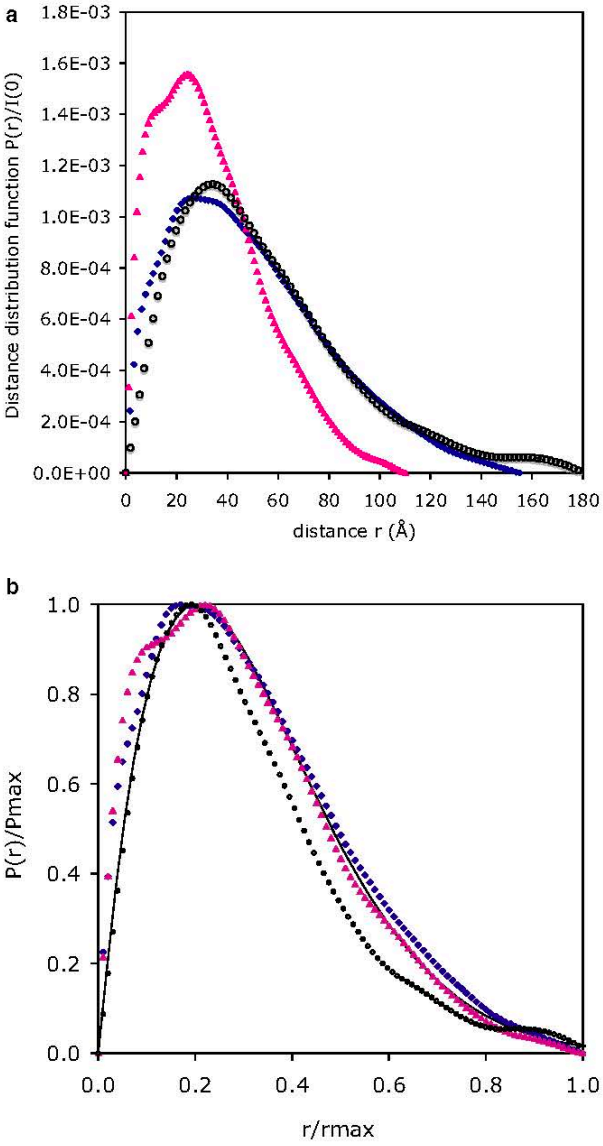

FIGURE 3 Pair distances distribution functions $P(r)$ for the proteins IB5 (*pink triangles*), II-1ng (*blue dots*), and II-1 (*open circles*). (*a*) Horizontal axis, distance r; vertical axis, distance distribution $P(r)/I(0)$. (*b*) Reduced coordinates r/r_{max} where r_{max} is the largest distance within each protein and $P(r)/P_{max}$ where P_{max} is the maximum value of $P(r)$. (*Solid line*) Theoretical distributions of freely jointed chains with the same radii of gyration.

Overall dimensions

Table 1 presents the radii of gyration R_g and maximum distances r_{max} of the three PRPs. The values of R_g were calculated from the pair distance distribution $P(r)$ according to the classical expression:

TABLE 1 Characteristic dimensions of the salivary proteins

Protein	M (Da)	L (Å)†	r_{max} (Å)*	R_g(Å)*, R_g (Å)†	b (Å)†	R_c (Å)†
IB5	7481, 7238, 7080, 6923	188 ± 10	110 ± 10	27.9 ± 1* 27.5 ± 1†	29.7 ± 1	2.7 ± 0.2
II-1ng	14,480, 14,095	364 ± 20	155 ± 10	41.0 ± 1* 40.3 ± 1†	29.9 ± 1	2.7 ± 0.2
II-1	20,000 (average)		178 ± 10	45.9 ± 2		2.7 ± 0.2

The radius of gyration of the cross section, R_c, was determined through Eq. 5 and the radius of gyration of the whole protein, R_g, was calculated according to $R_g^2 = (R_g^{SB})^2 + (3/2)R_c^2$ with R_g^{SB} given by Eq. 4.
*Structural parameters for the nonglycosylated proteins IB5 and II-1ng according to the $P(r)$.
†Structural parameters for the nonglycosylated proteins IB5 and II-1ng according to fits by Eqs. 2, 4, and 5.

$$R_g^2 = \frac{\int_0^D r^2 P(r)dr}{2\int_0^D P(r)dr}. \quad (1)$$

In the case of an extended protein it is more appropriate to use this relation rather than the well-known Guinier approximation that is valid only within a very restricted q range. These radii of gyration are much larger than those of globular proteins with comparable molar mass. Indeed, for globular proteins, the radius of gyration follows the law $R_g \approx 3(n)^{(1/3)}$ where n is the number of residues in the polypeptide backbone. Given the sequences of IB5 ($n \approx 70$) and II-1 ($n \approx 140$), this would yield $R_g = 12.4$ and 15.6 Å respectively, instead of the much larger values found here. On the other hand, an analysis of literature values for IDPs yields $R_g \approx 2.54(n)^{0.522}$ (8). For IB5, this would yield $R_g = 23.3$ Å, and for II-1ng, $R_g = 33.5$ Å. The experimental values for IB5 and II-1ng are still larger, indicating that these proteins have strongly extended conformations.

It is also instructive to compare the maximum distances. These are quite large (about half the end-to-end distance of a polyproline PPII helix), indicating again that the conformations are quite extended. There is also an interesting effect of the glycosylation on the overall dimensions. Indeed, comparing II-1 with II-1ng, we find that the maximum distance is 11% larger and the radius of gyration 15% larger. This reflects the contribution of the polyoside sidegroup, and is consistent with a location near the end rather than near the center of the macromolecule. Indeed, if the sidegroup was located near the center of the macromolecule, the maximum distance r_{max} of the glycosylated protein would be the same as that of the nonglycosylated one, and its radius of gyration R_g would be shorter rather than larger.

Shorter distances

The very large average dimensions of these proteins in solution must result from properties of the amino acid sequence. This is a question regarding finer details of the chain conformations, and the relevant information is contained in the high q part of the experimental spectra. These features are best seen in the Kratky-Porod representation, which enhances the high q part of the spectra. In this representation, a freely jointed chain yields a plateau at high q values because its scattering curve decays according to a q^{-2} power law. Fig. 4 compares the spectra of the three proteins, plotted in reduced coordinates, i.e., $I(q)/I(0)$ as a function of the reduced scattering vector $x^{1/2} = qR_g$. For comparison, the theoretical scattering curves of a dense sphere and a freely jointed chain are also traced. The scattering curve of the freely jointed chain is given by the Debye function $g_D(x)$:

$$I(q)/I(0) = g_D(x) = 2\left(e^{-x} + x - 1\right)/x^2. \quad (2)$$

At low q values, all spectra are superimposed, because of the use of reduced coordinates. At high q values, the spectra of the proteins IB5 and II-1ng rise above the theoretical curve for a freely jointed chain (Eq. 2). Accordingly, the

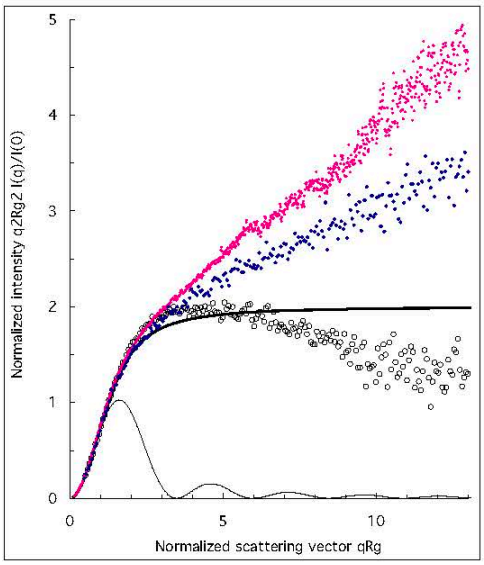

FIGURE 4 SAXS spectra for the proteins IB5 (*pink dots*), II-1ng (*blue dots*), and II-1 (*circles*), dissolved in ammonium acetate 50 mM pH 5.5 buffer. Horizontal axis: normalized scattering vector qR_g. Vertical axis: normalized intensity $(qR_g)^2\, I(q)/I(q \to 0)$. (*Thin full line*) Scattering curve for a dense homogenous sphere. (*Thick full line*) Scattering curve for a freely jointed chain (Eq. 2).

scattered intensity $I(q)$ has a decay that is in between that of a rod (q^{-1} power law) and that of freely jointed chain (q^{-2} power law). The classical way to describe such configurations is to introduce a persistence length that measures the orientational correlations between successive monomers. At large scales, a chain with a persistence length is equivalent to a random chain with a statistical element b that is twice the persistence length (49).

The spectrum of the glycosylated protein II-1 decays faster than the q^{-2} power law of a freely jointed chain. Because it has the same backbone as II-1ng, this faster decay must be an effect of the sugar groups. As indicated above (primary structures), II-1 has one large branched polyoside located at one of the potential glycosylation sites (most likely N_{35}). Hence the structure of the glycosylated protein is a branched chain, because the polyoside branches out from the chain at one location and because the polyoside is itself a branched chain. It is well known that branched chains yield faster decays at high q (50).

Chain models

To characterize the conformations by average geometrical parameters, we attempted to fit the experimental spectra with specific models. For the nonglycosylated proteins, the Kratky-Porod plot (Fig. 4) suggests that the appropriate model is a chain with a persistence length (51). We used the model proposed by Sharp and Bloomfield (52), which yields the following scattering function:

$$I_{SB}(q)/I(0) = g_D(x) + \frac{b}{L}\left[\frac{4}{15} + \frac{7}{15x} - \left(\frac{11}{15} + \frac{7}{15x}\right)e^{-x}\right], \quad (3)$$

where b is the length of the statistical element, L the contour length of the chain, x is equal to $q^2Lb/6$, and $g_D(x)$ is the Debye function given in Eq. 2. In this model, the radius of gyration of the Debye function $R_g = (Lb/6)^{(1/2)}$ is corrected with a function of the ratio $y = L/b$:

$$\left(R_g^{SB}\right)^2 = b^2\left[\frac{y}{6} - \frac{1}{4} + \frac{1}{4y} - \frac{1}{8y^2}\left(1 - e^{-2y}\right)\right]. \quad (4)$$

L and b are used as fitting parameters. They are related by $L = Nb$, where N is the number of statistical elements. Note that the contour length L of a disordered chain is the length at maximum physically possible extension and is always larger than the largest dimension of the protein, r_{max}, unless the chain is a rigid rod (49). An upper limit for L is given by $L = n \times a \times f$, where n is the number of amino acids in the sequence, $a = 3.78$ Å is the length per amino acid, and f accounts for geometrical constraints of the polypeptide chain ($f = 0.95$) (53). If the polypeptide chain contains secondary structure elements, the contour length must be smaller than this value.

To fit the whole spectrum, it is also necessary to take into account the thickness of the chain through R_c, the radius of gyration of its cross section. The fitting function for a thick filament is then that of a thick worm-like chain (WLC):

$$I_{TF}(q) = I_{SB}(q)\exp\left(\frac{-q^2R_c^2}{2}\right). \quad (5)$$

However, L and R_c are not independent parameters. They are related to the dry volume of the chain, V, which is known from the protein molar mass, M, the density $d = 1.4 \pm 0.1$ g/cm^3 and Avogadro's number N_{Av}:

$$2\pi R_c^2 = V/L \text{ and } V = M/(N_{Av}d). \quad (6)$$

Finally, the whole scattering curve was fitted according to Eqs. 3, 5, and 6 with Eq. 3 parameters only, i.e., $I(q \to 0)$, L and b. The range of validity of Eq. 3 is expected to be $0.01 < q < 0.1$ Å^{-1}. However, the fits are actually quite good over the whole range of q, i.e., up to $q = 0.4$ Å^{-1}. The parameters extracted from the fits are listed in Table 1 and the fits are presented in Fig. 5.

Rather satisfactorily, the radii of gyration listed in Table 1 and obtained from the fits of the experimental spectra by the WLC model are identical to those obtained from the pair distance distribution function $P(r)$, which is model independent.

The fitting L values of 188 and 364 Å for IB5 and II-1ng respectively are significantly lower than the high bound values $L = naf$ of 251 and 503 Å, which suggests strongly the presence of secondary structure elements that could be very short PPII- or PPI-type helical fragments. Indeed, the L/n values derived from curve fitting (2.6 Å for both IB5 and II-1ng respectively) are intermediary between the helical rise per residue values for a PPI-type helix (1.7 Å) and a PPII-type helix (3.1 Å) (54).

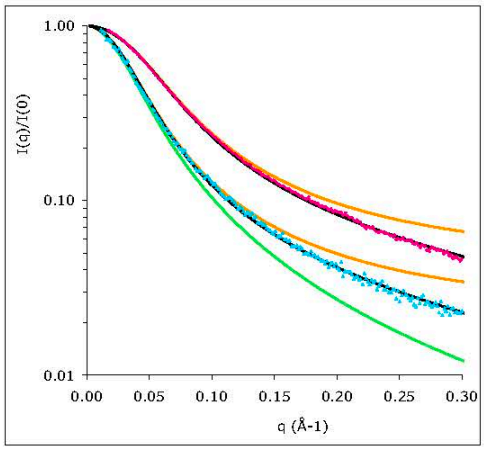

FIGURE 5 Scattering from the nonglycosylated proteins IB5 (*pink diamonds*) and II-1ng (*blue triangles*), compared with the scattering curves calculated according to the Debye model (Eq. 2, *green line* fit of II-1ng), the Sharp-Bloomfield model (Eq. 3, *orange lines*), and the WLC model with thickness (Eq. 5, *black lines*). The structural parameters extracted from the WLC fits are given in Table 1.

The existence of secondary structure elements is corroborated by the values of the statistical length of the order of 30 Å for both proteins, significantly higher than that expected for a completely unfolded polypeptide chain found in the literature, which is ~18–20 Å.

Finally, the cross-section radius of gyration values R_c resulting from the fits was compared to the value directly calculated from the sequence using the expression

$$R_c^2 = \left\langle \frac{\sum_i m_i |\vec{x}_i|^2}{\sum_i m_i} \right\rangle, \quad (7)$$

where the sum runs over all residues, and $\vec{x}_i$ gives the position of the projection of atom i with mass m_i on the plane normal to $C_\alpha^{\,i}-C_\alpha^{\,i+1}$ axis.

For both proteins, the calculated value for R_c is found close to 1.9 Å, whereas the fitting value is slightly higher (2.7 for both proteins). This is quite satisfactory in view of the purely atomic character of the calculation that does not take into account the excess of water molecules in the vicinity of the protein nor thermal motion of the protein atoms that entails a thermal volume around the protein. A thickness of at least 0.5 Å is generally found in the literature for this thermal volume (55). Furthermore, the presence of PPI- or PPII-type helices should increase the average R_c value with respect to the value of 1.9 Å calculated for a chain with the same sequence but no such secondary structure elements.

Glycosylated protein

For the glycosylated protein, II-1, the scattering curve can be fitted using the WLC model with the same contour length (325 Å) than for the nonglycosylated protein, indicating that both proteins have similar polypeptide backbones. On the contrary, the value of R_c is significantly higher ($\approx$6.5 Å). This is of course an effect of the large polyoside sidegroups, which are not described properly by the WLC model. Another approach in this case is to describe this protein as a branched macromolecule. Accordingly, the spectrum has been compared with that of disordered structures that repeat at every scale with a fractal exponent d_f up to a scale characterized by a radius of gyration R_g. The simplest way of doing this is to use the Fisher-Burford approximation (56,57):

$$I(q)/I(0) = \left(1 + \frac{(qR_g)^2}{3d_f/2}\right)^{-d_f/2}. \quad (8)$$

A good fit is obtained with the calculated scattering curve of fractal objects that have a radius of gyration of 45.9 ± 2 Å, a fractal dimension $d_f = 2.43$, which is indeed appropriate for branched macromolecules, and the same cross section as for the other proteins (Fig. 6). This is the most information that can be obtained without entering detailed information about the primary structure of the protein.

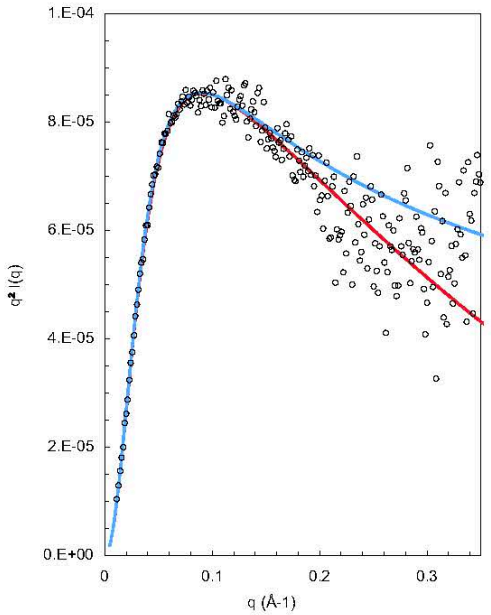

FIGURE 6 Scattering from the glycosylated protein II-1 in solution (*open circles*), compared with the calculated scattering curve for branched chains with a radius of gyration $R_g = 45.9$ Å, a fractal dimension $d_f = 2.43$ (*blue line*) or the same with a cross section $R_c = 2.7$ Å (*red line*).

Reconstruction of data-compatible conformations

The numbers given above for r_{max}, R_g, b, and R_c contain all the information that is available for the proteins in solution. Still, it is instructive to reconstruct some typical conformations that reproduce the experimental spectra, and therefore match these average parameters. Here there is a choice between constructing a single conformation that reproduces the experimental spectrum (58) (BUNCH approach), or choosing a subset of all possible conformations of the protein (59) (EOM approach). The first choice is somewhat restrictive, because a single conformation cannot give a fair view of the astronomical number of all conformations that are explored by the protein during its thermal motions. The second choice has the potential of better representing the variety of actual conformations. However, there is the possibility that the subset of chosen conformations results from a biased choice, and that it does not represent fairly the ensemble of actual conformations. We have tried both approaches, and found that both reproduce the data for protein IB5. In the second approach, however, the subset of conformations that was chosen by the program appeared to depend on the level of noise of the data and on the number of chosen conformations. Fig. SI-3 *a* shows various types of distributions of R_g, that are bimodal or monomodal depending on initial conditions. At present, we are not able to derive a physical interpretation from these distributions. In this article, we present the first type of reconstruction, and in the Supporting Material we present the second approach.

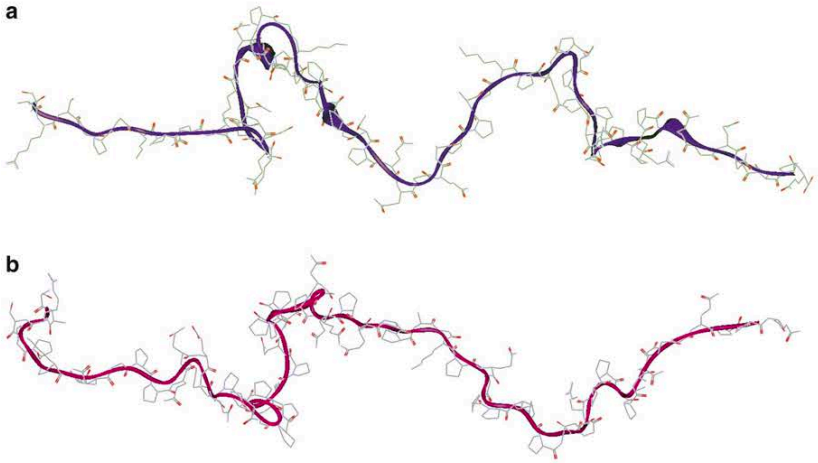

FIGURE 7 Two examples of data-compatible conformations obtained using the BUNCH program for the protein IB5.

We used the program BUNCH that was developed by Petoukhov and Svergun to describe a protein as a combination of rigid bodies joined by flexible linkers (58). For IB5, three polyproline repeats in the sequence (PPPP, PPP, and PPPPP) were taken as rigid bodies and described as pieces of a polyproline II helix. The other residues were replaced with dummy residues centered at C_α positions, separated by 3.78 Å, and treated as linkers. The program adjusts the positions of the rigid bodies and of the dummy residues to obtain the best agreement with the experimental spectrum. Then we used another program (SABBAC) (60) to take into account steric constraints due to sidegroups of the amino acids, and add these sidegroups to the backbone. In this way, we obtained a proper polypeptidic chain with all the sidegroups. Finally, a last adjustment was made using the program CRYSOL (61) to verify that the conformation produced by SABBAC does reproduce the experimental spectrum.

We carried out 20 runs of BUNCH. The agreement between experimental data and the scattering curve calculated from the coordinates of the dummy atoms in the model is excellent in each run, with $\chi = 1.1$ (Fig. SI-2). The results of each run provide an image of an equivalent conformation that reproduces the average distribution of distances within the protein (Fig. 7). These conformations are all different but share the common property of being extremely extended, in agreement with the overall dimensions listed in Table 1, more precisely compatible with a chain constituted by six or seven ($=L/b$) rigid elements of mean length 30 Å ($=b$).

CONCLUSIONS

The PRPs IB5 and II-1ng have conformations that are unusually extended, compared with other IDPs. Their values of R_g are significantly higher than those given by the expression $R_g \approx 2.54(n)^{0.522}$ valid for several IDP (8). The ratio of the radius of gyration to the contour length of the chain ($R_g/L \approx 0.11$ for II-1ng) is also significantly higher than that found recently using the same formalism for a thermally denatured protein ($R_g/L \approx 0.08$) (53).

This very strong extension is due to the length of the statistical segment (twice the persistence length), which is 30 Å, also unusually large for intrinsically disordered proteins (the usual value is on the order of 18 Å). The radius of gyration of the chain cross section is 2.7 ± 0.2 Å. These characteristics are presumably related to the numerous short polyproline repeats within the polypeptidic backbones. The glycosylated PRP II-1 has similar conformations but the presence of a large polyoside sidegroup yields an overall structure in solution that is closer to that of a self-similar branched macromolecule.

The conformations of these proteins in solution may reflect an evolutionary adaptation to the capture of plant tannins in the oral cavity. IB5 is known to precipitate when the tannin concentration in solution exceeds a threshold (31). This may be related to the feeling of astringency, which is a tactile perception associated with a loss of lubrication in the oral cavity. In this respect, the extended conformations in solution must optimize the accessibility of hydrophobic amino acids (mainly proline) to which the tannin molecules may bind. These extended conformations may also make it possible to bind stacks of tannin molecules, or polymerized tannins. II-1 is known to form limited aggregates on binding tannins, which do not precipitate. In previous work, we have shown that these aggregates are dense globules with an average radius of 100 Å, in between the radius of gyration (45 Å) and the largest distance (178 Å) of the free protein in solution (33). This type of aggregation may result from the amphiphilic nature of this protein because the hydrophobic residues of the protein backbone may form the core of the globule whereas the large polyoside sidegroups remain at the surface, as in the case of surfactant micelles. This behavior may have three possible functions: 1), a regulation of the tannin concentration in the oral cavity; 2), a reduction of the viscosity of saliva, due to the loss of macromolecules with extended conformations; and 3), a change in the

interfacial properties of saliva, because this protein has an overall configuration that is characteristic of an amphiphile. These functions may contribute to the perception of astringency when the tannin concentration in the oral cavity exceeds a level that is safe for the host.

SUPPORTING MATERIAL

Three figures are available at http://www.biophysj.org/biophysj/supplemental/S0006-3495(10)00548-5.

We thank Patrice Vachette for illuminating discussions.

This work was supported by the French Agence Nationale de la Recherche (07-BLAN-02 to A.N.R.), and the European Commission Sixth Framework Programme (RIDS 011934 to J.P.).

REFERENCES

1. Uversky, V. N. 2002. Natively unfolded proteins: a point where biology waits for physics. *Protein Sci.* 11:739–756.
2. Dunker, A. K., J. D. Lawson, …, Z. Obradovic. 2001. Intrinsically disordered protein. *J. Mol. Graph. Model.* 19:26–59.
3. Tompa, P. 2003. The functional benefits of protein disorder. *J. Mol. Struct. THEOCHEM.* 666–667:361–371.
4. Tompa, P. 2003. Intrinsically unstructured proteins evolve by repeat expansion. *Bioessays.* 25:847–855.
5. Ward, J. J., J. S. Sodhi, …, D. T. Jones. 2004. Prediction and functional analysis of native disorder in proteins from the three kingdoms of life. *J. Mol. Biol.* 337:635–645.
6. Dyson, H. J., and P. E. Wright. 2005. Intrinsically unstructured proteins and their functions. *Nat. Rev. Mol. Cell Biol.* 6:197–208.
7. Receveur-Bréchot, V., J. M. Bourhis, …, S. Longhi. 2006. Assessing protein disorder and induced folding. *Proteins.* 62:24–45.
8. Bernadó, P., and M. Blackledge. 2009. A self-consistent description of the conformational behavior of chemically denatured proteins from NMR and small angle scattering. *Biophys. J.* 97:2839–2845.
9. Liu, J., J. R. Faeder, and C. J. Camacho. 2009. Toward a quantitative theory of intrinsically disordered proteins and their function. *Proc. Natl. Acad. Sci. USA.* 106:19819–19823.
10. Wright, P. E., and H. J. Dyson. 1999. Intrinsically unstructured proteins: re-assessing the protein structure-function paradigm. *J. Mol. Biol.* 293:321–331.
11. Edgar, W. M. 1992. Saliva: its secretion, composition and functions. *Br. Dent. J.* 172:305–312.
12. Azen, E. A., E. Amberger, …, R. L. Niece. 1996. PRB1, PRB2, and PRB4 coded polymorphisms among human salivary concanavalin-A binding, II-1, and Po proline-rich proteins. *Am. J. Hum. Genet.* 58:143–153.
13. Cid, H., V. Vargas, …, S. Bustos. 1986. Secondary structure prediction of human salivary proline-rich proteins. *FEBS Lett.* 198:140–144.
14. Simon, C., I. Pianet, and E. J. Dufourc. 2003. Synthesis and circular dichroism study of the human salivary proline-rich protein IB7. *J. Pept. Sci.* 9:125–131.
15. Pascal, C., F. Paté, …, M. A. Delsuc. 2009. Study of the interactions between a proline-rich protein and a flavan-3-ol by NMR: residual structures in the natively unfolded protein provides anchorage points for the ligands. *Biopolymers.* 91:745–756.
16. Chan, M., and A. Bennick. 2001. Proteolytic processing of a human salivary proline-rich protein precursor by proprotein convertases. *Eur. J. Biochem.* 268:3423–3431.
17. Baxter, N. J., T. H. Lilley, …, M. P. Williamson. 1997. Multiple interactions between polyphenols and a salivary proline-rich protein repeat result in complexation and precipitation. *Biochemistry.* 36: 5566–5577.
18. Lu, Y., and A. Bennick. 1998. Interaction of tannin with human salivary proline-rich proteins. *Arch. Oral Biol.* 43:717–728.
19. Mehansho, H., L. G. Butler, and D. M. Carlson. 1987. Dietary tannins and salivary proline-rich proteins: interactions, induction, and defense mechanisms. *Annu. Rev. Nutr.* 7:423–440.
20. Hagerman, A. E. 1989. Chemistry of tannin-protein complexation. *In* Chemistry and Significance of Condensed Tannins. R. W. Hemingway and J. J. Karchesy, editors. Plenum Press, New York, NY. 323–331.
21. Sarni-Manchado, P., J.-M. Canals-Bosch, …, V. Cheynier. 2008. Influence of the glycosylation of human salivary proline-rich proteins on their interactions with condensed tannins. *J. Agric. Food Chem.* 56:9563–9569.
22. Yokotsuka, K., and V. L. Singleton. 1995. Interactive precipitation between phenolic fractions and peptides in wine-like model solutions: turbidity, particle size, and residual content as influenced by pH, temperature and peptide concentration. *Am. J. Enol. Vitic.* 46:329–338.
23. Haslam, E. 1998. Practical Polyphenolics: From Structure to Molecular Recognition and Physiological Action. Cambridge University Press, Cambridge, UK.
24. Jöbstl, E., J. O'Connell, …, M. P. Williamson. 2004. Molecular model for astringency produced by polyphenol/protein interactions. *Biomacromolecules.* 5:942–949.
25. Hatton, M. N., R. E. Loomis, …, L. A. Tabak. 1985. Masticatory lubrication. The role of carbohydrate in the lubricating property of a salivary glycoprotein-albumin complex. *Biochem. J.* 230:817–820.
26. Asquith, T. N., J. Uhlig, …, L. Butler. 1987. Binding of condensed tannins to salivary proline-rich glycoproteins: the role of carbohydrates. *J. Agric. Food Chem.* 35:331–334.
27. Loomis, R. E., E. J. Bergey, …, L. A. Tabak. 1985. Circular dichroism and fluorescence spectroscopic analyses of a proline-rich glycoprotein from human parotid saliva. *Int. J. Pept. Protein Res.* 26:621–629.
28. Kauffman, D. L., and P. J. Keller. 1979. The basic proline-rich proteins in human parotid saliva from a single subject. *Arch. Oral Biol.* 24: 249–256.
29. Oho, T., F. Rahemtulla, …, A. Hjerpe. 1992. Purification and characterization of a glycosylated proline-rich protein from human parotid saliva. *Int. J. Biochem.* 24:1159–1168.
30. Pascal, C., F. Bigey, …, P. Sarni-Manchado. 2006. Overexpression and characterization of two human salivary proline rich proteins. *Protein Expr. Purif.* 47:524–532.
31. Pascal, C., C. Poncet-Legrand, …, A. Vernhet. 2007. Interactions between a nonglycosylated human proline-rich protein and flavan-3-ols are affected by protein concentration and polyphenol/protein ratio. *J. Agric. Food Chem.* 55:4895–4901.
32. Canon, F., F. Paté, …, P. Sarni-Manchado. 2009. Characterization, stoichiometry, and stability of salivary protein-tannin complexes by ESI-MS and ESI-MS/MS. *Anal. Bioanal. Chem.* 395:2535–2545.
33. Pascal, C., C. Poncet-Legrand, …, A. Vernhet. 2008. Aggregation of a proline-rich protein induced by epigallocatechin gallate and condensed tannins: effect of protein glycosylation. *J. Agric. Food Chem.* 56:6724–6732.
34. Bretthauer, R. K., and F. J. Castellino. 1999. Glycosylation of *Pichia pastoris*-derived proteins. *Biotechnol. Appl. Biochem.* 30:193–200.
35. Laemmli, U. K. 1970. Cleavage of structural proteins during the assembly of the head of bacteriophage T4. *Nature.* 227:680–685.
36. Beeley, J. A., D. Sweeney, …, K. S. Khoo. 1991. Sodium dodecyl sulphate-polyacrylamide gel electrophoresis of human parotid salivary proteins. *Electrophoresis.* 12:1032–1041.
37. Reference deleted at proof.
38. Tschopp, J. F., G. Sverlow, …, L. Grinna. 1987. High-level secretion of glycosylated invertase in the methylotrophic yeast, *Pichia Pastoris. Nat. Biotechnol.* 5:1305–1308.

39. Doco, T., M. A. O'Neill, and P. Pellerin. 2001. Determination of the neutral and acidic glycosyl-residue compositions of plant polysaccharides by GC–EI-MS analysis of the trimethylsilyl methyl glycoside derivatives. *Carbohydr. Polym.* 46:249–259.

40. Harris, P. J., R. J. Henry, …, B. A. Stone. 1984. An improved procedure for the methylation analysis of oligosaccharides and polysaccharides. *Carbohydr. Res.* 127:59–73.

41. Dennis, J. W., M. Granovsky, and C. E. Warren. 1999. Protein glycosylation in development and disease. *Bioessays.* 21:412–421.

42. Helmerhorst, E. J., and F. G. Oppenheim. 2007. Saliva: a dynamic proteome. *J. Dent. Res.* 86:680–693.

43. Reddy, M. S., M. J. Levine, and L. A. Tabak. 1982. Structure of the carbohydrate chains of the proline-rich glycoprotein from human parotid saliva. *Biochem. Biophys. Res. Commun.* 104:882–888.

44. Gillece-Castro, B. L., A. Prakobphol, …, S. J. Fisher. 1991. Structure and bacterial receptor activity of a human salivary proline-rich glycoprotein. *J. Biol. Chem.* 266:17358–17368.

45. He, B., K. Wang, …, A. K. Dunker. 2009. Predicting intrinsic disorder in proteins: an overview. *Cell Res.* 19:929–949.

46. Guinier, A., and G. Fournet. 1955. Small Angle Scattering of X Rays. Wiley, New York, NY.

47. Glatter, O., and O. Kratky. 1982. Small Angle X-Ray Scattering. Academic Press, New York, NY.

48. Svergun, D. 1992. Determination of the regularization parameter in indirect-transform methods using perceptual criteria. *J. Appl. Cryst.* 25:495–503.

49. Grosberg, A. Y., and A. R. Khokhlov. 1994. Statistical Physics of Macromolecules. AIP Press, New York.

50. Burchard, W. 1974. Statistics of star-shaped molecules. I. Stars with polydisperse side chains. *Macromolecules.* 7:835–841.

51. Rawiso, M., R. Duplessix, and C. Picot. 1987. Scattering function of polystyrene. *Macromolecules.* 20:630–648.

52. Sharp, P., and V. A. Bloomfield. 1968. Light scattering from wormlike chains with excluded volume effects. *Biopolymers.* 6:1201–1211.

53. Pérez, J., P. Vachette, …, D. Durand. 2001. Heat-induced unfolding of neocarzinostatin, a small all-β protein investigated by small-angle x-ray scattering. *J. Mol. Biol.* 308:721–743.

54. Gu, W., and V. Helms. 2005. Dynamical binding of proline-rich peptides to their recognition domains. *Biochim. Biophys. Acta.* 1754: 232–238.

55. Bánó, M., and J. Marek. 2006. How thick is the layer of thermal volume surrounding the protein? *Biophys. Chem.* 120:44–54.

56. Fisher, M. E., and R. J. Burford. 1967. Theory of critical-point scattering and correlations. I. The Ising model. *Phys. Rev.* 156:583–622.

57. Kallala, M., C. Sanchez, and B. Cabane. 1993. Structures of inorganic polymers in sol-gel processes based on titanium oxide. *Phys. Rev. E Stat. Phys. Plasmas Fluids Relat. Interdiscip. Topics.* 48:3692–3704.

58. Petoukhov, M. V., and D. I. Svergun. 2005. Global rigid body modeling of macromolecular complexes against small-angle scattering data. *Biophys. J.* 89:1237–1250.

59. Bernadó, P., E. Mylonas, …, D. I. Svergun. 2007. Structural characterization of flexible proteins using small-angle x-ray scattering. *J. Am. Chem. Soc.* 129:5656–5664.

60. Maupetit, J., R. Gautier, and P. Tuffery. 2006. SABBAC: online Structural Alphabet-based protein BackBone reconstruction from Alpha-Carbon trace. *Nucleic Acids Res.* 34(Web Server issue):W147-W51 (http://bioserv.rpbs.jussieu.fr/SABBAC.html).

61. Svergun, D., C. Barberato, and M. H. J. Koch. 1995. CRYSOL—a program to evaluate x-ray solution scattering of biological macromolecules from atomic coordinates. *J. Appl. Cryst.* 28:768–773.

Publication n°5: Characterization, stoichiometry and stability of salivary protein-tannin complexes by ESI-MS and ESI-MS/MS.

Canon, F.; Paté, F.; Meudec, E.; Marlin, T.; Cheynier, V.; Giuliani, A.; Sarni-Manchado, P.

Anal. Bioanal. Chem. ***2009,*** *395 (8), 2535-2545.*

Anal Bioanal Chem (2009) 395:2535–2545
DOI 10.1007/s00216-009-3180-3

ORIGINAL PAPER

Characterization, stoichiometry, and stability of salivary protein–tannin complexes by ESI-MS and ESI-MS/MS

Francis Canon · Franck Paté · Emmanuelle Meudec · Thérèse Marlin · Véronique Cheynier · Alexandre Giuliani · Pascale Sarni-Manchado

Received: 9 June 2009 / Revised: 16 September 2009 / Accepted: 21 September 2009 / Published online: 18 October 2009

Abstract Numerous protein–polyphenol interactions occur in biological and food domains particularly involving proline-rich proteins, which are representative of the intrinsically unstructured protein group (IUP). Noncovalent protein–ligand complexes are readily detected by electrospray ionization mass spectrometry (ESI-MS), which also gives access to ligand binding stoichiometry. Surprisingly, the study of interactions between polyphenolic molecules and proteins is still an area where ESI-MS has poorly benefited, whereas it has been extensively applied to the detection of noncovalent complexes. Electrospray ionization mass spectrometry has been applied to the detection and the characterization of the complexes formed between tannins and a human salivary proline-rich protein (PRP), namely IB5. The study of the complex stability was achieved by low-energy collision-induced dissociation (CID) measurements, which are commonly implemented using triple quadrupole, hybrid quadrupole time-of-flight, or ion trap instruments. Complexes composed of IB5 bound to a model polyphenol EgCG have been detected by ESI-MS and further analyzed by MS/MS. Mild ESI interface conditions allowed us to observe intact noncovalent PRP–tannin complexes with stoichiometries ranging from 1:1 to 1:5. Thus, ESI-MS shows its efficiency for (1) the study of PRP–tannin interactions, (2) the determination of stoichiometry, and (3) the study of complex stability. We were able to establish unambiguously both their stoichiometries and their overall subunit architecture via tandem mass spectrometry and solution disruption experiments. Our results prove that IB5·EgCG complexes are maintained intact in the gas phase.

Keywords Polyphenol · Interaction · Proline-rich protein · Saliva · Astringency · IUP

Abbreviations

CID	collision-induced dissociation
EgCG	epigallocatechin gallate
ESI	electrospray ionization
IUP	intrinsically unstructured protein
MS	mass spectrometry
MS/MS	tandem mass spectrometry
PRP	proline-rich protein
Q-TOF	quadrupole/time-of-flight

Introduction

Demonstrations of proteins having little or no ordered structure under physiological conditions have increased exponentially over the past 15 years. Particular terms have been proposed to describe these proteins: intrinsically disordered proteins (IDPs), natively unfolded or intrinsically unstructured proteins (IUPs) [1–3]. Proline-rich proteins

F. Canon · F. Paté · E. Meudec · T. Marlin · V. Cheynier · P. Sarni-Manchado (✉)
UMR 1083 Sciences Pour l'Oenologie,
Polyphenol Interaction Research Group, INRA,
Bât 28, 2 place Viala,
F-34060 Montpellier, France
e-mail: sarni@supagro.inra.fr

A. Giuliani
DISCO beamline, Synchrotron Soleil,
l'Orme des Merisiers,
91192 Gif sur Yvette, France

A. Giuliani
CEPIA, INRA,
BP 71627, F-44316 Nantes, France

(PRPs), which are IUPs, are particularly abundant in human saliva and may constitute 70% of total secreted proteins in parotid saliva [4]. The salivary proteins play various roles (e.g., lubrication, digestion, taste, protection) as saliva is the first fluid which interacts with food constituents. Herbivorous and omnivorous mammals have developed the ability to synthesize salivary basic proline-rich proteins whose only known role is to bind tannins [5].

Plants synthesize a diverse group of phenolic compounds (*syn*. polyphenols) [6]. Among them, proanthocyanidins (*syn*. condensed tannins) are ubiquitous in plants and they are major components of foods (e.g., fruit, cocoa), beverages (e.g., wine, tea, beer, cider), animal feeds (e.g., pasture legumes), and herbal remedies. These molecules have attracted considerable interest because of their major contribution to organoleptic and biological properties. One of their prominent characteristics is their ability to interact with proteins, which can be either detrimental or beneficial. For example, haze developments are observed in beverages [7–9], reducing their quality. Inactivation of digestive enzymes and/or tanning of diet proteins impede their digestibility and assimilation, and thus lower nutritional value of some feeds (e.g., legumes) [10]. On the other hand, polyphenol–protein interactions are also involved in the beneficial antioxidant activity of polyphenols as enzyme inhibitors that limit superoxide and uric acid formation [11]. Recently, the participation of polyphenols in the regulation of gene expression, due to their ability to interact with receptors and nuclear factors, has been demonstrated [11].

According to Red Queen hypothesis[1] [12], animals developed shunning mechanisms along with the ability to perceive astringency. Astringency is a tactile sensation [13–16] resulting from interactions of tannins and showing some specificity [17] for which salivary PRPs are often evoked [18]. However, its physicochemical bases are still poorly understood. Protein–tannin interactions have been extensively studied using a variety of techniques and experimental models in relation to astringency and anti-nutritional effects and are reported to generate insoluble and soluble complexes [19–22]. Earlier works have measured protein and/or tannins remaining in solution after precipitation. Particular proteins have been proposed for use in studying protein–polyphenol interactions [23, 24]. However, these measurements may not reflect astringency as salivary protein–tannin interactions show some specificity [17], nor do they take into account the formation of soluble complexes. The first information on the structure of soluble complexes was provided by spectrometric methods such as nuclear magnetic resonance (NMR) [25–28] sometimes in association with molecular modeling [20, 29], circular dichroism (CD) [20, 21], and mass spectrometry [20, 30–32]. However, only peptides have been considered in these studies because of the unavailability of a model of natively unstructured PRPs.

Mass spectrometric procedures have greatly evolved and became methods of choice for characterization of biological macromolecules as well as their interactions. Electrospray ionization (ESI) has been demonstrated to be efficient to probe weak associations of molecules in solution such as receptor–ligand and protein–nucleic acid interactions [33, 34]. ESI-MS offers speed and sensitivity in monitoring components of mixtures. Determination of dissociation or relative binding affinities of noncovalent complexes is now well established [35–37]. The stabilities of noncovalent complexes have been assessed by their resistance to dissociation in the mass spectrometer using collision-induced dissociation (CID) or thermal denaturation experiments [38–40]. Recently, Xie and Loo wrote that "The direct detection of protein–ligand noncovalent complexes using ESI mass spectrometry can be challenging, depending on the types of compounds tested and the types of physical interactions necessary to maintain a stable complex in both solution and in the gas phase." This is certainly one of the reasons why few mass spectrometry publications concern protein–polyphenol complexes. Although these experiments have to be carefully interpreted with regards to solution-phase studies, they can provide information that is difficult to determine otherwise: the contribution of intermolecular interactions to ligand binding, free of any solvent contribution. MS and MS/MS allow one to probe intermolecular interactions experimentally [41].

We report here the first study of noncovalent complexes of the human salivary protein IB5 with tannins by using ESI-MS and MS/MS. IB5 is an intrinsically unstructured proteins of human saliva, whose interactions with tannins may be involved in astringency.

Materials and methods

Samples

Epigallocatechin gallate (EgCG) and reserpine (Fig. 1) were purchased from Sigma (Sigma Chemical Co., Poole, UK).

The human salivary proline-rich protein, IB5, was produced by use of the yeast *Pischia pastoris* as a host organism and purified as previously described [42].

EgCG and protein stock solutions were prepared in water/ethanol (88:12 v/v) acidified to pH 3.1 with acetic acid and were immediately frozen (−20 °C) to prevent

[1] Van Valen's Red Queen hypothesis is a model of coevolution driven by competitive interactions between species. It contrasts with the stationary or 'lost world' model, in which evolution is driven primarily by environmental change.

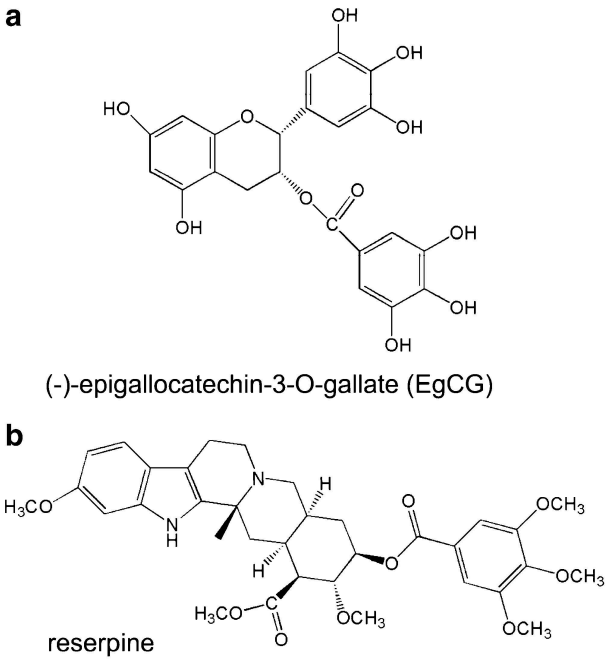

Fig. 1 Structures of **a** epigallocatechin-3-*O*-gallate (EgCG) and **b** reserpine

EgCG oxidation and proteolysis. Before use, they were diluted at room temperature to the desired concentrations.

EgCG–protein interactions

Formation of complexes was studied at pH 3.1, which corresponds to the average pH value of the mouth in the presence of a red wine. For IB5–EgCG interactions, the protein concentration was kept constant at 5 μM in the water/ethanol medium described above. EgCG and protein solutions were mixed extemporaneously at room temperature (regulated at 24 °C) so as to obtain a protein/polyphenol molar ratio of 1:10.

IB5 was mixed with EgCG (final concentration 5 μM and 50 μM, respectively) and allowed to equilibrate at room temperature for at least 5 min before ESI-MS analysis. All samples were prepared in triplicate and analyzed by ESI-MS.

Electrospray ionization mass spectrometry

MS spectra were obtained on a AccuTOF (JEOL, Tokyo, Japan) mass spectrometer equipped with an ESI source and a time-of-flight (TOF) mass analyzer, providing a resolving power of 6,000 at *m/z* 609. Each solution was injected into the mass spectrometer by means of a syringe infusion pump at a flow rate of 20 μL min^{-1}. The source voltage was set at 2,350 V in positive ion mode, the orifice 1 voltage at 35 V, the orifice 2 voltage at 5 V, the ring voltage at 10 V, and the capillary temperature at 150 °C. Spectra were acquired in positive ion mode from *m/z* 300 to 1,800. Each mass spectrum was acquired with an integration time of 1 s. The signal from 28 scans was accumulated in the multichannel acquisition mode and averaged.

Tandem mass spectrometry

Tandem mass spectrometry experiments were performed on a hybrid quadrupole time-of-flight (Q-TOF) Qstar Pulsar i mass spectrometer (Applied Biosystems, Forster City, CA), providing a resolving power of 10,000 at *m/z* 1,080.8. The Q-TOF was operated with the Turbospray (electrospray ion source). The interface was fitted with the IonCooler Guide to preserve the noncovalent complexes upon transfer into the gas phase. The IonCooler Guide is fitted around the initial ion entrance region of Q0 and increases the local pressure to greater than 30 mTorr, which greatly improves detection of weakly bound complexes [43]. The sample was injected into the mass spectrometer by means of a syringe infusion pump at a flow rate of 7 μL min^{-1}. The source voltage was set to 5,800 V in positive ion mode, the declustering potential at 47 V, the focusing potential at 209 V, the declustering potential 2 at 17 V, the ion source gas 1 set at 22, the ion source gas 2 at 0, the curtain gas at 10, and the capillary was not heated up. Nitrogen from a generator, containing less than 6 ppm oxygen, was used both as nebulizing and desolvation gas. During MS/MS experiments, nitrogen was used as collision gas in the collision cell (Linac) with CAD gas setting of 5. The collision-set energy voltage V_c was increased from 0 to 50 V. The kinetic energy of the precursor ion in the laboratory frame of reference is $E_{Lab} = z \times e \times V_c$, where z is the number of charges on the ion and e is the charge of an electron [44]. Data were acquired by the TOF analyzer at 1 acquisition/s with *m/z* ranging from 250 to 1,800.

Analysis of ESI-MS and ESI-MS/MS experiments and calculations

All experiments were repeated at least three times. Ion pattern and intensities were compared. ESI-MS and collision MS/MS data were analyzed with Analyst QS [45] and MagTran [46] software.

A procedure adapted from Jørgensen et al. [47] and Wan et al. [48] was used to establish the dissociation curves. The 50% dissociation energy is defined as the energy giving a 50% loss of precursor complex ions. Based on the data of Akashi et al. [49], one of the multiprotonated molecules of the IB5·EgCG complex (M), $[M+6H]^{6+}$, was selected and submitted to CID.

Results and discussion

ESI analysis of the protein solution

Figure 2a shows a representative positive electrospray ionization spectrum of purified IB5 (5 μM in H_2O/EtOH, 88:12 v/v, pH 3.1). The theoretical average molecular mass (MM) of IB5 is 6,923.74 Da (Table 1). The positive ESI mass spectra of IB5 showed a series of ion peaks from *m/z* 1,385 to 630, with charge states ranging from +5 to +11 which was confirmed by TOF-MS analysis (data not shown). Peaks have been assigned to protonated molecules. The IB5 spectrum analysis and deconvolution resulted in three molecular mass values of 6,923.70, 6,642.63, and 6,360.39 Da. It reveals the presence of three sequences of IB5, namely IB5a, IB5b, and IB5c, which correspond respectively to the whole protein and to N-terminal proteins with three and six amino acids (aa) deleted (Fig. 2b), with IB5a being the main form (>65%). Each form of IB5 exhibits the same charge state distribution (CSD). Typical protein purification techniques (and particularly for IUPs [1]) do not allow the separation of proteins with such small differences in length, the overall sequence remaining exactly the same. Edman sequencing experiments confirmed that IB5b and IB5c are not the result of fragmentation during the ionization but coexist in the purified fraction with IB5a. They may result from proteolytic activity of *Pichia pastoris* during protein expression or remaining during the protein purification procedure. It is worth noticing that peaks corresponding to multimers (i.e., aggregates) of IB5 were not observed, consistent with the absence of contribution from nonspecific association under the solution and instrumental conditions selected.

Under acidic conditions, the basic residues Arg, Lys, His and the NH_2 terminus are often the only sites of protonation, but in the gas phase [50, 51], Pro and Gln behave as basic residues that can be protonated. The high charge states observed for IB5 can thus be related to the ability of Pro residues to be easily protonated. Investigations on the effect of pH and organic solvent on the CSD of IB5 performed from pH 2.6 to 5.7 in the experimental medium and at a pH value of 1.3 in acetonitrile/water/TFA (80:20:0.1% v/v) showed no difference in the MS spectra. The natively unfolded nature of IB5 explains these data as evidenced earlier by CD experiments

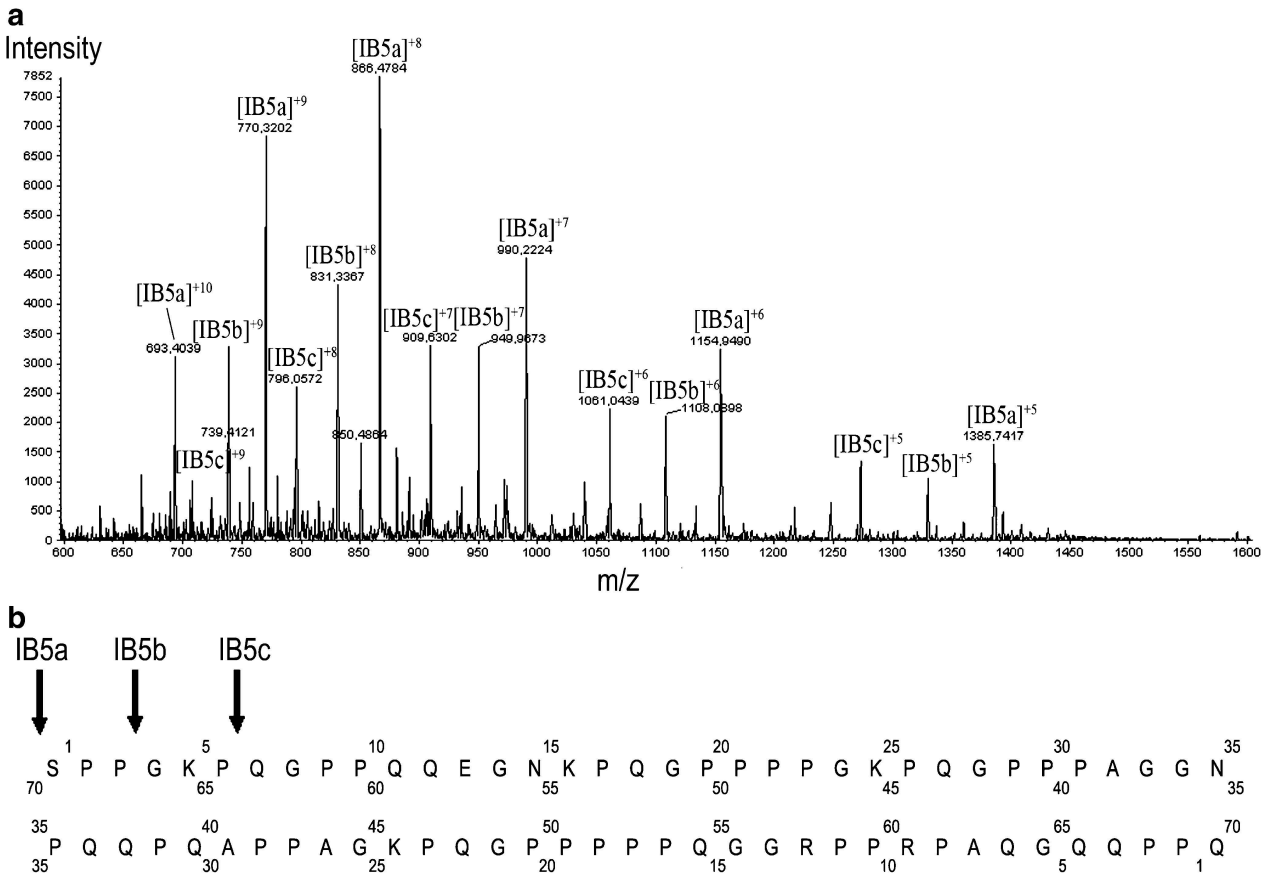

Fig. 2 **a** Positive-ion ESI mass spectrum of salivary PRP IB5 purified from PRPs produced by PRB4S transformant *Pichia pastoris* yeast. **b** Deduced primary sequences of the purified IB5*x*

Table 1 Theoretical and measured mass (Da) of IB5 purified from heterologous *Pichia pastoris*-expressed PRPs

	IB5a	IB5b	IB5c
Theoretical average mass	6,923.74	6,642.43	6,360.08
Measured average mass	6,923.70	6,642.63	6,360.39

[21]. The highest charged ions may represent extensively unfolded solution conformers, whereas the low charge states are assigned to more "compact" series [52].

IB5 fragmentation experiments via CID MS/MS performed on the Q-TOF instrument demonstrated that the highest charged ions were less stable than the lowest charged ones as reported for other proteins and according to the theory of proton mobility [53]. Whereas most investigations on proline-rich sequences under CID have concerned peptides [54, 55], we examined the fragmentation of a whole PRP, IB5, 70-aa long. The ESI-MS/MS spectrum of the $IB5^{7+}$ ion is shown in Fig. 3, which also presents cleavages that occur on the IB5 sequence. The CID spectra of the parent ion are primarily composed of singly, doubly, triply, and some quadruply charged fragments, and the C-terminal y series dominates. The y_{29} and y_{32} ions, corresponding to cleavages on the N-terminal side of proline residues, are the most abundant product ions. The y sequence ions are mainly observed in the center part of the protein backbone. The b_{38}, b_{37}, and b_{35} ions are present with their respective corresponding c ions. Moreover, many internal fragment ions are detected. Their interpretation remains difficult because of repeated sequences and proline abundance in IB5. This protein presents a low-complexity primary sequence, with only 9 different residues, and within the 70 amino acids, 29 are P, 13 are G, and 13 are K, with repeats of KPQGPP(P). P, G, and K residues are interesting from a mass spectrometry point of view [56]. Indeed, the presence of proline in a peptide induces the so-called proline effect which is characterized by the presence of a labile amide bond on the N-terminal side of proline and a stable amide bond on its C-terminal side which is associated with the abundance of y sequence ions [55]. Fragmentation of proline-containing peptides, particularly when poly-Pro stretches exist, produces unusual fragment ions in high-energy experiments, some of which are suggested to be produced by charge-remote cleavage [54]. Complete sequence information cannot be obtained because fragment ions arising from cleavages occurring not adjacent to proline amide bonds have very low abundances or are missing [57].

ESI-MS analysis of IB5·EgCG complexes

Concentrations of condensed tannin in red wine are approximately 1–2 g L^{-1}, corresponding to a mean molar concentration of 0.5–1 mM. In biological media as well as in processing media, polyphenols are often present together with proteins. For example, fining treatment, consisting in the addition of a protein fining agent, is applied to precipitate tannins from plant-derived beverages, so as to decrease haze and/or astringency. Fining agents are gelatin fractions submitted to different hydrolysis leading to different protein sizes. In the case of a red wine, addition of 8–20 g of protein per hectoliter of wine is of general use [58]. Thereby, the concentration of a fining protein showing a 10-kDa apparent MM at 10 g hL^{-1} can be estimated to be around 20 μM. The presence of food in the mouth initiates both mechanical and chemical stimuli via neural reflexes that result in an increased secretion of saliva with taste being the main stimulant for this secretion. Thus, the confrontation between polyphenols and salivary proteins is the first step of ingestion of plant products. The concentration of proteins in saliva is approximately 1 mg mL^{-1}, circa 83 μM. Polyphenols are present in large excess compared with proteins both in wine and in the mouth after sipping of wine, making the protein/polyphenol ratio always in favor of polyphenols. On this basis, to investigate soluble protein–polyphenol complexes we use a protein/polyphenol ratio of 1:10 that does give rise neither to the formation of precipitate nor cloudiness.

Premixed interaction medium with a 1:10 IB5/EgCG molar ratio (5 μM of IB5 with 50 μM of EgCG in H_2O/EtOH, 88:12 v/v, pH 3.1) was introduced into the ESI mass spectrometer. The successful analysis of noncovalent assemblies by MS requires the preservation of the native state of the complex in solution. It is crucial to use aqueous solutions containing only volatile buffers [59]. The MS analysis was performed in water/ethanol, allowing satisfactory levels of desolvation [59]. Analysis of the ESI mass spectrum (Fig. 4a) revealed three distinct entities, IB5, EgCG, and noncovalent soluble complexes in agreement with earlier isothermal titration microcalorimetry (ITC) and CD experiments [21]. It is noteworthy that no indication about their stoichiometries was obtained by other approaches. The CSD of these ions ranged from +6 to +10, like those of individual IB5 proteins. IB5a complexes remain predominant as expected from the protein sample analysis. Figure 4b presents a blowup of the region of the spectrum corresponding to the +7 ions. This is the main charge state for both IB5 and IB5·EgCG complexes. It can be noted that numerous stoichiometries ranging from 1:1 to 1:5 are observed. ESI mass spectra of a mixture of IB5 and reserpine, the latter having a chemical structure with aromatic rings and a molecular mass close to that of EgCG, did not give rise to complex peaks (data not shown). If the interaction is not driven by polyphenols, ESI-MS should have generated complexes between IB5 and reserpine. Use of reserpine allows us to confirm that the formation of complexes is related to tannins.

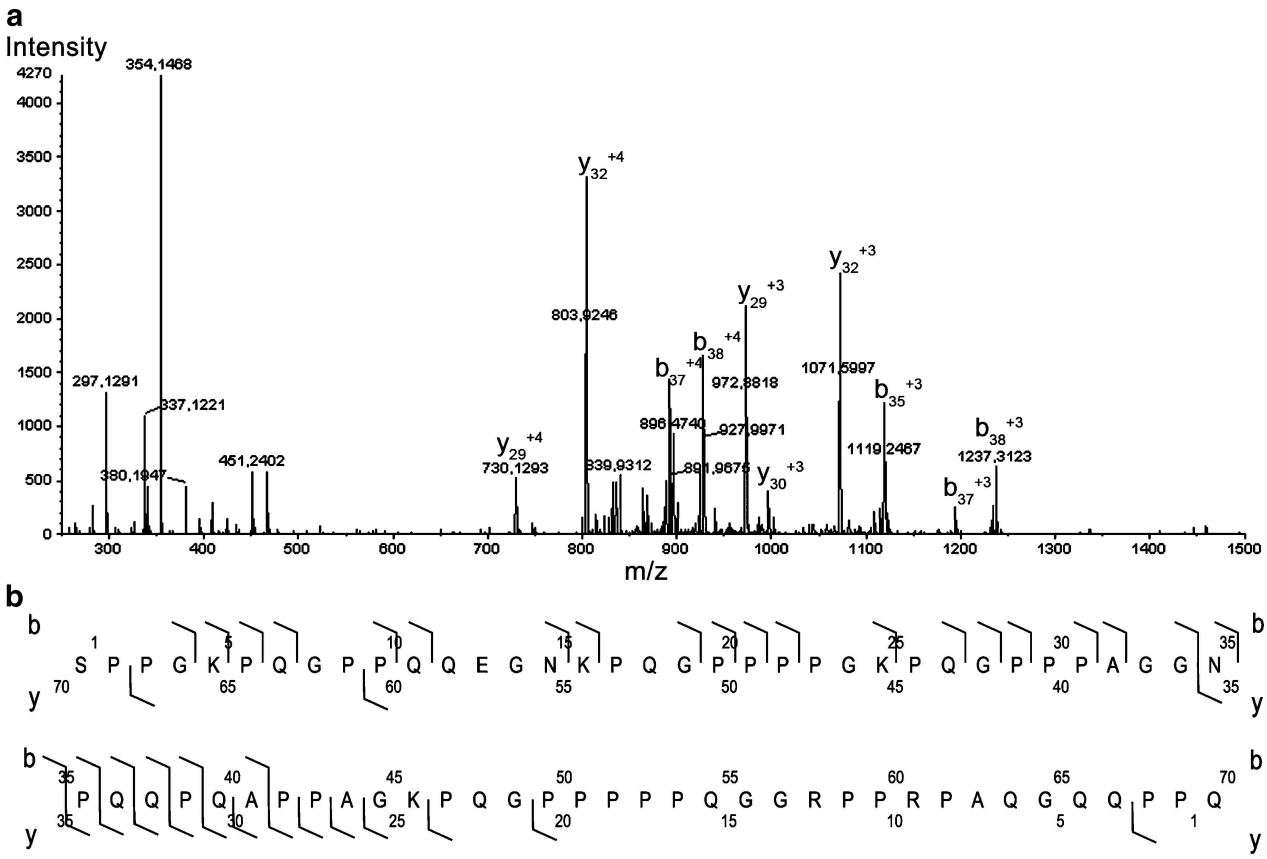

Fig. 3 **a** MS/MS spectrum of product ions obtained by CID of the 7+ charged ion of IB5, collision energy 280 eV. **b** Primary CID fragmentation reactions of IB5

From previous solution studies, proline-rich peptide–tannin interaction involves stacking of the planar proline ring with the phenolic ring, stabilized by hydrogen bonding interactions with the peptide bonds next to the proline and with other amino acids like glycine [20, 26, 60]. Involvement of both enthalpy-driven (attributed to hydrogen bonding) and entropy-driven (associated with the hydrophobic effect and conformational changes) phenomena in interactions of flavan-3-ols with poly-L-proline was confirmed by ITC [61]. The former phenomenon is prevalent in the case of monomers and the latter in that of polymers. Survival of small protein–ligand complexes is largely dictated by the nature of the interaction. In the gas phase, electrostatic and hydrogen bonding interactions are enhanced, whereas hydrophobic interactions are partly or completely lost [62, 63]. Full-scan simple mass spectra with soft ionization conditions obtained in our study probe the composition of the solution and relative abundance of the species. We show that IB5·EgCG complexes are preserved and may involve more than one tannin. The preservation of supramolecular complexes formed by IB5 and EgGC, a model of biological interest with regards to astringency, in the gas phase demonstrates the strength and the contribution of hydrogen bonding [62], in agreement with previous studies using the medium considered here [20]. As previously stated, the main function described for basic salivary PRPs, like IB5, is to be a scavenger which binds tannins [22, 64–66]. Scavenger IUPs function by molecular recognition and often can bind several partners at the same time [67]. Observation of multiple stoichiometries ranging from 1:1 to 1:5 is consistent with IB5's proposed function. Basic PRPs have to bind more than one molecule of tannins to counteract their effects, especially when tannin concentration is rather high.

ESI-MS/MS analysis of IB5·EgCG complexes

Collision-induced dissociation is a process whereby precursor ions are activated upon collision with an unreactive gas, such as argon or nitrogen in the present case. Each collision increases the overall vibrational energy of the molecule until there is enough internal energy accumulated within the molecule to overcome the bond energy, thus causing dissociation [68]. Different cases need to be

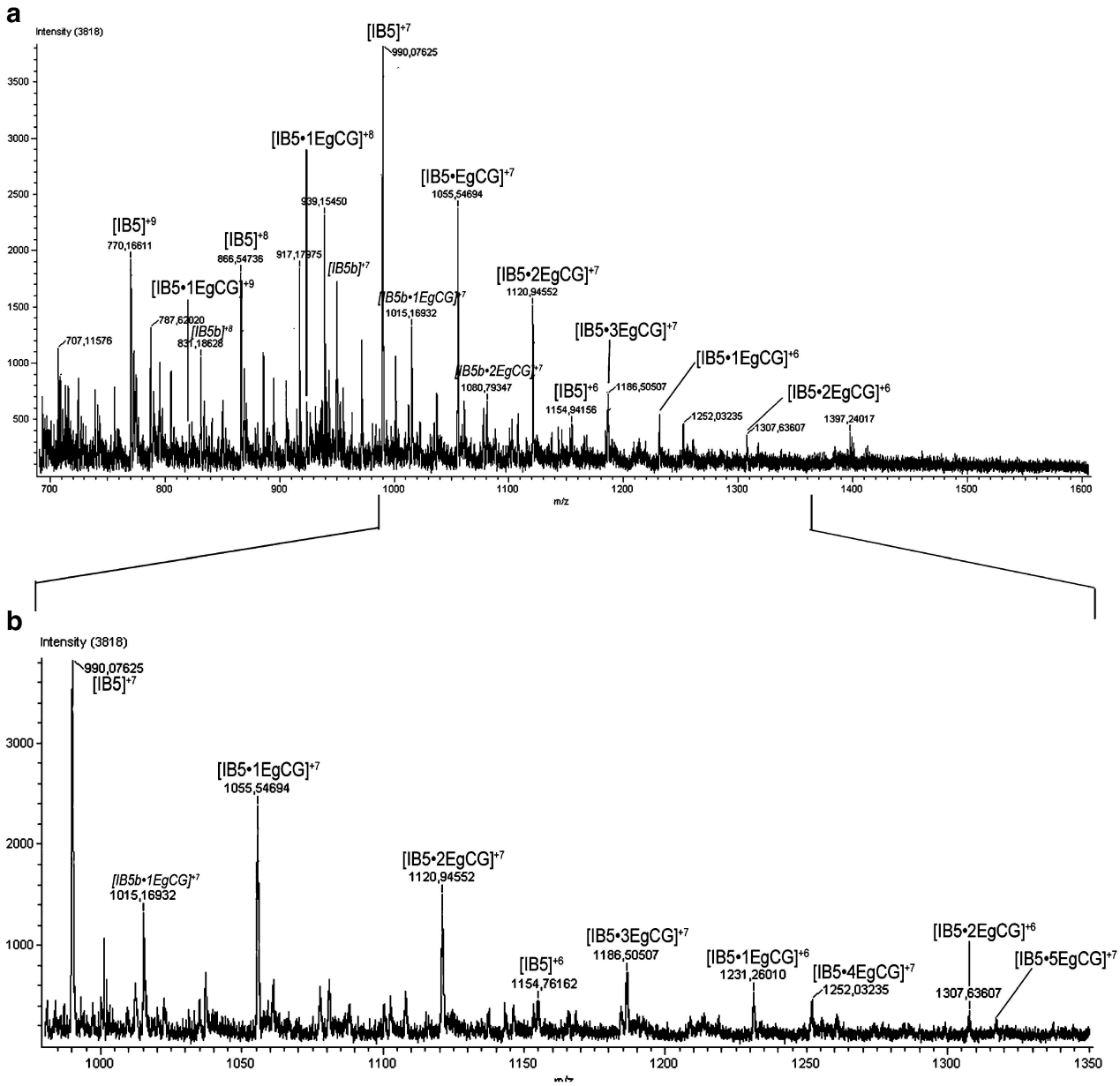

Fig. 4 **a** Positive-ion ESI mass spectrum obtained from mixture of IB5 and EgCG (5 μM:50 μM). **b** Expanded mass region of the 7+ complex ions

considered. Proteins with the lowest charge states are reported to have a conformation close to that in solution [69]. Therefore ESI conditions must be controlled, but also the charge state of the complex ion selected. ESI-MS/MS was performed on IB5·EgCG mixtures. Low-energy CID investigated the relative gas phase stability of the non-covalent IB5·EgCG complexes with 1:1 and 1:2 stoichiometries in the +6 charge state. The same experiments performed on +7 ions gave similar results but IB5 fragmentation was observed. During CID experiments, complex ions are accelerated with voltage offsets up to the 50-V range into the gas-filled collision cell where their translational energy is partly converted into internal energy in a multicollisional process. As mentioned earlier, the kinetic energy of the precursor ion in the laboratory frame of reference is obtained from $E_{\mathrm{Lab}}=z\times e\times V_{\mathrm{c}}$, where z is the number of charges on the ion and e is the charge of an electron [44]. Therefore, the collision energy for the +6 precursor was increased from 0 eV to 300 eV. Collision-induced total dissociation of both complexes (1:1 and 1:2) gave rise to the ions corresponding to $[IB5]^{6+}$ and a neutral EgCG (Fig. 5). The ion retains the overall charge

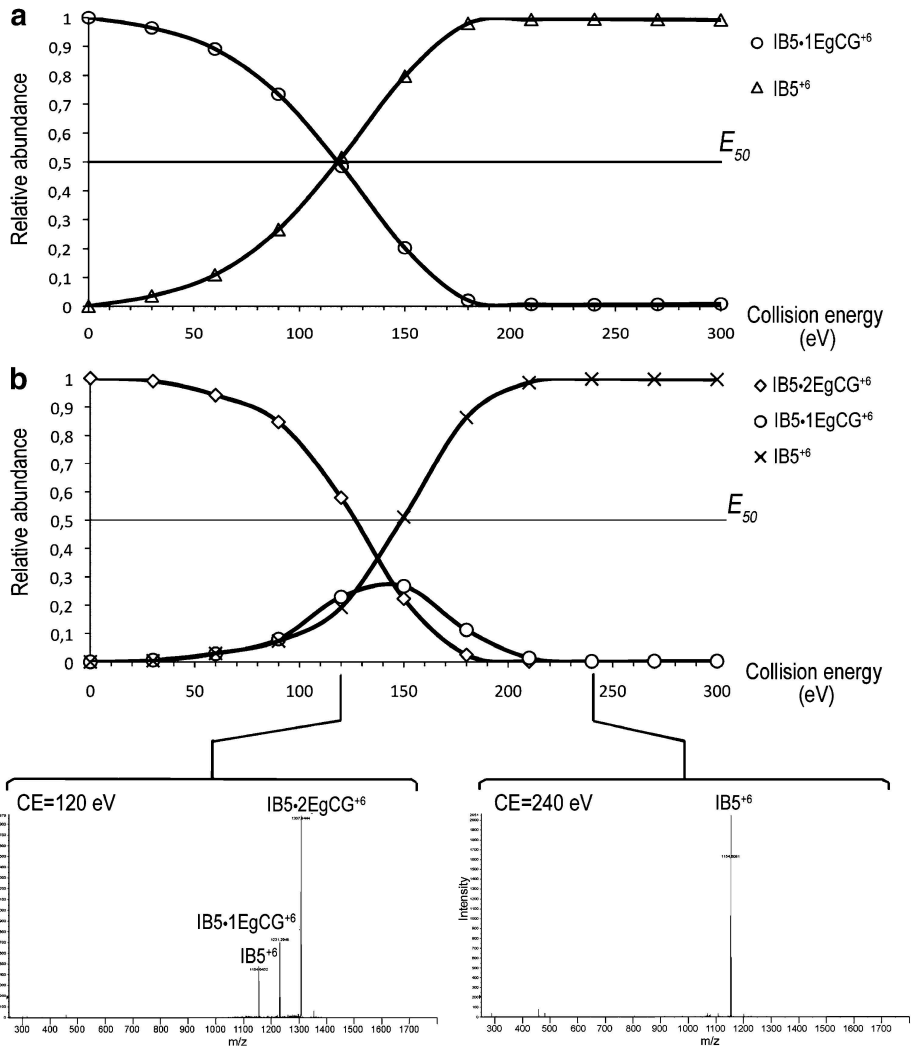

Fig. 5 **a** Plots of dissociation of $[IB5{\cdot}EgCG]^{6+}$ ion and appearance of the $[IB5]^{6+}$ ion. **b** Plots of dissociation of $[IB5{\cdot}2EgCG]^{6+}$ ion, appearance and dissociation of $[IB5{\cdot}EgCG]^{6+}$ ion, and appearance of the $[IB5]^{6+}$ ion. The *y*-axis represents relative abundance of ions; *insets* are CID-MS/MS spectrum of the selected $[IB5{\cdot}2EgCG]^{6+}$ complex ion (*m/z* 1,307) for collision energy 120 eV and collision energy 240 eV

as expected, whereas EgGC is released as a neutral species. Moreover, collision energy thresholds of total dissociation of [IB5·EgCG] and [IB5·2 EgCG] complex ions are 180 eV and 210 eV, respectively, showing the greater stability of the latter. Spectra obtained at CID lower collision energies allowed detection of both the remaining parent complex and $IB5^{6+}$ ions (Fig. 5a). In the case of 1:2 complexes, ions corresponding to the 1:1 complex are also detected. Precursor and product ions exhibit the same charge state (Fig. 5b). Thus, dissociation pathways for $[IB5{\cdot}2EgCG]^{6+}$ result from neutral loss of EgCG:

$$[IB5 \cdot 2EgCG]^{6+} \rightarrow [IB5 \cdot EgCG]^{6+} + EgCG$$
$$\rightarrow [IB5]^{6+} + 2EgCG$$

Table 2 Collision energy corresponding to 50% abundance of the precursor ions (E_{50}) in the laboratory frame (E_{Lab}) and in the center of mass (E_{CoM})

E_{50}(eV)	IB5·EgCG (1:1)	IB5·2EgCG (1:2)
E_{Lab}	120	127.5
E_{CoM}	0.45	0.45

Dissociation of the precursor complex ions leads to a decrease in stoichiometry down to the protein alone. Increasing energy on the parent ion releases the first tannin before the second one. Both tannins do not dissociate together from IB5. Nonetheless, this observation alone does not allow us to conclude whether tannins are bound on two different sites over IB5 or not.

Dissociation energies for $[IB5{\cdot}x\text{EgCG}]$ ions (x=1 or 2) were determined to give a measurement of the relative EgCG binding energies in these complexes. Relative abundance of the precursor ion was calculated as $I_p/(I_p + \sum I_{frag})$, where I_p is the peak intensity of the precursor ion,

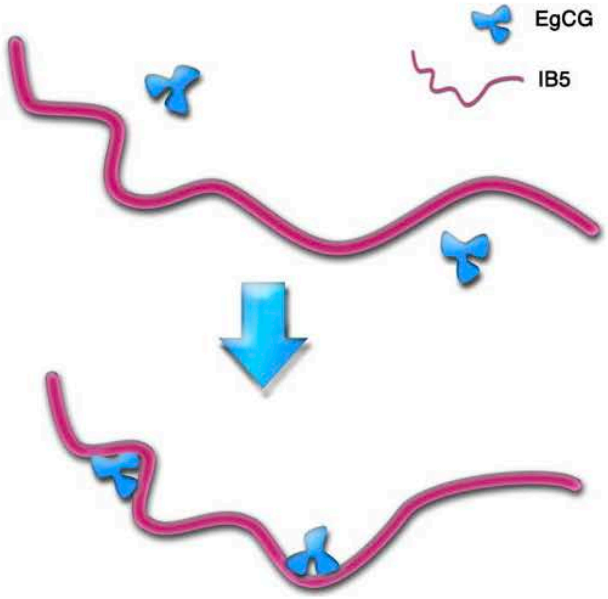

Fig. 6 Schematic illustrating the interaction between IB5 and EgCG

and $\sum I_{frag}$ is the sum of the peak intensities corresponding to all fragments [70]. This ratio is used to monitor the internal energy added to the complex ions to dissociate. The maximum energy that ions can acquire in the collision cell is the center-of-mass collision energy (E_{CoM}) of each collision summed over all. Laboratory frame collision energies (E_{Lab}) are converted to center-of-mass energies by using the equation

$$E_{CoM} = E_{Lab}\frac{m_g}{m_g + m_i} \quad (1)$$

where m_g and m_i are the mass of the target gas and of the complex ion, respectively.

The number of collisions (N_{col}) is determined by three parameters, the gas number density (n) , the length of the collision cell (l), and the collision cross section (σ) of the selected ion :

$$N_{col} = n \times \sigma \times l \quad (2)$$

Finally, the internal energy E_{Int} can be calculated from equation

$$E_{Int} = E_{CoM} \times N_{col} \quad (3)$$

As a first-order approximation, both complexes are expected to present very similar collision cross section because of the mere modification of their MM and their similar charge state [71]. Equation (2) shows that ions with similar cross section experience an identical number of collisions, thus from Eq. (3) their E_{Int} can be directly compared. From Eqs. (1) and (3), direct access to E_{Int} can be obtained via measurement of E_{CoM} for each species present in the spectrum. Moreover, previous works on proteins by the Douglas group provided evidence of the efficiency of energy transfer in a quadrupole, showing that almost 90% of the center-of-mass-energy is converted to internal energy [72]. Thus E_{Int} is approximately given by the center-of-mass energy E_{CoM} [72, 73]. For $[IB5{\cdot}EgCG]^{6+}$ and $[IB5{\cdot}2\ EgCG]^{6+}$ complex ions, dissociation curves as a function of collision energy were plotted, and the half-wave collision energy (E_{50}) was defined. E_{50} in the laboratory frame is the collision energy required to disrupt 50% of the parent complex ions. From the dissociation curves, E_{50} values have been established at 120 eV and 127.5 eV, respectively (Table 2). From these measurements, E_{50} in the center of mass (referred to as E_{CoM}) for $[IB5{\cdot}EgCG]^{6+}$ and $[IB5{\cdot}2\ EgCG]^{6+}$ ions are obtained (Table 2). The magnitude of that energy is related to the stability of the complex. Hence, we find that both $[IB5{\cdot}EgCG]^{6+}$ and $[IB5{\cdot}2\ EgCG]^{6+}$ ions (Table 2) have the same E_{CoM}. This implies that the same energy is required to either dissociate one EgCG from the IB5·2 EgCG complex or to dissociate the 1:1 complex. This feature highlights that EgCGs are involved within the complex with the same strength, indicating that they are bound on equivalent sites on IB5. These data support the presence of at least two potential equivalent interaction sites on IB5, as schematically illustrated in Fig. 6. Moreover, the intrinsic disorder of IB5 makes room for quite a large interaction surface, thus increasing the number of tannins that IB5 can bind [3].

Conclusions

Our experiments have demonstrated the ability of ESI-MS and ESI-MS/MS to detect and characterize noncovalent protein polyphenol complexes with a charge state distribution similar to that of the protein alone. Direct access to the complex stoichiometry has been reached through ESI-MS analysis, where a maximum of 5 EgCG for 1 protein has been observed. For the first time, this approach affords an opportunity to estimate the ability of polyphenols to form soluble complexes with a protein different stoichiometry and to evaluate their stability. Our results indicate that IB5 possesses several interaction sites to bind tannins. In the light of both observed stoichiometries and IB5 sequence, the repeated motif "KPQGPP" could be the main site for interaction. This study confirms that the stability of protein tannin complexes increases with the number of bound tannins and presumably with the number of repeated amino acid sequences [74]. Moreover, EgCG is likely to interact simultaneously through several sites of IB5. Another interesting consequence is that only PRP tannin complexes made with full-length PRP sequences resist degradation under conditions such as encountered in

digestion [75]. This study is part of a general theme centered on the relevance of ESI-MS to probe protein–tannin solution-phase properties. Indeed, it clearly demonstrates that ESI-MS is well suited to detect associated polyphenols and will be used in further work to evaluate the ability of structurally distinguishable tannins to interact with peptides or proteins keeping in mind their astringency.

Acknowledgement The authors thank Hélène Boze and Claire Bouchut (UMR 1083 SPO) for their help in protein production and purification and MS experiments. We acknowledge synchrotron SOLEIL and thank all staff for assistance in using beamline DISCO. AG thanks Applied Biosystems (Les Ullis, France) for the loan of the IonCooler Guide. This work is supported by grant 07-BLAN-0279 from the French Agence Nationale de la Recherche (A.N.R.).

References

1. Tompa P (2002) Trends Biochem Sci 27:527–533
2. Dyson HJ, Wright PE (2005) Nat Rev Mol Cell Biol 6:197–208
3. Dunker AK, Brown CJ, Lawson JD, Iakoucheva LM, Obradovic Z (2002) Biochemistry 41:6573–6582
4. Bennick A (1982) Mol Cell Biochem 45:83–99
5. Robbins CT, Hagerman AE, Austin PJ, Arthur CM, Hanley TA (1991) J Mammal 72:480–486
6. Haslam E, Lilley TH, Cai Y, Martin R, Magnolato D (1989) Planta Med 55:v
7. McMurrough I, Madigan D, Kelly RJ, Smyth MR (1996) J Am Soc Brew Chem 54:141–148
8. McMurrough I, Hennigan GP, Loughrey MJ (1983) J Inst Brew 89:15–23
9. Waters EJ, Peng Z, Pocock KF, Williams PJ (1995) Aust J Grape Wine Res I:86–93
10. Butler LG (1992) In: Hemingway RW, Laks PE (eds) Antinutritional effects of condensed and hydrolyzable tannins. Plenum, New York
11. Dangles O (2006) Agro Food Ind Hi-Tech 17:64–67
12. van Valen L (1973) Evol Theory 1:1–30
13. Breslin PA, Gilmore M, Beauchamp GK, Green BG (1993) Chem Senses 18:405–417
14. Green BG (1993) Acta Psychol 84:119–125
15. Clifford MN (1997) In: Tomas-Barberan F, Robins R (eds) Astringency. Clarendon, Oxford
16. Noble A (1998) In: Waterhouse AL, Eberler S (eds) Why do wines taste bitter and feel astringent ? American Chemical Society, Washington
17. Hagerman AE (1989) In: Hemingway RW, Karchesy JJ (eds) Chemistry of tannin-protein complexation. Plenum, New York, London
18. Bate-Smith EC (1954) Food 23:124–135
19. Haslam E (1996) J Nat Prod 59:205–215
20. Simon C, Barathieu K, Laguerre M, Schmitter JM, Fouquet E, Pianet I, Dufourc EJ (2003) Biochemistry 42:10385–10395
21. Pascal C, Poncet-Legrand C, Imberty A, Gautier C, Sarni-Manchado P, Cheynier V, Vernhet A (2007) J Agric Food Chem 55:4895–4901
22. Sarni-Manchado P, Canals-Bosch J, Mazerolles G, Cheynier V (2008) J Agric Food Chem 56:9563–9569
23. Porter LJ, Woodruffe J (1984) Phytochemistry 23:1255–1256
24. Okuda T, Mori K, Hatano T (1985) Chem Pharm Bull 33:1424–1433
25. Baxter NJ, Lilley TH, Haslam E, Williamson MP (1997) Biochemistry 36:5566–5577
26. Hatano T, Hemingway RW (1996) J Chem Soc Chem Comm:2537–2538
27. Luck G, Liao H, Murray NJ, Grimmer HR, Warminski EE, Williamson MP, Lilley TH, Haslam E (1994) Phytochemistry 37:357–371
28. Murray NJ, Williamson MP, Lilley TH, Haslam E (1994) Eur J Biochem 219:923–935
29. Vergé S, Richard T, Moreau S, Nurich A, Merillon J-M, Vercauteren J, Monti J-P (2002) Biochim Biophys Acta 1571:89–101
30. Sarni-Manchado P, Cheynier V (2002) J Mass Spectrom 37:609–616
31. Vergé S, Richard T, Moreau S, Richelme-David S, Vercauteren J, Promé J-C, Monti J-P (2002) Tetrahedron Lett 43:2363–2366
32. Chen Y, Hagerman AE (2004) J Agric Food Chem 52:4008–4011
33. Loo JA, Sannes-Lowery KA (1997) Mass Spectrom Rev 16:1–23
34. Pramanik BN, Bartner PL, Mirza UA, Liu YH, Ganguly AK (1998) J Mass Spectrom 33:911–920
35. Jorgensen TJD, Roepstorff P, Heck AJR (1998) Anal Chem 70:4427–4432
36. Kapur A, Beck JL, Brown SE, Dixon NE, Sheil MM (2002) Protein Sci 11:147–157
37. Bligh SWA, Haley T, Lowe PN (2003) J Mol Recognit 16:139–148
38. Gupta R, Kapur A, Beck JL, Sheil MM (2001) Rapid Commun Mass Spectrom 15:2472–2480
39. de Brouwer APM, Versluis C, Westerman J, Roelofsen B, Heck AJR, Wirtz KWA (2002) Biochemistry 41:8013–8018
40. Benesch JLP, Sobott F, Robinson CV (2003) Anal Chem 75:2208–2214
41. Rosu F, De Pauw E, Gabelica V (2008) Biochimie 90:1074–1087
42. Pascal C, Bigey F, Ratomahenina R, Boze H, Moulin G, Sarni-Manchado P (2006) Protein Expr Purif 47:524–532
43. Yin S, Xie Y, Loo JA (2008) J Am Soc Mass Spectrom 19:1199–1208
44. Haller I, Mirza UA, Chait BT (1996) J Am Soc Mass Spectrom 7:677–681
45. Robinson CV (2001) J Am Soc Mass Spectrom 12:126–126
46. Zhang J, Kashket S (1998) Caries Res 32:233–238
47. Jørgensen TJD, Delforge D, Remacle J, Bojesen G, Roepstorff P (1999) Int J Mass Spectrom Ion Process 188:63–85
48. Wan KX, Gross ML, Shibue T (2000) J Am Soc Mass Spectrom 11:450–457
49. Akashi S, Osawa R, Nishimura Y (2005) J Am Soc Mass Spectrom 16:116–125
50. Harrison AG (1997) Mass Spectrom Rev 16:201–217
51. Bleiholder C, Suhai S, Paizs B (2006) J Am Soc Mass Spectrom 17:1275–1281
52. Yi SL, Boys BL, Brickenden A, Konermann L, Choy WY (2007) Biochemistry 46:13120–13130
53. Engel BJ, Pan P, Reid GE, Wells JM, McLuckey SA (2002) Int J Mass Spectrom Ion Process 219:171–187
54. Breci LA, Tabb DL III, JRY WVH (2003) Anal Chem 75:1963–1971
55. Vaisar T, Urban J (1996) J Mass Spectrom 31:1185–1187
56. Zhang X, Jai-nhuknan J, Cassady CJ (1997) Int J Mass Spectrom Ion Process 171:135–145
57. Leymarie N, Berg EA, McComb ME, O'Connor PB, Grogan J, Oppenheim FG, Costello CE (2002) Anal Chem 74:4124–4132
58. Flanzy C (1998) Oenologie — Fondements scientifiques et technologiques. Lavoisier, Paris
59. Sharon M, Robinson CV (2007) Annu Rev Biochem 76:167–193
60. Hagerman AE, Rice ME, Richard NT (1998) J Agric Food Chem 46:2590–2595
61. Poncet-Legrand C, Gautier C, Cheynier V, Imberty A (2007) J Agric Food Chem 55:9235–9240

62. Robinson CV, Chung EW, Kragelund BB, Knudsen J, Aplin RT, Poulsen FM, Dobson CM (1996) J Am Chem Soc 118:8646–8653
63. Sobott FM, Hernández H, McCammon MG, Robinson CV (2005) Phil Trans R Soc A 363:379–391
64. Mehansho H, Hagerman A, Clements S, Butler LG, Rogler JC, Carlson DM (1983) Proc Natl Acad Sci USA 80:3948–3952
65. Carlson DM (1993) Crit Rev Oral Biol Med 4:495–502
66. Sarni-Manchado P, Cheynier V, Moutounet M (1999) J Agric Food Chem 47:42–47
67. Tompa P (2003) J Mol Struc (Theochem) 361–371
68. Khalsa-Moyers G, McDonald WH (2006) Brief Funct Genomic Proteomic 5:98–111
69. Ruotolo BT, Robinson CV (2006) Curr Opin Chem Biol 10:402–408
70. Ham BM, Cole RB (2005) Anal Chem 77:4148–4159
71. Chen Y-LC, JM, Collings BA, Konermann L, Douglas DJ (1998) Rapid Commun Mass Spectrom 12:1003–1010
72. Chen Y-L, Collings BA, Douglas DJ (1997) J Am Soc Mass Spectrom 8:681–687
73. Wells JM, McLuckey SA (2005) In: Collision induced dissociation (CID) of peptides and proteins. Academic, New York
74. Charlton AJ, Baxter NJ, Lilley TH, Haslam E, McDonald CJ, Williamson MP (1996) FEBS Lett 382:289–292
75. Lu Y, Bennick A (1998) Arch Oral Biol 43:717–728

Publication n°6: Ability of a salivary intrinsically unstructured protein to bind different tannin targets revealed by mass spectrometry.

Canon, F.; Giuliani, A.; Paté, F.; Sarni-Manchado, P.

Anal. Bioanal. Chem. ***2010,*** *398, 815-822.*

Anal Bioanal Chem (2010) 398:815–822
DOI 10.1007/s00216-010-3997-9

ORIGINAL PAPER

Ability of a salivary intrinsically unstructured protein to bind different tannin targets revealed by mass spectrometry

Francis Canon · Alexandre Giuliani · Franck Paté · Pascale Sarni-Manchado

Received: 23 April 2010 / Revised: 28 June 2010 / Accepted: 1 July 2010 / Published online: 28 July 2010

Abstract Astringency is thought to result from the interaction between salivary proline-rich proteins (PRP) that belong to the intrinsically unstructured protein group (IUP), and tannins, which are phenolic compounds. IUPs have the ability to bind several and/or different targets. At the same time, tannins have different chemical features reported to contribute to the sensation of astringency. The ability of both electrospray ionization mass spectrometry and tandem mass spectrometry to investigate the noncovalent interaction occurring between a human salivary PRP, IB5, and a model tannin, epigallocatechin 3-*O*-gallate (EgCG), has been reported. Herein, we extend this method to study the effect of tannin chemical features on their interaction with IB5. We used five model tannins, epigallocatechin (EgC), epicatechin 3-*O*-gallate (ECG), epigallocatechin 3-*O*-gallate (EgCG), procyanidin dimer B2 and B2 3′-*O*-gallate, which cover the main tannin chemical features: presence of a gallate moiety (galloylation), the degree of polymerization, and the degree of B ring hydroxylation. We show the ability of IB5 to bind these tannins. We report differences in stoichiometries and in stability of the IB5•1 tannin complexes. These results demonstrate the main role of hydroxyl groups in these interactions and show the involvement of hydrogen bonds. Finally, these results are in line with sensory analysis, by Vidal et al. (J Sci Food Agric 83:564–573, 2003) pointing out that the chain length and the level of galloylation are the main factors affecting astringency perception.

Keywords Polyphenol · Noncovalent interaction · Proline-rich protein · Saliva · Astringency · Intrinsically unstructured protein

Abbreviations

CID	Collision-induced dissociation
EgC	Epigallocatechin
ECG	Epicatechin gallate
EgCG	Epigallocatechin gallate
B2 3′-OG	B2 3′-*O*-gallate
ESI	Electrospray ionization
IUP	Intrinsically unstructured protein
MS	Mass spectrometry
MS/MS	Tandem mass spectrometry
PRP	Proline-rich protein
*b*PRP	Basic proline-rich protein
*a*PRP	Acidic proline-rich protein
Q-TOF	Quadrupole/time-of-flight
T	Tannin
UGT	Ungalloylated tannin
GT	Galloylated tannin
M	Monomer
GM	Galloylated monomer
D	Dimer
GD	Galloylated dimer
DP	Degree of polymerization

F. Canon · F. Paté · P. Sarni-Manchado (✉)
INRA, UMR 1083 Sciences Pour l'Oenologie,
2, place Viala,
F-34060 Montpellier, France
e-mail: sarni@supagro.inra.fr

A. Giuliani
DISCO Beamline, Synchrotron Soleil,
l'Orme des Merisiers,
91192 Gif sur Yvette, France

A. Giuliani
CEPIA, INRA,
BP 71627, 44316 Nantes Cedex 3, France

Introduction

Over the last decade, the sequence-to-structure-to-function paradigm based on the view that proteins need to have a well-defined three-dimensional structure for their function, has been re-assessed. Numerous proteins do have a well-defined function that requires intrinsic disorder, and the term of intrinsically unstructured protein (IUP) has been proposed to describe this group [1]. IUPs appear to be rather common in living organisms, especially in higher eukaryotes: primary sequence analyses indicate that about 25% of full-length mammal proteins belong to this class [2]. The intrinsic lack of structure can confer functional advantages such as the ability to bind several and/or different ligands [1, 3, 4]. This ability often leads to mixtures of complexes with heterogeneous composition. While techniques are emerging for the characterization of flexible proteins [5, 6], the study of complexes of IUP is highly challenging and requires new approaches. Electrospray ionization (ESI) has demonstrated its efficiency to probe weak associations of molecules in solution such as receptor-ligand and protein-nucleic acid interactions [7, 8]. ESI-MS offers speed and sensitivity in monitoring components of mixtures and allows the determination of supramolecular edifices stoichiometry. Determination of relative binding affinities of noncovalent complexes is now well established [9–11]. Tandem mass spectrometry (MS/MS) provides access to noncovalent interaction strengths, and qualitative information on the complex structure [12, 13]. Herein, the ability of a model IUP, namely IB5, to form supramolecular edifices with different ligands is explored through MS and MS/MS approaches.

The IUP IB5 is a human salivary protein belonging to the class of proline-rich proteins (PRPs). For numerous mammals, PRPs are the most prevalent group of proteins in the saliva; they may constitute 70% of all proteins in human parotid saliva [14]. The salivary proteins play various roles (lubrication, digestion, taste, protection…) as saliva is the first fluid which interacts with food constituents. Salivary PRPs are classically divided in two groups, acidic PRPs (*a*PRPs) and basic PRPs (*b*PRPs) [15]. *a*PRPs act primarily in maintaining oral homeostasis, whereas the only known function of *b*PRPs is to bind and to scavenge tannins [16–18]. Moreover, in rats and mice, synthesis of salivary PRPs is stimulated by a tannin rich diet [19, 20]. PRPs affinity for tannins is estimated to be 5–80 and 1,000 times higher than that of bovine serum albumin and lysozyme, respectively [21–23]. PRP involvement in adaptation to tannin rich diet either as astringency mediator or/and as scavenger, is related to their ability to establish noncovalent interactions with tannins [15, 24].

Tannins are phenolic compounds ubiquitous in plant and plant-based foods and beverages. From a biological point of view, tannins act in plant defense mechanisms as molecules that protect against herbivores [25]. This role has been attributed to their ability to interact with proteins, to precipitate them and to inhibit gastrointestinal enzymes, thereby reducing the digestibility of plant proteins [26]. Proanthocyanidins are the main tannins in plant-based food (e.g., fruit, cocoa) and beverages (e.g. wine, tea, beer, cider…). These molecules have attracted considerable interest because of their quantitative importance and major contribution to organoleptic and biological properties. The chemical characteristics of proanthocyanidins are believed to affect their organoleptic properties, in particular their degree of polymerization, their level of B ring hydroxylation and their level of galloylation [27]. Numerous studies on the impact of these chemical characteristics over the protein•tannin interaction, were realized on poly L-proline [28] or peptides [29]. Since the affinity for tannins differs among proteins [22], PRPs [21] and with the length of PRP [30], it is essential to examine the effect of tannin chemical features on tannin interaction with a full basic salivary proline-rich protein (*b*PRP).

Our previous work on the interaction between IB5, a 70-a.a.-long human *b*PRP, and EgCG, a model tannin, revealed the presence in solution of IB5•EgCG supramolecular edifices with several stoichiometries [31]. The gas-phase stability of complex ions corresponding to two stoichiometries was investigated, and demonstrated the presence of several interaction sites on IB5. This approach affords the opportunity to estimate the ability of polyphenols to form different stoichiometry soluble complexes with a protein and to evaluate their stability. Since PRP–tannin interactions are thought to be involved in astringency [32], it is important to understand how the tannin chemical features have an effect on the stoichiometry, and on the strength of these interactions. To address these questions, we investigated the interactions between IB5, and five model tannins (T): three are monomers (M) epigallocatechin (EgC), epicatechin gallate (ECG), epigallocatechin gallate (EgCG), and two are dimers (D): B2 and B2 3′-*O*-gallate (B2 3′-OG; Fig. 1a). They cover the main chemical characteristics of tannins: number of units (DP), hydroxylation pattern of the B ring and presence of a galloylated moiety on position 3.

This paper describes the use of the ESI-MS CID approach developed previously, which has proven its efficiency to probe protein–tannin solution-state properties, to gain deeper understanding on the relation between tannin structure and astringency perception.

Materials and methods

Samples

Epigallocatechin (EgC), epicatechin gallate (ECG), epigallocatechin gallate (EgCG), and reserpine (Fig. 1a and b)

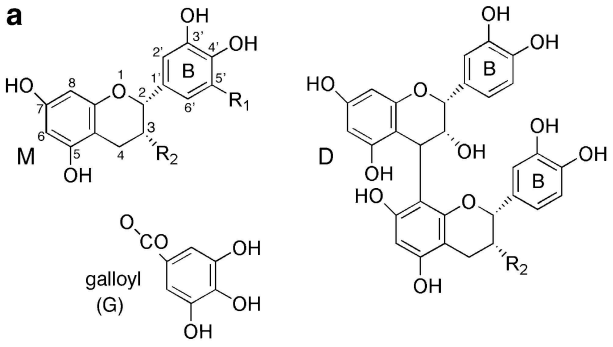

Tannins	skeleton	R_1	R_2
Epigallocatechin	M	OH	OH (UG)
Epicatechin gallate	M	H	galloyl (G)
Epigallocatechin gallate	M	OH	galloyl (G)
B2	D		OH (UG)
B2 3'OG	D		galloyl (G)

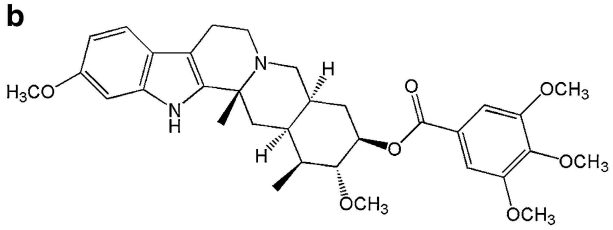

Fig. 1 Structures of **a** studied tannins (*T*) and **b** reserpine

were purchased from Sigma (Sigma Chemical Co., Poole, Dorset, U.K.). B2 and B2 3′-O-gallate were purified as previously described [33].

The human salivary proline-rich protein, IB5, was produced by use of the yeast *Pischia pastoris* as a host organism and purified as previously described [34].

Tannin and protein stock solutions were prepared in the following medium: water/ethanol, 88:12 (*v*/*v*) acidified to pH 3.2 with acetic acid. They were immediately frozen (−20 °C) to prevent protein proteolysis and tannin oxidation. Prior to use, they were diluted at room temperature to the desired concentrations.

Protein–tannin interactions

For IB5-tannin interactions, the protein concentration was kept constant at 5 μM in the water/ethanol medium described above. Tannins and protein solutions were mixed extemporaneously at room temperature (regulated at 24 °C) to obtain a protein/polyphenol molar ratio of 1:10.

The control solution, addressing the issue of nonspecific aggregates that could form during electrospray ionization, was prepared by mixing IB5 and reserpine at the same 1:10 final ratio as the IB5-T mixtures.

Electrospray ionization mass spectrometry and tandem mass spectrometry

Mass spectrometry and tandem mass spectrometry experiments were performed on a hybrid quadrupole time-of-flight (Q-TOF) Qstar Pulsar I mass spectrometer (Applied Biosystems, Forster City, CA), providing a resolving power of 10,000 at *m*/*z* 1080.8. The interface was fitted with the ion cooler guide to preserve the noncovalent complexes upon transfer into the gas phase. The ion cooler guide is mounted after the skimmer around Q0 and increases the local pressure to greater than 30 mTorr, which greatly improves preservation of weakly bound complexes [35]. The Q-TOF was operated with the Turbospray (electrospray ion source). The sample was infused in the mass spectrometer by means of a syringe infusion pump at 7 μL.min^{-1} flow rate. The source voltage was set to 5,800 V in positive ion mode, the declustering potential at 47 V, the focusing potential at 209 V, the declustering potential 2 at 17 V, the ion source gas 1 set at 22, the ion source gas 2 at 0, the curtain gas at 10 and the capillary was not heated up. Nitrogen from a generator, containing less than 6 ppm oxygen was used both as nebulizing and desolvation gas. During MS/MS experiments, nitrogen was used as a collision gas in the collision cell (Linac) with CAD gas setting of 5. The collision-set energy voltage V_c was increased from 0 to 50 V. The kinetic energy of the precursor ion in the laboratory frame of reference is $E_{\mathrm{Lab}} = z \times e \times V_c$, where z is the number of charges on the ion and e is the charge of an electron [36].

Analysis of ESI-MS and MS/MS experiments and calculations

ESI-MS and collision MS/MS data were analyzed with Analyst QS [37] and MagTran [38] softwares.

A procedure adapted from Jørgensen et al. [39] and Wan et al. [40] was used to establish the dissociation curves. The 50% dissociation energy is defined as the energy giving a 50% loss of precursor complex ions. Based on the data of Akashi et al. [41], one of the multiprotonated molecules of the IB5•1tannin complex (M), $[M+6H]^{6+}$ was selected and submitted to CID.

Results and discussion

ESI-MS analysis of IB5•tannin complexes

The mass spectrum obtained by electrospraying the protein solution displayed a series of peaks corresponding to protonated isoforms of IB5 (a 6923.70, b 6642.63, and c 6360.39 Da) with charge states ranging from +5 to +10 as previously observed [31].

The concentrations chosen for protein and tannin reflect biological conditions. Concentrations of condensed tannins in red wine are approximately 1–2 g.L ^{1}, corresponding to a mean molar concentration of 0.5–1 mM. The concentration of proteins in saliva is approximately 1 mg.mL ^{1} circa 83 μM. Polyphenols are present in large excess compared to proteins both in wine and in the mouth after sipping wine, making the protein/polyphenol ratio always in the benefit of polyphenols. On this basis, to investigate soluble protein–polyphenol complexes we use a protein/polyphenol ratio of 1:10 that gives rise neither to the formation of precipitate nor to cloudiness.

The interaction medium mimics the mouth condition during red wine consumption. As wine is more abundant than saliva, the buffering ability of wine tartaric acid leads to an acidic pH. The pH value of 3.2 used during this experiment is in the range of wine pH values, which are comprised between 2.8 and 3.8 [42, 43]. Moreover, the function of PRPs is to bind and scavenge tannins to protect digestive enzymes, for example in the stomach where pH is approximately 1.5 and PRP•tannin complexes are stable [44]. Thus, the pH used in this study reflects the biological pH of PRP–tannin interaction medium.

Premixed interaction medium with a 1:10 IB5/tannin molar ratio was submitted to ESI mass spectrometry. MS analysis reveals IB5•nT complex ion peaks for each mixture with several stoichiometries (n being the number of T molecules involved in the complexes, Fig. 2). Complexes involving galloylated tannins (IB5•nGT) show the highest stoichiometries and also the highest relative intensities. The presence of a galloylated moiety favors the interaction with IB5. Closer analysis of MS spectra shows that IB5•nUGT complexes (ungalloylated tannins) present similar stoichiometries, while stoichiometries of IB5•nGM complexes (galloylated monomers) are higher than those of IB5•nGD (galloylated dimers). This result may be related to the bulkier size of the dimers, which may restrict the number of sites that can be reached simultaneously on IB5. To address the issue of nonspecific aggregates, which could form during electrospray ionization, ESI mass spectra of mixtures of IB5 and reserpine have been recorded. Reserpine presents a chemical structure and a molecular mass close to those of our model tannins (Fig. 1). These spectra did not give rise to complex peaks. If the interaction was not driven by polyphenols, ESI-MS should have generated complexes between IB5 and reserpine. The absence of IB5•reserpine peak, and the presence of IB5•T peaks, demonstrated that the observed noncovalent complexes were not some ESI artifacts, sustaining the specificity of the protein–tannin interaction. The observation of IB5•T complexes demonstrates the ability of IB5 to bind different tannins. This result is in agreement with the characteristics of IUPs, which have often enough malleability to bind different partners [45, 46]. Observation of multiple and high stoichiometries is consistent with IB5 alleged function. The main function described for basic salivary PRPs, like IB5, is to be a scavenger that binds tannins [16–18, 47]. The extended structure of PRPs [48] allows them to bind more than one molecule of tannins to counteract their effects, especially when tannin concentration is rather high. These results confirm that PRP belong to the IUP functional class of scavenger [3, 49]. Scavenger IUPs work by molecular recognition and, can bind several partners at the same time [1, 3]. However, the stoichiometry differences observed among the complexes involving the different tannins reveal an impact of the tannin chemical features on the interaction. To pursue the investigation on this effect, the stability of IB5•1T complexes has been evaluated by MS/MS.

ESI-MS/MS analysis of IB5•1tannin complexes

The relative stability of IB5•1T complexes was investigated by monitoring $[IB5•1T]^{+6}$ ion dissociation by CID MS/MS experiments. Collision-induced dissociation is a multi-collisions process whereby precursor ions are activated upon collision with a non-reactive gas, nitrogen in the present case. Each collision increases the overall vibrational energy of the ion until there is enough internal energy accumulated within the species to overcome the bond dissociation energy, thus causing fragmentation [50]. In the present study, low-energy CID investigated the relative gas-phase stability of the noncovalent complexes $[IB5•1T]^{+6}$.

Ions were injected into the collision cell with increasing energies to dissociate them through collisions with nitrogen. Collision-induced total dissociation of all IB5•1T complexes gave rise to the ions corresponding to $[IB5]^{6+}$ and a neutral tannin.

$$[IB5 \bullet 1T]^{6+} \rightarrow [IB5]^{6+} + 1T$$

Dissociation curves for each parent complex ion were derived and correlated the relative abundance of the parent ion to the collision energy (Fig. 3).

The maximum energy that ions can acquire in the collision cell is the center-of-mass collision energy (E_{CoM}) of each collision summed over all. Laboratory frame collision energies (E_{Lab}) are converted to center-of-mass energies by using the equation

$$E_{CoM} = E_{Lab}\frac{m_g}{m_g + m_i} \quad (1)$$

where m_g and m_i are the mass of the target gas and of the complex ion, respectively.

The number of collision (N_{col}) is determined by three parameters, the gas number density (n), the length of the

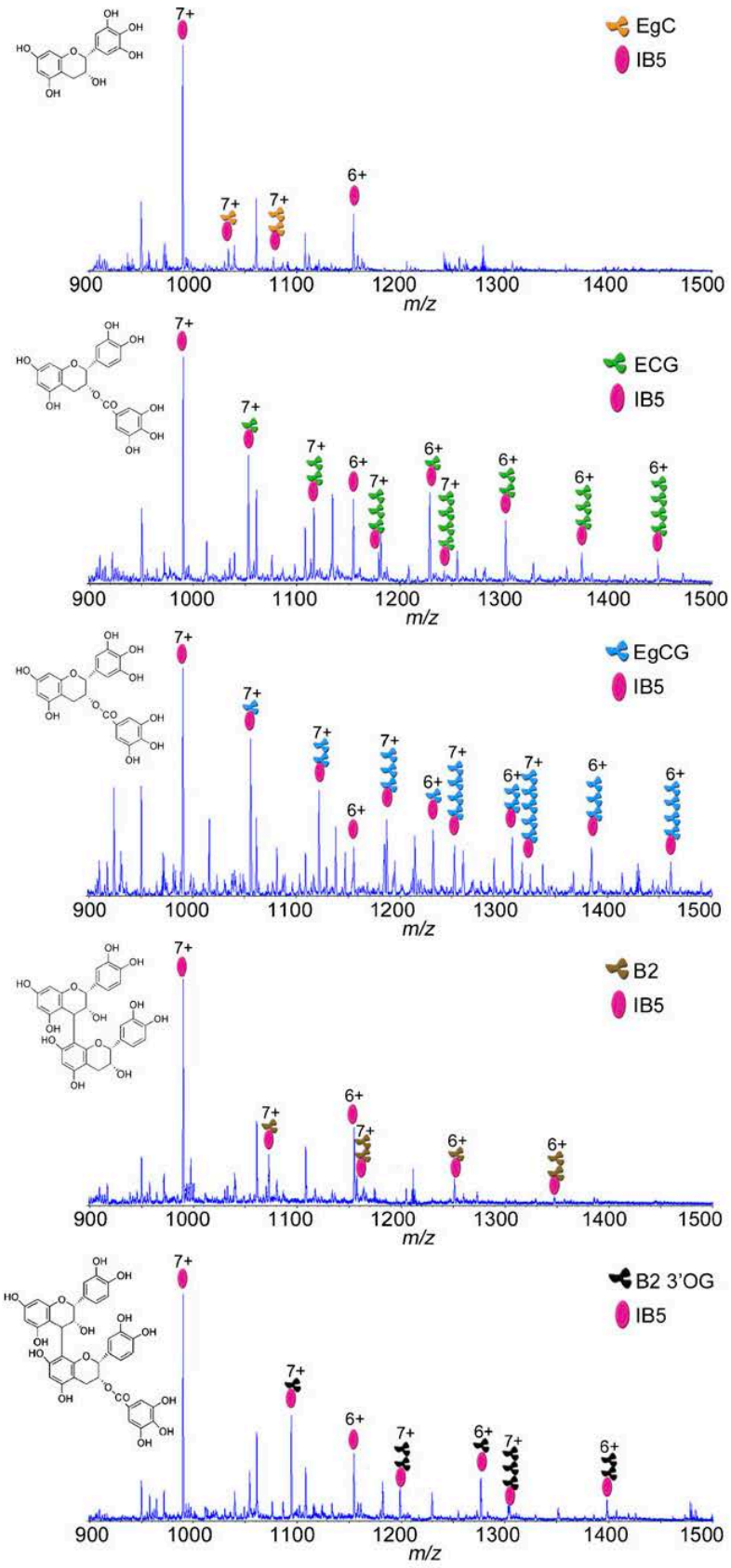

Fig. 2 Positive ion mass spectra of IB5:T (1:10) interaction mixtures. Peaks of IB5a and its complexes are labeled

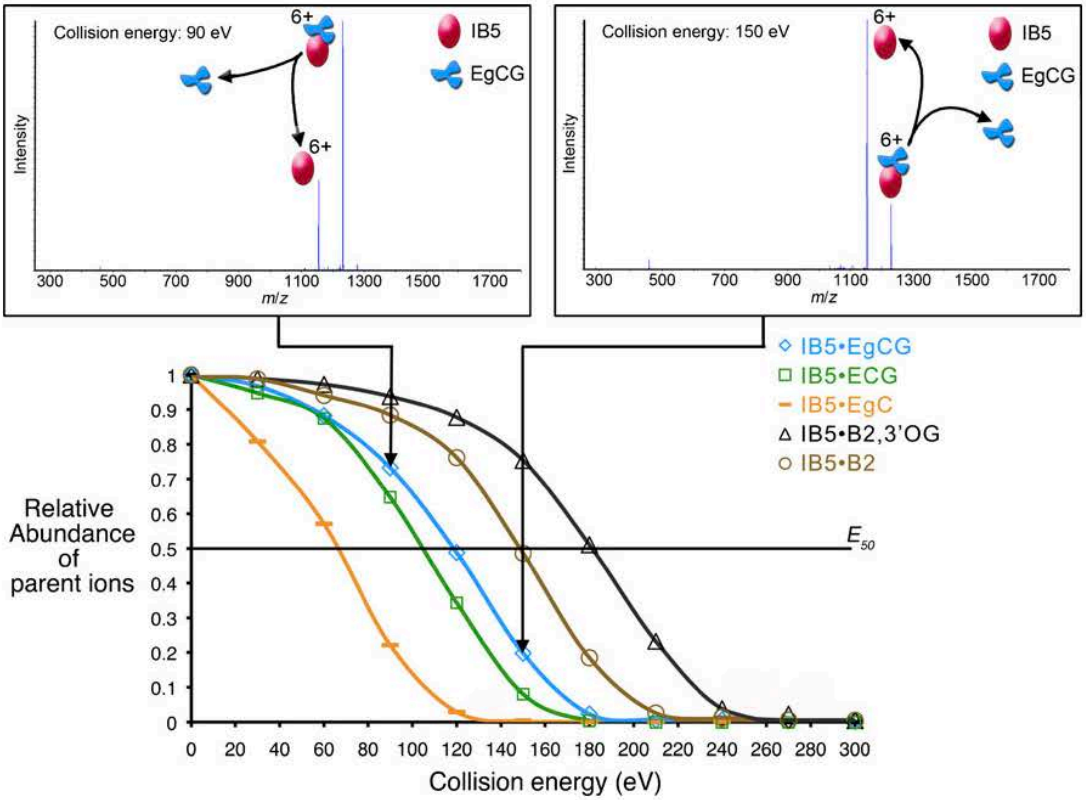

Fig. 3 Dissociation curves of $[IB5{\cdot}1T]^{+6}$ and MS/MS spectra of $[IB5{\cdot}1EgCG]^{+6}$ at collision energies of respectively 90 and 150 eV

collision cell (l) and the collision cross-section (σ) of the selected ion:

$$N_{col} = n \times \sigma \times l \quad (2)$$

Finally, the internal energy E_{Int} can be calculated from equation

$$E_{Int} = E_{CoM} \times N_{col} \quad (3)$$

Equation 2 shows that ions with similar cross-section experience the same number of collisions, on average. Thus from Eq. 3, direct comparison of E_{Int} can be realized via comparison of E_{CoM} for complexes with a similar collision cross-section. Given the slight modification of the molecular mass between $[IB5{\cdot}1T]^{+6}$ complexes and their similar charge state [31, 51], we expect complex ions to present similar collision cross sections. Consequently, the center-of-mass energy of the complex (E_{CoM}) is likely to fit the scaling of the internal energy transferred to the complex upon dissociation.

The dissociation curves show similar sigmoid shape for each $[IB5{\cdot}1T]^{+6}$, indicating that the interaction of IB5 with each tannin involves a similar mechanism independently of the tannin structure. During a first phase, dissociation curves depict an upper plateau where dissociation is minimal. Ions accumulate internal energy. Then, the curves bend downward into a log-linear dissociation region. Finally, the curves bend into a plateau toward the total complex dissociation. E_{50} in the laboratory frame is the

Table 1 E_{50} and E_{CoM} of the $[IB5{\cdot}1T]^{+6}$ complexes

	IB5•EgC	IB5•ECG	IB5•EgCG	IB5•B2	IB5•B2, 3′-OG
E_{50} (eV)	67.5	105	120	150	165
E_{CoM} (eV)	0.26	0.40	0.45	0.55	0.65

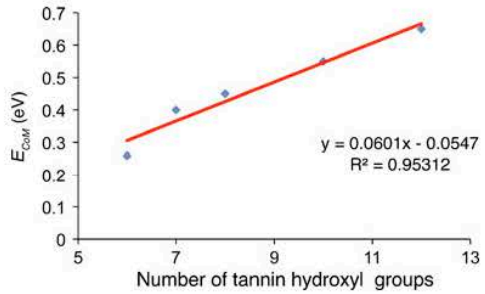

Fig. 4 Relation between the E_{CoM} of IB5•tannin complexes and the number of tannin hydroxyl groups

collision energy required to disrupt 50% of the parent complex ions. E_{50} are determined graphically from the dissociation curves (Fig. 3, Table 1). We used them to calculate the corresponding E_{CoM} (Table 1) reflecting complex stability [31, 51]. The higher the E_{CoM}, the stronger the interaction. Thus, classification of the complexes as a function of their stability can be drawn as:

$$[IB5 \bullet 1EgC]^{+6} < [IB5 \bullet 1ECG]^{+6} < [IB5 \bullet 1EgCG]^{+6} < [IB5 \bullet 1B2]^{+6} < [IB5 \bullet 1B2, 3'OG]^{+6}$$

It is worth noting that IB5•dimer complexes are more stable than those formed with monomers. Moreover, IB5•GT are more stable than IB5•UGT for a same degree of polymerization. The extra OH group on the B ring leads to a higher E_{CoM} (EgCG vs ECG). Through analysis of this set of tannins, we have shown the impact of chemical features on the stability of the complexes, and on the ability of IB5 to adapt to ligands, as previously observed for other IUPs [52]. Hence, we are able to classify these chemical characteristics as a function of their impact on the interaction strength with IB5:

B ring hydroxylation degree < galloylation < DP

Figure 4 shows that a linear relationship exists between the number of tannin hydroxyl groups and the E_{CoM} of IB5•tannin complexes. The more hydroxyl groups on tannins, the more stable the interaction with IB5. This indicates that interactions between IB5 and tannins mainly involve hydrogen bonds in the gas phase as stated earlier [31]. Electrostatic and hydrogen bonding interactions are enhanced in the gas phase whereas hydrophobic interactions are partly or completely lost [53, 54]. Therefore, the involvement of hydrophobic effect may not be excluded as it may occur in solution. Our results are in agreement with those of Simon [55], who has shown the importance of hydrogen bonding in the interaction between a proline-rich peptide (PRp: 14 a.a.) and tannins, with different techniques such as NMR, MS, CD, and molecular modeling.

Higher protein affinity has been reported for prodelphinidins (tannins with EgC units) compared to procyanidins (tannins mainly composed with EC and C units) [56]. In agreement with this finding, epigallocatechin gallate exhibited a stonger interaction than epicatechin gallate with immobilized salivary proteins [57]. The same trend was found when studying their complexation with the human salivary PRP IB5 by mass spectrometry but the reverse was found when calculating their binding constants with poly L-proline [58]. This difference can be explained by different affinities for tannins as observed between PRPs from various species [21] and by the random coil nature of *b*PRPs [48], which probably gives them enough malleability to be adaptable for different ligands in contrast with the polyproline helix conformation of poly L-proline.

Moreover, the astringency sensory analysis of different tannins has shown that DP and galloylation are major factors driving astringency perception [27]. This is parallel with our finding here, for which such factors are involved in the interaction strength with salivary proteins.

Conclusion

It is often asked why wine astringency sensation and intensity are dependent upon the wine itself and the wine taster. On one hand, wine molecules involved in astringency are tannins that gather a very large family of compounds with numerous and peculiar chemical structures. On the other hand, taster saliva holds a high level of proteins and particularly the so-called *b*PRPs whose only reported function is to bind tannins. Astringency is supposed to be related to their interactions and the stability of the arising complexes may have an impact on this perception. The stability of the complexes formed between tannins and *b*PRPs comes from the strength of the interaction forces. At this point, it makes compulsory to watch for them with regards to tannin chemical features. In this work, we used MS technologies benefiting from MS instrumentation developments to detect and characterize soluble noncovalent complexes involving a model *b*PRP, IB5, and tannins. The results show the effect of the tannin structure and highlight the involvement of hydrogen bounding on PRP–tannin interactions. The conformational rearrangement of PRP may favor the establishment of more hydrogen bonds. These results demonstrate the ability of PRP to universally bind tannins that have a variety of shapes and sizes and are in agreement with the tannin-scavenging function of IB5. Moreover, sensory analyses and MS studies have revealed that DP and galloylation are major factors driving tannin astringency perception [27] and PRP–tannin interaction respectively. This parallel is of particular interest because PRP–tannin interactions are thought to contribute to astringency mechanisms.

Acknowledgments The authors thank Dr. Véronique Cheynier for helpful scientific discussions, Thérèse Marlin for protein purification, Jean-Paul Mazauric for tannin purification and Emmanuelle Meudec for mass spectrometry assistance. Francis Canon was supported by a grant of French Ministry of Research. This work is supported by grant 07-BLAN-0279 from the French Agence Nationale de la Recherche (A.N.R.). We acknowledge synchrotron SOLEIL and thank all staff for assistance in using beamline DISCO. AG thanks ABSciex (Les Ullis, France) for the loan of the IonCooler Guide.

References

1. Dyson HJ, Wright PE (2005) Nat Rev Mol Cell Biol 6:197–208
2. Dunker AK, Silman I, Uversky VN, Sussman JL (2008) Curr Opin Struct Biol 18:756–764

3. Tompa P (2003) J Mol Struc (Theochem):361-371
4. Wright PE, Dyson HJ (1999) J Mol Biol 293:321–331
5. Bernstein SL, Dupuis NF, Lazo ND, Wyttenbach T, Condron MM, Bitan G, Teplow DB, Shea J-E, Ruotolo BT, Robinson CV, Bowers MT (2009) Nat Chem 1:326–331
6. Murray MM, Bernstein SL, Nyugen V, Condron MM, Teplow DB, Bowers MT (2009) J Am Chem Soc 131:6316–6317
7. Loo JA, Ogorzalek-Loo RR (1997) In: Cole RB (ed) Electrospray ionization mass spectrometry of peptides and proteins. Wiley, New York
8. Pramanik BN, Bartner PL, Mirza UA, Liu YH, Ganguly AK (1998) J Mass Spectrom 33:911–920
9. Jorgensen TJD, Roepstorff P, Heck AJR (1998) Anal Chem 70:4427–4432
10. Kapur A, Beck JL, Brown SE, Dixon NE, Sheil MM (2002) Protein Sci 11:147–157
11. Bligh SWA, Haley T, Lowe PN (2003) J Mol Recognit 16:139–148
12. Sobott F, McCammon MG, Robinson CV (2003) Int J Mass Spectrom Ion Processes 230:193–200
13. Jorgensen TJD, Hvelplund P, Andersen JU, Roepstorff P (2002) Int J Mass Spectrom Ion Processes 219:659–670
14. Mehansho H, Butler LG, Carlson DM (1987) Annu Rev Nutr 7:423–440
15. Bennick A (2002) Crit Rev Oral Biol Med 13:184–196
16. Carlson DM (1993) Crit Rev Oral Biol Med 4:495–502
17. Sarni-Manchado P, Canals-Bosch J, Mazerolles G, Cheynier V (2008) J Agric Food Chem 56:9563–9569
18. Sarni-Manchado P, Cheynier V, Moutounet M (1999) J Agric Food Chem 47:42–47
19. Mehansho H, Carlson DM (1983) J Biol Chem 258:6616–6620
20. Mehansho H, Clements S, Sheares BT, Smith S, Carlson DM (1985) J Biol Chem 260:4418–4423
21. Mole S, Butler LG, Iason G (1990) Biochem Syst Ecol 18:287–293
22. Asquith TN, Uhlig J, Mehansho H, Putnam L, Carlson DM, Butler L (1987) J Agric Food Chem 35:331–334
23. Austin PJ, Suchar LA, Robbins CT, Hagerman AE (1989) J Chem Ecol 15:1335–1347
24. McArthur C, Sanson GD, Beal AM (1995) J Chem Ecol 21:663–691
25. Dixon R, Xie D, Sharma S (2005) New Phytol 165:9–28
26. Zucker WV (1983) Am Nat 121:335–365
27. Vidal S, Francis L, Guyot S, Marnet N, Kwiatkowski M, Gawel R, Cheynier V, Waters EJ (2003) J Sci Food Agric 83:564–573
28. Poncet-Legrand C, Edelmann A, Putaux J-L, Cartalade D, Sarni-Manchado P, Vernhet A (2006) Food Hydrocoll 20:687–697
29. Sarni-Manchado P, Cheynier V (2002) J Mass Spectrom 37:609–616
30. Charlton AJ, Baxter NJ, Lilley TH, Haslam E, McDonald CJ, Williamson MP (1996) FEBS Lett 382:289–292
31. Canon F, Paté F, Meudec E, Marlin T, Cheynier V, Giuliani A, Sarni-Manchado P (2009) Anal and Bioanal Chem 395:2535–2545
32. Jobstl E, O'Connell J, Fairclough JPA, Williamson MP (2004) Biomacromolecules 5:942–949
33. Ricardo da Silva JM, Rigaud J, Cheynier V, Cheminat A, Moutounet M (1991) Phytochemistry 30:1259–1264
34. Pascal C, Bigey F, Ratomahenina R, Boze H, Moulin G, Sarni-Manchado P (2006) Protein Expr Purif 47:524–532
35. Yin S, Xie Y, Loo JA (2008) J Am Soc Mass Spectrom 19:1199–1208
36. Haller I, Mirza UA, Chait BT (1996) J Am Soc Mass Spectrom 7:677–681
37. Robinson CV (2001) J Am Soc Mass Spectrom 12:126–126
38. Zhang J, Kashket S (1998) Caries Res 32:233–238
39. Jørgensen TJD, Delforge D, Remacle J, Bojesen G, Roepstorff P (1999) Int J Mass Spectrom Ion Processes 188:63–85
40. Wan KX, Gross ML, Shibue T (2000) J Am Soc Mass Spectrom 11:450–457
41. Akashi S, Osawa R, Nishimura Y (2005) J Am Soc Mass Spectrom 16:116–125
42. Flanzy C (1998) Oenologie—Fondements scientifiques et technologiques. Lavoisier, Paris
43. Champagnol F (1986) Rev Fr Oenol 26:26–57
44. Shimada T (2006) J Chem Ecol 32:1149–1163
45. Fuxreiter M, Simon I, Friedrich P, Tompa P (2004) J Mol Biol 338:1015–1026
46. Oldfield C, Meng J, Yang J, Yang MQ, Uversky V, Dunker AK (2008) BMC Genomics 9:S1
47. Mehansho H, Hagerman A, Clements S, Butler LG, Rogler JC, Carlson DM (1983) Proc Natl Acad Sci USA 80:3948–3952
48. Boze H, Marlin T, Durand D, Pérez J, Vernhet A, Canon F, Sarni-Manchado P, Cheynier V, Cabane B (2010) Biophys J 99:656–665
49. Tompa P (2003) BioEssays 25:847–855
50. Khalsa-Moyers G, McDonald WH (2006) Brief Funct Genomic Proteomic 5:98–111
51. Chen Y-LC JM, Collings BA, Konermann L, Douglas DJ (1998) Rapid Commun Mass Spectrom 12:1003–1010
52. Wright PE, Dyson HJ (2009) Curr Opin Struct Biol 19:31–38
53. Robinson CV, Chung EW, Kragelund BB, Knudsen J, Aplin RT, Poulsen FM, Dobson CM (1996) J Am Chem Soc 118:8646–8653
54. Sobott FM, McCammon MG, Hernández H, Robinson CV (2005) Phil Trans R Soc A 363:379–391
55. Simon C, Barathieu K, Laguerre M, Schmitter JM, Fouquet E, Pianet I, Dufourc EJ (2003) Biochemistry 42:10385–10395
56. Hagerman AE (1989) In: Hemingway RW, Karchesy JJ (eds) Chemistry of tannin–protein complexation. Plenum, New York
57. Bacon JR, Rhodes MJC (1998) J Agric Food Chem 46:5083–5088
58. Poncet-Legrand C, Gautier C, Cheynier V, Imberty A (2007) J Agric Food Chem 55:9235–9240

Publication n°7: Folding of a Salivary Intrinsically Disordered Protein upon Binding to Tannins.

Canon, F.; Ballivian, R.; Chirot, F.; Antoine, R.; Sarni-Manchado, P.; Lemoine, J. r. m.; Dugourd, P.

J. Am. Chem. Soc. ***2011,*** *133 (20), 7847-7852.*

JACS
JOURNAL OF THE AMERICAN CHEMICAL SOCIETY

ARTICLE

pubs.acs.org/JACS

Folding of a Salivary Intrinsically Disordered Protein upon Binding to Tannins

Francis Canon,[†] Renaud Ballivian,[†,‡] Fabien Chirot,[‡] Rodolphe Antoine,[§] Pascale Sarni-Manchado,[†] Jérôme Lemoine,[‡] and Philippe Dugourd*[,§]

[†]INRA, UMR1083 Science Pour l'Oenologie, Polyphenol Interaction, Bât 28, 2 place Viala F-34060 Montpellier, France

[‡]Université de Lyon, F-69622, Lyon, France

[§]Université Lyon 1, F-69622, Villeurbanne; CNRS, F-69622, Lyon, France

Supporting Information

ABSTRACT: We used ion mobility spectrometry to explore conformational adaptability of intrinsically disordered proteins bound to their targets in complex mixtures. We investigated the interactions between a human salivary proline-rich protein IB5 and a model of wine and tea tannin: epigallocatechin gallate (EgCG). Collisional cross sections of naked IB5 and IB5 complexed with $N = 1-15$ tannins were recorded. The data demonstrate that IB5 undergoes an unfolded to folded structural transition upon binding with EgCG.

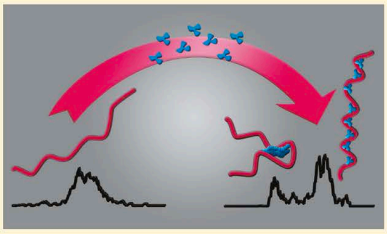

INTRODUCTION

The basic concept regarding the activity of proteins was dominated by the view that proteins need to have a well-defined three-dimensional structure for their function. However, during the past decade this view has changed,[1,2] and the sequence-to-structure-to-function paradigm had to be reassessed. Numerous proteins do have a well-defined function that requires intrinsic disorder, and the term of intrinsically disordered protein (IDP) has been proposed to describe this group.[1,3−5] IDPs appear to be rather common in living organisms especially in higher eukaryotes: primary sequence analyses indicate that about 10−20% of full-length proteins belong to this class and that 25−40% of all residues fall into such regions. The intrinsic lack of structure can confer functional advantages like the ability to bind several and/or different ligands. Moreover, many IDPs undergo coupled binding and folding processes that are intrinsically related to their dedicated function.[1−3] Now, the ability of IDPs to bind several ligands and in some cases to aggregate in large supramolecular edifices leads to mixtures of complexes with different stoichiometries and heterogeneous conformations. While several strategies are emerging for the characterization of flexible proteins, the study of mixed IDP−target complexes and of their assembly processes is highly challenging and requires new approaches. Besides heteronuclear multidimensional NMR[4,6] and small angle diffraction techniques[7,8] that are now used for IDPs, spectroscopy was used to get structural information on binding of tannins to proteins and spin relaxation measurements to get insight into molecular dynamics of the complexes.[9,10] Mass spectrometry combined to ion mobility (IMS) has the great advantage to allow determination of complex distributions and the qualitative structure of each of the species.[11−13] While much of the early IMS work on protein unfolding was performed using denaturing conditions,[14] measurements following electrospray ionization from "native" conditions support the use of ion mobility-mass spectrometry as a tool for structural biology.[15,16] For example, this method was recently applied with success to study the aggregation of a number of the amyloid-beta protein isoforms of A beta 40 and A beta 42,[17,18] prion,[19] and of α-synuclein proteins,[20] which are IDPs involved in several neurodegenerative diseases. Here, we explore the potentiality of IMS to study the structure of IDPs bound to their targets.

We investigated the interactions between the human salivary proline rich protein IB5 and a model of wine and tea tannin: epigallocatechin gallate (EgCG) (IB5 sequence and chemical structure of EgCG are given in the Supporting Information).[21,8] Tannins are phenolic compounds ubiquitous in plant and plant-based food.[22] The major part of plant/fruit tannins occurs through condensed forms. These condensed tannins continuously rearrange, polymerize, and break. They undergo different intra- and intermolecular reactions, among which oxidation reactions are the most important[23] and, through nucleation and growth processes, they can form colloidal particles.[24] They bind efficiently to salivary proline-rich proteins (PRPs) and thereby form soluble and nonsoluble tannin protein complexes.[25−27] These properties are considered to be responsible for astringency.[28,29] From a biological point of view, tannins act as protecting molecules toward herbivore species. This role has been attributed to their ability to interact with proteins, to precipitate them, and to inhibit gastrointestinal enzymes thereby reducing the digestibility of plant proteins.[30]

Received: January 19, 2011
Published: April 27, 2011

IB5 is a human protein which only known function is to bind and to scavenge tannins. Structurally speaking, IB5 belongs to the extendedly disordered family characterized by low sequence complexity and peculiar hydrodynamic dimensions.[4,31] Indeed, IB5 has a hydrodynamic dimension typical of considerably extended polypeptide chain and does not possess any ordered secondary structures.[32] The involvement of PRPs in the adaptation to a tannin diet as an astringency mediator and as a scavenger is related to their ability to establish noncovalent interactions with tannins. High tannin concentrations lead to insoluble IB5−tannin complexes, whereas lower ones give rise to soluble tannin−IB5 complexes with several stoichiometries.[27,33] These data suggest different recruitment schemes of binding partners related to conformational variability and adaptability. In the present work, ion mobility experiments show an unfolded to folded transition of IB5 protein induced by tannin binding.

MATERIALS AND METHODS

Epigallocatechin gallate (EgCG) was purchased from Sigma (Sigma Chemical Co., Poole, Dorset, U.K.). The IB5 human salivary proline rich protein was produced by the use of the yeast *Pischia pastoris* as a host organism and purified as previously described.[33] EgCG and protein stock solutions were prepared in the following medium: water/ethanol, 88:12 (v/v) acidified to pH 3.2 with acetic acid, which corresponds to the mouth conditions in the presence of red wine. IMS spectra were obtained with a home-built ESI ion mobility mass spectrometer.[34] Electrosprayed ions enter the instrument through a heated capillary interface held at 473 K and are accumulated in a small cylindrical ion trap.[35] Ion packets are periodically injected into a one meter long drift cell containing ≈10 Torr of He and travel through the influence of a uniform electric field (E = 770 V m^{-1}). At the exit of the cell, species are separated in drift-time according to their diffusion cross section. Compact ions display shorter drift-times than ions with extended structures. Then, the ions go through a quadrupole and a collision cell and are accelerated into a perpendicular reflectron time-of-flight mass spectrometer. 2-D maps (drift time, m/z) are recorded.

The ion mobility K is given by (eq 1):

$$t_d = \frac{L}{KE} \quad (1)$$

where L is the length of the drift cell, E is the electric field value in the cell, and t_d is the drift time across the cell. The ion mobility resolution of our instrument is ∼50. The experimental uncertainties on the determined K values are estimated to be 1%.

The mobility is related to the averaged collision cross section Ω_{avg} of the ion and buffer gas atom via eq 2:[36]

$$K = \frac{3}{16}\frac{ze}{N}\left(\frac{1}{m}+\frac{1}{M}\right)^{1/2}\left(\frac{2\pi}{kT}\right)^{1/2}\frac{1}{\Omega_{avg}} \quad (2)$$

where T is the temperature, ze the charge on the ion, N the buffer gas number density, and m and M, the masses of the neutral atom and ion, respectively .

Circular dichroism (CD) spectra were recorded on a Chirascan circular dichroism spectrometer (Applied Photophysics Ltd., Leatherhead, U.K.) using a 0.5 mm path length cell and analyzed with the CDtool software (Birkbeck College, London, U.K.).[37] The spectra of pure EgCG solutions at the desired concentration were subtracted from those of IB5:N EgCG to obtain the CD spectrum of the complexed protein.

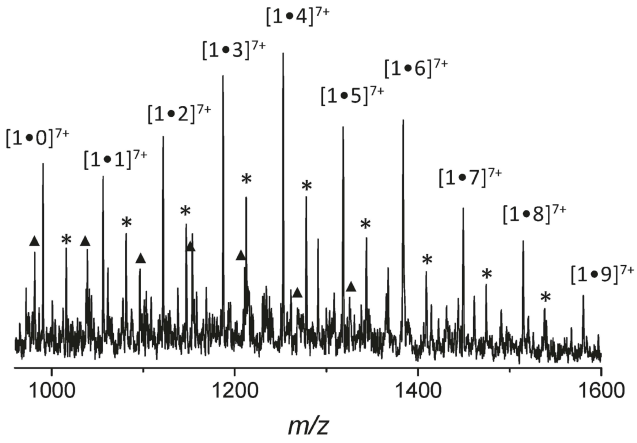

Figure 1. Positive ion mass spectrum of 1:20 IB5/EgCG (molar ratio) interaction mixture. Peaks for $[IB5a \cdot N\ EgCG]^{7+}$ are labeled. ▲ correspond to $[IB5a \cdot N\ EgCG]^{8+}$ complexes starting at N = 2. ∗ correspond to $[IB5b \cdot N\ EgCG]^{7+}$ complexes starting at N = 1.

RESULTS AND DISCUSSION

MS and IMS Data. The mass spectrum obtained by electrospraying the protein solution displayed a series of protonated peaks corresponding to three IB5 isoforms (a, 6923.70 Da; b, 6642.63 Da; and c, 6360.39 Da) with charge states ranging from 5+ to 10+ (see the Supporting Information, Figure S1). For interaction studies, IB5 and EgCG solutions were combined at a molar ratio of 1:20 (IB5/EgCG). Though crowded, the mass spectrum reveals free IB5 and IB5 supramolecular complexes with stoichiometries ranging from 1 up to 9 tannins (Figure 1). The abundance of the stoichiometries seems to follow a Poisson-like distribution. As a Poisson process is a stochastic process in which events occur continuously and independently of one another, this observation is in favor of a noncooperative sticking process.[38] The fragmentation spectrum (MS/MS) obtained after isolation and collision excitation of the supramolecular complex of IB5 with 9 tannins (charge state 7+) is shown in Figure S2 in the Supporting Information. The different fragment ions correspond to the free protein and complexes containing 1−8 tannins as well as the free tannin ion. It shows that the sequential loss of tannins is the preferred fragmentation pathway of the initial complex. The IMS contribution allows a study of the conformation of each complex and the resolution of eventual conformers. Figure 2 displays collisional cross sections of selected stoichiometries recorded for charge state 7+. For the naked protein, one broad peak is observed, which corresponds to a collision cross section centered at 1350 Å^2. The peak is much broader than what would be obtained from the diffusion equation assuming a single mobility,[13,36,39] which has to be correlated to the unstructured character of this type of proteins. Note that this value is, for example, much larger than the one (1050 Å^2) measured for the $(M + 7H)^{7+}$ ion of BPTI, a globular structured protein with a close molecular weight (M_w 6512 Da) used here as a standard. Binding of 1−7 EgCG ligands does not modify the general shape of the cross section profile. As expected, an increase in the collision cross section is observed as the number of bound ligands grows. The peaks are still broad in agreement with the expected non-specificity of protein−tannin interactions. From 10 ligands, a second feature appears in the collision cross section profile beside the one following the initial trend from the naked

protein. The two populations correspond to structural families that do not interconvert during the travel through the drift cell (drift time of ~60 ms). The second one is shifted to lower collisional cross section values (~1200 Å^2). Thereby, this new population corresponds to more compact conformations. Though the mass of IB5 complexed with 13 EgCG is twice the mass of the naked protein (12 877 Da versus 6 923 Da), the collision cross section of this more compact oligomer is smaller than the one of the protein. Interestingly, the cross section of the compact state increases little as the number of bound tannins grows, in contrast with the expended structures. The ratio of folded to unfolded states grows with the stoichiometry indicating the requirement of several tannins to stabilize the folded state. IMS results for charge states 6+ to 9+ are plotted in Figure 3. A transition was also observed for charge state 6+ and its onset for charge state 8+. The comparison of the results recorded for the different charge states shows that low charge states favor folded structures. This indicates that the role of the tannin molecules here is at least partially related to the screening of Coulombic forces that, in the gas phase, favor an elongated ensemble of conformations. High-charge state IB5 ions requires a larger amount of ligand molecules to convert down to the smaller structure. Though the structures may be stretched by Coulombic repulsion, the gas phase data presented here demonstrate that IB5 undergoes a structural transition upon binding with EgCG.

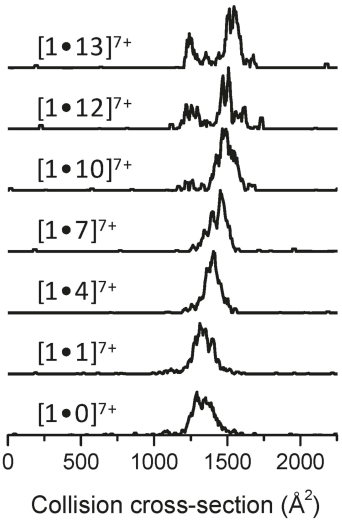

Figure 2. Collision cross section distributions for the 7+ charge state of IB5a and IB5a·*N* EgCG complexes (*N* = 0, 1, 4, 7, 10, 12, and 13).

Circular Dichroism. Circular dichroism (CD) experiments recorded on pure IB5 solution and on two 1:N IB5/EgCG (N = 10 and 40) mixtures further support the gas phase observation (Figure 4). The IB5 CD spectrum is characteristic of a wholly unfolded structure. An important modification of the CD curve shape of the protein occurs for N = 40 while for N = 10 the CD curve remains almost unchanged from the pure protein one. For 1:40 IB5/EgCG mixture, the band at 202 nm is red-shifted and the intensity of the band at 230 nm increases. These changes in the spectrum demonstrate a modification of the shape of the IB5 protein when involved in the complex in solution. The positive band that appears in the 220−240 nm region and may correspond to a higher extent of structure (disorder to order transition).[40] However, it cannot be directly related to the compaction of IB5 and thus cannot be used to quantify the effects seen in the IMS data set. This outlines the need for complementary methods and the potential role of IMS in structural biology, in particular, for protein complexes displaying polydispersity, heterogeneity, and eventually insolubility.

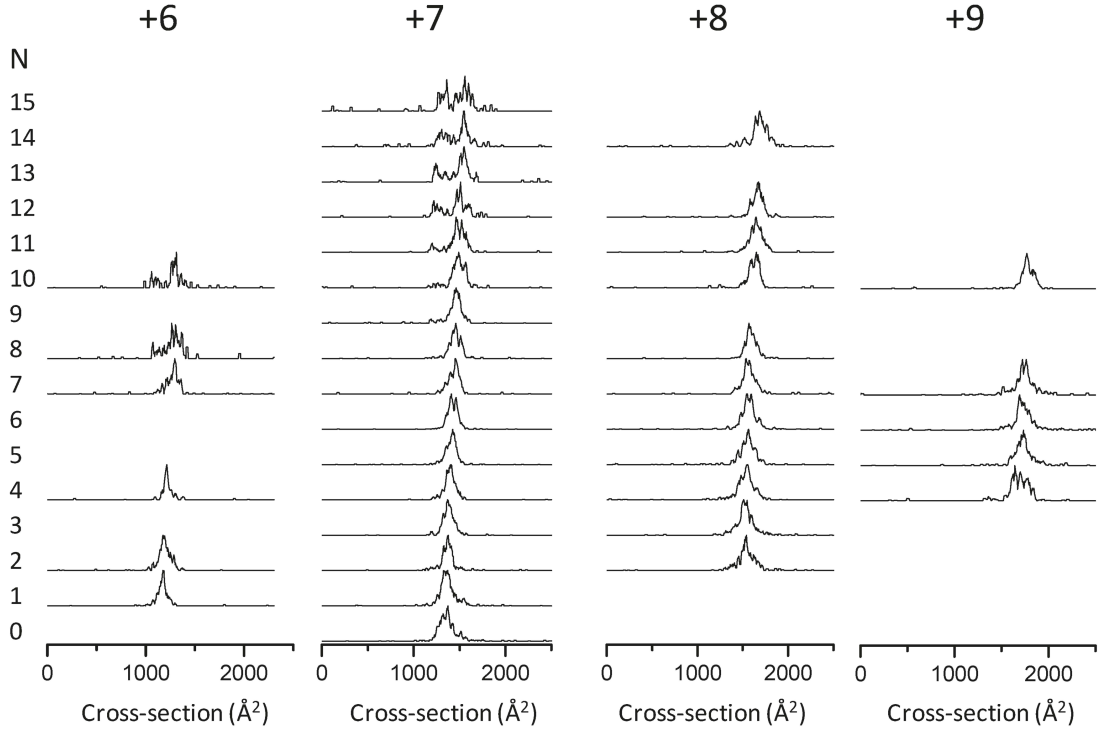

Figure 3. Collision cross section distributions of IB5a·*N* EgCG complexes recorded for charge states 6+, 7+, 8+, and 9+.

Modeling. IMS measurements are usually analyzed by calculating cross sections for unsolvated trial conformations obtained from molecular modeling. However, predicting the structure of noncovalent complexes with hundreds of atoms is clearly still out of reach. We chose to qualitatively interpret the experimental results using a coarse grained force field in which each amino acid and each tannin were replaced by single beads. The force field includes bonds, angles, van der Waals terms between amino acid beads, and a van der Waals term between tannins and amino acids (see Table S1 in the Supporting Information). Either a van der Waals term or a purely repulsive one was used between tannins in order to generate structures where tannins are, respectively, aggregated or separated. We want to outline that the only aim of this simple beads approach is to generate various model structures but that it cannot provide any energetic scale between them or binding information at the atomic level. For our purpose, the most significant parameters are the distance between two beads in the force field, as well as the size of each bead for the collisional cross section calculation. The distance between two amino acid beads was chosen to reflect the average distance between C_α atoms obtained from a sample of structures of IB5 optimized using Amber 99. We then generated structures by a Replica Exchange Monte Carlo simulation algorithm.[41] A total of 20 replicas were used and distributed according to an arithmetic progression in the temperature range 250—600 K. Representative samples of 400 configurations per replica were saved. Their cross sections were calculated using the exact hard sphere model[42] with a radius of 3.5 Å for an amino acid bead and of 7 Å for a tannin. These values were chosen to reproduce the calculated cross section values obtained with an all atom representation for different structures of IB5 and for the calculated cross section of an isolated tannin. Comparison between experimental and calculated cross section values allows the identification of structures that may account for experimental results.

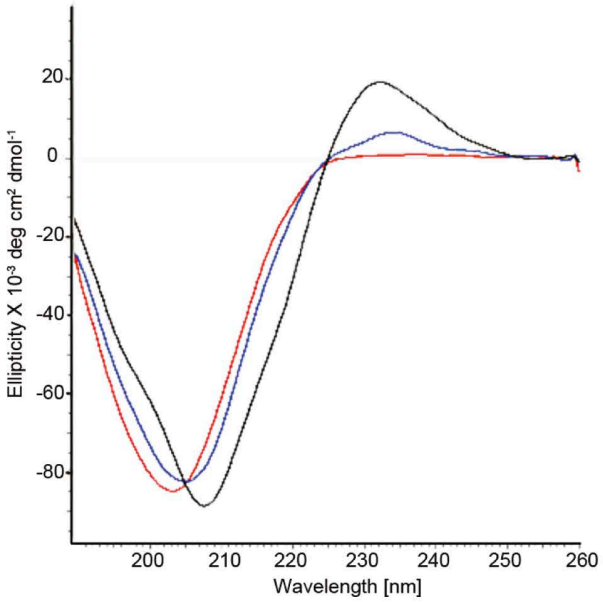

Figure 4. Circular dichroism spectra of IB5 solution (red) and the interaction mixtures 1:N IB5/EgCG (N = 10 (blue) and 40 (black) molar ratio).

Before discussing the simulation results, we want to outline that the model of an organized proline helix leads to much larger collision cross section than any of the two IMS peaks observed. Examples of calculated structures for the naked IB5 protein, 1·9 and 1·14 complexes that are in agreement with the experimental cross section values are shown in Figure 5. The measured cross-section for the bare IB5 corresponds to the open conformation expected for a proline-rich protein and is close to the one deduced from small-angle X-ray scattering (SAXS) measurements in solution.[32] The first family of peaks of 1·9 and 1·14 complexes can be reproduced by calculated structures where the tannins stick separately on the protein (Figure 5b,d). The principal forces driving in-solution association are governed by hydrogen bonding between the carbonyl function of proline residues and the tannin OH groups,[43−45] which leads in solution at low tannin concentration to a binding of a few number of individual tannins as proposed here. Theoretically, each additional tannin induces a significant increase in the collision cross section of the IB5 complex due to the extended geometry of EgCG (Table S2 in the Supporting Information). The comparison of IMS experimental results and simulations suggests that each added tannin induces a slight folding of IB5.

The latter model cannot account for the second peak with an apparent more compact conformation. While juxtaposed tannins show a large calculated collision cross section, IMS measurements on stacks of two and three tannins show that they have close collision cross sections (see the Supporting Information). This is confirmed by simulations performed on three-dimensional stacks of tannins (see Table S2 in the Supporting Information). Therefore, we propose that the second population peaks

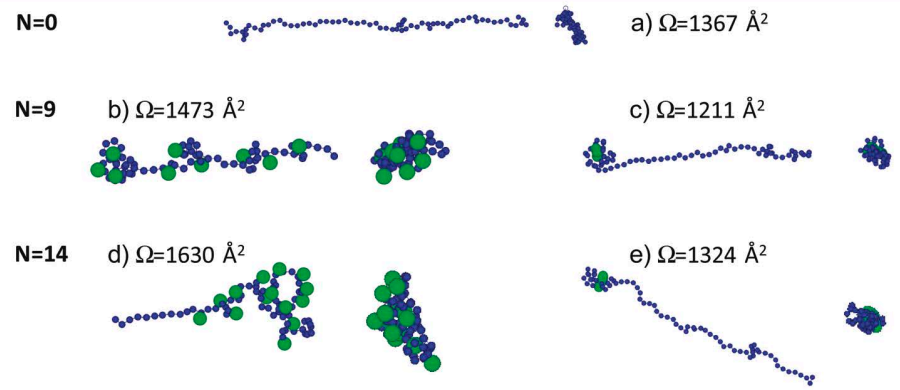

Figure 5. Examples of calculated structures for IB5a (a), IB5a·9 EgCG (b and c), and IB5a·14 EgCG complexes (d and e) which display experimental cross sections in agreement with experimental results (a top and a side view are displayed). In parts b and d, the tannins are dispersed while in parts c and e they are stacked. The blue circles correspond to amino acid beads, while the green ones correspond to tannin beads.

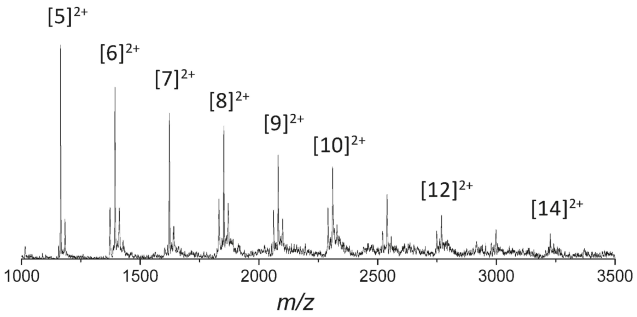

Figure 6. Positive ion mass spectrum of EgCG tannins. The most intense peak for each size corresponds to $[N\ EgCG + 2Na]^{2+}$ species.

characterized by a low cross section correspond to IB5 folded around compact aggregates of tannins. The folding is favored by multiple hydrogen bonds between IB5 and the different hydroxyl groups available on a stack of tannins.[45] This hypothesis is reinforced by the observation of aggregates of tannins when electrospraying a solution of tannins without IB5 (Figure 6), which demonstrates the availability of soluble aggregates of tannins in the experimental solution. These structures may be the first step toward the formation of large colloids of tannins and proteins. Indeed, a common view on tannin−protein complexation and precipitation is that, first, tannins aggregate on proteins. In secondary interactions, protein−tannin complexes self-associate via further hydrogen bonding between tannins acting as linker between several proteins. This triggers the formation of insoluble complexes that precipitate.[25,26,44] This mechanism was particularly well characterized in solution for polyphenol and β-casein interactions,[28] which highlighted the compaction of the protein upon binding to tannins, then aggregation leading to precipitation. Our results show that a similar mechanism involving first a compaction is also probable for salivary proteins. The family of structures with dispersed tannins (less compact) might correlate to the bimodal distributions observed in solution,[25] although they may be here enhanced by coloumbically driven unfolding. Finally, we outline that the broadness of the peaks in the collision cross section shows that each peak does not correspond to a single structure but to a family of structures. These may correspond to different binding sites of tannins on the protein leading to a wide range of conformers. A partial mixing of two complexation pathways (addition of single tannins and addition of an aggregate of tannins) cannot be excluded and may allow a fast binding of numerous tannins, which is in agreement with the biological roles of salivary proteins.

CONCLUSIONS

In summary, IMS was used to get a snapshot of the conformational distribution within a complex mixture of one model of salivary IDP protein bound to its natural target and of its conformational adaptability. The first important result is that a single protein can bind up to 15 tannins. IMS measurements show a transition from extended to more compact structures as the number of tannins bound to the protein increases. We propose that this transition is due to a competition between the binding of individual tannins and the binding of aggregated tannins. Both pathways of complexation coexist at high tannin concentration, which illustrates the capability of IDPs to efficiently bind targets in different manners. In the near future, IMS could be part of integrated approaches, which have to be developed to evolve from a static picture of functional IDPs to a dynamic one, in which several conformations are consistent with various aspects of function.

ASSOCIATED CONTENT

Supporting Information. Chemical structure of EgCG and sequence of IB5; MS/MS spectrum of the IB5a·9 EgCG complex; and cross sections for assemblies of tannins. This material is available free of charge via the Internet at http://pubs.acs.org.

AUTHOR INFORMATION

Corresponding Author
dugourd@lasim.univ-lyon1.fr

ACKNOWLEDGMENT

The authors thank Dr. Véronique Cheynier and Dr. Franck Paté for helpful scientific discussions and Thérèse Marlin for protein purification. Francis Canon was supported by a grant of French Ministry of Research. This work is supported by Grants 07-BLAN-0279 and 05-BLAN-0086 from the French Agence Nationale de la Recherche (A.N.R.).

REFERENCES

(1) Wright, P. E.; Dyson, H. J. *J. Mol. Biol.* **1999**, *293*, 321–331.
(2) Dunker, A. K.; Silman, I.; Uversky, V. N.; Sussman, J. L. *Curr. Opin. Struct. Biol.* **2008**, *18*, 756–764.
(3) Dyson, H. J.; Wright, P. E. *Nat. Rev. Mol. Cell Biol.* **2005**, *6*, 197–208.
(4) Tompa, P. *Trends Biochem. Sci.* **2002**, *27*, 527–533.
(5) Cortese, M. S.; Uversky, V. N.; Dunker, A. K. *Prog. Biophys. Mol. Biol.* **2008**, *98*, 85–106.
(6) Dyson, H. J.; Wright, P. E. . In *Nuclear Magnetic Resonance of Biological Macromolecules, Part B*; Methods in Enzymology, Vol. 339; Academic Press: San Diego, CA, 2001; pp 258−270.
(7) Bernado, P.; Mylonas, E.; Petoukhov, M. V.; Blackledge, M.; Svergun, D. I. *J. Am. Chem. Soc.* **2007**, *129*, 5656–5664.
(8) Svergun, D. I. *Biol. Chem.* **2010**, *391*, 737–743.
(9) Charlton, A. J.; Haslam, E.; Williamson, M. P. *J. Am. Chem. Soc.* **2002**, *124*, 9899–9905.
(10) Edelmann, A.; Lendl, B. *J. Am. Chem. Soc.* **2002**, *124*, 14741–14747.
(11) Bowers, M. T.; Kemper, P. R.; von Helden, G.; van Koppen, P. A. M. *Science* **1993**, *260*, 1446–1451.
(12) Clemmer, D. E.; Jarrold, M. F. *J. Mass Spectrom.* **1997**, *32*, 577–592.
(13) Dugourd, P.; Hudgins, R. R.; Clemmer, D. E.; Jarrold, M. F. *Rev. Sci. Instrum.* **1997**, *68*, 1122–1129.
(14) Clemmer, D. E.; Hudgins, R. R.; Jarrold, M. F. *J. Am. Chem. Soc.* **1995**, *117*, 10141–10142.
(15) Faull, P. A.; Florance, H. V.; Schmidt, C. Q.; Tomczyk, N.; Barlow, P. N.; Hupp, T. R.; Nikolova, P. V.; Barran, P. E. *Int. J. Mass Spectrom.* **2010**, *298*, 99–110.
(16) Politis, A.; Park, A. Y.; Hyung, S. J.; Barsky, D.; Ruotolo, B. T.; Robinson, C. V. *PLoS ONE* **2010**, *5*, 11.
(17) Murray, M. M.; Bernstein, S. L.; Nyugen, V.; Condron, M. M.; Teplow, D. B.; Bowers, M. T. *J. Am. Chem. Soc.* **2009**, *131*, 6316.
(18) Bernstein, S. L.; Dupuis, N. F.; Lazo, N. D.; Wyttenbach, T.; Condron, M. M.; Bitan, G.; Teplow, D. B.; Shea, J. E.; Ruotolo, B. T.; Robinson, C. V.; Bowers, M. T. *Nat. Chem.* **2009**, *1*, 326–331.
(19) Grabenauer, M.; Wyttenbach, T.; Sanghera, N.; Slade, S. E.; Pinheiro, T. J. T.; Scrivens, J. H.; Bowers, M. T. *J. Am. Chem. Soc.* **2010**, *132*, 8816–8818.

(20) Bernstein, S. L.; Liu, D.; Wyttenbach, T.; Bowers, M. T.; Lee, J. C.; Gray, H. B.; Winkler, J. R. *J. Am. Soc. Mass Spectrom.* **2004**, *15*, 1435–1443.
(21) Pascal, C.; Poncet-Legrand, C.; Imberty, A.; Gautier, C.; Sarni-Manchado, P.; Cheynier, V.; Vernhet, A. *J. Agric. Food Chem.* **2007**, *55*, 4895–4901.
(22) Quideau, S.; Deffieux, D.; Douat-Casassus, C.; Pouységu, L. *Angew. Chem., Int. Ed.* **2011**, *50*, 586–621.
(23) Poncet-Legrand, C.; Cabane, B.; Bautista-Ortín, A. B.; Carrillo, S.; Fulcrand, H.; Perez, J.; Vernhet, A. *Biomacromolecules* **2010**, *11*, 2376–2386.
(24) Zanchi, D. e.; Vernhet, A.; Poncet-Legrand, C. l.; Cartalade, D.; Tribet, C.; Schweins, R.; Cabane, B. *Langmuir* **2007**, *23*, 9949–9959.
(25) Charlton, A.; Baxter, N. J.; Khan, M. L.; Moir, A. J. G.; Haslam, E.; Davis, A. P.; Williamson, M. P. *J. Agric. Food Chem.* **2002**, *50*, 1593–1601.
(26) Zanchi, D.; Poulain, C.; Konarev, P.; Tribet, C.; Svergun, D. I. *J. Phys.: Condens. Matter* **2008**, *20*, 4224.
(27) Sarni-Manchado, P.; Canals-Bosch, J.-M.; Mazerolles, G.; Cheynier, V. *J. Agric. Food Chem.* **2008**, *56*, 9563–9569.
(28) Jobstl, E.; O'Connell, J.; Fairclough, J. P. A.; Williamson, M. P. *Biomacromolecules* **2004**, *5*, 942–949.
(29) Vidal, S.; Francis, L.; Noble, A.; Kwiatkowski, M.; Cheynier, V.; Waters, E. *Anal. Chim. Acta* **2004**, *513*, 57–65.
(30) Zucker, W. V. *Am. Nat.* **1983**, *121*, 335–365.
(31) Dunker, A. K.; Oldfield, C. J.; Meng, J.; Romero, P.; Yang, J. Y.; Walton-Chen, J.; Vacic, V.; Obradovic, Z.; Uversky, V. N. *BMC Genomics* **2008**, *16*, 1–26.
(32) Boze, H.; Marlin, T.; Durand, D.; Pérez, J.; Vernhet, A.; Canon, F.; Sarni-Manchado, P.; Cheynier, V.; Cabane, B. *Biophys. J.* **2010**, *99*, 656–665.
(33) Canon, F.; Paté, F.; Meudec, E.; Marlin, T.; Cheynier, V.; Giuliani, A.; Sarni-Manchado, P. *Anal. Bioanal. Chem.* **2009**, *395*, 2535–2545.
(34) Albrieux, F.; Calvo, F.; Chirot, F.; Vorobyev, A.; Tsybin, Y. O.; Lepère, V.; Antoine, R.; Lemoine, J.; Dugourd, P. *J. Phys. Chem. A* **2010**, *114*, 6888–6896.
(35) Albrieux, F.; Antoine, R.; Chirot, F.; Lemoine, J.; Dugourd, P. *Eur. J. Mass Spectrom.* **2010**, *16*, 557–565.
(36) Revercomb, H. E.; Mason, E. A. *Anal. Chem.* **1975**, *47*, 970–983.
(37) Lees, J. G.; Smith, B. R.; Wien, F.; Miles, A. J.; Wallace, B. A. *Anal. Biochem.* **2004**, *332*, 285–289.
(38) Culard, F.; Laine, B.; Sautiere, P.; Maurizot, J. C. *FEBS Lett.* **1993**, *315*, 335–339.
(39) Wyttenbach, T.; von Helden, G.; Bowers, M. T. *Int. J. Mass Spectrom. Ion Processes* **1997**, *165/166*, 377–390.
(40) Receveur-Bréchot, V.; Bourhis, J. M.; Uversky, V. N.; Canard, B.; Longhi, S. *Proteins* **2006**, *62*, 24–45.
(41) Sugita, Y.; Okamoto, Y. *Chem. Phys. Lett.* **1999**, *314*, 141–151.
(42) Shvartsburg, A. A.; Jarrold, M. F. *Chem. Phys. Lett.* **1996**, *261*, 86–91.
(43) Simon, C.; Barathieu, K.; Laguerre, M.; Schmitter, J. M.; Fouquet, E.; Pianet, I.; Dufourc, E. J. *Biochemistry* **2003**, *42*, 10385–10395.
(44) Hagerman, A. E.; Rice, M. E.; Ritchard, N. T. *J. Agric. Food Chem.* **1998**, *46*, 2590–2595.
(45) Canon, F.; Giuliani, A.; Paté, F.; Sarni-Manchado, P. *Anal. Bioanal. Chem.* **2010**, *398*, 815–822.

Publication n°8: Photodissociation and dissociative photoionization mass spectrometry of proteins and noncovalent protein-ligand complexes.

Canon, F.; Milosavljević, A. R.; van der Rest, G.; Réfrégiers, M.; Nahon, L.; Sarni-Manchado, P.; Cheynier, V.; Giuliani, A.

Angew. Chem. Int. Ed. 2013, *52* (32), 8377-8381.

Angewandte International Edition Chemie

DOI: 10.1002/anie.201304046

Mass Spectrometry of Proteins

Photodissociation and Dissociative Photoionization Mass Spectrometry of Proteins and Noncovalent Protein–Ligand Complexes**

*Francis Canon, Aleksandar R. Milosavljević, Guillaume van der Rest, Matthieu Réfrégiers, Laurent Nahon, Pascale Sarni-Manchado, Véronique Cheynier, and Alexandre Giuliani**

Tandem mass spectrometry (MS2) is a widely used method in structural analysis and biopolymer sequencing.[1] In MS2, an ion of interest is isolated, activated, and brought to dissociation. After analysis, the generated fragments provide structural information on the precursor ion.[2] Among the different activation methods, low-energy collision induced dissociation (CID), which relies on slow heating of ions through multiple inelastic low-energy collisions with a neutral gas, is the most widely used.[3] Another set of activation techniques, referred to as the EXD methods (electron capture dissociation (ECD) or electron-transfer dissociation (ETD)), involves the dissociative recombination reaction of multiply protonated ions with electrons.[4] The EXD set of techniques preserve labile bonds, which makes them particularly suited to localize post-translational modifications (PTM) and noncovalent binding sites on protein backbones.[3,5] Another way to increase the internal energy of an ion is by absorption of energetic photons. Methods involving ultraviolet (UV) laser-based photodissociation (PD) of electrosprayed ions are attracting a growing interest since the pioneering work of Williams and McLafferty[6] and have recently found promising applications in proteomics analysis.[7] Indeed, UV activation produces fragments complementary to those generated by other methods and provides high coverage in peptide sequence, that is almost the complete sequence can be determined from the experiments. Among the different wavelengths used, vacuum ultraviolet (VUV) photons of 193 nm (6.2 eV) and 157 nm (7.8 eV) have demonstrated the highest potential to be of use.[7,8]

However, very little is known about fragmentations induced above 8 eV. This problem pertains to the limitations in terms of photon energy delivered by lasers. Surprisingly, synchrotron radiation (SR), which is a widely tunable photon source in the VUVs, has been used only very recently for ion activation. Preliminary work has indicated some potential to bring sequence information on small peptides.[9]

Herein, we report on the potential of SR as a credible activation method in MS2 for structural analysis. The performances of photon activation over a wide energy range are compared to those of CID and ECD in terms of protein sequence coverage. More interestingly, the ability of this new method to preserve noncovalent interactions and to permit identification of the binding sites of a ligand on a protein is investigated and its outcomes are compared to those obtained by ECD.

This study has been performed on a human intrinsically disordered protein (IDP), named IB5. The only known function of IB5 and other basic proline-rich proteins (PRPs) is to bind and scavenge tannins, and thus constitute a first-line of defense against tannin anti-nutritional effects. These interactions are also thought to play a role in the sensation of astringency,[10] which is one of the most important organoleptic properties of food regarding consumer acceptability. Hitherto, the tannin binding sites on IB5 could not be precisely determined by classical structural approaches, such as X-rays diffraction or NMR spectroscopy, because of the lack of crystals for diffraction and of difficulties in spectra interpretation for spectroscopy because of the multiple repeated sequences of this protein. In contrast, the SR-based tandem mass spectrometry activation method presented herein has achieved, for the first time, unambiguous determination of the binding site of the tannin procyanidin B2 3′OG ((−)-epicatechin (4β-8)-(−)-epicatechin 3-O-gallate) on IB5.

[*] Dr. F. Canon, Dr. M. Réfrégiers, Dr. L. Nahon, Dr. A. Giuliani
Synchrotron SOLEIL
L'Orme des Merisiers, Saint Aubin
91192 Gif-sur-Yvette (France)
E-mail: giuliani@synchrotron-soleil.fr
Dr. F. Canon
INRA, UMR1324 Centre des Sciences du Goût et de l'Alimentation
21065 Dijon Cedex (France)
Dr. A. Giuliani
UAR1008 CEPIA, INRA
44316 Nantes (France)
Dr. A. R. Milosavljević
Institute of Physics Belgrade, University of Belgrade
Pregrevica 118, 11080 Belgrade (Serbia)
Dr. P. Sarni-Manchado, Dr. V. Cheynier
INRA, UMR1083 Sciences pour l'Œnologie
2 place Viala, 34060 Montpellier Cedex (France)
Dr. G. van der Rest
Laboratoire de Chimie Physique, Université Paris Sud
91405 Orsay Cedex (France)

[**] This work was supported by the Agence Nationale de la Recherche, France, under the projects ANR-08-BLAN-0065 and ANR-BLAN-0279. A.R.M. acknowledges support by the Ministry of Education, Science and technical development of Republic of Serbia (Projects No. 171020). Financial support from the TGE FT-ICR for conducting ECD dissociation experiments is gratefully acknowledged. The SOLEIL synchrotron radiation facility is acknowledged for providing beamtime under project 20090862.

Supporting information for this article is available on the WWW under http://dx.doi.org/10.1002/anie.201304046.

The experimental set up, described in detail elsewhere,[11] is based upon the coupling of a linear ion-trap mass spectrometer (LTQ XL, Thermo Finnigan) with a VUV beamline[12] at the SOLEIL synchrotron radiation facility (Figure 1). The mass spectrometer is equipped with a nano-

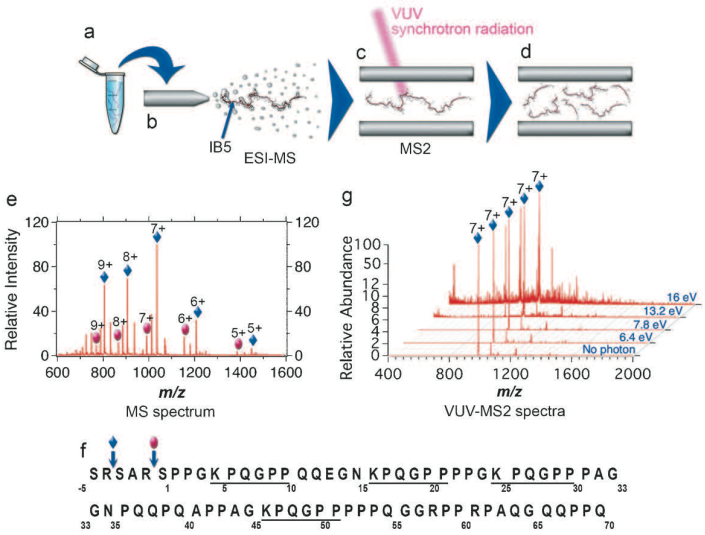

Figure 1. Synchrotron-radiation-based photon-induced activation. Solutions containing the protein, IB5, or its noncovalent complexes (a) are ionized (b), transferred into the ion trap (c), where the ions of interest are isolated and irradiated to generate fragment ions (d). The mass spectrum (e) shows a charge state distribution ranging from +5 to +9 for the two protein isoforms. The sequences of the isoforms are indicated in (f) by the red (IB5b) and blue (IB5a) symbols. Tandem mass spectra recorded at several photon energies (6.4, 7.8, 13.2, and 16 eV) are shown in (g) for $[IB5a]^{7+}$, spectra offset for clarity.

spray ion source allowing soft ionization of native proteins and noncovalent supramolecular complexes. The targeted protein or noncovalent complex can then be selected and activated with energetic VUV photons (Figure 1c) delivered by the beamline, thereby generating MS2 spectra. The fragments may eventually be activated in a subsequent tandem MS step (MS3) upon further VUV irradiation or CID.

The mass spectrum of the protein (Figure 1e), shows a charge-state distribution characteristic of a disordered protein. It also reveals that several protein isoforms have been co-purified.[13] The two isoforms, whose sequences are indicated in the Figure 1f have been activated with photons during 500 ms. The resulting MS2 spectra for IB5a (Figure 1g) reveal that the fragmentation patterns are strongly dependent on the photon energy. Figure 2 shows both the nature and the location of the bond cleavages on the protein backbone as a result of VUV irradiation at 6.4, 7.8, 13.2, and 16 eV, and ECD and CID, respectively. As expected, CID generates mainly y- and b-type ions, whereas ECD sequence ions are mainly c and z-type in nature. In contrast, both MS2 spectra of $[IB5a]^{7+}$ at 6.4 and 7.8 eV are dominated by a-type ions, which result from C_α–C bond cleavages as observed from laser-based PD experiments at the same photon energies on protonated peptides.[7,8b] At 13.2 and 16 eV, the mass spectra exhibit significantly richer fragmentation patterns (Figure 2a) into a, b, c, x, y and z-type ions, which resembles the outcomes of electron ionization dissociation (EID).[14] The abundances of the precursor (Figure 3a) and the product ions (Figure 3b,c) reveal that the fragmentation efficiency of the protein increases with the photon energy, which is consistent with the energy dependence of the photoabsorption cross-section of ions.[9] It leads us to distinguish between two different photon energy regimes. The fundamental difference between the low-photon-energy range (6.4 and 7.8 eV) and the high-energy one (13.2 and 16 eV) lies in the appearance of the $[M+7H]^{8+}$ and $[M+7H]^{\bullet 9+}$ radical cations produced upon photoionization of the precursor. These characteristics are similar to those reported[14] under EID conditions of protein ions. From the relative abundances of $[M+7H]^{8+}$ and $[M+7H]^{\bullet 9+}$ displayed for different photon energies in Figure 3b, it clearly appears that the ionization threshold of IB5 lies in between 7.8 and 13.2 eV. Above this threshold, photon activation leads to the ionization of the precursor ion and generates fragments through dissociative photoionization (DPI), with abundant formation of sequence ions of various natures. It has been shown theoretically that the removal of an electron from the peptidic backbone significantly weakens all the bonds, making them prone to fragmentation,[15] which is consistent with the present observations. Below the ionization threshold, photon absorption populates electronic excited state, which relax partly through dissociation. This regime, usually referred to as photodissociation (PD), has been shown to lead mainly to C_α–C bond cleavage.[8b] Tuning the photon energy below or above the ionization onset provides control over the extent and the nature of fragmentation pattern.

The following sequence coverage of the IB5 protein has been obtained: 46% for PD at 6.4 eV, 56% for PD at 7.8 eV, 58% for CID, 68% for ECD, and 91% for DPI at 16 eV. Although the CID spectrum is dominated by fragments resulting from cleavages close to proline residues, known as the proline effect[16] and previously described for this protein,[13] DPI leads to cleavage evenly spread along the backbone. The improved sequence coverage of ECD over CID remains however inferior to that obtained from DPI, because the abundant proline residues preclude the formation of c- and z-type fragments[16] under ECD conditions.

The photoabsorption cross-section is proportional to the number of electrons involved in the process.[17] Above the ionization threshold, photoionization is the main relaxation process following photoabsorption. This feature has the important practical consequence that the probability of ionizing a target increases with its mass or its size, which is totally opposite to CID which loses efficiency as the size of the target increases.[3]

The mass spectra of a solution containing IB5 and B2 3′OG typically show IB5·B2 3′OG supramolecular edifices with several stoichiometries in agreement with the tannin-

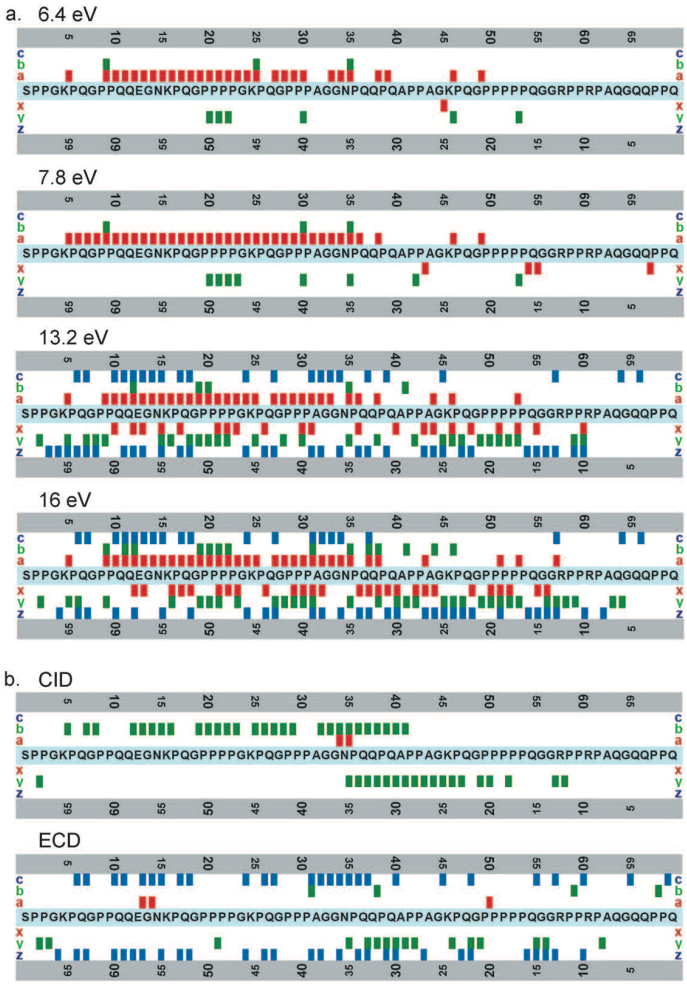

Figure 2. a) pattern of $[IB5]^{7+}$ fragmentation as a function of photon energy; b) pattern of $[IB5]^{7+}$ fragmentation resulting from CID and ECD experiments.

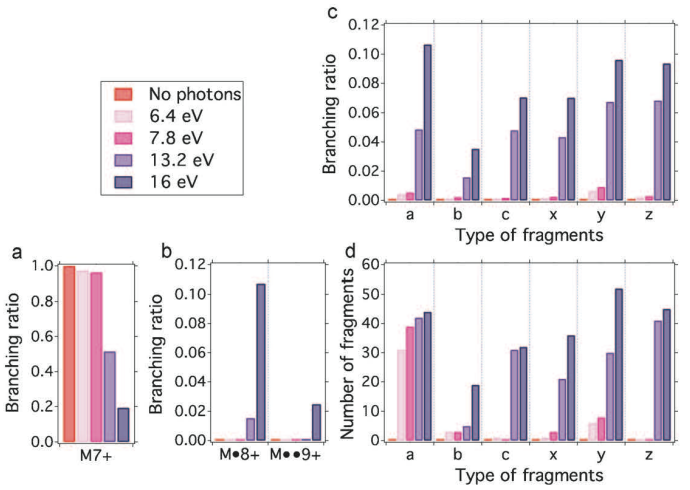

Figure 3. Branching ratio of the parent ion (a), the photo-ionized $[IB5]^{\bullet 8+}$ and $[IB5]^{\bullet\bullet 9+}$ (b), and the a, b, c, x, y, and z sequence ions (c) as a function of the photon energy. (d) Histogram of the number of fragment ions produced as a function of photon energy.

scavenging function of IB5.[18] The clusters of proline present in the IB5 sequence (Figure 1 f), as in other salivary PRPs, are believed to provide multiple tannin binding sites.[19] NMR experiments have confirmed the involvement of proline clusters in these interactions, but were not able to identify precisely which part of the sequence was involved.[20] To assess the potential of photon activation to localize the binding sites of the ligand (B2 3′OG) to the protein, IB5 1 B2 3′OG has been submitted to 16 eV DPI (Figure 4). This regime was chosen because of the large sequence coverage and abundance of fragments it had provided on the bare protein. The comparison with the MS2 spectrum of the bare protein (Figure 4 a) revealed peaks that are shared by both spectra and others that are not. Analysis of the specific peaks revealed that the masses of these fragments correspond to that of the specific fragments identified in the MS2 spectrum of $[IB5+7H]^{7+}$ shifted by the mass of the ligand. These fragments have been selected (Figure 4 b) and a subsequent CID analysis has been conducted. This MS3 step unambiguously confirmed the presence of the ligand through its detachment from the protein fragment (Figure 4 c). The list of fragments exhibiting such behavior is presented in Figure 4 d. This procedure has been repeated for the second isoform of the protein, IB5b (Figure 1 f), and the results are given in Figure 4 e. As expected, the fragmentation patterns of $[IB5a{\cdot}B2\ 3'OG+7H]^{7+}$ and $[IB5b{\cdot}B2\ 3'OG+7H]^{7+}$ are very similar, showing the reliability of our method (Figure 4 d,e). In both experiments more than fifty peaks have been identified and interpreted as fragments of IB5 noncovalently bound to B2 3′OG, contrasting with the four fragments identified using ECD (Figure 4 f). It appears that all these fragments from both N- and C-terminal series contain the KPQGPPPPPQGG segment of the sequence, indicating therefore a strong interaction between B2 3′OG and this part of the protein. Note that comparison of the DPI fragmentation patterns obtained for the bare and the complexed protein, as shown in the Supporting Information, reveals that the presence of the tannin does not affect significantly the fragmentation pattern of the protein, the ligand appearing as a spectator of the fragmentation process. This observation is consistent with the DPI mechanism suggested herein, where most of the photon absorption is ascribed to the protein. The sequence identified with a cluster of five prolines very likely adopts a PPI or a PPII helix conformation in solution.[20b,21] Such structural elements are thought to be crucial for IDPs in the binding with their partner,[22] as this stable segment might provide an initial contact point.[19a,20b] Moreover, the phenolic rings of the tannins can stack on the Pro-S face of proline.[20a] Therefore, the sequence identified displays all the features required for it to be the preferential binding site of B2 3′OG on IB5 and the role of the proline clusters in PRPs sequence is thus unequivocally confirmed.

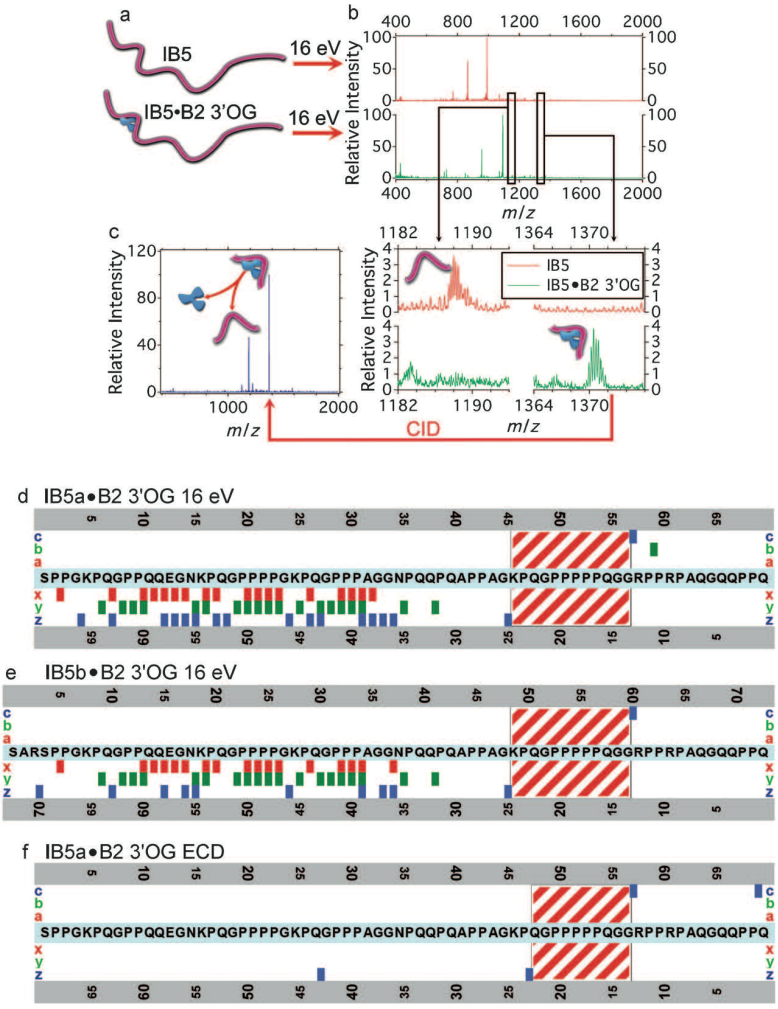

Figure 4. Localization of the tannin (B2 3'OG) binding site on IB5. a) MS2 spectra of $[IB5+7H]^{7+}$ and $[IB5{\cdot}B2\ 3'OG+7H]^{7+}$ after dissociative photoionization (DPI) at 16 eV. b) Enlargement on two parts of the DPI MS2 spectra for the bare and the complexed protein showing the shift in mass of one fragment as a result of the conservation of the ligand on it. c) DPI/CID MS3 spectrum of the *m/z* 1369.95 ion confirming the presence of the ligand on the DPI fragment ion. Patterns of the fragments linked to B2 3'OG for d) $[IB5a{\cdot}B2\ 3'OG+7H]^{7+}$ and e) $[IB5b{\cdot}B2\ 3'OG+7H]^{7+}$ after 16 eV DPI. f) Patterns of the fragments linked to B2 3'OG for $[IB5a{\cdot}B2\ 3'OG+7H]^{7+}$ after ECD activation. The binding site of B2 3'OG is highlighted by the dashed rectangle.

In summary, the present study shows that the nature of the fragments generated upon VUV photon activation is controlled by the photon energy. Therefore, synchrotron radiation, by providing access to a wide variety of photon activation regimes, ranging from PD to DPI, clearly appears to be very promising sequencing method, complementary to laboratory activation techniques. The sequence coverage, obtained both in PD and DPI regimes, makes synchrotron-radiation activation an appealing method for sequencing. DPI allowed the determination of the ligand binding site on an IDP. Therefore the new method, based upon DPI, should aid research in the growing and challenging field of protein noncovalent interactions.

Experimental Section

IB5 and B2 3'-O-gallate were produced and purified as described elsewhere.[18] Stock solutions of B2 3'-O-gallate were prepared in water/ethanol, 88:12 (v/v) acidified to pH 3.3 with acetic acid, mimicking the consumption of red wine. Final solutions of 10 μM of IB5 were electrosprayed, giving an overall consumption of 300 fmol per tandem mass spectrum. For IB5-B2 3'OG interactions, tannin and protein solutions were mixed extemporaneously at room temperature (regulated at 24°C) to obtain a protein/polyphenol molar ratio of 1:10 (10 μM:100 μM).

The experimental setup is based upon a linear ion-trap mass spectrometer (LTQ XL, Thermo Electron, San Jose, CA, USA)[11] coupled to the DESIRS beamline[12] of the SOLEIL synchrotron radiation facility (France). The synchrotron radiation beam was injected along the ion-trap axis. An MgF_2 window (below 10 eV) and gas filter filled with argon (8–16 eV) were used to suppress the high harmonic content delivered by the undulator that would be transmitted by the monochromator's grating. An electromechanical shutter was placed along the SR beams, allowing synchronization of the SR beam with the LTQ time sequence. For MS2 experiments, the precursor ions were irradiated during 500 ms. For MS3 experiments, a supplementary step of CID was applied on the targeted VUV product ion during which the shutter was kept close.

Mass spectra were analyzed using mMass software[23] and Igor Pro (Wavemetrics, Portland, USA). For each spectrum, the relative abundance (R) of the different ions has been established by the measurement of their peak area (A). The contribution of fragments formed without photon activation has been subtracted. Each of the peak areas was normalized by the sum of the area of all ions, and to the photon flux.

The ECD experiments were carried out with a 7-T APEX III FT-ICR mass spectrometer (Bruker Daltonik GmbH, Germany) equipped with an electrospray ion source. The isolated precursor ions were irradiated with electrons having less than 1 eV kinetic energy during 150 ms.

Received: May 11, 2013
Published online: July 19, 2013

Keywords: dissociative photoionization · mass spectrometry · proteins · tannins · VUV photon activation

[1] R. Aebersold, M. Mann, *Nature* **2003**, *422*, 198–207.
[2] F. W. McLafferty, *Science* **1981**, *214*, 280–287.
[3] N. L. Kelleher, *Anal. Chem.* **2004**, *76*, 196A–203A.
[4] a) R. A. Zubarev, N. L. Kelleher, F. W. McLafferty, *J. Am. Chem. Soc.* **1998**, *120*, 3265–3266; b) J. E. P. Syka, J. J. Coon, M. J. Schroeder, J. Shabanowitz, D. F. Hunt, *Proc. Natl. Acad. Sci. USA* **2004**, *101*, 9528–9533.
[5] Y. Xie, J. Zhang, S. Yin, J. A. Loo, *J. Am. Chem. Soc.* **2006**, *128*, 14432–14433.
[6] E. R. Williams, F. W. McLafferty, *J. Am. Soc. Mass Spectrom.* **1990**, *1*, 361–365.

[7] J. A. Madsen, D. R. Boutz, J. S. Brodbelt, *J. Proteome Res.* **2010**, *9*, 4205 – 4214.
[8] a) H. Zhou, Z. Ning, A. E. Starr, M. Abu-Farha, D. Figeys, *Anal. Chem.* **2012**, *84*, 720 – 734; b) L. Zhang, J. P. Reilly, *J. Proteome Res.* **2010**, *9*, 3025 – 3034.
[9] S. Bari, O. Gonzalez-Magana, G. Reitsma, J. Werner, S. Schippers, R. Hoekstra, T. Schlatholter, *J. Chem. Phys.* **2011**, *134*, 024314 – 024319.
[10] E. C. Bate-Smith, *Phytochemistry* **1973**, *12*, 907 – 912.
[11] A. R. Milosavljević, C. Nicolas, J.-F. Gil, F. Canon, M. Refregiers, L. Nahon, A. Giuliani, *J. Synchrotron Radiat.* **2012**, *19*, 174 – 178.
[12] L. Nahon, N. de Oliveira, G. A. Garcia, J.-F. Gil, B. Pilette, O. Marcouille, B. Lagarde, F. Polack, *J. Synchrotron Radiat.* **2012**, *19*, 508 – 520.
[13] F. Canon, F. Paté, E. Meudec, T. Marlin, V. Cheynier, A. Giuliani, P. Sarni-Manchado, *Anal. Bioanal. Chem.* **2009**, *395*, 2535 – 2545.
[14] a) Y. M. E. Fung, C. M. Adams, R. A. Zubarev, *J. Am. Chem. Soc.* **2009**, *131*, 9977 – 9985; b) R. A. Zubarev, H. Yang, *Angew. Chem.* **2010**, *122*, 1481 – 1483; *Angew. Chem. Int. Ed.* **2010**, *49*, 1439 – 1441.
[15] R. Parthasarathi, Y. He, J. P. Reilly, K. Raghavachari, *J. Am. Chem. Soc.* **2010**, *132*, 1606 – 1610.
[16] N. Leymarie, E. A. Berg, M. E. McComb, P. B. O'Connor, J. Grogan, F. G. Oppenheim, C. E. Costello, *Anal. Chem.* **2002**, *74*, 4124 – 4132.
[17] T. N. Olney, G. Cooper, W. F. Chan, G. R. Burton, C. E. Brion, K. H. Tan, *Chem. Phys.* **1997**, *218*, 127 – 149.
[18] a) F. Canon, A. Giuliani, F. Paté, P. Sarni-Manchado, *Anal. Bioanal. Chem.* **2010**, *398*, 815 – 822;b) F. Canon, R. Ballivian, F. Chirot, R. Antoine, P. Sarni-Manchado, J. Lemoine, P. Dugourd, *J. Am. Chem. Soc.* **2011**, *133*, 7847-7852.
[19] a) A. J. Charlton, N. J. Baxter, T. H. Lilley, E. Haslam, C. J. McDonald, M. P. Williamson, *FEBS Lett.* **1996**, *382*, 289 – 292; b) F. Canon, F. Paté, V. Cheynier, P. Sarni-Manchado, A. Giuliani, J. Pérez, D. Durand, J. Li, B. Cabane, *Langmuir* **2013**, *29*, 1926 – 1937.
[20] a) N. J. Baxter, T. H. Lilley, E. Haslam, M. P. Williamson, *Biochemistry* **1997**, *36*, 5566 – 5577; b) C. Pascal, F. Paté, V. Cheynier, M.-A. Delsuc, *Biopolymers* **2009**, *91*, 745 – 756.
[21] H. Boze, T. Marlin, D. Durand, J. Pérez, A. Vernhet, F. Canon, P. Sarni-Manchado, V. Cheynier, B. Cabane, *Biophys. J.* **2010**, *99*, 656 – 665.
[22] M. Fuxreiter, I. Simon, P. Friedrich, P. Tompa, *J. Mol. Biol.* **2004**, *338*, 1015 – 1026.
[23] M. Strohalm, D. Kavan, P. Novák, M. Volný, V. r. Havlíček, *Anal. Chem.* **2010**, *82*, 4648 – 4651.

Publication n°9: Binding site of different tannins on a human salivary proline-rich protein evidenced by dissociative photoionization tandem mass spectrometry.

Canon, F.; Ployon, S.; Mazauric, J.-P.; Sarni-Manchado, P.; Réfrégiers, M.; Giuliani, A.; Cheynier, V.

Tetrahedron ***2015,*** *71 (20), 3039-3044.*

Tetrahedron 71 (2015) 3039–3044

Contents lists available at ScienceDirect

Tetrahedron

journal homepage: www.elsevier.com/locate/tet

Binding site of different tannins on a human salivary proline-rich protein evidenced by dissociative photoionization tandem mass spectrometry

Francis Canon [a,b,c,*], Sarah Ployon [a,b,c], Jean-Paul Mazauric [d,e,f], Pascale Sarni-Manchado [d,e,f], Matthieu Réfrégiers [g], Alexandre Giuliani [g,h], Véronique Cheynier [d,e,f]

[a] INRA, UMR1324 Centre des Sciences du Goût et de l'Alimentation, F-21000 Dijon, France
[b] CNRS, UMR6265 Centre des Sciences du Goût et de l'Alimentation, F-21000 Dijon, France
[c] Université de Bourgogne, UMR Centre des Sciences du Goût et de l'Alimentation, F-21000 Dijon, France
[d] INRA, UMR1083 Sciences Pour l'Oenologie, F-34060 Montpellier, France
[e] Montpellier SupAgro, UMR1083 Sciences Pour l'Oenologie, F-34060 Montpellier, France
[f] Université Montpellier I, UMR1083 Sciences Pour l'Oenologie, F-34060 Montpellier, France
[g] Synchrotron SOLEIL, F-91192 Gif Sur Yvette, France
[h] INRA, CEPIA, UAR1008, F-44316 Nantes, France

ARTICLE INFO

Article history:
Received 29 May 2014
Received in revised form 12 October 2014
Accepted 6 November 2014
Available online 13 November 2014

Keywords:
Proline-rich proteins
Tannins
Non-covalent interaction
Binding site
Astringency
Mass spectrometry

ABSTRACT

The sensation of astringency is thought to originate from the interaction occurring between tannins and the salivary proline-rich proteins (PRPs). Astringency perception can be modified by the structure of tannins. Herein, we study the interactions occurring between the human salivary PRP, IB5, and three model tannins with different structure, epigallocatechin gallate and the procyanidin dimers B2 and B2 3′*O*-gallate, using the coupling of mass spectrometry and VUV-synchrotron radiation. The results obtained indicate that the structure of tannins, in particular the degree of polymerization and the galloylation, does not modify the binding site on IB5 involved in the interaction.

1. Introduction

Astringency is a major sensory attribute of wines and especially of red wines,[1] elicited primarily by tannins. It is usually accepted that tannin astringency results from their interaction with salivary proteins and subsequent aggregation and/or precipitation, causing a loss of the lubricating ability of saliva, although it may also involve adsorption of tannins on the oral mucosa.[2–4]

Tannins are ubiquitous in plants and believed to play a role in plant defense against pests and herbivores. Proanthocyanidins, i.e., oligomers and polymers of flavan-3-ols, also called condensed tannins, are the major tannins in foods and beverages, and particularly abundant in grapes and in red wine. They exhibit large structural diversity arising from the presence of several constitutive units and linkage positions, substitution, especially with galloyl groups, and varying degrees of polymerization. These structural features determine tannin properties, including astringency[5,6] and affinity for proteins and peptides that increase with chain length and galloylation[7–10] and are also impacted by tannin conformation.[11]

Among salivary proteins, proline-rich proteins (PRP) are particular prone to interact with tannins.[12] It has been suggested that secretion of PRPs, and especially of basic PRPs, whose only known function is tannin binding, is the first line of defense of herbivores against dietary tannins. Indeed, tannins inhibit digestive enzymes and impede assimilation of dietary proteins and other nutrients. Their binding by PRPs is believed to prevent these processes and could also reduce tannin consumption by triggering astringency. The high affinity of PRPs for tannins is associated to their structural characteristics. PRPs belong to intrinsically disordered proteins, and

* Corresponding author at present address: INRA, UMR CSGA, 17 Rue Sully, F-21065 Dijon Cedex, France. Tel.: +33 3 80 69 35 29; e-mail address: francis.canon@dijon.inra.fr (F. Canon).

http://dx.doi.org/10.1016/j.tet.2014.11.013
0040-4020/

show random coil structure except for small polyproline helix segments. The most accepted model of PRP–tannin interactions describes three different stages as tannin concentration increases: (i) tannins, which are multidentate ligands, bind to several sites on the free protein, (ii) the stoichiometries of the complexes increase and tannins cross-link different protein molecules, (iii) the resulting multimeric aggregates grow until precipitation.

A human salivary PRP, referred to as IB5, and its interactions with tannins have been particularly investigated. Its sequence (Fig. 1A) presents tandem repeats of KPQGPP(P) and eight clusters of 2–5 proline residues. Experiments involving small angle X-ray scattering (SAXS),[13] circular dichroism (CD),[14,15] nuclear magnetic resonance (NMR),[16] and mass spectrometry (MS)[17] have shown that IB5 exhibits a random coil structure and undergoes disorder to order transition upon interaction with epigallocatechin gallate (EgCG), selected as a model tannin ligand.[14,15] Molecular modeling performed on a smaller truncated PRP, $IB9_{37}$, also indicated that structural rearrangement of the peptide occurs during the interaction.[18] Folding of the peptide chain around the tannin, as first proposed by Charlton et al.,[19] may explain the higher tannin affinity of $IB9_{37}$ and IB5 compared to a single proline-rich repeat.

precise binding sites of tannins could not be determined by NMR on full length PRP proteins because of the abundance of proline and repeated sequences. A new method using tandem mass spectrometry coupled to synchrotron radiation as an activation method has recently allowed unambiguous determination of demonstration of binding of the procyanidin dimer B2 3′OG (epicatechin-(4β-8)-epicatechin-3-*O*-gallate, Fig. 1) on the KPQGPPPPPQGG segment of IB5 sequence.[23] In the case of $IB7_{14}$ and $IB9_{37}$, the same three binding sites, corresponding to PP and GG clusters, were involved for all tannin dimers and trimers tested but the binding force was higher for tannins showing extended conformation and longer chain length.[18,11] Once three tannins are linked to the peptide, regardless of its chain length, non-specific cross-linking occurs.[18,11] Similarly, upon, binding with EgCG, the full length protein IB5 forms aggregates with a core structure containing proteins that have bound at least three EgCG molecules and a less dense corona with fewer bound tannins.[21]

Regarding these different observations, it appears important to know if, as for shorter $IB9_{37}$, the same binding site on IB5 is involved in the interaction with tannins having different structures. Therefore, in the present paper, we apply the recent introduced method,

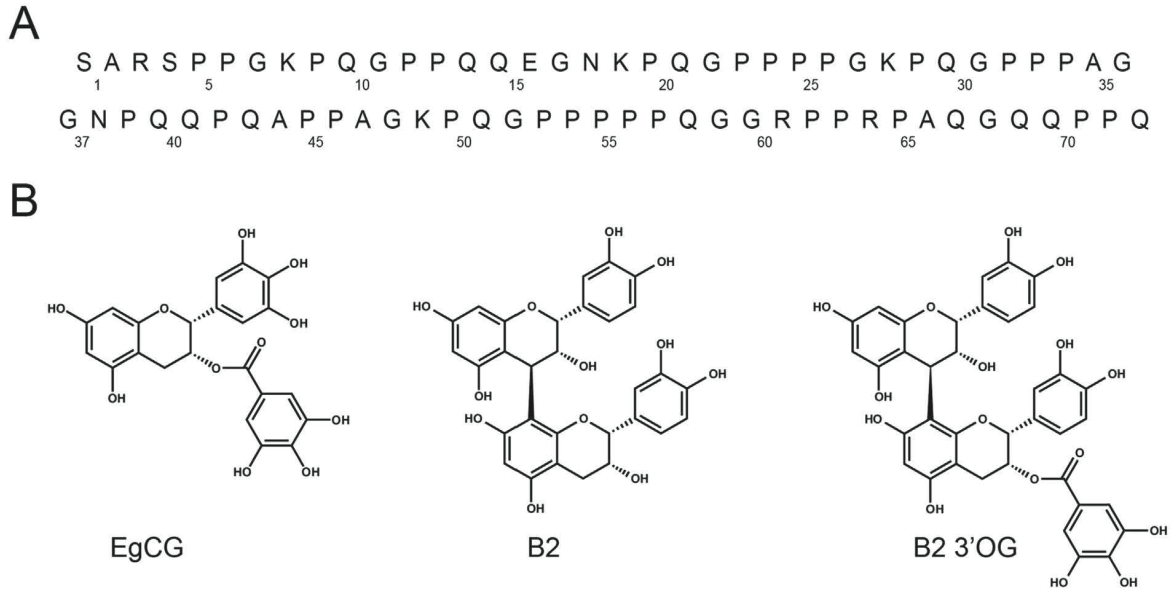

Fig. 1. (A) Sequence of the IB5 human salivary protein. (B) Molecular structure of the epigallocatechin gallate (EgCG), (epicatechin-4β-8)-epicatechin (B2) and epicatechin-(4β-8)-epicatechin-3-*O*-gallate (B2 3′OG).

NMR[20] and a multitechnique approach involving MS and SAXS[21] indicated that at least three EgCG molecules per protein or peptide are required to form PRP–EgCG aggregates. Comparison of different tannins showed that the stability of IB5·tannin complexes increases with the number of hydroxyl groups in the molecule, indicating the involvement of hydrogen bonds.[10] NMR studies performed on two proline-rich peptides ($IB7_{14}$ and $IB9_{37}$) also showed specific hydrophilic interaction at low tannin concentration.[18,11] Mass spectrometry has revealed that IB5·EgCG complexes are present in solution under a distribution of various stoichiometries and fragmentation experiments of complexes with stoichiometries from 1:1 to 1:9 suggested the presence of eight equivalent and independent binding sites on the protein, matching the number of proline clusters.[21] NMR data on complexes of tannins with IB5 or PRP peptides indicated the involvement of Pro and Gly residues in specific non-covalent interactions.[22,18,11,16] However, the coupling MS and vacuum-ultraviolet (VUV) radiation, to localize the binding sites of EgCG and B2 ((epicatechin-4β-8)-epicatechin, Fig. 1B.) on the full PRP, IB5, in 1:1 complexes, and to compare them to that of B2 3′OG.

2. Results and discussion

IB5 is a model of basic salivary PRP, which has been obtained by heterologous expression of the human gene PRB4S in the yeast *Pichia pastoris*.[24] The mass spectrum obtained by electrospraying the protein solution displayed a series of protonated peaks corresponding to four IB5 isoforms with charge states ranging from 5+ to 10+. IB5 isoforms differ from each other by few amino acids at their N-terminal end as previously observed.[23] The sequence of the main isoform is presented in Fig. 1A. Fig. 2A presents a close-up of the mass spectra of IB5 solution and IB5/tannin mixtures for the

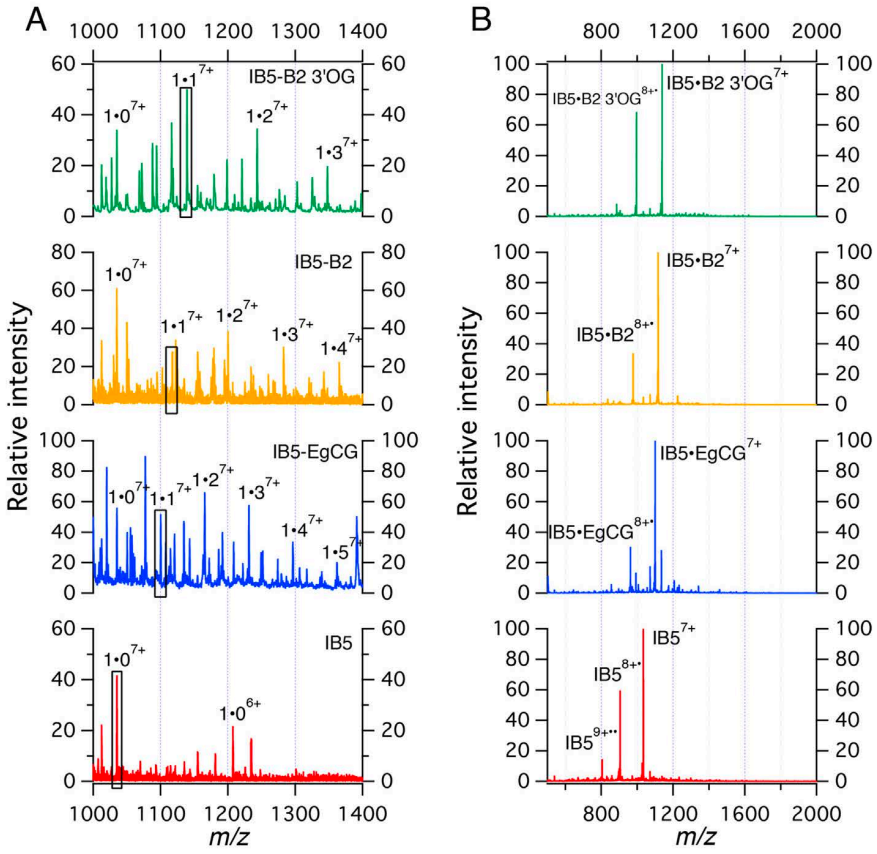

Fig. 2. (A) Electrospray mass spectra of IB5 (bottom line) and IB5/tannins mixtures. Stoichiometries corresponding to the 7+ charge state are labeled. The boxes indicate the stoichiometries selected for subsequent tandem mass spectrometry analysis. (B) DPI tandem mass spectra at 16 eV of the selected precursors.

following tannins: EgCG, B2, B2 3′OG. For each tannin studied here, the corresponding mass spectrum reveals the presence of peaks corresponding to IB5·*n*Tannin complexes with several stoichiometries, as described earlier.[10]

2.1. Mass spectrometry and tandem mass spectrometry analysis of the complexes

In order to localize the binding site of the three tannins on IB5, IB5·1Tannin complexes with the 7+ charge state were selected, and then activated using a 16 eV VUV radiation from a synchrotron radiation beamline. This photon energy has been chosen because of the large sequence coverage and the abundance of fragments it has previously provided on the bare protein.[23] The resulting VUV MS/MS spectra are presented in Fig. 2B. Each spectrum reveals the appearance of the $[M+7H]^{8+\bullet}$ radical cation produced upon the photoionization of the precursor ion. Two regimes of fragmentation have been previously reported using UV and VUV-irradiation.[25] Below the ionization threshold, photon absorption populates electronic excited states, which relax partly through dissociation. This regime, usually referred to as photodissociation, has been shown to lead mainly to the C_α–C bond cleavage. Activation at photon energies above the ionization threshold generates fragments through dissociative photoionization (DPI), with abundant formation of sequence ions of various natures.[26] This regime (DPI) has been shown to provide the highest sequence coverage for IB5 in comparison to the other activation techniques: collision induced dissociation (CID), electron capture dissociation (ECD), and photodissociation (PD).[23]

Comparison of the 16 eV DPI MS/MS spectra of $[IB5{\cdot}1Tannin+7H]^{7+}$ with that of the bare protein ($[IB5+7H]^{7+}$) revealed the presence of peaks shared with the bare proteins (i.e., without retention of the ligand) and of specific peaks that are only present on one spectrum (i.e., that may have retained the ligand). Fig. 3 presents an example of such fragment ions. The x_{48}^{4+} fragment ion of the bare protein is shifted to higher *m*/*z* when associated with the different tannins, as seen in Fig. 3, indicating that the same sequence of the protein is involved for each three tannins.

Analysis of all fragment ions retaining the tannins allows a map of the bound fragments to be established for each $[IB5{\cdot}1Tannin+7H]^{7+}$ precursor ion. The different maps of the fragmentation patterns are presented in Fig. 4 along with that of the bare protein.

For each of the tannins studied here, abundant fragment ions bound with the tannin are revealed upon DPI tandem mass spectrometry. The same experiments performed using ECD has revealed only four fragments retaining B2 3′OG[23] and 0 fragments conserving EgCG (data not shown). We have previously reported that $[IB5{\cdot}B2\ 3'OG+7H]^{7+}$ is more stable than $[IB5{\cdot}EgCG+7H]^{7+}$,[10] which might explain this observation. These observations confirm that DPI is a powerful activation method able to preserve the tannin–protein non-covalent associations. The fragmentation maps obtained for the three tannins show that all fragments from both N- and C-terminal series bearing the tannin ligands contain the QPQAPPAGKPQGPPPPPQGG segment of the sequence.

2.2. Interaction region of the protein with the tannins

This result indicates that this part of the sequence (i.e., QPQAPPAGKPQGPPPPPQGG) is the preferred binding site for EgCG, B2, and B2 3′OG. The sequence identified from the present result

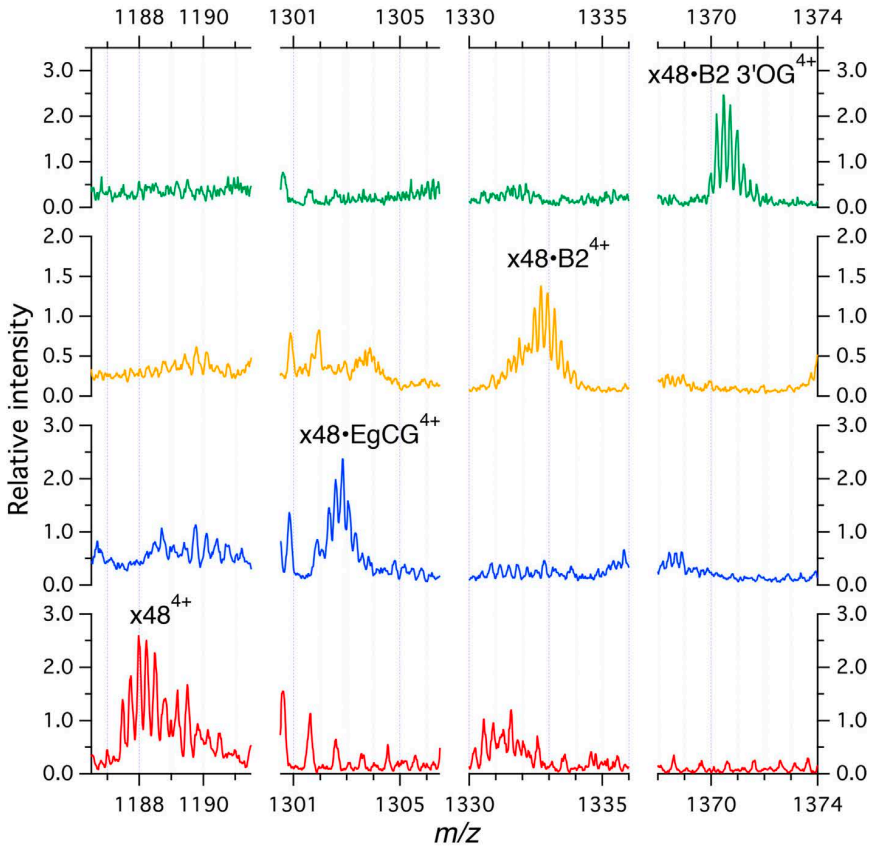

Fig. 3. Close-up of the *m/z* range corresponding to the x_{48}^{4+} fragment of IB5 (bottom panel) and of the x_{48}^{4+} fragment complexed with EgCG, B2, and B2 3′OG showing the gradual mass shift due to tannin binding on the fragment.

contains the longest cluster of proline, which very likely adopts a PPI or a PPII helix conformation in solution.[27,13,16] Clusters of proline have been previously suggested to be the preferential binding site of tannins on PRPs,[19,16] as this firm segment might provide an initial contact point for the binding.[19,16] Moreover, this segment is surrounded by clusters of glycine and alanine residues, which provide flexible regions allowing establishment of additional hydrogen bonds.[28] The current model of interaction between PRPs and tannins proposes that the clusters of proline are rigid regions, providing initial anchoring points favorable for effective tannin binding. Moreover, the carbonyl function in tertiary amides of proline residues is a more effective hydrogen bond acceptor than that in primary and secondary amides.[29] This firm region are linked by flexible hinges, allowing the reeling of the peptidic chain and the establishment of additional contact points. This model has been proposed to explain that full PRP have higher affinity for tannins as compared to shorter PRP peptides.[18,19] In agreement with this model, ion mobility experiments performed on the IB5·EgCG complexes have shown a transition from an extended conformation to more compact ones upon the binding of tannins,[15] confirming earlier results obtained by NMR and circular dichroism.[16] Molecular modeling calculations have also suggested a notable change in $IB9_{39}$ conformation during its interaction with tannins.[18] Interestingly, this model of interaction seems to be common for IDPs in the binding with their partner.[30] However, the conformational change was not observed with the shorter $IB7_{14}$[27,11] suggesting that it involves folding of the peptide chain around the tannin(s).

Identical sites, involving Pro and Gly residues, have been reported for the binding of three tannins (procyanidin dimers B1 and B3 and trimer C2) on peptides of PRP ($IB9_{37}$ and $IB7_{14}$). The affinity for all tannin molecules increased with the peptide chain length, as observed earlier for IB5[19] while the number of binding sites found for $IB9_{37}$ was slightly lower than for $IB7_{14}$,[18] again suggesting wrapping of the tannin by the PRP chain. The tannin affinity increased with the tannin molecular weight but was also higher for B2 than for the other procyanidin dimers tested, owing to its more extended structure.[18,11] The predominant conformation of B2 3′OG is also more compact than that of B2.[31] Although it does not result in a lower affinity for IB5, as shown by comparing the stability of IB5·tannin complexes,[10] this compact structure, which is able to establish a higher number of hydrogen bonds,[10] probably explains why the binding site of B2 3′OG on the IB5 sequence appears more defined that those of B2 and EgCG.

3. Conclusion

Astringency is an important sensory driver of intrinsic quality of red wines.[1] On one hand, it is known that the structure of tannins, in particular the degree of polymerization and the galloylation, affects astringency.[6] On the other hand, it is generally accepted that salivary PRPs play a role in the astringency sensation due to their ability to interact with tannins. PRP are able to bind several tannins at the same time. Moreover, investigation on interaction between PRP and EgCG have revealed that the proteins, which have bound at least three EgCG molecules connect to each other through EgCG bridges and build PRP·EgCG aggregates.[21] It has been also reported that PRPs undergo a structural rearrangement upon the binding.[15] Herein we investigated the effect of the tannin structure on their binding site onto PRP and we demonstrated that EgCG, B2, and B2 3′OG, which exhibit structural differences, i.e., degree of

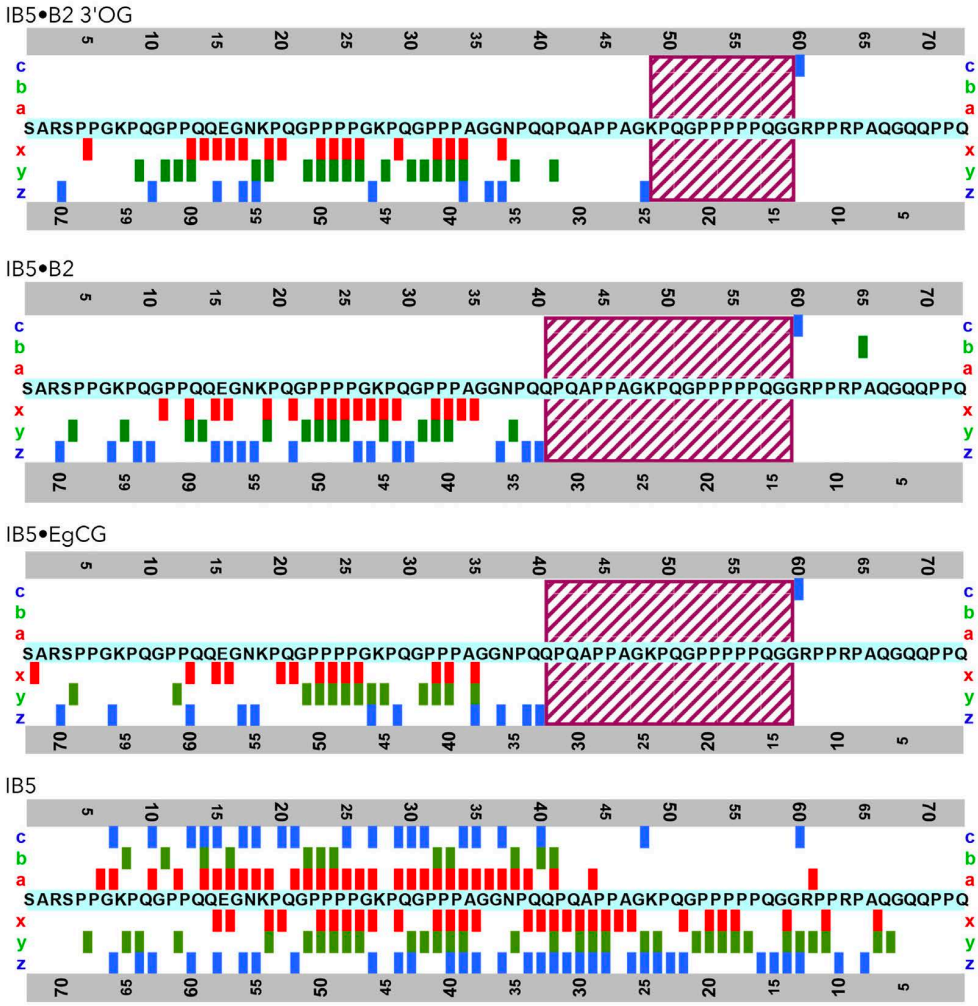

Fig. 4. Fragmentation patterns of IB5 alone and in association with B2 3′OG,[23] B2, and EgCG. The binding sites identified for the tannins on the backbone are indicated by a box.

polymerization and galloylation, bind to the same binding site. This binding site is constituted by a rigid cluster of five proline residues providing an initial contact point, surrounded by flexible hinges allowing structural rearrangements and the establishment of additional hydrogen bonds. Indeed, we previously reported that the structure of tannins modifies the strength of the PRP–tannin interaction as a function of the number of hydroxyl groups of tannins. It is interesting to notice that the structure of tannins affects both the strength of their interactions with PRP and the perception of astringency.[10,6]

4. Experimental section

4.1. Samples

Epigallocatechin gallate (EgCG) has been purchased from Sigma–Aldrich. B2 and B2 3′*O*-gallate were purified as previously described.[32] The human salivary proline-rich protein, IB5, was produced by use of the yeast *P. pastoris* as a host organism and purified as previously described.[13]

Tannin and protein stock solutions were prepared in the following medium: water/ethanol, 88:12 (v/v) acidified at pH 3.3 with acetic acid, mimicking the consumption of red wine.

The stock solutions were diluted to final solutions of 10 μM of IB5 before electrospray analysis. The tannin and protein solutions were mixed at room temperature prior to mass spectrometry analysis to obtain a protein/polyphenol molar ratio of 1:10.

4.2. Mass spectrometry

Mass spectrometry analyses have been performed on linear ion trap fitted with a nanospray ion source (LTQ XL) from Thermo Scientific (San Jose, CA, USA). The mass spectrometer has been coupled to DISCO,[33] a VUV beamline of the SOLEIL synchrotron radiation facility. This coupling is similar to that described previously,[34] with some differences. The APEX branch line was used, with the last stage of the differential pumping system[35] removed. The beamline was set to deliver 16 eV photons with 20 meV energy resolution. An electromechanical shutter was triggered by the activation signal from the mass spectrometer to allow irradiation of the precursor for 2000 ms during the activation stage.

Mass spectra were analyzed using mMass software[36] and Igor Pro (Wavemetrics, Portland, USA).

Acknowledgements

This work was supported by the L' Agence Nationale de la Recherche, France, under the projects ANR-08-BLAN-0065 and ANR-BLAN-0279, and by the Regional Council of Burgundy (FABER AIB 29000622), Européen de Développement Régional (FEDER) (European Union).

References and notes

1. Sáenz-Navajas, M.-P.; Ballester, J.; Pêcher, C.; Peyron, D.; Valentin, D. *Food Res. Int.* **2013**, *54*, 1506–1518.
2. Bajec, M. R.; Pickering, G. J. *Crit. Rev. Food Sci. Nutr.* **2008**, *48*, 858–875.
3. de Freitas, V.; Mateus, N. *Curr. Org. Chem.* **2012**, *16*, 724–746.
4. Gibbins, H. L.; Carpenter, G. H. *J. Texture Stud.* **2013**, *44*, 364–375.
5. Noble, A. C. In *Chemistry of Taste: Mechanisms, Behaviors, and Mimics*; Given, P., Paredes, D., Eds.; American Chemical Society: Washington, DC, 2002; pp 192–201.
6. Vidal, S.; Francis, L.; Guyot, S.; Marnet, N.; Kwiatkowski, M.; Gawel, R.; Cheynier, V.; Waters, E. J. *J. Sci. Food Agric.* **2003**, *83*, 564–573.
7. Sarni-Manchado, P.; Cheynier, V. *J. Mass Spectrom.* **2002**, *37*, 609–616.
8. Poncet-Legrand, C.; Edelmann, A.; Putaux, J.-L.; Cartalade, D.; Sarni-Manchado, P.; Vernhet, A. *Food Hydrocolloids* **2006**, *20*, 687–697.
9. Poncet-Legrand, C.; Gautier, C.; Cheynier, V.; Imberty, A. *J. Agric. Food Chem.* **2007**, *55*, 9235–9240.
10. Canon, F.; Giuliani, A.; Paté, F.; Sarni-Manchado, P. *Anal. Bioanal. Chem.* **2010**, *398*, 815–822.
11. Cala, O.; Pinaud, N.; Simon, C.; Fouquet, E.; Laguerre, M.; Dufourc, E.; Pianet, I. *FASEB J.* **2010**, *24*, 4281–4290.
12. Hagerman, A. E.; Butler, L. G. *J. Biol. Chem.* **1981**, *256*, 4494–4497.
13. Boze, H.; Marlin, T.; Durand, D.; Pérez, J.; Vernhet, A.; Canon, F.; Sarni-Manchado, P.; Cheynier, V.; Cabane, B. *Biophys. J.* **2010**, *99*, 656–665.
14. Pascal, C.; Poncet-Legrand, C.; Imberty, A.; Gautier, C.; Sarni-Manchado, P.; Cheynier, V.; Vernhet, A. *J. Agric. Food Chem.* **2007**, *55*, 4895–4901.
15. Canon, F.; Ballivian, R.; Chirot, F.; Antoine, R.; Sarni-Manchado, P.; Lemoine, J. r. m.; Dugourd, P. *J. Am. Chem. Soc.* **2011**, *133*, 7847–7852.
16. Pascal, C.; Paté, F.; Cheynier, V.; Delsuc, M.-A. *Biopolymers* **2009**, *91*, 745–756.
17. Canon, F.; Paté, F.; Meudec, E.; Marlin, T.; Cheynier, V.; Giuliani, A.; Sarni-Manchado, P. *Anal. Bioanal. Chem.* **2009**, *395*, 2535–2545.
18. Cala, O.; Dufourc, E.; Fouquet, E.; Manigand, C.; Laguerre, M.; Pianet, I. *Langmuir* **2012**, *28*, 17410–17418.
19. Charlton, A. J.; Baxter, N. J.; Lilley, T. H.; Haslam, E.; McDonald, C. J.; Williamson, M. P. *FEBS Lett.* **1996**, *382*, 289–292.
20. Charlton, A. J.; Baxter, N. J.; Lokman Khan, M.; Moir, A. J. G.; Haslam, E.; Davies, A. P.; Williamson, M. P. *J. Agric. Food Chem.* **2002**, *50*, 1593–1601.
21. Canon, F.; Paté, F.; Cheynier, V.; Sarni-Manchado, P.; Giuliani, A.; Pérez, J.; Durand, D.; Li, J.; Cabane, B. *Langmuir* **2013**, *29*, 1926–1937.
22. Baxter, N. J.; Lilley, T. H.; Haslam, E.; Williamson, M. P. *Biochemistry* **1997**, *36*, 5566–5577.
23. Canon, F.; Milosavljević, A. R.; van der Rest, G.; Réfrégiers, M.; Nahon, L.; Sarni-Manchado, P.; Cheynier, V.; Giuliani, A. *Angew. Chem., Int. Ed.* **2013**, *52*, 8377–8381.
24. Pascal, C.; Bigey, F.; Ratomahenina, R.; Boze, H.; Moulin, G.; Sarni-Manchado, P. *Protein Expr. Purif.* **2006**, *47*, 524–532.
25. Bari, S.; Gonzalez-Magana, O.; Reitsma, G.; Werner, J.; Schippers, S.; Hoekstra, R.; Schlatholter, T. *J. Chem. Phys.* **2011**, *134*, 024314–024319.
26. Giuliani, A.; Milosavljevic, A. R.; Canon, F.; Nahon, L. *Mass Spectrom. Rev.* **2014**, *33*, 424–441.
27. Simon, C.; Barathieu, K.; Laguerre, M.; Schmitter, J. M.; Fouquet, E.; Pianet, I.; Dufourc, E. J. *Biochemistry* **2003**, *42*, 10385–10395.
28. Chatterjee, A.; Kumar, A.; Chugh, J.; Srivastava, S.; Bhavesh, N. S.; Hosur, R. V. *J. Chem. Sci.* **2005**, *117*, 3–21.
29. Haslam, E. *J. Nat. Prod.* **1996**, *59*, 205–215.
30. Fuxreiter, M.; Simon, I.; Friedrich, P.; Tompa, P. *J. Mol. Biol.* **2004**, *338*, 1015–1026.
31. Tarascou, I.; Barathieu, K.; Simon, C.; Ducasse, M. A.; Andre, Y.; Fouquet, E.; Dufourc, E. J.; de Freitas, V.; Laguerre, M.; Pianet, I. *Magn. Reson. Chem.* **2006**, *44*, 868–880.
32. Ricardo da Silva, J. M.; Rigaud, J.; Cheynier, V.; Cheminat, A.; Moutounet, M. *Phytochemistry* **1991**, *30*, 1259–1264.
33. Giuliani, A.; Jamme, F.; Rouam, V.; Wien, F.; Giorgetta, J. L.; Lagarde, B.; Chubar, O.; Bac, S.; Yao, I.; Rey, S.; Herbeaux, C.; Marlats, J. L.; Zerbib, D.; Polack, F.; Refregiers, M. *J. Synchrotron Radiat.* **2009**, *16*, 835–841.
34. Milosavljevic, A. R.; Nicolas, C.; Gil, J. F.; Canon, F.; Refregiers, M.; Nahon, L.; Giuliani, A. *J. Synchrotron Radiat.* **2012**, *19*, 174–178.
35. Giuliani, A.; Yao, I.; Lagarde, B.; Rey, S.; Duval, J. P.; Rommeluere, P.; Jamme, F.; Rouam, V.; Wein, F.; De Oliveira, C.; Ros, M.; Lestrade, A.; Desjardins, K.; Giorgetta, J. L.; Laprevote, O.; Herbaux, C.; Refregiers, M. *J. Synchrotron Radiat.* **2011**, *18*, 546–549.
36. Strohalm, M.; Kavan, D.; Novák, P.; Volný, M.; Havlíček, V. *Anal. Chem.* **2010**, *82*, 4648–4651.

Publication n°10: Aggregation of the salivary proline-rich protein IB5 in the presence of the tannin EgCG.

Canon, F.; Paté, F.; Cheynier, V.; Sarni-Manchado, P.; Giuliani, A.; Pérez, J.; Durand, D.; Li, J.; Cabane, B.

Langmuir **2013,** *29 (6), 1926-1937.*

Langmuir

Article

pubs.acs.org/Langmuir

Aggregation of the Salivary Proline-Rich Protein IB5 in the Presence of the Tannin EgCG

Francis Canon,[†,‡] Franck Paté,[§] Véronique Cheynier,[§] Pascale Sarni-Manchado,[§] Alexandre Giuliani,[†,⊥] Javier Pérez,[¶] Dominique Durand,[&] Joaquim Li,[#] and Bernard Cabane*[,#]

[†]DISCO beamline, Synchrotron Soleil, l'Orme des Merisiers, 91192 Gif sur Yvette, France

[‡]INRA, UMR1324 Centre des Sciences du Goût et de l'Alimentation, F-21000 Dijon, France

[§]INRA, UMR1083 Sciences pour l'Oenologie, F-34060 Montpellier, France

[⊥]UAR 1008, CEPIA, INRA, BP 71627, F-44316 Nantes, France

[¶]SWING beamline, Synchrotron SOLEIL, BP 48, 91192 Gif-sur-Yvette, France

[&]IBBMC, CNRS UMR 8619, Université Paris-Sud, 91405 Orsay, France

[#]PMMH, CNRS UMR 7636, Université Pierre et Marie Curie, Université René Diderot, ESPCI, 10 rue Vauquelin, 75231 Paris cedex 05, France

Supporting Information

ABSTRACT: In the mouth, proline-rich proteins (PRP), which are major components of stimulated saliva, interact with tannins contained in food. We report in vitro interactions of the tannin epigallocatechin gallate (EgCG), with a basic salivary PRP, IB5, studied through electrospray ionization mass spectrometry (ESI-MS), small-angle X-ray scattering (SAXS), and dynamic light scattering (DLS). In dilute protein (IB5) solutions of low ionic strength (1 mM), the proteins repel each other, and the tannins bind to nonaggregated proteins. ESI-MS experiments determine the populations of nonaggregated proteins that have bound various numbers of tannin molecules. These populations match approximately the Poisson distribution for binding to $n = 8$ sites on the protein. MS/MS experiments confirm that complexes containing $n = 1$ to 8 EgCG molecules are dissociated with the same energy. Assuming that the 8 sites are equivalent, we calculate a binding isotherm, with a binding free energy $\Delta\mu = 7.26RT_a$ ($K_d = 706\ \mu$M). In protein solutions that are more concentrated (0.21 mM) and at higher ionic strength (50 mM, pH 5.5), the tannins can bridge the proteins together. DLS experiments measure the number of proteins per aggregate. This number rises rapidly when the EgCG concentration exceeds a threshold (0.2 mM EgCG for 0.21 mM of IB5). SAXS experiments indicate that the aggregates have a core−corona structure. The core contains proteins that have bound at least 3 tannins and the corona has proteins with fewer bound tannins. These aggregates coexist with nonaggregated proteins. Increasing the tannin concentration beyond the threshold causes the transfer of proteins to the aggregates and a fast rise of the number of proteins per aggregate. A poisoned growth model explains this fast rise. Very large cationic aggregates, containing up to 10 000 proteins, are formed at tannin concentrations (2 mM) slightly above the aggregation threshold (0.2 mM).

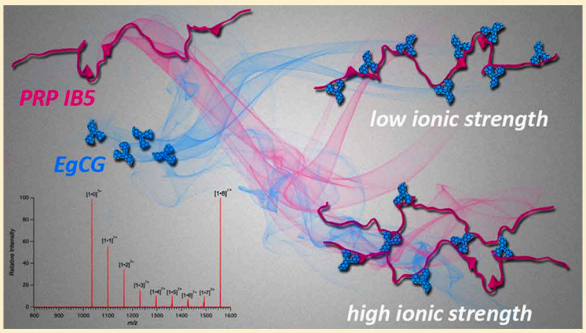

INTRODUCTION

About 25% of all proteins in higher eukaryotic organisms are intrinsically disordered proteins (IDPs), i.e. they lack well-structured 3D conformation and do not form a compact globular structure but instead populate dynamic conformational ensembles.[1−5] This is a consequence of their peculiar sequences, which have sometimes a bias toward charged and polar amino acids and away from bulky hydrophobic residues, and often a low sequence complexity with repeated short amino acid sequences.[6] Despite their lack of a well-defined 3D conformation, IDPs perform a variety of essential functions that are related to their lack of ordered conformations.[1−5]

Salivary proline-rich proteins (PRPs), which constitute about two-thirds of proteins secreted by the human parotid gland, have this type of sequence signature.[6−8] Salivary PRPs are divided into acidic and basic types that contain repeated sequences with high proportions of Pro, Gly, and Glu or Gln residues, respectively.[8−10] Despite their structural similarities, they have different functions. While acidic PRPs also bind to hydroxyapatite, the only described function of basic PRPs is to

Received: October 21, 2012
Revised: January 6, 2013
Published: January 8, 2013

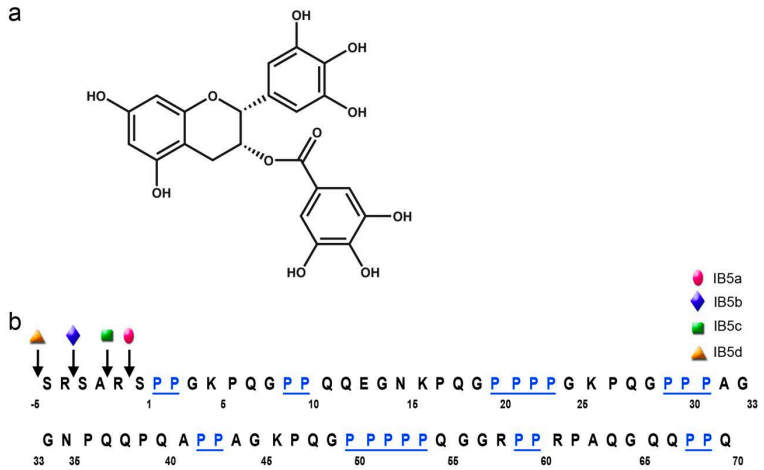

Figure 1. (a) Molecular structure of the tannin EgCG and (b) sequence of the salivary protein IB5.

bind tannins and protect the organism against their antinutritional effects.[9,10]

Tannins are phenolic compounds ubiquitous in plants and plant-derived products, known to reduce protein assimilation, because they bind digestive enzymes and dietary proteins.[9−13] The protective role of PRPs against dietary tannins may take place through either of two distinct mechanisms: (a) capture of tannins that thus become unable to inhibit digestive enzymes[9−13] and (b) astringency, a tactile perception in the mouth that signals an excessive concentration of tannins.[13−21] There is a debate regarding the mechanism of astringency.[18,19] The most generally accepted view is that it results from tannin aggregation with salivary proteins, causing a loss in the lubricating power of saliva.[10,17,20−23] An alternative hypothesis is that tannins act on receptors in the mucosa, like other primary tastes such as sourness or bitterness.[24−26] However, astringency increases upon repeated exposure, in contrast to taste sensations,[20] suggesting that it involves mechanical rather than chemosensory (gustatory) processes. Moreover astringency perception occurs on nongustatory mucosal surfaces and requires tissue movement to be perceived,[21] in agreement with a tactile mechanism involving an increase of in-mouth friction.

The present work explores the interactions of a common tannin, epigallocatechin gallate (EgCG), with a recombinant human salivary basic PRP, IB5. The sequence of IB5 and the structure of EgCG are shown in parts a and b of Figure 1. EgCG is a multidentate ligand able to bridge two proteins.[27] SAXS experiments have shown that IB5 takes unusually extended conformations compared to other IDPs.[28] Circular dichroism and NMR have given indications of disordered structures with short polyproline II helical sections that serve as anchorage for the binding of EgCG.[29] Studies of EgCG-IB5 interaction by dynamic light scattering, microcalorimetry, and circular dichroism led to the proposal of a three-stage mechanism involving binding of tannins to proteins, aggregation of the proteins when the tannin/protein molar ratio exceeds a threshold, and precipitation at still higher molar ratios.[30]

In the present work we address the following questions: (1) How strongly do EgCG molecules bind to IB5, how many binding sites are there on each protein, and what is the distribution of EgCG on these sites? (2) How many tannins are needed to cause aggregation of the proteins, what is the average number of proteins per aggregate, and what is the structure of these aggregates?

The answers to these questions should provide a microscopic basis for understanding the physiological functions of proline-rich proteins, particularly the phenomena that take place in the mouth upon ingestion of tannin-rich foods or drinks.

Addressing these questions is challenging because IB5 has several binding sites leading to complex mixtures composed of IB5•EgCG complexes with several stoichiometries that may then react with each other. We used an approach combining mass spectrometry (MS), small-angle X-ray scattering (SAXS), and dynamic light scattering (DLS). At first we sorted out the single-protein complexes using MS. Indeed, MS distinguishes the different noncovalent complexes that coexist in solution.[31,32] Its performance in PRP−tannin interactions has been previously demonstrated.[33−37] Then we used SAXS to determine the conformations of the complexes, the structures of the aggregates, and their relative compositions. Finally we used DLS to determine the mass of protein per aggregate.

These phenomena depend on the concentrations of the various species. We note T the molar concentration of tannins (EgCG) in a solution, of which T_{bound} are bound to proteins and $T_{free} = T - T_{bound}$ remain free in solution. We note P the total protein concentration, of which $P_{solution}$ are nonaggregated proteins and $P - P_{solution}$ are proteins forming multiprotein aggregates. The nonaggregated proteins comprise both free proteins and complexes made of one protein and different numbers (0, 1, 2, ...) of tannins. We note (T/P) the overall ratio of tannins to proteins in the solution, and (T_{bound}/P) the ratio of bound tannins to total proteins in the solution.

■ MATERIALS

The human salivary proline-rich protein IB5 was produced by the use of the yeast *Pichia pastoris* as a host organism and purified as previously described.[28,38] It was then freeze-dried and stored at −20 °C until use. Epigallocatechin gallate (EgCG) was purchased from Sigma (Poole, UK) and ammonium acetate from Merck (Darmstadt, Germany). The ammonium acetate 50 mM buffer was prepared in Milli-Q-purified water, acidified to pH 5.5 with acetic acid, filtered at 0.22 μm, and stored at 4 °C.

For SAXS and light scattering, filtered buffer was added to dry protein powder to yield a stock protein solution, and to EgCG powder to yield a stock tannin solution; both solutions were filtered again at 0.45 μm, and then centrifuged until SAXS spectra indicated that no

dx.doi.org/10.1021/la3041715 | *Langmuir* 2013, 29, 1926−1937

protein aggregates remained in the stock IB5 solution. The protein solution in buffer was prepared at twice the final protein concentration, and the tannin solution at twice the final EgCG concentration. Then equal volumes of each were mixed and agitated on a vortex to reach final concentrations. The protein concentration was determined from the SAXS intensity at $q \rightarrow 0$ (Supporting Information, section 3.1) and from the molar mass of the protein: it was 2.4 mg/mL or $P = 0.336$ mM. For MS the concentrations of the protein solutions were 0.005 and 0.05 M and an ammonium acetate 1 mM buffer acidified to pH 5.5 was used.

The compositions of the solutions were varied over ranges that overlap the physiological ranges of concentrations. The total concentration of protein in saliva is in the range 1−3.5 mg/mL. Most of these proteins originate from the parotid gland. The PRPs are a large fraction (up to 70%) of this total. The concentration of IB5 used in SAXS experiments (2.4 mg/mL) was near the top of this range, and the concentrations used for MS were much below. For tannins, we know that the average concentration of EgCG in green tea is 0.27 mg/mL (0.1−1 range) or 0.590 mM (0.2−2 range). The SAXS and DLS experiments were performed in this range. The pH was slightly lower than that of stimulated saliva, which is comprised between 5.8 and 7.2,[39] as is the case when drinking wine or fruit juice. As the isoelectric point of IB5 is 11.2, the charge state of IB5 is expected to be the same in saliva and in our buffer. The ionic strength used is comprised in the saliva natural variations.[40]

METHODS

At low protein concentration (0.005 and 0.050 mM) and low ionic strengths (1 mM) we observed the IB5•EgCG complexes using electrospray ionization mass spectrometry (ESI-MS) and confirmed their identity by tandem mass spectrometry (MS/MS) using a collision gas to activate precursor ions. At higher protein concentrations (0.21 to 0.42 mM) and high ionic strength (50 mM) we observed protein aggregation through dynamic light scattering (DLS) and small angle X-ray scattering (SAXS).

Mass spectrometry experiments were realized by using a linear ion-trap mass spectrometer (LTQ XL, Thermo Electron, San Jose, CA, USA) and a hybrid quadrupole time-of-flight (Q-TOF) Qstar Pulsar i mass spectrometer (ABSciex, Framingham, MA). Both instruments are equipped with an ESI ion source [56]. The solutions were infused directly into the mass spectrometer at a flow rate of 4 μL/min in the positive ion mode. The mass spectrometer parameters were optimized to transfer the noncovalent complexes from the solution to the gas phase. The source voltage and tube lens voltage of the ion trap were set at 4.2 kV and 100 V, respectively, while the heated capillary temperature was set at 200 °C and the sheath gas flow rate at 20. The following parameters were used on the Q-TOF: the source voltage was set to 5.8 kV in positive ion mode, the declustering potential at 47 V, the focusing potential at 209 V, the declustering potential 2 at 17 V, the ion source gas 1 set at 22, the ion source gas 2 at 0, the curtain gas at 10, and the capillary was not heated up. Mass spectra were studied by using *mMass* software and Igor Pro (Wavemetrics, Portland, OR).

MS/MS experiments have been performed with use of both mass spectrometers. However, experiments with the ion-trap have been realized to confirm ion identification, while the Q-TOF has been used to establish the dissociation curves of the noncovalent complexes. For MS/MS experiments with the ion-trap, collision-induced dissociation (CID) was performed with helium as collision gas. Precursor ions were activated during 30 ms and at a percentage of normalized collision energy (% NCE) giving enough dissociation for ion identification. During MS/MS experiments in the Q-TOF, nitrogen was used as collision gas in the collision cell (Linac) with a CAD gas setting of 5. The collision-set energy voltage V_c was increased from 0 to 50 V. The kinetic energy of the precursor ion in the laboratory frame of reference is $E_{Lab} = zeV_c$, where z is the number of charges on the ion and e is the charge of an electron.

SAXS experiments were performed with the SWING beamline at the synchrotron SOLEIL. The incident beam energy was 12.0 keV (wavelength 1.033 Å), the distance from the sample to the Aviex CCD detector was 1, 2, and 5 m, and the scattering vector q ranged from 0.002 to 1 $Å^{-1}$. Experiments were performed at 20 °C. Several successive frames (typically 10) of 0.5 s each were recorded for both sample and solvent. We checked that X-rays did not damage the proteins by comparing successive frames. The average intensity and experimental error of each set of frames were subsequently computed. Scattering from the solvent was measured and subtracted from the corresponding intensity of protein + tannin solution. DLS experiments were performed with a Malvern Nano ZS instrument, using 2 μL scattering cells.

RESULTS

Visual Observations and Light Scattering. *Visual Observations.* Immediately after mixing tannin (EgCG) solutions and protein (IB5) solutions, the samples were examined visually. For solutions made at high ionic strength (50 mM buffer), a slight turbidity was observed whenever the tannin concentration was above 1 mM, indicating that extensive aggregation took place. Precipitation was observed at 2 mM EgCG. Over times of the order of a day, the turbidity increased further, went through a maximum, and then decreased. On the other hand, there was no turbidity in samples made at low ionic strength (in 1 mM buffer). Also, we did not observe any aggregation in pure EgCG solutions at concentrations up to 2 mM and beyond. To obtain more precise and quantitative data on these aggregation processes, we used light scattering.

Light Scattering from Protein + Tannin Solutions. DLS experiments were performed to determine the number of proteins per aggregate. The solutions were made in the 50 mM buffer with $P = 0.21$ and 0.42 mM protein and $T = 0.05$ to 2.18 mM EgCG. Figure 2 presents the scattered intensities measured right after mixing, normalized by the intensity of a pure protein solution as follows. First the value of intensity/protein

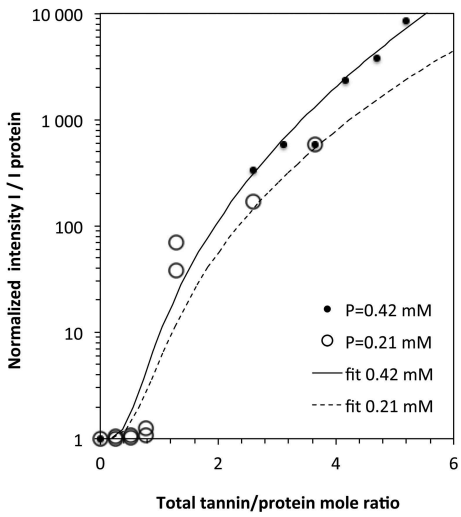

Figure 2. Light scattering by solutions of protein IB5 and tannin EgCG in the acetate buffer. The intensity values have been normalized by the intensity scattered by a pure protein solution of the same protein concentration P. The large values of the normalized intensities are from protein aggregates. The aggregation starts at a threshold in tannin concentration $T = 0.2$ mM. Beyond this threshold, the normalized intensity grows nearly exponentially with T. The lines are theoretical predictions from a model in which dense aggregates have a core made of proteins that have bound at least 3 tannins each, and a surface made of proteins that have bound fewer tannins.

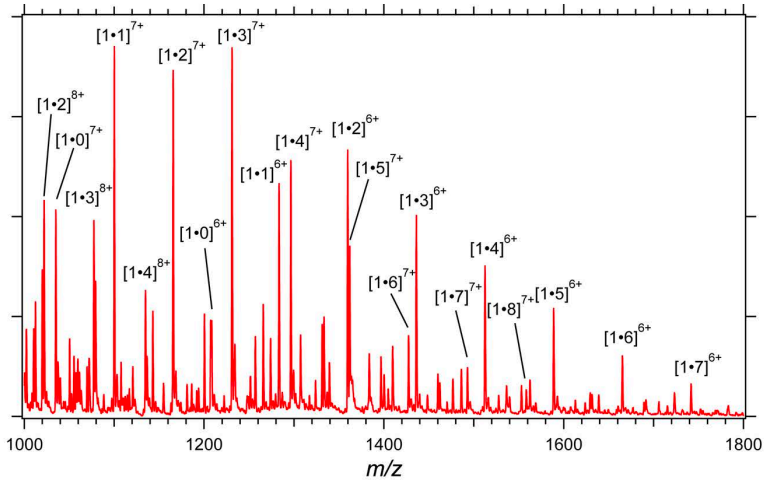

Figure 3. Positive ESI-MS spectrum of IB5 (0.05 mM)−EgCG (0.5 mM) mixture. The following caption is used $[P\bullet K]^{C+}$ with respectively P and K the number of proteins and tannins involved in the molecular and supramolecular ions and C the charge state of ions.

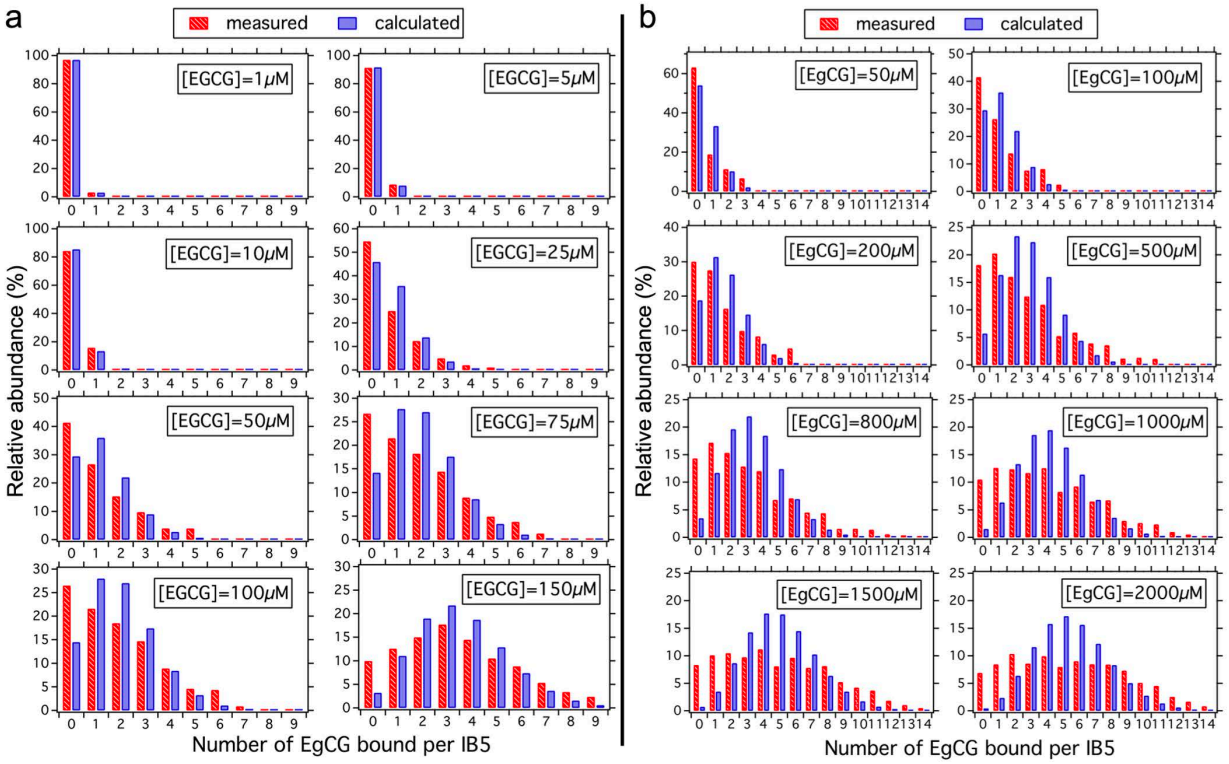

Figure 4. Distributions of bound EgCG on IB5 with (a) IB5 at 5 μM and (b) IB5 at 50 μM. Horizontal scale: number of bound tannins per protein. Vertical scale: frequencies of proteins that have respectively 0, 1, ..., 14 bound tannins. The red bars are the measured frequencies and the blue ones are the frequencies expected from the Poisson distribution. Each graph is for one concentration of EgCG.

concentration, I_{prot}/P, was determined for pure protein solutions and extrapolated to low protein concentrations. Then the values of I/P for the mixed protein + tannin solutions were measured and divided by that of the pure protein solution.

Three remarkable features emerged from these results. First, there was a threshold in tannin concentration T, below which the scattered intensities were practically identical with that of the pure protein solution. For solutions at P = 0.21 mM, this threshold was at T = 0.2 mM (Supporting Information, section 1.1). Then, beyond this threshold, the scattered intensities were much higher (×100 to ×10 000) than those of the pure protein solutions, and they increased nearly exponentially with the tannin concentration T. At higher protein concentrations (0.42 mM) it took more EgCG to reach the same number of proteins per aggregate. Also, the hydrodynamic radii of these aggregates

dx.doi.org/10.1021/la3041715 | *Langmuir* 2013, 29, 1926−1937

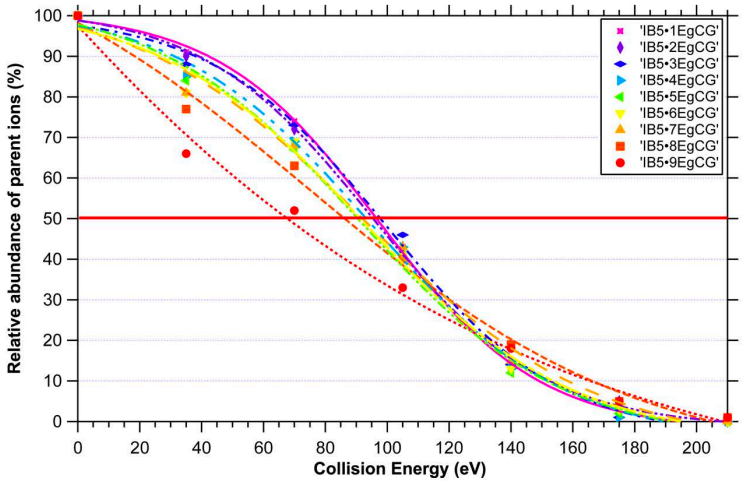

Figure 5. Dissociation curves of IB5•*k*EgCG complexes from k = 1 to 9.

were quite large, in the range 100−10000 Å (Supporting Information, section 1.3).

Kinetic Effects. At each composition, the intensity increased with time over a few hours, went through a maximum at about 4 times the initial intensity, and then decreased. The kinetics of restructuring was faster for lower EgCG concentrations (Supporting Information, section 1.2). At longer times, the intensity of light scattered by the aggregates decreased slowly but steadily, and the hydrodynamic diameters increased, indicating that the aggregates continued to dissociate and reorganize.

Binding through Mass Spectrometry. *Mass Spectrometry Experiments.* Mass spectrometry experiments were performed in order to follow the binding of EgCG on IB5. The experiments were performed by using a buffer with a weak ionic strength (1 mM) to conserve the IB5 cationic charges and therefore prevent the aggregation.

The mass spectrum obtained by electrospraying the protein solution displayed a series of protonated peaks corresponding to four IB5 isoforms (a, 6923.70 Da; b, 7238.60 Da; c, 7080.60 Da; d, 7481.80 Da) with charge states ranging from +5 to +10 (Supporting Information, section 2.1). We performed two series of experiments using solutions containing respectively 0.005 and 0.05 mM IB5 and tannin/protein ratios ranging from 1/5 to 40/1. Figure 3 shows the mass spectrum of the IB5−EgCG 0.05−0.5 mM mixture. Though crowded, the spectrum reveals free IB5 and IB5•*k*EgCG supramolecular complexes with several charge states. Complexes with stoichiometries ranging from k = 1 up 8 tannins can be observed on this spectrum. However, mixtures having higher tannin concentration show complexes having k values up to 14. For high tannin concentration, the k value might not correspond to the number n of binding sites on IB5 as molecules of EgCG can stack on top of each other.

Distributions of Tannins on Proteins. For each mixture, the relative abundance (R) of the different species has been established via the measurement of their respective peak areas (A). Each peak area was normalized by the sum of the areas of all major species (eq 1).

$$R = \frac{A}{\sum_{i=1}^{x} A_i} \times 100 \qquad (1)$$

As free IB5 and IB5•*kEgCG* complexes have different charge states, their relative abundance is the sum of the relative abundances of all charge states. The concentrations of bound and free EgCG were subsequently calculated knowing the IB5 concentration. Figure 4 shows the relative frequencies of proteins that have respectively 0, 1, ..., 14 bound EgCG molecules.

These populations can be compared with those expected for a purely statistical distribution of the EgCG molecules on independent and equivalent binding sites. Accordingly, if N_P proteins capture λN_P EgCG molecules, where $\lambda = T_{bound}/P$ is the average number of bound tannins per protein, the relative populations $f(k)$ of proteins that have captured k EgCG are given by the Poisson distribution:

$$f(k) = \frac{\lambda^k \exp(-\lambda)}{k!} \qquad (2)$$

We know the values of the binding ratio λ for each ESI/MS experiment, hence we can calculate the expected population distribution $f(k)$ according to eq 2, and compare it with the measured distribution. This comparison is presented in Figure 4.

Study of the IB5•EgCG Complexes through Tandem Mass Spectrometry Experiments. As molecules of EgCG can stack on each other, the stoichiometries of IB5•*k*EgCG complexes cannot correspond to the number of binding sites. To determine the number of EgCG binding sites on IB5, we have performed CID MS/MS experiments using a Q-TOF. The IB5•kEgCG complexes from k = 1 to 9 have been selected and then activated by collision with a neutral gas (azote). For each complex, the collision energy was progressively increased until the full dissociation of the precursor ions. The relative intensity of the precursor ions was plotted against the collision energy giving the dissociation curves of each complex (Figure 5). The curves were fitted by using a Boltzmann sigmoidal function. From the curves, the collision energy at which half of the precursor ions are dissociated (E50) was determined to compare the stability of the complexes. IB5•kEgCG complexes from k = 1 to 8 present similar E50, while IB5•9EgCG complexes exhibit a smaller value. This observation indicates that above 8 tannins bound on IB5 a different type of

dx.doi.org/10.1021/la3041715 | *Langmuir* 2013, 29, 1926−1937

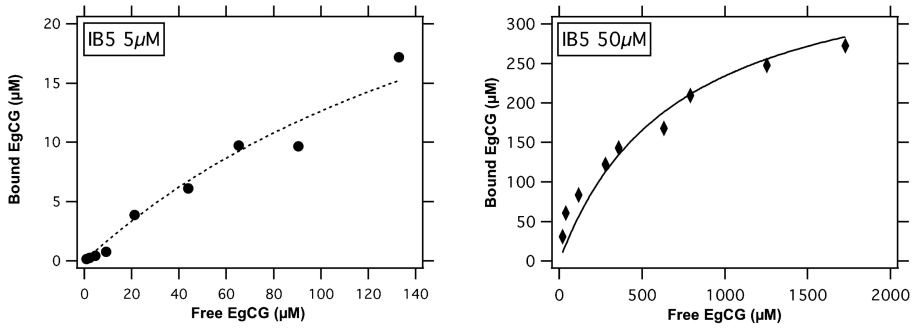

Figure 6. Binding isotherms of the tannins (EgCG) on the proteins (IB5, concentration P). Horizontal scales: concentration of free tannins T_{free} in μM. Vertical scales: concentration of bound tannins T_{bound}. Left: P = 0.005 mM. The data (dots) are fitted by the Langmuir model (dashed line) with n = 8 binding sites per protein and a binding energy $\Delta\mu_2 = 8.44RT_a$. Right: P = 0.05 mM. The data (diamonds) are fitted by the Langmuir model (solid line) with n = 8 binding sites per protein and a binding energy $\Delta\mu_2 = 7.26RT_a$.

interaction, which is more labile, is involved. This second type of interaction could be the stacking of tannins.

Binding Isotherms. From the relative frequencies of proteins that have bound 1, 2, ..., 14 tannins, we have calculated the concentration T_{bound} of bound tannins, and then the concentration of free tannins $T_{free} = T - T_{bound}$.[41,42] These concentrations are presented in Figure 6.

The Langmuir model is the simplest way to describe the binding equilibrium of small molecules to a set of identical independent sites located on a macromolecule.[43] This model has two parameters, which are the concentration T_{free} of free tannins in the solution and the binding free energy per mole of bound tannins, $\Delta\mu_{free\text{-}bound}$, normalized by the energy of thermal agitation, RT_a. The equilibrium condition yields the fraction X_{bound} of sites on the proteins that are occupied by bound tannins:

$$X_{bound} = \frac{T_{bound}}{nP} = \frac{KT_{free}}{KT_{free} + 1}$$
$$\text{with } K = \exp\left(\frac{\Delta\mu_{free-bound}}{RT_a}\right) \quad (3)$$

This is a relation between T_{bound} and T_{free}, with parameters n, P, and K. We know the actual values of the concentrations T_{bound} and T_{free} from the MS experiments. Consequently we can search which values of n and K reproduce the actual relation between T_{bound} and T_{free}. The fit of the data shown in Figure 6 yields n = 8 and $\Delta\mu/RT_a$ = 8.44 or K = 0.216 mM for the solution with P = 0.005 mM protein, and n = 8 and $\Delta\mu/RT_a$ = 7.26 or K = 0.706 mM for the solution with P = 0.05 mM protein. The fact that the parameters n and $\Delta\mu$ are so similar in both cases suggests that the Langmuir model is appropriate, i.e., the binding sites are independent and they have similar free energies.

Small Angle X-ray Scattering. *Aggregation of IB5 Caused by EgCG.* SAXS experiments were performed in order to study protein aggregation that occurred at higher ionic strength (50 mM acetate buffer), for the more concentrated protein solutions (P = 0.336 mM), in the presence of tannins (T = 0.2 to 4 mM). Two series of experiments were done at different times after the preparation of the solutions: 17 h at 10 °C for the first set of samples (presented below), and 6 h at 20 °C for the second set (Supporting Information, section 3.7), i.e., about the time of the maximum intensity according to light scattering. In both cases SAXS experiments were performed at 20 °C. Both series gave very similar results.

Figure 7 presents the SAXS spectra for a series of solutions containing a fixed protein concentration (P = 0.336 mM) and

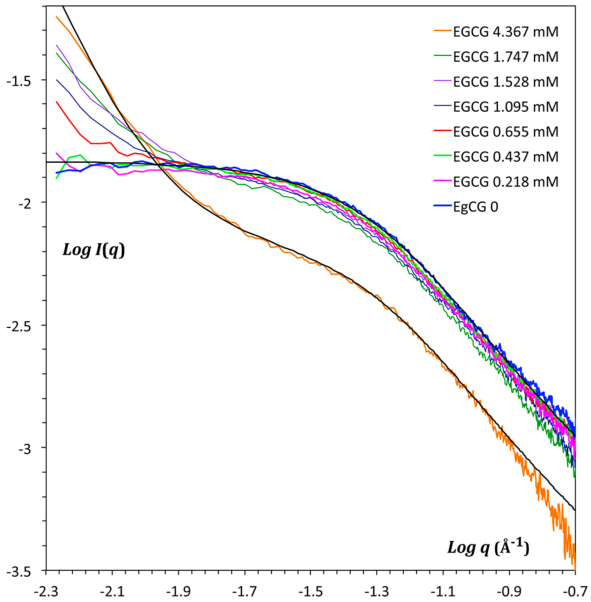

Figure 7. SAXS spectra from samples with the same protein concentration (P = 0.336 mM) but different tannin concentrations (indicated in the figure). The scattering at $q > 0.01$ Å^{-1} is mainly from nonaggregated proteins. The excess scattering at $q < 0.01$ Å^{-1} signals the presence of dense protein aggregates. The spectrum of the solution containing proteins only (blue line) is fitted by the theoretical scattering curve for worm-like chains with parameters given in Table 1. A linear combination of nonaggregated proteins and large dense aggregates fits all other spectra. These samples were equilibrated for 17 h at 10 °C (see also the Supporting Information, section 3.7, for other equilibration times).

increasing concentrations of tannins (T = 0 to 4.36 mM). The high-q part of these spectra ($q > 0.01$ Å^{-1}) is slowly varied with q (slower than q^{-2}); we argue below that it is characteristic of nonaggregated proteins with highly extended conformations.[28] The low-q part ($q < 0.01$ Å^{-1}, dimensions $r > 600$ Å) has a fast variation with q (close to q^{-3}), which signals the presence of

dx.doi.org/10.1021/la3041715 | Langmuir 2013, 29, 1926–1937

very large objects, i.e., aggregates. In this q range the intensities rise rapidly with EgCG concentration when it exceeds T = 0.5 mM.

Conformations of Proteins with Bound Tannins. We found that each spectrum could be fitted by a linear combination of the scattering from aggregates (first term) and that from nonaggregated proteins in solution (second term):

$$I(q) = CK(q) + DH(q) \tag{4}$$

The following analysis aims to reproduce the complete set of spectra with the smallest number of parameters, while keeping these parameters meaningful. Regarding the first term, we found that all $K(q)$ functions can be approximated by power laws with the same exponent $-d_f = -3$. Since we do not know precisely the aggregates sizes, $K(q)$ is an empirical function chosen to match the scattering, and C is proportional to the concentration of aggregates.

Regarding the second term, it must contain contributions from proteins that have bound either 0, 1, 2, ... or k tannins:

$$H(q) = f_0 H_0(q) + f_1 H_1(q) + \ldots + f_k H_k(q) \tag{5}$$

The frequencies f_k can be deduced from the MS results, and the form factors $H_k(q)$ could be calculated for thick worm-like chains similar to the pure protein in solution, but taking into account the contribution of the bound tannins. However, the number of parameters of this model would be excessively large. Indeed, it takes 3 parameters to describe each form factor, so that if the solution contained proteins with, say, 0, 1, 2, 3, and 4 bound tannins, it would take 15 parameters to determine the second term of eq 5. The precision of the data does not warrant this. We notice that the spectra obtained at different compositions are nearly identical at high q values (Figure 7). Therefore, at each composition, we can use a single form factor $H(q)$, calculated for a thick worm-like chain with a persistence length, as we did previously for the pure protein solutions,[28] and a single coefficient D (discussed in the next section):

$$\frac{H^{SB}(q)}{H^{SB}(q \to 0)} = g(x) + \frac{b}{L}\left[\frac{4}{15} + \frac{7}{15x} - \left(\frac{11}{15} + \frac{7}{15x}\right)\exp(-x)\right] \tag{6}$$

$$g(x) = 2(e^{-x} + x - 1)/x^2 \tag{7}$$

where x is equal to $(q^2Lb)/6$, b is the length of the statistical element, and L is the contour length of the chain.[28] Finally we take into account the thickness of the worm-like chain through a factor that depends on the radius R_c of its cross section:

$$H(q) = H^{SB}(q)\exp\left(\frac{-q^2 {R_c}^2}{2}\right) \tag{8}$$

Figure 8 shows the fits to two spectra according to eqs 4–8, with the parameters C, D, L, b, and R_c adjusted for each spectrum (as in Figure 7). The spectra are from a solution at low EgCG concentration (T = 0.437 mM) and a solution at high EgCG concentration (T = 1.747 mM). They are plotted in the Kratky representation, $q^2I(q)$ vs q, which enhances the effects of structural differences between chains with different numbers of bound tannins. The other spectra have been fitted in the same way. Table 1 lists the values of the structural parameters extracted from all such fits. Only one of these parameters has systematic variations: as the number of bound tannins per protein increases, the chains become thicker (larger cross-section). This makes sense, since the tannins have a high contrast and are bound as side groups of the main polypeptide chain.

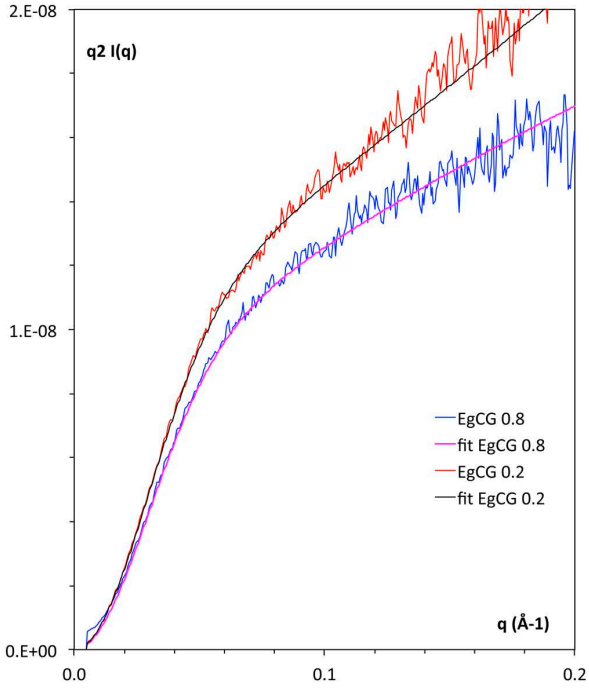

Figure 8. SAXS spectra of IB5–EgCG solutions, plotted in the Kratky representation, $q^2I(q)$ vs q. This representation enhances the high q part of the spectra, where the scattering originates from nonaggregated proteins that have remained in the solution. Upper set of data: solution containing T = 0.437 mM of the tannin EgCG and P = 0.336 mM of the salivary protein IB5. Lower set of data: T = 1.747 mM and P = 0.336 mM.

Table 1. Geometrical Parameters Used to Fit the SAXS Spectra with a "Thick Worm-Like Chain" Model[a]

T, mg/mL	T, mM	T_{bound}/P	L	b	R_g	R_c
0	0	0	207 ± 10	30 ± 1	29.2	2.7 ± 0.4
0	0	0	207 ± 10	32 ± 1	29.9	2.4 ± 0.4
0.1	0.218	0.507	207 ± 15	31 ± 2	29.6	2.7 ± 0.4
0.2	0.437	1	207 ± 15	31 ± 2	29.6	2.8 ± 0.4
0.3	0.655	1.473	207 ± 15	30 ± 2	29.2	2.9 ± 0.4
0.5	1.095	2.371	207 ± 15	29 ± 2	28.9	3.3 ± 0.4
0.7	1.528	3.168	190 ± 15	33 ± 2	28.8	3.2 ± 0.4
0.8	1.747	3.533	200 ± 15	32 ± 2	29.5	3.7 ± 0.4
2	4.367	6.124	200 ± 15	30 ± 2	28.8	3.8 ± 0.4

[a]The parameters are in Å: L, contour length of the chain, b, length of the statistical segment, R_g, overall radius of gyration, and R_c radius of the cross-section of the chain. The compositions are specified by T, total tannin concentration, and P = 0.336 mM; T_{bound}/P is the molar ratio of bound tannins to total proteins, calculated from the adsorption isotherm determined through MS. For the pure protein solutions there are slight differences with respect to the value of L given previously,[28] due to differences in the populations of the four IB5 isoforms. The two rows at T = 0 correspond to different experiments, and the differences between them give an idea of their precision.

dx.doi.org/10.1021/la3041715 | *Langmuir* 2013, 29, 1926–1937

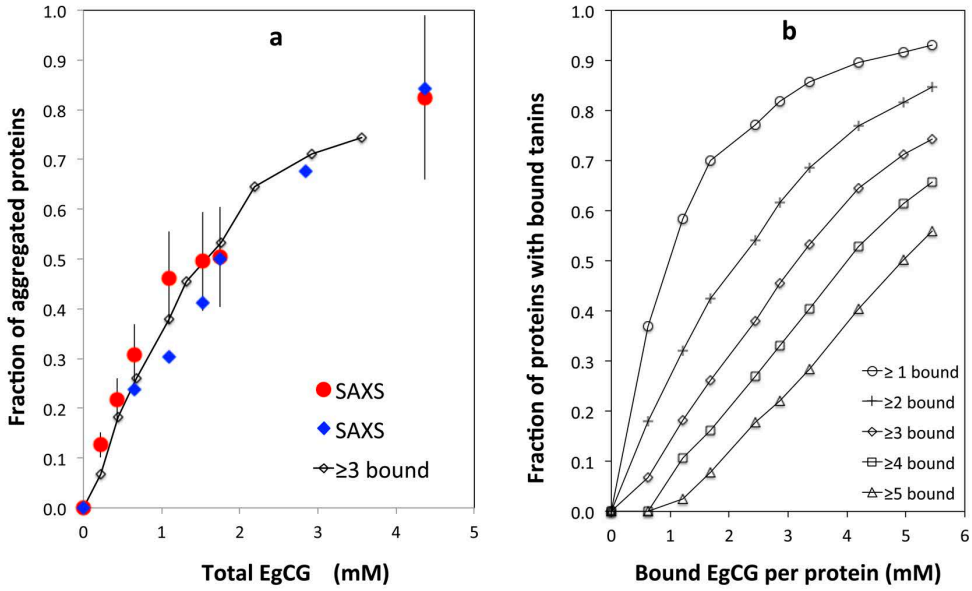

Figure 9. (a) Fraction of proteins that are aggregated, calculated from SAXS (filled dots and filled diamonds are from two experiments), and comparison with MS results from solutions that do not aggregate (open diamonds, proteins that have bound at least 3 EgCG molecules). Horizontal scale: total tannin (EgCG) concentration in mM. It is argued that it takes at least 3 tannins per protein to collapse the proteins into dense aggregates. (b) Fraction of proteins that have bound a set number of tannin molecules, from mass spectrometry. The horizontal axis is the average number of bound tannins per protein, T_{bound}/P, calculated from the Langmuir fit to the MS data.

Protein Aggregation. We calculate the fraction of nonaggregated proteins from the relative magnitude of the scattered intensities. For this purpose we extract from the worm-like chain fit (eqs 6–8) the intensity scattered by the proteins in the solution containing T tannins, and compare it with that from the pure protein solution. If proteins that have 0, 1, ..., k bound tannins coexist in the solution, the intensity scattered at $q \to 0$ by these proteins is:

$$H(T, q \to 0) = H(T = 0, q \to 0)\frac{P_{solution}}{P}\frac{\sum_{i=0}^{i=k}\alpha_i f_i}{\sum_{i=0}^{i=k} f_i} \quad (9)$$

where $P_{solution}$ is the concentration of nonaggregated proteins in the solution, $H_i(q\to0)$ is the intensity extrapolated to $q \to 0$ from proteins that have bound i tannins, f_i is the fraction of such proteins, from MS, and α_i is the ratio of scattered intensity between a protein that has bound i tannins and a protein that has none (Supporting Information, sections 3.1 to 3.4):

$$\alpha_i = \frac{H_i(q \to 0)}{H_0(q \to 0)} = \left[1 + i\frac{\nu_t \Delta\rho_t}{\nu_p \Delta\rho_p}\right]^2 \quad (10)$$

where ν_t is the volume of a tannin and ν_p is that of a protein, and $\Delta\rho_t$ is the scattering density of a tannin and $\Delta\rho_p$ is that of a protein. Thus we extract $P_{solution}/P$ from eqs 9 and 10 and obtain the fraction of aggregated proteins as $1 - P_{solution}/P$ (Supporting Information, sections 3.5 to 3.9). The variation of this fraction is presented in Figure 9a and Table 2, as a function of the total tannin concentration. At this point we note that adding 0.2 mM EgCG is enough to aggregate a significant fraction of the proteins, in agreement with the light-scattering result (Figure 2).

Kinetics of Aggregation and Dissociation. Similar sets of SAXS spectra were obtained at different times after mixing the protein solutions with the tannin solution (Figure 8, Supporting Information). In all cases, a linear combination of nonaggregated proteins and dense aggregates fits all spectra, according to eqs 4–10. The amounts of aggregated proteins were highest at short times after mixing. At very long times, on the order of a day, all these aggregates were found to dissociate spontaneously to some extent, as also observed through DLS (Supporting Information, section 1.2).

Table 2. Concentrations of Aggregated and Nonaggregated Proteins According to SAXS Data[a]

T, mM	T_{free}, mM	T_{bound}, mM	T_{bound}/P	$P_{aggregated}$, mM	$P_{solution}$, mM
0	0	0	0	0.000	0.336
0.218	0.048	0.170	0.51	0.043	0.293
0.437	0.101	0.336	1.00	0.073	0.263
0.655	0.160	0.495	1.47	0.103	0.233
1.095	0.298	0.797	2.37	0.155	0.181
1.528	0.463	1.065	3.17	0.166	0.170
1.747	0.559	1.188	3.53	0.169	0.167
4.367	2.309	2.058	6.13	0.277	0.059

[a] T is the total tannin concentration (EgCG). T_{free} and T_{bound} are the concentrations of free and bound tannins, calculated according to the MS results. T_{bound}/P is the number of bound tannins per protein with P = 0.336 mM the total protein concentration. $P_{aggregated}$ is the concentration of aggregated proteins and $P_{solution}$ the concentration of nonaggregated proteins, both calculated by fitting the experimental spectra according to eqs 4–10.

DISCUSSION

Aggregating and Nonaggregating Solutions. The aim of this discussion is to relate binding data, obtained from MS, and structural data, obtained from SAXS and DLS. Scattering experiments have been performed in 50 mM acetate buffer, which has an ionic strength similar to that occurring in the

dx.doi.org/10.1021/la3041715 | Langmuir 2013, 29, 1926–1937

mouth. In these conditions, the cationic charges of the proteins are screened, and the proteins may aggregate through bridges created by bound EgCG molecules. The MS data were obtained under 1 mM salt added to the protein + tannin mixture, owing to the poor tolerance of electrospray ionization to salts. However, mass spectrometry has been used only to study the interaction of the ligands to proteins, which is not affected by ionic strength. The results from both sets of experiments may then be related with confidence.

The Population of Protein Aggregates. When two species combine to form aggregates, the first question is: How many different types of aggregates are there, in terms of compositions and structures? This question is quite difficult to answer, since there must be variations in the numbers of tannins (EgCG) and proteins (IB5) per aggregate, and in the resulting structures. Hence a detailed description of the ensemble of aggregates is out of reach. However, we can answer a simpler question, which is whether the collection of aggregates can be meaningfully described as a single population, or else as two coexisting populations.

The SAXS data presented in Figure 7 and the fits according to eq 4 show that the solutions contain two populations, i.e., "dense" aggregates coexisting with nonaggregated proteins. Let us first discuss the population of nonaggregated proteins. The SAXS results show that these proteins have similar conformations to the proteins in pure IB5 solutions. However, the increasing values of the cross section of the polypeptide chains (Table 1) indicate that these proteins have bound a significant number of tannin molecules. The scattered intensities have been analyzed according to a simplified model where these proteins have bound the numbers of tannins that are predicted by the adsorption isotherm. This is adequate when most proteins are still nonaggregated. We find that the population of nonaggregated proteins decays continuously with rising tannin concentrations (Table 2 and Figure 9a). This decay matches the growth of the population of proteins that have bound at least 3 tannins (determined from MS), suggesting that they vanish from the solution.

Next, we consider the population of aggregates. First we focus on the composition P = 0.336 mM, T = 0.5 mM, for which the scattering from aggregates shows up in the low-q part of the spectra (Figure 7). According to the analysis of SAXS data (Table 2), 20% of the proteins were aggregated and no longer contributed to the high-q solution scattering. We know from MS how the tannins were initially distributed on the proteins before aggregation took place: for the corresponding composition with the same concentration of free EgCG, the frequencies of proteins that have respectively 1, 2, 3, 4, 5 bound EgCG molecules are 26%, 14%, 8%, 8%, and 3% (Table V, Supporting Information). The SAXS result is recovered if it is assumed that all proteins with at least 3 bound tannins did aggregate. The same correspondence is obtained at other compositions, indicating that the proteins with at least 3 bound tannins form the aggregates.

This result is in quantitative agreement with those of Pascal et al.[29] and Poncet-Legrand et al. obtained with polyproline as a protein[30,44] and those of Charlton et al. with proline-rich peptides.[45] As EgCG is a multidentate ligand, it may form bridges between proteins within aggregates, leading to the collapse of highly connected aggregates. This is in agreement with the fractal exponent of the aggregate structure, measured by SAXS, which is d_f = 3, characteristic of dense particles. At first, this dense structure may seem to conflict with the large hydrodynamic radii measured through DLS, which grow as the square root of the mass per aggregate (rather than the cube root law expected for dense particles). This conflict is resolved by considering that the aggregates have a dense core (seen by SAXS) and a less dense corona, which controls their hydrodynamic properties measured by DLS.

A Simple Poisoned Growth Model for Calculating the Aggregate Size. Here we present a simple model of the protein + tannin aggregates, in order to calculate the number of proteins per aggregate, and predict the intensity of scattered light. This model is based on the idea that aggregates recombine (and therefore grow to larger sizes) until their surfaces are "poisoned" by unreactive species.[46] To keep the numbers of parameters to a minimum, we assume that all aggregates are identical, with the same radius and the same number of proteins. We further assume that each aggregate is made of a dense core that contains a high concentration of bridging tannins, and a corona made of proteins with few bridging tannins. Two aggregates may recombine during their collisions, if their surfaces carry enough tannin molecules to bridge them together. However, there is a large pool of proteins that carry few tannin molecules. As the aggregates grow, their surfaces capture a small fraction of these proteins, and they become unable to make permanent bonds to each other. Consequently the final sizes of aggregates are limited by the abundance of "poisons", i.e., proteins that do not carry enough tannin molecules to continue the growth process.

Consider a solution containing N proteins, with a distribution $f(k)$ of tannin molecules on these proteins. The proteins with $k > k_0$ are aggregated, and they have formed a set of N_{ag} aggregates. Let n_{core} be the number of proteins in the core of each aggregate, V_{core} the volume of this core, and V^* the volume per protein in this core. Some of the proteins with $k < k_0$ are at the aggregate surface (fraction α), but most of them are free in the bulk solution (fraction $1 - \alpha$). Let $n_{surface}$ be the number of proteins at the surface of the aggregate, A_{core} the area of the core surface, and A^* the surface area per protein in this surface layer. Let $n_{solution}$ be the number of free proteins per aggregate. The distribution of proteins must verify the following sum rules:

$$n_{core} = \frac{V_{core}}{V^*} = \frac{N}{N_{ag}}\left[1 - \sum_{k=0}^{k=k_0} f(k)\right] \tag{11}$$

$$n_{surface} = \frac{A_{core}}{A^*} = \alpha\frac{N}{N_{ag}}\left[\sum_{k=0}^{k=k_0} f(k)\right] \tag{12}$$

$$n_{solution} = (1 - \alpha)\frac{N}{N_{ag}}\left[\sum_{k=0}^{k=k_0} f(k)\right] \tag{13}$$

$$n_{core} + n_{surface} + n_{solution} = \frac{N}{N_{ag}} \tag{14}$$

For a globular aggregate, the volume and surface area are related by ${V_{core}}^2\,{A_{core}}^{-3} = 1/36\pi$, which may be rewritten as:

$$V_{core} = 36\pi\left(\frac{V_{core}}{A_{core}}\right)^3 \tag{15}$$

Hence it is easy to calculate n_{core} and $n_{surface}$

$$n_{core} = 36\pi \frac{(V^*)^2}{(\alpha A^*)^3}[\phi(k)]^3$$
$$\text{with } \phi(k) = [1 - \sum_{k=0}^{k=k_0} f(k)]/[\sum_{k=0}^{k=k_0} f(k)] \quad (16)$$

$$n_{surface} = 36\pi \frac{(V^*)^2}{\alpha^2 (A^*)^3}[\phi(k)]^2 \quad (17)$$

Beyond this point, it is necessary to obtain some information on the parameter α, which contains the information on the poisoning process. Fortunately this problem has already been studied in another context, for the poisoned growth of oil droplets in surfactant solutions.[46] The conclusions from that work are that α and n_{core} are power laws of the poisoning ratio $\phi(k)$, so that:

$$n_{core} = n_0[\phi(k)]^{\beta} \quad (18)$$

The exponent obtained for n_{core} through numerical simulation is $\beta = 2.5$.[46] To apply these predictions to the growth of protein aggregates bridged by tannin molecules, we assume that the distribution $f(k)$ is the Poisson distribution given in eq 2. With this distribution, the data are best fitted by $n_{core} + n_{surface}$ with $\alpha \ll 1$, $k_0 = 3 \pm 1$, and $\beta = 2 \pm 0.5$ (Figure 2). This power law reproduces the aggregation threshold and also provides a good fit to the rest of the data for both protein concentrations. The aggregation threshold is rather insensitive to the choice of parameters, and determined mainly by the tannin concentration at which there is a substantial frequency of proteins with at least 3 bound tannins (Figure 9b). Moreover the model reproduces well the fact that, beyond the aggregation threshold, the aggregates readily reach very large aggregation numbers. Accordingly the poisoned growth model does reproduce the aggregation of proteins by tannins.

Aggregation Followed by Dissociation. Over very long times, the mixed solutions show a slow rise in turbidity followed by an even slower decay of turbidity. The rise in turbidity may be caused by the continued recombination of aggregates, due to their Brownian collisions. Indeed the rate of increase of the intensity of scattered light matches that expected for a cluster−cluster aggregation process with a low efficiency of encounters (1 successful recombination in 3×10^6). This is not surprising, given that the proteins and tannins must be in particular configurations in order to create a bridge.

The slow dissociation observed at long times, followed by spontaneous redispersion, may be caused by a redistribution of the tannins among the available proteins. Indeed, molecular dynamics simulations of the binding of EgCG to IB5 suggest that the tannin molecules may move fairly easily along the polypeptide chain.[47] For a tannin concentration that is twice the aggregation threshold, the total number of bound tannins amounts to $T_{bound}/P = 1$ tannin per protein. If the tannins do redistribute uniformly among all proteins, there will no longer be any proteins with 3 or more bound tannins, and therefore the aggregates will dissociate, expand, and dissolve, as observed. In addition, some tannins may change their connectivity from a configuration where they bridge two distinct proteins to a configuration where they bridge two sites of the same protein. This will reduce the number of bridges holding the aggregate together and lead to dissociation and dissolution of the aggregates.

CONCLUSION

In this work we examined the binding of molecules of the tannin EgCG to a basic proline-rich salivary protein, IB5, the subsequent aggregation of the protein through bridging tannins, and the growth of the aggregates, determined by the distribution of tannins on the proteins (poisoned growth). We obtained a quantitative description of these processes, at the microscopic scale. These processes appear to be general. Thus this description could serve as a model for the interactions of other disordered proteins (e.g., other salivary proteins) with tannins or with other bridging ligands.

(1) In very dilute IB5−EgCG solutions of low ionic strength (1 mM) the proteins repel each other. In these conditions the tannins bind to individual proteins but do not cause any aggregation. Using mass spectrometry, we have determined the distribution of bound EgCG among all the proteins in solution, i.e., how many proteins have 1, or 2, or 3, ... bound EgCG molecules. This distribution is close to the Poisson (= random) distribution, thereby indicating that the sites on the protein are equivalent and independent. The number of binding sites is n = 8, which matches the number of short proline repeats on the polypeptide chain. The number of bound EgCG molecules follows a Langmuir adsorption isotherm with an equilibrium constant $K_d = 0.706$ mM, or a free energy of $7.26 \pm 0.5\ RT_a$, where RT_a is the energy of thermal agitation at 20 °C. This free energy is in between those found previously for proline-rich peptides by Charlton et al.[45] and for poly(L-proline) by Poncet-Legrand et al.[44] The differences are presumably due to the lengths of the polyproline sequences in each case.

(2) In solutions that are more concentrated and at higher ionic strength (acetate buffer 50 mM, pH 5.5), the binding of the tannins causes the protein to aggregate. DLS experiments indicate that the aggregation threshold is at a tannin concentration of 0.2 mM (with 0.21 mM protein). Comparing SAXS and MS results, we found that the proteins that have bound at least 3 EgCG molecules connect to each other through EgCG bridges and build the aggregates, in good agreement with the results of Poncet-Legrand et al.[30,44] and Charlton et al.[45] These aggregates recombine into larger ones until their growth is limited by adsorption of proteins that have bound fewer EgCG molecules, as described by the poisoned growth model. Through this process, the aggregates become quite large at concentrations that are not much higher than the threshold (up to 1000 proteins per aggregate at a total EgCG concentration of 1 mM). These results are consistent with the observation of hazes in protein−polyphenol systems.[48]

(3) The threshold for the formation of these aggregates is in a range of compositions that matches the physiological ranges: it is at 0.2 mM EgCG for 0.21 mM protein, and 0.5 mM EgCG for 0.42 mM IB5. This suggests that the aggregation of salivary proteins by tannins in the mouth could have a physiological function. An obvious function could be the regulation of the amount of free tannins in the ingested food and drinks.

(4) Another function for the aggregation of salivary proteins by tannins in the mouth could be to cause astringency. From the present results, we can find out if the ranges of concentration for the perception of astringency correlate with those where aggregation and precipitation take place. Astringency perception has been reported at EgCG concentrations in the range 0.2 mM[49] to 0.4 mM.[50] These values are remarkably close to the aggregation threshold that we found (0.2 mM EgCG in an IB5 solution of concentration 0.21 mM).

Moreover, we have demonstrated that this aggregation process readily leads to massive aggregates when tannins concentrations exceed the threshold. These cationic aggregates could then bind to the salivary film that covers the mucosa,[51] and trigger the astringency perception. Experiments on acid-treated saliva have evidenced a pathway that involves the preferential binding of tannins to acidic PRPs and statherins, which are also involved in the salivary film,[52] causing their aggregation.[53] This aggregation may then lead to a cascade of other phenomena at the colloidal scale, with involvement of the cationic *b*PRP at a later stage, and then precipitation or deposition of the cationic aggregates on the anionic mucosa. Experiments similar to those reported here but involving mixtures of 2 or more proteins could make it possible to find out which ones of these pathways are active in the mouth.

■ ASSOCIATED CONTENT

Supporting Information

Additional results including time evolution of the scattered intensities in light scattering and SAXS, mass spectra of IB5 solutions, tables of frequencies of all protein populations as determined through MS, and expressions for the scattering by proteins in solution with bound tannins. This material is available free of charge via the Internet at http://pubs.acs.org.

■ AUTHOR INFORMATION

Corresponding Author

*Email: bcabane@pmmh.espci.fr.

Notes

The authors declare no competing financial interest.

■ ACKNOWLEDGMENTS

We thank Thérèse Marlin for production and purification of protein IB5. This work was supported by grant 07-BLAN-02 "PROTANIN" from Agence Nationale de la Recherche.

■ REFERENCES

(1) Wright, P. E.; Dyson, H. J. Intrinsically Unstructured Proteins: Re-assessing the Protein Structure−Function Paradigm. *J. Mol. Biol.* **1999**, *293*, 321−331.

(2) Dunker, A. K.; Brown, C. J.; Lawson, J. D.; Iakoucheva, L. M.; Obradovic, Z. Intrinsic Disorder and Protein Function. *Biochemistry* **2002**, *41*, 6573−6582.

(3) Ward, J. J.; Sodhi, J. S.; McGuffin, L. J.; Buxton, B. F.; Jones, D. T. Prediction and Functional Analysis of Native Disorder in Proteins from the Three Kingdoms of Life. *J. Mol. Biol.* **2004**, *337*, 635−645.

(4) Uversky, V. N.; Dunker, A.K. Understanding Protein Non-Folding. *Biochim. Biophys. Acta* **2010**, *1804*, 1231−1264.

(5) Brown, C. J.; Johnson, A. K.; Dunker, A. K.; Daughdrill, G. W. Evolution and Disorder. *Curr. Opinion Struct. Biol.* **2011**, *21*, 441−446.

(6) Williamson, M. P. The Structure and Function of Proline-Rich Regions in Proteins. *Biochem. J.* **1994**, *297*, 249−260.

(7) Tompa, P. Intrinsically Unstructured Proteins Evolve by Repeat Expansion. *BioEssays* **2003**, *25*, 847−855.

(8) Carlson, D. M. Salivary Proline-Rich Proteins: Biochemistry, Molecular Biology, and Regulation of Expression. *Crit. Rev. Oral Biol. Med.* **1993**, *4*, 495−502.

(9) Bennick, A. Interaction of Plant Polyphenols with Salivary Proteins. *Crit. Rev. Oral Biol. Med.* **2002**, *13*, 184−196.

(10) Lu, Y.; Bennick, A. Interaction of Tannin with Human Salivary Proline-Rich Proteins. *Arch. Oral Biol.* **1998**, *43*, 717−728.

(11) Mehansho, H.; Butler, L. G.; Carlson, D. M. Dietary Tannins and Salivary Proline-Rich Proteins. Interactions, Induction and Defense Mechanisms. *Annu. Rev. Nutr.* **1987**, *7*, 423−440.

(12) Mehansho, H.; Ann, D. K.; Butler, L. G.; Rogler, J. C.; Carlson, D. M. Induction of Proline-Rich Proteins in Hamster Salivary Glands by Isoproterenol Treatment and Unusual Growth Inhibition by Tannins. *J. Biol. Chem.* **1987**, *262*, 12344−12350.

(13) Haslam, E. Polyphenol−Protein Interactions. *Biochem. J.* **1974**, *139*, 285−288.

(14) Haslam, E.; Lilley, T. H.; Cai, Y.; Martin, R.; Magnolato, D. Traditional Herbal Medicines − The Role of Polyphenols. *Planta Med.* **1989**, *55*, 1−8.

(15) Breslin, P. A. S.; Gilmore, M. M.; Beauchamp, G. K.; Green, B. G. Psychophysical Evidence that Oral Astringency is a Tactile Sensation. *Chem. Senses* **1993**, *18*, 405−417.

(16) Baxter, N. J.; Lilley, T. H.; Haslam, E.; Williamson, M. P. Multiple Interactions between Polyphenols and a Salivary Proline-Rich Protein Repeat Result in Complexation and Precipitation. *Biochemistry* **1997**, *36*, 5566−5577.

(17) Bate-Smith, E. C. Astringency in Foods. *Food* **1954**, *23*, 124.

(18) Freitas, V. D.; Mateus, N. Protein/Polyphenol Interactions: Past and Present Contributions. Mechanisms of Astringency Perception. *Curr. Org. Chem.* **2012**, *16*, 724−746.

(19) Bajec, M. R.; Pickering, G. J. Astringency: Mechanisms and perception. *Crit. Rev. Food Sci. Nutr.* **2008**, *48*, 858−875.

(20) Lee, C. B.; Lawless, H. T. Time Course of Astringent Sensations. *Chem. Senses* **1991**, *16*, 225−238.

(21) Rossetti, D.; Yakubov, G. E.; Stokes, J. R.; Williamson, A.-M.; Fuller, G. G. Interaction of Human whole Saliva and Astringent Dietary Compounds Investigated by Interfacial Shear Rheology. *Food Hydrocolloids* **2008**, *22*, 1068−1078.

(22) Rossetti, D.; Bongaerts, J. H. H.; Wantling, E.; Stokes, J. R.; Wiliamson, A.-M. Astringency of Tea Catechins: More than an Oral Lubrication Tactile Percept. *Food Hydrocolloids* **2009**, *23*, 1984−1992.

(23) Obreque-Slier, E.; Lopez-Solís, R.; Pena-Neira, A.; Zamora-Marín, F. Tannin-Protein Interaction is more closely Associated with Astringency than Tannin-Protein Precipitation: Experience with two Oenological Tannins and a Gelatin. *Int. J. Food Sci. Technol.* **2010**, *45*, 2629−2636.

(24) Schiffman, S. S.; Suggs, M. S.; Sostman, A. L.; Simon, S. A. Chorda Tympani and Lingual Nerve Responses to Astringent Compounds in Rodents. *Physiol. Behav.* **1992**, *51*, 55−63.

(25) Critchley, H. D.; Rolls, E. T. Responses of Primate Taste Cortex Neurons to the Astringent Tastant Tannic Acid. *Chem. Senses* **1996**, *21*, 135−145.

(26) Iiyama, S.; Ezaki, S.; Toko, K.; Matsuno, T.; Yamafuji, K. Study of Astringency and Pungency with Multichannel Taste Sensor Made of Lipid Membranes. *Sens. Actuators, B* **1995**, *24*, 75−79.

(27) Jöbstl, E.; O'Connell, J.; Fairclough, P. A.; Williamson, M. P. Molecular Model for Astringency Produced by Polyphenol/Protein Interactions. *Biomacromolecules* **2004**, *5*, 942−949.

(28) Boze, H.; Marlin, T.; Durand, D.; Perez, J.; Vernhet, A.; Canon, F.; Sarni-Manchado, P.; Cheynier, V.; Cabane, B. Proline-Rich Salivary Proteins have Extended Conformations. *Biophys. J.* **2010**, *99*, 656−665.

(29) Pascal, C.; Pate, F.; Cheynier, V.; Delsuc, M. A. Study of the Interactions Between a Proline-Rich Protein and a Flavan-3-ol By NMR: Residual Structures in the Natively Unfolded Protein Provides Anchorage Points for the Ligands. *Biopolymers* **2009**, *91*, 745−756.

(30) Pascal, C.; Poncet-Legrand, C.; Imberty, A.; Gautier, C.; Sarni-Manchado, P.; Cheynier, V.; Vernhet, A. Aggregation of a Proline-Rich Protein Induced by Epigallocatechin Gallate and Condensed Tannins: Effect of Protein Glycosylation. *J. Agric. Food Chem.* **2007**, *55*, 4895−4901.

(31) Pramanik, B. N.; Bartner, P. L.; Mirza, U. A.; Liu, Y.-H.; Ganguly, A. K. Electrospray Ionization Mass Spectrometry for the Study of Non-Covalent Complexes: an Emerging Technology. *J. Mass Spectrom.* **1998**, *33*, 911−920.

(32) Gabelica, V.; Rosu, F.; Houssier, C.; Pauw, E. D. Gas Phase Thermal Denaturation of an Oligonucleotide Duplex and its Complexes with Minor Groove Binders. *Rapid Commun. Mass Spectrom.* **2000**, *14*, 464.

(33) Sarni-Manchado, P.; Cheynier, V. Study of Noncovalent Complexation between Catechin Derivatives and Peptide by Electrospray Ionization-Mass Spectrometry (ESI-MS). *J. Mass Spectrom.* **2002**, *37*, 609−616.
(34) Simon, C.; Barathieu, K.; Laguerre, M.; Schmitter, J. M.; Fouquet, E.; Pianet, I.; Dufourc, E. J. Three-Dimensional Structure and Dynamics of Wine Tannin-Saliva Protein Complexes. A Multitechnique Approach. *Biochemistry* **2003**, *42*, 10385−10395.
(35) Canon, F.; Paté, F.; Meudec, E.; Marlin, T.; Cheynier, V.; Giuliani, A.; Sarni-Manchado, P. Characterization, Stoichiometry, and Stability of Salivary Protein-Tannin Complexes by ESI-MS and ESI MS/MS. *Anal. Bioanal. Chem.* **2009**, *395*, 2535−2545.
(36) Canon, F.; Giuliani, A.; Pate, F.; Sarni-Manchado, P. Ability of a Salivary Intrinsically Unstructured Protein to Bind Different Tannin Targets Revealed by Mass Spectrometry. *Anal. Bioanal. Chem.* **2010**, *398*, 815−822.
(37) Canon, F.; Ballivian, R.; Chirot, F.; Antoine, R.; Sarni-Manchado, P.; Lemoine, J.; Dugourd, P. Folding of a Salivary Intrinsically Unstructured Protein upon Binding to Tannins. *J. Am. Chem. Soc.* **2011**, *133*, 7847−7852.
(38) Pascal, C.; Bigey, F.; Ratomahenina, R.; Boze, H.; Moulin, G.; Sarni-Manchado, P. Overexpression and Characterization of two Human Salivary Proline Rich Proteins. *Protein Expression Purif.* **2006**, *47*, 524−532.
(39) Neyraud, E.; Heinzerling, C. L; Bult, J. H. F.; Mesmin, C.; Dransfield, E. Effects of Different Tastants on Parotid Saliva Flow and Composition. *Chemosensory Perception* **2009**, *2*, 108−116.
(40) Macakova, L.; Yakubov, G. E.; Plunkett, M. A.; Stokes, J. R. Influence of Ionic Strength on the Tribological Properties of Pre-Adsorbed Salivary Films. *Tribol. Int.* **2011**, *44*, 956−962.
(41) Daniel, J. M.; Friess, S. D.; Rajagopalan, S.; Wendt, S.; Zenobi, R. Quantitative Determination of Noncovalent Binding Interactions using Soft Ionization Mass Spectrometry. *Int. J. Mass Spectrom.* **2002**, *216*, 1−27.
(42) Greig, M. J.; Gaus, H.; Cummins, L. L.; Sasmor, H.; Griffey, R. H. Measurement of Macromolecular Binding Using Electrospray Mass Spectrometry. Determination of Dissociation Constants for Oligonucleotide: Serum Albumin Complexes. *J. Am. Chem. Soc.* **1995**, *117*, 10765.
(43) Evans, D. F.; Wennerström, H. *The Colloidal Domain: Where Physics, Chemistry, Biology, and Technology Meet*; Wiley-VCH: New York, NY, 1994; eq 2.4.14
(44) Poncet-Legrand, C.; Gautier, C.; Cheynier, V.; Imberty, A. Interactions between Flavan-3-ols And Poly(L-Proline) Studied by Isothermal Titration Calorimetry: Effect of the Tannin Structure. *J. Agric. Food Chem.* **2007**, *55*, 9235−9240.
(45) Charlton, A. J.; Baxter, N. J.; Lokman Khan, M.; Moir, A. J. G.; Haslam, E.; Davies, A. P.; Williamson, M. P. Polyphenol/Peptide Binding and Precipitation. *J. Agric. Food Chem.* **2002**, *50*, 1593−1601.
(46) Lannibois, H.; Hasmy, A.; Botet, R.; Aguerre Chariol, O.; Cabane, B. Surfactant limited aggregation of hydrophobic molecules in water. *J. Phys. II* **1997**, *7*, 319−342.
(47) Golebiowski, J.; Fiorucci, S.; Adrian-Scotto, M.; Fernandez-Carmona, J.; Antonczak, S. Molecular Features Underlying the Perception of Astringency as Probed by Molecular Modeling. *Mol. Inf.* **2011**, *30*, 410−414.
(48) Siebert, K. J.; Troukhanova, N. V.; Lynn, P. Y. Nature of Polyphenol−Protein Interactions. *J. Agric. Food Chem.* **1996**, *44*, 80−85.
(49) Scharbert, S.; Holzmann, N.; Hofmann, T. Identification of the Astringent Taste Compounds in Black Tea Infusions by Combining Instrumental Analysis and Human Bioresponse. *J. Agric. Food Chem.* **2004**, *52*, 3498−3508.
(50) Rinaldi, A.; Gambuti, A.; Moio, L. Precipitation of Salivary Proteins After the Interaction with Wine: The Effect of Ethanol, pH, Fructose, and Mannoproteins. *J. Food Sci.* **2012**, *77*, C485−C490.
(51) Macakova, L.; Yakubov, G. E.; Plunkett, M. A.; Stokes, J. R. Influence of Ionic Strength Changes on the Structure of Pre-Adsorbed Salivary Films. A Response of a Natural Multi-Component Layer. *Colloids Surf., B* **2010**, *77*, 31−39.
(52) Bradway, S. D.; Bergey, E. J.; Jones, P. C.; Levine, M. J. Oral Mucosal Pellicle. Adsorption and Transpeptidation of Salivary Components to Buccal Epithelial Cells. *Biochem. J.* **1989**, *261*, 887−896.
(53) Soares, S.; Vitorino, R.; Osorio, H.; Fernandes, A.; Venancio, A.; Mateus, N.; Amado, F.; Freitas, V. D. Reactivity of Human Salivary Proteins Families Toward Food Polyphenols. *J. Agric. Food Chem.* **2011**, *59*, 5535−5547.

Publication n°11: Retention effect of human saliva on aroma release and respective contribution of salivary mucin and a-amylase.

Pagès-Hélary, S.; Andriot, I.; Guichard, E.; Canon, F.

Food Res. Int. **2014,** *64, 424-431.*

Food Research International 64 (2014) 424–431

Contents lists available at ScienceDirect

Food Research International

journal homepage: www.elsevier.com/locate/foodres

Retention effect of human saliva on aroma release and respective contribution of salivary mucin and α-amylase

Sandy Pagès-Hélary, Isabelle Andriot, Elisabeth Guichard, Francis Canon *

INRA, UMR1324 Centre des Sciences du Goût et de l'Alimentation, F-21000 Dijon, France
CNRS, UMR6265 Centre des Sciences du Goût et de l'Alimentation, F-21000 Dijon, France
Université de Bourgogne, UMR Centre des Sciences du Goût et de l'Alimentation, F-21000 Dijon, France

ARTICLE INFO

Article history:
Received 16 April 2014
Accepted 20 July 2014
Available online 28 July 2014

Keywords:
Saliva
Mucin
α-Amylase
Aroma
Air/liquid partition coefficient
Hydrophobic effect

ABSTRACT

As great differences were observed in the amount of α-amylase in human saliva, there is a need to better understand the effect of this protein alone or in mixture with mucin on aroma compound partitioning. We report the respective role of mucin and α-amylase on the air/liquid partition coefficients of two series of 5 methyl-ketones and 5 ethyl-esters. We confirm that mucin affects the release of aroma compounds and, for the first time, we demonstrate the ability of α-amylase to decrease the release of aroma compounds. For both proteins, we report the involvement of hydrophobic effects. Interestingly, no cumulative effect was observed when both proteins were mixed together in solution. We hypothesize that protein–protein interactions occur between the two proteins and decrease the total number of available binding sites for aroma compounds. The effect of human saliva is also investigated and compared to that of artificial salivas. In the presence of human saliva the release of ketones is lower than in water and slightly higher than in the presence of artificial saliva composed of α-amylase and/or mucin. Esters are more affected by the presence of human saliva than ketones. This observation is due to the presence of an esterase activity in saliva, which activity increases with the hydrophobicity of esters. The difference observed in aroma release between artificial and human salivas could be explained by the presence of other salivary proteins in human saliva.

1. Introduction

Flavour is one of the most important organoleptic properties of food regarding consumer acceptability. Therefore, the mechanisms involved in the release of flavour compounds during food consumption are a particular subject of interest. Regarding the release of aroma compounds, the global mechanism could be divided into three steps. During the first step, aroma compounds are released from food to saliva during food breakdown in the mouth. Then, they are partitioned between saliva and the air phase in the oral cavity. The intermittent aperture of the velum allows the transfer of aromatized air from the oral to the nasal cavity (Buettner, Beer, Hannig, & Settles, 2001), mostly during masticatory activity and swallowing events (Repoux, Labouré, et al., 2012; Repoux, Semon, Feron, Guichard, & Laboure, 2012). Finally, they reach the olfactory mucosa, where they bind to the olfactory receptors (Gaillard, Rouquier, & Giorgi, 2004).

Several studies have reported a difference between retronasal and orthonasal perception of the same odorant molecule, indicating an influence of the oral processing and physiology on aroma perception (Burdach, Kroeze, & Koster, 1984; Kuo, Pangborn, & Noble, 1993; Linforth, Martin, Carey, Davidson, & Taylor, 2002; Voirol & Daget, 1986). Among the different factors influencing the release of volatile compounds, the impacts of saliva (Genovese, Piombino, Gambuti, & Moio, 2009) and of oral volume (Mishellany-Dutour et al., 2012) were evidenced. Saliva, which results from blood filtration, not only is composed of 99% of water, but it also contains numerous inorganic salts and organic compounds such as proteins (Humphrey & Williamson, 2001). The total protein concentration ranged between 1 and 3.5 $mg \cdot mL^{-1}$ (Bennick, 1982; Neyraud, Heinzerling, Bult, Mesmin, & Dransfield, 2009), although higher concentrations have been reported (Ferguson, 1999). The proteomic analyses of saliva have identified 1166 proteins (Denny et al., 2008). Some of these proteins are able to interact with food molecules and play a role in flavour. For example, proline rich-proteins are involved in astringency as these proteins can bind and aggregate tannins, which are at the origin of this sensation (Canon, Milosavljević, et al., 2013; Canon, Paté, et al., 2013b). Therefore, different investigations on flavour perception have evoked the variation in salivary protein composition to explain inter-individual variability in flavour perception (Dsamou et al., 2012; Mounayar et al., 2013; Poette et al., 2014). Regarding aroma release from food matrices, a lot of studies have demonstrated that proteins

* Corresponding author at: Centre des Sciences du Goût et de l'Alimentation, UMR1324 INRA, UMR6265 CNRS, Université de Bourgogne, Dijon, 17 rue Sully, BP 85610, F-21065 Dijon, France. Tel.: +33 380693529; fax: +33 380693227.
E-mail address: francis.canon@dijon.inra.fr (F. Canon).

http://dx.doi.org/10.1016/j.foodres.2014.07.013
0963-9969/

can interact and bind to aroma compounds and that the nature and strength of the interactions depend on both the type of macromolecules and aroma compounds (Guichard, 2006; Lorrain et al., 2013; Mitropoulou, Hatzidimitriou, & Paraskevopoulou, 2011; Rodriguez-Bencomo et al., 2011; Villamor, Evans, Mattinson, & Ross, 2013). The effect of saliva addition to model wine modified the release of aroma compounds in the vapour phase (Mitropoulou et al., 2011). This effect depends on the type of wine and differs between human and artificial salivas suggesting that other salivary proteins than mucin can affect the release of aroma compounds (Genovese et al., 2009). Moreover, there is an important variability in saliva composition between individuals (Quintana et al., 2009). For example, Perry et al. (2007) have reported great differences in the amounts of α-amylase in saliva through the study of different populations. In addition, the composition of the salivary peptidome is modified with the age of the subject and with his diet (Morzel et al., 2012). Therefore, it has been suggested that differences in salivary protein composition could be at the origin of inter-individual variation in aroma release (Piombino et al., 2014; Repoux, Semon, Feron, Guichard, & Laboure, 2012). As different proteins can interact with aroma compounds and as there is an important variability in protein saliva composition, it is of interest to understand if the protein composition of saliva impacts the release of aroma compounds. Surprisingly, previous investigations in simple model systems have reported no significant difference between human saliva and artificial saliva containing only mucin on aroma release (Benjamin, Silcock, Beauchamp, Buettner, & Everett, 2012; van Ruth, Grossmann, Geary, & Delahunty, 2001). These results suggest that the effect of salivary proteins on aroma release can be assimilated to the effect of one protein: mucin. Among the few results on the effect of other salivary proteins on aroma compound partitioning, it has been reported that the addition of α-amylase to an artificial saliva containing mucin does not significantly affect aroma release (van Ruth, Roozen, & Cozijnsen, 1995). To our knowledge, besides this study, the effect of α-amylase on aroma release has never been clearly investigated, despite the fact that α-amylase is one of the most abundant proteins in saliva (Schenkels, Veerman, & Nieuw Amerongen, 1995). Therefore, to address the lack of clear information on the effect of α-amylase, we have investigated the effect of this protein alone or in mixture with mucin on the air/liquid partitioning of aroma compounds. As hydrophobic effects are generally the main non-covalent interactions driving the binding of aroma compounds onto proteins (Damodaran & Kinsella, 1980; Damodaran & Kinsella, 1981; Guichard, 2006; Tavel, Andriot, Moreau, & Guichard, 2008), two series of linear aliphatic volatile compounds, five methyl ketones and five ethyl esters, were chosen in order to determine the role of these aroma–protein interactions on aroma compound partitioning. These molecules cover a wide-range of hydrophobicity, characterized by the log *P* value (octanol–water partition coefficient). Their air/liquid partition coefficients were determined in water, in buffer solution, in human saliva and in three artificial salivas containing mucin, α-amylase or a mixture of mucin and α-amylase.

2. Materials and methods

2.1. Human saliva

Human saliva (hs) was constituted by a pool of stimulated saliva coming from 15 volunteers (6 females and 9 males, aged 24–60). The subjects were asked to avoid eating or drinking (although water was allowed) for at least 1 h before saliva collection. Stimulated saliva was collected by asking the subjects to chew a piece of Parafilm (American National Can, Chicago, IL) and then to spit out their saliva at regular intervals (Neyraud, Palicki, Schwartz, Nicklaus, & Feron, 2012). Two saliva collections were organized the same day: one in the morning and one in the afternoon. All saliva samples were immediately stored at 4 °C after each individual collection and then pooled, the same day as the collection, to obtain a total volume of 800 mL. This pool was divided into aliquots of 20 mL stored at −20 °C until use and for a maximal time of two weeks. Before freezing and after defrost of the saliva, the pH was 8.3 ± 0.01 and the viscosity was 6.9 mPa·s at 20.7 °C, 1500 s^{-1}, 30 s. Usually, the pH of human saliva is comprised between 5.56 and 7.41, but pH values up to 8.5 have been reported (Neyraud et al., 2009). Variation in pH can affect the charge of proteins and therefore their conformation (Canon et al., 2011; Giuliani et al., 2012). However, Friel et al. did not find any significant difference on the retention of aroma compounds by mucin for pH values comprised between 6.5 and 8.5. The basicity of the saliva observed here is probably due to the fact that bicarbonate is the main buffer of saliva and could be converted into CO_2 by carbonic anhydrase. As the partial pressure of CO_2 is higher in saliva than in air, the loss of CO_2 leads to a decrease in bicarbonate and therefore an increase in pH (Bardow, Moe, Nyvad, & Nauntofte, 2000). Regarding the effect of the storage on saliva, we verified that the retention of ethyl heptanoate and 2-heptanone by human saliva was not modified after storage at −20 °C.

The protocol for saliva collection was submitted to an Ethics Committee and was approved on 17th April of 2008 by the Comité de Protection des Personnes Est-1 (No. 2008/15) and on 8th August of 2008 by the Direction Générale de la Santé — France (No. DGS2008-0196).

2.2. Preparation of artificial salivas

Water solution (w) was deionized MilliQ water (18.2 $m\Omega \cdot cm^{-1}$, Millipore Corporation Billerica, MA, USA). A buffer solution was made-up using the following components: $NaHCO_3$ (5.208 $g \cdot L^{-1}$), K_2HPO_4, $3H_2O$ (1.369 $g \cdot L^{-1}$), NaCl (0.877 $g \cdot L^{-1}$), KCl (0.477 $g \cdot L^{-1}$), and $CaCl_2$, $2H_2O$ (0.441 $g \cdot L^{-1}$) (van Ruth et al., 2001). Three artificial salivas were constituted by addition in the buffer solution of mucin (2.16 $g \cdot L^{-1}$) for the mucin artificial saliva (m), α-amylase (200,000 $U \cdot L^{-1}$) for the α-amylase artificial saliva (a) and α-amylase (200,000 $U \cdot L^{-1}$) with mucin (2.16 $g.L^{-1}$) for the artificial saliva composed of mucin and α-amylase (ma) in the concentrations used by van Ruth et al. (2001). Mucin from bovine submaxillary salivary glands and human α-amylase were purchased from Sigma Aldrich (Sigma Aldrich, St Quentin Fallavier, France). Before each experiment, fresh artificial salivas were prepared, therefore NaN_3, usually used as a bacterial growth inhibitor, was not added to the solution in order to avoid any effect of this molecule on aroma release (direct interactions or modifications of the protein structure).

The pH of the artificial saliva and buffer solution was adjusted using sodium hydroxide NaOH to 8.3 ± 0.01, which was the pH of the defrosted human saliva. The viscosity of artificial saliva solutions was comprised between 6.6 and 7 mPa·s (20.7 °C, 1500 s^{-1}, 30 s).

2.3. α-Amylase activity

The α-amylase activity was measured in human and artificial salivas containing α-amylase using the amylase CNPG3 assay kit (BIOLABO, Maizy, France), in order to compare the amount of α-amylase in all saliva samples. After the addition of a solution of 2-chloro-p-nitrophenyl-α-D-maltotrioside (CNPG3) at 2.25 · 10^{-3} $mol \cdot L^{-1}$, the tested solution was diluted 4000-fold in NaCl solution at 9 g/L. The degradation of CNPG3 by α-amylase activity is directly proportional to 2-chloro-4-nitrophenol (CNP) concentration, which can be determined by absorbance measurement at 405 nm. A standard curve was established with six different concentrations using a serum containing α-amylase with an activity comprised between 2.25 $U \cdot mL^{-1}$ and 42 $U \cdot mL^{-1}$ (Exatrol-N, BIOLABO, Maizy, France). The α-amylase activity was expressed in International Enzyme Unit Activity (U) per L. One U is defined as the amount of the enzyme that catalyses the conversion of 1 μmol of substrate per minute.

2.4. Aroma compounds

Aroma compounds were purchased from Sigma Aldrich (Sigma Aldrich, St Quentin Fallavier, France): 2-propanone, 2-hexanone, 2-heptanone, 2-octanone, 2-nonanone, ethyl propanoate, ethyl butanoate, ethyl pentanoate, ethyl hexanoate, and ethyl heptanoate (Table 1). A gas chromatography–flame ionization detector (GC–FID) analysis confirmed the purity of all aroma compounds (>99%).

Stock solutions of aroma compounds were prepared in propylene glycol at a concentration of 0.1 $mol \cdot L^{-1}$ and stored at 4 °C.

2.5. Static equilibrium headspace analysis

Stock solutions of aroma compounds were further diluted into water, buffer, artificial saliva solutions and human saliva to obtain a final aroma compound concentration of 1.10^{-4} $mol \cdot L^{-1}$, which is below the solubility threshold of the tested compounds in water. The final pH was 8.3 ± 0.01 for all solutions. In order to avoid any aroma competition for protein binding sites, we chose to analyse aroma compounds one by one. The final solutions (5 mL) were put into 20.46 mL headspace vials (Supelco, Bellefonte, PA, USA). The headspace vials were immediately sealed with silicone septa in magnetic caps (Supelco). The experiments were performed at a temperature of 30 °C, which is in the range of the temperature measured in the mouth when consuming cold beverages (between 22 and 33 °C) (Engelen et al., 2003). Moreover many air/liquid partition coefficients are available at this temperature. The time needed to reach the static equilibrium was determined in all artificial salivas during preliminary experiments with a mixture of aroma compounds from different chemical classes and log *P* values, including ethyl propanoate, octan-2-one and nonan-2-one. The headspace vials were placed in the incubator of an automatic headspace sampler (GERSTEL MPS 2, Gerstel Inc., Mülheim an der Ruhr, Germany) and equilibrated at 30 °C until a static equilibrium was attained (40 min). A one millilitre sample of headspace was taken automatically using a preheated (35 °C) 2.5 mL gas-tight syringe (Gerstel, manufactured by SGE, Victoria, Australia) and analysed by gas chromatography (TRACE GC Ultra, Thermo Electron, Milan, Italy). The injector temperature was set at 240 °C. A capillary DB-Wax column (30 m, 0.32 mm i.d., 0.5 μm; Agilent J&W Scientific, Folsom, CA, USA) and a flame ionization detector set at 250 °C were used. The carrier gas was hydrogen at a velocity of 0.03 $cm^3 \cdot s^{-1}$ in split mode (1/10). For each aroma compound, an oven isothermal temperature was preliminarily determined in order to obtain a retention time comprised between 2 and 5 min and used during the present experiments (Table 1). All experiments were performed in triplicate. In order to compare the effect of saliva composition on aroma release and to avoid day-to-day variations, for each aroma compound, all the studied media were analysed on the same day.

Table 1
List of aroma compounds with their molecular weight in $g \cdot mol^{-1}$ (Mw), hydrophobic constant (log *P*), solubility in water at 25 °C in $mol \cdot L^{-1}$ (Sol), enthalpy of vaporisation ($\Delta_{vap}H°$) in $kJ \cdot mol^{-1}$, GC oven temperature.

Aroma compound	Mw[a]	log *P*[a]	Sol[a]	$\Delta_{vap}H°$[b]	GC oven temperature
Methyl ketones					
2-Propanone	58	−0.24	3.79E+00	31	45 °C
2-Hexanone	100	1.24	7.75E−02	43	80 °C
2-Heptanone	114	1.73	1.88E−02	47.2	95 °C
2-Octanone	128	2.22	6.91E−03	39.8	100 °C
2-Nonanone	142	2.71	1.20E−03	56.4	125 °C
Ethyl esters					
Ethyl propanoate	102	1.36	1.05E−01	39.1	60 °C
Ethyl butanoate	116	1.85	2.37E−02	42	70 °C
Ethyl pentanoate	130	2.34	7.12E−03	46.1	90 °C
Ethyl hexanoate	144	2.83	2.14E−03	51.7	95 °C
Ethyl heptanoate	158	3.32	6.45E−04	55.8	110 °C

[a] Values were calculated by EPISUITE 4.00 software (US Environmental Protection Agency).
[b] http://webbook.nist.gov/chemistry.

2.6. Calculation of air/liquid partition coefficient

For each aroma compound, a calibration curve was established by GC/FID in the same analytical conditions reported above and using a liquid injection (1 μL) of a solution of aroma compounds in CH_2Cl_2 (10^{-5} to 10^{-2} $mol \cdot L^{-1}$). The calibration curves were used to determine the concentration of each aroma compound in the gas phase (Chana, Tromelin, Andriot, & Guichard, 2006). Then, the partition coefficient of compound i in medium m, $K_{im} = C_{ivap}/C_{im}$, where C_{ivap} is the molar concentration of compound i in the gas phase and C_{im} is the molar concentration of compound i in the medium, was calculated. As $C_{ivap} \ll C_{im}$, C_{im} can be approximated by the initial concentration in the medium.

2.7. Analysis of ester degradation in human saliva

To test the hypothesis that esters are transformed into acid due to the presence of an esterase activity in the human saliva, the concentration of esters was measured in the headspace at 30 °C at different times (20, 40, 60, 80, 100, 120, 140, 160, 180, and 200 min).

Simultaneously, the production of acid from the degradation of esters was quantified in the liquid phase after dichloromethane extraction. Human saliva samples containing ester were thawed and extracted three times with 1 mL CH_2Cl_2 under stirring for 15 min. After extraction, the 3 mL of CH_2Cl_2 was pooled and concentrated with a 5 mL Kuderna Danish apparatus to obtain a final volume of 300 μL. Extracts were then analysed by GC/EI–MS (Agilent Technologies, 78 90A GC system, Les Ulis, France). The injector temperature was set at 240 °C and a capillary FFAP column (30 m, 0.32 mm, 0.5 μm; Agilent J&W Scientific, Folsom, CA, USA) was used. The carrier gas was helium at a flow rate of 0.03 $cm^{-3} \cdot s^{-1}$ in splitless mode. The GC oven temperature started at 40 °C and was increased to 120 °C at a rate of 6 °C·min^{-1} then to 140 °C at a rate of 1 °C·min^{-1}, maintained for 10 min at 140 °C, then increased to 160 °C at a rate of 4 °C·min^{-1}, then to 240 °C at a rate of 6 °C·min^{-1}.

A calibration curve of heptanoic acid ($1.58 \cdot 10^{-10}$ to $7.00 \cdot 10^{-9}$ mol acid in 1 μL CH_2Cl_2, $r^2 = 0.993$) was used to calculate the amount of acid produced by the ethyl heptanoate degradation.

2.8. Data analyses

Air/liquid partition coefficient calculated in the various media that were studied was submitted to univariate analysis of variance (ANOVA), followed by a mean comparison test (Neuman-Keuls test, 5%), by using R® Software (Version 2.14.1. Ink, Foundation for Statistical Computing, Vienna, Austria).

The ratios of the partition coefficient saliva/water were calculated and then plotted against the log *P* value of aroma compounds. The resulting curves were then fitted using the line curve fitting function in Igor Pro (Version 6.22A, WaveMetrics, Portland, USA).

3. Results and discussion

3.1. Air/liquid partition coefficients of ketones and esters in artificial and human saliva

Air/liquid partition coefficients (K) are reported in Fig. 1A for ketones and Fig. 1B for esters. As expected, no significant difference was observed between the air/water (Kw) and air/buffer (Kb) partition coefficients for all molecules (data not shown), thus only Kw values are reported and water constitutes the reference medium. For ketones, Fig. 1A shows an increase in the air/liquid partition coefficients as a function of the ketone aliphatic chain length for all studied media.

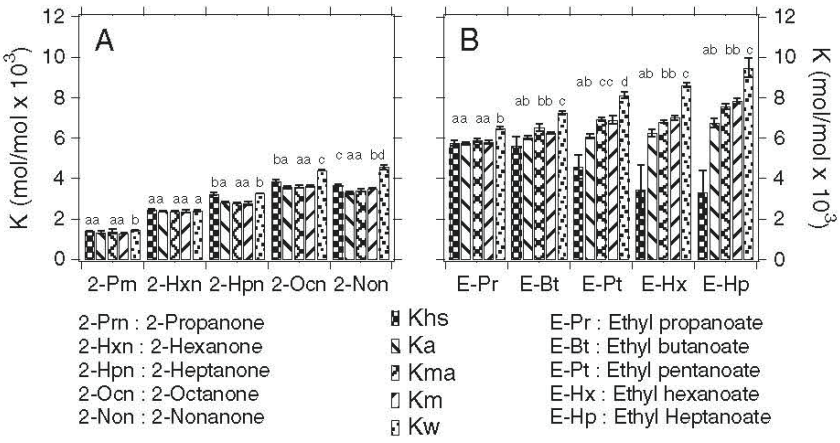

Fig. 1. Air/liquid partition coefficients (K) of aroma compounds for (A) ketones and (B) esters in the presence of water (Kw), mucin in buffer (Km), mucin and α-amylase in buffer (Kma), α-amylase in buffer (Ka), and human saliva (Khs). For each aroma compound, values with different letters are significantly different ($P < 0.05$) after mean comparison (Newman–Keuls-test).

This increase in air/liquid partition coefficients in the function of log *P* value for homologous series of aroma compounds has already been established at a temperature of 25 °C by Buttery, Ling, and Guadagni (1969) and at 30 °C by Merabtine, Lubbers, Andriot, Tromelin, and Guichard (2010). No significant difference was observed between all media for 2-propanone (*P* value > 0.06) and 2-hexanone (*P* value > 0.1). For the other ketones, 2-heptanone, 2-octanone and 2-nonanone, the air/mucin (Km), air/α-amylase (Ka) and air/(mucin + α-amylase) (Kma) partition coefficients are not significantly different from each other, while Km, Ka and Kma are significantly lower than both Kw and air/human saliva partition coefficient (Khs) (*P* values < 0.001) and Khs is significantly lower than Kw (*P* value < 0.001). In Fig. 1B in water and artificial salivas, the air/liquid partition coefficients of esters increase also as a function of ester hydrophobicity, whereas the opposite trend is observed in the presence of human saliva. As for ketones, the air/liquid partition coefficients of esters in artificial salivas (Km, Ka and Kma) are not significantly different from each other and significantly lower than the air/water partition coefficient (Kw) (*P* value < 0.001). But contrary to ketones, the air/human saliva partition coefficients (Khs) of all the esters are significantly lower than the air/liquid partition coefficients in other media (*P* value < 0.001). Results obtained in artificial salivas suggest that the salivary proteins mucin and α-amylase are both able to retain methyl ketones and ethyl esters and that these interactions are not specific to a family of proteins as previously observed for several proteins in food matrices (Guichard, 2006). The present observation of the retention of aroma compounds in a solution containing only α-amylase seems in contradiction with the previous data reported by van Ruth et al. (1995). Moreover, while previous investigations suggest that artificial saliva containing mucin only and human saliva have similar effects on the behaviour of aroma compounds (van Ruth & Roozen, 2000), our results show significant differences between artificial and human salivas in the function of the protein composition and the nature of aroma compound. Therefore, in the following parts, we will both compare the effect of proteins alone in solution, proteins in mixture and total salivary proteins on aroma partitioning.

3.2. Effect of artificial saliva composition on aroma compound release

In order to gain a deeper understanding on the protein–aroma interactions and the role of hydrophobic effects in such interactions, the relative partition coefficients between saliva media (m, ma, a and hs) and water (w) were calculated for molecules whose the partition coefficients are significantly affected by artificial or human saliva and, then, plotted as a function of the hydrophobicity (log *P* value) of the compounds. The relative partition coefficients give a direct access to the effect of proteins on aroma release.

3.2.1. Effect of isolated mucin and α-amylase on aroma release

The ratio between air/mucin and air/water partition coefficients (Km/Kw) is plotted for esters and ketones as a function of their log *P* value on Fig. 2A. All ratios are lower than 1, which indicates that mucin has a retention effect on all aroma compounds. A linear fit function was used to correlate the relative partition coefficients Km/Kw with the corresponding log *P* value, for aroma compounds which were significantly affected by the presence of salivary protein (i.e. aroma compounds presenting log *P* values above 1.3). The slope of the linear correlation is -0.041 ± 0.017 and its y-intercept is 0.930 ± 0.034. The correlation coefficient (r) is −0.71 and the coefficient of determination (r^2) is 0.50. This negative correlation indicates an increase in the retention of aroma compounds by mucin as a function of their hydrophobicity suggesting that aroma molecules interact with mucin mainly due to hydrophobic effects. Mucins have molecular weights ranging from 0.5 to 20 MDa (Bansil & Turner, 2006). They are composed of a long polypeptidic chain highly glycosylated in the central region. This structure presents hydrophobic domains (Bansil & Turner, 2006), which could constitute binding sites of small molecules such as aroma compounds. Van Ruth et al. also reported a higher retention of the more hydrophobic aroma compounds by salivary proteins at 37 °C (van Ruth et al., 2001). However, it should be noticed that the hydrophobic effect does not explain all the variability of our results because the coefficient of determination r^2 is only of 0.50. Therefore, other non-covalent interactions such as electrostatic interactions could be also involved between aroma compounds and the mucin glycosylations (Tromelin, Merabtine, & Andriot, 2010). Indeed, for a similar log *P* value methyl-ketones exhibit a higher dipole-moment than ethyl-ester, which could be in favour of electrostatic interactions in addition to hydrophobic effects. In their investigation on the effect of mucin on aroma partitioning from solution adjusted at pH 7.0, at 25 °C, Friel and Taylor (2001) did not observe such correlation between the relative concentration of aroma compounds from different chemical classes in air and the corresponding log *P* value. This suggests that this relation is only valid within homologous series and that other types of interactions could be involved.

For similar log *P* value, ketones seem slightly more retained than esters. For example, 2-nonanone is significantly more retained by mucin than ethyl heptanoate (*P* value < 0.05). Separated analysis of the

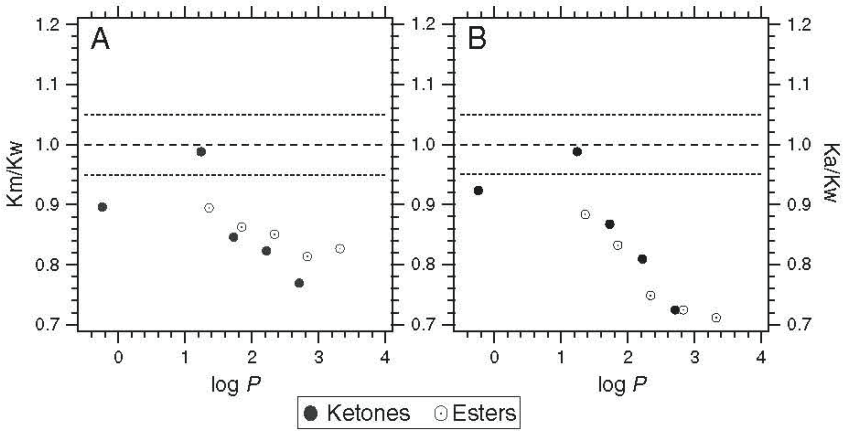

Fig. 2. Relationship between hydrophobicity (log *P* value) of aroma compounds and the ratio of the air/liquid partition coefficient in the presence of (A) mucin (Km/Kw) and (B) α-amylase (Ka/Kw) to the one in water. Dotted horizontal lines represent the ±5% interval around the ratio equal to 1.

correlation between the relative partition coefficients Km/Kw of ester with their log *P* value gives a better negative correlation: $y = -0.037x\ (\pm 0.0091) + 0.0937\ (\pm 0.022)$ ($r = -0.92$ and $r^2 = 0.85$). For ketones, it is too speculative to discuss the negative correlation obtained, as only three molecules are significantly affected and studied in this analysis.

Fig. 2B presents the ratio of K values between α-amylase medium (a) and water (w) as a function of aroma log *P* value. As for mucin, an increase of the aroma retention is observed with the log *P* value for all the esters and for ketones with log *P* values higher than 1.3. Therefore, a linear fit function was used to correlate the relative partition coefficients Ka/Kw of compounds with their corresponding log *P* value (in the range from 1.3 to 3.5). The slope of the curve is -0.101 ± 0.013 and the y-intercept is 1.02 ± 0.032 ($r = -0.95$ and $r^2 = 0.90$). This negative correlation can explain almost all the variability observed, which clearly indicates the involvement of hydrophobic effects in the retention of aroma compounds with a linear hydrophobic chain by α-amylase. Regarding the structure of the proteins, α-amylase is a globular protein with a well-defined three-dimensional structure (Kandra & Gyémánt, 2000; Ramasubbu, Paloth, Luo, Brayer, & Levine, 1996) contrary to mucin. Our results suggest that one or several hydrophobic domain(s) in the α-amylase structure are available for the binding of hydrophobic molecules such as aroma compounds. The correlations observed for mucin and α-amylase with the log *P* value of molecules suggest that aroma compounds with a log *P* value higher than 1.5 are more affected by α-amylase than by mucin. By using a mouth model system under a nitrogen gas flow, van Ruth et al. (1995) did not observe any significant effect of the addition of α-amylase to artificial saliva containing mucin. However these authors observed different trends according to their experimental conditions. It appears thus necessary to analyse the results obtained with artificial saliva containing both mucin and α-amylase.

3.2.2. Effect of mixed mucin and α-amylase on aroma release

We thus investigated the effect of mucin and α-amylase mixed together in solution on the release of aroma compounds. Fig. 3A presents the relative partition coefficient between the medium containing both mucin and α-amylase (ma) and water (w). As for isolated proteins, a decrease in the Kma/Kw ratio as a function of aroma compound hydrophobicity is observed. The application of a linear fit function gives: $y = -0.067x\ (\pm 0.021) + 0.0989\ (\pm 0.050)$ ($r = -0.80$ and $r^2 = 0.63$). The slope obtained with the mixture of the two proteins is intermediate between the ones obtained for isolated mucin or α-amylase. It indicates that the retention of aroma compounds by artificial saliva containing α-amylase and mucin is not the sum of the effects of isolated proteins. Fig. 3B presents the evolution of the relative partition coefficient

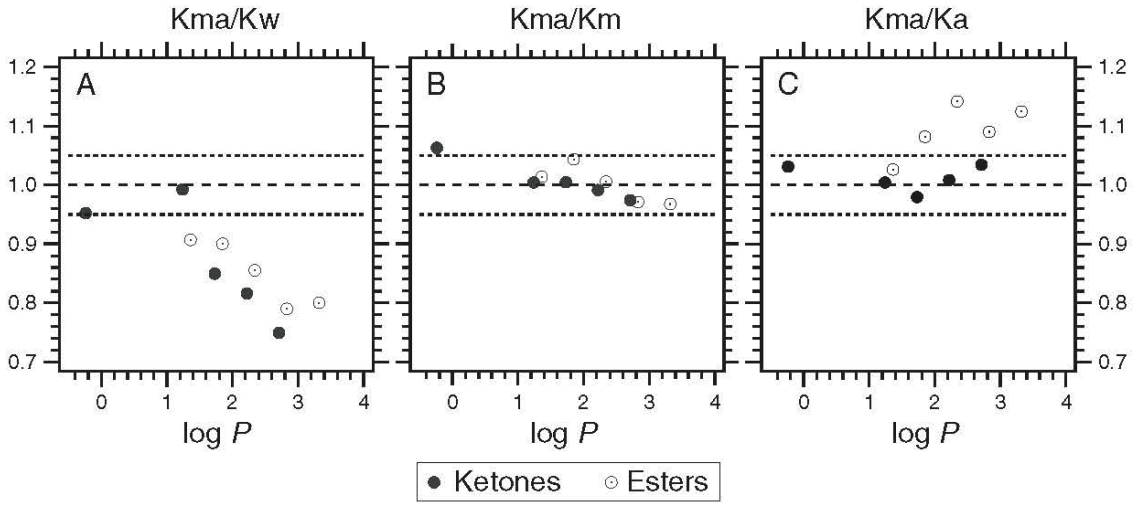

Fig. 3. Relationship between hydrophobicity (log *P* value) of aroma compounds and their relative air/liquid partition coefficient (K) between mucin and α-amylase and (A) water (Kma/Kw), or (B) mucin (Kma/Km) or (C) α-amylase (Kma/Ka). Dotted horizontal lines represent the ±5% interval around the ratio equal to 1.

between the medium containing both mucin and α-amylase and mucin (Kma/Km) as a function of molecule hydrophobicity (log *P* value), which brings information on the effect of the addition of α-amylase to a mucin solution on the release of aroma compounds. Almost all ratio values are comprised between 0.95 and 1.05 indicating that the addition of α-amylase to mucin does not change the retention of aroma compounds. This observation is in agreement with the result obtained by van Ruth et al. (1995). Fig. 3C shows the evolution of the relative partition coefficient between the medium containing both mucin and α-amylase and α-amylase (Kma/Ka) as a function of molecule hydrophobicity (log *P* value) and highlights the effect of the addition of mucin to artificial saliva containing only α-amylase. It appears that the addition of mucin does not affect the retention of ketones but reduces the retention of esters. Mucin has the ability to interact with other proteins and to form supramolecular edifices (Soares et al., 2004). Interestingly, interactions between mucin and α-amylase have been previously reported in saliva (Iontcheva, Oppenheim, & Troxler, 1997). Therefore, protein–protein interactions could be at the origin of our results, as they can modify the protein properties and the ability of each individual protein to interact with other molecules such as aroma compounds. The number of available binding sites of aroma compounds can decrease and consequently affect the retention of aroma compounds by proteins. In the same time, in the presence of mucin in artificial saliva containing α-amylase the retention of esters is decreased while no effect is observed for ketones.

3.3. Effect of human saliva on aroma compound partitioning

In order to compare the effects of artificial salivas and human saliva on aroma retention, the partition coefficient ratios between human saliva and water (Khs/Kw) were also determined. They are reported as a function of the molecule hydrophobicity (log *P* value) in Fig. 4. Ketones and esters seem to be differently affected by human saliva.

For ketones, the effect of human saliva on the air/liquid partition coefficient is only significant (Fig. 1) for 2-octanone and 2-nonanone, which have log *P* values higher than 2. The comparison between the 2 molecules shows that 2-nonanone, which has the highest hydrophobicity, is more retained by human saliva than 2-octanone. The effect of human saliva on ketone release is probably due to retention by salivary proteins. The Khs values of all ketones are higher than their Ka, Km or Kma. Therefore, ketones are less retained by human saliva than artificial saliva. This difference could be due to different amounts of proteins between artificial and human salivas. However, the concentrations in mucin in the artificial salivary media correspond to those typically observed in human saliva. The activity of α-amylase was 180 ± 3 UI·mL^{-1} in human saliva and 144 ± 2 UI·mL^{-1} in artificial saliva. Therefore, the amount of α-amylase is probably higher in human saliva and could not explain the lower retention of ketones in human saliva than that in artificial salivas. As hypothesize in the case of the artificial saliva containing a mixture of mucin and α-amylase, this observation could be explained by protein–protein interactions. Such interactions could decrease the amount of available binding sites for aroma compounds onto proteins. In agreement with this hypothesis, the presence of heterogeneous protein supramolecular edifices in saliva has been previously described (Soares et al., 2004).

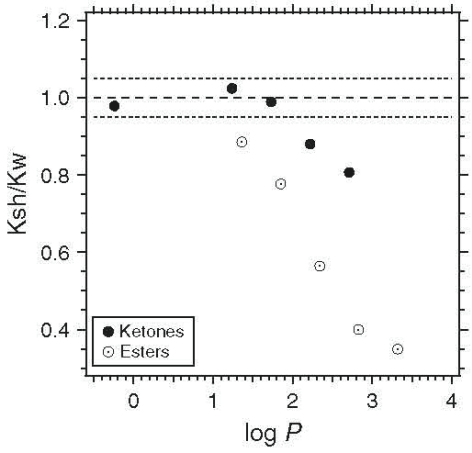

Fig. 4. Relationship between hydrophobicity (log *P* value) of aroma compounds and their relative air/liquid partition coefficient (K) between human saliva and water (Khs/Kw). Dotted horizontal lines represent the ±5% interval around the ratio equal to 1.

For all the studied esters, their air/liquid partition coefficient in the presence of human saliva (Khs) is lower than the one obtained in the presence of water (Kw) (Fig. 1). Fig. 4 shows a decrease of the Ksh/Kw ratio of ester as a function of their log *P* value. A linear relation was found between the Khs/Kw ratio and log *P* values (Fig. 4): $y = -0.296x\ (\pm 0.031) + 1.28\ (\pm 0.075)$ ($r = -0.98$ and $r^2 = 0.97$). This negative correlation indicates that an increase in molecule hydrophobicity induces a decrease in the amount of aroma compounds released in the air phase in the presence of human saliva.

The comparison between esters and ketones indicates that esters exhibit a lower Ksh/Kw value than ketones for a similar log *P* value. The difference of behaviour between esters and ketones in the presence of human saliva could be due to the strongest interactions between esters and salivary proteins, involving other types of non-covalent interaction in addition to hydrophobic effects, or to ester degradation by human saliva. Indeed, Buettner has previously reported an esterase activity of saliva (Buettner, 2002), corresponding to the hydrolysis of ester into the corresponding acid and alcohol. To confirm this hypothesis, we have recorded the concentration of esters in the air phase as a function of time (Fig. 5A). This figure reveals that the ester concentration increases from 5 to 40 min, which is the required time to get the thermodynamic equilibrium. From 40 min, except for ethyl propanoate, the ester concentration decreases as a function of time. It confirms that in the presence of human saliva there is a degradation of esters as a function of time. The composition of the liquid phase was followed through the GC–MS analysis of a dichloromethane extract. This analysis reveals a decrease in ester concentration and the apparition of the corresponding acid (data not shown). The decrease in ester concentrations in the headspace as a function of time and the identification of the corresponding acid in the aqueous phase confirm the hypothesis of an esterase activity in human saliva.

Taking ethyl heptanoate as an example we then calculated the amount of acid produced by the degradation of the ester after 180 min. The initial amount of ethyl heptanoate in the 5 mL human saliva sample was of $5.5 \cdot 10^{-7}$ mol. The production of heptanoic acid was calculated from the calibration curve. A total of $1.85 \cdot 10^{-7}$ mol of heptanoic acid was produced in the 5 mL sample after 180 min, which corresponded to the loss of $3.11 \cdot 10^{-7}$ mol of ethyl heptanoate at the same time, calculated from the GC data. We checked that no acid was produced from the ester solution without the addition of human saliva and that the incubation of human saliva without ethyl heptanoate did not produce the acid. This result confirms the production of heptanoic acid by enzymatic hydrolysis of ethyl heptanoate in the presence of human saliva.

From Fig. 5A, the rate of ester degradation was determined for each ester by determining the slope value of the concentration curve between 40 and 200 min. The rates of ester degradation are reported in Fig. 5B. as a function of the ester log *P* value. It shows a linear correlation between the rate of ester degradation and their log *P* value. The maximal rate of degradation is reached at a log *P* value of three. It should be noticed that the log *P* value is linearly correlated with the carbon number of the ester aliphatic chain. Therefore, the enzymatic activity is also correlated to the length of the aliphatic chain. This observation is in agreement with the study performed by Buettner on the influence of saliva enzymes on esters (Buettner, 2002). As the Khs/Kw ratio of ethyl heptonate is lower than that of ethyl hexanoate, we cannot

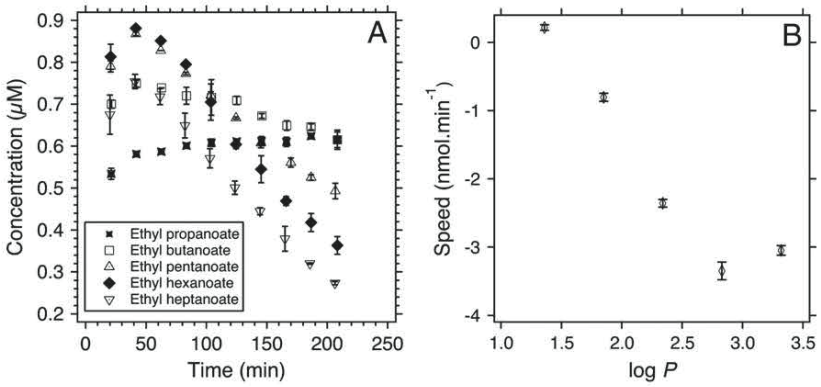

Fig. 5. (A) Concentration of ester in air above the human saliva as a function of time. (B) Relationship between the rate of ester degradation in human saliva and hydrophobicity of aroma compounds (log *P* value).

exclude an additional effect of aroma compound retention by other proteins involving hydrophobic effects. Even if the hydrolysis of esters in our conditions is relatively slow in comparison with real times of consumption, which can vary from a few seconds to a few minutes, this decrease in the amount of esters can impact aroma persistence. During cheese consumption, the analysis of the expired air has revealed a lower persistence of ethyl propanoate than 2-nonanone (Repoux, Labouré, et al., 2012; Repoux, Semon, Feron, Guichard and Laboure, 2012). The persistence of 2-nonanone in the expired air could be due to its retention by the oral, pharyngeal and/or nasal lubricated mucosa, as observed previously (Doyennette et al., 2014) and suggested by Normand, Avison, and Parker (2004) and Buettner and Beauchamp (2010). Until now no experimental results have been obtained on the in vivo persistence of esters. We could suppose that aroma persistence of esters could be also modified due to their degradation by salivary esterases present in the salivary film.

4. Conclusions

This investigation highlights the effect of salivary proteins on aroma release and more particularly on ketone and ester release. For the first time, it is clearly demonstrated that both mucin and α-amylase have the ability to retain aroma molecules. In both cases, hydrophobic effects are involved in these aroma–protein interactions. Regarding the effect of α-amylase on aroma release, the inter-individual variation of α-amylase concentration in saliva (Perry et al., 2007) could be at the origin of variations in aroma release between individuals (Piombino et al., 2014; Repoux, Labouré, et al., 2012; Repoux, Semon, Feron, Guichard and Laboure, 2012). As hydrophobic effects seem mainly at the origin of these protein effects, the differences in the perception of aroma during food consumption by different subjects are more likely to occur for the most hydrophobic molecules. However, the interactions that can occur between mucin and α-amylase could decrease the total number of available binding sites for aroma compounds on proteins. This study shows also that human saliva has the ability to influence the release of volatile molecules and this effect cannot be totally resumed by using artificial saliva containing only mucin and α-amylase. It appears important in the future to have a better understanding of both the protein binding sites involved in the retention of aroma compounds and the protein–protein interactions occurring in saliva. Indeed, the difference observed between artificial and human salivas could be explained not only by the interactions with both mucin and α-amylase, but also by the presence of other salivary proteins, which could impact the release of specific aroma compounds.

Acknowledgements

We thank Hélène Brignot for the measurement of α-amylase activity, the volunteers for saliva collection and the ChemoSens analytical platform. This work received financial support from the Regional Council of Burgundy (FABER AIB 29000622, FEDER European Union 33759), INRA-CEPIA department. Sandy Pages-Helary received a Giract bursary for first year PhD students.

References

Bansil, R., & Turner, B.S. (2006). Mucin structure, aggregation, physiological functions and biomedical applications. *Current Opinion in Colloid & Interface Science, 11*(2–3), 164–170.

Bardow, A., Moe, D., Nyvad, B., & Nauntofte, B. (2000). The buffer capacity and buffer systems of human whole saliva measured without loss of CO_2. *Archives of Oral Biology, 45*, 1–12.

Benjamin, O., Silcock, P., Beauchamp, J., Buettner, A., & Everett, D. W. (2012). Tongue pressure and oral conditions affect volatile release from liquid systems in a model mouth. *Journal of Agricultural and Food Chemistry, 60*(39), 9918–9927.

Bennick, A. (1982). Salivary proline-rich proteins. *Molecular and Cellular Biochemistry, 45*, 83–99.

Buettner, A. (2002). Influence of human salivary enzymes on odorant concentration changes occurring in vivo. 1. Esters and thiols. *Journal of Agricultural and Food Chemistry, 50*(11), 3283–3289.

Buettner, A., & Beauchamp, J. (2010). Chemical input–sensory output: Diverse modes of physiology–flavour interaction. *Food Quality and Preference, 21*(8), 915–924.

Buettner, A., Beer, A., Hannig, C., & Settles, M. (2001). Observation of the swallowing process by application of videofluoroscopy and real-time magnetic resonance imaging-consequences for retronasal aroma stimulation. *Chemical Senses, 26*(9), 1211–1219.

Burdach, K. J., Kroeze, J. H. A., & Koster, E. P. (1984). Nasal, retronasal, and gustatory perception — An experimental comparison. *Perception & Psychophysics, 36*(3), 205–208.

Buttery, R. G., Ling, L. C., & Guadagni, D.G. (1969). Volatilities of aldehydes, ketones, and esters in dilute water solution. *Journal of Agricultural and Food Chemistry, 17*(2), 385–389.

Canon, F., Ballivian, R., Chirot, F., Antoine, R., Sarni-Manchado, P., Lemoine, J. r. m, & Dugourd, P. (2011). Folding of a salivary intrinsically disordered protein upon binding to tannins. *Journal of the American Chemical Society, 133*(20), 7847–7852.

Canon, F., Milosavljeviĉ, A.R., van der Rest, G., Réfrégiers, M., Nahon, L., Sarni-Manchado, P. , Cheynier, V., & Giuliani, A. (2013). Photodissociation and dissociative photoionization mass spectrometry of proteins and noncovalent protein–ligand complexes. *Angewandte Chemie International Edition in English, 52*(32), 8377–8381.

Canon, F., Paté, F., Cheynier, V., Sarni-Manchado, P., Giuliani, A., Pérez, J., Durand, D., Li, J., & Cabane, B. (2013). Aggregation of the salivary proline-rich protein IB5 in the presence of the tannin EgCG. *Langmuir, 29*(6), 1926–1937.

Chana, A., Tromelin, A., Andriot, I., & Guichard, E. (2006). Flavor release from ι-carrageenan matrix: A quantitative structure—property relationships approach. *Journal of Agricultural and Food Chemistry, 54*(10), 3679–3685.

Damodaran, S., & Kinsella, J. E. (1980). Flavor protein interactions. Binding of carbonyls to bovine serum albumin: Thermodynamic and conformational effects. *Journal of Agricultural and Food Chemistry, 28*(3), 567–571.

Damodaran, S., & Kinsella, J. E. (1981). Interaction of carbonyls with soy protein: Thermodynamic effects. *Journal of Agricultural and Food Chemistry, 29*(6), 1249–1253.

Denny, P., Hagen, F. K., Hardt, M., Liao, L., Yan, W., Arellanno, M., Bassilian, S., Bedi, G. S., Boontheung, P., Cociorva, D., Delahunty, C. M., Denny, T., Dunsmore, J., Faull, K. F., Gilligan, J., Gonzalez-Begne, M., Halgand, F., Hall, S.C., Han, X., Henson, B., Hewel, J., Hu, S., Jeffrey, S., Jiang, J., Loo, J. A., Loo, R. R. O., Malamud, D., Melvin, J. E.,

Miroshnychenko, O., Navazesh, M., Niles, R., Park, S. K., Prakobphol, A., Ramachandran, P., Richert, M., Robinson, S., Sondej, M., Souda, P., Sullivan, M.A., Takashima, J., Than, S., Wang, J., Whitelegge, J. P., Witkowska, H. E., Wolinsky, L., Xie, Y., Xu, T., Yu, W., Ytterberg, J., Wong, D. T., Yates, J. R., III, & Fisher, S. J. (2008). The proteomes of human parotid and submandibular/sublingual gland salivas collected as the ductal secretions. *Journal of Proteome Research, 7*(5), 1994–2006.

Doyennette, M., Deleris, I., Feron, G., Guichard, E., Souchon, I., & Trelea, I. C. (2014). Main individual and product characteristics influencing in-mouth flavour release during eating masticated food products with different textures: Mechanistic modelling and experimental validation. *Journal of Theoretical Biology, 340*, 209–221.

Dsamou, M., Palicki, O., Septier, C., Chabanet, C., Lucchi, G., Ducoroy, P., Chagnon, M. -C., & Morzel, M. (2012). Salivary protein profiles and sensitivity to the bitter taste of caffeine. *Chemical Senses, 37*(1), 87–95.

Engelen, L., de Wijk, R. A., Prinz, J. F., Janssen, A.M., Weenen, H., & Bosman, F. (2003). The effect of oral and product temperature on the perception of flavor and texture attributes of semi-solids. *Appetite, 41*(3), 273–281.

Ferguson, D. B. (1999). The flow rate and composition of human labial gland saliva. *Archives of Oral Biology, 44*(Suppl. 1), S11–S14.

Friel, E. N., & Taylor, A. J. (2001). Effect of salivary components on volatile partitioning from solutions. *Journal of Agricultural and Food Chemistry, 49*(8), 3898–3905.

Gaillard, I., Rouquier, S., & Giorgi, D. (2004). Olfactory receptors. *Cellular and Molecular Life Sciences, 61*(4), 456–469.

Genovese, A., Piombino, P., Gambuti, A., & Moio, L. (2009). Simulation of retronasal aroma of white and red wine in a model mouth system. Investigating the influence of saliva on volatile compound concentrations. *Food Chemistry, 114*(1), 100–107.

Giuliani, A., Milosavljevic, A.R., Hinsen, K., Canon, F., Nicolas, C., Refregiers, M., & Nahon, L. (2012). Structure and charge-state dependence of the gas-phase ionization energy of proteins. *Angewandte Chemie International Edition, 51*(38), 9552–9556.

Guichard, E. (2006). Flavour retention and release from protein solutions. *Biotechnology Advances, 24*(2), 226–229.

Humphrey, S. P., & Williamson, R. T. (2001). A review of saliva: Normal composition, flow, and function. *The Journal of Prosthetic Dentistry, 85*(2), 162–169.

Iontcheva, I., Oppenheim, F. G., & Troxler, R. F. (1997). Human salivary mucin MG1 selectively forms heterotypic complexes with amylase, proline-rich proteins, statherin, and histatins supramolecular edificies. *Journal of Dental Research, 76*(3), 734–743.

Kandra, L., & Gyémánt, G. (2000). Examination of the active sites of human salivary α-amylase (HSA). *Carbohydrate Research, 329*(3), 579–585.

Kuo, Y. -L., Pangborn, R. M., & Noble, A.C. (1993). Temporal patterns of nasal, oral, and retronasal perception of citral and vanillin and interaction of these odourants with selected tastants. *International Journal of Food Science & Technology, 28*(2), 127–137.

Linforth, R., Martin, F., Carey, M., Davidson, J., & Taylor, A. J. (2002). Retronasal transport of aroma compounds. *Journal of Agricultural and Food Chemistry, 50*(5), 1111–1117.

Lorrain, B., Tempere, S., Iturmendi, N., Moine, V., de Revel, G., & Teissedre, P. -L. (2013). Influence of phenolic compounds on the sensorial perception and volatility of red wine esters in model solution: An insight at the molecular level. *Food Chemistry, 140*(1–2), 76–82.

Merabtine, Y., Lubbers, S., Andriot, I., Tromelin, A., & Guichard, E. (2010). Retention/release equilibrium of aroma compounds in fat-free dairy gels. *Journal of the Science of Food and Agriculture, 90*(9), 1403–1409.

Mishellany-Dutour, A., Woda, A., Laboure, H., Bourdiol, P., Lachaze, P., Guichard, E., & Feron, G. (2012). Retro-nasal aroma release is correlated with variations in the in-mouth air cavity volume after empty deglutition. *PLoS ONE, 7*(7), e41276.

Mitropoulou, A., Hatzidimitriou, E., & Paraskevopoulou, A. (2011). Aroma release of a model wine solution as influenced by the presence of non-volatile components. Effect of commercial tannin extracts, polysaccharides and artificial saliva. *Food Research International, 44*(5), 1561–1570.

Morzel, M., Jeannin, A., Lucchi, G., Truntzer, C., Pecqueur, D., Nicklaus, S., Chambon, C., & Ducoroy, P. (2012). Human infant saliva peptidome is modified with age and diet transition. *Journal of Proteomics, 75*(12), 3665–3673.

Mounayar, R., Morzel, M., Brignot, H., Tremblay-Franco, M., Canlet, C., Lucchi, G., Ducoroy, P., Feron, G., & Neyraud, E. (2013). Salivary markers of taste sensitivity to oleic acid: A combined proteomics and metabolomics approach. *Metabolomics, 10*(4), 688–696.

Neyraud, E., Heinzerling, C. I., Bult, J. H. F., Mesmin, C., & Dransfield, E. (2009). Effects of different tastants on parotid saliva flow and composition. *Chemosensory Perception, 2*(2), 108–116.

Neyraud, E., Palicki, O., Schwartz, C., Nicklaus, S., & Feron, G. (2012). Variability of human saliva composition: Possible relationships with fat perception and liking. *Archives of Oral Biology, 57*(5), 555–566.

Normand, V., Avison, S., & Parker, A. (2004). Modeling the kinetics of flavour release during drinking. *Chemical Senses, 29*(3), 235–245.

Perry, G. H., Dominy, N. J., Claw, K. G., Lee, A. S., Fiegler, H., Redon, R., Werner, J., Villanea, F. A., Mountain, J. L., Misra, R., Carter, N.P., Lee, C., & Stone, A.C. (2007). Diet and the evolution of human amylase gene copy number variation. *Nature Genetics, 39*(10), 1256–1260.

Piombino, P., Genovese, A., Esposito, S., Moio, L., Cutolo, P. P., Chambery, A., Severino, V., Moneta, E., Smith, D. P., Owens, S. M., Gilbert, J. A., & Ercolini, D. (2014). Saliva from obese individuals suppresses the release of aroma compounds from wine. *PLoS ONE, 9*(1), e85611.

Poette, J., Mekoué, J., Neyraud, E., Berdeaux, O., Renault, A., Guichard, E., Genot, C., & Feron, G. (2014). Fat sensitivity in humans: Oleic acid detection threshold is linked to saliva composition and oral volume. *Flavour and Fragrance Journal, 29*(1), 39–49.

Quintana, M., Palicki, O., Lucchi, G., Ducoroy, P., Chambon, C., Salles, C., & Morzel, M. (2009). Inter-individual variability of protein patterns in saliva of healthy adults. *Journal of Proteomics, 72*(5), 822–830.

Ramasubbu, N., Paloth, V., Luo, Y., Brayer, G. D., & Levine, M. J. (1996). Structure of human salivary [alpha]-amylase at 1.6 A resolution: Implications for its role in the oral cavity. *Acta Crystallographica Section D, 52*(3), 435–446.

Repoux, M., Labouré, H., Courcoux, P., Andriot, I., Sémon, É., Yven, C., Feron, G., & Guichard, E. (2012). Combined effect of cheese characteristics and food oral processing on in vivo aroma release. *Flavour and Fragrance Journal, 27*(6), 414–423.

Repoux, M., Semon, E., Feron, G., Guichard, E., & Laboure, H. (2012). Inter-individual variability in aroma release during sweet mint consumption. *Flavour and Fragrance Journal, 27*(1), 40–46.

Rodriguez-Bencomo, J. J., Munoz-Gonzalez, C., Andujar-Ortiz, I., Martin-Alvarez, P. J., Moreno-Arribas, M. V., & Pozo-Bayon, M.A. (2011). Assessment of the effect of the non-volatile wine matrix on the volatility of typical wine aroma compounds by headspace solid phase microextraction/gas chromatography analysis. *Journal of the Science of Food and Agriculture, 91*(13), 2484–2494.

Schenkels, L. C., Veerman, E. C., & Nieuw Amerongen, A. V. (1995). Biochemical composition of human saliva in relation to other mucosal fluids. *Critical Reviews in Oral Biology and Medicine, 6*(2), 161–175.

Soares, R. V., Lin, T., Siqueira, C. C., Bruno, L. S., Li, X., Oppenheim, F. G., Offner, G., & Troxler, R. F. (2004). Salivary micelles: Identification of complexes containing MG2, sIgA, lactoferrin, amylase, glycosylated proline-rich protein and lysozyme. *Archives of Oral Biology, 49*(5), 337–343.

Tavel, L., Andriot, I., Moreau, C. I, & Guichard, E. (2008). Interactions between β-lactoglobulin and aroma compounds: Different binding behaviors as a function of ligand structure. *Journal of Agricultural and Food Chemistry, 56*(21), 10208–10217.

Tromelin, A., Merabtine, Y., & Andriot, I. (2010). Retention–release equilibrium of aroma compounds in polysaccharide gels: Study by quantitative structure–activity/property relationships approach. *Flavour and Fragrance Journal, 25*(6), 431–442.

van Ruth, S. M., Grossmann, I., Geary, M., & Delahunty, C. M. (2001). Interactions between artificial saliva and 20 aroma compounds in water and oil model systems. *Journal of Agricultural and Food Chemistry, 49*(5), 2409–2413.

van Ruth, S. M., & Roozen, J. P. (2000). Influence of mastication and saliva on aroma release in a model mouth system. *Food Chemistry, 71*(3), 339–345.

van Ruth, S. M., Roozen, J. P., & Cozijnsen, J. L. (1995). Changes in flavour release from rehydrated diced bell peppers (*Capsicum annuum*) by artificial saliva components in three mouth model systems. *Journal of the Science of Food and Agriculture, 67*(2), 189–196.

Villamor, R. R., Evans, M.A., Mattinson, D. S., & Ross, C. F. (2013). Effects of ethanol, tannin and fructose on the headspace concentration and potential sensory significance of odorants in a model wine. *Food Research International, 50*(1), 38–45.

Voirol, E., & Daget, N. (1986). Comparative study of nasal and retronasal olfactory perception. *Food Science and Technology - Lebensmittel - Wissenschaft & Technologie, 19*, 316–319.

Publication n°12: Understanding the release and metabolism of aroma compounds using micro-volume saliva samples by ex vivo approaches.

Muñoz-González, C.; Feron, G.; Brulé, M.; Canon, F.

Food Chem. **2018,** *240*, 275-285.

Food Chemistry 240 (2018) 275–285

Contents lists available at ScienceDirect

Food Chemistry

journal homepage: www.elsevier.com/locate/foodchem

Understanding the release and metabolism of aroma compounds using micro-volume saliva samples by *ex vivo* approaches

Carolina Muñoz-González *, Gilles Feron, Marine Brulé, Francis Canon

Centre des Sciences du Goût et de l'Alimentation, UMR1324 INRA, UMR6265 CNRS Université de Bourgogne, Agrosup Dijon, F-21000 Dijon, France

ARTICLE INFO

Article history:
Received 12 March 2017
Received in revised form 23 June 2017
Accepted 11 July 2017
Available online 15 July 2017

Keywords:
Aroma compounds
Carbonyl compounds
Enzymatic conversion
Saliva composition
Salivary proteins
Total antioxidant capacity

ABSTRACT

This study investigated the behaviour of key aroma compounds in the presence of human saliva (200 μL) from different individuals ($n = 3$) submitted or not to centrifugation (whole *vs* clarified saliva). HS-GC results showed that human saliva strongly decreased the release of carbonyl compounds (aldehydes and ketones). This effect was dependent on i) the structure of the aroma compounds and ii) the saliva composition. Whole saliva exerted a higher effect than clarified saliva on aroma compounds. Moreover, this effect was individual-dependent and related to the total protein content and the total antioxidant capacity of saliva. HS-SPME and LLE-GC/MS analyses revealed that metabolism of the compounds by salivary enzymes was involved. This observation indicates that some aroma compounds could be metabolized in the oral cavity in an individual manner, which could have implications for aroma perception (e.g., formation of new metabolites with different odor thresholds and qualities) and/or organisms' health status (e.g., compound detoxification).

1. Introduction

Since aroma perception is one of the most important aspects driving food consumption and it can be modulated during the oral processing of the food, the impact of oral parameters such as saliva on aroma compounds has received great attention in recent years (Ployon, Morzel, & Canon, 2017). In this regard, it has been recently shown that saliva composition is related to *in vivo* aroma release (Feron et al., 2014) and aroma perception (Guichard, Repoux, Qannari, Laboure, & Feron, 2017) during the consumption of model cheeses. However, *in vivo* experiments are subjected to the influence of other physiological factors that could affect the transfer of the aroma compounds to the olfactory receptors. Therefore, the effect of saliva in such an approach is difficult to unravel. Consequently, most of the studies performed to elucidate the effects of saliva on aroma compounds have been performed under well-controlled *in vitro* or *ex vivo* conditions. These studies have highlighted effects of different nature of saliva on aroma compounds. The retention of aroma compounds by salivary proteins in the presence of artificial (Friel & Taylor, 2001; Pages-Helary, Andriot, Guichard, & Canon, 2014; van Ruth, Grossmann, Geary, & Delahunty, 2001) or human salivas (Genovese, Piombino, Gambuti, & Moio, 2009; Munoz-Gonzalez, Feron et al., 2014; Pages-Helary et al., 2014) is well-documented. Moreover, other mechanism such as the metabolism of aroma compounds (Buettner 2002a, 2002b; Lasekan, 2013) by salivary enzymes, has also been strongly suggested. Interestingly, it has been described that the same compound can be submitted to both effects; e.g., ethyl hexanoate can be retained by mucin solutions (Friel & Taylor, 2001) whilst it is also susceptible to metabolism by salivary enzymes (Buettner, 2002b; Pages-Helary et al., 2014). In addition, an increase in the release of some aroma compounds in the presence of specific salivary constituents (called the salting-out effect) has also been observed (Friel & Taylor, 2001).

However, most of the above-mentioned studies have been carried out with artificial salivas (Friel & Taylor, 2001; Pages-Helary et al., 2014; van Ruth et al., 2001) or pooled salivas submitted or not to a clarification process (Genovese et al., 2009; Munoz-Gonzalez, Feron et al., 2014; Pages-Helary et al., 2014), which could have not completely represented the complexity of human saliva composition as is found in the human mouth (whole saliva). Indeed, human saliva is composed of a wide number of different components, such as electrolytes, proteins and microorganisms, whose profile and proportion is highly individual-dependent (Leake, Pagni, Falquet, Taroni, & Greub, 2016; Neyraud, Palicki, Schwartz, Nicklaus, & Feron, 2012).

In spite of this well-known inter-individual variability on saliva composition, the possible effects of this variability on aroma compounds (release, metabolism) by *ex-vivo* approaches have received very little attention and very few studies have tackled this question

* Corresponding author.
E-mail address: carolina.munoz@inra.fr (C. Muñoz-González).

http://dx.doi.org/10.1016/j.foodchem.2017.07.060
0308-8146/

(Buettner, 2002a, 2002b; Piombino et al., 2014). This could be related to analytical constraints, such as the collection of suitable volumes of saliva to carry out these studies. Indeed, works on this topic have employed different techniques that require relative high volumes of saliva (6–10 mL/assay) that would be difficult to obtain from one individual. Among them, static headspace methodology has been the preferred approach. This approach is based on the analysis of the headspace (HS) above a solution after an equilibrium time. The headspace can be taken with a syringe (HS) or concentrated in a polymer-coated fiber (headspace solid-phase microextraction; HS-SPME) before being analysed by gas chromatography (GC), gas chromatography-mass spectrometry (GC–MS) or other on-line techniques like proton transfer reaction-mass spectrometry (PTR-MS). Moreover, liquid-liquid extractions (LLE) coupled to GC–MS have also been employed to study the transformations of aroma compounds in the presence of saliva (Buettner, 2002a, 2002b). In fact, due to the complexity of human saliva composition and the wide type of biochemical reactions (e.g., non-covalent interactions, enzymatic conversion) that could occur between salivary and food components, the use of complementary methodologies seems mandatory to elucidate the effects of human saliva on aroma compounds.

With this background, the aim of the present study was to investigate the effects of human saliva composition on aroma compounds. In order to reach this goal, an HS-GC method adapted to low volumes of saliva (200 μL) was firstly developed, validated and then independently applied to 17 key aroma compounds in the presence of saliva from three individuals and submitted to different treatments (whole *vs* clarified). The selected aroma compounds belonged to three different chemical families (ketones, aldehydes and alcohols), possessed different structures (carbonyl position, presence of double bonds, linear *vs* branched) and a range of physicochemical properties (hydrophobicity, volatility). Control samples with water were employed to evaluate the extent of the saliva effect. The relationship between some saliva compositional parameters and HS-GC data was examined. Finally, HS-SPME-GC/MS and LLE-GC/MS analyses allowed us to investigate the nature of the observed effects.

2. Material and methods

2.1. Aroma compounds

Seventeen compounds were chosen on the basis of their different physicochemical characteristics (chemical family, functional group, carbonyl count, structure, chemical properties), their aroma impact (key food and beverage aroma compounds) and because of their suitability for the analysis technique (sensitivity, solubility). The list of compounds included three main chemical families (ketones, aldehydes and alcohols) and two functional groups (carbonyl *vs* alcohol) (Table 1). The aroma compounds were of analytical grade (Aldrich, Steinheim, Germany; Fluka, Buchs, Switzerland; Firmenich, Geneva, Switzerland). A gas chromatography-flame ionization detector (GC-FID) analysis confirmed the purity of all aroma compounds (>95%) that was taken into account for calculations. Stock solutions (1%) of the single aroma compounds were prepared in propylene glycol at room temperature under magnetic stirring for 2 h. They were stored at 4 °C for a maximum of three months.

2.2. Saliva samples

2.2.1. Saliva collection

Unstimulated saliva samples were freshly collected from three healthy subjects (two men, one woman), aged between 30 and 52 years old. All subjects were non-smokers and had not taken any antibiotics or other medical treatments during the three months previous to sampling. Participants were asked not to consume any food or drink two hours before saliva was collected. They let the saliva naturally be accumulated in the mouth and then spat it directly into a collection tube. Different saliva collections for each individual were organized over several days and pooled together in order to: i) avoid interday variability in saliva composition among individuals (Buettner, 2002a, 2002b; Neyraud et al., 2012), and ii) get a suitable volume of saliva from each individual to perform the whole investigations while avoiding their fatigue.

From the pooled saliva from each individual, half of the crude saliva (whole saliva) was separated and the other half centrifuged at 15,000*g* for 15 min at 4 °C (clarified saliva). Clarification of human saliva is a treatment frequently employed in the literature to remove excessive mucus, cells and facilitate biochemical analysis. Therefore, two saliva types (whole and clarified saliva) from each of the three individuals were employed for this study. Saliva samples were aliquoted and stored at −80 °C until use. Previously, it was verified that the storage of saliva under these conditions did not modify its effect on aroma compounds. To do that, the release of aroma compounds in presence of fresh saliva or saliva submitted to storage (frozen at −80 °C and thawed) was studied and no significant differences were observed between samples.

The experimental protocol was approved by the French Ethics Committee for Research (CPP Est I, Dijon, #14.06.03, ANSM #2014-A00071-46).

2.2.2. Saliva biochemical analyses

2.2.2.1. Protein concentration. The protein concentration was determined using the Bradford protein assay with bovine serum albumin (BSA) used as the standard for calibration.

2.2.2.2. Total antioxidant capacity (TAC). The total antioxidant capacity was determined using an ORAC Assay kit (Zen-bio, Research Triangle Park, NC). This assay measures the loss of fluorescein fluorescence over time due to peroxyl radical formation resulting from the breakdown of AAPH (2,2′-azobis-(2-amidinopro pane) dihydrochloride). Trolox (6-hydroxy-2,5,7,8-tetramethyl chroman-2-carboxylic acid), a water-soluble vitamin E analog, serves as a positive control to inhibit fluorescein decay in a dose-dependent manner. The intensity of fluorescence was measured (excitation filter, 485 nm; emission filter, 538 nm) using a microtiter plate fluorometer (Victor 3-V, PerkinElmer, France). The total antioxidant capacity was expressed in micromolar Trolox equivalents.

2.2.2.3. pH. pH was determined using a pH meter (Mettler Toledo, Schwerzenbach, Switzerland).

2.3. HS-GC analyses

To follow the release of aroma compounds in micro-volume samples, aqueous aroma solutions were freshly prepared by dilution of the stock solutions with water to obtain single solutions of each odorant at 10 mg/L. This concentration is far below the solubility threshold of the assayed compounds in water (Table 1). A 300-μL aliquot of this aroma solution was added to 200 μL of water or saliva. Vials were immediately closed with a PTFE/silicone septum (Supelco, Bellefonte, PA), stirred and incubated at 37 °C. The time needed to reach equilibrium was determined for all the compounds in the control samples with water at 5, 15, 30, and 45 min. From the analysis of the kinetic profiles it was found that 30 min of incubation was enough for the equilibration of the selected aroma compounds. After the incubation time, two hundred microliters of headspace were taken automatically using a preheated (45 °C)

Table 1
List of the 17 aroma compounds employed in this study together with their molecular weight (MW), hydrophobic constant (log P), boiling point (BP), solubility in water, GC oven temperature, aroma descriptor, CAS number and structure.

Compound	MW (g/mol)[a]	log P[b]	BP (°C)[c]	Water solubility (mg/L)[d]	GC oven temperature (°C)	Descriptor[e]	CAS number	Type[f]
Ketones								
2-butanone	72.11	0.26	70.36	76100	50	Butterscotch	78-93-3	L
2,3-butanedione	86.09	−1.34	117.70	1000000	60	Buttery	431-03-8	U
2-pentanone	86.13	0.75	95.03	21200	60	Sweet, fruit	107-87-9	L
2,3-pentanedione	100.12	−0.85	140.60	615900	70	Butter, cream	600-14-6	U
2-octanone	128.22	2.22	163.60	884	100	Fruity	111-13-7	L
1-octen-3-one	126.2	2.37	161.99	895	120	Mushroom, metal	4312-99-6	U
Alcohols								
1-pentanol	88.15	1.33	136.95	20890	90	Fruit, balsamic	71-41-0	L
1-hexanol	102.17	1.82	159.09	6885	100	Fatty, floral, green	111-27-3	L
(*Z*)-3-hexen-1-ol	100.00	1.61	165.73	16000	110	Fruity, green, leaves	928-97-2	U
1-octanol	130.23	2.81	200.67	814	130	Green herbaceous	111-87-5	L
1-octen-3-ol	128.22	2.60	180.31	1836	100	Mushroom, earthy, fungal	3391-86-4	U
Linalool	154.25	3.38	204.05	684	130	Aniseed, citrus, floral	78-70-6	C
Menthol	156.27	3.38	218.94	434	140	Carraway, sweet	89-78-1	C
Aldehydes								
Hexanal	100.16	1.80	132.2	3527	70	Grass, fat	66-25-1	L
Octanal	128.22	2.78	132.20	394	100	Fat, lemon, green	124-13-0	L
Octenal	126.20	2.35	117.37	945	115	Green	25447-69-2	U
Benzaldehyde	106.13	1.71/1.48	181.22	6100	130	Almond, burnt sugar	100-52-7	C

[a] Molecular weight.
[b] Hydrophobic constant estimated using molecular modeling software EPI Suite (U.S. EPA 2000–2007).
[c] Boiling point estimated using molecular modeling software EPI Suite (U.S. EPA 2000–2007).
[d] Water solubility estimated at 25° C using molecular modeling software *EPI* Suite (U.S. EPA 2000–2007).
[e] From Flavornet database (http://www.flavornet.org; accessed October 2009), from NIST web chemistry book (2005) (http://www.webbook.nis.gov/chemistry).
[f] Chemical structure (L: linear, U: unsaturated; C: cyclic).

1-mL gas-tight syringe (Gerstel, manufactured by SGE, Victoria, Australia) and analysed by gas chromatography (Agilent 7890B). The injector temperature was set at 240 °C and the flame ionization detector at 250 °C. A DW-Wax capillary column (30 m × 0.32 mm i.d. × 0.5 μm; Agilent J&W Scientific, Folsom, CA) was used. The carrier gas was helium at a velocity of 30 cm^3/s in splitless mode. For each aroma compound, an oven isothermal temperature was preliminary determined in order to obtain a retention time between 2 and 5 min (Table 1). In order to avoid any aroma competition for protein binding or catalytic sites in the saliva samples, aroma compounds were analysed one by one. Each sample was analysed in triplicate (one injection per sample vial). A total of 408 injections was carried out.

To validate the methodology, linearity and repeatability of the procedure were determined in an aqueous solution composed of a mixture of 17 aroma compounds at four levels of concentration (1, 5, 10, 25 mg/L). Each sample was analysed in triplicate (one injection per sample vial).

2.4. HS-SPME-GC/MS analyses

HS-SPME-GC/MS analyses were performed to identify the possible formation of new volatile metabolites in the presence of saliva. This technique was chosen since it is a very sensitive technique frequently employed in the literature because of its powerful concentration of the headspace, and therefore suitable to follow metabolites at low concentrations (can reach parts per trillion (ppt) levels for certain compounds). A mixture composed of pooled whole saliva from the three individuals was incubated in the presence of single aroma solutions and the headspace above the samples extracted by HS-SPME-GC/MS. Moreover, control samples with water (water + aroma solution) and blanks of saliva were analysed in parallel and under exactly the same analytical conditions to discard the presence of possible artefacts. The extraction was automatically performed by using a CombiPal system (CTC Analytics, Zwingen, Switzerland) provided with a 50/30 μm DVB/CAR/PDMS fiber of 2 cm length (Supelco). After the incubation time (25 min), the extraction was performed in the headspace of the vials for 5 min at 37 °C. Desorption was performed in the injector of a gas chromatograph (Agilent 6890 N; Agilent, Santa Clara, CA) in splitless mode for 1.5 min at 240 °C. After each injection the fiber was cleaned for 30 min at 240 °C to avoid any memory effects. The oven temperature was programmed to increase from 40 to 240 °C at 4 °C/min and held for 1 min. After desorption of the SPME fiber, volatile compounds were separated on a DB-Wax polar capillary column (30 m × 0.32 mm i.d. × 0.50 μm film thickness) from Agilent (J&W Scientific, Folsom, CA, USA). Helium was the carrier gas at a flow rate of 1 mL/min. The coefficient of variation (CV) of the technique was calculated after analyzing six times an aroma mixture containing the 17 selected compounds under the conditions reported above. The mean CV was 5.7% (with values ranging from 1.6% for (*Z*)-3-hexen-1-ol to 13.1% for 1-pentanol).

For the MS system (Agilent 5973N), the temperatures of the transfer line, quadrupole, and ion source were 250, 150, and 230 °C, respectively. Electron impact mass spectra were recorded at 70 eV ionization voltage and the ionization current was 10 μA. The acquisitions were performed in scan mode (from *m/z* 35 to 350). The identification of compounds was based on the comparison of retention times and mass spectra from two databases: NIST 2.0 and WILEY 138.

2.5. LLE-GC/MS analyses

In an attempt to confirm the enzymatic metabolism of aroma compounds by saliva, LLE-GC–MS analyses were carried out after submitting the whole saliva samples to different treatments to obtain non enzymatic saliva, sterile saliva and saliva without microorganisms, cells or enzymes. Moreover, the effect of the reducing agent NADH (1 mM; Sigma-Aldrich, Steinheim, Germany) in the presence of whole and non-enzymatic saliva was also evaluated. This technique allows the determination in the liquid phase of a broad range of aroma compounds with very different polarities. Moreover, it does not take into account the possible weak

interactions between aroma compounds and salivary components whilst providing a high sensitivity.

After incubation of the samples at 37 °C for 30 min, liquid-liquid extractions were carried out. Methodologies based on methods already published by Buettner (2002a), and Esteban-Fernandez and coworkers (Esteban-Fernandez, Rocha-Alcubilla, Munoz-Gonzalez, Moreno-Arribas, & Pozo-Bayon, 2016) were adapted to the present experimental conditions. Briefly, 500 μL of a saturated $CaCl_2$ solution were immediately added to the samples to inhibit possible enzymatic reactions. The solutions were extracted twice with 1 mL of dichloromethane (Carlo Erba, Val de Reuil, France) then centrifuged (5000g, 4 °C, 15 min) to separate the two phases. Prior to the extraction, samples were spiked with 100 μL of the internal standard, methyl nonanoate (10 mg/L). The combined organic extracts were dried over anhydrous Na_2SO_4, then concentrated to a total volume of 200 μL. One microlitre was injected into the GC/MS in splitless mode following the same method described above for the HS-SPME/GC–MS analysis. The same LLE procedure was carried out with the salivas and water samples without added aroma compounds, in order to detect any possible compounds coming from the salivas or any artefact formed during the extraction procedure. Relative peak areas (RPAs) were obtained by dividing the area of the peak of interest by the area of the internal standard.

2.6. Statistical analyses

Linear regression analyses were performed on the static HS-GC experiments to establish the linearity of each aroma compound and the lack of fit test was used to judge the adequacy of the linear models. ANOVA analyses were employed to determine significant effects among the studied factors. In addition, for each aroma compound and individual (water, S1, S2 or S3) differences between saliva type (whole *vs* clarified saliva) were subsequently examined by least significant difference (LSD) test. The significance level was $0.01 < p < 0.1$ throughout the study. The STATISTICA program for Windows version 7.1 and the XLSTAT program were used for data processing (StatSoft, Inc., 2005; www.statsoft.com).

3. Results and discussion

It has been previously demonstrated that human saliva impacts the release of aroma compounds (Genovese et al., 2009; Mitropoulou, Hatzidimitriou, & Paraskevopoulou, 2011; Munoz-Gonzalez, Feron et al., 2014; Pages-Helary et al., 2014; Piombino et al., 2014). However, to study the impact of differences in human saliva composition among individuals on aroma compounds, it is necessary to take into account that the collection of suitable volumes of human saliva for experimental purposes is tedious, unpleasant and sometimes (e.g. hyposalivation) very difficult (Friel & Taylor, 2001). In this work, an HS-GC methodology using small volumes of saliva (200 μL) has been developed, its analytical performance determined and then applied to evaluate the effects of human saliva composition on aroma compounds.

3.1. Analytical performance of the HS-GC method

The repeatability of this methodology was studied by the calculation of the relative standard deviation (RSD) ($n = 6$) and results are presented in Supplementary material (Table 1). The RSD average of the method was very low (3.8%) which means a good repeatability across analyses. Among the chemical classes, ketones (mean RSD = 3.2%) and alcohols (mean RSD = 3.3%) presented the lowest RSDs while aldehydes (mean RSD = 5.8%) the highest. This could be due to the higher positive charge of the carbonyl carbon of aldehydes that confers a higher reactivity to these molecules.

For each compound, a linear regression was calculated to determine the linearity of the analytical method (Table 1: Supplementary material). A lack of fit test was also applied to determine whether the calculated model was adequate for the experimental data. As can be seen, a clear linear relationship between the amount of aroma compounds in the headspace and the concentration of aroma compounds added to the vials was obtained. The linear models showed determination coefficients higher than 99% for all the assayed compounds and adequate values of residual standard deviation (*s*) over the concentration range assayed (Table SM 1). The lack of fit test also showed the adequacy of the proposed regression models (p values > 0.01 for all aroma compounds).

3.2. Effects of human saliva on aroma compounds by HS-GC

Once the validity of the method was proven, the methodology was applied to measure the HS of 17 aroma compounds in the presence of salivas from three individuals (n = 3) submitted or not to a clarification process (whole *vs* clarified). Results are shown in Table 2 as a function of the aroma chemical family, saliva treatment (whole *vs* clarified) and assayed sample (w, S1, S2, S3). To facilitate data interpretation, headspace data are expressed relative to water, so that values >100% represent an increase of the compound release in the headspace compared to the water samples, while values <100% denote a decrease. As shown in Table 2, both types of behaviour (decrease or increase of HS concentration compared to water) were observed depending on the molecule.

3.3. Differences on aroma release by compound type

Previous studies have reported that aroma compounds can interact with proteins (Tavel, Moreau, Bouhallab, Li-Chan, and Guichard (2010) and salivary proteins through hydrophobic effects (Pages-Helary et al., 2014). Therefore, physicochemical properties, such as hydrophobicity, have been frequently employed to predict the release of aroma compounds in the presence of other compounds. In an attempt to explain the results observed in this study, the hydrophobicity (log *P* values) of the compounds and their relative headspace concentrations above the saliva samples (mean of whole saliva values) (Supplementary material Fig. 1) were plotted. As can be observed in the figure, and in spite of the selected molecules covering a wide range of log *P* values (from −1.34 to +3.38) no clear correlation between the log *P* and the relative headspace values could be observed ($r^2 = 0.017$). In their study, Friel and Taylor (2001) also reported the absence of a correlation between log *P* and the relative headspace values of aroma compounds in the presence of artificial saliva solutions containing only mucin. Therefore, non-covalent interactions between salivary proteins and aroma compounds involving hydrophobic effects seem not to be the main or unique mechanism explaining the effects of saliva on aroma compounds.

The impact of human saliva on aroma air–solution partition has been found to be highly chemical family-dependent (Table 2). Aldehydes and ketones, chemical families containing a carbonyl group, were the most affected compounds. Among them, aldehydes were more affected than ketones by the presence of different salivas. This higher effect of saliva on partitioning of aldehydes compared to ketones has already been observed by Friel and Taylor (2001), and van Ruth et al. (2001), in the presence of artificial salivas. Alcohols were less affected than the other chemical families by the presence of saliva (Table 2). Within a chemical family, different effects were observed as a function of the compound structure (e.g. linear *vs* cyclic/ramified, saturated *vs* unsaturated).

Table 2
Relative headspace aroma values determined above water and saliva samples by HS-GC. Data represent the comparison of the same aroma compound determined in water or saliva samples and are expressed as percentages (considering the value determined in the water sample as 100% and comparing it with the value of the same compound determined in the saliva sample of each individual). The coloured columns represent the mean values of each saliva type (whole *vs* clarified saliva).

Compounds	whole saliva					clarified saliva				
	w	S1	S2	S3	mean whole saliva	w	S1	S2	S3	mean clarified saliva
Ketones										
2-butanone	100 b	106 a	104 a	105 a	105	100 a	103 a	101 a	99 a	101
2,3-butanedione	100 a	93 b	90 b	52 c	78	100 a	95 bc	98 ab	94 c	96
2-pentanone	100 a	101 a	99 a	99 a	100	100 b*	105 a*	103 ab*	100 a*	103
2,3-pentanedione	100 a	94 b	92 b	72 c	86	100 a	92 b	91 b	92 b	92
2-octanone	100 a	105 a	101 a	102 a	103	100 a	99 a	97 a	100 a	99
1-octen-3-one	100 a	86 b	85 b	40 c	70	100 a	85 b	85 b	49 c	73
Alcohols										
1-pentanol	100 b*	103 ab*	105 ab*	110 a*	106	100 b	106 a	106 a	103 ab	105
1-hexanol	100 a	103 a	101 a	101 a	102	100 a	103 a	103 a	103 a	103
(Z)-3-hexen-1-ol	100 a	103 a	101 a	101 a	102	100 a	105 a	105 a	105 a	105
1-octanol	100 c	104 b	109 a	107 ab	107	100 b*	103 ab*	105 a*	105 a*	104
1-octen3-ol	100 a*	100 a*	100 a*	96 b*	99	100 a	99 a	102 a	98 a	100
linalool	100 a	102 a	99 a	102 a	101	100 a	103 a	105 a	106 a	105
menthol	100 b*	104 ab*	105 a*	99 b*	103	100 a	102 a	99 a	100 a	100
Aldehydes										
Hexanal	100 a	96 a	88 b	39 c	74	100 a	100 a	98 a	90 b	96
Octanal	100 a	89 b	77 c	23 d	63	100 a	100 a	102 a	94 b	99
Octenal	100 a	105 a	100 a	71 b	92	100 a	101 a	99 a	89 b	96
Benzaldehyde	100 ab	96 b	103 a	73 c	91	100 a	99 a	100 a	103 a	101

Different letters across the different assessors denotes statistical differences ($p < 0.05$ or * $0.05 < p < 0.1$) after application of the LSD test.

3.3.1. Ketones

Three classes of ketones were studied: linear saturated (2-butanone, 2-pentanone and 2-octanone), or unsaturated monoketones (1-octen-3-one) and diketones (2,3-butanedione, 2,3-pentanedione). To the authors' knowledge, the only work specifically studying the *ex-vivo* effect of human saliva on ketones is the one carried out by Pages-Helary et al. (2014). This work focused on the effect of saliva on a series of five linear methylketones (2-propanone, 2-hexanone, 2-heptanone, 2-octanone and 2-nonanone). They showed that the two most hydrophobic ketones assayed in their study (2-octanone and 2-nonanone) presented lower partition coefficients in human saliva than in water solutions. The origin of this observation was attributed to the retention of these compounds by human salivary proteins through non-covalent interactions. In the present study, no significant effects on the assayed linear methyl ketones (2-butanone, 2-pentanone, 2-octanone) have been observed, which could be due to differences in the composition of salivas employed between the two studies. Indeed, in their study Pages-Helary et al. (2014) used pooled human saliva provided by several volunteers. Moreover, they also found different effects of artificial saliva on aroma compounds as a function of its composition. To explain their results, authors proposed that some salivary proteins interact with each other, precluding the access of aroma compounds to the binding sites.

Interestingly, a significant effect of human saliva was found for the diketones (2,3-butanedione and 2,3-pentanedione) and the unsaturated monoketone (1-octen-3-one) assayed in the present study. For example, 2,3-butanedione was reduced on average by 13% in the HS above saliva compared to the control samples. The same trend was observed for 2,3-pentanedione (11% average reduction) and 1-octen-3-one (28% average reduction). The presence of more than one functional group or double bonds in these molecules could have increased their reactivity, making them more susceptible to action by salivary components. To our knowledge this is the first time that an effect of human saliva on these compounds has been described. Only a few works (Friel & Taylor, 2001; van Ruth et al., 2001) have studied the behaviour of one of these molecules (2,3-butanedione) in the presence of artificial saliva, showing contradictory effects. In solutions with mucin, alpha-amylase and salts, van Ruth et al. (2001) did not find any significant effect of saliva on 2,3-butanedione. In contrast, Friel and Taylor (2001) showed that 2,3-butanedione was reduced by up to 50% in the headspace when artificial saliva (mucin and salts) was present. The disparity in these results could be due to the different techniques (HS-GC *vs* HS-APCI/MS), equilibrium times (6 min *vs* 5 h), or more probably to the different compositions of the salivas employed in these studies. Indeed, the artificial salivas used in the previous studies contained only mucin with/without alpha-amylase.

3.3.2. Alcohols

In the case of alcohols three different classes were also studied and divided into linear (saturated and unsaturated) and cyclic molecules. However, the effects of human saliva on these compounds were almost negligible and when observed, a salting-out effect was in general the behaviour detected. The limited effect of saliva on alcohols is also in agreement with the results found in different publications (Buettner 2002a; Friel & Taylor, 2001; Genovese, Moio, Sacchi, & Piombino, 2015; Munoz-Gonzalez, Feron et al., 2014; van Ruth et al., 2001) carried out with diverse techniques, matrix (model solutions *vs* food) and saliva types (human or artificial salivas).

3.3.3. Aldehydes

All the aldehydes assayed in this study were affected by the presence of saliva. The linear saturated molecules (hexanal, octanal) were the most affected molecules, and hydrophobic effects could explain the differences observed between both linear aldehydes: the release of hexanal (log $P = 1.80$) was reduced to a lesser extent than that of octanal (log $P = 2.78$) in the presence of saliva. This result was already observed by van Ruth et al. (2001), which stated that a larger molecule size or higher hydrophobicity could

result in a higher affinity for salivary proteins. This observation appears to contradict the general trend observed in this study for which hydrophobicity seems not to be the main or unique determinant explaining HS data. However, it could be possible that all the molecules are not subjected to the same mechanism, and hydrophobicity could be one factor causing the affinity of a serious of analogous compounds for a specific protein *via* hydrophobic effects as reported previously (Pages-Helary et al., 2014).

The aldehydes less affected were the cyclic benzaldehyde and the unsaturated 2-octenal. In fact, the unsaturated 2-octenal was less affected than its analogue saturated octanal, which was contrary to the effect observed for the ketones. This fact also suggests that different mechanisms could be involved as a function of the structure of the molecule. This could explain the different behaviour observed between aldehydes and ketones in the presence of saliva.

3.4. Differences in aroma release due to saliva type

Table 2 shows the mean headspace data of each aroma compound determined for the whole and clarified saliva samples. Interestingly, the effects of human saliva on the affected compounds (carbonyl compounds) were more marked in the presence of whole than clarified saliva. One compound (benzaldehyde), was affected by whole saliva but not affected by clarified saliva while 1-octen-3-one was similarly affected by whole and clarified saliva. During the centrifugation process carried out at 4 °C for 15 min at 15,000*g*, components in suspension and/or with high molecular weight (like aggregates or supramolecular complexes of proteins, mucins, cells, microorganism and food debris or salivary micelles) are separated from saliva solutions. Therefore, some of those components that had been completely or totally removed from clarified saliva could participate in the observed effects. These results pointed out the necessity to apply the minimum treatment on saliva samples, in order to be able to study the effect of human saliva composition on aroma compounds.

In order to explore more deeply our results, relative headspace data obtained for each individual and saliva type were independently submitted to one-way ANOVA and LSD tests (Table 2). As can be seen, large variations in the aroma air–solution distribution between individuals have been found. However, these differences were much less important in clarified than in whole saliva, probably due to a reduction in the amount of proteins after centrifugation as mentioned above. This observation suggests that the centrifugation tended to standardize saliva samples across individuals. Interestingly, the compounds affected by the presence of human saliva, presented an aroma distribution pattern quite similar for the affected compounds: S3 showed the highest reduction of aroma compounds in the headspace, while S1 and S2 behaved mostly in the same way and presented values between water and S3. The existence of *in vivo* inter-individual differences on aroma release patterns during food consumption has been extensively described, both in solid (Feron et al., 2014; Pionnier, Chabanet, Mioche, Le Quere, & Salles, 2004) and liquid food matrices (Deleris et al., 2011; Frank, Appelqvist, Piyasiri, Wooster, & Delahunty, 2011; Munoz-Gonzalez, Martin-Alvarez, Moreno-Arribas, & Pozo-Bayon, 2014) and have been attributed to anatomical and physiological differences across individuals. Among the factors that can influence *in vivo* retronasal aroma, respiratory flows (Munoz-Gonzalez, Feron et al., 2014; Pionnier et al., 2004), masticatory parameters (Feron et al., 2014; Pionnier et al., 2004), saliva flow and composition (Feron et al., 2014), oral and pharyngeal mucosa (Buettner, Beer, Hannig, & Settles, 2001; Deleris, Saint-Eve, Saglio, Souchon, & Trelea, 2016; Esteban-Fernandez et al., 2016), and in-mouth oral cavity volume (Mishellany-Dutour et al., 2012) have been suggested to explain these effects. Therefore, the present results reinforced the idea that inter-individual differences in saliva composition could be one factor affecting retronasal aroma, which would explain differences in aroma perception across individuals, as has been recently shown in model cheeses (Guichard et al., 2017).

3.5. Whole saliva composition and its relationship with aroma release among individuals

In an attempt to understand which parameters from whole saliva were more involved on the differences in the HS data observed among individuals, the biochemical characterization of the whole saliva samples (the one showing the more important effects on aroma compounds) was performed and is shown in Table 3. The biochemical characterization was based on three general measurements: total protein content, pH of the medium and total antioxidant capacity. These three parameters were selected for their potential contribution to the observed HS-GC results.

As stated above, aroma compounds can interact with salivary proteins through non-covalent and covalent interactions. Moreover, a wide number of proteins presents in saliva could show potential enzymatic properties on aroma compounds. To investigate the effect of salivary proteins on aroma release, the total salivary content of whole saliva samples ($n = 3$) was analysed and is shown in Table 3. As can be seen, the three individuals exhibited significant differences in their protein content. S3 showed the highest protein value that was significantly different from S1 and S2. In our study, this individual was the one showing the lowest relative headspace concentrations of carbonyl compounds (aldehydes and some ketones). S1 and S2 presented however a lower effect on aroma compounds and their behaviour was quite similar. Therefore, it seems that a high total protein content was related to a high reduction of carbonyl compounds in the headspace. These results are in agreement with the ones from Piombino et al. (2014), who showed a link between aroma release and protein content in salivas from obese and normal-weight individuals. Therefore, and although proteomic analyses would be needed to confirm the proteins involved in these interactions, the total protein content could be a first parameter to evaluate the potential effect of saliva on aroma release.

The pH of the medium can modify the protein conformation and as a result, the affinity of aroma–protein interactions or the enzymatic activity. In this regard, it has been shown that variations of pH (ranging from 3 to 9) can modify the partition coefficients of some aroma compounds in beta-lactoglobulin solutions (van Ruth & Villeneuve, 2002). Nevertheless, the differences in pH across the saliva samples used in this study were not large (Table 3). S1 presented the highest pH values (7.5), followed by S3 (7.2) and S2 (7.1). Therefore, it is unlikely that the small differences in pH found in the present study could explain the observed results. Moreover, the final pH of all the aroma solutions containing saliva was measured and ranged from 7.2 to 7.5, probably due to the buffering capacity of human saliva (data not shown). Therefore, pH is unlikely the cause of the differences observed in this study. However, it is important to take in mind that in certain consumption situations in which the pH of the product dominates over the oral pH (e.g., consumption of liquid foods, such as wine, characterized by an acidic pH and slight oral processing (high food:saliva ratio, low residence time)), the effects of this variable on aroma release could be different.

Finally, the determination of the total antioxidant capacity (TAC) of the whole saliva samples was carried out, as this parameter has been previously related to the aroma release behaviour in the presence of saliva (Piombino et al., 2014). In that study, authors showed that salivas from obese individuals presented significantly higher TAC values and lower aroma release than salivas from

Table 3
Biochemical composition of the whole saliva samples employed in this study.

	TPC[1] (mg/mL)		pH		TAC[2] (μM Trolox)	
	Mean	SD	Mean	SD	Mean	SD
S1	0.42 b	0.00	7.50 a	0.01	605b	259
S2	0.49 b	0.22	7.10 b	0.00	998 ab	330
S3	1.38 a	0.20	7.20 b	0.01	1277 a	243

Different letters across the different assessors denotes statistical differences ($p < 0.1$).
[1] Total Protein Content.
[2] Total Antioxidant Capacity.

normal-weight individuals. For example, the headspace concentration of the aldehyde furfural was reduced up to 40% in the saliva from the obese group compared to the saliva from the normal-weight group. Authors suggested that these effects were the result of the induction of a systemic antioxidant response in the saliva from obese individuals. This could be especially relevant for compounds prone to be submitted to redox reactions (e.g., lipid oxidation products, such as aldehydes and ketones). In this regard, it has been previously stated that saliva may constitute a first line of defense against oxidative stress (Terao & Nagao, 1991). It has also been speculated that TAC is related to the total amount of reducing agents in saliva (Kohen, Tirosh, & Kopolovich, 1992). Therefore, the higher the TAC is, the higher the reducing power of saliva to control oxidative stress. Our results are in agreement with these findings. As can be seen in Table 3, S3 possessed the highest TAC value, followed by S2 and S1. Therefore, it is likely that, the higher the TAC is, the higher is the ability of saliva to reduce the concentration of carbonyl compounds in the headspace. However, the fact that S3 also showed the highest protein content makes difficult to understand which variable (TPC or TAC) is more related to the aroma release data. Therefore, further studies with a higher number of individuals would be needed to understand the mechanisms at the origin of these effects.

3.6. Metabolism of aroma compounds by whole saliva

Some previous works have shown that human saliva is able to metabolize different groups of aroma compounds, like esters, thiols or aldehydes (Buettner, 2002a, 2002b). Therefore, the possible metabolism of the assayed aroma compounds by saliva was investigated by HS-SPME-GC/MS. These analyses revealed the presence of new metabolites in the HS above the saliva samples that were not present in the controls with water or blanks of saliva samples. Table 4 shows the aroma compounds significantly affected by the presence of human saliva (namely the assayed aldehydes, the diketones and the unsaturated 1-octen-3-one) together with the corresponding new metabolites identified. As can be seen, the main observed effect was the reduction of the carbonyl group to an alcohol group, which is in agreement with the results found by Buettner who observed the reduction of aldehydes to their corresponding alcohols (Buettner, 2002a). However, to the authors' knowledge, this is the first time that the reduction of ketones by human saliva is reported. Moreover for some compounds more than one metabolite was detected. For example, the analysis of the headspace of 1-octen-3-one resulted in the detection of two compounds: 3-octanone and 1-octen-3-ol. This transformation has already been described in mushrooms (Chen & Wu, 1984). Authors suggested the existence of two separated enzymes responsible for the formation of each compound or the existence of only one enzyme whose activity is affected by pH. Other compounds that led to the detection of more than one metabolite were 2,3-pentanedione and 2-octenal, although in these cases others hypotheses like isomerization of aroma compounds in the injector cannot be excluded (Le-Quéré, unpublished results).

In an attempt to confirm the enzymatic nature of these transformations, four types of saliva and controls with water were incubated at 37 °C in the presence of octanal and then extracted and analysed by a previously optimized LLE-GC/MS methodology. Octanal was chosen since it was the compound affected to the highest extent in the previous HS experiments. The four types of saliva assayed were: i) whole saliva, ii) whole saliva submitted to a thermal treatment of 100 °C for 10 min (non-enzymatic saliva), iii) whole saliva centrifuged at 2800*g* for 10 min (4 °C), pasteurized (60 °C for 60 min) and clarified by a final centrifugation (2800*g*, 4 °C, 10 min) (sterile saliva) and iv) sterile saliva submitted to a thermal treatment of 100 °C for 10 min (saliva without microorganisms, cells and enzymes). As can be observed in Fig. 1, the recovery of octanal was only significantly different from water in the whole saliva samples. Moreover, the formation of its metabolite octanol was only observed in this saliva type. Therefore, it appears that the only saliva with metabolizing capacity (enzymatic activity) was the whole saliva (saliva without any treatment). The enzymes responsible for the observed effects could most probably belong to the oxidoreductase superfamily, enzymes NAD(P)H+ dependent. Among them, the aldoketoreductases (AKR), short-chain dehydrogenases (SDR) or alcohol dehydrogenases (ADH) are good candidates to carry out these reactions (Marchitti, Brocker, Stagos, & Vasiliou, 2008), although to the authors' knowledge the secretion of these enzymes by human salivary glands has not been described yet (Denny et al., 2008). Therefore these enzymes could come from different sources (oral tissues or microbiota) and be present in the complex mix of fluids called whole saliva. Indeed, ADH expression and activities have been shown in human gingival and lingual mucosa (Dong, Peng, & Yin, 1996).

To further support the hypothesis that the observed effects were of enzymatic nature, whole and non-enzymatic saliva (100 °C – 10 min) were incubated in the presence or absence of NADH. NADH is the reduced form of the coenzyme NAD, working as a reducing agent and found in all living cells to involved in redox reactions. The presence of NADH is essential to the correct efficiency of NAD(P)H-dependent enzymes. As can be seen in Fig. 2a, whole saliva caused a higher degradation of octanal than non-enzymatic saliva. Moreover, the presence of NADH provoked a further reduction of octanal in whole saliva, while in non-enzymatic saliva no significant effects were observed. This strongly suggests the action of an enzymatic mechanism on the metabolism of this compound.

Finally, whole salivas from the three individuals were independently incubated in the presence or absence of NADH (Fig. 2b). As can be seen, salivas incubated in the presence of NADH showed a lower octanal and a higher octanol formation for all the individuals. Interestingly, saliva from S1 (saliva showing the lowest TAC value and possibly the lowest amount of reducing agents) seemed to be most affected by the presence of NADH. It seems for this saliva that the presence of the reducing agent has helped the enzymatic conversion take place at a higher rate. However, for saliva from S3 (saliva showing the highest TAC and possibly the highest amount of reducing agents) no differences on octanol formation

Table 4
Compounds and corresponding metabolites detected by HS-SPME-GC/MS in presence of saliva. Sensory characteristics (attribute and odor thresholds (OT)) are also included in the table.

Compounds significantly reduced by the presence of saliva	Metabolites identified in the HS above saliva samples	
2,3-butanedione (diacetyl)  «Buttery» OT: 2,3-6,5 ppb	3-hydroxy-2-butanone (acetoin)  «Sour milk» OT: 800 ppb	
2,3-pentanedione  «Butter, cream» OT: 78 ppb	3-hydroxypentan-2-one  «Herbaceous, truffle» OT: ?	2-hydroxypentan-2-one
1-octen-3-one 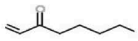 «Mushroom-like» OT: 0,005 ppb	3-octanone 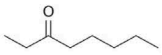 «Fruity, floral» OT: 28 ppb	1-octen-3-ol 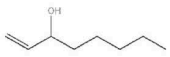 «Mushroom» OT : 1 ppb
Hexanal 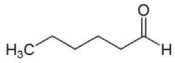 «Green, grassy» OT: 4,5 ppb	1-hexanol 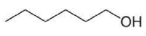 «Fatty, floral, green» OT: 2500 ppb	
Octanal 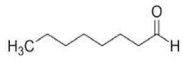 «Green grassy» OT: 0,7 ppb	1-octanol 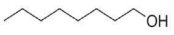 «Green» OT: 110 ppb	
Octenal 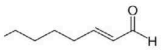 «Green» OT: 3 ppb	(E)-2-octen-1-ol  «?» OT: ?	1-octanol, (Z)-3-octen-1-ol, and others
Benzaldehyde  «Almond, burnt sugar» OT: 350 ppb	Benzyl alcohol 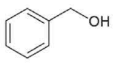 «Sweet, flower» OT: 10000 ppb	

Molecular structures from webbook.nist.gov; descriptors from flavornet.com and leffingwell.com; odor thresholds (OT) from leffingwell.com.

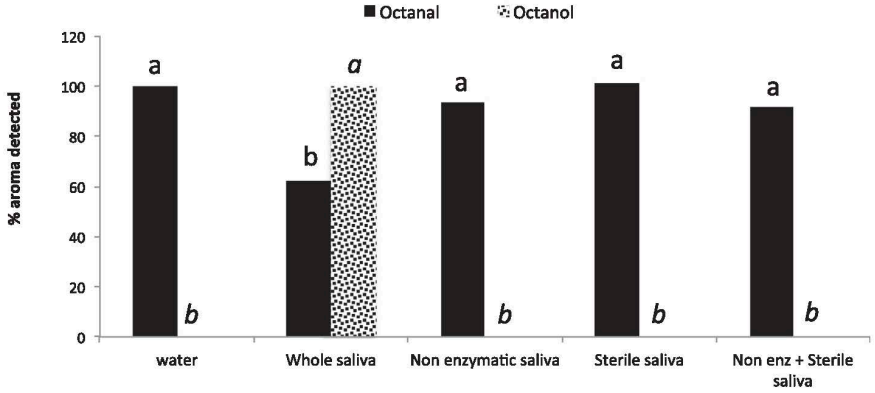

Fig. 1. Average values of octanal and octanol in presence of water and the four saliva types by LLE-GC/MS. Data represent the comparison of the same aroma compound determined in the different saliva/water samples and are expressed as percentages (considering the highest value of the specific compound as 100% and comparing this value with the amounts of the same compound determined in the other samples).

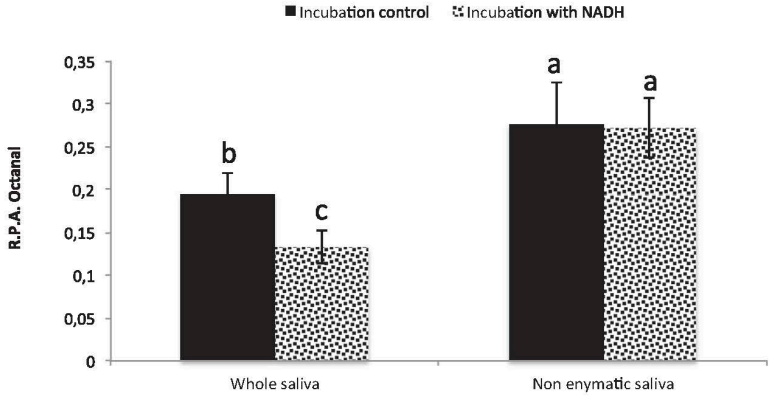

Fig. 2a. Average values of octanal (relative peak areas) in the presence of whole saliva and non-enzymatic saliva with/without NADH by LLE-GC/MS.

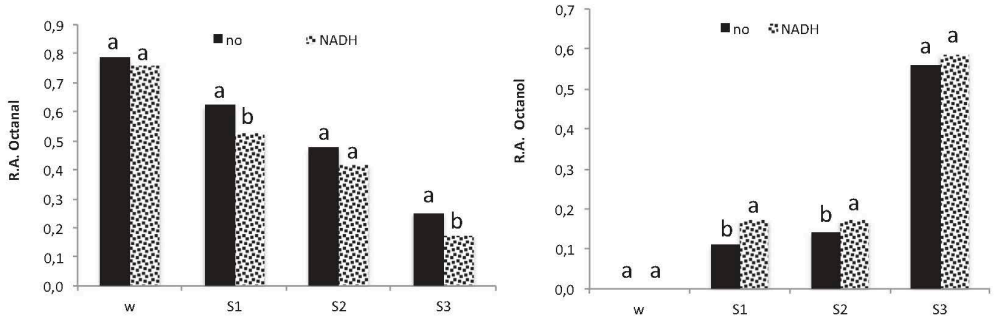

Fig. 2b. Average values of octanal and octanol (relative peak areas) in presence of water or whole salivas ($n = 3$) with/without NADH by LLE-GC/MS.

in the presence or absence of NADH were observed, possibly because a plateau for the conversion was already reached.

Finally, it is important to underline that although the reduction of the carbonyl group has been proven, it may not be the only mechanism occurring. Therefore, the existence of alternative processes like the retention of aroma compounds by salivary proteins through non-covalent interactions or the formation of conjugates with glutathione or other proteins to form condensed products cannot be discarded from the present investigation. Moreover these experiments have been carried out at pH closer to 7. Therefore the metabolic capacity of human saliva during food consumption in which saliva pH might drop or rise depending on the food should be evaluated in further experiments.

4. Conclusions

In conclusion, the new HS-GC method developed in this study adapted to small sample volumes of saliva has allowed the study of the effects of human saliva composition on 17 aroma compounds. The results showed a decrease of carbonyl compounds (ketones, aldehydes) in the headspace, while alcohols were mostly

unaffected by the presence of saliva. These effects were more important for whole than clarified salivas, revealing the necessity to use the most representative saliva possible to elucidate the effects of human saliva on aroma compounds. Even if the saliva of only three individuals was studied, the present study clearly demonstrates an effect of inter-individual variation of saliva composition on the release of aroma compounds. Salivary biochemical parameters, like the total protein content and the total antioxidant activity determined in whole saliva samples, seemed to be related to the HS data. Finally, HS-SPME-GC/MS and LLE-GC–MS analyses confirmed the reduction of the carbonyl group with the corresponding formation of an alcohol group in the presence of whole saliva and strongly suggested that this was of enzymatic nature. The metabolites formed are in general less odoriferous than the initial compounds and with possibly different sensory attributes. Moreover, by converting carbonyl (xenobiotic) compounds to less reactive products (alcohols), the organism would decrease the overall chemical reactivity of these molecules and prevent their possible toxicity. Therefore, the ability of human saliva to catalyze these reactions could represent one mode of inactivation and detoxification of toxic compounds at the entrance of the organism. Consequently, these results could have implications both in aroma perception and/or an individual's health status.

It should be emphasized that these data were obtained in *ex vivo* conditions, which could never represent all the complex mechanisms occurring *in vivo*. For example, incubation times employed cannot be compared to the consumption situation, occurring generally at shorter times. However, under *in vivo* conditions odorants are continuously exposed to a constant flow of freshly saliva so that the turnover might be considerably higher. Also, the reaction rate *in vitro* might be decreased by depletion of the reducing agent during incubation. As a result, the effects here shown could have over/under estimated the role of saliva on aroma compounds. Further work, considering different groups of populations (old *vs* young or hyposalivator *vs* normal salivator) and matrix effects (non-volatile components) are needed to describe in more detail the observed phenomena, and to determine whether they are significant *in vivo*.

Funding

This work has been written with the support of the Agreenskills fellowship programme which has received funding from the EU's Seventh Framework Programme under grant agreement N° FP7-609398 (AgreenSkills + contract). The work was also funded by the projects: MUFFIN N° 14-CE20-0001-01 and AlimaSSenS N° 14-CE20-0003-01.

Conflict of interest

The authors declare no conflict of interest in publishing this work.

Acknowledgements

We give a special thank you to Hélene Brignot for technical assistance, to the volunteers for providing us the saliva samples, and to the ChemoSens Platform (CSGA, Dijon, France).

Appendix A. Supplementary data

Supplementary data associated with this article can be found, in the online version, at http://dx.doi.org/10.1016/j.foodchem.2017.07.060.

References

Buettner, A. (2002a). Influence of human saliva on odorant concentrations. 2. Aldehydes, alcohols, 3-alkyl-2-methoxypyrazines, methoxyphenols, and 3-hydroxy-4,5-dimethyl-2(5H)-furanone. *Journal of Agricultural and Food Chemistry, 50*, 7105–7110.

Buettner, A. (2002b). Influence of human salivary enzymes on odorant concentration changes occurring in vivo. 1. Esters and thiols. *Journal of Agricultural and Food Chemistry, 50*, 3283–3289.

Buettner, A., Beer, A., Hannig, C., & Settles, M. (2001). Observation of the swallowing process by application of videofluoroscopy and real-time magnetic resonance imaging-consequences for retronasal aroma stimulation. *Chemical Senses, 26*, 1211–1219.

Chen, C., & Wu, C. (1984). Studies on the enzymic reduction of 1-octen-3-one in mushroom (agaricus-bisporus). *Journal of Agricultural and Food Chemistry, 32*, 1342–1344.

Deleris, I., Saint-Eve, A., Guo, Y. L., Lieben, P., Cypriani, M. L., Jacquet, N., ... Souchon, I. (2011). Impact of swallowing on the dynamics of aroma release and perception during the consumption of alcoholic beverages. *Chemical Senses, 36*, 701–713.

Deleris, I., Saint-Eve, A., Saglio, A., Souchon, I., & Trelea, J. C. (2016). Insights in aroma compound retention by mucosa during consumption through mathematical modelling. *Journal of Food Engineering, 190*, 123–138.

Denny, P., Hagen, F. K., Hardt, M., Liao, L. J., Yan, W. H., Arellanno, M., ... Fisher, S. J. (2008). The proteomes of human parotid and submandibular/sublingual gland salivas collected as the ductal secretions. *Journal of Proteome Research, 7*, 1994–2006.

Dong, Y. J., Peng, T. K., & Yin, S. J. (1996). Expression and activities of class IV alcohol dehydrogenase and class III aldehyde dehydrogenase in human mouth. *Alcohol, 13*, 257–262.

Esteban-Fernandez, A., Rocha-Alcubilla, N., Munoz-Gonzalez, C., Moreno-Arribas, M. V., & Pozo-Bayon, M. A. (2016). Intra-oral adsorption and release of aroma compounds following in-mouth wine exposure. *Food Chemistry, 205*, 280–288.

Feron, G., Ayed, C., Qannari, E. M., Courcoux, P., Laboure, H., & Guichard, E. (2014). Understanding Aroma Release from Model Cheeses by a Statistical Multiblock Approach on Oral Processing. *PloS one, 9*.

Frank, D., Appelqvist, I., Piyasiri, U., Wooster, T. J., & Delahunty, C. (2011). Proton transfer reaction mass spectrometry and time intensity perceptual measurement of flavor release from lipid emulsions using trained human subjects. *Journal of Agricultural and Food Chemistry, 59*, 4891–4903.

Friel, E. N., & Taylor, A. J. (2001). Effect of salivary components on volatile partitioning from solutions. *Journal of Agricultural and Food Chemistry, 49*, 3898–3905.

Genovese, A., Moio, L., Sacchi, R., & Piombino, P. (2015). Sip volume affects oral release of wine volatiles. *Food Research International, 77*, 426–431.

Genovese, A., Piombino, P., Gambuti, A., & Moio, L. (2009). Simulation of retronasal aroma of white and red wine in a model mouth system. Investigating the influence of saliva on volatile compound concentrations. *Food Chemistry, 114*, 100–107.

Guichard, E., Repoux, M., Qannari, E. M., Laboure, H., & Feron, G. (2017). Model cheese aroma perception is not only explained by in vivo aroma release but also by salivary composition and oral processing parameters. *Food & Function*.

Kohen, R., Tirosh, O., & Kopolovich, K. (1992). The reductive capacity index of saliva obtained from donors of various ages. *Experimental Gerontology, 27*, 161–168.

Lasekan, O. (2013). A comparative analysis of the influence of human salivary enzymes on odorant concentration in three palm wines. *Molecules, 18*, 11809–11823.

Leake, S., Pagni, M., Falquet, L., Taroni, F., & Greub, G. (2016). The salivary microbiome for differentiating individuals: Proof of principle. *Microbes and Infection, 18*, 399–405.

Marchitti, S., Brocker, C., Stagos, D., & Vasiliou, V. (2008). Non-P450 aldehyde oxidizing enzymes: The aldehyde dehydrogenase superfamily. *Expert Opinion on Drug Metabolism & Toxicology, 4*, 697–720.

Mishellany-Dutour, A., Woda, A., Laboure, H., Bourdiol, P., Lachaze, P., Guichard, E., & Feron, G. (2012). Retro-Nasal Aroma Release Is Correlated with Variations in the In-Mouth Air Cavity Volume after Empty Deglutition. *PloS one, 7*.

Mitropoulou, A., Hatzidimitriou, E., & Paraskevopoulou, A. (2011). Aroma release of a model wine solution as influenced by the presence of non-volatile components. Effect of commercial tannin extracts, polysaccharides and artificial saliva. *Food Research International, 44*, 1561–1570.

Munoz-Gonzalez, C., Feron, G., Guichard, E., Rodriguez-Bencomo, J. J., Martin-Alvarez, P. J., Moreno-Arribas, M. V., & Pozo-Bayon, M. A. (2014a). Understanding the role of saliva in aroma release from wine by using static and dynamic headspace conditions. *Journal of Agricultural and Food Chemistry, 62*, 8274–8288.

Munoz-Gonzalez, C., Martin-Alvarez, P. J., Moreno-Arribas, M. V., & Pozo-Bayon, M. A. (2014b). Impact of the nonvolatile wine matrix composition on the in vivo aroma release from wines. *Journal of Agricultural and Food Chemistry, 62*, 66–73.

Neyraud, E., Palicki, O., Schwartz, C., Nicklaus, S., & Feron, G. (2012). Variability of human saliva composition: Possible relationships with fat perception and liking. *Archives of Oral Biology, 57*, 556–566.

Pages-Helary, S., Andriot, I., Guichard, E., & Canon, F. (2014). Retention effect of human saliva on aroma release and respective contribution of salivary mucin and alpha-amylase. *Food Research International, 64*, 424–431.

Piombino, P., Genovese, A., Esposito, S., Moio, L., Cutolo, P., Chambery, A., ... Ercolini, D. (2014). Saliva from Obese Individuals Suppresses the Release of Aroma Compounds from Wine. *PloS one*, *9*.

Pionnier, E., Chabanet, C., Mioche, L., Le Quere, J. L., & Salles, C. (2004). 1. In vivo aroma release during eating of a model cheese: Relationships with oral parameters. *Journal of Agricultural and Food Chemistry*, *52*, 557–564.

Ployon, S., Morzel, M., & Canon, F. (2017). The role of saliva in aroma release and perception. *Food Chemistry*, *226*, 212–220.

Tavel, L., Moreau, C., Bouhallab, S., Li-Chan, E., & Guichard, E. (2010). Interactions between aroma compounds and beta-lactoglobulin in the heat-induced molten globule state. *Food Chemistry*, *119*, 1550–1556.

Terao, J., & Nagao, A. (1991). Antioxidative effect of human saliva on lipid-peroxidation. *Agricultural and Biological Chemistry*, *55*, 869–872.

van Ruth, S., Grossmann, I., Geary, M., & Delahunty, C. M. (2001). Interactions between artificial saliva and 20 aroma compounds in water and oil model systems. *Journal of Agricultural and Food Chemistry*, *49*, 2409–2413.

van Ruth, S., & Villeneuve, E. (2002). Influence of beta-lactoglobulin, pH and presence of other aroma compounds on the air/liquid partition coefficients of 20 aroma compounds varying in functional group and chain length. *Food Chemistry*, *79*, 157–164.

Publication n°13: Association between salivary hypofunction and food consumption in the elderlies. A systematic literature review.

Muñoz-González, C.; Vandenberghe-Descamps, M.; Feron, G.; Canon, F.; Labouré, H.; Sulmont-Rossé, C.,

The journal of nutrition, health & aging **2018,** *22* (3), 407-419.

J Nutr Health Aging

ASSOCIATION BETWEEN SALIVARY HYPOFUNCTION AND FOOD CONSUMPTION IN THE ELDERLIES. A SYSTEMATIC LITERATURE REVIEW

C. MUÑOZ-GONZÁLEZ, M. VANDENBERGHE-DESCAMPS, G. FERON, F. CANON, H. LABOURÉ, C.SULMONT-ROSSÉ

Centre des Sciences du Goût et de l'Alimentation, AgroSup Dijon, CNRS, INRA, Univ. Bourgogne Franche-Comté, F-21000 Dijon, France. Corresponding author: Claire Sulmont-Rossé, INRA, CSGA, 17 rue Sully, F-21000 Dijon, France, Telephone: +33 380 69 32 71, E-mail address: claire.sulmont-rosse@inra.fr

Abstract: *Objectives:* This systematic literature review aims to summarize the existing scientific evidence about the association between a reduced salivary function and food consumption in elderly people. *Methods:* A validated search strategy in two databases (PubMed and ISI Web of Knowledge) was carried out and retrieved papers together with their reference lists were screened by two independent reviewers. The quality of the included studies was critically appraised via the Quality Assessment Criteria for Evaluating Primary Research Papers. *Results:* From the originally identified studies (n=391), only 15 articles (all cross-sectional studies) met the pre-fixed inclusion/exclusion criteria. The methodological quality of the included studies was in general good, although only 3 from 15 obtained the maximum score. The control of confounding factors was the quality variable more poorly rated in the selected studies. Salivary hypofunction was associated with a decrease of the objective chewing and swallowing abilities and taste perception. Moreover, most of the selected studies showed a relationship between salivary hypofunction and food consumption (in terms of appetite loss, unbalanced dietary intake and malnutrition), although no causality could be established. *Conclusions:* This study highlights the fact that salivary hypofunction definition and measurements are different across the studies. Therefore, future research efforts should focus on establishing a gold standard to define and identify salivary hypofunction throughout life and on performing longitudinal studies controlling for confounding factors to establish causality. .

Key words: Hyposalivation, dietary intake, appetite, nutritional status, elderly.

Introduction

Saliva is a complex biological fluid composed by water, inorganic and organic molecules (1). Secreted by several salivary glands, saliva plays an important role in the preservation and maintenance of oral health and functions (2). First, saliva is known to be essential in fulfilling daily activities such as speaking. Second, it exerts a key role maintaining oral health under normal conditions: tooth and oral mucosa integrity, protection against dental caries, periodontal diseases, etc. (3; 4; 5). Third, as the first digestive fluid in contact with food, saliva is a key factor assisting the oral processing of food, whereby food is transformed into a bolus to be swallowed. During the mastication process, the lubrication function of saliva allows moistening of food and supports the creation of a bolus which in turn facilitates the ability to chew (6). Furthermore, some food components are released from the food matrix and dissolved in saliva, where they can be influenced by the presence of salivary components such as salivary enzymes that begin the process of food digestion (i.e. alpha-amylase) or metabolize flavor compounds (i.e. esterases, glycosidases) (7; 8).

In consequence, an alteration in the composition or amount of saliva released to the human mouth, produced as a consequence of a diminished salivary gland function, could have serious consequences. A reduced salivary output could induce a defect in lubrication, compromising the comfort while chewing and swallowing (3). These dysfunctions could be accompanied by an unbalanced flavor perception that could provoke an unpleasant sensory experience. Besides these effects, if the situation of dry mouth is maintained in the long term, the decline (or absence) of salivation per se may change the oral environment, which could cause infections, destruction of taste receptors (9) and formation of dental caries, which can derive in tooth losses (4), thus compromising even more the food oral processing. The sum of these events could therefore provoke a decline in food interest and a loss of appetite, resulting in a modification of people's dietary habits. The quantity, quality and variety of food consumed could be altered, thus contributing to a diminished nutritional status.

This cascade of reactions possibly induced by a reduced salivary output is of especial relevance for elderly people, the population group most affected by salivary disorders. Older people are more likely to take medications compared to other generations, which is a well-known factor of hyposalivation as a side effect (10). A recent meta-analysis has shown that the aging process is associated with reduced salivary flow per se in a salivary-gland-manner (11), and this reduction can not be fully explained on the basis of medications (11) or dental status (12). In the same time, this age group is frequently associated with poor appetite, weight loss and malnutrition (13; 14). However, the relationship between food consumption and salivary hypofunction in elderly population remains unclear. This could be due to the fact that very often the studies on this topic have measured the subjective sensation of dry mouth (xerostomia) instead of performing real measurements of saliva deficiencies (3, 15-19). Indeed, xerostomia and hyposalivation are two separate entities, which are not always correlated (20;

Received January 30, 2017
Accepted for publication May 2, 2017

21). Whereas xerostomia relates to a subjective evaluation of dry mouth, hyposalivation represents a decrease in the amount of saliva secreted to the oral cavity. Therefore the aim of this work was to systematically review the original articles studying the associations between salivary hypofunction measured objectively and alterations in food consumption in elderly population. In this review, food consumption has been addressed by the study of i) food oral processing, ii) food behavior (appetite and dietary intake) and iii) nutritional status. Out of scope of this article are external factors affecting food consumption such as food availability, cultural factors, etc.

Method

Search strategy

A review of the literature was conducted in September 2016 for all published articles containing information about the association between salivary hypofunction and i) food oral processing, ii) food behavior (appetite and dietary intake), and iii) nutritional status in the elderlies. The electronic databases PubMed and ISI Web of Knowledge were used to search for relevant articles (without date restriction). The search strategy consisted of a set of Medical Subject Headings (MeSH) terms and free text words subsequently combined. Following groups of key words were introduced:

1) food oral processing, mastication, chewing, swallowing, flavo(u)r, taste, aroma, texture, flavo(u)r perception, taste perception, aroma perception, texture perception, chemosensory perception, orosensory perception, food sensory perception, texture modification, aroma release, taste release, trigeminal sensation(s), food texture;

2) food consumption, food behavio(u)r, nutrition, appetite, food intake, malnutrition, undernutrition, malnourishment, eating, nutrient intake, eating capability, food liking, dietary pattern, meal frequency, eating frequency;

3) elderly, senior, ag(e)ing, old age, older adult(s), old(er) people, old(er) person(s);

4) saliva, hyposalivation, salivary flow, salivary composition, salivary protein(s), salivary secretion(s), salivary hypofunction, xerostomia, dry mouth, oral mucosa, mucosal wetness, mucosa dryness, oral dryness.

Selection criteria and study selection

Articles were included if they explored the association between an objective measure of salivary deficiencies and i) food oral processing (mastication, swallowing, orosensory perception), ii) food behavior (appetite and food intake) or iii) nutritional status. Only articles that defined salivary hypofunction were included in this systematic literature review (SLR). Therefore articles that did not explore populations with salivary disorders or that did not specify cut-off values of saliva deficiencies were not included in this SLR. Study design and settings were not defined as exclusion criteria because of the exploratory character of the review. Only articles written in English were included, no date limitation was performed.

Two reviewers (CMG and MVD) independently screened the titles and abstracts based on the selection criteria. If the abstract did not provide enough information to decide upon inclusion/exclusion, the full paper was retrieved for further screening. Disagreements about inclusion or exclusion were discussed between the reviewers until consensus was reached.

Data abstraction and synthesis

Two reviewers (CMG and MVD) independently extracted data from the included articles. The extracted data included study characteristics (author and year of publication, study design, sample size, settings (living condition), determinant, outcome, methods, main results and conclusions), and participant characteristics (age, gender, country/ethnicity, functional status). A synthesis of the data is reported in Table 1.

Quality assessment

The quality assessment of the review is based on "The quality assessment criteria for evaluating primary research papers from a variety of fields" (22). The used checklist contains the following items:

1. Is the objective of the study sufficiently described?
2. Is the study design evident and appropriate?
3. Is the method of subject selection described and appropriate?
4. Are subject characteristics sufficiently described (functional status, health, etc.)?
5. Are outcome measures well defined and robust to measurement?
6. Is the sample size appropriate?
7. Are analytic methods described, justified and appropriate?
8. Is some estimate of variance reported for main results?
9. Are they controlled for confounding?
10. Are the results reported in sufficient detail?
11. Are the conclusions supported by results?

Each question can be answered with 'yes', 'partial', 'no' and 'not applicable'. The summary score is the total sum ((number of 'yes' x 2) + (number of 'partial' x 1)) / total possible sum (28 – (number of 'not applicable' x 2). The associated scoring manual (22) was used to guide the scoring process. When the quality of a paper was debatable, a discussion between two independent reviewers was held until consensus was reached.

Results

Selected articles

Figure 1 shows the overview of the search strategy. A total of 391 articles were identified: PubMed (n=219), and ISI Web of Knowledge (n=172). Duplicate articles (n=102) were excluded. Additionally, 248 articles were excluded because the inclusion criteria (based on title and/or abstract) were not met. The full texts of 41 articles were reviewed in detail.

Table 1

Description of the 15 selected studies concerning salivary hypofunction and associated parameters related to food consumption

Reference	Study design*	Study population	Country	Functional status**	Parameter studied and method(s)	Results of the association between the parameter studied and salivary hypofunction
Dormenval et al., 1998	CS	sample size: 99 mean age ± SD (years) 82.5 ± 4.0 gender (% female): 70	Switzerland	H	Nutritional status: Anthropometric (BMI, triceps skinfold thickness and mid-arm circumference), and biological measurements (serum albumin concentration)	- BMI<21 (p<0.05) - triceps skinfold thickness: (p=0.01) - mid-arm circumference: (p<0.05) - serum albumin concentration: (p=0.01)
Dormenval et al., 1999	CS	sample size: 99 mean age ± SD (y/o): 82.5 ± 4.0 gender (% female): 70	Switzerland	H	Appetite: questionnaire	- Lack of appetite (p=0.05)
Samnieng et al., 2012	CS	sample size: 612 mean age ± SD (y/o): 68.8 ± 5.9 gender (% female): 74	Thailand	C	i) Oral function (tasting, speaking, swallowing, chewing): questionnaire ii) Nutritional status: MNA	- Oral function problems (p<0.05) - Low MNA score (p<0.05).
Syrjälä et al., 2013	CS	sample size: 157 mean age ± SD (y/o): 79.2± 3.6 gender (% female): 70	Finland	C	Nutritional status (risk of malnutrition): MNA-SF	- Risk of malnutrition (n.s)
Samnieng, 2014	CS	sample size: 612 mean age ± SD (y/o) : 68.8 ± 5.9 gender (% female): 74	Thailand	C	Appetite: questionnaire	- Appetite loss (p<0.05)
Iwasaki et al., 2016	CS	sample size: 352 mean age ± SD (y/o): 80.0 ± 0.0 gender (% female): 51	Japan	C	i)Dietary intake: validated food frequency questionnaire ii) Subjective capacities to eat and swallow: questionnaire	- Self-reported chewing difficulties (p<0.001) - Self-reported swallowing difficulties (p<0.036) -Total energy intake (n.s) - Low intake of n-3 polyunsaturated fatty acid, potassium, vitamin D, vitamin E, vitamin B6 and folate (p<0.05) - Low consumption of vegetable, fish and shellfish consumption (p<0.05)
Ikebe et al., 2006	CS	sample size: 328 mean age ± SD (y/o): 66.2 ± 4.1 gender (% female): 47	Japan	C	Masticatory performance: Gummy jellies test	- Masticatory ability: bivariate level (p=0.006) and multivariate level (p=0.046) - Masticatory performance: no support zone (p<0.003), 1 to 3 support zones (p=0.047), 4 support zones (n.s)

Table 1 (contined)

Reference	Study design*	Study population	Country	Functional status**	Parameter studied and method(s)	Results of the association between the parameter studied and salivary hypofunction
Mesas et al., 2010	CS	sample size: 267 mean age ± SD (y/o): 66.5 ± 4.1 gender (% female): 60	Brazil	C	Nutritional status: MNA	- Nutritional deficit (OR: 2.18, 95% CI: 1.06 – 4.50) (considering stimulated salivary flow <0.7 ml/min)
Poisson et al., 2014	CS	sample size: 159 mean age ± SD (y/o): 85.3 ± 5.7 gender (% female): 68	France	H	i) Dysphagia: swallowing abilities ii) Nutritional status: BMI, serum albumin concentration, MNA-SF iii) Dietary intake: 3-day records	-Dysphagia: univariate level ($p<0.001$) and multivariate level (n.s) - Malnutrition (n.s) - Protein and energy intake (n.s)
Soini et al., 2003	CS	sample size: 51 mean age ± SD (y/o): 83.7 ± 4.4 gender (% female): 78	Finland	C	Nutritional status (risk of malnutrition): MNA	- Risk of malnutrition ($p = 0.049$)
Solemdal et al., 2012	CS	sample size: 174 mean age ± SD (y/o): 83.5 ± 6.1 gender (% female): 68	Norway	H	Taste ability: taste strips method	- Total taste score ($p=0.001$), sweet sum score ($p=0.007$) and salty sum score ($p=0.009$) related to friction with mirror test - Total taste score ($p=0.007$), sweet sum score ($p=0.001$) and salty sum score ($p=0.030$) related to dry tongue - Salty sum score ($p=0.023$) related to salivary flow
Srinivasulu et al., 2014	CS	sample size: 81 mean age ± SD (y/o): 70.0 ± 7.1 gender (% female): 58	India	I	Nutritional status: MNA	- Nutritional status ($p<0.001$)
Ikebe et al., 2002	CS	sample size: 351 mean age ± SD (y/o): 66.7 ± 4.3 gender (% female): 46	Japan	C	Dissatisfaction with tasting; self-assessed chewing ability: questionnaire	- Dissatisfaction with tasting food ($p<0.05$) - Self-assessed chewing ability ($p<0.01$)
Shinkawa et al., 2009	CS	sample size: 502 mean age ± SD (y/o): 72.3 ± 6.7 gender (% female): 51	Japan	C	Satisfaction with chewing and swallowing abilities: questionnaire	- Subjective chewing ability ($p=0.002$) - Swallowing ability (n.s)

* CS: cross-sectional studies; ** C: community dwelling volunteers (independently living); I: Institutionalized volunteers; H: hospitalized patients

Twenty eight articles were excluded due to different reasons: not an objective measurement of the saliva flow but a subjective sensation of dry mouth (n=11), the relationship between the variables was not explored (n=3), cut-off value to determine salivary hypofunction not specified (n=7), the outcome measurements were not focused specifically on our research topic (n=3), redundant information due to a publication on the same data (n=2), or not original papers but reviews (n=2). The reference lists of all included articles were checked for additional articles. In consequence, four new papers were found to be of interest for this review but two of them (23, 24) were not written in English, so not included in the final list. The final group consisted of 15 articles. All of them were subjected to a methodological quality assessment.

Figure 1

Overview of the research strategy

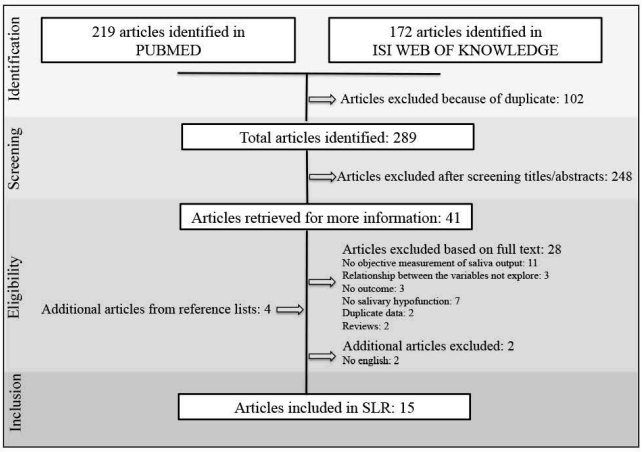

Methodological quality

The methodological quality of the included studies was in general good: of the 15 selected articles the quality scores varied between 0.77 and 1 in a 0-to-1 rating scale (Table 2). Three articles (25-27) obtained the maximum score according to the above-mentioned manual scoring (22). On the contrary, the lowest score was attributed to the one (28) with the smallest sample size (n=51) (item n° 6). Moreover, in this work the study design (item n° 2), the analytical methods employed (item n° 7) and the results (item n° 10) were not sufficiently described. Furthermore, confounding factors (item n° 9) were partially taken into account.

In fact, the control of confounding factors (item n° 9) was the quality variable more poorly rated in the selected studies. This was due to the fact that most of the studies did not take into account all the factors established as confounding in this study: age, gender, drug intake, diseases, mental status, socio-economic status, dental status and place to live. Therefore this item was often rated as "partial".

Study characteristics

Table 1 gives an overview of the 15 selected articles. Publication year of the studies ranged from 1998 to 2016, showing that the interest on this topic is held and even increased over time (from 1998 to 2004: 4 studies; from 2005 to 2011: 4 studies; from 2012 to 2016: 7 studies). All the studies had a cross-sectional design. The studies were based on populations from all over the world (Brazil: 1, Finland: 2, Japan: 5, Norway: 1, Switzerland: 2, Thailand: 2; France:1; India:1), with exception of the African and Oceanic continent and north America. The sample size varied from 51 (28) to 640 (29) subjects. The gender distribution of subjects varied between 46% (30) and 78% (28) of females. Eighty per cent of the studies presented however, a higher percentage of women compared to men. The mean age was highly dispersed in the selected studies, ranging from 66 to 84 years old. The recruited populations were located either in institutions (5 studies) or in their own homes (10 studies). The subjects recruited in the selected studies were in good general health except for three studies: one study with hospitalized very sick volunteers (31), one study which included subjects receiving home care nurses visits (28) and one study (27) where the elderlies were living in their own homes prior to hospitalization for acute medical problems.

Analytical methods

Salivary hypofunction was determined differently across the selected studies (Table 3). Fourteen of the 15 studies measured the salivary flow rate either at rest, under stimulation by chewing a piece of paraffin-wax during saliva collection or both at rest and under stimulation. Most of these studies used the spitting method for the salivary collection but some preferred to measure the salivary flow using the draining method or the sterile compress method. The draining method consists in allowing saliva to drain out between parted lips into a test tube held near the mouth. The sterile compress method consists in placing a sterile compress under the tongue, then weighting the compress after a certain time to evaluate the amount of saliva incorporated. These studies have defined salivary hypofunction when the salivary flow was below a certain cut-off value. This reference value was 0.1 ml/min of saliva determined at rest in all the selected studies. However, the cut-off values employed to define salivary hypofunction under stimulation were not consensual and varied from 0.5 ml/min to 1.0 ml/min in the different studies. Very few studies have determined salivary hypofunction using alternative methods. Four over fifteen articles employed (besides the determination of salivary flow) additional measures to determine salivary hypofunction, such as the mirror test (that consists of measuring the stickiness of buccal mucosa when passing through it the back of a dental mirror) or the registration of dry tongue (presence of moisture or not). Only one study (32) did not use salivary flow to define hyposalivation. Authors measured the moisture of the buccal mucosa by using a device that evaluates the weight

Table 2
Quality assessment of the 15 selected studies

Reference	Question/ objective sufficiently described?	Study design evident and appropriate?	Method of subject selection is described and appropriate?	Subject characteristics are sufficiently described?	Outcome measures(s) well defined and robust to measurement/ misclassification bias? Means of assessment reported?	Sample size appropriate?	Analytic methods described/ justified and appropriate?	Some estimate of variance is reported for main results?	Controlled for confounding? (age, gender, drug intake, diseases, mental status, socio-economic status, dental status and place to live)	Results reported in sufficient detail?	Conclusions supported by results?	Sum Score
Dormenval et al., 1998	Yes	Yes	Yes	Yes	Yes	Yes	Yes	Yes	Partial	Partial	Yes	0.91
Dormenval et al., 1999	Yes	Partial	Yes	Yes	Yes	Yes	Partial	Yes	Partial	Yes	Partial	0.82
Samnieng et al., 2012	Yes	Yes	Yes	Yes	Yes	Yes	Yes	Yes	Partial	Yes	Yes	0.95
Syrjälä et al., 2013	Yes	Yes	Yes	Yes	Yes	Yes	Yes	Yes	Partial	Partial	Partial	0.86
Samnieng, 2014	Yes	Yes	Yes	Yes	Yes	Yes	Partial	Yes	Yes	Yes	Yes	0.95
Iwasaki et al., 2016	Yes	Yes	Yes	Yes	Yes	Yes	Yes	Yes	Yes	Yes	Yes	1.00
Ikebe et al., 2006	Yes	Yes	Yes	Partial	Yes	Yes	Yes	Yes	Partial	Yes	Yes	0.91
Yoshinaka et al., 2007	Yes	Yes	Yes	Partial	Yes	Yes	Partial	Yes	Partial	Partial	Yes	0.82
Mesas et al., 2010	Yes	Yes	Yes	Yes	Yes	Yes	Yes	Yes	Yes	Yes	Yes	1.00
Poisson et al., 2014	Yes	Yes	Yes	Yes	Yes	Yes	Yes	Yes	Partial	Partial	Yes	0.91
Soini et al., 2003	Yes	Partial	Yes	Yes	Yes	Partial	Partial	Yes	Partial	Partial	Yes	0.77
Solemdal et al., 2012	Yes	Yes	Yes	Yes	Yes	Yes	Yes	Yes	Yes	Yes	Yes	1.00
Srinivasulu et al 2014	Yes	Partial	Yes	Yes	Yes	Partial	Yes	Yes	No	Yes	Yes	0.82
Ikebe et al., 2002	Yes	Yes	Yes	Yes	Yes	Yes	Partial	Yes	Partial	Yes	Yes	0.91
Shinkawa et al, 2009	Yes	Yes	Yes	Yes	Yes	Yes	Partial	Yes	Partial	Yes	Yes	0.91

Table 3

Objectives measurements to determine salivary hypofunction and corresponding cut-off values in the 15 selected studies

Article	Parameters measured	Methodology	Number of measures	Cut-off value to determine hyposalivation	References of the methodology
		Articles that performed the measure of salivary flow to determine hyposalivation			
Dormenval et al., 1998	Unstimulated salivary flow rate, stimulated salivary flow rate	Measured during 6 min, spitting out each 2 min; collected between 9h and 11h	2	Unstimulated salivary flow rate < 0.1ml/min, Stimulated salivary flow rate < 0.5ml/min	(61)
Dormenval et al., 1999	Unstimulated salivary flow rate, stimulated salivary flow rate	Measured during 6 min, spitting out each 2 min; Collected between 9h and 11h	2	Unstimulated salivary flow rate < 0.1ml/min, Stimulated salivary flow rate < 0.5ml/min	(61)
Samnieng et al., 2012	Unstimulated salivary flow rate, stimulated salivary flow rate	Measured during 5 minutes	1	Unstimulated salivary flow rate < 0.1 ml/min Stimulated salivary flow rate < 0.5 ml/min	-
Syrjälä et al., 2013	Unstimulated salivary flow rate, stimulated salivary flow rate	Measured during 5 minutes (draining method)	1	Unstimulated salivary flow rate < 0.1ml/min, stimulated salivary flow rate < 1ml/min	(40, 62)
Samnieng, 2014	Unstimulated salivary flow rate	Measured during 5 minutes	1	Unstimulated salivary flow rate < 0.1 ml/min	
Iwasaki et al., 2016	Stimulated salivary flow rate	Measured during 3 minutes; Collected between 9h to 15h	1	Stimulated salivary flow rate < 0.5 ml/min	(58)
Ikebe et al., 2006	Stimulated salivary flow rate	Measured during 2 minutes at their own pace; collected between 10:00 am and 3:00 pm	1	Stimulated salivary flow rate < 0.5 ml/min	(30, 63)
Yoshinaka et al., 2007	Stimulated salivary flow rate	Measured during 2 minutes at their own pace	1	Stimulated salivary flow rate < 0.5 ml/min	(64)
Mesas et al., 2010	Stimulated salivary flow rate	No information provided	1	Stimulated salivary flow rate < 0.5 ml/min; Stimulated salivary flow rate < 0.7ml/min	(30, 36, 62, 66)
Poisson et al., 2014	flow under the tongue	Measured by placing a sterile compress under the tongue for 5 min	1	Salivary flow < 0.1 g/min	-
		Articles that combined the measure of salivary flow rate with other measures of oral dryness			
Soini et al., 2003	Unstimulated salivary flow rate, stimulated salivary flow rate, Objective dry mouth	Measured during 5 min (Unstimulated salivary flow rate: let the saliva flow into the tube ; Stimulated salivary flow rate: spitting out each 1 min) ; collected between 9h and 11h	1	Unstimulated salivary flow rate < 0.1 ml/min, stimulated salivary flow rate < 0.8 ml/min Clinical dentist criteria	(67)
Solemdal et al., 2012	Stimulated salivary flow rate, mirror test, dry tongue	Measured during 3 minutes at their own pace	1	Stimulated salivary flow rate < 0.6 g/min Dental mirror sticked to the mucosa Tongue completely devoid of moisture	(68, 69)
Srinivasulu et al 2014	Stimulated salivary flow rate, Total protein content, calcium, pH, buffering capacity	Measured during 5 minutes at their own pace; collected early in the morning	1	Stimulated salivary flow rate < 0.5ml/min	(70)
Ikebe et al., 2002	Stimulated salivary flow rate, pH of saliva	Measured during 2 minutes at their own pace: Collected between 10:00 am and 3:00 pm	1	Stimulated salivary flow rate < 0.5 ml/min	(3, 20, 64, 71)
		Articles that used other method to determine hyposalivation			
Shinkawa et al., 2009	Moisture of oral mucosa	Measured at the right buccal mucosa, during 2 sec	3	28.3% of the MCM value	(33)

percentage of water found in the mucosa, and determined salivary hypofunction when the moisture of oral mucosa was below 28.3% according to a previous study that validated the method (33).

Association between salivary hypofunction and food oral processing (8 studies)

The relationship between a diminished salivary function and food oral processing (mastication/chewing, swallowing, orosensory perception) has been examined in 8 articles (25, 27, 29-32, 34, 35). Only 3 studies measured objectively chewing, swallowing and taste abilities (27, 31, 34), while the others (n=5) employed questionnaires. The objective measurements consisted of the determination of masticatory performance, signs of dysphagia and taste ability. The evaluation of masticatory performance was achieved by measuring the amount of dissolved glucose after the mastication of test gummy jellies. The signs of dysphagia were reported using the water test during which the volunteers were asked to swallow four times an increasing volume of water to report any abnormal signs (coughing or voice modification). Finally, the taste ability test consisted in impregnating some strips with sweet, salty and bitter taste, then asking the volunteers to identify the tastes by putting the strips in the anterior region of the tongue.

Six of the eight studies investigated the association between salivary hypofunction and the chewing and/or swallowing abilities (25, 30-32, 34, 35). Ikebe and coworkers (2006) (34) found a significant association between lower values of masticatory performance and hyposalivation in independently living older adults. In another study with hospitalized very sick older patients, Poisson and collaborators (2014) (31) found a strong relationship at univariate level between individuals presenting a low salivary flow (<0.1 g/min) and dysphagia. However this effect was not observed at multivariate level, when considering other independent variables in the model. The rest of the studies evaluated chewing and/or swallowing abilities through questionnaires. Two works (25, 35) found a significant association between reduced saliva flow rate and perceived chewing and swallowing difficulties. Ikebe and collaborators (2002) (30) also found a relationship between hyposalivation and poor self-assessed chewing ability though it was not of statistical level. Finally, Shinkawa et al., (2009) (32) found a significant association between oral dryness (measured via the level of moisture of oral mucosa) and poor self-assessed chewing ability but no with swallowing.

The association between salivary gland hypofunction and orosensory perception was evaluated in four studies (27, 29, 30, 35). However, it is important to notice that all of them were only focused on one modality of flavor perception: taste. In these studies, taste ability was evaluated either objectively (taste detection through the filter-paper disc method) or by questionnaires considering taste as a marker for oral function (dissatisfaction with tasting). Only Solemdal et al., (2012) (27) studied the association of salivary hypofunction on the objective taste ability. These authors reported a significant and markedly reduced total taste score, particularly for sweet and salty taste, in patients with objective dry mouth (measured by the friction with mirror and dry tongue tests). Low sum score for salty taste was also related to low stimulated salivary flow rate. The rest of the studies evaluated taste ability through global questionnaires including self-assessed items on oral function, with contradictory results. Two studies (30, 35) found that hyposalivation was negatively and significantly correlated to self-assessed taste satisfaction, whilst Yoshinaka and coworkers (2007) (29) failed to find this correlation. In addition to the measure of salivary flow rate, Ikebe et al., (2002) (30) measured the pH of the stimulated saliva but no correlation between the pH and taste satisfaction could be established.

In summary, most of the studies on this topic have shown a relationship between a reduced salivary function and alterations in food oral processing (mastication, swallowing, orosensory perception). It should be noted that this relationship seems clearer when the outcomes were measured objectively rather than by questionnaires.

Association between salivary hypofunction and food behavior (4 studies)

Two studies (36, 37) examined the possible relationship between hyposalivation and appetite, and two others between hyposalivation and dietary intake (25, 31). For both categories, the outcomes were evaluated throughout the use of four different questionnaires: a questionnaire related to dietary intakes/nutrition and masticatory function (36), a single question-item on appetite (37); a 3-day record on food intake (31); a brief-type self-administered diet history questionnaire (25). The use of questionnaires could be justified by the fact that appetite is the subjective desire of eating foods. In 1999, Dormenval and coworkers (36) found that lack of appetite was associated with hyposalivation (stimulated salivary flow rate < 0.5 ml/min) in hospitalized Swiss patients. More recently, Samnieng (2014) (37) also found a positive correlation between lack of appetite and low resting salivary flow in independently living older Norwegians.

Regarding dietary intake, the two selected studies found no association between total energy intake and hyposalivation. However, when studying specific nutrient and food intake, Iwasaki and collaborators (2016) (25) found that the hyposalivation group had significantly lower intake of n-3 poly-unsaturated fatty acids, potassium, vit E, D, B6 and folate, which was in line with the observed reduction in the consumption of vegetables, fish and shellfish. Moreover, mean dietary intake of protein and vitamin B12 in the hyposalivation group tended to be lower than in the control group ($0.05 < P < 0.10$).

In summary, the scarce literature available on this topic showed an association between hyposalivation and appetite loss and unbalanced dietary intake in elderly people.

Association between salivary hypofunction and nutritional status (7 studies)

The association between salivary gland hypofunction and nutritional status has been evaluated in 7 studies. Five of them (26, 28, 35, 38, 39) evaluated the nutritional status using the Mini Nutritional Assessment (MNA). Meanwhile, Dormenval and coworkers, (1998) (40) assessed the nutritional status by quantifying biological malnutrition markers (BMI, level of serum albumin) and anthropometric measurements. Finally, Poisson et al., (2014) (31) employed both the MNA and the values of serum albumin concentration.

The results showed that hyposalivation was significantly associated with malnutrition in 4 studies (26, 35, 39, 40). Additionally, Syrjälä and co-workers (2013) (38) showed that subjects with low salivary flow (at rest or under stimulation) were slightly more at risk of malnutrition than subjects with normal salivary flow though their results were not statistically significant. Besides, Soini et al., (2003) (28) stated that no relation was found between hyposalivation and malnutrition. However, they found a significant association between the clinical dentist evaluation of dry mouth and the risk of malnutrition ($p=0.049$). On the contrary, Poisson and coauthors (2014) (31) did not find any relationship between hyposalivation (determined as salivary flow under the tongue <0.1 g/min) and MNA and/or biological malnutrition either at univariate or multivariate level. In addition to the measure of salivary flow rate, Srinivasulu et al., (2014) (39) measured the pH, the buffer capacity, the total protein and the total calcium of saliva samples. However, the authors did not highlight any significant correlation between the saliva composition and nutritional status.

In summary, five studies found a correlation between hyposalivation and malnutrition. Another study observed a relationship between the objective evaluation of dry mouth and the risk of malnutrition. Only one article did not find any association between the two variables. Therefore, and although most of the studies have shown some associations between salivary hypofunction and nutritional status, up to date this relationship is still controversial.

Discussion

Salivary hypofunction refers to alterations in the quality (composition) or quantity (salivary flow, residual saliva in the mouth) of saliva secreted into the human mouth (41). This situation could alter the orosensory perception while eating, which is one of the most recognized determinants for consumer's preferences and food consumption (7). As a result, the appetite, dietary intake and nutritional status of an individual could be compromised. This is of special relevance for elderly people, a population group frequently affected by both salivary and nutritional deficiencies. The aim of this work was to systematically review all the existing papers on this topic, in order to explore the relationships between a reduced salivary output and food consumption in the elderlies. In this paper only objective measurements of salivary hypofunction were considered, since the subjective complaint of dry mouth (xerostomia) is not always associated with an objective evidence of reduced salivary secretions (20; 42).

In total, 15 articles met the criteria for inclusion in this work (see Table 1). Eight of them studied the relationship of salivary hypofunction with food oral processing, 2 with appetite, 2 with dietary intake and 7 with nutritional status. In general, the selected studies clearly showed some associations between salivary hypofunction and the studied parameters. However, some controversial results have also been observed. It should also be noticed that the study characteristics are very different from one study to another, and the presence of not controlled confounding factors or methodological issues should be taken into account to interpret the results.

Discussion on the methods used to measure salivary hypofunction.

This review focuses on studies that objectively measured symptoms of salivary hypofunction. The prevalence of the population suffering these symptoms ranged from 14% (35) to around 50% (26; 28) in the selected articles. These differences were most likely dependent to the different characteristics of the studied populations (such as age, race, living place (community, institutions, and hospitals), functional status (healthy vs ill), drugs consumption, etc.) but also on the methods and cut-off values employed to determine salivary hypofunction.

For most of the selected studies (14 out of 15), the determination of the salivary flow below a cut-off value was the tool used to determine salivary hypofunction (see Table 3). However, a lack of consensus was observed regarding the type of saliva collected (at rest or under stimulation), the protocol employed to measure the salivary flow rate (spitting, draining method, cotton roll), and the cut-off value to determine hyposalivation. Of the 14 studies that measured saliva flow, five of them performed both resting and stimulated measurements (28; 35; 36; 38; 40), seven studies based their results on the measure of stimulated salivary flow (25; 26; 27; 29; 30; 34; 39), one study only measured the resting salivary flow rate (37) whilst one study performed the measure of salivary flow under the tongue (31). The use of resting or stimulated salivary flow rates provides different information since saliva is not delivered to the human mouth by the same salivary glands and in the same proportions under the two conditions. Therefore, whole saliva at rest, where the submandibular gland predominates, differs from that secreted during stimulation (more related to parotid gland function). Consequently, and in spite of the scarce literature on this topic, it is not surprising that the two measures are not always correlated (43).

Moreover, two studies used additional methods (dentist evaluation, mirror test and tongue moisture) to measure salivary hypofunction besides the determination of the salivary flow (27; 28). These methods could show a more advance phase of salivary hypofunction where the oral integrity (mucosa, tongue)

has already been affected due to a prolonged hyposalivation situation held over time. In addition, only two studies (30; 39) reported, additionally to the measure of stimulated salivary flow, changes in saliva composition. This could be due to the fact that these analyses are time consuming and expensive, and therefore difficult to be performed to study big populations, as those employed in the selected articles.

Otherwise, one study (32) did not use the measure of salivary flow to determine salivary hypofunction but evaluated it by measuring the moisture of the buccal mucosa. The device used for this evaluation determined the weight percentage of water found in the mucosa. Originally developed to measure the moisture of the skin, the device was modified specifically for this study. As it is not a common method used to measure hyposalivation, it is not possible to compare the results of this study to the results of the other selected studies.

In addition to the different parameters employed to determine hyposalivation (salivary flow at rest or under stimulation, moisture of mucosa, etc), within the same parameter, the protocol was not always performed in the same way. Table 3 highlights the differences observed in collection times (from 1 to 6 minutes), hours of collection (respecting or not the circadian rhythms), collection protocols (free spitting vs controlled), etc., employed to measure salivary hypofunction. Moreover, only three articles (32, 36, 40) measured the selected parameters two or three times, whilst the other studies only performed the measures once. Therefore, no information about the accuracy of the methods could be obtained, that in the worst scenario could be traduced in a misclassification of people across the groups.

The cut-off value to determine salivary hypofunction was consensual across the studies for the saliva at rest. A value lower than 0.1 ml/min was considered hyposalivation. However for the salivary flow under stimulation a high dispersion on the cut-off values was encountered among studies. Indeed, there is no universally accepted reference value to determine hyposalivation using stimulated salivary flow rate. Most of the authors employed a cut-off value of 0.5 ml/min to define hyposalivation (25, 26, 29, 34, 35, 36, 40), whilst others employed values ranged from 0.5 to 1 ml/min (27, 38). The differences in the cut-off points could derive in an erroneous assignation of the participants to the groups and in a misinterpretation of the results, making difficult the comparison of the studies. This was displayed in the study of Mesas et al., (2010) (26). Authors employed two cut-off levels (stimulated salivary flow rate < 0.5 and stimulated salivary flow rate < 0.7 ml/min) to define hyposalivation, and they only found a significant association with nutritional status when using the value of 0.7 ml/min. For the other methods employed to define salivary hypofunction, like the "mirror test'' and dry tongue methods, the comparison across studies is difficult because they are less frequently employed and dependent on the dentist's criteria. The moisture of oral mucosa cannot be either compared since the method was only employed in one article.

All these remarks highlight the idea that the diagnosis of salivary hypofunction is not consensual across the studies. Therefore, guidelines to measure salivary flow hypofunction with one or several complementary methods to evaluate the degree of dysfunction would be appropriate to allow an international standardization and a better comparison across the studies. Moreover longitudinal studies observing secretory function over time are required to establish causality. This would acknowledge setting up normal ranges or cut-off points to distinguish normal from abnormal salivary function. That amount is probably different across cultures (depending on gland sizes) (44).

Discussion on the relationship between salivary hypofunction with food oral processing, food behavior and nutritional status

Figure 2 represents schematically the associations between salivary hypofunction and food consumption found in the 15 selected articles. As a consequence of the cross-sectional design employed in the studies, no causal-effect relation can be established. Therefore, it cannot be concluded if salivary hypofunction is a cause or a consequence of the studied consumption parameters.

Figure 2

Schema resuming the main correlations found in this SLR between salivary hypofunction and the selected outcomes. The ratio (x/n) indicates the number of articles that highlighted a positive association between salivary hypofunction and the specific outcome (x) from the total number of articles that treated the topic (n)

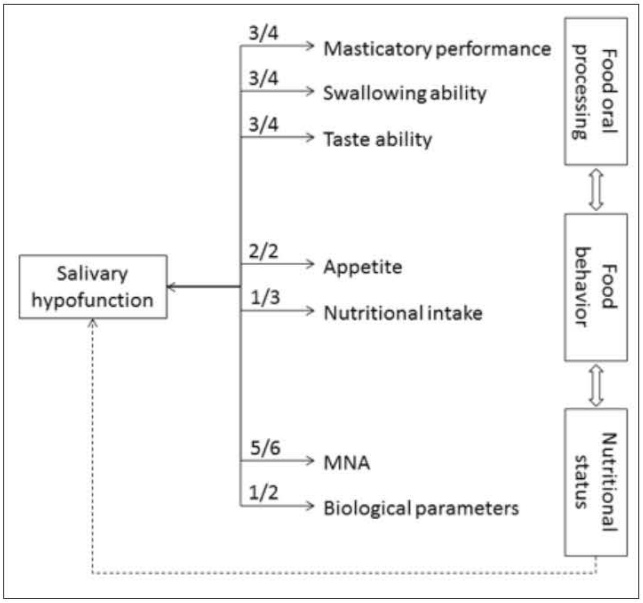

As can be seen in Figure 2, salivary hypofunction was related to food oral processing, and in particular to mastication. It has been shown that elderly with hyposalivation had a

reduced ability to break down foods into discrete portions by chewing to permit swallowing (34). This effect was more important in denture wearers with a lack of posterior occlusal contacts. Moreover, a relationship between hyposalivation and poor self-assessed chewing ability has been shown in four articles. Authors suggested that although presenting an altered masticatory performance is a multifactorial problem, salivary flow is a critical factor for masticatory function. However, the associations with dysphagia or swallowing have been less studied and results were controversial (31, 32).

In spite of chemosensory perception is a key factor for food enjoyment and one of the factors that motivate food consumption, its association with salivary gland hypofunction in the elderlies have received little attention. This could be due to the fact that food science has historically focused on the food and only in the later years some research groups have started to consider the interaction between food and human physiology to explain food perception. Moreover, to date most of the studies regarding the relation between the role of saliva on flavor release and perception have been conducted on healthy and young individuals (<65 y/o), while elderly population remains underexplored. Therefore only 4 articles met the inclusion criteria and they were all based on taste. While it has been found that salivary hypofunction is related to the objectively measured taste perception (27, 45), for the self-assessed taste ability results are controversial. However, most epidemiological studies do not include objective measurements of taste perception, probably because the evaluation through tests is more time-consuming than performing questionnaires.

To the author's knowledge the association between hyposalivation and texture or other modalities of orosensory perception (e.g aroma) in the elderlies has not been addressed by the scientific community yet. Some studies reported age-related loss of texture sensation (46, 47) and ultimately texture preference changes (48), but these studies have not investigated the role of a diminished saliva secretion in the observed results.

Assuming that a reduced salivary output produces an impaired food experience, the desire for food or drink known as appetite could be altered. This is in agreement with the findings of the two selected articles on this topic which shown a relationship between hyposalivation and loss of appetite (37, 40), even when the settings employed were very different in both of them. Consequently, this appetite loss could provoke a diminished food intake. However, the two studies on this topic found that the total energy intake was not impaired in elderly with hyposalivation. Nevertheless, when specific nutrients and/or group of foods were studied, the hyposalivator group presented a reduced consumption of vegetables, fish and seafood which was related to the lower intake of n-3 polyunsaturated fatty acids, potassium, vit C, E, B6 and folate after adjusting for confounders (number of teeth, denture use, sex, income, education, body mass index, smoking status, alcohol use, diabetes, medication, activities of daily living, depression and total calorie intake) (25). A reduced consumption of such specific nutriments/or groups of food, which are recognized for their health benefits (49-51), could have a negative impact on the health of this population.

Finally, an alteration of the dietary intake (quantitative or qualitative) could provoke an impairment of the nutritional status of the elderly population. Numerous studies have been conducted during the last decade to study the relationship between nutritional status and oral conditions in elderly, but to the authors' knowledge, only 7 studies have assessed the relationship between salivary hypofunction and nutritional status. However, some contradictory results have been found. While four articles found a significant correlation between MNA and hyposalivation, one did not. Although the method used to measure salivary flow was similar in the five studies, the cut-off values differed among them, which could explain the differences found in their results. On the other hand, the other two selected articles (28, 38) encountered only weak associations between nutritional status and hyposalivation or the dentist's estimation of dry mouth. Although other reasons (different cut-off levels, circadian rhythms not controlled, differences across populations) could explain these differences, it is interesting to observe that in these last two studies none of the subjects were malnourished but at risk of malnutrition. This is of importance since probably nutritional disturbances held over time can cause atrophy of salivary glands (39), producing a reduction of their function. If this is truth, alterations on saliva would be a consequence of an altered nutritional status. Unfortunately, as all the selected studies presented a cross sectional design no causality could be established and more studies are needed to validate this hypothesis.

Finally, the measure of the food consumption parameters was mostly performed by using subjective than objective methods. This could be due to the fact that the use of self-report questionnaires is less time consuming than performing objective determinations. However, as many studies have shown no correlation between the subjective feeling of dry mouth (xerostomia) and hyposalivation, there are no evidences of links between objective and subjective evaluations of the outcomes (29).

Limitations and strengths of the present SLR

The main strength of this work is that it is a solid literature search, with a complete overview of the relationship between an objective measurement of salivary hypofunction and the determinants of food consumption among the elderly population. Moreover, the selected studies represent the wide heterogeneity found in this population group (from healthy elderly individuals to chronically ill hospitalized old-people). The analysis of the quality of the selected articles let us to identify the most frequent risks across the studies and suggest new ideas for future works. For example, future studies on this topic should control better for confounding factors like gender, age, drug intake, diseases, mental status, socioeconomic status, dental status and place to live, because they are well-known

factors that can alter salivary function (52-55) but also food consumption (56-59).

However, this study presents some limitations. Unfortunately, we were not able to perform a meta-analysis due to the obvious heterogeneity among the studies in relation to definitions and measurements as explained above. Also, we could not establish causality due to the cross-sectional nature of the selected studies. Therefore it cannot be concluded if hyposalivation is a cause or a consequence of the selected food consumption parameters.

Implication of this study

This study has revealed the urgent need to introduce and implement universal guidelines to assess salivary hypofunction. Moreover, cohort studies (with comparable groups following the same population for a longer period of time) and statistical control of the confounding factors are required to establish causality. Even if this review has pointed out some evidences about the relationship between salivary hypofunction and food consumption in the elderlies, the literature available on this topic is scarce. This is particularly obvious in some cases such as in the study of the relationship between hyposalivation and flavor perception. Therefore, there is a big opportunity for researchers, clinicians and food industry to better understand this association and if so, give nutritional recommendations and/or conceive products with sensory and nutritional properties adapted for people with salivary dysfunction.

Conclusions

The main findings of this review can be summarized in the following points: 1) to date, salivary hypofunction is mainly based on measures of salivary flow 2) definition and measures of hyposalivation are different across the studies; 3) salivary hypofunction has been related to a decrease of objective chewing and swallowing abilities and taste perception; very little is known about other modalities of chemosensory perception (e.g. aroma) 4) hyposalivation has been associated with appetite loss; 5) hyposalivation has been related to an unbalanced dietary intake but not with total intake; 6) it has been seen a relationship between saliva deficiencies and malnutrition, though some controversial results have also been shown. Although it is not possible to completely eliminate the potential effects of underlying methodological issues and in spite of the scarce number of publications on this topic it is suggested a relationship between salivary hypofunction and food consumption in the elderlies. Unfortunately, due to the cross-sectional nature of the articles, no causality could be established. Therefore longitudinal studies on this topic controlling for confounding factors are needed.

Acknowledgments: CMG thanks the support of the Agreenskills fellowship program which has received funding from the EU's Seventh Framework Program under grant agreement N° FP7-609398 (AgreenSkills+ contract). Authors thank the French National Research Agency for financial support through the AlimaSSenS project [ANR-14-CE20-0003-01] and the MuFFIn project [ANR-14-CE20-0001-01].

Conflict of Interest: No conflicts of interest to report on all authors.

References

1. Mese H, Matsuo R. Salivary secretion, taste and hyposalivation. J Oral Rehabil, 2007;34, 711-723.
2. Mandel I D. The role of saliva in maintaining oral homeostasis. J Am Dental Assoc, 1989;119, 298-304.
3. Loesche W J, Schork A, Terpenning M S, Chen Y M, Stoll J. Factors which influence levels of selected organisms in saliva of older individuals. J Clin Microb, 1995;33, 2550-2557.
4. Caplan D J, Hunt R J. Salivary flow and risk of tooth loss in an elderly population. Commun Dent Oral Epidemiol, 1996;24, 68-71.
5. Narhi T O, Kurki N, Ainamo A. Saliva, salivary micro-organisms, and oral health in the home-dwelling old elderly - A five-year longitudinal study. J Dent Res, 1999;78, 1640-1646.
6. Prinz J F, Lucas P W. An optimization model for mastication and swallowing in mammals. Proceed Royal Society B-Biol Sci, 1997;264, 1715-1721.
7. Buettner A. Influence of human saliva on odorant concentrations. 2. aldehydes, alcohols, 3-alkyl-2-methoxypyrazines, methoxyphenols, and 3-hydroxy-4,5-dimethyl-2(5H)-furanone. J Agric Food Chem, 2002;50, 7105-7110.
8. Buettner A. Influence of human salivary enzymes on odorant concentration changes occurring in vivo. 1. Esters and thiols. J Agric Food Chem, 2002;50, 3283-3289.
9. Spielman A I. Interaction of saliva and taste. J Dent Res, 1990;69, 838-843.
10. Sreebny L M, Schwartz S S. A reference guide to drugs and dry mouth. Gerodontology, 1986;5, 75-99.
11. Affoo R H, Foley N, Garrick R, Siqueira W L, Martin R E. Meta-Analysis of Salivary Flow Rates in Young and Older Adults. J Am Geriatr Soc, 2015;63, 2142-2151.
12. Vandenberghe-Descamps M, Laboure H, Prot A, Septier C, Tournier C, Feron G, Sulmont-Rosse C. Salivary flow decreases in healthy elderly people independently of dental status and drug intake. J Texture St, 2016;47, 353-360.
13. Mowe M, Bohmer T, Kindt E. Reduced nutritional-status in an elderly population (greater-than-70y) is probable before disease and possibly contributes to the development of disease. Am J Clin Nut, 1994;59, 317-324.
14. McWhirter J P, Pennington C R, Jebb S A. Incidence and recognition of malnutrition in-hospital. Clin Nut, 1994;13, 267-268.
15. Quandt S A, Chen H Y, Bell R A, Savoca M R, Anderson A M, Leng X Y, Kohrman T, Gilbert G H, Arcury T A. Food Avoidance and Food Modification Practices of Older Rural Adults: Association With Oral Health Status and Implications for Service Provision. Gerontologist, 2010;50, 100-111.
16. Quandt S A, Savoca M R, Leng X Y, Chen H Y, Bell R A, Gilbert G H, Anderson A M, Kohrman T, Arcury T A. Dry Mouth and Dietary Quality in Older Adults in North Carolina. J Am Geriatr Soc, 2011;59, 439-445.
17. Stenman U, Ahlqwist M, Bjorkelund C, Hakeberg M. Oral health-related quality of life - associations with oral health and conditions in Swedish 70-year-old individuals. Gerodontology, 2012;29, E440-E446.
18. Nykanen I, Lonnroos E, Kautiainen H, Sulkava R, Hartikainen S. Nutritional screening in a population-based cohort of community-dwelling older people. Eur J Public Health, 2013;23, 405-409.
19. Porter J, Ntouva A, Read A, Murdoch M, Ola D, Tsakos G. The impact of oral health on the quality of life of nursing home residents. HQLF, 2015;13.
20. Narhi T O, Meurman J H, Ainamo A. Xerostomia and hyposalivation - Causes, consequences and treatment in the elderly. Drugs Aging, 1999;15, 103-116.
21. Ohara Y, Hirano H, Yoshida H, Obuchi S, Ihara K, Fujiwara Y, Mataki S. Prevalence and factors associated with xerostomia and hyposalivation among community-dwelling older people in Japan. Gerodontology, 2016;33, 20-27.
22. Kmet L M, Robert C. Lee, and Linda S. Cook. Standard quality assessment criteria for evaluating primary research papers from a variety of fields, 2004.
23. Satoh-Kuriwada S, Sasano, T., Saito, M., Hasimoto, K., Simeno, Y., Oba, M., Sakamoto, M., Aizawa, K. and Watanabe, M. Epidemiological study on taste disorders in the elderly. Part 1: Influence of systemic disease and medication on gustatory disorder. Jpn. J. Oral Diag. Oral Med., 2003;16, 1-8.
24. Satoh-Kuriwada S, Sasano, T., Saito, M., Simeno, Y., Oba, M., Sakamoto, M., Aizawa, K. and Watanabe, M. Epidemiological study on gus- tatory disorders in the elderly. Part 2: Influence of hyposalivation on gustatory disorder. Jpn. J. Oral Diag. Oral Med., 2005;18, 14-18.
25. Iwasaki M, Yoshihara A, Ito K, Sato M, Minagawa K, Muramatsu K, Watanabe R, Manz M C, Ansai T, Miyazaki H. Hyposalivation and dietary nutrient intake among community-based older Japanese. Geriatr Gerontol Int, 2016;16, 500-507.
26. Mesas A E, Andrade S M, Cabrera M A, Bueno V L. Oral health status and nutritional deficit in noninstitutionalized older adults in Londrina, Brazil. Rev Bras Epidemiol, 2010;13, 434-445.
27. Solemdal K, Sandvik L, Willumsen T, Mowe M, Hummel T. The impact of oral health on taste ability in acutely hospitalized elderly. PLoS One, 2012;7, e36557.
28. Soini H, Routasalo P, Lauri S, Ainamo A. Oral and nutritional status in frail elderly. Spec Care Dentist, 2003;23, 209-215.

29. Yoshinaka M, Yoshinaka M F, Ikebe K, Shimanuki Y, Nokubi T. Factors associated with taste dissatisfaction in the elderly. J Oral Rehabil, 2007;34, 497-502.
30. Ikebe K, Sajima H, Kobayashi S, Hata K, Morii K, Nokubi T, Ettinger R L. Association of salivary flow rate with oral function in a sample of community-dwelling older adults in Japan. Oral Surg Oral Med Oral Pathol Oral Radiol Endod, 2002;94, 184-190.
31. Poisson P, Laffond T, Campos S, Dupuis V, Bourdel-Marchasson I. Relationships between oral health, dysphagia and undernutrition in hospitalised elderly patients. Gerodontology, 2014;33, 161-168.
32. Shinkawa T, Hayashida N, Mori K, Washio K, Hashiguchi K, Taira Y, Morishita M, Takamura N. Poor chewing ability is associated with lower mucosal moisture in elderly individuals. Tohoku J Exp Med, 2009;219, 263-267.
33. Yamada H, Nakagawa Y, Nomura Y, Yamamoto K, Suzuki M, Watanabe N Y, Saito I, Seto K. Preliminary results of moisture checker for Mucus in diagnosing dry mouth. Oral Dis, 2005;11, 405-407.
34. Ikebe K, Matsuda K, Morii K, Furuya-Yoshinaka M, Nokubi T, Renner R P. Association of masticatory performance with age, posterior occlusal contacts, occlusal force, and salivary flow in older adults. Int J Prosthodont, 2006;19, 475-481.
35. Samnieng P, Ueno M, Shinada K, Zaitsu T, Wright F A, Kawaguchi Y. Association of hyposalivation with oral function, nutrition and oral health in community-dwelling elderly Thai. Community Dent Health, 2012;29, 117-123.
36. Dormenval V, Mojon P, Budtz-Jorgensen E. Associations between self-assessed masticatory ability, nutritional status, prosthetic status and salivary flow rate in hospitalized elders. Oral Dis, 1999;5, 32-38.
37. Samnieng P. Appetite loss and related factors in community-dwelling elderly thai. Int. J Clin. Prev. Dent., 2014;10, 23-30.
38. Syrjala A M, Pussinen P I, Komulainen K, Nykanen I, Knuuttila M, Ruoppi P, Hartikainen S, Sulkava R, Ylostalo P. Salivary flow rate and risk of malnutrition - a study among dentate, community-dwelling older people. Gerodontology, 2013;30, 270-275.
39. Srinivasulu G, Fareed, N., Sudhir, K.M., Kumar, K. Relationship between Stimulated Salivary Factors, Dental Caries Status and Nutritional Condition among Institutionalized Elderly People. OHDM, 2014;13, 49-53.
40. Dormenval V, Budtz-Jorgensen E, Mojon P, Bruyere A, Rapin C H. Associations between malnutrition, poor general health and oral dryness in hospitalized elderly patients. Age Ageing, 1998;27, 123-128.
41. Glore R J, Spiteri-Staines K, Paleri V. A patient with dry mouth. Clinical Otolaryngology, 2009;34, 358-363.
42. Villa A, Abati S. Risk factors and symptoms associated with xerostomia: a cross-sectional study. Aust Dent J, 2011;56, 290-295.
43. Neyraud E, Palicki O, Schwartz C, Nicklaus S, Feron G. Variability of human saliva composition: Possible relationships with fat perception and liking. Arch Oral Biol, 2012;57, 556-566.
44. Ship J A, Fox P C, Baum B J. How much saliva is enough - normal function defined. J Am Dental Assoc, 1991;122, 63-69.
45. Satoh-Kuriwada S, Shoji N, Kawai M, Uneyama H, Kaneta N, Sasano T. Hyposalivation Strongly Influences Hypogeusia in the Elderly. J Health Sci, 2009;55, 689-698.
46. Kremer S, Bult J H F, Mojet J, Kroeze J H A. Compensation for age-associated chemosensory losses and its effect on the pleasantness of a custard dessert and a tomato drink. Appetite, 2007;48, 96-103.
47. Kremer S, Mojet J, Kroeze J H A. Perception of texture and flavor in soups by elderly and young subjects. J Texture St, 2005;36, 255-272.
48. Forde C G, Delahunty C M. Examination of chemical irritation and textural influence on food preferences in two age cohorts using complex food systems. Food Qual Pref, 2002;13, 571-581.
49. Carr A C, Frei B. Toward a new recommended dietary allowance for vitamin C based on antioxidant and health effects in humans. Am J Clin Nut, 1999;69, 1086-1107.
50. Lemaitre R N, King I B, Mozaffarian D, Kuller L H, Tracy R P, Siscovick D S. n-3 polyunsaturated fatty acids, fatal ischemic heart disease, and nonfatal myocardial infarction in older adults: the Cardiovascular Health Study. Am J Clin Nut, 2003;77, 319-325.
51. Rimm E B, Willett W C, Hu F B, Sampson L, Colditz G A, Manson J E, Hennekens C, Stampfer M J. Folate and vitamin B-6 from diet and supplements in relation to risk of coronary heart disease among women. JAMA, 1998;279, 359-364.
52. Bardow A, Nyvad B, Nauntofte B. Relationships between medication intake, complaints of dry mouth, salivary flow rate and composition, and the rate of tooth demineralization in situ. Arch Oral Biol, 2001;46, 413-423.
53. Kreher J M, Graser G N, Handelman S L. The relationship of drug-use to denture function and saliva flow-rate in a geriatric population. J Prosthetic Dent, 1987;57, 631-638.
54. Ship J A, Baum B J. Is reduced salivary flow normal in old-people?. Lancet, 1990;336, 1507-1507.
55. Ship J A, Decarli C, Friedland R P, Baum B J. Diminished submandibular salivary flow in dementia of the alzheimer type. J Gerontology, 1990;45, M61-M66.
56. Dean M, Raats M M, Grunert K G, Lumbers M, Food Later Life T. Factors influencing eating a varied diet in old age. Public Health Nut, 2009;12, 2421-2427.
57. Johnson A E, Donkin A J M, Morgan K, Neale R J, Page R M, Silburn R L. Fruit and vegetable consumption in later life. Age Ageing, 1998;27, 723-728.
58. Mioche L, Bourdiol P, Peyron M A. Influence of age on mastication: effects on eating behaviour. Nut Res Rev, 2004;17, 43-54.
59. Moreira N C F, Krausch-Hofmann S, Matthys C, Vereecken C, Vanhauwaert E, Declercq A, Bekkering G E, Duyck J. Risk Factors for Malnutrition in Older Adults: A Systematic Review of the Literature Based on Longitudinal Data. Adv Nut, 2016;7, 507-522.
60. Savoca M R, Arcury T A, Leng X Y, Chen H Y, Bell R A, Anderson A M, Kohrman T, Frazier R J, Gilbert G H, Quandt S A. Severe tooth loss in older adults as a key indicator of compromised dietary quality. Public Health Nut, 2010;13, 466-474.
61. Sreebny L M, Yu A, Green A, Valdini A. Xerostomia in diabetes-mellitus. Diabetes Care, 1992;15, 900-904.
62. Flink H, Bergdahl M, Tegelberg A, Rosenblad A, Lagerlof F. Prevalence of hyposalivation in relation to general health, body mass index and remaining teeth in different age groups of adults. Community Dent Oral Epidemiol, 2008;36, 523-531.
63. Hirotomi T, Yoshihara A, Ogawa H, Ito K, Igarashi A, Miyazaki H. A preliminary study on the relationship between stimulated saliva and periodontal conditions in community-dwelling elderly people. J Dent, 2006;34, 692-698.
64. Sreebny L M, Zhu W T. Anti-SS-A and anti-SS-B Ab's in the saliva and blood of patients with dry mouth and dry eyes. J Dent Res, 1996;75, 2031-2031.
65. Michael E C D, Denis O. Saliva and oral health. London.
66. Cabrera M A S, Mesas A E, Rossato L A, De Andrade S M. Salivary flow and psychoactive drug consumption in elderly people. Revista Da Associacao Medica Brasileira, 2007;53, 178-181.
67. Narhi T O, Tenovuo J, Ainamo A, Vilja P. Antimicrobial factors, sialic-acid, and protein-concentration in whole saliva of the elderly. Scand J Dent Res, 1994;102, 120-125.
68. Henricsson V, Svensson A, Axell T. Evaluation of some electrical methods for objective assessment of oral mucosal dryness. Scand J Dent Res, 1990;98, 520-528.
69. Navazesh M. Methods for collecting saliva. Annals of the New York Academy of Sciences, 1993;694, 72-77.
70. Navazesh M, Kumar S K S. Measuring salivary flow - Challenges and opportunities. Journal of the American Dental Association, 2008;139, 35S-40S.
71. Osterberg T, Landahl S, Hedegard B. Salivary flow, saliva, ph and buffering capacity in 70-year-old men and women - correlation to dental-health, dryness in the mouth, disease and drug-treatment. J Oral Rehabil, 1984;11, 157-170.

Publication n°14: Does interindividual variability of saliva affect the release and metabolization of aroma compounds ex vivo? The particular case of elderly suffering or not from hyposalivation.

Muñoz-González, C.; Brulé, M.; Feron, G.; Canon, F.

Journal of Texture Studies 2018, *50* (1), 36-44.

Received: 4 June 2018 | Revised: 11 October 2018 | Accepted: 22 November 2018

DOI: 10.1111/jtxs.12382

RESEARCH ARTICLE

WILEY Journal of Texture Studies

Does interindividual variability of saliva affect the release and metabolization of aroma compounds ex vivo? The particular case of elderly suffering or not from hyposalivation

Carolina Muñoz-González | Marine Brulé | Gilles Feron | Francis Canon

Centre des Sciences du Goût et de l'Alimentation, UMR1324 INRA, UMR6265 CNRS Université de Bourgogne, Agrosup Dijon, Dijon, France

Correspondence
Carolina Muñoz-González, Centre des Sciences du Goût et de l'Alimentation, UMR1324 INRA, UMR6265 CNRS Université de Bourgogne, Agrosup Dijon, F-21000 Dijon, France.
Email: carolina.munoz@inra.fr

Funding information
Agence Nationale de la Recherche, Grant/Award Number: MUFFIN N° 14-CE20-0001-01 and AlimaSSenS N°14-CE; Agreenskills fellowship , Grant/Award Number: N°FP7-609398 (AgreenSkills+ contract); Research prize, Grant/Award Number: French Nutrition Society; AlimaSSenS, Grant/Award Number: N°14-CE20-0003-01; MUFFIN, Grant/Award Number: N° 14-CE20-0001-01; French Nutrition Society; EU's Seventh Framework Programme, Grant/Award Number: N°FP7-609398

Abstract

The aim of this work was to study the effects of interindividual variability of human elderly saliva on aroma release and metabolization by ex vivo approaches. Thirty individuals suffering or not from hyposalivation were selected from a panel formed by 110 elderly people (aged >65 years old) that were matched by age and sex. Then, their stimulated saliva samples were independently incubated in presence of three aroma compounds (ethyl hexanoate, octanal, 2-nonanone) to perform headspace-gas chromatography and liquid/liquid extraction-gas chromatography mass spectrometry analyses. These assays revealed that the extent of saliva effect on the release and metabolization of aroma compounds was highly dependent on the chemical family of the compounds (octanal>ethyl hexanoate>2-nonanone). Moreover, salivas from the hyposalivator (HPS) group exerted a significant lower release and/or higher metabolization than those of the control group for the three assayed compounds. Regarding the biochemical characterization of the saliva samples, no significant differences were found in the total protein content between the two groups. This does not preclude the involvement of specific proteins on the observed results that need to be clarified in further experiments. Saliva from the HPS group presented a significantly higher total antioxidant capacity than that of the control group, which suggests that this parameter could be related to the metabolization of aroma compounds by saliva. Such effects might alter aroma perception in individuals suffering from hyposalivation.

Practical applications

The world population is getting older so fast that most countries are not prepared to handle this demographic challenge, characterized by an increasing prevalence of noncommunicable chronic diseases (e.g., diabetes, gastrointestinal disorders) associated to inadequate eating patterns. Thus, supporting a balanced diet is one of the most cost-effective strategies to maintain a good quality of life. A suitable diet needs to take into account both, specific sensory and nutritional individual needs. However, aging is often accompanied by deterioration in oral health (e.g., low salivary secretions), which could alter the capacities to taste and smell. Results from this work contribute to a better understanding of the role of human saliva in aroma release and metabolization, a first step to comprehend retronasal aroma release and perception. This knowledge will help to propose innovative solutions for the reformulation of food products better adapted to the elderly's needs, thus allowing delayed onset of dependency.

KEYWORDS

aroma release, elderly, hyposalivation, metabolization, saliva, total antioxidant capacity

This article was published on AA publication on: 06 December 2018.

1 | INTRODUCTION

The interest in the role of human saliva on the food oral processing is growing in last years (Mosca & Chen, 2017; Muñoz-González et al., 2017; Muñoz-González, Feron, & Canon, 2018a; Ployon, Morzel, & Canon, 2017). In several studies, a particular attention is turned to the functions that saliva may play on aroma compounds (Buettner, 2002a, 2002b; Genovese, Piombino, Gambuti, & Moio, 2009; Munoz-Gonzalez et al., 2014; Munoz-Gonzalez, Feron, Brule, & Canon, 2018b; Pages-Helary, Andriot, Guichard, & Canon, 2014; Piombino et al., 2014). These studies, carried out ex vivo, have demonstrated that human saliva and its components can increase or decrease the release of aroma compounds via different mechanisms such as noncovalent interactions, salting-out effects or enzymatic conversion. Thus, it is believed that the variability of human saliva might be one of the factors explaining interindividual variation in retronasal aroma release and aroma perception (Feron et al., 2014; Guichard, Repoux, Qannari, Laboure, & Feron, 2017).

However, most of the studies on this topic have employed pooled salivas or individual salivas from a limited number of subjects (Buettner, 2002a, 2002b; Genovese et al., 2009; Munoz-Gonzalez et al., 2018b; Munoz-Gonzalez et al., 2014; Pages-Helary et al., 2014) that do not represent properly the well-known interindividual variability of human saliva composition in healthy individuals (Leake, Pagni, Falquet, Taroni, & Greub, 2016; Neyraud, Palicki, Schwartz, Nicklaus, & Feron, 2012). Additionally, different pathologies or functional states can provoke biochemical and microbiological changes in salivary parameters raising the differences in specific populations (Castagnola, Cabras, Vitali, Sanna, & Messana, 2011; Schipper, Silletti, & Vinyerhoeds, 2007). This fact leads to hypothesize that people experiencing salivary disorders might present an altered retronasal release and perception of aroma. Hereof, it should be mentioned an original study that showed that saliva from obese people (body mass index [BMI] > 30) suppressed aroma release from wine compared to saliva from normal-weight subjects (18.5 < BMI < 24.9; Piombino et al., 2014). Authors observed that saliva from obese individuals (n = 28) presented a higher total antioxidant capacity (TAC) compared to that of the controls (n = 28). They suggested the induction of a systemic antioxidant response in the saliva from obese subjects that might have affected the release of aroma compounds in that group.

Elderly people are another specific population affected by salivary disorders. A recent meta-analysis has shown that the aging process is associated per se with a reduced secretion of the salivary-glands (Affoo, Foley, Garrick, Siqueira, & Martin, 2015). In the elderlies, such salivary hypofunction could have a negative influence on food consumption as it has been recently reviewed (Muñoz-González et al., 2017). In that article, authors systematically reviewed the existing articles on this topic and they found that most of them showed an association between hyposalivation and a decrease in the chewing and swallowing abilities, but also in taste perception (Iwasaki et al., 2016; Samnieng et al., 2012; Solemdal, Sandvik, Willumsen, Mowe, & Hummel, 2012). A relationship between salivary hypofunction and appetite loss (Dormenval, Mojon, & Budtz-Jorgensen, 1999; Iwasaki et al., 2016) and unbalanced dietary intake was also underlined. However, in spite of the relevance of this topic, and the increased of this population group, to the authors' knowledge the effects of saliva on aroma release in elderlies have never been investigated.

For that reason, in this article, the role of interindividual differences of saliva from elderly people on aroma compounds has been studied. Thirty individuals (15 suffering from hyposalivation, 15 with normal salivary flow) were selected from a panel formed by 110 older individuals. Both groups were matched by age and sex. Saliva samples (n = 30) were independently incubated in presence of three aroma compounds (ethyl hexanoate, octanal and 2-nonanone). Aroma release was measured by HS-GC. Moreover, LLE-GC/MS analyses were performed to investigate the possible metabolization of aroma compounds by saliva. Biochemical analyses of the saliva samples were carried out to compare the two groups and to understand the relationship between data on saliva composition and the release and metabolization of aroma compounds.

2 | MATERIAL AND METHODS

2.1 | Aroma compounds

Three compounds were chosen on the basis of their physicochemical characteristics (similar log P and boiling point), their aroma impact, and because of their suitability for the analyses techniques regarding the detection limits and solubility (Table 1). They belong to three chemical families (ketones, aldehydes, and esters), known to be affected by saliva (Buettner, 2002a, 2002b; Munoz-Gonzalez et al., 2018b; Pages-Helary et al., 2014). The aroma compounds were of analytical grade (Aldrich, Steinheim, Germany). A gas chromatography-flame ionization detector analysis confirmed the purity of all aroma compounds (>98%), which was take into account for the calculations. Stock solutions (1%) of single aroma compounds were freshly prepared in propyleneglycol at room temperature under magnetic stirring for 2 hr. They

TABLE 1 Physicochemical properties of the aroma compounds used in this study

Aroma compounds	CAS number	Chemical family	Chemical formula	MW[a] (g/mol)	Log P[b]	BP[c] (C)	Solubility[d] (mg/L)	Aroma descriptor[e]
Ethyl hexanoate	123-66-0	Ester	$C_8H_{16}O_2$	144	2.8	168	308	Fruity
Octanal	124-13-0	Aldehyde	$C_8H_{16}O$	128	2.8	176	394	Fat, lemon, green
2-Nonanone	821-55-6	Ketone	$C_9H_{18}O$	142	2.7	185	171	Blue cheese, fatty, fruity

[a] Hydrophobic constant estimated using molecular modeling software EPI Suite (U.S. EPA 2000–2007).
[b] Boiling point estimated using molecular modeling software EPI Suite (U.S. EPA 2000–2007).
[c] Solubility in water estimated using molecular software EPI Suite (U.S. EPA 2000–2007).
[d] From Flavornet database (http://www.flavornet.org; accessed October 2009).
[e] Molecular weight.

were stored at 4C throughout the study, and their stability was periodically checked. The final concentration of the aroma compounds in the water solutions was 3 ppm.

2.2 | Saliva samples

2.2.1 | Panel of elderly individuals

A panel of 110 elderly volunteers formed the initial population (AlimaSSenS project: toward an adapted and healthy food supply for elderly people). The AlimaSSens panel was recruited from a population of elderly people living at home in Dijon (France). The recruitment criteria were the following: older than 65 years old, no acute pathological episodes at the time of the experiment, and scoring at least 24 on the mini mental state evaluation, which indicates normal cognition (Folstein, Folstein, & McHugh, 1975). An interview was carried out with each volunteer to ensure that they met the inclusion criteria. Interested people followed a dentist evaluation and completed a questionnaire asking them about medications and food habits. Exclusionary criteria included any physiological condition or taking medications that could influence salivation (e.g., antidepressants and antihistamines). Finally, their weight and their height were measured and used to calculate their body mass index (BMI = weight [kg]/height^2 [m^2]). All subjects gave written informed consent to participate in the experiment after receiving oral and written information. The experimental protocol was approved by the French Ethics Committee for Research (CPP Est I, Dijon, #14.06.03, ANSM #2014-A00071-46).

2.2.2 | Saliva collection and salivary flow rates calculation

Participants were asked not to consume any food or drink at least 1 hr before saliva was collected. Unstimulated salivary flow was measured by instructing the participants to let the saliva naturally be accumulated in the mouth and then spat it directly into a collection tube during 10 min. Stimulated salivary flow was measured by instructing the participants to masticate a piece of pre-weighed parafilm while spitting out the saliva into a pre-weighed screw-cap cup every time they felt like swallowing over a period of 5 min. Cups were weighed, and salivary flow rates were expressed in ml/min assuming that 1 g of saliva corresponds to 1 ml. Only stimulated saliva samples were analyzed in this study, since this is the saliva secreted during food consumption. Moreover, it has been previously reported that this type of saliva was correlated to aroma release during food consumption (Feron et al., 2014). Saliva samples were alliquoted and stored at −80C until use.

2.3 | Saliva biochemical analysis

2.3.1 | Protein concentration

The protein concentration was determined using the Bradford protein assay with bovine serum albumin used as the standard for calibration.

2.3.2 | Protein profile

Salivary samples were separated by electrophoresis using analytical 4–20% precast polyacrylamide gels (Biorad, France). The samples (10 μg of total protein content) were diluted into a mixture (vol/vol) of 2× Laemmli buffer and Dithiothreitol (100 mM; final volume = 50 μl). Then, they were heated at 100C during 5 min. The gels were performed on a Mini-PROTEAN Tetra Cell (BioRad). A control of saliva and a molecular weight marker Precision Plus Protein Unstained (Biorad) were loaded in each of the gels. The running buffer 1× TGS was added into the gels and a separation voltage of 200 V was applied during 40 min. After that, the gels were rinsed into the deionized water for 10 min. Gel images were acquired on a ChemiDoc MP imaging system (Biorad) for fluorescently stained gels. The time of exposure was 10 s. Molecular weight and intensity of each protein band were calculated on the normalized gels using the ImageLab software (Biorad). Spot volumes were normalized within one gel by the total volume of all valid spots for that particular gel and used for statistical analysis.

2.3.3 | Total antioxidant capacity

The total antioxidant capacity was determined using an ORAC Assay kit (Zen-bio, Research Triangle Park, NC). This assay measures the loss of fluorescein fluorescence over time due to peroxyl radical formation resulting from the breakdown of AAPH (2,2′-azobis-2-methyl-propanimidamide, dihydrochloride). Trolox (6-hydroxy-2,5,7,8-tetramethylchroman-2-carboxylic acid), a water soluble vitamin E analogue, serves as a positive control to inhibit fluorescein decay in a dose-dependent manner. The intensity of fluorescence was measured (excitation filter, 485 nm; emission filter, 538 nm) using a microtitre plate fluorometer (Victor 3-V, PerkinElmer, France). The total antioxidant capacity was expressed in micromolar Trolox equivalent.

2.4 | Release of aroma compounds by HS-GC

A previously validated method adapted to microvolumes of saliva was employed (Munoz-Gonzalez et al., 2018b). Briefly, 300 μl of the aroma solution (containing the three aroma compounds at 3 ppm) were placed into a 10 ml headspace vial (Agilent Technologies, Palo Alto, CA). Then, water or stimulated saliva samples (n = 30) were added to the vial until a final volume of 500 μl. Vials were immediately sealed with a PTFE/silicone septum (Supelco, Bellefonte, PA), vortexed and then incubated at 37C during 30 min. After the incubation time, 200 μl of headspace were taken automatically using a preheated (45C) 1-ml gas-tight syringe (Gerstel, manufactured by SGE, Victoria, Australia) and analyzed by gas chromatography (Agilent 7890B) in splitless mode at 240C. A capillary DW-Wax column (30 m x 0.32 mm i.d. x 0.5 μm; Agilent J&W Scientific, Folsom, CA) and a flame ionization detector set at 250C were used. The carrier gas was helium at a velocity of 30 cm^3/s. Aroma compounds were analyzed at 110C (isothermal temperature). Each salivary sample (n = 30) was analyzed independently and in triplicate (one injection per sample vial). Salivary samples were analyzed in random order.

Linearity and repeatability (calculated in three different days) of the procedure were determined in the mix of the three aroma compounds at five levels of concentration (0.6, 1.2, 2.5, 5, and 10 mg/L), with determination coefficients higher than 0.99 and relative standard deviations lower than 7% for the three assayed compounds. Absence of interference (competition, interaction…) between the aroma compounds was checked for both water and saliva (p > .05). Stability of the aroma compounds and that of the GC system was checked during

all the analysis period with no significant differences obtained across days ($p > .05$).

2.5 | Recovery of aroma compounds after incubation by LLE-GC/MS

After incubation at 37C during 30 min, 500 μl of a saturated $CaCl_2$ solution were added to the samples to inhibit possible enzymatic reactions (Buettner, 2002a, 2002b). Moreover, samples were acidified with HCl to protonate acids and increase their extraction. The solutions were extracted twice with 1 ml of dichloromethane (Carlo Erba, Val de Reuil, France) then centrifuged (5,000g, 4C, 15 min) to separate the two phases. Prior to the extraction, samples were spiked with 100 μl of the internal standard, methyl nonanoate (10 mg/L). The combined organic extracts were dried over anhydrous Na_2SO_4, then concentrated to a total volume of 100 μl. Two microliters were injected into the GC/MS in splitless mode for 1.5 min at 240C. The oven temperature was programmed to increase from 40 (5 min) to 240C at $4C/min^{-1}$ and held 5 min. Aroma compounds were separated on a DB-Wax polar capillary column (30 m × 0.32 mm i.d. × 0.50 μm film thickness) from Agilent (J&W Scientific, Folsom, CA). Helium was used as the carrier gas at a flow rate of 1.5 ml/min. For the MS system (Agilent 5973N), the temperatures of the transfer line, quadrupole, and ion source were 250, 150, and 230C, respectively. Electron impact mass spectra were recorded at 70 eV ionization voltages, and the ionization current was 10 μA. The acquisitions were performed in scan (from 35 to 350 amu) and SIM modes. The identification of compounds was based on the comparison of retention times and mass spectra from three databases: NIST 2.0 and WILEY 138. Relative peak areas (RPAs) were obtained by calculating the relative peak area in relation to that of the internal standard. The use of RPAs data to express aroma release was sufficient for this type of analysis as the aim of the work was to compare the extent of aroma recovery between saliva samples. Each salivary sample ($n = 30$) was analyzed independently and in triplicate (one injection per sample vial).

Linearity and repeatability of the procedure were determined in the aqueous solution at four levels of concentration (0.1, 1, 5, and 10 mg/L), with coefficients of determination (R^2) higher than 0.99 and relative standard deviations lower than 3% for all the assayed compounds. The same LLE procedure was carried out with the salivas and water samples without added aroma compounds to detect any possible compound coming from the salivas or any artifact formed during the extraction procedure. Stability of the aroma compounds and that of the GC/MS was checked in controls during all the analysis period and no significant differences were obtained across days ($p > .05$).

2.6 | Statistical analyses

Linear regression analyses were performed to establish the linearity of the response of each aroma compound by GC and GC/MS. Normality test on the two populations (HPS versus control) regarding the SSFR confirmed that both groups were normally distributed. ANOVA analyses and the least significant differences (LSD) test were used to determine significant differences between the groups. The significance level was $p < .05$ throughout the study. The XLstat program was used for data processing (StatSoft, Inc., 2005, www.statsoft.com).

3 | RESULTS AND DISCUSSION

3.1 | Description of the panel

As it can be seen in Table 2, the initial population was formed by 110 persons aged between 65 and 87 year olds (mean age = 72 year olds). Averaged unstimulated salivary flow rate determined for the whole group was 0.31 (±0.18) and averaged stimulated salivary flow rate was 1.63 (±0.82) ml/min.

From this population, 15 individuals presented hyposalivation (measured as the presence of a SSFR lower than 0.8 ml/min Soini, Routasalo, Lauri, & Ainamo, 2003). Therefore, these 15 individuals formed the hyposalivator group (mean SSFR for the hyposalivator group = 0.61 ± 0.18 ml/min). The control group was constituted by individuals ($n = 15$) presenting a SSFR similar to the mean SSFR of the initial population (mean SSFR for the control group = 1.69 ± 0.17 ml/min). Both groups were matched by age and sex. This resulted in a higher proportion of women than men in this study. This is because people suffering from hyposalivation in the initial population were mostly women. This gender difference on salivary flow rate has already been described in several articles, and it could be due to the smaller salivary gland size of women comparing to men (Inoue et al.,

TABLE 2 Description of the elderly panel

	Initial population	Hyposalivator group	Control group	*p* Value
Number of subjects	110	15	15	
Sex (male; female)	51; 59	3; 12	3; 12	
Mean age (±SD)	71.6 (±5.5)	72.3 (±5.6)	71.4 (±4.3)	
Mean BMI[1] (kg/m^2)	27.4 (±4.3)	**28.6 (±5.1)[a]**	**25.2 (±3.9)[b]**	**.0500**
USFR[2] (min; max) (ml/min)	0.05; 0.90	0.05; 0.41	0.16; 0.51	
Mean USFR (ml/min)	0.31 (±0.18)	**0.15 (±0.10)[b]**	**0.32 (±0.11)[a]**	**.0002**
SSFR (min; max) (ml/min)	0.23; 4.55	0.23; 0.80	1.35; 1.93	
Mean SSFR[3] (ml/min)	1.63 (±0.82)	**0.61 (±0.18)[b]**	**1.69 (±0.17)[a]**	**≤.0001**

In bold, statistical differences between the hyposalivator and control groups. Different letters across the different groups denotes statistical differences after the application of the LSD test.
[1]Body mass index (BMI, Kg/m^2).
[2]USFR, Unstimulated salivary flow rate.
[3]SSFR, stimulated salivary flow rate.

2006). Table 2 shows that, as expected, the hyposalivator group presented significantly lower unstimulated and stimulated salivary flow rates than the control group. Moreover, the body mass index (BMI) of people forming the hyposalivator group was significantly higher than that of those from the control group (Table 2). An association between high BMI and hyposalivation has already been found by Flink, Bergdahl, Tegelberg, Rosenblad, and Lagerlof (2008). However, the explanations for this association are so far inconclusive. It has been suggested that both parameters could be related to malnutrition, by the appearance of diabetes, cardiovascular diseases, cancer, osteoporosis and caries, or other chronic diseases that might affect both the weight and/or the salivary gland function of the people (Flink et al., 2008).

3.2 | Aroma release after the interaction of the selected aroma compounds with water or with salivas from the hyposalivator and control groups

Figure 1 shows the aroma release values obtained for each of the three aroma compounds in the water and saliva samples (hyposalivator and control groups) together with the results of the LSD test. As it can be seen, all the assayed compounds were significantly less released in the hyposalivator group compared to the control group and the water samples, although the extent of the effect varied among compounds. Interestingly, octanal was the compound most affected by saliva and the only significantly different between the control group and the water samples. The differences observed among compounds cannot be only explained on the basis of some physicochemical properties of the aroma compounds, such as hydrophobicity or boiling point, as these characteristics were similar for the tested molecules (see Table 1). The effect of saliva on aroma compounds varied as a function of their chemical family. The higher effect of human saliva on aldehydes and esters than on monoketones has been previously reported in several publications performed under ex vivo conditions (Buettner, 2002a, 2002b; Munoz-Gonzalez et al., 2018b; Pages-Helary et al., 2014).

The decrease in the release could be mostly due to two phenomena. On the one hand, aroma compounds might be retained by salivary components (such as proteins), as it has been previously suggested (Pages-Helary et al., 2014). On the other hand, these results could be explained by a transformation of the aroma compounds (Buettner, 2002a, 2002b; Munoz-Gonzalez et al., 2018b; Pages-Helary et al., 2014) through enzymatic or nonenzymatic reactions by saliva. In any case, the fact that in average, salivas from elderly people suffering from hyposalivation decreased more the release of aroma compounds than saliva from individuals presenting a normal salivary flow could be at the origin of aroma perception anomalies in this population. To the best of the authors' knowledge, this is the first time that this finding has been shown. However, in our study, people from the hyposalivator group presented also a higher BMI compared to those of the control group. In this regard, Piombino et al. (2014) have already shown that saliva from young obese individuals (high BMI) supresses aroma release compared to saliva from normal-weight subjects. Therefore, in vivo studies controlling for confounding factors (such as BMI) will be needed to elucidate the role of hyposalivation on retronasal aroma release and perception.

3.3 | Metabolization of aroma compounds by salivas from the hyposalivator and control groups

The possible metabolization of the assayed aroma compounds by saliva was investigated by LLE-GC/MS. After incubating the aroma compounds in the presence of each of the 30 saliva samples or water during 30 min at 37C, aroma compounds were extracted with dichloromethane and analyzed by GC–MS. Blanks of saliva without the

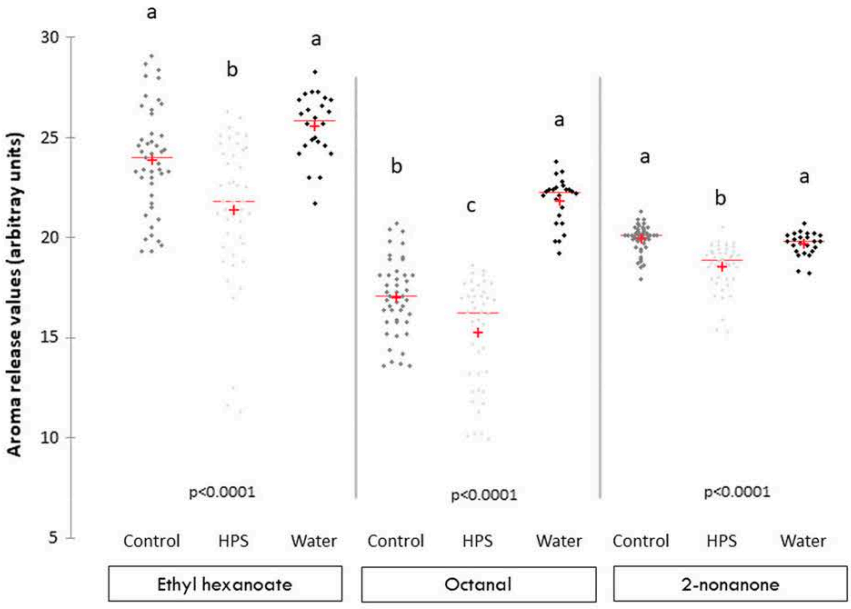

FIGURE 1 Aroma release values obtained after the incubation of the three aroma compounds at 37C during 30 min with water or with salivas (n = 30) from the HPS or control groups and analyzed by HS-GC. Different letters across the different groups denote statistical differences after application of the LSD test

aroma compounds or the aroma compounds without saliva were also analyzed in the same conditions.

A one-way ANOVA analysis was performed on the extracted amounts of octanal, ethyl hexanoate, 2-nonanone after their incubation in the presence of the 30 saliva samples or water. These results are shown in Table 3. As it can be observed, the three assayed compounds presented a significantly lower recovered quantity of the three aroma compounds in the saliva samples from the hyposalivator group compared to the water samples and to the salivas from the control group. In agreement with the aroma release analyses, octanal was the only compound significantly different between the control group and the water samples. Table 3 also shows that the recovered quantity of the three aroma compounds was significantly lower in the salivas from the hyposalivator group compared to those of the control group. Assuming the fact that the addition of the solvent to the samples would loss the integrity of salivary proteins, noncovalent interactions between protein and aroma compounds are unlikely to survive to the solvent changes. Therefore, they are unlikely to explain the different recovery between the two groups. Therefore, a stronger metabolization of the three compounds in the hyposalivator group compared to the control group is the most plausible mechanism to explain our results, despite that the involvement of noncovalent interactions cannot be excluded.

Additionally, the presence of metabolites was checked to investigate which type of conversion suffered the aroma compounds by saliva. The type of reaction was clearly confirmed for octanal that was reducted to 1-octanol (Figure 2). In agreement, no octanol was found in the water samples and a significant lower production of 1-octanol was obtained in the control group compared to the hyposalivator group (Table 3). In the case of ethyl hexanoate, its expected metabolite (the hexanoic acid) was also detected in the blanks of saliva without aroma compounds added (Figure 2). Therefore, its formation by the effect of salivary components could not be definitely proven in the present study. Finally, no metabolite was detected for the 2-nonanone (Figure 2), which was possibly due to a limitation on the sensibility of our method.

Overall, these findings confirm a different metabolization rate of aroma compounds in the two salivary groups. Therefore, these results suggest that elderly people suffering from hyposalivation could present an altered aroma perception (e.g., due to a lower availability of aroma compounds to reach the olfactory receptors retronasally and/or to a higher formation of new aroma compounds [i.e., metabolites] which might present different odor thresholds and qualities). This relevant finding needs to be verified in vivo.

TABLE 3 Relative peak areas (related to the internal standard) of the aroma compounds extracted after the incubation at 37°C during 30 min with water or the salivas from the hyposalivator and control groups and determined by LLE-GC/MS

	Ethyl hexanoate	Octanal	2-Nonanone	Octanol
Water	0.41^{a}	0.27^{a}	1.66^{a}	0.00^{c}
Control	0.37^{a}	0.19^{b}	1.54^{a}	0.24^{b}
Hyposalivator	0.25^{b}	0.15^{c}	1.39^{b}	0.33^{a}
p Value	<.0001	<.0001	.0003	<.0001

Different letters across the different groups denote statistical differences after application of the LSD test.

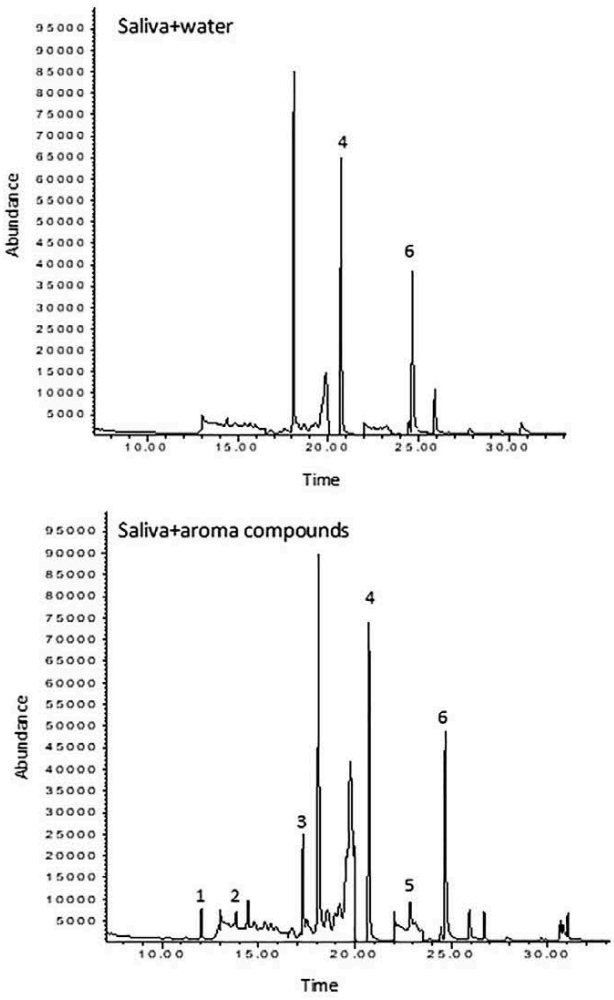

FIGURE 2 Chromatograms corresponding to one saliva sample incubated with water or the same saliva incubated with the aroma compounds selected for this study. Numbers in the chromatogram correspond to the compounds: 1. Ethyl hexanoate, 2. Octanal, 3. 2-nonanone, 4. Methyl nonanoate (IS), 5. Octanol, and 6. Hexanoic acid

3.4 | Researching the origin of the differences observed on aroma release and metabolism between the hyposalivator and the control groups

In a previous study performed with artificial or pooled human saliva, it has been suggested that salivary proteins such as mucin and alpha-amylase could interact with aroma compounds, affecting their release to the headspace (Pages-Helary et al., 2014). In another work, Piombino et al. (2014) showed that saliva from obese individuals presented a significantly higher total antioxidant capacity and lower ex vivo aroma release than saliva from normal-weight subjects. In agreement with those papers, Munoz-Gonzalez et al. (2018b) observed that the highest the total protein content and the total antioxidant capacity of the saliva samples, the lowest the ex vivo aroma release. However, the latter study was performed with a limited number of saliva samples (n = 3). Consequently, the protein content and the total antioxidant seem to be two factors affecting the behavior of aroma compounds in presence of saliva. To validate this hypothesis,

these parameters were analyzed in the 30 saliva samples selected for this study and results are shown below.

3.4.1 | Total protein content and protein profile of saliva from hyposalivators or control subjects

As it can be seen in Figure 3, the total protein content (TPC) values between the hyposalivator and control groups were not significantly different (p = .710). Therefore, this parameter did not seem to be enough to explain the differences in the aroma release and metabolization observed in the two salivary groups of the present study. These differences could be more likely due to specific noncovalent interactions or enzymatic reactions. In this regard, Pages-Helary et al. (2014) suggested that specific salivary proteins such as mucin and alpha-amylase affect the release of esters and monoketones. Consequently, we further explored the protein profile of the 30 saliva samples through electrophoresis to know if the relative amount of specific proteins could better explain the aroma release and metabolization data. One example of the protein profiles obtained is shown in Figure 4. From that analysis, seven spots were identified in more than the 80% of the saliva samples and their relative abundances determined. However, the determination of mucins could not be possible due to the high molecular weight of these proteins and no significant differences were observed between groups in the band corresponding to the protein alpha-amylase between groups (55 kDa). This could be due to the fact that different proteins could have comigrated in the same band of the gel, which could have masked the differences of specific proteins between groups. Interestingly, three bands, in the range of 10–15 kDa, were significantly different between the two salivary groups (p < .1). Consequently, these preliminary results open the door to new proteomics studies to identify the protein(s) involved in the observed results.

3.4.2 | Total antioxidant capacity of saliva from hyposalivators or control subjects

To check a possible role of TAC on the differences on aroma release and metabolism observed in the two groups, TAC was analyzed in the

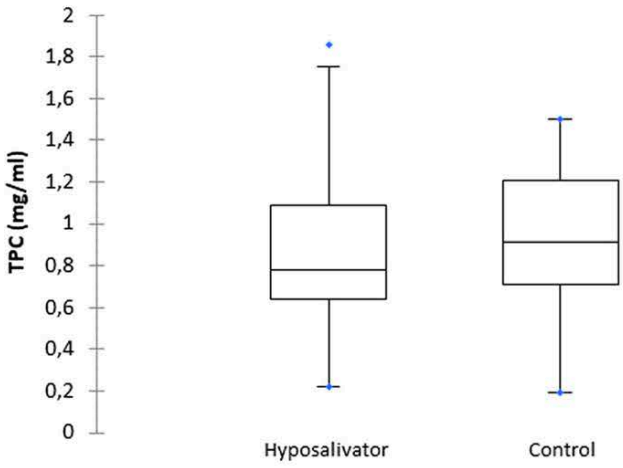

FIGURE 3 Box plot representation of the TPC determined in the salivas from the hyposalivator and control groups. Box outline represents lower and upper quartiles, the line inside the box is the median value and the circles correspond to the smallest and largest observations

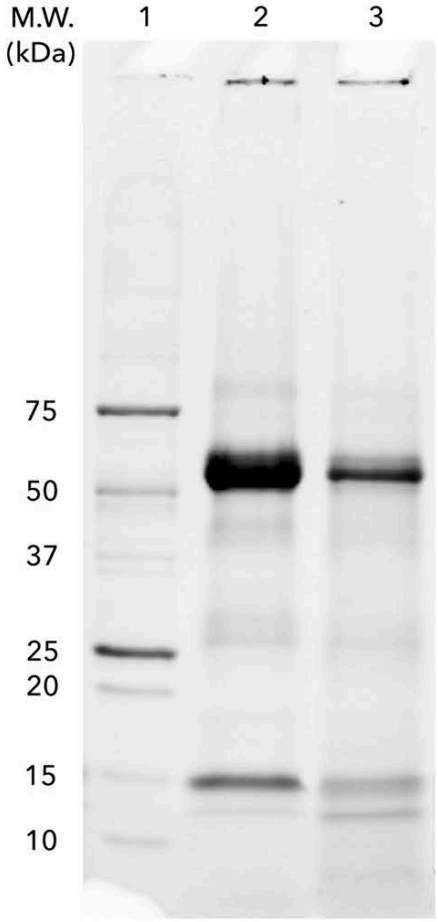

FIGURE 4 Protein profiles corresponding to the protein standard (1) and the stimulated salivary samples from two subjects: one hyposalivator (2) and one control (3)

30 saliva samples and results showed significant differences in the TAC values between both groups (Figure 5). In this regard, the hyposalivator group presented significantly higher TAC values than those of the control group, which might explain at least partially the higher metabolization rate and thus, the lower aroma release observed for this group. In previous papers, it has been suggested a negative association between the salivary TAC and the ex vivo release of aroma compounds (Munoz-Gonzalez et al., 2018b; Piombino et al., 2014). Although the mechanisms on how TAC impact aroma release are to date unclear, these effects could be related to the oxidative status of the saliva samples, which could affect the aroma compounds prone to redox reactions (Piombino et al., 2014). Recently, it was ascertained that the presence of NADH helped to take place at a higher rate the enzymatic conversion of aroma compounds (octanal) by saliva (Munoz-Gonzalez et al., 2018b). NADH is a coenzyme, which is used as a reducing agent. Moreover, it has been suggested a relation between the antioxidant status and the total amount of reducing agents in saliva (Kohen, Tirosh, & Kopolovich, 1992). Therefore, it is possible that people with high TAC have also high concentration of NADH in their saliva. However, further research is required to validate this hypothesis.

Finally, it should be mentioned that the effects of hyposalivation on aroma compounds need to be validated in vivo, taking into account

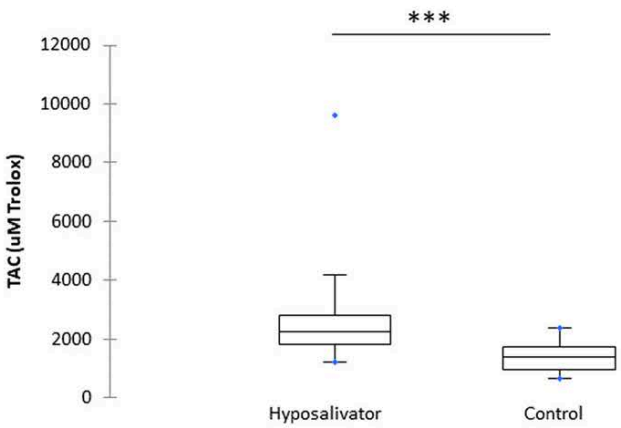

FIGURE 5 Box plot representation of the TAC determined in the salivas from the hyposalivator and control groups. Box outline represents lower and upper quartiles, the line inside the box is the median value and the arms of the box correspond to the smallest and largest observations (***Significant differences $p < .0001$)

the control of confounding factors (age, gender, BMI, drug intake, diseases, mental status, or dental status). As stated above, salivary parameters might be modified by the health status of individuals. For example, it has been seen that obese people presented higher TAC values than normal-weight subjects (Piombino et al., 2014) and that patients with dementia presented lower TAC values than control subjects (Choromanska et al., 2017). Moreover, hyposalivation is frequently present in diverse systemic diseases and immunological disorders, such as obesity (Flink et al., 2008), diabetes mellitus (Conner, Iranpour, & Mills, 1970), or dementia (e.g., Alzheimer's dementia; Choromanska et al., 2017; Flink et al., 2008), and it can be also an adverse effect of the treatments (such as radiotherapy) used to treat them (Narhi et al., 1992; Schubert & Izutsu, 1987; Sreebny & Valdini, 1988; Valdez, Atkinson, Ship, & Fox, 1993). Therefore, as hyposalivation might have different origins, the dispersion of saliva composition of the subjects suffering it (and therefore its effect on aroma perception) could also be very high. Moreover, some of these conditions (e.g., dementia) could affect directly the sensory integration in the brain, masking the contribution of saliva to aroma perception.

4 | CONCLUSIONS

In conclusion, from a panel formed by 110 elderly people, 15 of them suffered from hyposalivation (measured as presenting a salivary flow rate lower than 0.8 ml/min), which represented the 13.6% of the population. Most of them were women.

Moreover, this work has demonstrated for the first time that interindividual differences of saliva from elderly people affect aroma release and ex vivo metabolization of aroma compounds. In particular, saliva from elderly people suffering from hyposalivation presented a lower release and/or a higher metabolization of aroma compounds (octanal, ethyl hexanoate, and 2-nonanone) than saliva from the control group. Although no differences on the total protein content between groups were found, the involvement of specific proteins on the present results cannot be discarded. Moreover, saliva from the hyposalivator group presented a significantly higher TAC mean than that of the control group.

These findings could indicate that people suffering from hyposalivation could present an altered aroma perception due to a different amount of aroma compounds reaching the olfactory receptors by the retronasal pathway, concomitantly with the dissimilar formation of new metabolites with different sensory properties. However, this finding found under ex vivo conditions will need to be confirmed in an in vivo and more realistic situation, in which the influence of other orophysiological parameters can be taken into account and in times comparable with the eating process. Moreover, the control of confounding factors in future research is mandatory to assess if these differences among salivary groups observed ex vivo can have a sensory meaning.

ACKNOWLEDGMENTS

We give a special thanks to Chantal Septier and Aurelie Prot for technical assistance and to the volunteers for providing us the saliva samples. This work has been performed with the support of (1) the Agreenskills fellowship programme which has received funding from the EU's Seventh Framework Programme under grant agreement N°FP7-609398 (AgreenSkills+ contract), (2) the research prize awarded by the French Nutrition Society in 2017 to C.M-G, and (3) the projects: MUFFIN N° 14-CE20-0001-01 and AlimaSSenS N°14-CE20-0003-01.

ETHICAL STATEMENTS

Conflict of Interest: The authors declare no conflict of interest in publishing this work.

Ethical Review: This study was approved by the French Ethics Committee for Research (CPP Est I, Dijon, #14.06.03, ANSM #2014-A00071-46).

Informed Consent: Written informed consent was obtained from all study participants.

ORCID

Carolina Muñoz-González https://orcid.org/0000-0001-6185-7049

REFERENCES

Affoo, R. H., Foley, N., Garrick, R., Siqueira, W. L., & Martin, R. E. (2015). Meta-analysis of salivary flow rates in young and older adults. *Journal of the American Geriatrics Society*, *63*(10), 2142–2151. https://doi.org/10.1111/jgs.13652

Buettner, A. (2002a). Influence of human saliva on odorant concentrations. 2. Aldehydes, alcohols, 3-alkyl-2-methoxypyrazines, methoxyphenols, and 3-hydroxy-4,5-dimethyl-2(5H)-furanone. *Journal of Agricultural and Food Chemistry*, *50*(24), 7105–7110. https://doi.org/10.1021/jf020714o

Buettner, A. (2002b). Influence of human salivary enzymes on odorant concentration changes occurring in vivo. 1. Esters and thiols. *Journal of Agricultural and Food Chemistry*, *50*(11), 3283–3289. https://doi.org/10.1021/jf011586r

Castagnola, M., Cabras, T., Vitali, A., Sanna, M. T., & Messana, I. (2011). Biotechnological implications of the salivary proteome. *Trends in Biotechnology*, *29*(8), 409–418. https://doi.org/10.1016/j.tibtech.2011.04.002

Choromanska, M., Klimiuk, A., Kostecka-Sochon, P., Wilczynska, K., Kwiatkowski, M., Okuniewska, N., … Maciejczyk, M. (2017).

Antioxidant defence, oxidative stress and oxidative damage in saliva, plasma and erythrocytes of dementia patients. Can salivary AGE be a marker of dementia? *International Journal of Molecular Sciences*, *18*(10). pii: E2205. https://doi.org/10.3390/ijms18102205

Conner, S., Iranpour, B., & Mills, J. (1970). Alteration in parotid salivary flow in diabetes mellitus. *Oral Surgery Oral Medicine Oral Pathology Oral Radiology and Endodontics*, *30*(1), 55. https://doi.org/10.1016/0030-4220(70)90011-3

Dormenval, V., Mojon, P., & Budtz-Jorgensen, E. (1999). Associations between self-assessed masticatory ability, nutritional status, prosthetic status and salivary flow rate in hospitalized elders. *Oral Diseases*, *5*(1), 32–38.

Feron, G., Ayed, C., Qannari, E. M., Courcoux, P., Laboure, H., & Guichard, E. (2014). Understanding aroma release from model cheeses by a statistical multiblock approach on oral processing. *PLoS One*, *9*(4), e93113. https://doi.org/10.1371/journal.pone.0093113

Flink, H., Bergdahl, M., Tegelberg, A., Rosenblad, A., & Lagerlof, F. (2008). Prevalence of hyposalivation in relation to general health, body mass index and remaining teeth in different age groups of adults. *Community Dentistry and Oral Epidemiology*, *36*(6), 523–531. https://doi.org/10.1111/j.1600-0528.2008.00440.x

Folstein, M. F., Folstein, S. E., & McHugh, P. R. (1975). Mini-mental state - practical method for grading cognitive state of patients for clinician. *Journal of Psychiatric Research*, *12*(3), 189–198. https://doi.org/10.1016/0022-3956(75)90026-6

Genovese, A., Piombino, P., Gambuti, A., & Moio, L. (2009). Simulation of retronasal aroma of white and red wine in a model mouth system. Investigating the influence of saliva on volatile compound concentrations. *Food Chemistry*, *114*(1), 100–107. https://doi.org/10.1016/j.foodchem.2008.09.022

Guichard, E., Repoux, M., Qannari, E. M., Laboure, H., & Feron, G. (2017). Model cheese aroma perception is explained not only by in vivo aroma release but also by salivary composition and oral processing parameters. *Food & Function*, *8*(2), 615–628. https://doi.org/10.1039/c6fo01472k

Inoue, H., Ono, K., Masuda, W., Morimoto, Y., Tanaka, T., Yokota, M., & Inenaga, K. (2006). Gender difference in unstimulated whole saliva flow rate and salivary gland sizes. *Archives of Oral Biology*, *51*(12), 1055–1060. https://doi.org/10.1016/j.archoralbio.2006.06.010

Iwasaki, M., Yoshihara, A., Ito, K., Sato, M., Minagawa, K., Muramatsu, K., … Miyazaki, H. (2016). Hyposalivation and dietary nutrient intake among community-based older Japanese. *Geriatrics & Gerontology International*, *16*(4), 500–507. https://doi.org/10.1111/ggi.12500

Kohen, R., Tirosh, O., & Kopolovich, K. (1992). The reductive capacity index of saliva obtained from donors of various ages. *Experimental Gerontology*, *27*(2), 161–168. https://doi.org/10.1016/0531-5565(92)90040-7

Leake, S. L., Pagni, M., Falquet, L., Taroni, F., & Greub, G. (2016). The salivary microbiome for differentiating individuals: Proof of principle. *Microbes and Infection*, *18*(6), 399–405. https://doi.org/10.1016/j.micinf.2016.03.011

Mosca, A. C., & Chen, J. S. (2017). Food-saliva interactions: Mechanisms and implications. *Trends in Food Science & Technology*, *66*, 125–134. https://doi.org/10.1016/j.tifs.2017.06.005

Muñoz-González, C., Feron, G., & Canon, F. (2018a). Main effects of human saliva on flavour perception and the potential contribution to food consumption. *Proceedings of the Nutrition Society*, *77*, 423–431. https://doi.org/10.1017/S0029665118000113

Munoz-Gonzalez, C., Feron, G., Brule, M., & Canon, F. (2018b). Understanding the release and metabolism of aroma compounds using micro-volume saliva samples by ex vivo approaches. *Food Chemistry*, *240*, 275–285. https://doi.org/10.1016/j.foodchem.2017.07.060

Munoz-Gonzalez, C., Feron, G., Guichard, E., Rodriguez-Bencomo, J. J., Martin-Alvarez, P. J., Moreno-Arribas, M. V., Pozo-Bayon, M. A. (2014). Understanding the role of saliva in aroma release from wine by using static and dynamic headspace conditions. *Journal of Agricultural and Food Chemistry*, *62*(33), 8274–8288. https://doi.org/10.1021/jf503503b

Muñoz-González, C., Vandenberghe-Descamps, M., Feron, G., Canon, F., Labouré, H., & Sulmont-Rossé, C. (2017). Association between salivary hypofunction and food consumption in the elderlies. A systematic literature review. *The Journal of Nutrition, Health & Aging*, *22*, 407–419. https://doi.org/10.1007/s12603-017-0960-x

Narhi, T. O., Meurman, J. H., Ainamo, A., Nevalainen, J. M., Schmidtkaunisaho, K. G., Siukosaari, P., … Mäkilä, E. (1992). Association between salivary flow-rate and the use of systemic medication among 76-year-old, 81-year-old, and 86-year-old inhabitants in Helsinki, Finland. *Journal of Dental Research*, *71*(12), 1875–1880. https://doi.org/10.1177/00220345920710120401

Neyraud, E., Palicki, O., Schwartz, C., Nicklaus, S., & Feron, G. (2012). Variability of human saliva composition: Possible relationships with fat perception and liking. *Archives of Oral Biology*, *57*(5), 556–566. https://doi.org/10.1016/j.archoralbio.2011.09.016

Pages-Helary, S., Andriot, I., Guichard, E., & Canon, F. (2014). Retention effect of human saliva on aroma release and respective contribution of salivary mucin and alpha-amylase. *Food Research International*, *64*, 424–431. https://doi.org/10.1016/j.foodres.2014.07.013

Piombino, P., Genovese, A., Esposito, S., Moio, L., Cutolo, P. P., Chambery, A., … Ercolini, D. (2014). Saliva from obese individuals suppresses the release of aroma compounds from wine. *PLoS One*, *9*(1), e85611. https://doi.org/10.1371/journal.pone.0085611

Ployon, S., Morzel, M., & Canon, F. (2017). The role of saliva in aroma release and perception. *Food Chemistry*, *226*, 212–220.

Samnieng, P., Ueno, M., Shinada, K., Zaitsu, T., Wright, F. A. C., & Kawaguchi, Y. (2012). Association of hyposalivation with oral function, nutrition and oral health in community-dwelling elderly Thai. *Community Dental Health*, *29*(1), 117–123. https://doi.org/10.1922/CDH_2690Ueno07

Schipper, R. G., Silletti, E., & Vinyerhoeds, M. H. (2007). Saliva as research material: Biochemical, physicochemlical and practical aspects. *Archives of Oral Biology*, *52*(12), 1114–1135. https://doi.org/10.1016/j.archoralbio.2007.06.009

Schubert, M. M., & Izutsu, K. T. (1987). Iatrogenic causes of salivary-gland dysfunction. *Journal of Dental Research*, *66*, 680–688. https://doi.org/10.1177/00220345870660s213

Soini, H., Routasalo, P., Lauri, S., & Ainamo, A. (2003). Oral and nutritional status in frail elderly. *Special Care in Dentistry*, *23*(6), 209–215.

Solemdal, K., Sandvik, L., Willumsen, T., Mowe, M., & Hummel, T. (2012). The impact of oral health on taste ability in acutely hospitalized elderly. *PLoS One*, *7*(5), e36557. https://doi.org/10.1371/journal.pone.0036557

Sreebny, L. M., & Valdini, A. (1988). Xerostomia. 1. Relationship to other oral symptoms and salivary-gland hypofunction. *Oral Surgery Oral Medicine Oral Pathology Oral Radiology and Endodontics*, *66*(4), 451–458. https://doi.org/10.1016/0030-4220(88)90268-x

Valdez, I. H., Atkinson, J. C., Ship, J. A., & Fox, P. C. (1993). Major salivary-gland function in patients with radiation-induced xerostomia—Flow-rates and sialochemistry. *International Journal of Radiation Oncology Biology Physics*, *25*(1), 41–47. https://doi.org/10.1016/0360-3016(93)90143-j

How to cite this article: Muñoz-González C, Brulé M, Feron G, Canon F. Does interindividual variability of saliva affect the release and metabolization of aroma compounds ex vivo? The particular case of elderly suffering or not from hyposalivation. *J Texture Stud.* 2019;50:36–44. https://doi.org/10.1111/jtxs.12382